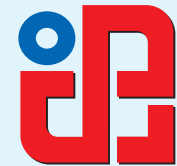




UNIVERSITY OF NOVI SAD
Faculty of Technical Sciences
Department of Production Engineering
Novi Sad, Serbia



12th INTERNATIONAL SCIENTIFIC CONFERENCE
MMA 2015 - FLEXIBLE TECHNOLOGIES



PROCEEDINGS

Novi Sad, 25-26 September 2015



UNIVERSITY OF NOVI SAD
FACULTY OF TECHNICAL SCIENCES
DEPARTMENT OF PRODUCTION ENGINEERING
NOVI SAD, SERBIA



12th INTERNATIONAL SCIENTIFIC CONFERENCE
MMA 2015 - FLEXIBLE TECHNOLOGIES



PROCEEDINGS

Novi Sad, 25-26 September 2015

PROCEEDINGS OF THE 12th INTERNATIONAL SCIENTIFIC CONFERENCE
MMA 2015 - FLEXIBLE TECHNOLOGIES
Andrievlje, 2015

Publisher: **FACULTY OF TECHNICAL SCIENCES
DEPARTMENT OF PRODUCTION ENGINEERING
21000 NOVI SAD, Trg Dositeja Obradovica 6
SERBIA**

Organization of this Conference was approved by Educational-scientific Council of Faculty of Technical Sciences in Novi Sad

Editor: **Dr Rade Doroslova ki, professor, dean**

Reviewers team:

Prof. dr Bojan BABI , MF Beograd, SRB
Prof. dr Jože BALI , Univerzitet Maribor, SLO
Prof. dr Miroslav BADIDA, TU Košice, SK
Assoc. Prof. dr Sebastian BALOŠ, FTN Novi Sad, SRB
Assoc. Prof. dr Igor BUDAK, FTN Novi Sad, SRB
Prof. dr Franc UŠ, Univerzitet Maribor, SLO
Prof. dr Goran DEVEDŽI , MF Kragujevac, SRB
Prof. dr Mircea VIOREL DRAGOI, UT Brasov, RO
Prof. dr Kornel EHMANN, NU Illinois, USA
Prof. dr Marin GOSTIMIROVI , FTN Novi Sad, SRB
Prof. dr Miodrag HADŽISTEVI , FTN Novi Sad, SRB
Prof. dr Janko HODOLI , FTN Novi Sad, SRB
Prof. dr Jerzy J DRZEJEWSKI, UT Wroclaw, PL
Prof. dr Vid JOVIŠEVI , MF Banja Luka, BIH
Prof. dr Janez KOPA , Univerzitet Ljubljana, SLO
Prof. dr Pavel KOVA , FTN Novi Sad, SRB
Assoc. Prof. dr Ognjen LUŽANIN, FTN Novi Sad, SRB
Prof. dr Vidosav MAJSTOROVI , MF Beograd, SRB
Prof. dr Miodrag MANI , MF Niš, SRB
Prof. dr Ildiko MANKOVA, TU Košice, SK
Prof. dr Dorian MARJANOVI , FSB Zagreb, HR
Prof. dr Dragan MILUTINOVI , MF Beograd, SRB

Prof. dr Zoran MILOJEVI , FTN Novi Sad, SRB
Prof. dr Ostoja MILETI , MF Banja Luka, BiH
Prof. dr Zoran MILJKOVI , MF Beograd, SRB
Prof. dr Slobodan NAVALUŠI , FTN Novi Sad, SRB
Prof. dr Bogdan NEDI , MF Kragujevac, SRB
Prof. dr Zoran PANDILOV, MF Skoplje, MK
Prof. dr Petar PETROVI , MF Beograd, SRB
Prof. dr. Milentije STEFANOVI , FIN Kragujevac, SRB
Prof. dr Goran ŠIMUNOVI , SF Slavonski Brod, HR
Prof. dr Branko ŠKORI , FTN Novi Sad, SRB
Assoc. Prof. dr Slobodan TABAKOVI , FTN Novi Sad, SRB
Prof. dr Ljubodrag TANOVI , MF Beograd, SRB
Prof. dr Miroslav TRAJANOVI , MF Niš, SRB
Prof. dr Ivica VEŽA, FESB Split, HR
Prof. dr Dragiša VILOTI , FTN Novi Sad, SRB
Assoc. Prof. dr or e VUKELI , FTN Novi Sad, SRB
Prof. dr Milan ZELJKOVI , FTN Novi Sad, SRB
Assist. Prof. Aleksandar ŽIVKOVI , FTN Novi Sad, SRB
Assist. Prof. dr Saša ŽIVANOVI , MF Beograd, SRB

Technical treatment and design: **Dr Mijodrag MILOSEVI , assistant professor
M.Sc Jovan VUKMAN, assistant**

Manuscript submitted for publication: **September 18, 2015**
Printing: **1st**
Circulation: **100 copies**

CIP classification:

CIP -

621.7/.9(082)
621.9(082)

INTERNATIONAL Scientific Conference MMA 2015 "Flexible Technologies" (12 ; 2015 ; Novi Sad)

Proceedings / 12th International Scientific Conference MMA 2015 "Flexible Technologies", Novi Sad, 25-26 September 2015 ; [editor Rade Doroslova ki]. - 1. izd. - Novi Sad : Faculty of Technical Sciences, 2015 (Novi Sad : Grid). - 301 str. : ilustr. ; 30 cm

Tiraž 100. - Bibliografija uz svaki rad. - Registar.

ISBN 978-86-7892-722-5

a) - b) - -

Printing by: **FTN, Graphic Centre
GRID, Novi Sad**

Financing of the Proceedings was sponsored by the Ministry of Education, Science and Technological Development of the Republic of Serbia and supported by the Provincial Secretariat for Science and Technological Development of AP Vojvodina.



12th INTERNATIONAL SCIENTIFIC CONFERENCE NOVI SAD, SERBIA, SEPTEMBER 25-26, 2015

CONFERENCE ORGANIZER

University of Novi Sad
Faculty of Technical Sciences
Department of Production Engineering
Novi Sad, Serbia

PROGRAMME COMMITTEE

Prof. dr Milan Zeljkovi , FTN Novi Sad, chairman
Prof. dr Sergei Alexandrov, IPM Moskva, RUS
Prof. dr Slavko Arsovski, FIN Kragujevac, SRB
Prof. dr Gustav Arz, BUTE Budapest, HU
Prof. dr Bojan Babi , MF Beograd, SRB
Prof. dr Miroslav Babi , FIN Kragujevac, SRB
Prof. dr Jože Bali , Univerzitet Maribor, SLO
Prof. dr Miroslav Badida , TU Košice, SK
Prof. dr Livia Dana Beju, US Sibiu, RO
Prof. dr Konstantinos Bouzakis, AU Thessaloniki, GR
Prof. dr Erhan Budak, FENS, Istanbul, TR
Prof. dr Ilija Čosi , FTN Novi Sad, SRB
Prof. dr Franc Čuš, Univerzitet Maribor, SLO
Prof. dr Goran Devedži , FIN Kragujevac, SRB
Prof. dr Cristian Doicin, UP Bucharest, RO
Prof. dr Dragan Domazet, UM Beograd, SRB
Prof. dr Ljubomir Dimitrov, TU Sofija , BG
Prof. dr Mircea Viorel Dragoi, UT Brasov, RO
Prof. dr Numan M. Durakbasa, TU Be , AT
Prof. dr Kornel Ehmann, NU Illinois, USA
Prof. dr Sabahudin Ekinovi , MF Zenica, BIH
Prof. dr Dušan Golubovi , MF Istočno Sarajevo, BIH
Prof. dr Marin Gostimirovi , FTN Novi Sad, SRB
Prof. dr Janko Hodoli , FTN Novi Sad, SRB
Prof. dr Jaromir Houša, FMEPrague, CZ
Prof. dr František Holešovský, JEPU Usti, CZ
Prof. dr Jerzy J. Drzejewski, UT Wroclaw, PL
Prof. dr Vid Jovišević , MF Banja Luka, BIH
Prof. dr Janez Kopa , Univerzitet Ljubljana, SLO
Prof. dr Pavel Kova , FTN Novi Sad, SRB
Prof. dr Ivan Kuric, FME Žilina, SK

Prof. dr Miodrag Lazi , FIN Kragujevac, SRB
Prof. dr Ljubomir Luki , FMG Kraljevo, SRB
Prof. dr Vidosav Majstorovi , MF Beograd, SRB
Prof. dr Miodrag Mani , MF Niš, SRB
Prof. dr Ildiko Mankova, TU Košice, SK
Prof. dr Dorian Marjanovi , FSB Zagreb, HR
Prof. dr Dragan Milutinovi , MF Beograd, SRB
Prof. dr Zoran Miljkovi , MF Beograd, SRB
Prof. dr Radivoje Mitrovi , MF Beograd, SRB
Prof. dr Nikolai Myshkin, NASB Gomel, BY
Prof. dr Bogdan Nedi , FIN Kragujevac, SRB
Prof. dr Zoran Pandilov, MF Skoplje, MK
Prof. dr Emil Radu Precup, PU Timisoara, RO
Prof. dr Petar Petrovi , MF Beograd, SRB
Prof. dr Goran Putnik, University of Minho, PT
Prof. dr Miroslav Radovanovi , MF Niš, SRB
Prof. dr Sreten Savićević , MF Podgorica, CG
Prof. dr Goran Šimunovi , SF Slavonški Brod, HR
Prof. dr Mirko Sokovi , Univerzitet Ljubljana, SLO
Prof. dr Ljubomír Šooš, STU Bratislava, SK
Prof. dr Dušan Šormaz, OH Athens, SAD
Prof. dr Tibor Szalay, BUTE Budapest, HU
Assoc. Prof. dr Slobodan Tabakovi , FTN Novi Sad, SRB
Prof. dr Ljubodrag Tanovi , MF Beograd, SRB
Prof. dr Peter Toth, Óbuda University, HU
Prof. dr Miroslav Trajanovi , MF Niš, SRB
Prof. dr Toma Udiljak, FSB Zagreb, HR
Prof. dr Ivica Veža, FESB Split, HR
Prof. dr Dragiša Viloti , FTN Novi Sad, SRB
Prof. dr Vojo Višekruna, MF Mostar, BIH



**12th INTERNATIONAL SCIENTIFIC CONFERENCE
NOVI SAD, SERBIA, SEPTEMBER 25-26, 2015**

HONORARY COMMITTEE

Mr Dragan Banjac, FTN Novi Sad, SRB

*Prof. dr Pavao Bojani , MF Beograd, SRB
Prof. dr Ljubomir Borojev, FTN Novi Sad, SRB
Prof. dr Branko Ivkovi , FIN Kragujevac, SRB
Prof. dr Milenko Jovi i , MF Beograd, SRB
Prof. dr Milisav Kalajdži , MF Beograd, SRB
Prof. dr Vu ko Me anin, FMG Kraljevo, SRB*

*Prof. dr Vladimir Mila i , MF Beograd, SRB
Prof. dr Dragoje Miliki , FTN Novi Sad, SRB
Prof. dr Ratko Mitrovi , FIN Kragujevac, SRB
Prof. dr Sava Sekuli , FTN Novi Sad, SRB
Prof. dr Bogdan Sovilj, FTN Novi Sad, SRB
Prof. dr Jelena Stankov, FTN Novi Sad, SRB
Prof. dr Velimir Todi , FTN Novi Sad, SRB
Prof. dr Dragutin Zelenovi , Academic, SRB*

ORGANIZING COMMITTEE

*Associate Professor Slobodan Tabakovi , chairman
dr Milenko Sekuli , Associate Professor
dr Igor Budak, Associate Professor
dr or e Vukeli , Associate Professor
dr Aco Anti , Assistant Professor
dr Mijodrag Miloševi , Assistant Professor*

*dr Dejan Luki , Assistant Professor
dr Aleksandar Živkovi , Assistant Professor
M.Sc. Cvijetin Mla enovi , Assistant
M.Sc. Goran Jovi i , Research Assistant
M.Sc. Jovan Vukman, Research Assistant, technical
secretary*



**12th INTERNATIONAL SCIENTIFIC CONFERENCE
NOVI SAD, SERBIA, SEPTEMBER 25-26, 2015**

ACKNOWLEDGEMENT

Organisation of 12th International Scientific Conference MMA 2015 – FLEXIBLE TECHNOLOGIES was made possible with understanding and financial help of following sponsors:

- **MINISTRY OF EDUCATION, SCIENCE AND TECHNOLOGICAL DEVELOPMENT OF THE REPUBLIC OF SERBIA** – Belgrade
- **PROVINCIAL SECRETARIAT FOR SCIENCE AND TECHNOLOGICAL DEVELOPMENT OF AP VOJVODINA** – Novi Sad
- **FACULTY OF TECHNICAL SCIENCES** - Novi Sad
- **DEPARTMENT FOR PRODUCTION ENGINEERING AT THE FACULTY OF TECHNICAL SCIENCES** - Novi Sad
- **INICAD DESIGN** – Bucharest
- **TEAM CAD** - Belgrade
- **MOLDEX** –
- **GASTEH** – Indjija
- **Gruji &** – Novi Sad
- **FKL** – Temerin

Conference MMA - FLEXIBLE TECHNOLOGIES, as well as other conferences with a long tradition, with its regular holding contribute to the continuity of application of the scientific results in the metal processing industry.

The last two decades in the world are characterized by very intensive development of production techniques and technologies. In our country, in addition to the bad situation in the metal industry in recent years, are still present, as bright spots, training of personnel and research work. It shows the vitality of research personnel in the region who wants, with their enthusiasm and persistence, provide a significant contribution to the development of production engineering in this region, both through the application of scientific results in practice and education of personnel in the field of production techniques and technologies.

At the Conference are represented current topics of production engineering with an emphasis on new technologies - effects and significance of their introduction into the production processes, the globalization of production and transfer of technologies . Conference MMA, as one of the most significant scientific and professional conferences in this field, aims to gather and exchange experiences of researchers from universities, institutes and experts from the industry, and thus to contribute to the revival of the metal processing industry in these regions.

Twelfth International Scientific Conference MMA 2015 - FLEXIBLE TECHNOLOGIES has been held for the ninth time as an international. So far conference by number of works, by their quality and by the participation of foreign authors acquired an enviable reputation among the scientific and professional workers from universities and industry.

Conference MMA - FLEXIBLE TECHNOLOGIES includes the following topics:

- ◆ *MATERIAL PROCESSING TECHNOLOGIES*
- ◆ *MACHINE TOOLS*
- ◆ *METROLOGY, QUALITY, FIXTURES, CUTTING TOOLS AND TRIBOLOGY*
- ◆ *AUTOMATIC FLEXIBLE TECHNOLOGICAL SYSTEMS, CAx AND CIM PROCEDURES AND SYSTEMS*
- ◆ *OTHER PRODUCTION ENGINEERING TECHNOLOGIES*
- ◆ *MECHANICAL ENGINEERING AND ENVIRONMENTAL PROTECTION*
- ◆ *BIO-MEDICAL ENGINEERING*

With about 60 papers, of which almost 30% coming from abroad, XII International Scientific Conference MAY 2015 - FLEXIBLE TECHNOLOGIES is keeping the level of the previous conferences. The participation of many authors from home and abroad, and issues covered in the papers, confirms the efforts for holding the conference and thus contribute to the exchange of knowledge, research results and experiences of experts from industry, research institutions and universities working in the field of production engineering.

On behalf of the Programme and Organization Committee of the Conference we would like to thank all home and foreign authors, reviewers, as well as institutions and individuals who contributed to the realization of high-quality program of the Conference.

Novi Sad, September 2015,

*Chairman of the Programme Committee
Prof. dr Milan Zeljkovi
Chairman of the Organization Committee
Prof. dr Slobodan Tabakovi ,*



Contents

Section A: METAL CUTTING

Muženi , D., Kramar, D., Sekuli , M., Gostimirovi , M., Kopa , J.: HYBRID MANUFACTURING; CUTTING PROCESSES WITH LASER ASSISTANCE	1
Kheifetz, M., Gaiko, V., Borodavko, V., Klimenko, S., Tanovi , Lj.: HIGH-PERFORMANCE METHODS OF DETAIL SURFACE PROCESSING	5
Kheifetz, M., Pynkin, A., Pozilova, N., Klimenko, S., Tanovi , Lj.: ANALYSIS OF INTENSIVE PROCESSING METHODS OF TREATMENT	9
Sekuli , M., Kova , P., Gostimirovi , M., Hadžistevi , M., Rodi , D., Pucovski, V.: MODELING OF THE MAIN CUTTING FORCE IN FACE MILLING HARDENED STEEL BY ROTATABLE CENTRAL COMPOSITE DESIGN OF EXPERIMENTS.....	13
Simonovi , S.: NANOMECHANICAL MODELLING OF A CUTTING PROCESS	17
Gostimirovi , M., Rodi , D., Kova , P., Ješi , D., Kulundži N.: AN EXPERIMENTAL STUDY OF THE CUTTING FORCES IN CREEP-FEED GRINDING	21
Barali , J., Nedi , B.: THE INFLUENCE OF ABRASIVE WATER JET PROCESSING PARAMETERS ON REACTION FORCE.....	25
Pucovski, V., Sekuli , M., Kramar, D., Gostimirovi , M., Kopa , J.: ULTRASONIC ASSISTED TURNING	29
Sekuli , S.: OPTIMIZATION OF CUTTING CONDITIONS IN DRILLING OPERATIONS BY SIMULATION.....	33

Section B: MACHINE TOOLS

Košarac, A., Zeljkovi M., Mla enovi , C., Živkovi , A.: CREATE SISO STATE SPACE MODEL OF MAIN SPINDLE FROM ANSYS MODEL	37
Knežev, M., Živkovi , A., Mla enovi , C.: ANALYSIS STATIC AND DYNAMIC BEHAVIOR OF HYDRODYNAMIC SPINDLE	43
Lazarevi D., Nedi B.: MEASUREMENT TECHNOLOGIES AND MACHINING ERRORS	47

Mitrovi , S, Dimi , Z, Vidakovi , J, Lutovac, M, Kvrđi , V.: SYSTEM FOR SIMULATION AND SUPERVISION OF ROBOTIC CELLS	51
Živkovi , A., Zeljkovi , M., Tabakovi , S., Mla enovi , C.: AN IMPROVED MODEL FOR DETERMINING THE THERMAL PRELOAD OF BALL BEARINGS WITH ANGULAR CONTACT	55
Tabakovi , S., Živanovi , S., Zeljkovi , M.: THE APPLICATION OF VIRTUAL PROTOTYPE IN DESIGN OF A HYBRID MECHANISM BASED MACHINE TOOLS	59
Anti , A., Šari , T., Miloševi , M.: A MODULE FOR FEATURE EXTRACTION WITHIN THE NEURO-FUZZY SYSTEM FOR TOOL WEAR RECOGNITION	63
Đi a , ., Zeljkovi , M., Sredanovi , B., Borojevi , S.: IDENTIFICATION OF DYNAMICAL CONTACT PARAMETERS FOR SPINDLEHOLDER-TOOL ASSEMBLY OPTIMIZATION OF THE SPINDLE-BEARING SYSTEM	67
Prodanovi , S., Nedi , N., Luki , Lj.: POSSIBILITIES FOR DISTURBANCE REJECTION IN THE DECOUPLED TITO PROCESS	71

Section C: METROLOGY, QUALITY, FIXTURES, METAL CUTTING TOOLS AND TRIBOLOGY

Luđi , R., Nikoli I., Juki , J., Šari , T., Šimunovi , G., Šimunovi , K., Galzina, V., Svalina I.: APPLICATION OF KAIZEN METHOD THROUGH IMPLEMENTATION OF VISUAL SYSTEM FOR PRODUCTION CONTROL.....	75
Beju, L.D., Brindasu,P.D., Navalusic, S.: OPTIMISATION OF THE INSERT TOP CLAMPING SYSTEM USED AT TURNING TOOLS.....	79
Bojani , M., Hadžistevi , M., Mla enovi , C.: STRAIGHTNESS EXAMINATION OF CMM AXES.....	83
Joti G., Hadžistevi M., Pejašinovi Ž., Štrbac B.: DETERMINATION OF CMM UNCERTAINTY USING CALIBRATED WORKPIECES	87
Majstorovi , D., V., Stojadinovi , M., S.: CYBER-PHYSIAL MANUFACTURING – INTELLIGENT MODEL FOR INSPECTION PLANNING ON CMM.....	93
Štrbac, B., Radlova ki, V., Spasi – Joki , V., Matin, I, Hadžistevi , M.: ESTIMATING TOTAL UNCERTAINTY OF MEASURING FLATNESS IN ACCORDANCE WITH GPS STANDARDS USING CMM	97

Section D: AUTOMATIC FLEXIBLE TECHNOLOGICAL SYSTEMS, CAx AND CIM PROCEDURES AND SYSTEMS

osi , I., Katalini , B., Teki , Ž., Lali , B.: RESHAPING THE FUTURE OF MANUFACTURING - 10 TRENDS FOR THE NEXT 10 YEARS	101
Wakhare, M., Šormaz, D.: RULE BASED AUTOMATED SETUP PLANNING WITH TOLERANCE CONSIDERATION	105

Cerjakovi , E., Top i , A., Lovri , S., Heri , M.: IMPACT OF PRODUCTION EQUIPMENT SELECTION ON PRODUCTION COSTS.....	113
ur ev, M., Miloševi , M., Luki , D., Jovi i , G., Vukman, J.: A REVIEW ON INTEGRATED PROCESS PLANNING AND PRODUCTION SCHEDULING APPROACH.....	117
Petronijevi , J., Petrovi , M., Vukovi , N., Miti , M., Babi , B., Miljkovi , Z.: MULTI-AGENT MODELING FOR INTEGRATED PROCESS PLANNING AND SCHEDULING	121
Petrovi , M., Petronijevi , J., Miti , M., Vukovi , N., Plemi , A., Miljkovi , Z., Babi , B.: THE ANT LION OPTIMIZATION ALGORITHM FOR FLEXIBLE PROCESS PLANNING	125
Šormaz, D., Wakhare, M.: AN EXTENDABLE CAPP KNOWLEDGE MODEL AND RULE-BASED METHOD OF PROCESS SELECTION FOR DIFFERENT MANUFACTURING FEATURES.....	129
Kokotovi , B., Živanovi , S., Jakovljević Ž.: VERIFICATION OF A PROCEDURE FOR FEEDRATE SCHEDULING FOR CONSTANT FORCE IN 2D MILLING OPERATIONS	137
Borojevi , S., Joviševi , V., Todi , V., Zeljkovi , M.: PARTS DESIGN BASED ON MANUFACTURING FEATURES.....	141
But, A.: VOLUMILL STRATEGY IN GROWING UP THE PRODUCTIVITY ON CNC MANUFACTURING.....	145
Jakovljevi , Ž., Markovi , V., Živanovi , S.: RECOGNITION OF QUADRICS FROM 3D POINT CLOUDS GENERATED BY SCANNING OF ROTATIONAL PARTS.....	149
Milojevi , Z., Tabakovi , S., Bojani , M., Zeljkovi , M.: MULTI AXIS NC CODE SIMULATION BASED ON THREE-DEXEL MODEL REPRESENTATION AND GPU	153
Petrovi , A., Ivanovi , S., Luki , Lj.; GENERATING PARAMETERS FROM THE NC CODE NEEDED FOR DEFINING THE OPTIMAL TOOL PATH.....	157
Živanovi , S., Kokotovi , B., Jakovljevi , Ž.: TURNING MACHINE SIMULATION FOR PROGRAM VERIFICATION	161
Section E: OTHER PRODUCTION ENGINEERING TECHNOLOGIES – METAL FORMING TECHNOLOGIES	
Stefanovi , M., Gulišija, Z., Mihailovi , M., Mandi , V., Patari , A.: THE IMPORTANCE OF TRIBO-MODELING IN DEVELOPMENT OF HOT FORGING TECHNOLOGY.....	165
Plan ak, M., Skakun, P., Ka mar ik I., Ivaniševi A., Milutinovi M., Viloti D.: SOME NEWER ACHIEVEMENTS IN COLD FORGING.....	169
Ran elovi , S., Nikoli , S., Milutinovi , M., Taniki , D.: ANALYSIS OF RUNNING SYSTEM AT INJECTION MOLDING TOOL FOR PRODUCTS WITH DIFFERENT GEOMETRY	173

Skakun, P., Planak, M., Karmar, I., Ivanišević, A., Movrin D., Vilotić, D., Milutinović, M.: FLOW RELIEF OPENINGS IN EXTRUSION OF GEAR-LIKE ELEMENTS - THEORETICAL AND NUMERICAL APPROACH	177
Sobotova, L., Badida, M.: CHARACTERIZATION OF LASER CLEANING OF STEEL SHEETS	181
Krašnik M., Vilotić, D., Štanić L., Stefanović, M.: EXPERIMENTAL AND NUMERIC ANALYSIS OF STEEL C45E FORMABILITY IN THE UPSETTING PROCESSES OF TAPERED SPECIMEN.....	185
Kovačević, L., Terek, P., Miletić, A., Kukuruzović, D., Kakaš, D.: APPLICATION OF CASTING SIMULATIONS IN OPTIMIZATION OF GATING SYSTEM WITH VERTICAL RUNNER EXTENSION	191
Reljić, V., Milenković, I., Šešlija, D., Dudić, S., Šulc, J.: DEVELOPMENT OF REMOTE CONTROLLED PNEUMATIC SPRING	195
Vukićević, M.: THERMITE WELDING.....	199

Section F: MECHANICAL ENGINEERING AND ENVIRONMENTAL PROTECTION

Vojinović Miloradov, M., Mihajlović, I., Miloradov, M., Radonić, J., Turk Sekulić, M., Španik, I.: MASS DISCHARGE OF EMERGING SUBSTANCES BASED ON CONCENTRATION LEVELS IN DANUBE IN THE VICINITY OF NOVI SAD	203
Adamović, D., Vojinović Miloradov, M., Dorić, J., Miloradov, M., Adamović S.: OPTIMAL WORKING REGIME OF IC ENGINE FROM THE POINT OF EMISSION CHARACTERISTICS	207
Gluvakov, Z., Agarski, B., Košut, Z., Hodolić, J., Kosec, B., Milijić, V.: MULTI-CRITERIA ASSESSMENT OF AGRICULTURAL AND WOOD BIOMASS PELLETS FROM ENVIRONMENTAL AND ENERGY PERSPECTIVE.....	211
Morača, S., Fajsić, A., Bekker, I., Šević, D.: THE SUSTAINABLE PRODUCT DESIGN AND MANUFACTURING PROCESS	215
Muránsky, J.: QUALITY OF ENVIRONMENT AND ITS QUANTITATIVE DETERMINATION IN MECHANICAL ENGINEERING	219

Section G: BIO-MEDICAL ENGINEERING - CAx

Luković, S., Devedžić, G., Luković, V., Anwer, N., Zečević Luković, T., Subburaj, K.: 3D MODELING OF SPINAL DEFORMITIES SHAPES USING 5TH DEGREE B-SPLINES.....	223
Grujić, J., Romek, A., Tabaković, N., Ličen, H.: CONTROL OF PROCESS OF MACHINING OF AN ARTIFICIAL FEMORAL HEAD	227
Movrin, D., Spasić, A., Ivanišević, A., Karmar, I., Vučajirić, V., Skakun, P., Milutinović M.: DETERMINATION OF INFILTRATION DEPTH IN 3D PRINTING TECHNOLOGY BY USING CT TECHNIQUE	231
Ranđelović, S., Mišić, D., Mišić, M., Kostić, I., Tanikić, D.: SOFTWARE SUPPORT FOR FMEA ANALYSIS IN ORTHOPEDIC SURGERY	235

Raspudi , V.: ROTATIONAL KINEMATICS OF LOWER LIMBS DURING STAIR ASCENT USING CAD/CAE	239
Spasi A., Vu aj irilovi V., Movrin D., Šokac M., Budak I., Till V.: CT DENSITY OF THE CORTICAL BONE OF ALVEOLAR PROCESS OF MAXILLA	243
Vasiljevi , D., Maravi , T., Kantardži , I., Lainovi , T., Blaži , L.: GENERATION OF A CT-SCAN BASED 3D SOLID MODEL OF A SECOND UPPER PREMOLAR TOOTH	247
AUTHOR INDEX	248
INFORMATION ABOUT DONATORS	251

12th INTERNATIONAL SCIENTIFIC CONFERENCE MMA 2015 -
FLEXIBLE TECHNOLOGIES

PROCEEDINGS



Section A:

METAL CUTTING

Novi Sad, 25-26 September 2015



12th INTERNATIONAL SCIENTIFIC CONFERENCE NOVI SAD, SERBIA, SEPTEMBER 25-26, 2015

Invited paper

Muženi , D., Kramar, D., Sekuli , M., Gostimirovi , M., Kopa , J.

HYBRID MANUFACTURING; CUTTING PROCESSES WITH LASER ASSISTANCE

Abstract: Hybrid manufacturing processes are based on the simultaneous and controlled interaction of process mechanisms and/or energy sources/tools having a significant effect on the process performance. Typical examples of hybrid processes are cutting processes (turning and milling) with laser assistance, also acknowledged as Laser Assisted Machining (LAM). With increasing demands for high-strength materials in industry and the recent development in laser technology, especially in terms of compactness, efficiency and flexibility, LAM processes have increased considerably during the last years. In this paper the state-of-the-art in the development of LAM systems for improving the machinability of different hard-to-machine materials are presented.

Key words: hybrid manufacturing, laser assisted machining, machinability, hard-to-machine materials

1. INTRODUCTION

Modern products, especially in the aviation industry, require high-performance materials that retain desired mechanical properties even at very high temperatures. Machinability of materials, which meet these requirements, is generally poor or economically unacceptable with the use of conventional machining processes. For the purpose of improving machinability and reducing machining costs, newer, hybrid approaches to the machining of such materials are being developed. Hybrid manufacturing processes are based on the simultaneous and controlled interaction of process mechanisms and/or energy sources/tools having a significant effect on the process performance [1]. Laser Assisted Machining (LAM) is a Hybrid Manufacturing Process, which consists of a conventional cutting tool and a laser beam (or more laser beams) that heats the to-be-machined material right in front of the cutting tool. Due to the laser heating the material is softened, which makes the cutting process easier and in some cases even the material removal mechanism changes. The changes in the temperature-dependent material properties significantly affect the machinability of some hard-to-machine materials in terms of cutting forces, tool wear, chip formation and machined surface integrity.

2. LASER SOURCES

There are three types of laser sources used for LAM, which differ in the active lasing medium: CO₂, Nd:YAG and High Power Diode Lasers (HPDL). In Table 1, the main characteristics of these types of lasers, including the absorptances for a metallic and a non-metallic material, are summarized. In terms of implementation of laser sources in an industrial LAM process, the most important characteristic of the laser source is efficiency, combined with the absorptance for the machined material. For example if we take a CO₂ laser, which has 10% efficiency in transforming electrical power into laser light, and use it for a LAM

process on carbon steel (0.1 absorptance), the final efficiency of laser heating is only about 1%. Very important characteristics in terms of implementation in an industrial process are also the size, rigidity and the possibility of using fibers for transmitting the laser light to the workpiece. The latter is a major advance in terms of flexibility. As seen in Table 1, HPDL-s have the highest efficiency and CO₂ laser systems cannot use fibers for transmitting the laser light to the workpiece. In terms of size a 1 kW CO₂, Nd:YAG and HPDL laser systems would have the volumes of about 1 m³, 100 dm³ and 100 cm³, respectively. Another advantage of HPDL-s is that the system needs almost no maintenance.

3. STATE-OF-THE-ART

As stated in [2], work material classes that are well suited to the application of LAM technology include: (i) hard and brittle materials such as engineering ceramics that can otherwise be subject only to cost-prohibitive abrasive processing, (ii) heat resistant materials like nickel alloys, (iii) materials with abrasive constituents such as high silicon content aluminum alloys, and (iv) materials with a propensity to significant strain hardening like austenitic stainless steels. In this paper, the review of the state-of-the-art in LAM is divided into five groups of materials: engineering ceramics, steel, superalloys, composite materials and cast iron.

3.1 Engineering ceramics

Engineering ceramics are known for their high hardness, brittleness and temperature resistance. Lei et al. [3] studied LAM of silicon nitride (Si₃N₄) and determined three mechanisms associated with ceramic material removal: (i) oxidation, melting and vaporization in a workpiece surface layer due to intense laser heating; (ii) material removal by a cutting tool due to plastic deformation in a shear zone, which is characterized by viscous flow of a glassy grain-boundary phase material and reorientation of the -

	CO ₂	Nd:YAG	HPDL
Wavelength [μm]	10,6	1,06	0,8-0,95
Output power [kW]	up to 30	up to 3	up to 3
Efficiency [%]	5-10	1-3 (F) 15-30 (D)	30-60
Spec. volume [l/kW]	1000	100	0,1
Using fibers	Impossible	Possible	Possible
Operating voltage [kV]	up to 20	up to 1	up to 0,1
Service intervals [h]	1000	500 (F)	No maintenance
Spec. price [€/W]	75-250	90-400	40-250
Absorptance of Si ₃ N ₄	0,9	0,6-0,8	0,7
Absorptance of carbon steel	0,1	0,35	0,4

Table 1. Types and characteristics of lasers [4, 5]

(F – flashtube-pumped, D – diode-pumped)

Si₃N₄ grains; (iii) segmentation of chips due to the initiation, coalescence and propagation of intergranular microcracks. The authors achieved tool life comparable to that of metal cutting and no surface/subsurface cracks on machined surfaces. Pfefferkorn et al. [6] studied LAM of magnesia partially stabilized zirconia and prolonged the PCBN tool life from 3 to 120 min and reduced the specific cutting energy from 6,6 to 2,6 J/mm³ by raising the material removal temperature (T_{mr}) from 530°C (conventional turning) to 1210°C (LAM). The authors determined the optimal range of T_{mr} between 900 and 1100°C. For determining T_{mr} a three dimensional heat transfer model was developed by Rozzi et al. [7] and extended by Tian et al. [8] to take into account workpieces with complex geometry. Si₃N₄ workpieces with complex geometry were successfully machined by LAM. The authors developed also a 2D multiscale finite element model [9] that considers the glassy intergranular phase and the Si₃N₄ grains separately. Tian et al. [10] developed a three dimensional heat transfer model for predicting the temperature distribution in a laser assisted milling process. Si₃N₄ were successfully milled using TiAlN coated solid carbide end mills with the T_{mr} being 1200-1300°C. The authors achieved good surface roughness of the machined surface and acceptable tool wear. Yang et al. [11] studied the mechanisms of edge chipping of Si₃N₄ workpieces undergoing a laser assisted milling process and determined the optimal range of T_{mr} , where edge chipping was significantly reduced, to be 1300-1400°C.

3.2 Steel

Types of steel suited to the use of LAM are high hardness steels like tool or bearing steel and steels that exhibit major strain hardening, like austenitic stainless steels. Dumitrescu et al. [2] studied LAM of AISI D2 tool steel with a hardness of 60 HRC. They avoided catastrophic tool failure and extended tool life for up to 100%. Anderson et al. [12] implemented LAM on P550 austenitic stainless steel and due to low absorptance used two laser sources to heat the workpiece material. For determining the T_{mr} the authors adapted the thermal model from Rozzi et al. [13] to consider two laser sources. The specific cutting energy was reduced by 25% compared to conventional machining and tool life of a ceramic tool was extended by 100%. No detrimental precipitates or changes in hardness were

found in the machined subsurface. Furthermore, an economic analysis showed economic savings of 20-50 % compared to conventional machining, even with the additional cost of operating and maintaining the laser. Germain et al. [14] studied LAM of 100Cr6 bearing steel with a HRC of 57. The authors observed a sharp decrease in the cutting force compared to conventional turning, an increase in residual stresses towards tensile and an increase in the fatigue limit of the machined specimens. Ding et al. [15] studied LAM of hollow shafts of varying thickness, made of quenched steel AISI 4130, with a HRC of 50. The authors developed a transient thermal model for predicting the temperature distribution in the hollow shafts and empirical equations to determine the process parameters for a given T_{mr} . At a T_{mr} of 200°C, the authors achieved a 20% reduction in specific cutting energy and no changes in the machined surface and subsurface microstructure and hardness. In another paper [16] Germain et al. report of LAM of 42CrMo4 steel and propose a numerical thermo-mechanical model that takes into account the nonlinearities that occur during chip formation for determining the temperature and stress fields in the workpiece during LAM. Kim et al. [17] implemented laser assisted milling on AISI 1045 steel and proposed empirical equations for determining the temperature of the workpiece material entering the cutting zone and the cutting forces. Panjehpour et al. [18] studied LAM of AISI 52100 bearing steel with a HRC of 54 and determined the surface temperature and the heat penetration into the workpiece can be controlled more efficiently with the use of a pulsed in comparison to a continuous wave laser source.

3.3 Superalloys

Superalloys are high-temperature materials that display excellent resistance to mechanical and chemical degradation in temperatures close to their melting points. In this chapter LAM of titanium and nickel based superalloys is presented.

Titanium alloys

Titanium alloys are divided into α , β and α/β alloys, according to their structure. Generally, titanium alloys are more ductile, whereas α alloys are stronger yet less ductile. Germain et al. [14] studied LAM on an titanium alloy, Ti6Al4V, and achieved a drastic decrease in cutting forces, but an increase in residual

stresses towards tensile. Due to tensile residual stresses, that facilitate the spread of microcracks, the fatigue limit diminishes slightly. Attempts of increasing machinability of Ti6Al4V by LAM with the additional component of cryogenic cooling of the machine tool were made by Dandekar et al. [19]. In both cases (LAM and the LAM/cryogenic combined process), there was a considerable improvement in the machinability of the material, in terms of lower specific cutting energy and machined surface roughness. An optimal T_{mr} of 250°C was established, at which tool life was improved by a factor of 1,7 and 2 for LAM and the combined process, respectively. With the combined process, the authors successfully machined the material with cutting speeds above 150 m/min, which has potential for high speed machining of this material. An economic analysis, based on estimated tool and labor costs, showed a 30 and 40% reduction in overall machining costs for LAM and the combined process, respectively. Sun et al. [20] studied laser assisted milling of Ti6Al4V and achieved a drastic decrease in feed force compared to conventional milling. The feed force was most reduced when the workpiece material, entering the cutting zone, was heated to 200-450°C. Rashid et al. [21] studied the effects of laser power in LAM of a titanium alloy, Ti-6Cr-5Mo-4Al. they established an optimal laser power of 1200-1600W when using cutting speeds of 25-125m/min. In an extensive research [22] the authors examined the effects of feed and cutting speed on cutting forces and temperature of the workpiece material in front of the cutting zone. They determined the optimal laser power, feed, cutting speed and temperature of the material in front of the cutting zone to be 1200W, 0,15-0,25 mm/rev, 25-100 m/min and 1050-1250°C, respectively.

Nickel alloys

Nickel or nickel-chrome alloys generally exhibit high toughness and strength and are subjected to high strain hardening. Anderson et al. [23] studied LAM of Inconel 718 and determined the low absorptance of the material to the laser light (~0,2) to be reason for the poor feasibility of LAM on this material. To raise the absorptance the authors performed experiments with different coatings and chose the most appropriate one that rose the absorptance to ~0,8. With LAM, they achieved longer tool life, lower specific cutting energy and a two-fold improvement in surface roughness. Germain et al. [24] studied the effect of cutting tool material in LAM of Inconel 718 and determined the ceramic tool are more suitable than carbide tools. The cutting forces were reduced by 40% in LAM and tool life of ceramic tools was improved by 25% in comparison with conventional turning. Shi et al. [25] developed a three dimensional numerical model with a new constitutional law for Inconel 718 that takes into account friction and heat transfer on the tool-workpiece contact. Tian et al. [10] developed a heat transfer model, which was already described in the section about engineering ceramics. By heating the workpiece material (Inconel 718) in front of the cutting zone to 520°C, the authors achieved 40-50% reduction in the cutting forces, a more than 50% reduction in cutting

tool chipping and two-fold improvement in machined surface roughness. Attia et al. [26] experimented on LAM high speed finish turning of Inconel 718 with ceramic cutting tools. They determined the optimal process parameters and achieved a considerable reduction in cutting forces, 25% improvement in machined surface roughness and an 800% increase in cutting speed, compared to conventional turning. Ding et al. [27] studied LAM of Waspaloy and determined an optimal T_{mr} in the range of 300-400°C. At this T_{mr} , the authors achieved a 50% increase in cutting tool life, compared to conventional turning. Kim et al. [17] implemented laser assisted milling of Inconel 718 and proposed empirical equations for determining the temperature of the workpiece material entering the cutting zone and the cutting forces.

3.4 Composite materials

Composite materials suitable to LAM are especially the ones that are composed of a soft matrix with hard inserts that have an abrasive effect on the cutting tool. Wang et al. [28] studied LAM of a composite that is composed of an aluminum matrix with Al_2O_3 inserts and achieved up to 50% reduction in cutting forces, longer tool life and increase in compressive residual stresses, compared to conventional turning. Dandekar et al. [29] studied LAM of a long Al_2O_3 fiber-reinforced aluminum matrix composite and developed a two dimensional finite element model that takes into account three different materials: Al_2O_3 fibers, crystal grains of the matrix material and cohesive zone elements. They achieved lower specific cutting energy, machined surface roughness, tool wear and grain pull-out occurrence. The authors also determined optimal machining parameters, T_{mr} , feed, depth of cut and cutting speed of 300°C, 0,02 mm/rev, 0,5 mm and 30 m/min, respectively. In another study [30] the authors studied LAM of a 20% by volume fraction SiC particle-reinforced aluminum matrix composite. They determined the optimal machining parameters for machining this material with a carbide tool; the T_{mr} , feed, depth of cut and cutting speed of 300°C, 0,1 mm/rev, 0,76 mm and 150 m/min, respectively.

3.5 Cast iron

Cast iron is not the usual material suitable for LAM, but a study [31] on LAM of compacted graphite iron (CGI) was performed by Skvarenina et al. At a T_{mr} of 400°C, carbide tool life was improved by 60%, compared to conventional turning. An economic analysis of cylinder liner manufacture showed a 20% decrease in machining costs.

4. CONCLUDING REMARKS

Many LAM studies were conducted and the beneficial effect of laser assistance on the conventional cutting process was demonstrated by numerous authors, however very few systems were implemented in an industrial process. In most of the studied cases CO_2 and Nd:YAG lasers were used. With the recent development of HPDL-s and their advantages, which enable the use of such systems not only in a research,

but also in an industrial environment, the possibility of mass implementation of LAM systems in an industrial environment opens up. On the other hand, the laser industry is evolving quickly in the last years and new types of laser sources, which would be suited for LAM, are being developed, for example fiber lasers.

5. REFERENCES

- [1] Lauwers, B.: *Surface Integrity in Hybrid Machining Processes*, 19, p.p. 241-251, 2011.
- [2] Dumitrescu, P., Koshy, P., Stenekes, J., Elbestawi, M. A.: *High-power diode laser assisted hard turning of AISI D2 tool steel*, Int J Mach Tool Manu, 46, p.p. 2009-2016, Dec 2006.
- [3] Lei, S., Shin, Y. C., Incropera, F. P.: *Experimental investigation of thermo-mechanical characteristics in laser-assisted machining of silicon nitride ceramics*, J Manuf Sci E-T Asme, 123, p.p. 639-646, Nov 2001.
- [4] Kim, K. S., Kim, J. H., Choi, J. Y., Lee, C. M.: *A Review on Research and Development of Laser Assisted Turning*, Int J Precis Eng Man, 12, p.p. 753-759, Aug 2011.
- [5] Diaci, J.: *Laserski sistemi*, University of Ljubljana (in Slovene), Ljubljana, 2006.
- [6] Pfefferkorn, F. E., Shin, Y. C., Tian, Y. G., Incropera, F. P.: *Laser-assisted machining of magnesia-partially-stabilized zirconia*, J Manuf Sci E-T Asme, 126, p.p. 42-51, Feb 2004.
- [7] Rozzi, J. C., Pfefferkorn, F. E., Shin, Y. C., Incropera, F. P.: *Experimental evaluation of the laser assisted machining of silicon nitride ceramics*, J Manuf Sci E-T Asme, 122, p.p. 666-670, Nov 2000.
- [8] Tian, Y. G., Shin, Y. C.: *Thermal modeling for laser-assisted machining of silicon nitride ceramics with complex features*, J Manuf Sci E-T Asme, 128, p.p. 425-434, May 2006.
- [9] Tian, Y. G., Shin, Y. C.: *Multiscale finite element modeling of silicon nitride ceramics undergoing laser-assisted machining*, J Manuf Sci E-T Asme, 129, p.p. 287-295, Apr 2007.
- [10] Tian, Y. G., Wu, B. X., Anderson, M., Shin, Y. C.: *Laser-assisted milling of silicon nitride ceramics and Inconel 718*, J Manuf Sci E-T Asme, 130, p.p. Jun 2008.
- [11] Yang, B., Shen, X., Lei, S.: *Mechanisms of edge chipping in laser-assisted milling of silicon nitride ceramics*, 49, p.p. 344-350, 3// 2009.
- [12] Anderson, M. C., Shin, Y. C.: *Laser-assisted machining of an austenitic stainless steel: P550*, P I Mech Eng B-J Eng, 220, p.p. 2055-2067, Dec 2006.
- [13] Rozzi, J. C., Pfefferkorn, F. E., Incropera, F. P., Shin, Y. C.: *Transient thermal response of a rotating cylindrical silicon nitride workpiece subjected to a translating laser heat source, part I: Comparison of surface temperature measurements with theoretical results*, J Heat Trans-T Asme, 120, p.p. 899-906, Nov 1998.
- [14] Germain, G., Morel, F., Lebrun, J. L., Morel, A.: *Machinability and surface integrity for a bearing steel and a titanium alloy in laser assisted machining - (Optimisation on LAM on two materials)*, Laser Eng, 17, p.p. 329-344, 2007.
- [15] Ding, H., Shin, Y. C.: *Laser-assisted machining of hardened steel parts with surface integrity analysis*, 50, p.p. 106-114, 1// 2010.
- [16] Germain, G., Dal Santo, P., Lebrun, J. L.: *Comprehension of chip formation in laser assisted machining*, Int J Mach Tool Manu, 51, p.p. 230-238, Mar 2011.
- [17] Kim, D. H., Lee, C. M.: *A study of cutting force and preheating-temperature prediction for laser-assisted milling of Inconel 718 and AISI 1045 steel*, Int J Heat Mass Tran, 71, p.p. 264-274, Apr 2014.
- [18] Panjehpour, A., Yazdi, M. R. S., Shoja-Razavi, R.: *An experimental investigation of pulsed laser-assisted machining of AISI 52100 steel*, Opt Laser Technol, 63, p.p. 137-143, Nov 2014.
- [19] Dandekar, C. R., Shin, Y. C., Barnes, J.: *Machinability improvement of titanium alloy (Ti-6Al-4V) via LAM and hybrid machining*, Int J Mach Tool Manu, 50, p.p. 174-182, Feb 2010.
- [20] Sun, S., Brandt, M., Barnes, J. E., Dargusch, M. S.: *Experimental investigation of cutting forces and tool wear during laser-assisted milling of Ti-6Al-4V alloy*, P I Mech Eng B-J Eng, 225, p.p. 1512-1527, Sep 2011.
- [21] Rashid, R. A. R., Sun, S., Wang, G., Dargusch, M. S.: *The effect of laser power on the machinability of the Ti-6Cr-5Mo-5V-4Al beta titanium alloy during laser assisted machining*, Int J Mach Tool Manu, 63, p.p. 41-43, Dec 2012.
- [22] Rashid, R. A. R., Sun, S., Wang, G., Dargusch, M. S.: *An investigation of cutting forces and cutting temperatures during laser-assisted machining of the Ti-6Cr-5Mo-5V-4Al beta titanium alloy*, Int J Mach Tool Manu, 63, p.p. 58-69, Dec 2012.
- [23] Anderson, M., Patwa, R., Shin, Y. C.: *Laser-assisted machining of Inconel 718 with an economic analysis*, Int J Mach Tool Manu, 46, p.p. 1879-1891, Nov 2006.
- [24] Germain, G., Lebrun, J. L., Braham-Bouchnak, T., Bellet, D., Auger, S.: *Laser-assisted machining of Inconel 718 with carbide and ceramic inserts*, Int J Mater Form, 1, p.p. 523-526, Apr 2008.
- [25] Shi, B., Attia, H., Vargas, R., Tavakoli, S.: *Numerical and Experimental Investigation of Laser-Assisted Machining of Inconel 718*, Mach Sci Technol, 12, p.p. 498-513, 2008.
- [26] Attia, H., Tavakoli, S., Vargas, R., Thomson, V.: *Laser-assisted high-speed finish turning of superalloy Inconel 718 under dry conditions*, Cirp Ann-Manuf Techn, 59, p.p. 83-88, 2010.
- [27] Ding, H. T., Shin, Y. C.: *Improvement of machinability of Waspaloy via laser-assisted machining*, Int J Adv Manuf Tech, 64, p.p. 475-486, Jan 2013.
- [28] Wang, Y., Yang, L. J., Wang, N. J.: *An investigation of laser-assisted machining of Al2O3 particle reinforced aluminum matrix composite*, J Mater Process Tech, 129, p.p. 268-272, Oct 11 2002.
- [29] Dandekar, C. R., Shin, Y. C.: *Laser-Assisted Machining of a Fiber Reinforced Metal Matrix Composite*, J Manuf Sci E-T Asme, 132, p.p. Dec 2010.
- [30] Dandekar, C. R., Shin, Y. C.: *Experimental evaluation of laser-assisted machining of silicon carbide particle-reinforced aluminum matrix composites*, Int J Adv Manuf Tech, 66, p.p. 1603-1610, Jun 2013.
- [31] Skvarenina, S., Shin, Y. C.: *Laser-assisted machining of compacted graphite iron*, Int J Mach Tool Manu, 46, p.p. 7-17, Jan 2006.

Authors: David Muzenic¹, dr. Davorin Kramar¹, assoc. prof. dr. Milenko Sekuli², prof. dr. Janez Kopa¹, ¹University of Ljubljana, Faculty of Mechanical Engineering, Laboratory for Cutting, Askerceva 6, 1000 Ljubljana, Slovenia, Phone.: +386 1 477-14-38 Fax: +386 1 251-85-67,
E-mail: David.Muzenic@fs.uni-lj.si;
Davorin.Kramar@fs.uni-lj.si;
Janez.Kopac@fs.uni-lj.si

²University of Novi Sad, Faculty of Technical Sciences, Institute for Production Engineering, Trg Dositeja Obradovica 6, 21000 Novi Sad, Serbia, Phone.: +381 21 450-366, Fax: +381 21 454-495.
E-mail: milenkos@uns.ac.rs;

Kheifetz, M., Dr. Gaiko, V., Borodavko, V.¹, Klimenko, S.², Tanovi, Lj.³

HIGH-PERFORMANCE METHODS OF DETAIL SURFACE PROCESSING

Abstract: At the automated designing intensive methods of processing of details of machines it is offered to use domination of properties of relations of technological decisions. On a basis synergetic the approach models of loss of serviceability of units are considered. Unification of combined treatment of surfaces of revolution and flat surfaces using additional units permits the creation of flexible treatment centers.

Key words: combined treatment, flexible technological complexes, electromagnetic and ion-beam treatment

In a technological system with high energy and matter concentration, the ion-beam effects are not fully absorbed by surface layers. At the same time the dissipation of ion-beam fluxes is not necessary connected with the dissipative structures formed in surface layers, but often is caused by a reflection, refraction, etc. of matter and energy withdrawal from work area.

1. ENERGY AND MATTER BALANCE EQUATION

Equations of hydrodynamic field, describing the technological factors of thermomechanical and electrophysical machining, should take into account chemical reactions and physical transformations, connected with phase transitions and structure formation. To prove it, let material density ρ be represented in equations of hydrodynamic field by a sum (Ebeling, 1979, Haken, 1991):

$$\rho = \sum_{i=1}^K M_i \cdot C_i, \quad (1)$$

where M_i is a molecular mass of i-component, C_i is a concentration of i-component, K is the number of components in a physical-chemical system.

As a result of transformations/manipulations, a system of equations of hydrodynamic field will be supplemented by equation (Ebeling, 1979)

$$\frac{\partial C_i}{\partial \tau} + \nabla \cdot (C_i v) + \nabla \cdot F_{d_i} = \sum_{r=1}^{R_0} \nu_{ir} w_r, \quad (2)$$

where v is a flow of matter rate, F_{d_i} – density of diffusion flow of i-component, ν_{ir} – stoichiometric coefficient of i-substance in r-reaction, w_r – rate of r-reaction, R_0 – number of proceeding reactions. In the equation of local entropy balance, when K

components in a physical-chemical system are considered, density of entropy flow will be equal to:

$$F_\varepsilon = \frac{1}{T} (F_q \sum_{i=1}^K F_{d_i} W_i), \quad (3)$$

where T is absolute temperature, F_q – density of thermal flow, W_i – chemical potential of i-component.

Entropy production will be described by the equation (Ebeling, 1979):

$$\begin{aligned} \sigma = & F_q \left[\nabla \frac{1}{T} \right] - \sum_{i=1}^K F_{d_i} \left[\nabla \left(\frac{W_i}{T} \right) \right. \\ & \left. - \frac{1}{T} \cdot F_{m_i} \right] - \frac{1}{T} P_g \cdot \nabla v + \\ & \frac{1}{T} \sum_{i=1}^K W_i \sum_{r=1}^{R_0} \nu_{ir} w_r, \end{aligned} \quad (4)$$

where F_{m_i} is mass force, applied to i-component, P_g – dissipative part of pressure tensor, describing, in particular, viscous forces.

Entropy production σ determines the evolution, steadiness and stability conditions; therefore different states of the technological system may be described by transfer criteria (Haken, 1991).

Stability criteria of ion-beam processes. To describe cooperative processes in a technological system at thermomechanical and electrophysical processing, the Peclet Pe and modified Reynolds Re^* criteria are recommended for use, which describe a surface layer in solid, elastic, plastic and viscous states. In ion-beam processing, the functional layers properties are usually formed under the intensive influence on free surface of a solid or melted material, with specified density ρ , coefficient of viscosity ν , coefficient of temperature conductivity ω , coefficient of volumetric expansion β^* , coefficient

of thermocapillarity σ_K , etc. Therefore, to describe the cooperative processes, in addition to Peclet and Reynolds criteria, there will be required criteria characterizing the surface and three-dimensional flows of matter.

The surface flows due to the thermocapillary phenomena, caused by surface tension depending on temperature, are described by Marangoni criterion (Haken, 1991; Gershuni et al., 1972):

$$Mr = \frac{\sigma_K \nabla T t^2}{\rho \nu \omega}. \quad (5)$$

The rotation of flows, influenced by the natural convection, with free motion of fluid flows within a forming layer, is characterized by Grashof criterion (Lykov, 1967; Reznikov, 1981):

$$Gr = \frac{\beta^* g \nabla T t^4}{\nu^2}, \quad (6)$$

where g is a free fall acceleration.

Formation of a spatially periodic system of toroidal vortexes within a melted layer, caused by buoyancy force $\rho \beta^* g \nabla T$, known as Benar cells, is represented by Rayleigh criterion (Gershuni et al., 1972; Lykov, 1967):

$$Rl = \frac{\beta^* g \nabla T t^4}{\nu \omega}. \quad (7)$$

The most stable indicator and the most mobile characteristic of the excitation mechanism, making the technological medium move, is the ratio of longitudinal and lateral cell sizes (Gershuni et al., 1972). In fact, change in boundary conditions does not affect this parameter, either when vortex flows are excited by buoyancy forces or when the flows are initiated by thermocapillary forces. The main exciting mechanism is changed with the change of the flowing layer thickness as Type II phase transition and results in abrupt change of cell sizes ratio.

Excitation of toroidal vortexes, making the Benard convection cells (Gershuni et al., 1972), is initiated by surface flows, influenced by thermocapillary forces. Surface flows in a molten pool are determined by a heating source moving (Lykov, 1967; Reznikov, 1981). Therefore, interconnection of layers, flows and vortexes regular motion, alternating with unstable turbulence and free convection of flows, is better to analyze with the Pe, Re, Mr, Gr and Rl criteria used (Table 1).

So, to describe the cooperative processes of surface layer formation during ion-beam processing, field equations are valid, supplemented by equations. It is expedient to represent structural changes and phase transitions by Mr, Gr and Rl criteria.

2. CONTROL OF ION-BEAM PROCESS STABILITY

Conditions for regular, dissipative structures formation were analyzed for electron-beam surfacing of VT9 and VT20 alloys. Cellular structures were found to be fixed in the surface layer after the ion-beam heating at $q=2\dots7$ kW/cm² specific capacity during $\tau = 0.2\dots0.3$ s. Smaller specific capacity impedes the convection flows separation into stable vortexes due to insufficient temperature gradient in the melt, those resulting in the dissipative structures formed; the effect of greater capacity is the same as above because of too deep melting (Table 1). Therefore, regular structures are formed only if affected by a developed electron beam, and the cellular structures are not formed in the nearby sections melted by heat conductivity (Shipko et al., 1995).

The cellular structure is formed in one-phase pseudo α -alloy VT20 on the basis of liquid dissipative structures (Shipko et al., 1995). Drop in size and number of cells in transition zones, as well as in their longitudinal and lateral dimensions ratio from 4.1 to 4.5 is indicative of the convective character of structure formation. Moreover, it is just

Stages	I	II	III	IV	V
Criteria	Pe → Re → Mr → Gr → Rl				
Surface layer condition	$\nu \left \frac{t}{\omega} \right \rightarrow \nu \left \frac{t}{\nu} \right \rightarrow \frac{\sigma_K \nabla T}{\rho \nu} \left \frac{t^2}{w} \right \rightarrow \frac{\beta^* g \nabla T}{\nu} \left \frac{t^4}{\nu} \right \rightarrow \frac{\beta^* g \nabla T}{\nu} \left \frac{t^4}{w} \right $				
Structure formation mechanisms	Heat conductivity of layers and media	Turbulence of flows and streams	Thermocapilla-ry surface flows	Free flows and layers convection	Spatially periodic vortexes

Table 1. Change in surface layer conditions during the structure formation processes

the narrower cells formed by the thermocapillary force (Gershuni et al., 1972), that are, first, initiated and then moved to the periphery being described by the Marangoni criterion Mr . If the intensity of the electron beam effect is higher, the natural convection, characterized by the Grashof criterion Gr , having excited vortex motion under the influence of the thermocapillary forces, smears vertical dissipative structures in the center of the heating area. There aren't any big, wider toroidal vortexes created by buoyancy forces and described by the Rayleigh criterion Rl , observed during the flowing by the electron beam (Shipko et al., 1995). The dissipative structures formed in a liquid phase are followed by the intensive redistribution of alloying elements.

Elements, reducing the surface tension, are accumulated in the corners and next to the cell walls. Intensive concentration stratification takes place in β -phase, proved by the alloyed α'' -martensite appearing in one-phase pseudo α -alloy VT20 in the areas of cellular structure. Structural parameters of $\alpha(\alpha')$ -phase change from $a=0.292$ nm; $c=0.467$ nm in the initial state and their close values at partial melting with slow recrystallization to $a=0.295$ nm; $b=0.529$ nm; $c=0.469$ nm (Shipko et al., 1995).

The analysis of the cellular structure surface S_0 area as related to the total melt area, depending on specific capacity q and time of heating τ (Fig. 3.1), has shown that the largest area of regular structure $S_0 = 40\%$ is formed at heating with specific capacity $q=2.5$ kW/cm² during $\tau=1.5$ s. The surface heating rate in this case exceeds 2500°C/s and the temperature gradient in the surface layer reaches $8 \cdot 10^5$ °C/m (Shipko et al., 1995).

The diagram (Fig. 1) enables to analyze the dissipative structures influencing the surface layer formation processes at beam processing. The technological system equilibrium states, such as an unstable node transforming in the result of restrictions into a limit cycle and unstable bow, varying from zero to maximum, which brings the system closer to the designed stable state, can also be observed at electron-beam processing.

Thus, the cellular structure forming on the maximal area is of the unstable node type transferring into a limit cycle. The cycle is limited, first, by an extremely deep melting, and, second, by the treated material transferring from solid into a liquid state. Surfacing – melting boundary formation is described as an unstable bow mode. The heat flows moving from interfacial area in the opposite directions due to heat conductivity and convection flows stabilize the technological system in different phases. At that time the translational mechanisms of the matter and energy transfer change for vortex ones in the interfacial area.

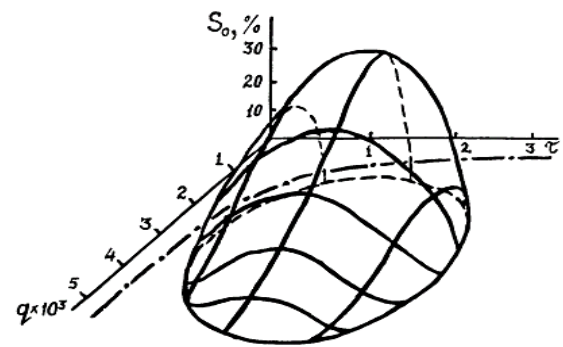


Fig. 1. Dependence of relative surface structure S_0 on specific capacity q (W/cm²) and duration (s)

The problem of order and chaos has been attracting attention for a long time. The task is to study and describe the collective phenomena which are observed on transition from disordered to ordered systems and vice versa. A general feature of these phenomena is that a system is becoming more complex (when heated), it acquires certain phenomenological features which are difficult to detect when investigating more simple subsystems.

The interaction of the subsystems determines the properties of the object. Synergetic properties of the object and its space-time periodicity are governed by both the instability and stabilization. But the actual properties of an object can be predicted and explained only if specific problems are solved and this solution is compared with the experimental results.

When these subsystems interact in an open thermodynamic system, there is observed a self-organization and appear the macroscopic space-time structures. As generally accepted, the transition occurs as a rise of fluctuations. Stochastic disturbances, rising, go over to the deterministic cellular motion. This transition occurs only over a certain range of values of the control parameters.

The above results of the investigation can be applied to numerous technological environments having different physicochemical properties. Only some of them have been investigated so far: liquid semiconductors and semimetals, certain types of liquid crystals, ambipolar media, etc. Other media, such as porous materials, gas-liquid mixtures, and many others, have to be investigated by the above method for to study the interaction of properties.

3. CONCLUSIONS

Analysis of combined surfacing methods that use diverse energy sources and combine different operations and stages makes it possible to give the fundamentals for to control the processes of the surface layers of the workpieces formation (Kheifetz, 2005; Vitiaz et al., 2011).

- 1) Greater capacity, energy concentration, additional degrees of freedom of the sources,

tools, technological media and surfaced materials, improved interaction are achieved through self-organization and is evolutionary. The processes of the combined electrophysical and ion-beam surface treatment of workpieces are determined by cooperative nonlinear phenomena and effects at various matter and energy fluxes interaction. Structures of the workpieces produced, such as phases, layers, and surfaces, are dissipative, self-organizing and are inherited in the process of formation and operation.

- 2) The structures location is described by boundary conditions and is determined by the position of technological and operational barriers, which can be defined as the second derivative of pulsed matter and energy transfer in time and space. The state of structures is described by the initial conditions and is determined by the magnitude of the barriers, while the transition from one state to another should be accompanied by pulsed matter and energy transfer that reorganizes the barriers. In the processes of the workpieces formation and operation, the open manufacturing system can be controlled through the interrelated boundary and initial conditions by changing the position and magnitude of the technological and operational barriers.
- 3) Dissipative self-organizing structures are inherited and reorganized during the workpieces surfacing and operation. It is useful that the structures be inherited or reorganized into a new state successively from operation to operation with minimum pulses of matter and energy transfer. In workpiece surfacing the technological barriers and surfacing operations should reasonably be arranged in the order inverse to that of the technological barriers and actions in the operation stages.

Based on the above given conclusions, the following stage sequence is advisable in designing combined physicochemical treatment methods:

- 1) Selection of chemical elements, compounds, phases and other states, which provide the dissipative inherited structures formation, corresponding to different operation stages.
- 2) Analysis of possible mutual transformation of dissipative self-organized structures at all stages of surfacing and operation.
- 3) Identifying the rational initial and boundary conditions of the manufacturing system operation and the respective positions and sizes of technological and operational barriers.
- 4) Considering possible variants of barriers reorganization at different surfacing and operation stages.
- 5) Selection of basic treatment techniques, operation conditions, matter and energy sources, equipment and tools providing the technological and operational barriers formation.
- 6) Study of sources and tools possibilities to control the barriers reorganization under production and operation.
- 7) Making the manufacturing and operation routing on the basis of chosen manufacturing technique, operation conditions, sources and tools.
- 8) Considering the possible variants for both different surfacing actions and running-in overlapping.
- 9) Determining the rational modes, parameters of surface formation and operation stage both in all operations and stages, and at successive change of operations and stages.
- 10) Study of possibilities to provide a manufacturing process with a fluent change of operations and stages.

4. REFERENCES

- [1] Ebeling, V. (1979). *Forming structures in irreversible processes. Introduction to the theory of dissipative structures*, Moscow.
- [2] Haken, H. (1991). *Information and self-organization. Macroscopic approach to complex systems*, Moscow.
- [3] Gershuni, G.Z. & Zhukhovitsky, E.M. (1972). *Convective stability of incompressible fluid*, Moscow.
- [4] Lykov, A.V. (1967). *Theory of heat conductivity*, Moscow.
- [5] Reznikov, A.N. (1981). *Thermophysics of material machining*, Moscow.
- [6] Shipko, A.A., Pobel, I.L. & Urban, I.G. (1995). *Strengthening of steels and alloys applying electron beam heating*, Minsk.
- [7] Kheifetz, M.L. (2005). *Designing of processes of the combined handling*, Moscow.
- [8] Vitiaz, P.A., Ilyushchenko, A.F., Kheifetz M.L. et al. (2011). *Technologies of nanostructured materials and coatings*, Minsk.

Authors: Prof. Michael Kheifetz, Dr. Victor Gaiko, Vladimir Borodavko, The State Scientific and Production Amalgamation "Center" of the National Academy of Sciences of Belarus, Nezavisimosti Avenue, 66, Minsk, Belarus, E-mail: kheifetz@presidium.bas-net.by; mlk-z@mail.ru,

Prof. Sergey Klimenko, Institute of Super Firm Materials it. V.N.Bakul of the National Academy of Sciences of Ukraine, Kiev, Ukraine,

Prof. Ljubodrag Tanovic, University of Belgrade, Kraljice Marije, 16, Belgrade, Serbia

Kheifetz, M., Pynkin, A., Pozilova, N., Klimenko, S., Tanovi, Lj.

ANALYSIS OF INTENSIVE PROCESSING METHODS OF TREATMENT

Abstract: Analysis of the self-organization processes in deposition, thermal treatment, deformation, and cutting of surface layers of items, as well as in combined methods of treatment, i.e. in deposition of coatings and thermal treatment combined with deformation and cutting, shows that a technological complex can work continuously and stably in an automatic mode requiring no external control. This gives reasons for the technological complexes designed as autonomous flexible production modules to be used for combined electromagnetic and thermomechanical treatment of workpieces.

Key words: self-organization, processes of deposition, thermal treatment, technological complex

The development and manufacturing application of new processing methods, based on combination of different kinds of energy or different ways of material treatment, is a promising trend in machine building. In general, a system model of a technology is represented by a combination of three input flows: matter, energy and information. It is worthwhile to consider a processing method in the form of energy and information subsystems. The first one supplies and converts energy, necessary to affect a work material in order to change its physical-mechanical properties, to remove or to deposit material. It is specified by a processing form. The second one controls energy and matter flows, providing them in required quantities to the prescribed place of the workspace so that certain form, size and properties of a component surface are ensured.

1. SURFACE LAYER FORMATION, USING HIGH-PERFORMANCE PROCESSING METHODS

It would be reasonable to consider processing as some energy system, affecting an intermediate product for to provide a transition from one state to another, corresponding to a new quality (Kheifetz & Chemisov, 2002; Ryzhov & Averchenkov, 1989).

This effect is achieved in several stages. At the first one, the supplied energy is converted into working energy, E_w , with the help of technological equipment. At the second one, the working energy is converted into energy of effect on the treated object, E_{eff} . At the third stage, the energy of the effect leads to formation of physicochemical mechanisms, $M_{ph.-ch.}$, of workpiece processing, which are the main element, transforming the basic parameters of processing method (efficiency, energy consumption, surface quality, etc.).

Thus, the process of treatment (PT) represents a chain of energy conversion (Poduraev, 1983)

$$PT = \{E_w \Rightarrow E_{eff} \Rightarrow M_{ph.-ch.}\}. \quad (1)$$

Shaping processes (Sh) are characterized by the following components:

$$Sh = \{M_{e.-s}, F_{d.e}, K_{sch.t.}\} \quad (2)$$

and their features are: for $M_{e.-s}$ – point, linear and surface characteristics, volumetric sources; for $F_{d.e}$ – continuous, pulse and impulse action; for $K_{sch.t}$ – rectilinear, rotary, two rectilinear, rotary-translational motion or its absence.

As a result, all methods are, first of all, divided into three classes: with or without removal of material and with deposition of material. Secondly, each class has subclasses, which characterize the types of energy, material processing. Thirdly, there are differences in character of physical-mechanical effect and, fourthly, in the type of applied instrumentation and in the processing kinematics.

Based on this classification, there are generalized models of processing method (PM), which are usually represented by the following analytic form (Averchenkov, 1997):

$$PT = \{N_{m.t}, RA_{m.t}, E_w, E_{eff}, M_{ph.-ch.}, K_{sch.t}, F_{d.e}, M_{e.-s}, S, G\}. \quad (3)$$

Formulas give rather complete and clear idea about the structure and composition of processing and shaping process components. It is convenient to use them, when developing new technological procedures and shaping methods, but they do not allow one to conduct any logical operations and transformations. To formalize the conditions of object-oriented formation of new processing methods, each complex of similar components r_i is described as some set of technological solutions R_i . This approach (Golodenko & Smolentsev, 1994)

allows each processing method $r_{m,t}$ to be represented as a tuple:

$$r_{m,t} = (r_{surf}, r_{mat}, r_f, r_{eff.mat}, r_{e.s.}, r_{m.e.s.}, r_{e.m.}, r_t, r_k, r_{st}). \quad (4)$$

Each element of the tuple is a component of the corresponding set of technological solutions, i.e.,

$$\{ r_i \} = R_i \text{ or } r_i \in R_i. \quad (5)$$

The presence of a specific property α in a technological solution r_i is expressed by the corresponding predicate

$$E_\alpha(r_i), \quad (6)$$

which confirms that the technological solution r_i possesses the property α .

Each property α can acquire range θ_α . Then the expression

$$E_\alpha(r_i) \wedge \theta_\alpha \quad (7)$$

indicates that the technological solution r_i possesses the property α and the value of the latter is θ_α .

Predicate allows choosing a technological solution with a given property, the value of which is determined by formula.

In general, a technological solution r_i is characterized by a set of properties $\alpha, \delta, \dots, \gamma$, each of them can acquire different values; that is expressed by formula

$$\forall r_i \exists \alpha \exists \delta \dots \exists \gamma \{ [E_\alpha(r_i) \wedge (\bigwedge_{j=1}^n \theta_{\alpha_j})] \wedge [E_\delta(r_i) \wedge (\bigwedge_{k=1}^m \theta_{\delta_k})] \wedge \dots \wedge [E_\gamma(r_i) \wedge (\bigwedge_{p=1}^q \theta_{\gamma_p})] \}. \quad (8)$$

A certain interconnection can exist between the property values of solution r_i , and not every combination of them is admissible, i.e., the technological solution r_i , possesses the property with the value θ_{α_n} and the property δ , the value of which is determined by the set $\theta_{\delta_{pj}}$. This situation is described by formula

$$\exists \alpha \exists \delta \forall r_i [E_\alpha(r_i) \wedge \theta_{\alpha_n} \rightarrow E_\delta(r_i) \wedge (\bigwedge_{j=1}^k \theta_{\delta_{pj}})]. \quad (9)$$

We assume that if any two components of the processing method possess at least one common property, then interconnection of property generality exists between them. This makes it possible to organize the selection of technological solutions by equivalency and preference. Dissimilar

solutions, the combinations of whose properties correspond to each other are chosen by the first characteristic:

$$\exists \alpha \forall r_i \forall r_j [E_\alpha(r_i) \wedge E_\alpha(r_j) \wedge (\theta_\alpha^{r_i} = \theta_\alpha^{r_j}) \rightarrow (r_i \approx r_j)] \quad (10)$$

and like solutions possessing the best values of the required properties are chosen by the second characteristic

$$\exists \theta_\alpha \forall r_{i1} \forall r_{i2} [E_\alpha(r_{i1}) \wedge E_\alpha(r_{i2}) \wedge (\theta_\alpha^{r_{i1}} \geq \theta_\alpha^{r_{i2}}) \rightarrow (r_{i1} \approx r_{i2})]. \quad (11)$$

According, this approach allows to formalize the search for a technological solution r_i by the specific value of the determined criterion of selection t_q :

$$(\theta_\alpha^{r_i} \geq t_q). \quad (12)$$

Then a combination of predicates of the type allows to select the solution r_i by several criteria of selection $t_{q1}, t_{q2}, \dots, t_{qn}$, which correspond to n different properties of the solution r_i . In this case the condition of selection of the solution r_i takes the form

$$\bigwedge_{j=1}^n (\theta_{\alpha_j}^{r_i} \geq t_{qj}). \quad (13)$$

Use of the expression in problems of selection of dissimilar technological solutions, possessing different but mutually dependent properties α and δ (i.e., the condition $E_\alpha(r_i) \rightarrow E_\delta(r_j)$ is valid) allows to organize the selection of solutions

$$\exists \theta_\alpha \forall r_i \forall r_j [E_\alpha(r_i) \wedge E_\delta(r_j) \wedge (\theta_\alpha^{r_i} \geq t_{q1}) \wedge (\theta_\delta^{r_j} \geq t_{q2}) \rightarrow (r_i \approx r_j)]. \quad (14)$$

However, in general, condition is not valid, since the interrelations of the properties $E_\alpha(r_i) \rightarrow E_\delta(r_j)$, of the solutions r_i , and r_j , are often unknown. Moreover, in substantiating the selection of technological solutions and the synthesis of combined methods one must allow for stability of formation of processing quality indexes and consider the control over stability of the technological process mechanisms using feedback. Therefore, it is suggested to use criteria of self-organization as an object function instead of specific values of the criteria of the selection $t_{q1}, t_{q2}, \dots, t_{qn}$ combination, since the conditions, providing self-organization of surface phenomena and stabilization of the processing quality indexes formation are a consequence of the considered technological system excess structural composition.

The Romanowski relation

$$R = (\lambda_p^2 - k) / \sqrt{2k}, \quad (15)$$

where λ_p^2 is a Pirson's criterion, k is a number of freedom degrees, i.e. the value of groups in a studied row, allows one to judge the degree of correspondence of the statistical data to the selected law of distribution (Pashver, 1974).

A statistical analysis of quality indexes of the studied processing methods makes it possible to distinguish the most substantial technological factors and to reveal the interrelations between them. Formation of manufacturing rules of studied processing methods only from narrow ranges of the modes, restricted by self-organization conditions, provides conditions for the quality indexes of a surface layer stabilization.

In selecting the number of elements and processes, realized by a technological complex, it may be expedient to consider the interrelation of conflicting requirements to a production system on its reliability and plausibility. The reliability -- stability and flexibility -- adaptability relation can serve as a criterion, which allows to decide on a rational structure of a technological complex.

In self-organizing systems the flexibility and reliability can be controlled by changing the number of subsystems. Each subsystem i has a strictly defined q_1 and a fluctuating with scattered characteristics q_2 . The total yield of the system to a first approximation with account for the adaptability of the material and information flows is

$$q^{(i)} = q_1^{(i)} + q_2^{(i)}. \quad (16)$$

Assuming that under the conditions of production q_i is an independent random quantity, we present the total yield as

$$Q = \sum_{i=1}^n q^{(i)}. \quad (17)$$

Total yield, according to the central limit theorem, increases in proportion to the number of subsystems n , whereas the degree of scattering increases in proportion to the square root \sqrt{n} , similar to relation.

Thus, it is expedient to create technological complexes of high-performance processing, providing stabilization of component quality indexes and automation of control of technological processes, with conditions ensured for surface self-organization.

According to the classification of processing methods, we consider self-organization in the

processes of deposition, thermal processing, deformation, and surface layers of components cutting, as well as in combinations of deposition of coatings and thermal processing with deformation and cutting in combined processing.

2. PROCESS MIX IN HIGH-PERFORMANCE COMBINED PROCESSING METHODS

Simultaneous use of several energy fluxes, transferred to workspace by both a technological medium and instrumentation with control elements, sharply increases the efficiency of technological operations. However, combined use of several fluxes creates technological limits to stability of combined methods. Therefore, principally new technological complexes for combined processing can now be created on the basis of self-organization processes in technological systems.

To produce components with technological complexes, it may be expedient to use thermo-mechanical and electromagnetic flows of matter and energy, since the processes of production objects surfacing, accurate within a micron, have basically a thermo-mechanical character, and electromagnetic flows (due to their simple formation and convenient monitoring) are most technological.

We study the whole range of technological operations: deposition of coatings, thermal processing, deformation and surface layers cutting of components, and the principal combinations of them, which should be realized by technological complexes in combined electromagnetic and thermomechanical processing of components. The method of electromagnetic fusion is used for deposition of a surface layer, in which particles of ferromagnetic powder are aligned with electrode chains in a constant magnetic field, and, as a result of electric-arc discharges, are welded to the surface of the blank. This method makes it possible to deposit coatings of only a certain thickness; then the formed layer loses stability, and protrusions are formed on the surface, which are destroyed in subsequent discharges. The process of surface formation is controlled by electromagnetic flows, which, besides the fixation of ferropowder particles, provide intense heat release at places of their contact and, regardless of the expenditure of powder, control the thickness of the weld layer, changing its electric resistance.

Local inductive electric-contact heating or electric-spark discharge, which, beside heating, allow to alloy a surface layer of components, using ferropowder particles or introducing additives to the lubricating and cooling fluids, are used for surface thermal processing of items. Electromagnetic flows in workspace are mainly those that allow to control

both the depth and degree of hardening of a surface layer in thermal processing.

Ball rollers are used in technological complexes for deformation hardening and to change the form of surface layers. In surface plastic deformation, additional degrees of freedom allow the ball, as a result of interaction with the processed surface, to rotate as well as to swing. Without additional heating, the degree of deformation is small and the trajectory of a ball has a loop-like character. In heating, the processed material passes over to a plastic state, due to which the degree of deformation and the coefficient of friction increase. This impedes rotation and decreases the length of, first, the peak-like and, then, sinusoidal trajectory of a ball, thus leading to the decreased intensity of plastic deformation. So the process of surface plastic deformation can be controlled by a thermal effect and additional rotation of a ball.

The process of cutting is exercised in the technological complex by traditional cutters, milling cutters, emery disks, and a free abrasive in a magnetic field (Yashcheritsyn et al, 1996).

When cutting is performed by traditional cutting tools in processing with preheating, the equilibrium of temperature softening and deformation hardening intensities is violated, and the zone of chip formation loses stability and begins to shift, changing the shear angle. In this case the process of chip formation can be controlled by additional displacement of rotating tools, which does not allow frozen volumes of metal to fasten on a blade and restores a working part of a cutting edge, thus preventing a sharp increase of temperature in a localized volume of chip formation zone.

At grinding by an emery disk, with greater depth of cutting in incision or oscillations of the allowance, the forces of cutting and friction increase, thus facilitating the active crumbling of the disk abrasive particles. Due to this, the intensity of the disk wear and the velocity of crumbled particles transfer accompanied by heating increase. As a result, the forces of cutting and friction decrease, thus leading to a decrease in intensity of crumbling. These oscillations of intensity enable to control the process of grinding, restoring the abrasive particles of a disk.

Processing of viscous and plastic materials by an emery disk leads to its greasing, thus impeding self-sharpening. In this case, the process of grinding is controlled by electromagnetic flows in magneto-abrasive processing, when metal is removed in a

mechanical-chemical way by unfastened grains of abrasive powder with a ferromagnetic coating under constant magnetic field.

3. CONCLUSION

Examination of self-organization processes in deposition, heat treatment, deformation and surface layer cutting, as well as when deposition of coatings and heat treatment are combined with deformation and cutting in combined processing methods carries the implication, that a technological complex can work stably in an automatic mode over a long period of time and needs no external control. This indicates that technological complexes should be designed as the autonomous flexible production modules for combined electromagnetic and thermomechanical processing of items.

4. REFERENCES

- [1] Kheifetz, M.L. & Chemisov, B.P. (ed.) (2002). Intellectual manufacturing: A condition status and developing prospects, Novopolotsk.
- [2] Ryzhov, E.V. & Averchenkov, V.I. (1989). Optimization of technological processes of mechanical treatment, Kiev.
- [3] Poduraev, V. N. (1983). Technology of physicochemical methods of treatment, Moscow.
- [4] Averchenkov, V.I. (1997). *Trenie i iznos*, 18, N 3, pp. 339-348.
- [5] Golodenko, B.A. & Smolentsev, V.P. (1994). *Vestn. mashinostr.*, N 4, pp. 25-28.
- [6] Paskhver, I. S. (1974). Law of large numbers and statistical regularities, Moscow.
- [7] Yashcheritsyn, P.I., Kozhuro, L.M. & Kheifetz, M.L. (1996). *Vestnik machinostroeniya*, N 3, pp.33-36.

Authors: **rof. Michael Kheifetz, Alexander Pynkin, Natalia Pozilova**¹, The State Scientific and Production Amalgamation "Center" of the National Academy of Sciences of Belarus, Nezavisimosti Avenue, 66, Minsk, Belarus,
E-mail: kheifetz@presidium.bas-net.by;
mlk-z@mail.ru,

Prof. Sergey Klimenko, Institute of Super Firm Materials it. V.N.Bakul of the National Academy of Sciences of Ukraine, Kiev, Ukraine,

Prof. Ljubodrag Tanovi, University of Belgrade, Kraljice Marije, 16, Belgrade, Serbia

Sekuli , M., Kova , P., Gostimirovi , M., Hadžistevi , M., Rodi , D., Pucovski, V.

MODELING OF THE MAIN CUTTING FORCE IN FACE MILLING HARDENED STEEL BY ROTATABLE CENTRAL COMPOSITE DESIGN OF EXPERIMENTS

Abstract: *The objective of this present study was to present the mathematical model for modeling and analysis on the effects of process parameters, including the feed per tooth, depth of cut and cutting speed on the main cutting force in hard milling of pre-annealed tool steel 3840 (EN 90MnCrV8) (hardness 57 HRC) using cemented carbide inserts. Reliable prediction of milling forces is significant for the simulation of the machinability, cutter breakage, cutter wear, chatter and surface quality. A central composite rotatable design with three factors and five levels was chosen to minimize the number of experimental conditions. The predicted values and measured values are fairly close which indicates that the developed the main cutting force prediction model can be effectively used to predict the main cutting force from the face milling process with 99,68% confident.*

Key words: modeling, main cutting force, hard face milling, DoE

1. INTRODUCTION

Design of experiments (DOE) is one of the many problem-solving quality tools that can be used for various investigations such as finding the significant factors in a process, the effect of each factor has on the outcome, the variance in the process, troubleshooting the machine problems, screening the parameters, and modeling the processes. By using strategically designed and statistically performed experiments, it is possible to study the effect of several variables at one time, and to study inter-relationships and interactions. DOE is a tool to develop an experimentation strategy that maximizes learning using a minimum of resources.

Cutting of hardened steel is a topic of high interest for today's industrial production and scientific research. The common disadvantages of hard milling are excessive tool wear and high cutting forces. Knowledge of the cutting forces owing to a predictive model is very interesting with respect to the choice of a machine tool power, the cutting tools, the optimization of cutting conditions for a given machining operation or the control of the occurrence of vibrations.

The aim of this research is to analyse dependence of the main cutting force F_v on three cutting parameters, namely the cutting speed v , the feed per tooth f and depth of cut a in the hard face milling process.

2. DESIGN OF EXPERIMENT

The planning of experiments means prior prediction of all influential factors and actions that will result from new knowledge utilizing the rational research. The experiments have been carried out using the factorial design of experiments. Response surface methodology (RSM) is a widely practiced approach for various fields, particularly in situations where several input variables influence a quality characteristic of the product or process. RSM attempts to analyze the influence of the independent variables on a specific

dependent variable (response). The most popular class of second-order designs called Central Composite Design (CCD) was used for RSM in the experimental design.

In this work, the design of experiments was achieved by the rotatable central composite design (RCCD). The RCCD models the response using the empirical second-order polynomial:

$$y = b_0 + b_1x_1 + b_2x_2 + b_3x_3 + b_{11}x_1^2 + b_{22}x_2^2 + b_{33}x_3^2 + b_{12}x_1x_2 + b_{13}x_1x_3 + b_{23}x_2x_3 + b_{123}x_1x_2x_3 \quad (1)$$

where b_0, b_i, b_{ij}, b_{ii} are regression coefficients, and x_i, x_j are the coded values of input parameters.

The required number of experimental points for RCCD is determined:

$$N = 2^k + 2k + n_0 = n_k + n_\alpha + n_0 = 2^3 + 6 + 6 = 20 \quad (2)$$

where k is the number of parameters, n_0 is the repeated design number on the average level, and n is the design number on central axes.

The required number of experimental points is $N=20$. There are eight factorial experiments (3 factors on two levels, 2^3) with added 6 star points and centre point (average level) repeated 6 times to calculate the pure error.

The theory of the design of experiments and mathematical statistical analyses use coded values of input factors of the face milling process. The coded values of three independent input factors have values on five levels, Table 1.

Experiments have been carried out according to the experimental plan based on central composite rotatable second order design. Experimental design matrix consisting of experiment run order and coded values of the process parameters is shown in Table 2.

Levels of factors	Cutting speed $x_1=v$ (m/min)	Feed per tooth $x_2=f$ (mm/tooth)	Depth of cut $x_3=a$ (mm)	Coded values		
Highest	54,95	0,444	0,63	1,682	1,682	1,682
High	43,96	0,352	0,50	1	1	1
Average	35,32	0,280	0,32	0	0	0
Low	27,86	0,223	0,20	-1	-1	-1
Lowest	21,98	0,178	0,16	-1,682	-1,682	-1,682

Table 1. Physical and coded values of input factors in hard face milling

N	X_1	X_2	X_3	X_1^2	X_2^2	X_3^2	X_1X_2	X_1X_3	X_2X_3	$X_1X_2X_3$
1	1	-1	-1	1	1	1	1	1	1	-1
2	1	1	-1	1	1	1	-1	-1	1	1
3	1	-1	1	1	1	1	-1	1	-1	1
4	1	1	1	1	1	1	1	-1	-1	-1
5	1	-1	-1	1	1	1	1	1	-1	-1
6	1	1	-1	1	1	1	-1	1	-1	-1
7	1	-1	1	1	1	1	-1	-1	1	-1
8	1	1	1	1	1	1	1	1	1	1
9	1	0	0	0	0	0	0	0	0	0
10 X_1	1	0	0	0	0	0	0	0	0	0
11	1	0	0	0	0	0	0	0	0	0
12	1	0	0	0	0	0	0	0	0	0
13	1	0	0	0	0	0	0	0	0	0
14	1	0	0	0	0	0	0	0	0	0
15	1	-1,682	0	0	2,828	0	0	0	0	0
16	1	1,682	0	0	2,828	0	0	0	0	0
17	1	0	-1,682	0	0	2,828	0	0	0	0
18	1	0	1,682	0	0	2,828	0	0	0	0
19	1	0	0	-1,682	0	0	2,828	0	0	0
20	1	0	0	1,682	0	0	2,828	0	0	0

Table 2. Experimental design matrix with coded values

3. EXPERIMENTAL WORK

The experimental work was carried out at the Department of Production Engineering, the Faculty of Technical Sciences in Novi Sad. The machining was conducted on a Vertical-spindle Milling Machine („Prvomajska“ FSS-GVK-3) in dry condition. A face milling cutter with $\varnothing 125$ mm diameter („Jugoalat“ G.717), with cemented carbide inserts („Sandvik Coromant“ type SPKR 12 03 ED R-WH 3040) with tool cutting edge angle $\kappa=75^\circ$ and rake angle $\gamma=7^\circ$ was used as a tool. All of the experiments were conducted with one insert.

Workpiece material was pre-annealed tool steel 3840 (EN 90MnCrV8) (hardness 57 HRC). Material composition of workpiece is as follows: C-0,9%; Si-0,3 %, Mn-2%; Cr-0,3%; V-0,15% by wt. Dimensions of experimental probe is 200x104,7 x50 mm.

The instrumentation package includes a three-force component dynamometer Kistler (model 9257), based on the piezoelectric effect and PC based data acquisition system with LabView 8.0 software. The samples were sent to a multichannel amplifier for analogical signals for a better integrity of F_x , F_y and F_z . Then the data was transferred to a computer with an AD card to convert the analogical signals to digital

format for analysis.

Figure 1 presents the cutting forces scheme in one-tooth face milling (a shaded area is a chip removed by one tooth per revolution).

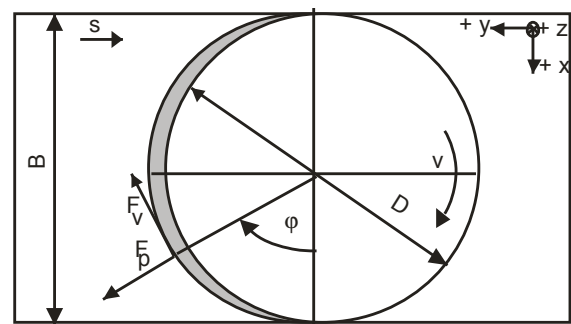


Fig. 1. The scheme of cutting forces

The results obtained through experiments have been presented in Figure 2. To eliminate the influence of random factors on change forces F_x , F_y and F_z during one revolution of cutter, requested their average values. The middle value was based on the values of cutting force for series of three full revolution of cutter (Figure 2).

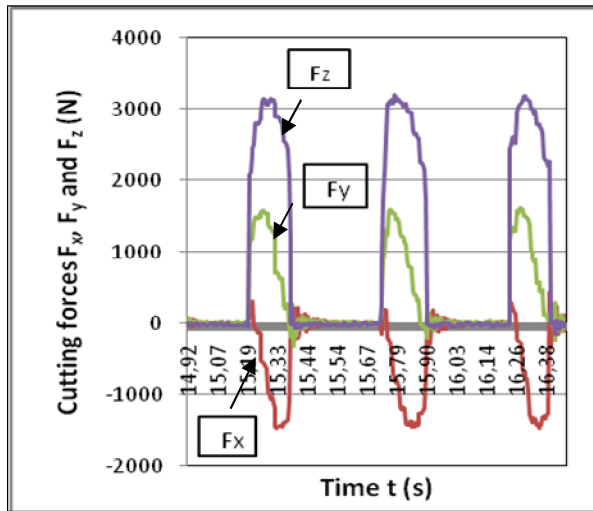


Fig. 2 Orthogonal cutting forces for three full revolution of cutter

The main cutting force F_v can be calculated on the basis of measured cutting forces in x and y direction using the following equation:

$$F_v = -F_x \sin \varphi + F_y \cos \varphi \quad (3)$$

Angle φ determines instantaneous position cutter insert on workpiece.

4. ANALYSIS OF RESULTS

Regression analysis (RA) have been performed using program package “Microsoft Office Excel”. By RA analysis the coefficients of regression, multi-regression factors, standard false evaluation and the value of the t -test have been assessed, Table 3. The measured values of the main cutting force and values obtained by regression analysis (RA) are presented in Table 4.

SUMMARY OUTPUT		Fv				
Regression Statistics						
Multiple R	0.996871366					
R Square	0.993752521					
Adjusted R Square	0.986810877					
Standard Error	28.5889688					
Observations	20					
ANOVA						
	df	SS	MS	F	Significance F	
Regression	10	1170072.841	117007.2841	143.1580973	1.12025E-08	
Residual	9	7355.962235	817.3291373			
Total	19	1177428.804				
	Coefficients	Standard Error	t Stat	P-value	Lower 95%	Upper 95%
Intercept	4256.983515	566.3142241	7.516999104	3.62752E-05	2975.891739	5538.075291
b1	-71.77546645	15.86490926	-4.524164954	0.001438177	-107.6643845	-35.88654841
b2	-16693.82032	1981.951446	-8.422920929	1.4633E-05	-21177.30597	-12210.33466
b3	-9867.036183	1436.919072	-6.866800208	7.33402E-05	-13117.57295	-6616.499419
b11	0.18360494	0.082455298	2.22672097	0.052979641	-0.002921901	0.370131782
b22	11001.92882	1272.410462	8.64652496	1.18354E-05	8123.536381	13880.32125
b33	3599.660571	383.719259	9.380974468	6.07469E-06	2731.627303	4467.693839
b12	237.1319876	49.34937924	4.805166574	0.000966735	125.4959361	348.7680391
b13	183.9814492	38.19615542	4.816753079	0.000951265	97.57574282	270.3871556
b23	35308.24018	4771.18346	7.400310735	4.10206E-05	24515.07336	46101.407
b123	-764.3710939	129.7563753	-5.89081725	0.000231695	-1057.900407	-470.8417807
RESIDUAL OUTPUT						
	Observation	Predicted Fv	Residuals	Standard Residuals		
	1	518.1687307	-11.58760546	-0.588912476		
	2	469.8174142	-2.327819397	-0.118305882		
	3	394.5039422	-16.86254064	-0.856998505		
	4	521.1475858	-8.481755833	-0.431065064		
	5	789.1639827	20.38290933	1.035912868		
	6	806.1466045	22.71727875	1.154551639		
	7	1207.796934	11.01045679	0.559580268		
	8	923.5178187	13.55857974	0.689082554		
	9	519.5637959	-10.64431763	-0.540972116		
	10	519.5637959	14.71688409	0.747950616		
	11	519.5637959	-0.963137621	-0.048949178		
	12	519.5637959	14.65209308	0.744657768		
	13	519.5637959	-38.94537991	-1.979306267		
	14	519.5637959	-10.57574341	-0.537486995		
	15	579.2140477	4.145597378	0.210690123		
	16	550.6169202	-7.273051253	-0.369635524		
	17	582.8064592	-13.73934044	-0.688269286		
	18	897.8276565	1.938643305	0.098526933		
	19	409.8024268	47.99549843	2.439257007		
	20	1256.696994	-29.7172492	-1.510308481		

Table 3. Regression analysis and ANOVA

Mathematical model for the main cutting force was obtained as follow:

$$F_v = 4256,98 - 71,77 \cdot v - 16693,82 \cdot f - 9867,04 \cdot a + 0,18 \cdot v^2 + 11001,93 \cdot s^2 + 3599,66 \cdot a^2 + 237,13 \cdot v \cdot f + 183,98 \cdot v \cdot a + 35308,24 \cdot s \cdot a - 764,37 \cdot v \cdot f \cdot a \quad (4)$$

No	Input parameters			F _v (N)		
	v (m/min)	f (mm/tooth)	a (mm)	Measured experimental data	Values obtained by regression analysis	Relative error (%)
1	27,86	0,223	0,2	506,581	518,169	2,287
2	43,96	0,223	0,2	467,489	469,817	0,498
3	27,86	0,352	0,2	377,641	394,504	4,465
4	43,96	0,352	0,2	512,665	521,148	1,654
5	27,86	0,223	0,5	809,546	789,164	2,518
6	43,96	0,223	0,5	828,863	806,147	2,741
7	27,86	0,352	0,5	1218,807	1207,797	0,903
8	43,96	0,352	0,5	937,076	923,518	1,447
9	35,32	0,280	0,32	508,919	519,564	2,092
10	35,32	0,280	0,32	534,280	519,564	2,755
11	35,32	0,280	0,32	518,600	519,564	0,186
12	35,32	0,280	0,32	534,215	519,564	2,743
13	35,32	0,280	0,32	480,618	519,564	8,103
14	35,32	0,280	0,32	508,988	519,564	2,078
15	21,98	0,280	0,32	583,359	579,214	0,711
16	54,95	0,280	0,32	543,343	550,617	1,339
17	35,32	0,178	0,32	569,067	582,806	2,414
18	35,32	0,444	0,32	899,766	897,828	0,215
19	35,32	0,280	0,16	457,797	409,802	10,484
20	35,32	0,280	0,63	1226,980	1256,697	2,422
				Average error:2,603		

Table 4. Measured values and values obtained by RA

The analysis of variance (ANOVA) and the F -ratio test have been performed to check the adequacy of the model as well as the significance of the individual model coefficients. It can be appreciated that the P -value is less than 0,05 which means that the model is significant at 95% confidence level. Also the calculated value of the F -ratio is more than the standard value of the F -ratio for F_v . It means the model is adequate at 95% confidence level to represent the relationship between the machining response and the machining parameters of the face milling process. ANOVA table for F_v also includes the individual model coefficients, interaction terms and the square terms, where it can be seen that there are all effects with a P -value less than 0.05 which means that they are significant at 95% confidence level. The R^2 value is high, close to 1, which is desirable.

5. CONCLUSION

The five level rotatable central composite design is employed for developing mathematical model for predicting the main cutting force in hard face milling. The experimentation is carried out considering three machining parameters, viz., cutting speed, feed per tooth and depth of cut as independent variables and the main cutting force. For prediction of the main cutting force within the selected experimental domain, the

quadratic model is developed. Regarding the results RCCD is found to be capable of accurate predictions of the main cutting force with approximate average relative error of 2,603%.

5. REFERENCES

- [1] Sekuli , M., Hadžistevi , M., Jurkovi , Z., Kova , P. Gostimirovi , M.: *Application of Taguchi method in the optimization of face milling parameters*, ICPE 2011, p.p. 57-60, Niš, September 28-30, 2011.
- [2] Cukor, G., Jurkovi , Z., Sekuli , M.: *Rotatable central composite design of experiments versus Taguchi method in the optimization of turning*, Metalurgija, Vol.50, No 1, pp 17-20, 2011.
- [3] Sekuli , M., Rodi , D., Kova , P. Gostimirovi , M., Savkovi , B.: *ANFIS predicting of the cutting forces in face milling hardened steel*, SLIM 2011, p.p. 346-349, Fiesa, September 25-27, 2011.

Authors: Assoc. Prof. M. Sekuli¹, Prof. P. Kova¹, Prof. M. Gostimirovi¹, Prof. M. Hadžistevi¹, D. Rodi¹ Ph.D. student, V. Pucovski¹ Ph.D. student

¹University of Novi Sad, Faculty of Technical Sciences, Department of Production Engineering, Trg Dositeja Obradovi a 6, 21000 Novi Sad, Serbia, Phone.: +381 21 450-366, Fax: +381 21 454-495.

E-mail: milenkos@uns.ac.rs;

Simonovi , S.

NANOMECHANICAL MODELLING OF A CUTTING PROCESS

Abstract: The Model of cutting process is reviewed based on molecular dynamic. Description of work-piece modeling, tools and environment modeling has been rendered taking into consideration thermodynamic aspects of the process. Modeling of the system boundaries has been described with regard to uniqueness of the cutting process.

Keywords: Molecular dynamic, Cutting

1. INTRODUCTION

Nanomechanics refers the study and characterization of the mechanical behavior of individual atoms, atomic-scale systems and structures in response to various types of forces and loading conditions.

There are three main methods used for modeling of the nano processes: Ab initio methods, semi empirical methods and classical dynamic.

Ab Initio calculations are based on the Schrödinger equation. The Schrödinger equation cannot be solved exactly for any molecule with more than one electron. Thus approximations are used; the less serious these are, the “higher” the level of the ab initio calculation is said to be. There are two methods that can be used to make the problem solvable without introducing any empirical material parameters: the density functional theory (DFT) and Hartree-Fock (HF) theory. At least, in the viewpoint of materials mechanics, the density functional methods have been more efficient and thus more popular than the Hartree-Fock calculations. Structural, mechanical, and electronic properties of materials obtained by DFT-based calculations are in general comparable with experimental values, as long as the relevant computational parameters are properly chosen. On the other hand, although Hartree-Fock calculations provide the high accuracy of results, they are much more demanding computationally than the density functional methods.

Semi empirical calculations are, like ab initio, based on the Schrödinger equation. However, the very complicated integrals that must be calculated in the ab initio method are not actually evaluated in semiempirical calculations: instead, the program draws on a kind of library of integrals that was compiled by finding the best fit of some calculated entity like geometry or energy (heat of formation) to the experimental values. This plugging of experimental values into a mathematical procedure to get the best calculated values is called parameterization. It is the mixing of theory and experiment that makes the method “semiempirical”: it is based on the Schrödinger equation, but parameterized with experimental values (empirical means experimental).

Molecular mechanics is based on a model of a molecule as a collection of balls (atoms) held together by springs (bonds). Molecular mechanics is fast.

Only slow motion (slower than thermal vibrations) of atoms, ions and molecules can be considered, and the internal electronic structure is ignored. The atoms and molecules exert internal forces on each other that are determined by instantaneous values of the total potential energy of the system. The potential energy is typically considered only as a function of the system spatial configuration and is described by means of **inter-atomic potentials**. These potentials are considered as known input information; they are either found experimentally or are computed by averaging over the motion of the valence electrons in the ion’s Coulomb field by means of quantum ab initio methods. Numerical methods of solving the classical equations of motion for multiparticle systems with known interatomic potentials are collectively referred to as **molecular dynamics**(MD). MD is regarded as a major practical application of the classical particle dynamics.

Here, only the more classical atomistic approach will be presented.

2. BASIC MACHINING MODEL

Figure 1. represents an often applied model for MD cutting process simulation, i.e. the orthogonal cutting layout, and includes the essential elements of MD modeling. In addition to the material properties and the interactions between its constituents, the contact and interface conditions, e.g. between tool tip and workpiece as well as with their environment, need to be described.

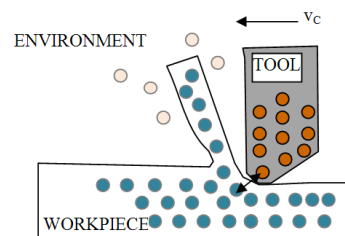


Figure 1.

The machining system is supposed to consist of the workpiece, the tool and the environment. All the three elements are represented by a discrete body or a certain material that is described by its chemical elements and by their coordinates. The coordinates provide the information about the atomic arrangement,

i.e. the structure of the material, which could be set up, e.g. for a metal on the basis of known lattice structures and lattice constants. The V_c is relative velocity between the tool and the workpiece.

In nano and micromachining processes the actual material removal can be limited to the surface of the workpiece, i.e. to only a few atoms or layers of atoms. At this range, inherent measurement problems and the lack of more detailed experimental data limit the possibility for developing analytical and empirical models as more assumptions have to be made. On the basis of atomistic contact models, the dynamics of the local material removal process and its impact on the material structure, as well as the surface generation, can be studied.

Taking into consideration the crystal size of typical metals, which range between a few tens to several hundred microns in diameter, single crystalline workpiece structures represent reasonable material structures for nanoscale cutting simulations as the tool tip will have to cut over a length of at least 30,000 unit cells before reaching a grain boundary area.

Although Figure 1. shows a 2D orthogonal cutting setup, the choice of material representation should always be 3D. With pure 2D models it is impossible to sufficiently describe the 3D crystalline structure of metals and, hence, no realistic slip system or dislocation motion seems possible and no realistic deformation behavior can be expected.

3. THE MODELLING OF CUTTING PROCESS INTERATOMIC INTERACTION

The interactions between particles are specified by functions that describe the potential energy. Depending on the complexity of a material and the chosen mathematical description respectively, the potential function may consider many parameters. The goal of the potential function development is that the functional description and the material-specific set of parameters lead to a self-organizing, known structure as a function of the state variables. This provides the basis as well as the necessary flexibility for carrying out not only phase and structure calculations, but also cutting process calculations at the nanoscale. Potential functions and sets of parameters have to be specified for all possible combinations of interactions that need to be considered. In the following, the principles of the necessary potential functions will be described using the widely applied so-called pair potential functions.

The best known pair potential functions is the Lennard-Jones (LJ)potentials (see equation (1)) for which the potential energy V_{ij} is only a function of the separation or bonding distance $r_{ij} = |\vec{r}_i - \vec{r}_j|$, between atoms i and j .

$$V_{ij}^{LJ} = 4\epsilon \left[\left(\frac{\sigma}{r_{ij}} \right)^{12} - \left(\frac{\sigma}{r_{ij}} \right)^6 \right] \dots (1)$$

There are two parameters, σ and ϵ , in LJ potential. However, using pair-potentials it is not possible to

correctly describe all elastic constants of a crystalline metal. For a better representation of metals, many-body interactions need to be included into the function as for example in the well-known potentials following the embedded atom method (EAM). In the following, the Finnis-Sinclair-type EAM potential by Ackland et al. was employed for the workpiece-workpiece interactions.

Metallic elements give up their valence electrons to form a "cloud" of electrons surrounding the atom nuclei. The valence electrons move freely within the electron cloud and become associated with several atom nuclei. The positively charged nuclei are held together by mutual attraction to the electrons. This attraction forms a strong metallic bond. The metallic bonding mechanism is quite different from both ionic bond and covalent bond, thus a different type of atomistic potential called Embedded Atom Method (EAM) has been developed.

In the formulation (2), the cohesive energy of metal consists of two parts: one is the summation of all the pairwise bonding energy, and the second is the energy which depends on the volume of metal after deformation. Compared to pair potentials, the latter part is the energy necessary to keep the metal in equilibrium, and corresponds to the elasticity energy, which is the energy based on the density of the background electron cloud.

E_i terms the embedded energy, which is the required energy to embed the atom i into the background of a local electron cloud at the atom position i . Introducing notation for the potential energy V_i of atom i and the total potential energy U_{tot} of the atomistic system, the EAM formulation can be given as follows:

$$U^{tot} = \sum_i E_i(\rho_i) + \frac{1}{2} \sum_i \sum_j V_{ij}(r_{ij}) \dots (2)$$

where ρ_i is the electronic density at the atom position i . This density is assumed to be the sum of the electronic density $\rho_j(r_{ij})$ as follows:

$$\rho_i = \sum_{j=1(\neq i)} \rho_j(r_{ij}) \dots (3)$$

where $\rho_j(r_{ij})$ is the electron density distribution of atom j at the position of atom i , before atom i is embedded into the electron cloud. In order to obtain the total energy of the system, we need to determine the pair potential V_{ij} , the embedded function E_i , and the electron cloud density function ρ_i . These functions are not calculated from QM such as the HF method or the electron density function theory, but fitted from experimental data and therefore remain in the category of empirical potential. Fitting these functions usually requires the following experimental data: lattice parameter, bonding energy, vacancy formation energy, and an elastic constant.

5. NANOMECHANICAL MODEL OF THE CUTTING PROCESS ENVIRONMENT

Most state-of-the-art material removal process simulations focus on the material removal mechanisms, chip and surface generation. Besides partially strong idealizations of the tool and workpiece properties as

well as the direct contact and boundary conditions, so far fluids have not been included in the environmental descriptions of workpiece and tool in MD-modeling. Hence, such an environment represents high vacuum conditions with no heat convection to an atmosphere or coolant. Therefore, an extension of MD machining process simulation has been proposed by considering fluids together with the tool tip and the workpiece [3]. The extension of MD machining process models by molecular gas and fluid dynamics (see [4, 5]) provide an opportunity for enabling a complete energy balance and for investigating the impact of adsorption and reaction layers at the workpiece surface and their contribution to the contact tribology beyond dry-machining at high vacuum. For this purpose the spaces above workpiece and tool surfaces need to be filled with particles that follow fluid particle dynamics. The fluid-fluid interactions as well as the tool (hard)-workpiece interactions usually are calculated on the basis of the Lennard-Jones (LJ) potential function. The wetting of the tool (fluid-tool) and workpiece surface (fluid-workpiece) are also described by the fluid-fluid potential function that represents a weak interaction like hydrogen bonding in water, but no chemical reaction.

6. THE MODEL OF MOLECULAR DYNAMIC UNDER CUTTING PROCESS

Molecular dynamics model of a cutting process takes into consideration macroscopic, irreversible thermodynamics and reversible nano-mechanics. The thermodynamic equations form a link between the nanomechanical state, a set of atoms and molecules, and the macroscopic surroundings, the environment. The thermodynamic equations yield the quantities, system temperature and hydrostatic pressure of the model and allow us to determine energy changes involving heat transfer. In mechanics, it is usual to consider energy changes caused by displacement and deformation. By the term “mechanical state” of a microscopic system we mean a list of present coordinates (r) and velocities (v) of the constituents [4]. For this information about the state of the system to be useful, equations of motion, capable of predicting the future, must be available. As the governing equations of motion for a system of constant total energy, the well-known Newton’s equations of motion can be chosen:

$$\frac{d\bar{v}_i(t)}{dt} = \frac{1}{m_i} \sum_{j \neq i} \bar{F}_{ij}(\bar{r}_{ij}) \dots (4)$$

$$\frac{d\bar{r}_i(t)}{dt} = \bar{v}_i(t) \dots (5)$$

$i, j = 1, 2, \dots, n$

where n denotes the number of nanosystem constituents.

The resulting force on an atom i is expressed by an integral over all force contributions F_{ij} . Numerically this is calculated as a sum over all forces acting on each atom i (equation (4)). Hence, two bodies at close

distance interact through this sum of force contributions in the equation of motion. To advance the atoms in space, the equation of motion has to be integrated with respect to time, once to obtain the new velocity and twice for the new position of each atom. Numerically, this operation is more efficiently carried out by approximation schemes, for instance using finite difference operators and the so-called Verlet or Stoermer algorithm [6, 4]:

$$\bar{r}_i(t + \Delta t) = \bar{r}_i(t) + \Delta t \cdot \bar{v}_i(t) + \frac{1}{2m_i} \Delta t^2 \bar{F}_i(t) \dots (6)$$

$$\bar{v}_i(t + \Delta t) = \bar{v}_i(t) + \frac{\Delta t}{2m_i} [\bar{F}_i(t + \Delta t) + \bar{F}_i(t)] \dots (7)$$

$$\bar{F}_i = - \frac{\partial U(\bar{r}_1, \bar{r}_2, \dots, \bar{r}_n)}{\partial \bar{r}_i} \dots (8)$$

$i=1, \dots, n$

With the present initial positions, initial velocities and applied forces, first the new positions and then the new velocities can be calculated. So, given the equations of motion, applied forces and boundary conditions, i.e. knowing the current mechanical state, it is possible to simulate the future behavior of a system. Mathematically, this represents an initial value problem. A reasonable distribution of the initial velocities can be obtained from the Maxwell-Boltzmann distribution function.

The dynamic development of the atomic system as a whole determines the instantaneous kinetic state of the system. By relating the average kinetic energy of the atoms E_{kin} (with average velocity v), i.e. their nanomechanical state, to the thermal energy E_{therm} of the system, which is the thermodynamic state, the gas kinetic definition of the system temperature is adopted:

$$E_{kin} = m \cdot \frac{1}{n} \sum_{i=1}^n v_i^2 = \frac{3}{2} k_B T = E_{therm} \dots (9)$$

where T is temperature and k_B – Boltzman’s constant

From equation (9) the temperature T of a 3D system of atoms can be directly observed or, for a given reference temperature, the kinetic energy in the system can be controlled.

Since the initial choice of the atom configuration is more or less idealistic, i.e. artificial, it does not fit into the Maxwell-Boltzmann distribution from the energetic point of view, the whole system needs to pass through an initial equilibration phase, during which the atom configuration adjusts to the invariants of the system, e.g. total system energy, volume, pressure and/or temperature, and thereby also to the boundary conditions.

7. THE BOUNDARY CONDITIONS MODELLING

Since the size of atomistic models is small a large percentage of atoms are located on the surfaces. These surface atoms have completely different surrounding conditions and forces from the atoms inside of the bulk.

Also, fixed atom boundary can be introduced by removing the dynamics of boundary atoms, but keeping the interactions with the freely moving atoms. The consequences of such infinitely hard boundaries for the simulation can be significant as no energy can be passed through the boundary and phonons will be reflected at it. The sole use of hard boundaries represents a poor representation of the surrounding environment/material. Some of the negative effects of hard boundaries can be corrected by placing thermally controlled atom layers between freely moving atoms and a hard boundary [7,8]. The problem of surface effects can be eliminated by introducing periodic boundary conditions (PBC). In a simulation model with PBC, a given number of atoms move within a supercell and interact with each other. The supercell is surrounded by a periodically repeated environment made up of an infinite number of its own images. Thus, the atoms in a supercell not only interact with atoms in the same cell, but with image atoms in adjacent mapped cells. The supercell can be viewed as a rectangular box, and the images of this simulation box are aligned periodically in all directions (Figure 2.). For two dimensional (2D) cases, each cell has eight neighbors, and for three dimensional (3D) cases, there are 26 neighbors. The system reacts as if there are identical systems at both sides of the PBC, exposed to the same conditions and changes. In practice, the system is connected to itself, and atoms at one side interact with atoms on the other side and form a continuous structure. If deformation in the system requires an atom to slip across the PBC, it transfers from one side of the model to the other. Figure 2 shows a sketch of an cutting process model (the cutting tool on the top of a workpiece), where a one-axis PBC is considered perpendicular to the horizontal axis.

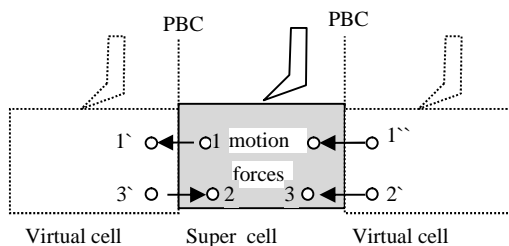


Figure 2.

A consequence of periodic boundaries is that energy and phonons are not reflected, but travel through the system by means of the PBCs. One or two-axis PBCs can be employed where symmetry axes are available and the lattice structure allows an undisturbed bonding through the PBC planes. Additionally, a deformation compatibility across a PBC has to be fulfilled by an appropriate alignment of preferred slip systems relative to the PBCs, in order to avoid artificial deformation patterns [9,10,11].

8. CONCLUSION

Nano modelling of the cutting process has following elements:

- initial configuration is determined by means of systems atomic coordinate determination
- nano-mechanics is constituted by means of atomic interaction
- determination of equation of motion by means of equation of classical dynamics
- mathematical description is determined by means of numerical integration (dynamics)
- energy balance of the system is determined by means of thermodynamics
- boundary conditions are determined by micromechanical boundaries of the model

9. LITERATURE

- [1] Fan, Jinghong: *Multiscale analysis of deformation and failure of materials*, John Wiley & Sons, Ltd, 2011
- [2] Davim J., Jackson J.: *Nano and micromachining* ISTE Ltd and John Wiley & Sons, Inc., Great Britain and the United States, 2009
- [3] Rentsch R., Brinksmeier E., "Tribology Aspects in State-of-the-art MD Cutting Simulations", 8th. CIRP Int. Workshop on Modeling of Machining Operations, Chemnitz, D, 2005, p. 401-408.
- [4] Hoover W.G., *Computational Statistical Mechanics*, Studies in Modern Thermodynamics 11, Elsevier Science, Amsterdam-Oxford-New York-Tokyo, 1991, 313
- [5] Rappaport D.C., *The Art of Molecular Dynamics Simulation*, Cambridge Univ. Press, Cambridge, UK, 1995.
- [6] Allen M.P., Tildesley D.J., *Computer Simulation of Liquids*, Clarendon Press, Oxford, 1987.
- [7] Belak J., Stowers I.F., "The Indentation and Scraping of a Metal Surface: A Molecular Dynamics Study", in *Fundamentals of Friction: Macroscopic and Microscopic*, Eds.: Singer, Pollock, ASI Series E, Vol. 220, 1991, p. 511-520.
- [8] Shimada Sh., Ikawa N., Ohmori G., "Molecular Dynamics Analysis as Compared with Experimental Results of Micromachining", *Annals of the CIRP*, Vol. 41/1, 1992, p. 117- 120.
- [9] Rentsch R., Inasaki I., "Indentation Simulation on Brittle Materials by Molecular Dynamics", in *Modeling, Simulation, and Control Technologies for Manufacturing*, SPIE Proc. Vol. 2596, Ed. R. Lumia, Philadelphia, PA, USA, 1995, p. 214-224.
- [10] Daw M.S., Baskes M.I., "Embedded-atom Method: Derivation and Application to Impurities, Surfaces, and other Defects in Metals", *Phys. Rev. B* 29 (12), 1984, p. 6443-6453.
- [11] Finnis M.W., Sinclair J.E., "A Simple Empirical N-body Potential for Transition Metals", *Philosophical Magazine*, A., Vol. 50, No. 1, 1984, p. 45-55.

Author: dr Svetomir Simonovi, professor of the Technical College, Bulevar Zorana in i a 152A, 11070 Novi Beograd

e-mail: svetomir@sezampro.rs

Gostimirovi , M., Rodi , D., Kova , P., Ješi , D., Kulundži N.

AN EXPERIMENTAL STUDY OF THE CUTTING FORCES IN CREEP-FEED GRINDING

Abstract: This paper examines the value and character of cutting forces in the creep-feed grinding. In order to identify the impact of cutting forces on the state of the process of deep grinding, according on the elements of the machining experimental tests were determined dependence of the tangential and normal components of the grinding forces and ratio grinding force. In comparison with the traditional multi-pass grinding results show the occurrence of higher cutting forces in creep-deep grinding, especially normal components.

Key words: creep-feed grinding, cutting forces, grinding force ratio, machining conditions

1. INTRODUCTION

Grinding is one of the most important methods of machining material. The basic advantages of grinding are high-accuracy machining and surface quality, the ability to process hard and machining difficult to cut materials or complex surfaces shapes [1].

In recent years, in addition to the classic multi-pass grinding, which is used for finishing operations, high productivity grinding processes are applied, which allow the use of grinding in the roughing and finishing operations [2, 3]. In these highly productive grinding procedures, increasing cutting speeds and / or depth of cut, significantly increasing productivity is relatively small, which has long been disadvantage of the classic grinding.

Deep grinding, as a representative of the highly productive grinding processes, increase productivity and reduce total processing time realizes one pass grinding with large depths of cut and low-speed auxiliary movement of the workpiece [4, 5]. On the other hand, due to the increase in the length and time of contact with the workpiece wheels, increases spending desktop grinding wheels, grinding temperature and cutting forces.

This paper analyzes the cutting forces in the creep-feed grinding and experimentally determined mean values of cutting force of abrasive grains that are currently in in the grip with the workpiece. Cutting forces are determined depending on the treatment regime for two types of corresponding wheels.

2. CUTTING FORCES IN GRINDING

The forces that occur in the processing of grinding as resistance to penetration into the workpiece by grinding grain, as a result of plastic deformation in the cutting zone and friction between the grinding surface and workpiece [6, 7]:

$$F = F_{deformation} + F_{friction} \quad (1)$$

Cutting force one abrasive grain F_{grain} and total force on grinding wheel were created at the same time by the number of active grains that are caught in the workpiece. In the research process dynamics processing grinding is used the total mean cutting

force, because the cutting force of one abrasive grain is not significant [8]:

$$F = \sum_1^{N_a} F_{grain} \quad (2)$$

The size and character of the grinding force depends on machining conditions, characteristics of the grinding wheel, workpiece material, stiffness of machining system, cooling conditions, the process of dressing etc.

Due to the greater depths of cut and intense wearing wheel in deep grinding appears to increase cutting force. However, as in deep grinding with increasing depth of cut takes less speed of the workpiece and the grinding wheel permanently sharp, level of growth the grinding forces compared to conventional grinding is not excessively high.

2.1. Mechanism of processing grinding

The cutting process in grinding is achieved through simultaneously a large number of abrasive grains catch a very thin layer of material that is placed in the space between two abrasive grains and pores, Figure 1. When abrasive grains come out of catch with the material, chips leave the area under the influence of centrifugal force, or due to flushing agent for cooling and lubrication.

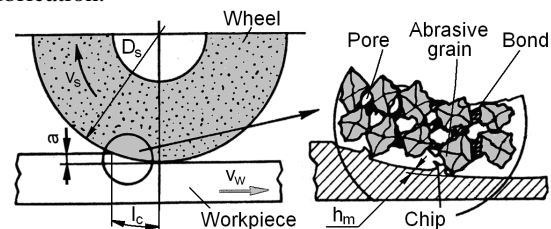


Fig. 1. Mechanism of processing grinding

Mechanism of processing grinding is different from other procedures of machining because of the different geometric shapes of abrasive grains. Therefore, in grinding each grain has a different and undefined cutting geometry, which is still unfavorable.

The process of cutting when grinding is defined by the kinematic and geometrical parameters. Kinematic parameters are: cutting speed v_s and workpiece speed

v_w , respectively, feed s if there is movement. The geometrical parameters are: wheels diameter D_s , workpiece diameter D_w , depth of cut a , the length of contact l_c and average chip thickness h_m .

The length of contact of surface grinding is distance that actively grain exceeds from the moment of contact with the workpiece exit from a contact:

$$l_c = \sqrt{a \cdot D_s} \quad (3)$$

The average chip thickness is imaginary thickness that each time cutting abrasive grains, and is determined by:

$$h_m = \frac{a \cdot v_w}{v_s} = \frac{Q'}{v_s} \quad (4)$$

where is $Z'=a \cdot v_w$ - specific productivity grinding.

2.2. Components of the grinding forces

Generally, in the processing of grinding occurs resulting cutting forces. For practical reasons, the resulting force is split into components in several interesting directions. In the case of surface grinding, where there is no lateral movement of the table, usually resulting force has been divided: tangential (extensive) component F_t and normal (radial) component F_n .

Tangential component acts in the direction of the tangent to the surface of the grinding wheel and workpiece contact, ie. in the direction of cutting speeds. The normal component acts normally to the surface of the wheels and workpiece. As the diameter of the wheels is far greater than the depth of cut, it can be assumed that the tangential and normal component supine in a horizontal or vertical plane, Figure 2.

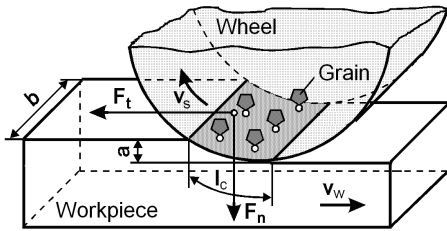


Fig. 2. Components of the grinding forces

The relationship of normal and tangential components of the grinding forces is defined as the grinding force ratio:

$$\lambda = \frac{F_n}{F_t} = \frac{F'_n}{F'_t} \quad (5)$$

In the previous equation, the components of the grinding forces are reduced per unit width of grinding b , referred to as the specific grinding force:

$$F'_t = \frac{F_t}{b} \quad (6)$$

$$F'_n = \frac{F_n}{b}$$

Tangential grinding force is authoritative for determining the driving power machine tools, while the normal force significant from the point of processing accuracy and high surface quality. These components of the cutting forces during grinding are determined by measurement and calculation. To measure applied dynamometers, to give the exact value of the force, but

the defined conditions of processing. Calculation of forces grinding through analytical dependences obtained for certain processing conditions during experimental tests, limited test area, while the use of theoretically derived forms, because of its generality usually unreliable.

Generally known empirical equation for determining tangential (main) grinding forces, analogous expressions by Kronenberg in 1927, reads as follows [1]:

$$F'_t = h_m \cdot k_{mc} \quad (7)$$

where is k_{mc} - main unit cutting force.

One of the most popular analytical model for assessing the normal components of the grinding forces was developed by Werner and is expressed by the following equation [9]:

$$F'_n = K \cdot \left(\frac{Q'}{v_s} \right)^{2\epsilon-1} \cdot a^\epsilon \cdot D_s^{1-\epsilon} \quad (8)$$

where is K - proportionality factor i ϵ - exponent whose value depends on the specific workpiece material.

Based on the grinding force can be expressed by specific grinding energy, which shows how much energy is consumed per unit volume of material removed:

$$u = \frac{P'}{Q'} = \frac{F'_t \cdot v_s}{a \cdot v_w} = \frac{F'_t}{h_m} \quad (9)$$

where is $P'=F'_t \cdot v_s$ - specific grinding energy.

2. EXPERIMENTAL SETUP

2.2. Conditions of the experimental setup

Workpiece material used in the experimental setup was the molybdenum high speed steel (HSS), which is widely used in the industry of cutting tools. Designation of the selected speed steel is DIN S 2-10-1-8. This steel belongs to a group of ledeburite steel with a microstructure consisting of martensite and fine mixtures of primary and secondary ledeburite cementite. The chemical composition of the test material was: 1,08 % C; 0,22 % Si; 0,23 % Mn; 0,014 % P; 0,019 % S; 4,1 % Cr; 1,5 % W; 9 % Mo; 1,1 % V and 8 % Co. Measured hardness on all samples ranged 66 ± 1 HRC. Experimental samples consisted of tiles measuring $40 \times 20 \times 16$ mm.

Based on the recommendations, the chosen material of the workpiece and set the conditions of processing, were selected two wheels similar characteristics: wheels »Norton« type 32A54 FV BEP and size $400 \times 80 \times 127$ mm, respectively »Winterthur« type 53A80 F15V PMF and size $400 \times 50 \times 127$ mm. The wheels is with high-quality abrasive grain, medium grain size, hardness soft, open structure with ceramic binder. All experiments were conducted with sharp wheels, and sharpening is done with a diamond planer alignment with a depth of 0.01 mm/speed and displacement of 0.1 mm/rev.

The machining conditions included variable depths of cut and workpiece speed. The depth of cut was $a = 0.05; 0.1; 0.25; 0.5; 1$ mm and the workpiece speed

was $v_w = 2.5; 5; 10; 25; 50$ mm/s. The adopted mean value of specific material removal rate is $Q' = 2,5$ mm³/mm·s. The wheel speed was held constant $v_s = 30$ m/s.

2.2. Experimental Procedures

Measuring the forces that occur during surface grinding was done using three component dynamometer »Kistler Instrumente AG", type 9257. Used dynamometer works on the piezoelectric principle, which is reflected in the emergence of electricity on the surface of the crystal plate embedded in the dynamometer when the same force is exerted pressure. Electricity is amplified by means of amplifiers capacitive "Kistler" type CA 5001 and then is converted into DC voltage in size from 0 to 10 V.

Measurement, analysis and control of the grinding force was performed using the information of the measuring system [10], where data acquisition is implemented by AD cards and cash integrated software package, Figure 3. The set information measurement data acquisition system is characterized by a high degree of accuracy, reliability, speed of response and the ability to reproduce measurement results. Allows real-time measurements, timely intervention if they appear illogical results, as well as comprehensive and rapid processing and analysis of results.

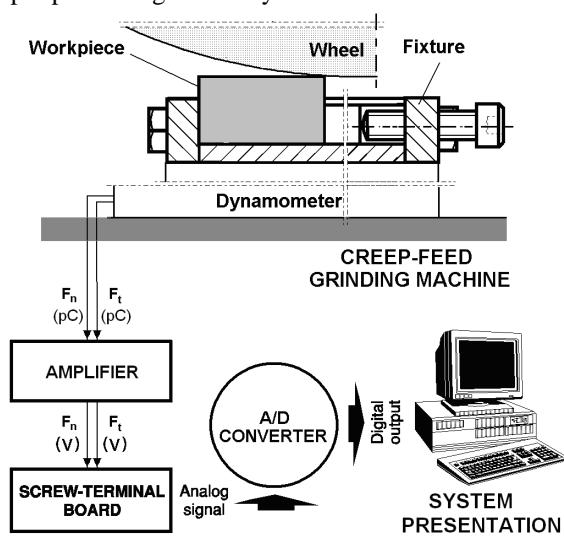


Fig. 3. Information system for measuring and processing of cutting forces during surface grinding

3. RESULTS

The measured values of the normal and tangential grinding force, depending on the mode of processing elements, point to a very reliable and safe measurement of the force components in the flat deep grinding. An example of measurement results of the cutting force during deep grinding, two wheels with similar characteristics but different manufacturers, is shown in Figure 4. It can be concluded that for the same processing conditions obtained different values of force components sanding, or about the same dynamic character.

Figure 5 and 6 are given depending on the specific

components of cutting forces, as well as their relationship F'_n/F'_t , depending on the cutting depth and workpiece speed for two selected wheels. With diagrams shown it can be concluded that with increased cutting depth grinding forces are rising and decrease with increasing rotation of the workpiece.

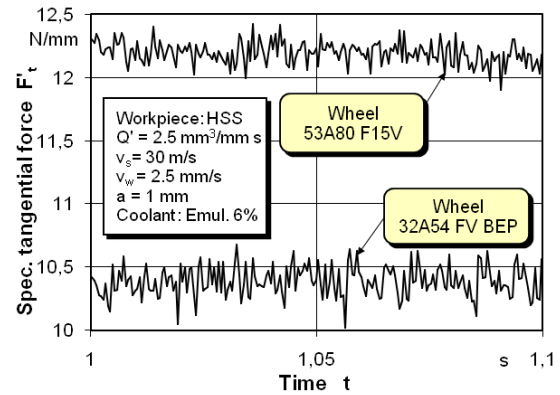


Fig. 4. Value and character of the measured tangential grinding force components

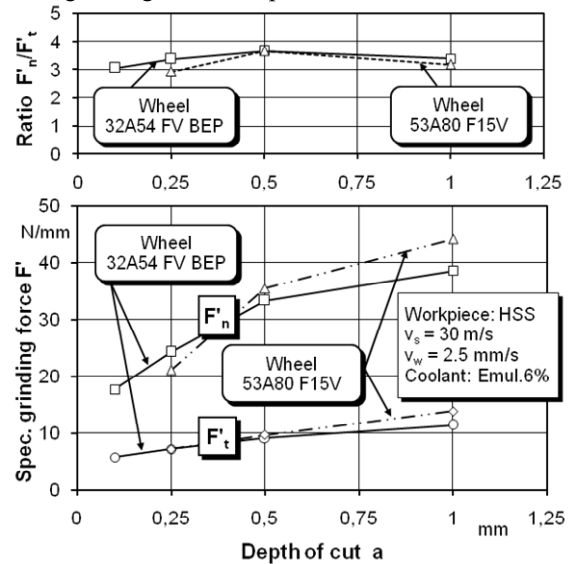


Fig. 5. The grinding forces, depending on the depth of cut

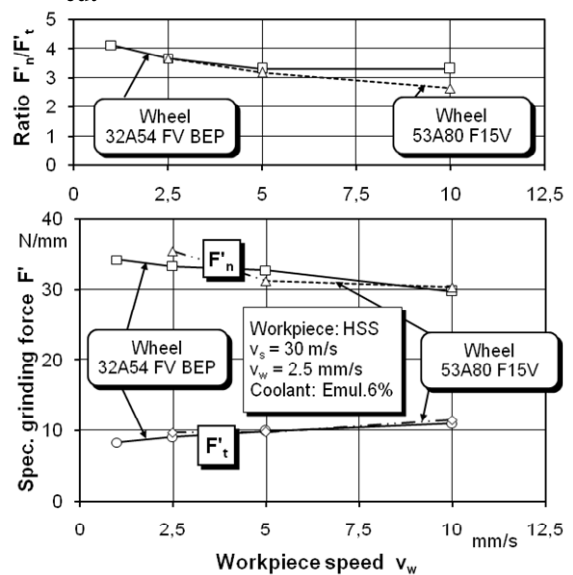


Fig. 6. The grinding forces, depending on the cutting speed

Changing of cutting force in grinding, depending on the elements of the treatment regime, and a constant specific productivity of grinding, is shown in Figure 7. The diagram shows that compared to conventional grinding, in creep-feed grinding appear higher cutting forces.

The ratio of normal and tangential grinding forces moved to within 2-4, except that higher values related to creep-feed grinding.

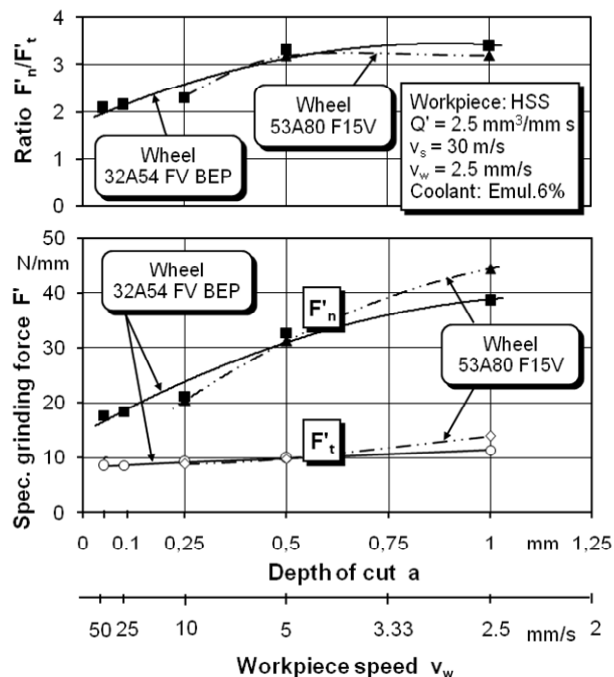


Fig. 7. Changing the cutting force depending on the elements of the treatment regime for creep-feed grinding

4. CONCLUSIONS

Based on the conducted experimental research and analysis can be performed the following conclusions:

- When creep-feed grinding reduces processing time, but also increase the cutting force;
- Cutting forces primarily depend on the type of workpiece material and elements of its processing;
- Cutting forces during creep-feed grinding, due to a greater number of active abrasive grains into engagement with the workpiece material, are significantly higher compared to conventional grinding;
- the grinding forces, the increasing length of contact of the grinding wheel and workpiece material, with increasing depth of cut growth;
- increase the speed of the workpiece grinding forces decrease because it reduces the cross-section of the affected layers of material by grinding grain;
- In creep-feed grinding can be observed greater grinding force ratio;

Cutting forces during creep-feed grinding allow identification of the energy balance of machine tools and estimation of the level of accuracy in different processing conditions;

5. ACKNOWLEDGEMENTS

The paper is the result of the research within the project TR 35015 (2011/15) financed by the Ministry of Education, Science and Technological Development of the Republic of Serbia and Ceopus III.

6. REFERENCES

- [1] König, W.: *Fertigungsverfahren, Band 2 - Schleifen, Honen, Läppen*. VDI-Verlag GmbH, Düsseldorf, 1980.
- [2] Kopac, J., Krajnik, P.: *High-performance grinding - A review*, Journal of Materials Processing Technology, Vol.175, No.1-3, pp. 278-284, 2006.
- [3] Kovac, P., Gostimirovic, M., Sekulic, M., Savkovic, B.: *A review of research related to advancing manufacturing technology*, Journal of Production Engineering, Vol.12, No.1, pp. 9-16, 2009.
- [4] Gostimirovic, M., Sekulic, M., Kopac, J., Kovac, P.: *Optimal control of workpiece thermal state in creep-feed grinding using inverse heat conduction analysis*, Strojniški vestnik - Journal of Mechanical Engineering, Vol.57, No.10, pp. 730-738, 2011.
- [5] Gostimirovic, M., Kovac, P., Jesic, D., Skoric, B., Savkovic, B.: *Surface layer properties of the workpiece material in high performance grinding*, Metalurgija, Vol.51, No.1, pp. 105-108, 2012.
- [6] Malkin, S., Guo, C.: *Grinding Technology - Theory and Applications of Machining with Abrasives*, Industrial Press, New York, 2008.
- [7] Mishra, V.K., Salonitis, K.: *Empirical estimation of grinding specific forces and energy based on a modified Werner grinding model*, Procedia CIRP, Vol.8, pp. 287-292, 2013.
- [8] Durgumahanti, U.S.P., Singh, V., Rao, P.V.: *A New Model for Grinding Force Prediction and Analysis*, International Journal of Machine Tools & Manufacture, Vol.50, pp. 231-240, 2010.
- [9] Werner, G.: *Influence of work material on grinding forces*, Annals of CIRP, Vol.27, pp. 243-248, 1978.
- [10] Gostimirovic, M., Kovac, P., Sekulic, M.: *An inverse heat transfer problem for optimization of the thermal process in machining*. Sadhana, Vol.36, No.4, pp. 489-504, 2011.

Authors: Prof. Dr Marin Gostimirovi¹, M.Sc Dragan Rodi¹, Prof. Dr Pavel Kova¹, Dr Dušan Ješi², M.Sc Nenad Kulundži¹.

¹University of Novi Sad, Faculty of Technical Sciences, Department for Production Engineering, Trg Dositeja Obradovica 6, 21000 Novi Sad, Serbia, Phone: +381 21 450-366, Fax: +381 21 454-495.

²Tribotehnik, Titov trg 6/4, 51000 Rijeka, Croatia.

E-mail: maring@uns.ac.rs

rodicdr@uns.ac.rs

pkovac@uns.ac.rs

dusan.jesic@ri.hiner.hr

nenadts@gmail.com

Baralić, J., Nedić, B.

THE INFLUENCE OF ABRASIVE WATER JET PROCESSING PARAMETERS ON REACTION FORCE

Abstract: Abrasive water jet is one of the newest unconventional methods of processing, which is now increasingly used for making different parts and processing of different materials. A tool that performs processing is abrasive water jet, produced by the abrasive grains mixed with pure, high pressure, water jet. Thus, the abrasive grain acquire speed, and abrasive water jet occurs. Abrasive grains in the water jet have great kinetic energy, but it is still a very small part of that energy in cutting use. One way to determine the coefficient of efficiency of abrasive waterjet cutting is the monitoring of reaction force when cutting materials.

This paper presents a method for measuring the reaction force in processing with abrasive water jet. Also, this paper shows the influence of various abrasive water jet processing parameters (such as operating pressure, abrasive flow, traverse speed and material thickness) on reaction force.

Key words: abrasive water jet, processing parameters, reaction force

1. INTRODUCTION

Abrasive water jet is the most recent nonconventional cutting technology used in a very large area of industrial applications. It was first time patented in 1968. by Norman Franz, researcher at University of Michigan, USA. Abrasive water jet processing has many advantages such as: no heat affected zone, high machining versatility, high flexibility, quick machining and small cutting forces [1]. It is used in processing of different materials such as steel, stone, brass, titanium, aluminum, any kind of glass and composites and many other materials [2]. The efficiency of processing depends on several abrasive water jet process parameters [3]. This paper presents experimental investigations of operating pressure, abrasive flow, traverse speed and material thickness influence on abrasive water jet reaction force.

For a better understanding of the influence of abrasive water jet processing parameters on reaction force, it is necessary to understand the principles of abrasive water jet processing, Fig. 1.

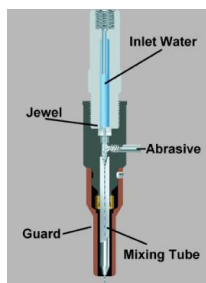


Fig. 1. Schematic view of abrasive water jet machining [4]

Energy of abrasive water jet, required for cutting materials is obtained by pressurizing water to high pressures (usually up to 400 MPa) and then forming a high-intensity cutting water stream by focusing through

a small orifice-jewel. A high-speed water jet (nearly 1000 m/s) transfers kinetic energy to the abrasive particles, which erode the material. Workpiece material is removed by the action of high-speed water mixed with abrasive particles.

2. ABRASIVE WATER JET REACTION FORCE

When cutting material by abrasive water jet, the initial phase of cutting occurs. For this form of cutting (in which the material thickness is less than the maximum depth of cut), on its way through the workpiece, abrasive water jet acts on the material with some force. That force has the same direction as the speed of the abrasive water jet, i.e. it is tangent to the path of the abrasive water jet, Fig. 2. Reaction force by its intensity and direction is equal to the cutting force, but having the opposite direction.

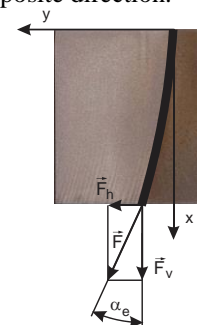


Fig. 2. Cutting force while processing with abrasive water jet [7]

When processing with abrasive water jet, reaction force decomposes into three components; F_1 , F_2 and F_3 . F_2 has two components, F_2' and F_2'' , which are mutually the same very low intensity, but with different directions, so that the resulting resistance value of F_2 is around zero. Because of that, this resistance can not be taken into consideration. F_1 is a component of reaction force that is equal in intensity to force F_v , which is the

most important component of the cutting force. Thus, the greatest attention was paid to this component of reaction force. F_3 is equivalent to an support motion resistance in classical processing on a lathe, and its intensity is equal to the force F_h . In general, the diagram change of resistance F_l with the time of cutting has a shape such as this illustrated in Fig. 3.

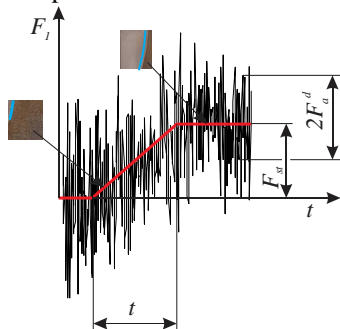


Fig. 3. Diagram of reaction force F_l [8]

The Fig. 3 shows that the reaction force F_l has its own dynamic and static component. Only the static component of reaction force has been analyzed in this paper. Due to the dynamic nature of abrasive water jet processing, reaction force has an extremely dynamic character. In some cases, it may manifest with significant deviation of reaction force signal, from its mean value.

Reaction force was measured using a three-component dynamometer for turning, KISTLER Type 9265A1, Fig. 4. Reaction force were measured for samples of X5CrNi 18-10 with various thicknesses.

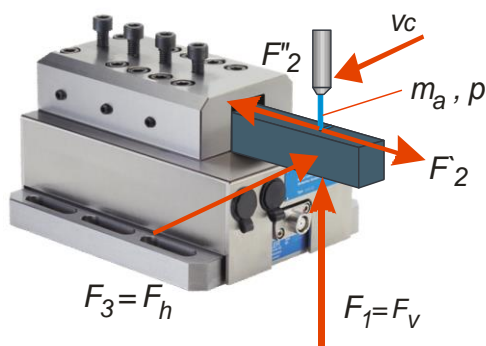


Fig. 4. Measurement of reaction force in abrasive water jet processing [8]

3. EXPERIMENTAL RESEARCH

Aim of the conducted experimental research was to define the influence of operating pressure, traverse speed, abrasive flow and thickness of material on the reaction force during processing with abrasive water jet.

Variable parameters in experimental research were:

- Traverse speed – v_c : 30, 50, 70, 90, 100, 110 and 150 mm/min,
- Operating pressure – p : 270, 320, 380 and 413 MPa,
- Abrasive flow – m_a : 200, 300, 350 and 400 g/min,
- Material thickness– s : 5, 10, 15, 20 and 25 mm,

Constant parameters in experimental research were:

- Distance of the cutting head from the sample surface – $h_0 = 3$ mm,
- Sample material - X5CrNi 18-10,
- Jewel diameter – $d_o = 0.3$ mm,
- Mixing tube diameter– $d_f = 1.02$ mm and
- Abrasive - Garnet #80.

Fig. 5 shows the workpiece in dynamometer during experimental research.



Fig. 5. Workpiece in dynamometer during experimental research [7]

The measuring chain for measuring of reaction force is shown in Fig. 6. It consists of three component dynamometer KISTLER Type 9265A1, measuring intensifier KISTLER Type Ca5001, AD converter Burb Brown type 2000 and the computer PC/AT. Signal acquisition of reaction force component was carried out with 300 Hz in a time interval of 10 seconds, using LT software/control v.5.02.



Fig. 6. Part of measuring equipment for experimental research [7]

4. RESULTS OF EXPERIMENTAL RESEARCH

In Fig. 7 is shown recording of the measurement signals of reaction force F_l , i.e. its change with time. It can be seen that an increase in the value of the reaction force component F_l occurs when cutting of sample with abrasive water jet begins. Values rise until the abrasive water jet is not completely cut through the material. After that point (about nine seconds from beginning) there is no further increase in value of the component of reaction force.

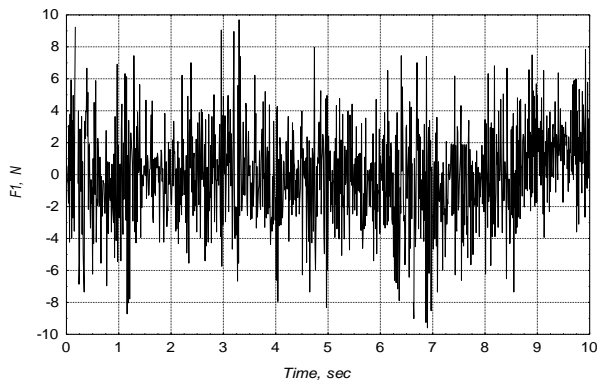


Fig. 7. A record of reaction force measurement signal, $p = 413$ MPa; $v_c = 50$ mm / min; $m_a = 400$ g / min

In Table 1 are given the values of reaction force component F_I , which are measured while the processing of samples of different thicknesses with different processing parameters values.

Sample	p , MPa	v_c , mm/min	m_a , g/min	s , mm	x_0 , mm	F_I , N
1.	270	50	400	20	3	0.97
2.	320	50	400	20	3	2.12
3.	380	50	400	20	3	1.92
4.	413	50	400	20	3	1.98
5.	413	50	200	20	3	1.86
6.	413	50	250	20	3	2.05
7.	413	50	300	20	3	1.81
8.	413	50	350	20	3	1.76
9.	413	50	400	20	3	1.86
10.	413	30	400	20	3	1.43
11.	413	50	400	20	3	1.98
12.	413	70	400	20	3	2.85
13.	413	90	400	20	3	1.98
14.	413	110	400	20	3	3.45
15.	320	50	300	20	3	1.85
16.	270	30	200	20	3	1.5
17.	413	150	400	5	3	1.57
18.	413	100	400	5	3	1.1
19.	413	70	400	5	3	0.93
20.	413	100	400	10	3	2.15
21.	413	70	400	10	3	1.4
22.	413	50	400	10	3	1.02
23.	413	100	400	15	3	3.64
24.	413	70	400	15	3	2.23
25.	413	50	400	15	3	1.38
26.	413	100	400	25	3	1.58
27.	413	70	400	25	3	3.34
28.	413	50	400	25	3	2.53

Table 1. Measured values of reaction force component F_I

Influence of some abrasive water jet processing parameters on reaction force component F_I are given in the following figures. Change of reaction force component F_I , depending on the operating pressure is

shown in Fig. 8. From the figure it can be noticed that the first measured value at point, $p = 270$ MPa, quite differs from the other measured values. By observing other measured values, it can be said that increase of the operating pressure leads to a slight decrease in the value of reaction force component F_I [7].

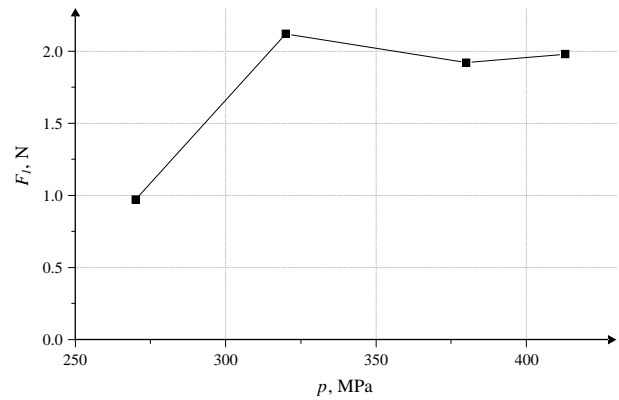


Fig. 8. Influence of operating pressure on F_I

Fig. 9 shows the influence of the abrasive flow on the value of the reaction force component F_I . By observation of the diagram, it can be seen that the change the abrasive flow does not significantly affect on the values of reaction force component F_I [7].

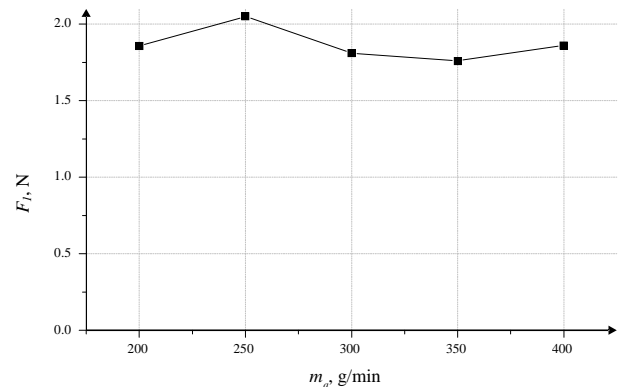


Fig. 9. Influence of abrasive flow on F_I

Influence of the traverse speed to the vertical component of the reaction force F_I is shown in Fig. 10.

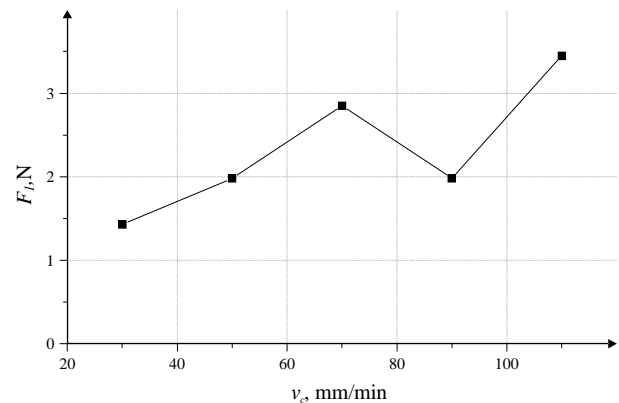


Fig. 10. Influence of traverse speed on F_I

The Fig. 10 shows that the traverse speed has a significant influence on reaction force F_I . When

processing with higher traverse speeds, there is a greater reaction force [7].

The influence of the thickness of the material which is being processed is also significant, Fig. 11. From Fig. 11 it can be observed that when processing with the same traverse speed, reaction force F_l has significantly higher values for processing of thicker materials [7].

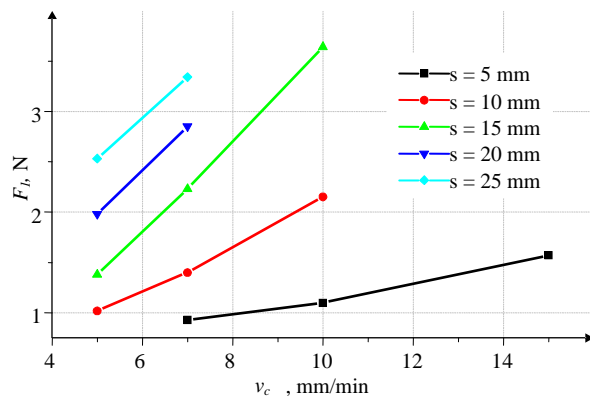


Fig. 11. Influence of material thickness on F_l

5. CONCLUSION

By analyzing the experimental results, it was found that an increase in the operating pressure leads to a reduction of reaction force. The influence of the abrasive flow on the reaction force is almost negligible, while the traverse speed and the thickness of the material to be processed have significant influence on the reaction force. Increase of the traverse speed as well as increase of the thickness of the material being processed leads to increase of reaction force.

Also, by analyzing the reaction force measurement signal, it was observed that with increase in depth of cut increases reaction force value. The maximum value of reaction force reaches only when the abrasive water jet completely cut through workpiece which has been processing.

For more precisely definition of the influence of certain abrasive water jet processing parameters on reaction force, it is necessary to carry out a larger number of experimental research.

6. REFERENCES

- [1] Wang, J., Guo, D.M.: *The cutting performance in multi pass abrasive water jet machining of industrial ceramics*, Journal of Materials Processing Technology, Volume 133, 371-377, 2003
- [2] Akkurt, A., Kulekci, M., K., Seker, U., Ercan, F.: *Effect of feed rate on surface roughness in abrasive water jet cutting applications*, Journal of Materials Processing Technology, Volume 147, 389-396, 2004
- [3] Pal, V., K., Tandon, P.: *Identification of the role of machinability and milling depth on machining time in controlled depth milling using abrasive water jet*,

International Journal of Advanced Manufacturing Technology, 2012

- [4] <http://www.omax.com/>, 02.07.2015.
- [5] Momber, W. A., Kovacevic, R.: *Principles of Abrasive Water Jet Machining*, Springer Verlag London, 1998
- [6] Chandra, B., Singh, J.: *A Study of effect of Process Parameters of Abrasive jet machining*, International Journal of Engineering Science and Technology (IJEST), Jan., Vol. 3 No. 1., 2011
- [7] Baralić, J., *Energija i kvalitet obrade abrazivnim vodenim mlazom*, doktorska disertacija, Fakultet inženjerskih nauka Univerzitet u Kragujevcu, Kragujevac, 2014.
- [8] Baralić, J., Nedić, B., Radovanović, M., Janković, P., *Obradivost materijala rezanjem abrazivnim vodenim mlazom*, monografija, Fakultet inženjerskih nauka Univerzitet u Kragujevcu, Kragujevac, 2015.

* This paper is part of project **TR35034** The research of modern non-conventional technologies application in manufacturing companies with the aim of increase efficiency of use, product quality, reduce of costs and save energy and materials, funded by the Ministry of Education, Science and Technological Development of Republic of Serbia

Authors: **dr Jelena Baralić**, docent, University of Kragujevac, Faculty of Technical Sciences, Čačak, **prof. dr Bogdan Nedić**, University of Kragujevac, Faculty of Engineering, Kragujevac

E-mail: jelena.baralic@ftn.kg.ac.rs; nedic@kg.ac.rs



Pucovski, V., Sekuli, M., Kramar, D., Gostimirovi, M., Kopa, J.

ULTRASONIC ASSISTED TURNING

Abstract: In this paper a brief review of ultrasonic assisted turning will be presented. This technology allows many hard-to-machine materials to be machined with greater material removal rate, prolonged tool life and less affected surface microstructure. Its benefits are beyond dispute and many authors have tested it and graded it as a positive upgrade for conventional machining process. At the end of the paper a possible technical solution, for ultrasonic assisted turning, will be presented.

Key words: ultrasonic assisted turning, hybrid machining system, machinability, hard-to-machine materials

1. INTRODUCTION

During ultrasonic vibration assisted turning (UAT), the cutting tool is induced with small vibrations, usually couple of microns, and high frequency, around 20 kHz. The result of this movement, is intermittent contact between the cutting tool and the workpiece. This leads to generation of cutting force only during one half-period of vibration. Mentioned force is usually higher than those during conventional turning (CT), but average forces in UAT are smaller than those in CT. UAT is a potential technology suitable for machining hard-to-machine metallic and nonmetallic materials. It leads to better surface of the machined workpiece, longer tool life and more favorable microstructure of the surface layer. The ultrasonic vibrations can be applied along any of the three cutting directions or along any combinations of them [1]. The most positive effect has been found to be generated during applying vibrations in the tangential direction, that is in the direction of the cutting force.

Main condition which has to be met, for vibration assisted cutting to take effect, is that the cutting speed have be greater than $v_c < 2af$, in which a is an amplitude and f is the frequency of vibrations.

In this paper a short review of existing literature will be presented. Review papers for this area exist [2] but older dated so many of the new improvements in this field are not mentioned. This gap is intended to be partly filled by this paper.

Ultrasonic vibrational cutting is long known and one of the first papers were [3] and [4]. As the time went by, the topic started expanding and soon many authors accepted the idea. For example influence on surface roughness in turning with ultrasonic vibrating tool has been later done by [5]. But the idea hit its peak only recently, with the development of technical equipment, mostly electronic controllers and powerful personal computers for simulations and modeling. One of the things that brought novelty is finite element numerical analysis. Among many areas it was also used for research on influence of ultrasonic vibrational cutting on occurrence of chatter during turning [6]. The obtained results from the numerical analysis for some selected points of the stability lobe were compared and

validated against the observed experimental results. It was shown that ultrasonic vibration can improve the stability for some cutting conditions, while degrading the stability in some other conditions. Hence, the proposed numerical analysis is a valuable tool to aid the designer to predict the effect of ultrasonic vibration on chatter stability [6]. Prior that, one paper analyzed the influence of ultrasonic turning on chatter [7] and came to the conclusion that chatter is effectively suppressed irrespective of the tool geometry by vibration cutting. However, in the case of conventional cutting the occurrence of chatter was strongly influenced by the tool geometry. Obviously, vibration cutting achieved a higher cutting stability as compared with conventional cutting. By applying the vibration cutting method, the occurrence of chatter can be reduced significantly [7].

Regarding theoretical basics of UAT, one of the most in depth paper which is dealing with this subject is [8]. A kinematics model has been developed in the mentioned study for the relative movement between the cutting tool and workpiece in UAT. Among others, the model predicts that the cutting tool does not disengage from the workpiece during its cyclic motion and inevitably rubs and presses against the lateral surface remaining after each revolution of the workpiece. [8]. In the second part of this [9] study, a dynamics model has been developed for UAT. The model can theoretically estimate the instantaneous cutting mechanics parameters and forces at various vibration frequencies and amplitudes and for different turning parameters. It is found out that the cutting process is carried out easier at large rake angles due to the lower cutting forces in UAT [9]. Third part [10], which is the final part of this study, is experimentally investigating claims of hypothesis and models stated in two previous works. There was a close agreement between the theoretical and experimental.

2. ELLIPTICAL TYPE OF MOVEMENT

Most equipment used for UAT is based on one dimensional movement. But the idea has been born to try and use two-way type of movement. It has been known as an elliptical type of movement. First to

exploit this idea was one group of researchers presented in [11] and the orthogonal cutting of copper was carried out by applying the ultrasonic elliptical vibration cutting. The conclusion was that the chip thickness and the cutting force are reduced significantly by applying the elliptical vibration as compared with the conventional cutting including the conventional vibration cutting. Also the formation of burrs is suppressed by the elliptical vibration cutting. The surface roughness generated by the elliptical vibration is small ($0,02 \mu\text{m } R_{\text{max}}$), while the geometrical shape accuracy is better in the elliptical vibration cutting. Later came other papers, in the area of elliptical vibrational cutting, carried out by many different researchers [12] [13] [14] [15] [16] [17]. They all reported improvements while using elliptical ultrasonic vibrations.

3. FINITE ELEMENT ANALYSIS

One of many fields in engineering, which benefited from rapid development of electronic equipment, is simulation and modeling with finite element analysis. One of the first ever finite element simulation was 2D simulation and is presented in [18]. In this paper an experimental and numerical (finite element) investigations have been carried out to study the process of ultrasonically assisted turning in comparison with the conventional turning process. An elasto-plastic finite element model for ultrasonic turning was proposed as an enhancement of the model for conventional turning to explore microstructural processes at the cutting tool-chip interface for both technologies. A detailed comparison based on numerical analyses of the transient stress distribution during the cycle of ultrasonic vibration and the steady-state stress distribution in conventional turning has shown that the mean level of stresses in the process zone and, consequently, cutting forces were considerably lower for the ultrasonically assisted technology, which correlates with known experimental results. In conventional turning the cutting tool stays in a permanent contact with the chip throughout the entire cutting process. In contrast, in ultrasonic turning the cutter remains in contact with the chip only about 40% of the time, according to FE simulations.

Upgrade in this field came with first 3D FE model of UAT that was developed as extension to the 2D model [19]. Up to then, a 3D FE models were used to simulate conventional cutting processes. Now it was used to compare obtained results from experimental use of UAT and simulated results obtained using FE. One of the main conclusions was that with the use of the coolant the cutting force is by 20–25% lower due to absence of the friction force at the tool–chip interface. The same is also reported in [20]. Others conclusions which could be drawn from others investigation in FEM area [21] [22] [23] was that in ultrasonic cutting, machining force and workpiece stress vary periodically and, in most part of the process are significantly less than those occurring in conventional turning. Machining force depends heavily on the cutting speed and increases with an increase in the latter. The effect

of tool clearance and rake angles in UAT is similar to that of conventional turning, i.e., clearance angle has no significant influence on the machining force while rake angle has an inverse effect. The amplitude of ultrasonic vibration of the cutting tool has a direct and significant influence on the machining force.

Some of the researchers focused on temperature problems in UAT [24]. Temperature distribution was analyzed in the cutting tool and workpiece during cutting. While no considerable differences were found in the workpiece temperatures for CT and UAT, the cutting tool temperatures were nearly two times lower for UAT. These differences are explained by reduced time of the thermal conductance to the tool during UAT due to the intermittent nature of contact conditions at the tool-chip interface for UAT. Other researchers have found similar results [25] [26] [27].

Most of the materials used as a workpiece during UAT are various types of metals, but some authors focused their research to non-metals. Test materials of epoxy, polyurethane foam and mild cheddar cheese have been used in FE models of ultrasonic cutting due to their availability and diversity [28]. The sliding friction at the blade and specimen interface has been shown to decrease markedly under ultrasonic excitation of the contact surface. Tests carried out using an ultrasonic block horn have recorded significant reductions in the coefficient of dynamic friction. The models could be used to adjust the cutting parameters, such as frequency and blade tip amplitude, to predict the excitation force or cutting speed required to cut effectively through different material layers. The validity of the model relies critically on an accurate assessment of the friction condition at the blade–material interface and accurate material models [28].

Eventually UAT become joined with other hybrid machining types. So for example in [29] a new hybrid machining technique called hot ultrasonically assisted turning (HUAT) is introduced for machining of a beta titanium alloy. In this technique, hot machining was combined with ultrasonically assisted turning (UAT) to achieve combine advantages of both techniques in turning of intractable alloys. The experiments and FE model were used to investigate this process in comparison with three other techniques. The conclusion was positive for mentioned new technique and the advice was that it can be used for machining of hard-to-cut alloys with lower average cutting forces.

4. HARD-TO-MACHINE MATERIALS

The development of new materials such as high-strength metals, composites and ceramics, which are very hard, brittle and abrasive, is demanding progress in the machining techniques. UAT is one of the promising techniques for machining intractable materials. These new materials include Ni and Ti based super alloys, composites, ceramics, glass etc. [30]. Some everyday hard-to-machine materials have been studied and machined with UAT, for example hardened steel SCM440 [31], stainless steel [32], low alloy steel (DF2) [33] and Ti-64 [34]. Others researches are focused on more complex materials like Inconel 718

[35] [36] [37], Ti-15333 [38] [39] or shape memory alloy Nitinol [40] [39]. Some focused their research on materials specially developed for certain purposes like for example Ti-676-0.9La [41] or Ti-15333Zr-0.9La [42]. Most above mentioned papers reported improvement in machinability of materials with UAT.

5. EQUIPMENT DEVELOPMENT FOR UAT

At the Faculty of Technical Sciences, Department for production Engineering a device is being developed for UAT. This project is being realized with cooperation with Telsonic d.o.o. Sonotrode, which is also the toolholder, is made from tool steel SPM10 and its dimensions are calculated with respect to acoustic properties given for frequency on which it will operate. Modeling of acoustic behavior of sonotrode is done in Solidworks and snapshot of final results is shown on Fig. 1.

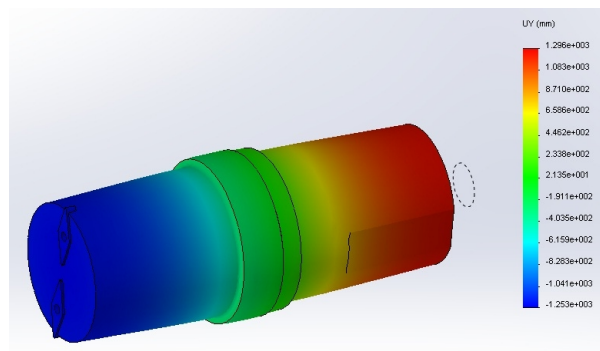


Fig. 1. Sonotrode, or toolholder, modeled in Solidworks and result from acoustic analysis

It can be seen that the ratio of input and output amplitude is 1:1, which should be 20 μm on 20 kHz. Tool insert will be VCGT 11 03 04 type, two pieces which should provide symmetric balance during oscillations. Through the brass ring the sonotrode will be mounted on steel holder, Fig. 2, custom made to fit on Kistler dynamometer and onto the conventional lathe.

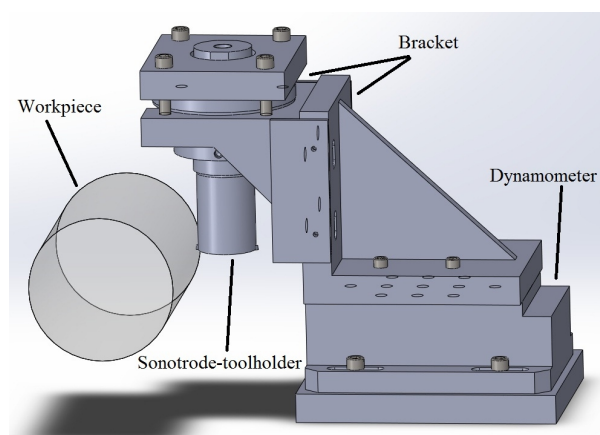


Fig. 2. Assembly of sonotrode mounted on holder with Kistler dynamometer

Classical piezo-electric ultrasonic transducer will be

used to drive the sonotrode. Suitable ultrasonic generator, with enough power to smoothly operate during machining, will be used.

6. CONCLUSION

Ultrasonic assisted turning is a promising technique to be used while machining various materials. This has proven to be most effective on hard-to-machine where it has reduced cutting forces and prolonged tool life while making minimal changes on the top layer microstructure of workpiece material. Its use is also justified on soft materials, where it enables the use of higher machining parameters without deforming the workpiece, and composite laminated materials, where it prevents formation of burrs and tearing the material in the cutting zone.

7. REFERENCES

- [1] Nategh, M. J., Amini, S., Soleimanimehr, H., Abdullah, A., Sadeghi, M. H.: *A Machining Force Model Developed for Ultrasonic Vibration-assisted Turning, through Statistical Analysis of Influential Parameters*, Aerospace Mechanics Journal, 4(4), p.p. 83-91, 2009.
- [2] Brehl, D. E., Dow, T. A.: *Review of vibration-assisted machining*, Precision Engineering, 32(3), p.p. 153-172, 2008.
- [3] Balamuth, L.: *Ultrasonic assistance to metal removal*, Ultrasonics, 4(3), p.p. 125-130, 1966.
- [4] Skelton, R. C.: *Effects of ultrasonic vibration on the turning process*, International Journal of Machine Tool Design and Research, 9(4), p.p. 363-374, 1969.
- [5] Wang, L., Zhao, J.: *Influence on surface roughness in turning with ultrasonic vibration tool*, International Journal of Machine Tools and Manufacture, 27(2), p.p. 181-190, 1987.
- [6] Tabatabaei, S. M. K., Behbahani, S., Mirian, S. M.: *Analysis of ultrasonic assisted machining (UAM) on regenerative chatter in turning*, Journal of Materials Processing Technology, 213(3), p.p. 418-425, 2013.
- [7] Xiao, M., Karube, S., Soutome, T., Sato, K.: *Analysis of chatter suppression in vibration cutting*, International Journal of Machine Tools and Manufacture, 42(15), p.p. 1677-1685, 2002.
- [8] Nategh, M. J., Razavi, H., Abdullah, A.: *Analytical modeling and experimental investigation of ultrasonic-vibration assisted oblique turning, part I: Kinematics analysis*, International Journal of Mechanical Sciences, 63(1), p.p. 1-11, 2012.
- [9] Razavi, H., Nategh, M. J., Abdullah, A.: *Analytical modeling and experimental investigation of ultrasonic-vibration assisted oblique turning, part II: Dynamics analysis*, International Journal of Mechanical Sciences, 63(1), p.p. 12-25, 2012.
- [10] Razavi, H., Nategh, M. J., Abdullah, A.: *Analytical modeling and experimental investigation of ultrasonic-vibration assisted oblique turning, part III: Experimental investigation*, International Journal of Mechanical Sciences, 63(1), p.p. 26-36, 2012.
- [11] Moriwaki, T., Shamoto, E.: *Ultrasonic Elliptical Vibration Cutting*, CIRP Annals - Manufacturing Technology, 44(1), p.p. 31-34, 1995.
- [12] Li, X., Zhang, D.: *Ultrasonic elliptical vibration transducer driven by single actuator and its application in precision cutting*, Journal of Materials Processing Technology, 180(1-3), p.p. 91-95, 2006.
- [13] Zhang, X., Senthil Kumar, A., Rahman, M., Nath, C., Liu, K.: *Experimental study on ultrasonic elliptical vibration cutting of hardened steel using PCD tools*, Journal

- of Materials Processing Technology, 211(11), p.p. 1701-1709, 2011.
- [14] Nath, C., Rahman, M., Neo, K. S.: *Machinability study of tungsten carbide using PCD tools under ultrasonic elliptical vibration cutting*, International Journal of Machine Tools and Manufacture, 49(14), p.p. 1089-1095, 2009.
- [15] Ma, C., Shamoto, E., Moriwaki, T., Wang, L.: *Study of machining accuracy in ultrasonic elliptical vibration cutting*, International Journal of Machine Tools and Manufacture, 44(12-13), p.p. 1305-1310, 2004.
- [16] Nath, C., Rahman, M., Neo, K. S.: *A study on the effect of tool nose radius in ultrasonic elliptical vibration cutting of tungsten carbide*, Journal of Materials Processing Technology, 209(17), p.p. 5830-5836, 2009.
- [17] Ma, C., Shamoto, E., Moriwaki, T., Zhang, Y., Wang, L.: *Suppression of burrs in turning with ultrasonic elliptical vibration cutting*, International Journal of Machine Tools and Manufacture, 45(11), p.p. 1295-1300, 2005.
- [18] Mitrofanov, A. V., Babitsky, V. I., Silberschmidt, V. V.: *Finite element simulations of ultrasonically assisted turning*, Computational Materials Science, 28(3-4), p.p. 645-653, 2003.
- [19] Ahmed, N., Mitrofanov, A. V., Babitsky, V. I., Silberschmidt, V. V.: *3D finite element analysis of ultrasonically assisted turning*, Computational Materials Science, 39(1), p.p. 149-154, 2007.
- [20] Mitrofanov, A. V., Ahmed, N., Babitsky, V. I., Silberschmidt, V. V.: *Effect of lubrication and cutting parameters on ultrasonically assisted turning of Inconel 718*, Journal of Materials Processing Technology, 162-163(p.p. 649-654), 2005.
- [21] Amini, S., Soleimanimehr, H., Nategh, M. J., Abudollah, A., Sadeghi, M. H.: *FEM analysis of ultrasonic-vibration-assisted turning and the vibratory tool*, Journal of Materials Processing Technology, 201(1-3), p.p. 43-47, 2008.
- [22] Kukkala, V., Sahoo, S. K.: *Finite element analysis of ultrasonic vibratory tool and experimental study in ultrasonic vibration assisted turning (uvt)*, International Journal of Engineering Science Invention, p.p. 73-77, 2013.
- [23] Ahmed, N., Mitrofanov, A. V., Babitsky, V. I., Silberschmidt, V. V.: *Analysis of forces in ultrasonically assisted turning*, Journal of Sound and Vibration, 308(3-5), p.p. 845-854, 2007.
- [24] Mitrofanov, A. V., Babitsky, V. I., Silberschmidt, V. V.: *Finite element analysis of ultrasonically assisted turning of Inconel 718*, Journal of Materials Processing Technology, 153-154(p.p. 233-239), 2004.
- [25] Muhammad, R., Ahmed, N., Roy, A., Silberschmidt, V. V.: *Numerical Modelling of Vibration-Assisted Turning of Ti-15333*, Procedia CIRP, 1(p.p. 347-352), 2012.
- [26] Mitrofanov, A. V., Babitsky, V. I., Silberschmidt, V. V.: *Thermomechanical finite element simulations of ultrasonically assisted turning*, Computational Materials Science, 32(3-4), p.p. 463-471, 2005.
- [27] Muhammad, R., Maurotto, A., Roy, A., Silberschmidt, V. V.: *Ultrasonically assisted turning of Ti-6Al-2Sn-4Zr-6Mo*, Journal of Physics: Conference Series, 382(p.p. 012016), 2012.
- [28] Lucas, M., MacBeath, A., McCulloch, E., Cardoni, A.: *A finite element model for ultrasonic cutting*, Ultrasonics, 44 Suppl 1(p.p. e503-9), 2006.
- [29] Muhammad, R., Roy, A., Silberschmidt, V. V.: *Finite Element Modelling of Conventional and Hybrid Oblique Turning Processes of Titanium Alloy*, Procedia CIRP, 8(p.p. 510-515), 2013.
- [30] Babitsky, V., Astashev, V.: *Nonlinear Dynamics and Control of Ultrasonically Assisted Machining*, Journal of Vibration and Control, 13(5), p.p. 441-460, 2007.
- [31] Xiao, M., Wang, Q. M., Sato, K., Karube, S., Soutome, T., Xu, H.: *The effect of tool geometry on regenerative instability in ultrasonic vibration cutting*, International Journal of Machine Tools and Manufacture, 46(5), p.p. 492-499, 2006.
- [32] Mahdy, S. M. A., Gouda, M. A., Silberschmidt, V. V.: *Study of ultrasonically assisted turning of stainless steel and brass alloys*, Journal of Physics: Conference Series, 451(p.p. 012037), 2013.
- [33] Nath, C., Rahman, M., Andrew, S. S. K.: *A study on ultrasonic vibration cutting of low alloy steel*, Journal of Materials Processing Technology, 192-193(p.p. 159-165), 2007.
- [34] Patil, S., Joshi, S., Tewari, A.: *Microstructural analysis of Ultrasonic Assisted Turning of Ti alloy Ti6Al-4V*, Proceedings of the 8th International Conference on MicroManufacturing, p.p. 539-544, March 25-28.
- [35] Ahmed, N., Mitrofanov, A. V., Babitsky, V. I., Silberschmidt, V. V.: *Analysis of material response to ultrasonic vibration loading in turning Inconel 718*, Materials Science and Engineering: A, 424(1-2), p.p. 318-325, 2006.
- [36] Babitsky, V. I., Mitrofanov, A. V., Silberschmidt, V. V.: *Ultrasonically assisted turning of aviation materials: simulations and experimental study*, Ultrasonics, 42(1-9), p.p. 81-6, 2004.
- [37] Babitsky, V., Kalashnikov, A. N., Meadows, A., Wijesundara, A. A. H. P.: *Ultrasonically assisted turning of aviation materials*, Journal of Materials Processing Technology, 132(1-3), p.p. 157-167, 2003.
- [38] Maurotto, A., Roy, A., Babitsky, V., Silberschmidt, V. V.: *Recent developments in ultrasonically assisted machining of advanced alloys*, Proceedings of 4th CIRP International Conference on High Performance Cutting, p.p. [39] Maurotto, A., Muhammad, R., Roy, A., Babitsky, V. I., Silberschmidt, V. V.: *Comparing Machinability of Ti-15-3-3-3 and Ni-625 Alloys in Uat*, Procedia CIRP, 1(p.p. 330-335), 2012.
- [40] Akbari, J., Chegini, A. G., Rajabnejad, A. R.: *Ultrasonic assisted turning of NiTi shape memory alloy*, 5th International Conference and Exhibition on Design and Production of Machines and Dies/Molds, p.p. Pine Bay Hotel-Kusadasi, Aydin, Turkey, 18-21 June.
- [41] Muhammad, R., Hussain, M. S., Maurotto, A., Siemers, C., Roy, A., Silberschmidt, V. V.: *Analysis of a free machining + titanium alloy using conventional and ultrasonically assisted turning*, Journal of Materials Processing Technology, 214(4), p.p. 906-915, 2014.
- [42] Maurotto, A., Siemers, C., Muhammad, R., Roy, A., Silberschmidt, V.: *Ti Alloy with Enhanced Machinability in UAT Turning*, Metallurgical and Materials Transactions A, 45(6), p.p. 2768-2775, 2014.

Authors: Vladimir Pucovski¹, assoc. prof. dr. Milenko Sekuli¹, dr. Davorin Kramar², prof. dr. Marin Gostimirovi¹, prof. dr. Janez Kopa²,

¹University of Novi Sad, Faculty of Technical Sciences, Institute for Production Engineering, Trg Dositeja Obradovica 6, 21000 Novi Sad, Serbia, Phone.: +381 21 450-366, Fax: +381 21 454-495.

E-mail: pucovski@uns.ac.rs; milenkos@uns.ac.rs; maring@uns.ac.rs

²University of Ljubljana, Faculty of Mechanical Engineering, Laboratory for Cutting, Askerceva 6, 1000 Ljubljana, Slovenia, Phone.: +386 1 477-14-38 Fax: +386 1 251-85-67,

E-mail: David.Muzenic@fs.uni-lj.si; Davorin.Kramar@fs.uni-lj.si; Janez.Kopac@fs.uni-lj.si

Sekuli , S.

OPTIMIZATION OF CUTTING CONDITIONS IN DRILLING OPERATIONS BY SIMULATION

Abstract: This paper discussed economic aspects of metal cutting conditions in drilling, on the basis: 1. maximum productivity, 2. minimum matching costs, and 3. minimum matching costs per unit time. The optimal cutting condition with the set of criteria are given with the simulation. For the purpose of computation and efficiency it is requested to develop the computer program.

Key words: drill, drilling, cutting condition, optimization, simulation.

1. INTRODUCTION

The elements of cutting condition have some certain influence on the machining time and tool life, that have implication which results in further statement: the cost of machining depends on both either of machining time or/and tool life.

Many authors have started from the above statements in order to determine the optimal machining condition on the lathe and the milling machine [1, 2, 3, 6, and 7]. There were comparatively few attempts to determine the optimal conditions for the drilling operation.

The optimal cutting conditions are identified on the different ways, e.g. using linear programming, convex programming or iterative procedure.

The article considered then the author's contribution to the optimal cutting conditions calculation with a view of economic aspects, developed later using simulation as a mathematical tool relying on the following criteria: 1. maximum productivity, 2. minimum costs and 3. minimum machining cost per unit machining time.

2. METHODOLOGY DEVELOPED FOR DETERMINING THE OPTIMAL CUTTING CONDITIONS IN DRILLING OPERATIONS

2.1 Maximal productivity as a criteria for identification of right cutting conditions

The productivity represents the quantity of work pieces in unit times [7]

$$q = \frac{1}{t_k} \quad (1)$$

where the time per piece is

$$t_k = t_g + t_a + t_p + t_m + t_{pz} + t_i$$

and t_g denote machining time, t_a tool changing time reduced on one workpiece, t_p handling time, t_m down time, t_{pz} setup time reduced on one workpiece and t_i idle time.

How is machining time

$$t_g = j \frac{L}{s_n} \quad (2)$$

and time to change cutting tool

$$t_a = t_z \frac{t_g}{T} \quad (3)$$

after substitution we have

$$t_k = t_g \left[1 + \frac{t_z}{T} \right] + B \quad (4)$$

where is

$$B = t_p + t_m + t_{pz} + t_i = \text{const.}$$

2.2 The machining costs as a criteria for proposed cutting condition determination

The machining cost for one operation can be presented with the sum [5, 8]

$$U_0 = R + M + A \quad (5)$$

Where the costs are:

- Manpower

$$R = (1+b) k_1 (t_g + t_a + t_p + t_m + t_{pz} + t_i) \quad (5.1)$$

(k_1 is the net wage per minute of workers, and b coefficient of indirect cost),

- Machine tool

$$M = \frac{c_M p}{F \eta_{100,60}} (t_g + t_a + t_p + t_m + t_{pz} + t_i) \quad (5.2)$$

(c_M is an initial value of a machine tool including standard accessories, cost of jigs and fixtures, p is depreciation rate, F is a work period for machines specifically, and η is a exploitations time coefficient of machine tool), and

- Cutting tool

$$A = A_1 + A_2 + A_3 \quad (5.3)$$

where cost of change of used tool are

$$A_1 = (1+b) k_1 t_1 \frac{t_g}{T} \quad (5.31)$$

regrinding cost

$$A_2 = (1+b_a) k_2 t_2 \frac{t_g}{T} \quad (5.32)$$

and the depreciation cost of the cutting tool

$$A_3 = \frac{c_A}{i_0+1} \frac{t_g}{T} \quad (5.33)$$

(k_2 is the net wage of regrinding, t_2 is the regrinding time of cutting tool, b_a coefficient of an indirect cost of tool shop and i_0 the number of cutting tool regrinding) and we then obtain the cutting tool cost

$$S_{\min} \quad S_i \quad S_{\max} \quad (8)$$

$$A = [(1+b) k_1 t_1 + (1+b_a) k_2 t_2 + \frac{C_A}{i_0+1}] \frac{t_g}{T} \quad (5.3')$$

We now proceed the substitution of equations (5.1), (5.2) and (5.3) in the equation (5) and after arranging we have the total machining cost

$$U_0 = E [B + t_g (1 + \frac{t_z + \frac{G}{E}}{T})] \quad (2')$$

where are

$$E = [(1 + b) k_1 + \frac{C_M p}{F_{\eta} 100.60}]$$

$$G = [(1 + b) k_1 t_1 + (1 + b_a) k_2 t_2 + \frac{C_A}{i_0+1}]$$

if we put that

$$H = t_z + \frac{G}{E}$$

we then conclude that

$$U_0 = E [B + t_g (1 + \frac{H}{T})] \quad (5'')$$

2.3 The machining cost per machining unit time

The machining cost per machining unit time is

$$U_{0,ij} = \frac{U_{0ij}}{t_{kij}} \quad (5.1)$$

3. DETERMINATION OF OPTIMAL CUTTING CONDITION BY DRILLING

Determination of optimal cutting condition by drilling has the following order:

- Diameter of hole

Oftenest diameter which drilling is known and is equal

$$D = D_1 = D_i \quad (6)$$

- Feed

Maximal value of feed connection with minimal value of clearance angle on critical place (on peripheral of cutting edge) can be determined from term [7].

$$s_i = C_s D_i^{p_s} \quad (7)$$

where C_s and p_s are constants related in function allow stress of working piece material. However, for smaller drill diameters it is necessary to determine the allowable offset value based on its allowed stress resistance, follows [7]

$$s_i = (\frac{k_C}{42 C_M})^{1/y} D_i^{(3-x)/y} \quad (7')$$

Where C_M , x , y are constants and k_C allowed stress), with respect on constrains of available feeds, which machine tool have.

s_{\min} and s_{\max} are value of minimum and maximum feeds of machine tool.

- Cutting speed

Cutting speed by drilling can be determined from term [7]

$$v_T = \frac{C_V D^{x_0} \mu_0}{T^m s^{y_0}} \quad (9)$$

(where C_V , x_0 , y_0 and m are constants dependent of cutting tool material and working piece material, T tool life of drill and μ_0 coefficient in function of ratio drilling depth and diameter of drill

$$\mu_0 = f\left(\frac{l}{D}\right)$$

However, if we will attain tool life T which correspond total depths of drilling L , that is

$$T = \frac{L}{s n} \quad (2')$$

and

$$n = \frac{1000 v}{\pi D} \quad (1')$$

cutting speed which correspond different total depths of cutting L_j after substitution (2') and (1') in term (9) [7]

$$v_{LL_j} = L_j^{-\frac{m}{1-m}} \left[\left(\frac{1000}{\pi} \right)^m \frac{C_V D_i^{x_0-1} \mu_0}{s_i^{y_0-m}} \right]^{\frac{1}{1-m}} \quad (10)$$

Where by

$$L_{\min} \quad L_j \quad L_{\max}; L_j \Big|_{L_{\max} \rightarrow J=\lambda}^{L_{\min} \rightarrow J=1} \quad (11)$$

Number of revolution which corresponds particular of cutting speed is in function of total drilling depths, i.e.

$$n_{ij} = \frac{1000 v_{LL_j}}{D_i} \quad (12)$$

By then must respect constrains connected for available number of revolution of machine tool

$$n_{\min} \quad n_{ij} \quad n_{\max} \quad (13)$$

(n_{\min} and n_{\max} are values of minimum and maximum number of revolution which have machine tool).

- Power needed for drilling

Power needed for drilling can be determined according to [6]

$$P = \frac{C_M D^x s^y n}{975000} \quad (14)$$

e.g. by variation of variables

$$P_{ij} = \frac{C_M D_i^x s_i^y n_{ij}}{975000} \quad (14.1)$$

taking into account that it must be

$$P_{ij} \leq \eta P_M \quad (15)$$

(where is P_M working power of machine tool motor and η coefficient of utilization) if

$$P_{ij} > P_M \quad (15')$$

machine cannot drill with diameter D_i , and previous must be with diameter

$$D_{i+1} = 0,6 D_i \quad [7]$$

and procedure must be repeated until condition (15) is fulfilled.

Taking in to account terms (7), (11) and (15) with respect of constrains (8), (13) and (15'), (2) and (3) for time per piece we have

$$t_{kij} = \frac{l}{s_i n_{ij}} + \frac{t_z}{L_j/l} + B \quad (4.1)$$

Total machining cost:

$$U_{oij} = E \left(B + \frac{l}{s_i n_{ij}} + \frac{H}{L_j/l} \right) \quad (5.2)$$

And after substitution (5.2) and (4.1) we have for total machining cost per unit of machining time

$$U_{oij} = \frac{E \left(B + \frac{l}{s_i n_{ij}} + \frac{H}{L_j/l} \right)}{\frac{l}{s_i n_{ij}} + \frac{t_z}{L_j/l} + B} \quad (16)$$

If we use, as a basis for decision making, the following values of the basic elements are relevant for cutting conditions and they give further term

$$U_{01ij} = (U_{o1ij})_{\min} \quad (5.3)$$

4. FLOW CHART FOR BASIC CUTTING CONDITIONS ELEMENTS DETERMINATION BY SIMULATION

Flow for determination of optimal elements for cutting condition by simulation via next criterions: 1. Maximal productivity, 2. Minimum costs, and 3. Minimal cost per unit time, is given on Fig. 1

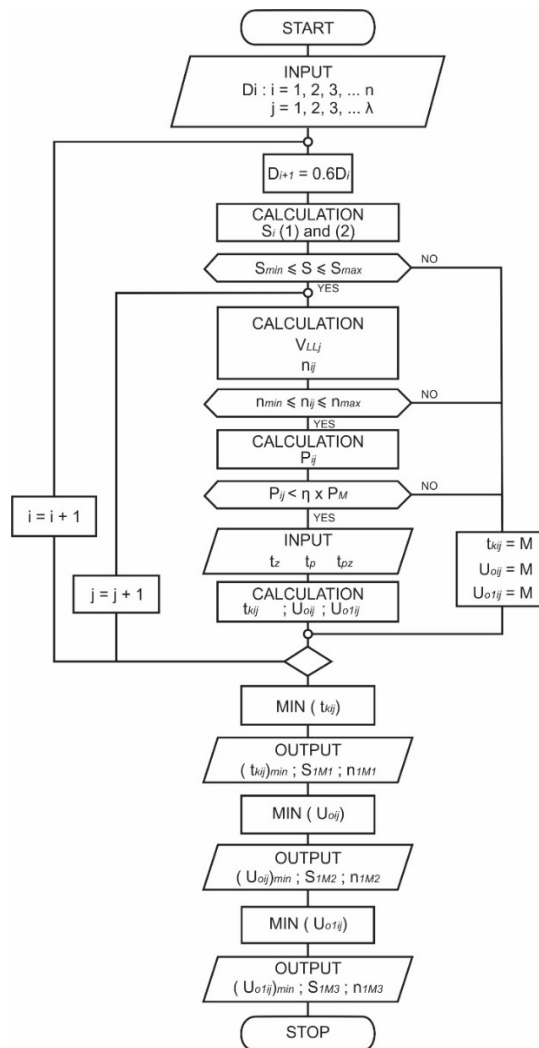


Fig. 1. Optimization of cutting condition in drilling operation by simulation

5. CONCLUSIONS

On the basis before mentioned we can conclude:

- aiming for optimal cutting conditions in drilling operations can use the previously discussed procedure based on economic criteria,
- the suggested simulation method has shown the great deal of efficiency and is relatively simple if we compare with those optimal technique in literature (linear or convex programming, iterative procedure, etc.)
- the criteria of minimum cost method per unit matching time is a result of two early presented conclusion, has its own elaboration, and
- optimization of the cutting conditions in drilling operations, based on economic principles by simulation represent one part of generalization, in application of the same criteria of the different kind of machining.

6. REFERENCES

- [1] Colding, B., 1969. Machining Economics and Industrial Data Manuals. Ann. C.I.R.P., No.1, 14.
- [2] Dipiereux, W.R., 1969. Ermittlung optimaler Schnittbedingungen insbesondere im Hinblick auf die wirtschaftliche Nutzen numerisch gegeschteueter Werkzeugmaschinen, Dissertation TH Aachen.
- [3] Draghici, G. and Platinea, C., 1975. Calculation by convex mathematical programming of the optimum cutting condition when cylindrical milling. Int. J. Mach. Tool Des. And Res., 2.
- [4] Hitomi, K., 1971. Optimization of multistage machining system: Analysis of optimal machining conditions for the flow-type machining system. Trans. A.S.M.E., J. of Eng. For Ind., B. 93, 2.
- [5] Ivkovi, B., 1974. The structure of the Production Costs in the Metal Processing, Mašinski fakultet, Kragujevac.
- [6] Popovi, B., 1966. Calculation of Optimum Processing Factors by Linear Programming Method and by Application of Digital Electronic Computer. Tehnika – Mašinstvo.
- [7] Stankovi, P., 1979. Machining, 1st part, 7th edit., Gra evinska knjiga, Beograd.
- [8] Todi, V., Banjac, D. and Malbaški, D., 1977. Application of iterative method for determination optimal parameters of the cutting conditions for turning. 3th JUPITER Conference Cavtat, Beograd.

Authors: Prof. dr Sava St. Sekuli,
Department for Industrial Engineering and
Management, Faculty of Technical Sciences, University
of Novi Sad, 21000 Novi Sad, Trg Dositeja Obradovica
7, 21000 Novi Sad, Serbia.
E-mail: dj.lazarevic@uns.ac.rs

12th INTERNATIONAL SCIENTIFIC CONFERENCE MMA 2015 -
FLEXIBLE TECHNOLOGIES

PROCEEDINGS



Section B:

MACHINES TOOLS

Novi Sad, 25-26 September 2015

Košarac, A., Zeljkovi M., Mladenovi, C., Živkovi, A.

CREATE SISO STATE SPACE MODEL OF MAIN SPINDLE FROM ANSYS MODEL

Abstract: This paper shows identification of dynamic characteristics of working unit module main spindle, based on application of APDL ANSYS and MATLAB software. Single Input Single Output (SISO) state space MATLAB model will be developed from an APDL ANSYS main spindle model. The first step in defining the state space model is to define the eigenvector elements for all modes for only the input and output degrees of freedom. The next step is analysing the each mode contribution and sort them from the largest to smallest. One of the modal reduction technique is then applied, and modes with smallest contribution are simply truncated.

Key words: Main spindle, modal parameters, model size reduction, state space

1. INTRODUCTION

One of the biggest obstacle in work with finite element models is system size. During a sequence of FEM analysis of complex mechatronic system like machine tool is, nodal displacement are computed for mesh which can have up to 10^5 , even 10^6 degree of freedom (DOF). Considering that design process is very interactive, so FEM analysis needs to be repeated frequently, it is obvious that perform finite element analysis repeatedly can be very time consuming. Although modern computers are becoming more and more powerful, dealing with such huge models is still a problem. Model order reduction (MOR) techniques reduces the size of the FEM model while input/output relationship remains preserved.

Using modal analysis eigenvalues (resonant frequencies) and eigenvectors (mode shape) are determined. Since the number of eigenvalues and eigenvectors is equal to number of DOF, it is obvious that this is too large to be inserted into state space in MATLAB model. Therefore, the goal to be achieved is not only obtaining a reliable dynamic model, since such a model exist and that is a FEM model. The objectives to be achieved are:

- Convert a large finite element model (by “large model” it is assume model with thousands of hundreds DOF) to a smaller MATLAB model which still provide correct response for the forcing input, i.e. still maintaining the input / output relationship, Fig1,
- Obtained MATLAB model can be inserted into complex control system models and be used do define system dynamic.

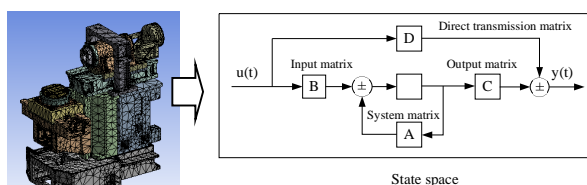


Fig. 1. Model size reduction

The mathematical model obtained by finite element

method is linear time-invariant model. The entire structure is described by the mass, damping and stiffness matrices and can be represented by linear ordinary differential equations with constant coefficients. This model can be transformed into state space representation where a system an n^{th} order differential equation is replaced with a single first order matrix differential equation.

When carrying out certain analysis, such as for example modal analysis, considered system has a highly complex mathematical model which solving can take a long time. In order to reduce the time required for the execution of the simulation, still maintaining the input / output relationship, different model reduction technique are applied. Maglie [3] used the FEM model to determine the relative movement of the tool tip to the workpiece under the influence of the cutting force. Maglie [3] presented a platform for the exchange of data between ANSYS WORKBNCH and simulation model developed in MATLAB / Simulink in which further static and dynamic analysis are performed. The platform integrates modules that contain characteristics of joints, while set of macros is exporting models from ANSYS WORKBNCH into MATLAB / Simulink, including the properties of the joints, stiffness and damping. Maglie [3] used MOR for ANSYS, commercial model order reduction software tool for reading ANSYS files and performing Krylov-based model reduction.

Vesely [5] analysed the impact of natural frequencies of the machine tool mechanical structure on the dynamic behaviour of the feed drive. Machine tool structure is being observed in two ways: as lumped mass in one, and as a finite element model in the second case. Machine tool is modelled as a system of elastic bodies, and model order reduction of FEM model is performed by applying Craig – Bamton reduction techniques. This technique allows the selection of a certain number of natural frequencies the reduced model will keep comparing to the original model, and the selection of so-called "interface" nodes that are used for coupling with other bodies. Also, Vesely [5] analysed two methods for determining the influence of the machine tool structure on the dynamic

behaviour, the first way - modal decomposition technique in which the transformation is performed on mass, damping and stiffness matrix obtained from the FEM system, and otherwise - by solving the equation of motion in modal coordinates.

2. MAIN SPINDLE MODAL ANALYSIS

In this paper, on the main spindle example, Fig.2, is shown how the model can be transformed from finite elements into state space representation, how to do modal reduction sorting modes by dc gain and peak gain, perform sorted modes modal truncation and finally find solution in physical coordinates through the next steps, [4]:

1. Perform modal analysis, and determination of natural frequencies and mode shapes in ANSYS (eigenvalues / eigenvectors),
2. Transformation of the FEM model so that the modal matrix include only those degrees of freedom where the force is applied and/or outputs desired,
3. Analysing the modal contribution of each mode and sort them in descending order, as well as reducing the number of modes by modal truncation including only modes which have significant contribution to desired response,
4. Create modal state space form equations of motion,
5. Find solution in physical coordinates in frequency or time domain.

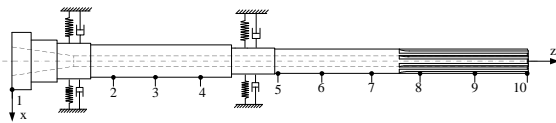


Fig. 2. Equivalent dynamic model of spindle with measurement points

Main spindle, shown in Fig 2., is supported by the two sets of angular contact ceramic ball bearings in front, SKF S7011 CD/HCP4A and two sets of angular contact ceramic ball bearings in rear SKF 7008 CD/HCP4A, installed back to back, Fig2. Values of bearing stiffness depending on the preload are provided in the table 1 [6], [2].

	Preload					
	Small		Middle		Big	
	Front brg set	Front brg set	Front brg set.	Front brg set	Front brg set	Front Brg set
Radial stiffness N/ μ m	400	280	560	387	690	475
Axial stiffness N/ μ m	69	48	115	82	170	120

Table 1. Stiffness of bearing [6], [2]

Considering that quill unit moves horizontally (feed movement), the main spindle assembly has a specific construction, with free end of the main spindle relatively large length, [6], [7]. Therefore, it is especially interesting to consider the dynamic behaviour of the main spindle free end. Fig.3. shows

main spindle modelled in APDL ANSYS with two elastic support on the bearing places. The material is linear isotropic structure steel. Young's modulus is $E=2 \cdot 10^{11}$ Pa, Poisson's ratio is $\nu=0.3$, material density $\rho = 7850$ N/m³. SOLID186 a higher order 3-D 20-node solid element is used to simulate main spindle. Total numbers of nodes and elements are 85032 and 17167 respectively. When assigned material to model in ANSYS, the spindle mass is 9.2 kg. Spring damper element COMBIN 14 is applied to simulate the elastic support of the two set of bearings. Eighteen elements was set along the circumferential direction of the spindle on each set of bearing, simulating rolling elements. Since the inertial force and the thermal expansion of bearing elements affect the balls, an uneven distribution of contact forces and an uneven contact angle change occurs. The consequence of the aforementioned is the uneven distribution in bearing stiffness, depending on the position of the ball [7].

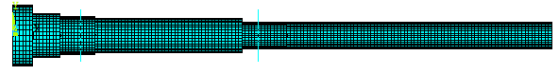


Fig. 3. Main spindle finite element model

The first ten eigenvalues (Tab. 2) and eigenvectors for bending motion of main spindle were extracted using Block-Lanczos method. Each of 10 column of modal matrix represent the eigenvector for that mode, normalized with respect to mass. Each row of the modal matrix show relative motion of points to which forces are applied and/or for which displacement are desired (measurement points from Fig. 2).

f_1 (Hz)	f_2 (Hz)	f_3 (Hz)	f_4 (Hz)	f_5 (Hz)
154,37	926,92	1641,06	2351,83	2538,17

f_6 (Hz)	f_7 (Hz)	f_8 (Hz)	f_9 (Hz)	f_{10} (Hz)
4533,14	5687,47	6972,75	8228,99	9637,48

Table 2. Eigenvalues for bending motion of main spindle, Hz

3. MAIN SPINDLE STATE SPACE REPRESENTATION

In the state space formulation, n second order differential equations are converted to 2n first order differential equations. The most general state-space representation of a linear system is

$$\begin{aligned} \dot{x} &= Ax + Bu \\ y &= Cx + Du \end{aligned} \quad (3.1)$$

where first equation is state equation, and second output equation, and

x is the state vector,

u is the input (or control) vector,

y is the output vector,

A is the state (or system) matrix,

B is the input matrix,

C is the output matrix,

D is the "feedthrough (or feedforward) matrix" (in cases where the system model does not have a direct feedthrough, D is the zero matrix.

Rewriting the equation 3.1 in matrix form as:

$$\begin{bmatrix} \dot{x}_1 \\ \dot{x}_2 \\ \dot{x}_3 \\ \dot{x}_4 \end{bmatrix} = \begin{bmatrix} 0 & 1 & 0 & 0 \\ 0 & 0 & 0 & 0 \\ 0 & 0 & 0 & 1 \\ 0 & 0 & -\omega_2 & -2\zeta_2\omega_2^2 \end{bmatrix} \begin{bmatrix} x_1 \\ x_2 \\ x_3 \\ x_4 \end{bmatrix} + \begin{bmatrix} 0 \\ F_{p1} \\ 0 \\ F_{p2} \end{bmatrix} \quad (3.2)$$

$$\dot{x} = Ax + Bu$$

It may be noted that along the diagonal two sets of uncoupled first order equations appear in block of 2x2 coefficients, where the first block 2x2 represent response of the first mode and second block represent response second mode.

$$\begin{array}{l} \text{Response of} \\ \text{the first} \\ \text{mode:} \\ \text{Response of} \\ \text{the second} \\ \text{mode:} \end{array} \begin{bmatrix} 0 & 1 \\ 0 & 0 \\ 0 & 1 \\ -\omega_2 & -2\zeta_2\omega_2^2 \end{bmatrix} \quad (3.3)$$

Damping ratio is known, either to be adopted as a single value for all modes, or column vector whose members are individual damping ratio for each mode. The natural frequencies (eigenvalues) are also known. This means that the process of determining the submatrix A can easily be expressed algorithmically, and thus the programmed. Uncoupled equation of motion of two first modes are

$$\begin{array}{l} \text{First} \\ \text{mode} \\ \text{Second} \\ \text{mode} \end{array} \begin{bmatrix} \dot{x}_1 \\ \dot{x}_2 \\ \dot{x}_3 \\ \dot{x}_4 \end{bmatrix} = \begin{bmatrix} 0 & 1 \\ 0 & 0 \end{bmatrix} \begin{bmatrix} x_1 \\ x_2 \end{bmatrix} + \begin{bmatrix} 0 \\ F_{p1} \end{bmatrix} u \quad (3.4)$$

$$\begin{bmatrix} \dot{x}_3 \\ \dot{x}_4 \end{bmatrix} = \begin{bmatrix} 0 & 1 \\ -\omega_2 & -2\zeta_2\omega_2^2 \end{bmatrix} \begin{bmatrix} x_3 \\ x_4 \end{bmatrix} + \begin{bmatrix} 0 \\ F_{p2} \end{bmatrix} u$$

The transformation of the dynamic behaviour of finite elements in the state space involves performing two types of reduction: reducing the number of DOF of the FEM model and the modal reduction.

Reducing the number of DOF of the FEM model means that new model analysed in MATLAB include only the degree of freedom to which forces are applied and/or for which displacement are desired.

If the new model still comprises a number of degrees of freedom bigger than needed, then modal reduction based on the set of criteria is carried out. Analysis of the modal contributions of each individual modes and sort them according to the relative importance is the criterion for performing modal reduction.

The procedure is the following: modes are first ranked on the basis of their relative importance, and then performs the elimination of modes with a lower value modal contributions, i.e. **modal truncation**. Parameters on which determines the sorting mode is the **damping ratio**. The criteria to be applied for sorting mode depends on whether the value of the damping ratio considered unique or different for each mode.

In the first case the criterion for ranking modes is “**dc gain**”, (3.5), while in the second case, the criterion used for ranking modes is “**pick gain**” (3.6) [1].

$$\frac{z_j}{F_k} = \sum_{i=1}^m \frac{z_{nji} z_{nki}}{\omega_i^2} \quad (3.5)$$

$$\frac{z_{ji}}{F_{ki}} = \frac{-j}{2\zeta_i} \left(\frac{z_{nji} z_{nki}}{\omega_i^2} \right) \quad (3.6)$$

Comparing (3.2) and (3.3) can be seen that peak gain is -90° phase shift at resonance, but to have greater amplitude for then dc gain. If relative damping has unique value for all modes, peak gain has larger amplitude but relative amplitude are the same. That means with unique relative damping both methods give the same order of modes regardless which of the ranking criterion is applied. If relative damping has different values for all modes, then peak gain ranking criterion needs to be applied.

Usually the value of damping ratio is between 0,005 (0.5% of the critical damping) to 0.02 (2% of the critical damping). If the experimental results are available, i.e. real and imaginary part of the transfer function, damping ratio can be determined for each mode, and in that case the obtained values of damping ratio are placed in a separate text file.

Fig.4 shows dc gain value for all modes versus mode number for direct frequency response function (FRF) measurement location (X1/F1), and Fig.5 for cross FRF (X10/F1). If the response is measured at the same location where force is applied then such FRF is called a direct, but if is measured at different location, this is cross FRF.

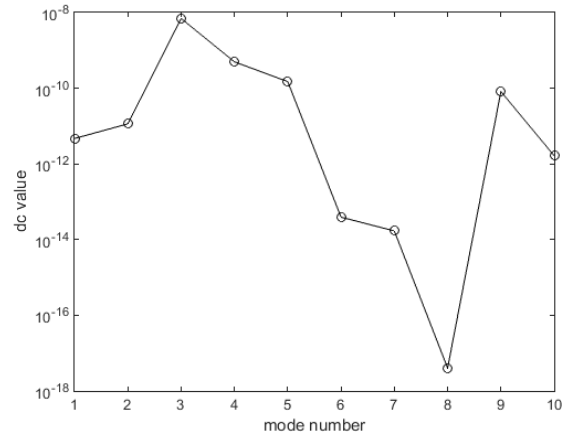


Fig. 4. dc value of each mode contribution versus mode number, direct FRF (X1/F1)

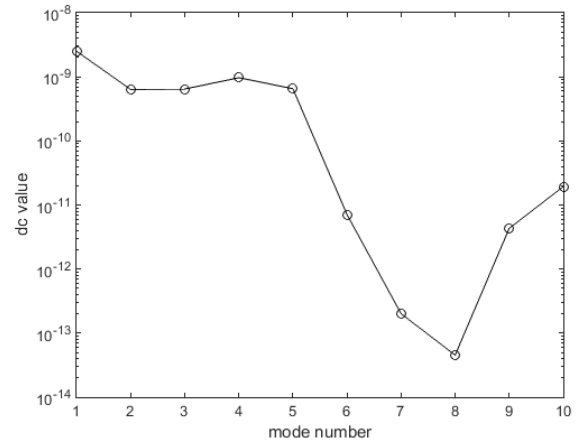


Fig. 5. dc value of each mode contribution versus mode number, cross FRF (X10/F1)

In this case constant damping ratio $\zeta = 0.001$ was considered as unique for all modes, so dc gain was used as a criterion for mode ranking. It can be seen that the mode 1 and 2 (frequencies 154.37 Hz and 926.92 Hz) have smaller modal contributions of modes 3,4 and 5. Accordingly, Fig.6 and Fig.7 show that the first two frequencies have such low gain that their resonant peaks are barely visible on the overall response.

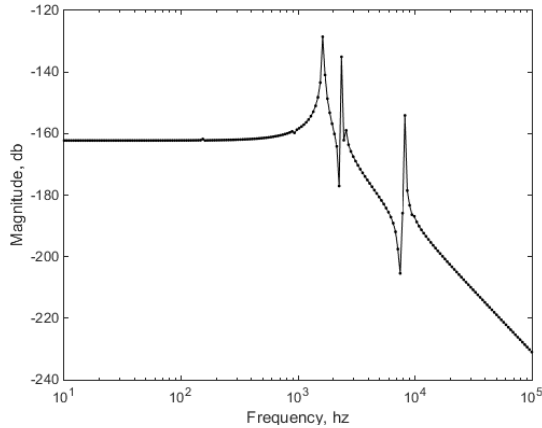


Fig. 6. Direct FRF, all 10 modes included

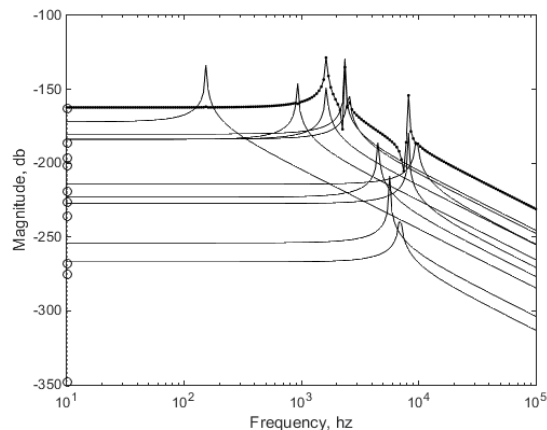


Fig. 7. Direct FRF, overlay of each individual mode contributions

Fig.7 show the overall frequency response with overlaid SDOF (Single Degree of Freedom) response of all the individual modes. Fig.8 shows overall mode contributions for four selected modes. It can be seen that modes 3,4,5 and 9 have the most significant modal contribution.

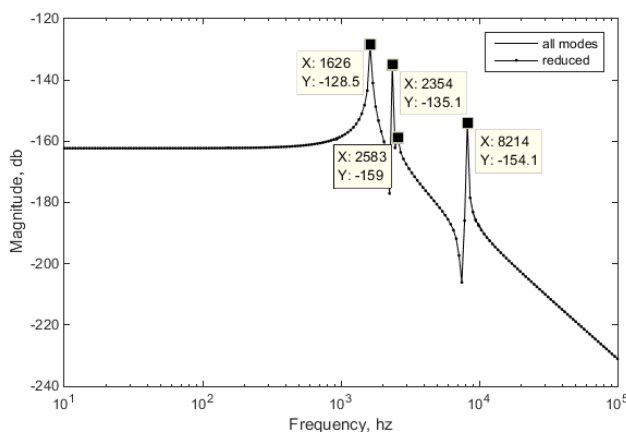


Fig. 8. Direct FRF – reduced sorted modal truncation frequency response –four modes included

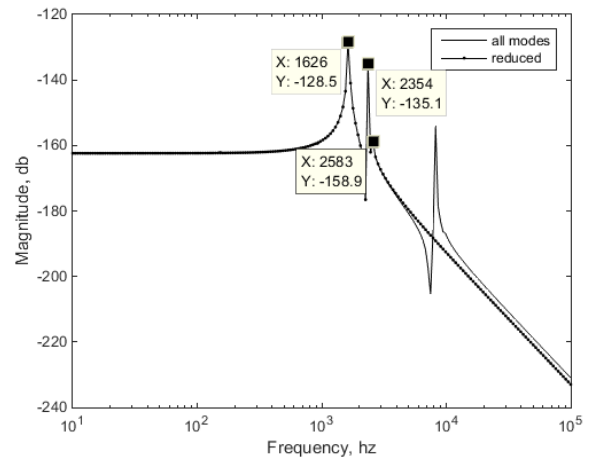


Fig. 9. Direct FRF – reduced sorted modal truncation frequency response –three modes included

If transfer function is plotted for three selected modes, it can be seen that the most significant modes are modes 3,4 and 5, Fig.9. However, in the case of cross FRF, modal contribution of the first four modes is significantly higher than in other modes, Fig.10. Fig.11 shows overall mode contribution for all ten modes and four sorted modes for cross FRF (X10/F1). It can be noted that it is necessary to create at least two different state space models, the first includes all modes extracted from ANSYS, and second only desired number of modes, i.e. reduced number of modes.

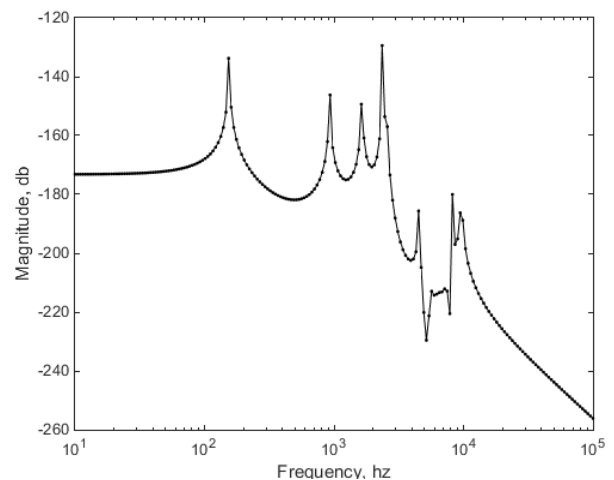


Fig. 10. Cross FRF (X10/F1)– all ten modes included

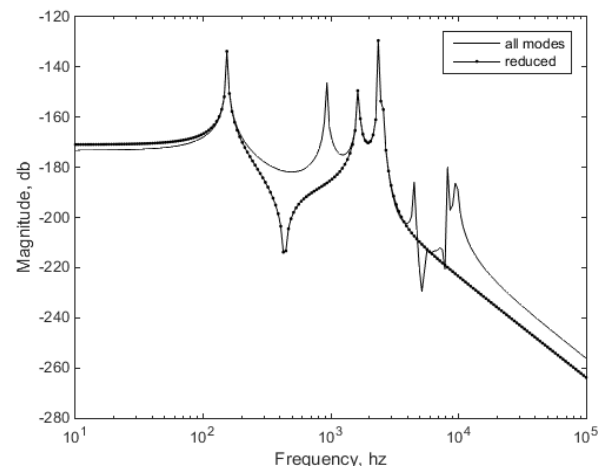


Fig. 11. Cross FRF (X10/F1), reduced sorted modal truncation, 4 modes included

From Fig.11 can be seen that there is an error in the low frequency portion of the frequencies response. This is because the influence of truncated modes on dc gain did not take into account. This influence can be replaced using other techniques of modal reduction, which will be the subject of further research.

4. FINAL REMARKS

This paper shows how to take the results of finite element main spindle model created in ANSYS and reduce the model size extracting lower order state space model in MATLAB (model reduction). Then number of modes can be reduced (modal reduction) by ranking relative importance of each mode to overall response. It was shown modal truncation, as one of techniques for modal reduction. A reduced solution provides very reliable dynamic of the model with a significant reduction in number of states.

Reduced mode can be further inserted into a more complex control system model and used to find system dynamics.

5. REFERENCES

- [1] Hatch, M. R.: *MATLAB and ANSYS*, Chapman & Hall/CRC, 2001.
- [2] Košarac, A., Zeljkovi, M., Mla enovi, C., Živkovi, A.: *Numerical-experimental identification of a working unit module dynamic characteristics*, VIII International Conference "Heavy Machinery-HM 2014", Zlatibor, 25-28 June 2014.
- [3] Maglie, P.: *Parallelization of Design and Simulation: Virtual Machine Tools in Real Product Development*, A dissertation submitted to the ETH ZURICH, 2012.
- [4] Schmitz, T. L., Smith, K.S.: *Mechanical Vibrations Modeling and Measurement*, Springer, 2012.
- [5] Vesely, J., Sulitka, M.: *Machine Tool Virtual Model*, MM Science Journal, December 2009, 146-151.
- [6] Zeljkovi, M.: *Sistem za automatizovano projektovanje i predikciju ponašanja sklopa glavnog vretena mašina alatki*, Doktorska disertacija, Fakultet tehničkih nauka, Novi Sad, 1996.
- [7] Živkovi, A., Zeljkovi, M., Tabakovi, S., Milojevi, Z.: *Mathematical modeling and experimental testing of high – speed spindle behaviour*, The International Journal of Advanced Manufacturing Technology, 2015.

Authors: Mr Aleksandar Košarac, University of East Sarajevo, Faculty of Mechanical Engineering,
Prof. dr Milan Zeljkovic, Assistant Professor,
Aleksandar Zivkovic. M.Sc. Cvijetin Mla enovic,
University of Novi Sad, Faculty of Technical Sciences,
Institute for Production Engineering, Trg Dositeja
Obradovica 6, 21000 Novi Sad, Serbia, Phone.: +381
21 450-366, Fax: +381 21 454-495.

E-mail: akosarac@gmail.com; milanz@uns.ac.rs;
acoz@uns.ac.rs; mladja@uns.ac.rs

Knežev, M., Živkovi, A., Mladenovi, C.

ANALYSIS STATIC AND DYNAMIC BEHAVIOR OF HYDRODYNAMIC SPINDLE

Abstract: *Becoming more stringent demands with regard to quality of ball bearings, as well as complexity of physical and chemical process that occur inside of them, which cannot be explained based on theoretical knowledge, caused intensive development of experimental methods and devices for testing and diagnostic of rolling bearings. Experimental tests are carried out on special for this purpose intended devices. The most important element of device is hydrodynamic spindle from who depend the accuracy of device. The objective of this work is to study the static and dynamic behavior of spindle supported by hydrodynamic bearings, using the FEM method.*

Key words: *hydrodynamic spindle, hydrodynamic bearings, static analysis, dynamic analysis, CAE*

1. INTRODUCTION

Experimental results have a major impact both on the resolving existing problems and the development of new designs and technologies throughout the life of the roller bearings, therefore is very important that results are accuracy [8]. The hydrodynamic spindle system is the most important element of a measuring device since its properties are closely related to the accuracy of the device, because during the test roller bearing is placed on spindle and every imperfection of spindle will reflect on results. The dimension of the spindle as well as the location, the stiffness of the hydrodynamic bearings, loads of tourniquet and driving system affect the spindle behavior. For the hydrodynamic bearings, the journal and the bearing surface are separated by the sliding action with a wedge pressure-generating mechanism to develop a pressure within the bearing [4]. So that stiffness depends on the pressure and thickness of the lubrication film [3], [6]. Spindle used in precision devices must have low error motion over a range of operation speeds, small temperature rise and minimum wear. The above requirements can be achieved by appropriate choice material and construction of the spindle and its bearings [2]. Hydrodynamic bearings are characterized by very high accuracy of work, running smoothness with high vibrations dumping, simply technology and low cost of making, economically maintenance and so on.

The purpose of static analysis is validation that the spindle deformations are in allowed limits and finding the force in bearings. On the other hand dynamic analysis is made with aim to analyze the dynamic behavior, for what is used modal analysis to determinate natural frequencies and mode shapes as well as harmonic analysis to determine the response of certain nodes at the effect of the load. Both analyzes are carried out using the finite element method.

2. STATIC AND DYNAMIC ANALYZES

The spindle is mounted in a housing of device via two radial and one axial hydrodynamic bearing for satisfying the high precision rotating of spindle. The Fig 1 shows the 3D model of hydrodynamic spindle

system with marked characteristic parts.

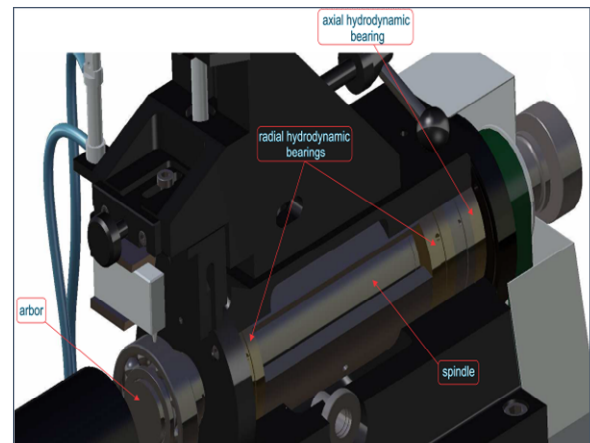


Fig. 1. 3D CAD model of hydrodynamic spindle system [7]

Due to simple Axial-symmetric nature of the spindle system, the spindle is represented by one dimensional element type with two nodes BEAM188, which is six degree element, based in Timoshenko beam theory, with circular annular cross-section, which is suitable for representing the stepped nature of spindle. Stiffness of hydrodynamic bearings is defined by equivalent spring-dumper element type COMBIN14 whereby value of initial stiffness both hydrodynamic bearings are $C_r=70 \text{ N}/\mu\text{m}$ [1]. The front conical surface of the spindle which is used to accept and positioning the arbor is replaced with cylindrical surface with the dimension of middle diameter of cone. The Fig. 2a shows model described with 16 nodes and 15 elements type BEAM 188 and 2 elements type COMBIN14 (Fig. 2b).

In reality, the spindle has a total length of 324 mm and its outside diameter is variable, on place where is spindle connected with bearings diameter is 60 mm. The spindle is connected with front and rear bearing with the isotropic bearing stiffness designated as nodes 15 and node 16 respectively.

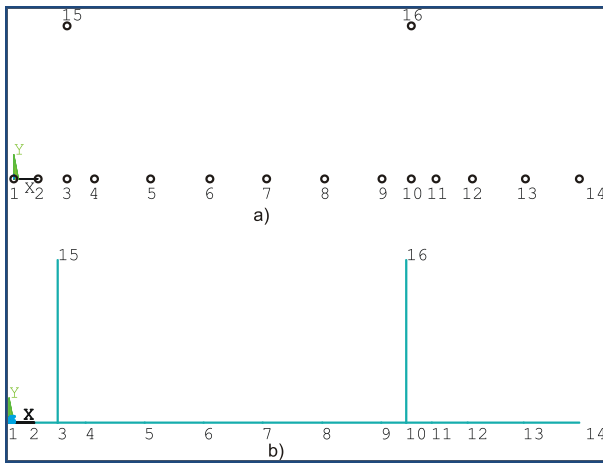


Fig. 2. Spindle described by; a) the nodes, b) BEAM188 elements

Using ANSYS APDL, a static model was built, consisting of a solid shaft rigidly connected to arbor and belt pulley and supported by the bearings hydrodynamic bearings.

The Fig. 3 shows model for analysis, the same model will be used for static and dynamic analysis, only the constraints will be changed.

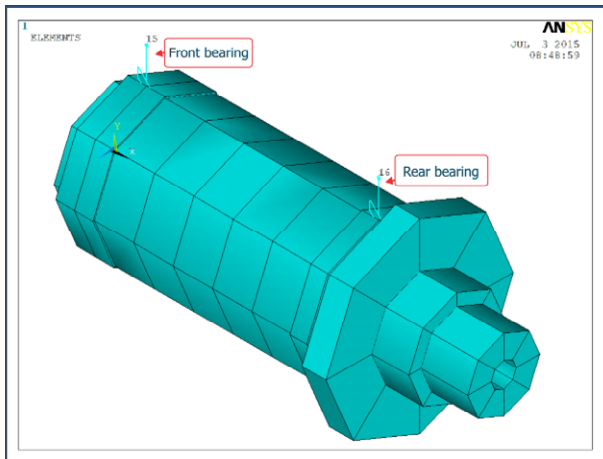


Fig. 3. 3D Representation model of spindle

Material of spindle is 20MnCr5, and his data are specified in Table 1.

Material	20MnCr5
Modulus of elasticity	2.1E+05 MPa
Density	7.8E-06 kg/mm ³
Tensile strength	800 MPa
Poisson Ratio	0.3

Table 1. Spindle material data

2.1 Static analysis

The static analysis is carried out with radial load on node of finite element mesh where is spindle in contact with belt pulley (node 14), and axial load on spindle nose (node 1). Applied forces are the result of the maximal axial force ($F_a=200$ N), which acting on the test bearing and the radial force ($F_r=430$ N) by the belt

transmissions.

The Fig. 4 shows deformations in Y direction, the biggest value of deformations is on the end of spindle, showed by blue color, what was expected because that is the place of radial force. The maximum of radial displacement occurs at the end of the spindle and is $16.9 \mu\text{m}$, while the minimum radial displacement occurs at the spindle nose and is $0.5 \mu\text{m}$ (Fig. 4). On the place where is spindle connected with a front hydrodynamic bearing deformation is $5.0 \mu\text{m}$, and on the rear bearing place is $12.0 \mu\text{m}$. Hydrodynamic bearings are designed with clearance of $20 \mu\text{m}$, so then mentioned displacements on front and rear bearing will not disturb proper work. Force reactions in bearings are: front and rear bearing $F_{rb}=203\text{N}$, and $F_{rb}=633\text{N}$ respectively.

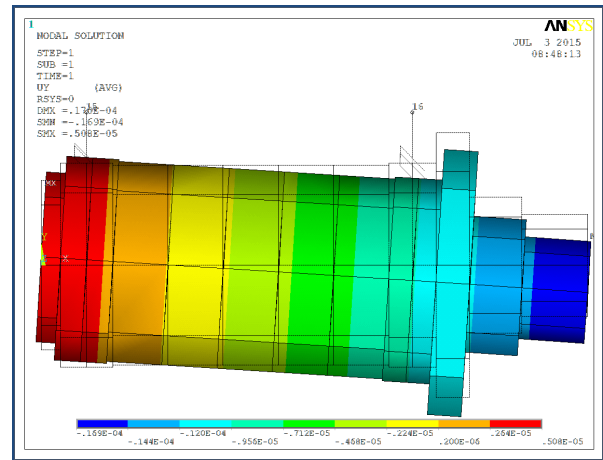


Fig. 4 Structural displacement due to loads

The spindle stiffness includes the axial and bending stiffness. In this operating condition, the axial stiffness is more important than bending stiffness. The axial stiffness (C_a) of the spindle unit is defined as follows: if the front part of the spindle generates unit axial displacement a , the force required to be imposed on the direction of the displacement is F_a . [5] The static axial stiffness of the spindle nose can be calculated as:

$$C_a = \frac{F_a}{a}; N / \mu\text{m} \quad (1)$$

$$C_a = \frac{200}{1.8} \cong 111; N/\mu\text{m}$$

On the basis of displacement from Figure 4, radial stiffness of the front ($C_{r,f}$) and rear bearing ($C_{r,r}$), under applied the radial load are:

$$C_{r,f} = \frac{203}{5} = 40.6; N/\mu\text{m} \quad (2)$$

$$C_{r,r} = \frac{633}{12} = 52.7; N/\mu\text{m}$$

Similar stiffness values for the given displacements are shown in the paper [1].

2.2 Dynamic analysis

For dynamic analysis spindle is freely supported, because mode frequencies as well as the natural frequencies are depend on the system parameters. In

order to find the spindle natural frequencies domain of the spindle was used finite element model represented in Fig. 5. Two nodes 15 and 16 are taken all degrees of freedom, to node 3 where is spindle connected with front bearing is taken rotational degree around X axis, and translation in Z direction, while to node 10 are taken translations in X and Z directions, and rotation around X axis.

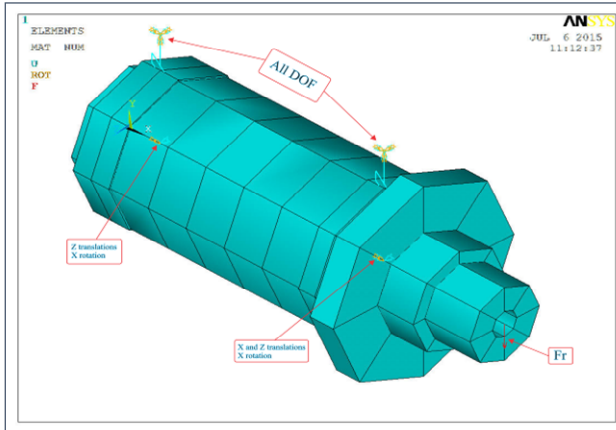


Fig. 5. Finite element model for dynamic analysis with constraints

Reason for that kind of limitations is radial on front and radial with axial bearings on rear side of spindle.

Accordingly numerical models were obtained the results for the first five natural frequencies of model (represented in Fig. 5.) values are given in Table 2.

Mode	Frequency [Hz]
f_{01}	355
f_{02}	504
f_{03}	5088
f_{04}	5580
f_{05}	9000

Table 2. Natural frequencies of the spindle

Based on the calculated values, plotted are the mode shapes for corresponding natural frequencies. Vibration modes according third and fifth natural frequencies are represented, Fig 6 shows third, and Fig. 7 shows fifth mode shapes. We can observe that the first spindle natural frequency of the spindle is about 355 Hz corresponding to 21300 rpm, and it is much higher than maximum spindle speed which is 1800 rpm.



Fig. 6 Third natural frequencies of the test spindle

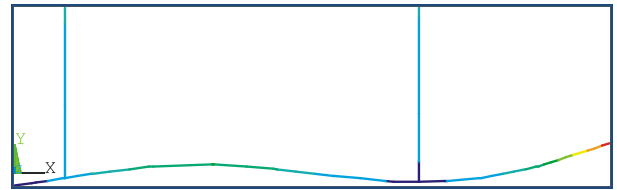


Fig. 7 Fifth natural frequencies of the test spindle

The spindle is modeled as a stationary reference frame where the general dynamic equation includes the rotational effects as follows:

$$[M] \{\ddot{u}\} + [G] \{\dot{u}\} + [K] \{u\} = \{F\} \quad (3)$$

Where:

$[M]$ = Structural mass matrix

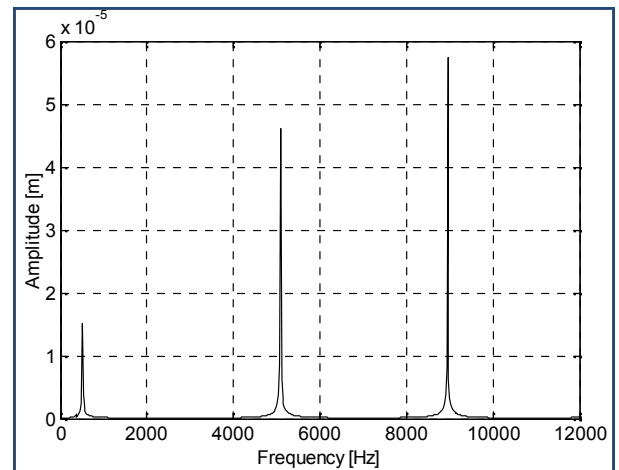
$[G]$ = Gyroscopic effect originated from the rotational angular velocity applied to the structure

$[K]$ = Stiffness matrix

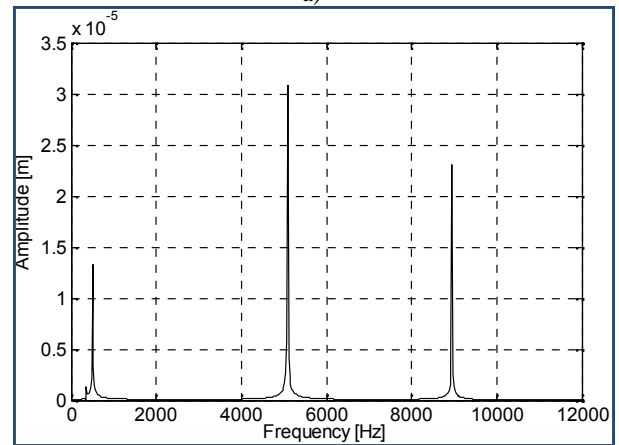
$\{F\}$ = External force vector

In this paper, damping is not considered.

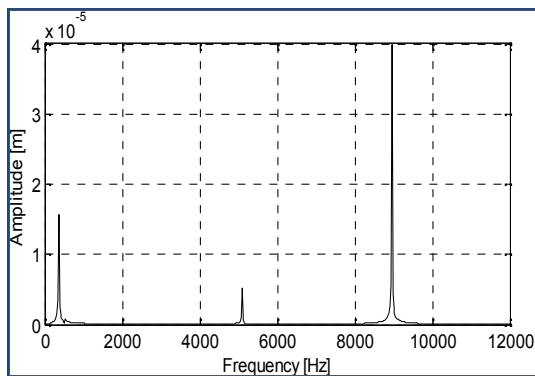
In the considered frequency interval 0 ÷ 10000 Hz, given by modal analysis, was performed harmonic response analysis spindle at the effect of loads. The Fig. 8 shows the displacement of characteristic nodes of spindle.



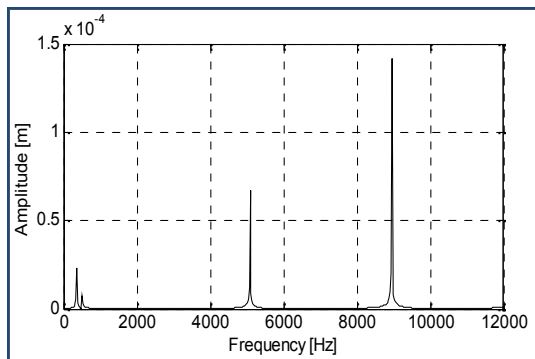
a)



b)



c)



d)

Fig. 8. Harmonic responses of characteristic nodes on: a) spindle nose (node 1), b) the front bearing (node 3), c) the rear bearing (node 10), d) the end of spindle (node 14)

The Fig. 8 shows harmonic response of the characteristic nodes, and can be seen that maximum responses are different for each node. All the maximum values are taking place above operational frequency of 30 Hz what corresponding to 1800 rpm. So in the normal conditions, the deformations will be with the limits.

3. CONCLUSION

The spindle made of multiple steps is modeled and analyzed for different boundary conditions for static and dynamic analysis. The analysis summary is as follows.

Initial static analysis shows minimum, maximum and deformations of significant parts of spindle, as well as the forces in both hydrodynamic radial bearings. The value of spindle stiffness is validated through theoretical calculations.

Modal analysis carried out with bearing supports under flexible conditions shows that natural frequencies of spindle are a much bigger than the operational frequency, so than they can not endanger measuring process.

Harmonic response analysis of characteristic nodes represented along with natural frequencies, shows that the maximum values of displacement are different for each node, because they are depended of vibration bending mode.

All the results shows that device can operate safe and accurately with the given bearing values and spindle dimensions.

Acknowledgments: In this paper some results of the project: *Contemporary approaches to the development of special solutions related to bearing supports in mechanical engineering and medical prosthetics* – TR 35025, carried out by the Faculty of Technical Sciences, University of Novi Sad, Serbia, are presented. The project is supported by the Ministry of Science and Technological Development of the Republic of Serbia.

4. REFERENCES

- [1] Bellakhdhar, B., Dogui, A., Ligier, J.L.: *Main Bearing Stiffness Investigation*, World Academy of Science, Engineering and Technology, Vol. 5, pp.1492-1496, 2001
- [2] Borovkov, A., Artamanov, I.: *3D Finite Element Modeling and Vibration Analysis of Gas Turbine Structural Elements*, St.Petersburg State Polytechnical University, Russia, 2015.
- [3] Badrway, S.: *Dynamic modeling and analysis of motorized milling spindles for optimizing the spindle cutting performance*, Technical papers Moore Nanotechnology Systems, LLC, 2015.
- [4] Chen, Y., S., Cheng, Y., D., Chiou, C., C.: *The critical speeds of a machine tool spindle bearing system with the high stiffness hydrostatic journal bearings*, Yuan-Ze University Chungli, Taoyuan, Taiwan, 2014.
- [5] Damodar, A., Kondayya, D., Prasad, B.: *Static and dynamic analysis of spindle of a CNC machining centre*, International Academy of Science, Engineering and Technology, Volume 2, 165-170, 5, Nov 2013.
- [6] Delgado, A., S., Ozturk, E., Sims, N.: *Analysis of Non-Linear Machine Tool Dynamic Behavior*, The Manufacturing Engineering Society International Conference, MESIC, ELSEVIER, Zaragoza, 26th-27th, June 2013
- [7] Knežev, M.: *Design of virtual device for measuring and control vibrations of rolling bearings*, Master thesis, Faculty of Technical Science, Novi Sad, July 2015.
- [8] Tomovi, R.: *Research of rolling bearings construction parameters impact to the condition of their labouring correctness*, Doctoral dissertation, Faculty of Mechanical Engineering, Niš 2009.

Authors: M.Sc. Miloš Knežev, Assistant Professor, Aleksandar Zivkovi, M.Sc. Cvijetin Mla enovi, University of Novi Sad, Faculty of Technical Sciences, Department for Production Engineering, Trg Dositeja Obradovica 6, 21000 Novi Sad, Serbia, Phone.: +381 21 485 2330, Fax: +381 21 454-495.

E-mail: milosknezev@gmail.com, acoz@uns.ac.rs, mladja@uns.ac.rs;



Lazarevi D., Nedi B.

MEASUREMENT TECHNOLOGIES AND MACHINING ERRORS

Abstract: *The ultimate goal of performing measurement in a manufacturing system is to gain close control of the machining process based on tolerance requirements and to adjust process errors as they occur. The key issue is to connect machining and tolerance requirements. What to measure and when to measure is another critical issue. The paper presents a short introduction in a closed-loop manufacturing from the basic methods of measurement technologies and a shorter description of the machine errors.*

Key words: *Manufacturing, Measurement technologies, Accuracy, Error compensation*

1. INTRODUCTION

Manufacturing operations are driven by cost requirements that relate to the value of a particular product to the marketplace. Given this selling price, the system works backwards to determine what resources can be allocated to the manufacturing portion of the cost equation. Then, production personnel set up the necessary resources and provide the workpieces that are consumed by the market. Everyone is happy until something changes. Unfortunately, the time constant associated with change in the manufacturing world has become very short. Requirements often change even before a system begins producing parts, and even after production is underway there are typically many sources of variability that impact on the cost/quality of the operation. Variability associated with scheduling changes are to be accommodated by designing flexibility into the basic manufacturing systems. However, the variability that is related to changing process conditions are best handled by altering system performance at a more basic level.

Error conditions often occur where one or more process parameters deviates significantly from the expected value and the process quality degrades. The sensitivity of the process to these variations in operation conditions depends on the point in the overall manufacturing cycle at which they occur as well as the specific characteristics of a particular process disturbance. Amplitude, a frequency of occurrence, and a direction typically characterize these process errors [2, 3]. In a machining operation, the typical result is a lack of synchronization between the tool and part locations so that erroneous dimensions are produced.

Over time, the amplitude of process errors is typically limited to a specific range either by their inherent nature or by the operator's actions. For example, shop temperature profiles tend to follow a specific pattern related to cutting forces, and cutting tools are replaced as they wear out. As multiple process error sources interact, the result is typically a seemingly random distribution of performance characteristics with a given "normal range" that defines the routine tolerances achievable within a given set of operations. On the other hand, trends such as increased operating temperatures due to a heavy workload, coolant

degradation, and machine tool component wear, have a non-random pattern that continue over time until an adjustment is made [2].

One solution to the problem of process variation is to build a system that is insensitive to all disturbances; unfortunately, this is rarely practical. A more realistic approach is to use a manufacturing model that defines the appropriate response to a particular process parameter change. This technique can be very successful if the necessary monitoring systems are in place to measure what is really happening within the various manufacturing operations. This approach works because manufacturing processes are deterministic in nature: a cause-and-effect relationship exists between the output of the process and the process parameters [2]. Events occur due to specific causes, not random chance, even though an observer may not recognize the driving force behind a particular action. If the key process characteristics are maintained at a steady-state level, then the process output will also remain relatively constant. Conversely, when the process parameters change significantly, the end product is also affected in a noticeable manner. By measuring the important process parameters in real time and performing appropriate adjustments in the system commands, great improvements can be achieved in increasing product quality and lowering production costs [3]. Closed-Loop Manufacturing (CLM) as such a method is widely employed in modern industry.

2. CLOSED-LOOP MANUFACTURING

Closed-loop manufacturing is a method for optimizing the efficiency of a manufacturing process. It involves the use of measurement technology (metrology), most often touch sensor probes, to determine actual part dimensions as well as coordinates of machine tool characteristics [4]. The elements of CLM are comprised of reliable machines, robust processes, automatic data collection, continuous improvement, and efficient and accurate analysis. Each element is supported by various methods which when combined deliver a complete closed-loop solution. The CLM cycles consist of measurement, data collection, data analysis, and process adjustment. Fig. 1 illustrates these elements and the cycle of CLM.

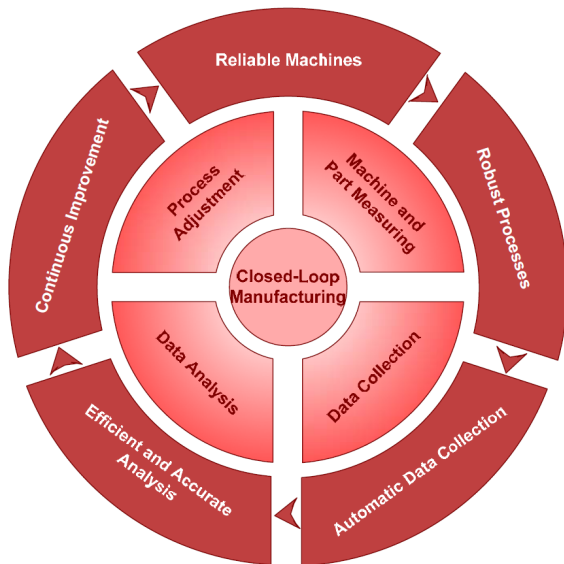


Fig. 1. Elements of CLM [1]

Using the measurement of workpiece as a check on the CLM process is well established but there are a number of issues as to where to measure, what to measure and when to measure. There are three types of measurement in manufacturing processes listed as follows, all of which can be used to provide measurement data for CLM processes:

- 1) In-process measurement
 - with On-Machine Measurement (OMM), which takes place as the workpiece is being made.
 - with portable measurement, where the workpiece surface is tested when the part has been made but not relocated. The surface instrument, which is hand-held, has somehow to be perched on the part when the machining has stopped and then the measurement recorded.
- 2) In situ measurement
 - The workpiece is removed from the machine and measured with an instrument located near the machine tool.
- 3) Remote measurement
 - The workpiece is taken to a properly equipped inspection room to be inspected on a Coordinate Measuring Machine (CMM).

2.1 In-process measurement

Inspection, including dimensional inspection, has commonly been an activity performed after, rather than during, a manufacturing step or process. In many instances, several steps may have been performed before a part is measured. If the part is found to deviate from the specified tolerances, it must either be rejected at a point where considerable value has been added or be reworked. In either case, the manufactured cost has been boosted. As aforementioned, in-process measurement is significant in that it ultimately allows a manufacturer to achieve a goal of zero scrap (i.e. the “first part correct” paradigm), since deviations in the manufacturing process measured by sensors can be used in a corrective manner to control the process before tolerances are exceeded. Advances in sensor technology and digital computers and controllers are

permitting a dramatic increase in the application of in-process measurement and control.

The concept of in-process measurement and control has to do with (a) measuring a process variable while that variable can still be influenced and (b) applying a corrective feedback to the machine that affects the process so as to encompass those sources of error that normally occur during the process and thus eliminate error from the variable on the resultant workpiece. Fig. 2 illustrates the basic concept of in-process measurement.

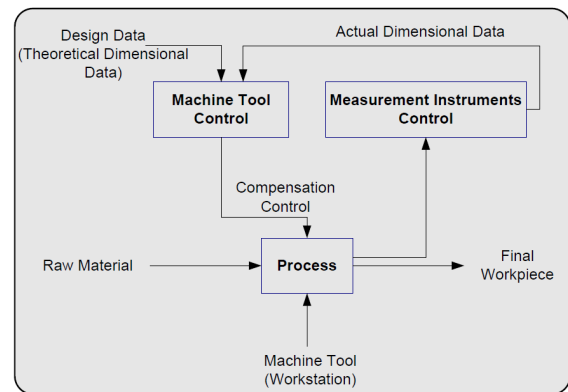


Fig. 2. Concept of In-process measurement [1]

In order to produce a workpiece, raw material is required, equipment such as a machine tool is needed to effect the process, and something to describe quantitatively the amount of material to be removed – the design drawing or data from the design – is required. During machining process, OMM instruments or portable measurement instruments provide a continuous measurement that can be in the form of an analog signal or a digital data work, which is compared with the required dimension derived from the part design. The result of the comparison is a compensatory signal which is applied to the machine control so as to restore the dimension within its allowable range on either the part being machined or subsequent parts. The use of limited in-process measurement coupled with the monitoring of the key process parameters of manufacturing process as a substitute for extensive postprocess inspection is becoming more realistic and attractive in achieving fully automated manufacturing process [3]. The two types of measuring devices commonly used in in-process measurement are OMM and portable measuring devices. Compared with portable measuring devices, OMM has been gradually used as the preferred measuring equipment for the purpose of direct inspections in manufacturing and quality control, which is a vital feature for an automated production system. In-process measurement with OMM operations is a process that integrates the design, machining, and inspection aspects of manufacturing to allow a product to be inspected and accepted directly on a machine tool. This process is accomplished by using the machine tool as the inspection device while the part is secured on the machining centre with its coordinate system intact. Using the machine tool as an inspection device eliminates the need for expensive inspection

equipment, allowing the manufacturer to divert resources to other uses. There is no need for inspection fixture either, because the machine tool part fixture serves as the inspection fixture. As the workpiece gets more complicated, the role of OMM becomes more significant as efficient dimensional measuring equipment [5]. Sensors present in a CNC system have the capability of providing accurate feedback for the different drive/motors. They are often limited to just perform these functionalities and not geared toward supporting those inspection tasks which are effectively what OMM is about. The advantages of employing OMM for in-process measurement are summarized as follows [6]:

- 1) Cost and time saving through
 - reducing lead-time required for gages and fixtures,
 - minimizing need for design, fabrication, maintenance of hard gages, fixtures & equipment,
 - reducing inspection queue time and inspection time, and
 - eliminating rework of nonconforming product.
- 2) Changing from “reactive” inspection to “proactive” control by
 - integrating quality control into product realization process,
 - using characterized and qualified processes to increase product reliability,
 - focusing resources on prevention of defects instead of detection in the end (a post-mortem process),
 - utilizing real-time process knowledge and control, and part acceptance/disposition, and
 - enhancing small lot acceptance capability.
- 3) Elimination of non-value added operations such as lot inspection, sampling plans, receiving inspection, design, fabrication and maintenance of hard gages, and reworking nonconforming parts;
- 4) Agile machining.
 - OMM enables quick responses to product design changes. Since inspection operations are carried out on the same machining centre, inspection gages and fixture changes are not required. New and existing technologies such as probing strategy, error compensation, data analysis software and fixture design technology can be integrated into the OMM system. As errors occurring during machining processes are detected and recorded as they appear, part distortion can be “corrected” promptly by adjusting the subsequent machining operations.

Therefore, in-process measurement with OMM operations presents a promising solution toward improving manufacturing processes.

3. THE ACCURACY OF A MACHINE TOOL

The demand for high precision component manufacturing is increasing because it offers substantial benefit to a wide range of applications with higher quality and better reliability. The realization of machines for such precision manufacturing depends on the possibility of completely monitoring the sometimes complex mechanisms of the machine, the peripheral devices and control with respect to their functioning so

that necessary correction could be made to enhance its accuracy.

As the functional requirements of the products become more sophisticated and their dimensional tolerance becomes tighter, the effectiveness and the accuracy of the manufacturing process become more critical. The accuracy of a machine tool is primarily affected by the geometric errors; non-uniform thermal expansion of the machine structure; and static/dynamic load induced errors. As a consequence, a resultant volumetric error which is the relative error between the cutting tool and the machined part is created. Hence, the reduction of the error to improve the accuracy of the machine tool is crucial. The errors/inaccuracies can be reduced with the structural improvement of the machine tool through better design, manufacturing and assembly practices. However, the method will result in very high manufacturing cost particularly when the accuracy requirements are beyond certain levels. Therefore, error compensation has been employed to improve machine tool accuracy cost-effectively. Machine tool accuracy enhancement through error compensation involves predicting and compensating the resulting machining errors. The system does not avoid errors but monitors continuously the condition of the machine and any error that may be generated is compensated for accordingly. The basic philosophy behind the concept is that it is difficult to construct a perfect machine tool. Despite perfect design, the accuracy of the machine changes when it is subjected to thermal loading, excessive cutting forces and other external excitations. It is therefore, a much easier task to measure the amount of inaccuracies and compensate for them through changes in the commanded position of the different axes of movement of the machine tool. Various works [7, 8, 9] have reviewed past efforts to improve machine tool accuracy through error compensation in serial kinematic machine. However, considerable work has been done after these reviews both in serial and parallel kinematic machines [11].

The accuracy of a machine depends on the deviation in the position of the tool cutting edge from the theoretically required value when compared with specified tolerance. The extent of this deviation in a machine gives a measure of its accuracy defined as the degree of agreement or conformance of a finished part with the required dimensional and geometrical specifications. Factors affecting the total volumetric accuracy of a machine tool and their relationships are given in Fig. 1 inspired from [7, 8] and completed. These include three main sources of errors namely:

1. geometric errors
2. thermally induced errors
3. load induced errors.

Other sources of error such as fixturing, instrumentation, material instability and controller errors also contribute to the dimensional and geometric aspect of the produced part.

On a closer look at the various types of errors, their components could be classified into systematic and random error. Systematic errors are those errors that occur in the same way at every measurement and cannot be discovered by examining the result of

measurements. Causes of systematic errors are usually known [10]. They possess constant relative magnitude and constant sign and correction can be applied. Random errors on the other hand exhibit some variability in both magnitude and sign and are affected by measured system; variation in operating and environmental conditions; measurement procedure; and technique. All categories of errors in machine tools possess systematic and random components.

4. CONCLUSION

Recognizing the deterministic nature of manufacturing operations paves the road for improvements in product quality and reduction of production costs. This is accomplished by measuring the important process parameters and by performing appropriate adjustments in the system commands; through this a CLM system is formed. The elements necessary to form an efficient CLM system are an operational strategy or model that establishes acceptable limits of variability and the appropriate response when these conditions are exceeded, a means of measuring change within the process, plus a mechanism for inputting the necessary corrective response. Three types of measurements exist in CLM systems serving three types of closed-loop in the manufacturing systems. Compared with in situ measurement and remote measurement, in-process measurement, commonly used for process control loop, has the benefits of being able to monitor manufacturing process in real time when a significant alteration has occurred within a manufacturing cycle. In process measurement can be used in two ways: process control (monitor key process parameters) and process qualification (monitor workpiece form/dimension acceptance). The data collected in both practices can be used in statistical analysis to improve manufacturing processes.

Error measurement and prediction are intricately interwoven; therefore, they could be considered and treated together as error prediction procedure. MTAEC phases could be divided into two broad categories. One is offline approach where the error is measured either before or after a machining process and the same is used to alter or re-calibrate the process during subsequent operations. This category assumes that the entire process of machining and measurement is highly repeatable. The other method known as online error compensation does not assume process repeatability. In online error compensation, the error as monitored during the machining process is used to alter the process during the same operation. The latter is conducted continuously when the machine is in operation to constantly correct for the inaccuracies. The advantage of this method is that a higher grade of accuracy could be achieved in a relatively lower grade machine tool through the use of error compensation techniques [7, 8]. This is desirable in industry today as it involves a combination of high accuracy, low cost and high production rate. To enhance the machine tool accuracy by compensation technique, it is preferred to measure the error of the machined part directly under

cutting conditions and correct the deviated tool path online. Unfortunately, it is very difficult to measure part error in real-time due to lack in dedicated probe

5. REFERENCES

- [1] Yaoyao, Z.: *An Integrated Process Planning System for Machining and Inspection*. Chemical and Process Engineering. University of Auckland, 2009.
- [2] Barkman, W. E.: *In-process Measurement*, in *Handbook of Industrial Automation*, E.L.H. Richard L. Shell, Editor. 2000, Marcel Dekker: New York.
- [3] Barkman, W. E.: *In-Process Quality Control for Manufacturing*. 1989: New York : M. Dekker.
- [4] Jesse, C.: *Process Controlled Manufacturing at Pratt & Whitney*. Society of Automotive Engineers transactions, 2001. 110(01): p. 227-232.
- [5] Kim, K. D., Chung, S. C.: *Synthesis of the measurement system on the machine tool*. International Journal of Production Research, 2001. 39(11): p. 2475-2497.
- [6] Kamath, R.: *On-Machine Inspection and Acceptance (OMIA)*. 2000, Master of Engineering Thesis, University of Missouri-Rolla, USA.
- [7] Ramesh, R., Mannan, M. A. and Poo, A. N. (2000a) 'Error compensation in machine tools – a review Part I: geometric, cutting-force induced and fixture dependent errors', International Journal of Machine Tools & Manufacture, Vol. 40, pp.1235–1256.
- [8] Ramesh, R., Mannan, M. A. and Poo, A. N. (2000b) 'Error compensation in machine tools – a review part II: thermal errors', International Journal of Machine Tools & Manufacture, Vol. 40, pp.1257–1284.
- [9] Yuan, J. and Ni, J. (1998): 'The real-time error compensation technique for CNC machining systems', Mechatronics, Vol. 8, pp.359–380.
- [10] Slocum, A. H. (1992): 'Precision machine design', Society of Manufacturing Engineers, Michigan.
- [11] Samir M., Tunde O. (2010): *A review of machine tool accuracy enhancement through error compensation in serial and parallel kinematic machines*, Int. J. Precision Technology, Vol. 1, Nos. 3/4.

Authors:

Dragan Lazarevi, Higher Technical School of Professional Studies Zvečan,

Prof. dr Bogdan Nedi, Faculty of Engineering University of Kragujevac,

E-mail: lazarevicddragan@yahoo.com
nedic@kg.ac.rs

Acknowledgments: This paper is part of project TR35034 The research of modern non-conventional technologies application in manufacturing companies with the aim of increase efficiency of use, product quality, reduce of costs and save energy and materials, funded by the Ministry of Education, Science and Technological Development of Republic of Serbia

Mitrovi , S, Dimi , Z, Vidakovi , J, Lutovac, M, Kvrqi , V.

SYSTEM FOR SIMULATION AND SUPERVISION OF ROBOTIC CELLS

Abstract: Flexible and user-friendly virtual environment, Lola Robot Simulator, was developed to simulate and supervise robot cells. 3D graphic visualisation of robots and their environment, automatic and manual movement of virtual robot axes and end-effector trajectory tracing are implemented through open-source tools on Linux platform. In this paper, a short presentation of the Lola Robot Simulator will be given, with emphasis on main features of the system. Lola Robot Simulator was successfully applied to a robot cell comprised of two industrial robots – “Lola15” and “Lola50” and a track guided vehicle “Robo1000”.

Keywords: 3D virtual robot model, simulation, program verification.

1. INTRODUCTION

The state-of-the-art robot programming methods in industrial applications are tedious and time-consuming tasks that require technical expertise. As stated in [1] robot programming represents the main obstacle for utilization of robots in machining applications, especially in small and medium-sized enterprises (SMEs). Robot programming, as well as any other type of programming, is error-prone process that can result in unwanted effects. It is hazardous to use unverified and untested robot programs, since property damage and personal injuries may occur. Finding skilled personnel, capable of operating industrial robots is the main difficulty for SMEs.

In an attempt to facilitate tasks of robot programmers and operators and to make robot programming a less daunting task, a flexible 3D virtual environment for simulation and verification of robot programs was developed using open-source tools. Robot simulation is very important in modern industrial applications [2], [3]. There are modern specialised CAD/CAM systems for robots, such as the Robotmaster [4], Robot Studio [5], and others.

The state-of-the-art virtual robots can be classified into three main types: (i) virtual robots in CAD/CAM systems, (ii) virtual robots in control systems, and (iii) virtual reality robots [6]. The subjects of our study are virtual robots integrated in control and programming systems.

From the vast variety of available open-source software, only few were used in the design of the proposed system – OpenGL [7], OmniORB [8], [9] and QGLViewer [10]. OpenGL has already found its place in production engineering, especially in the area of graphical modelling of machine tools and robots [11], [12]. EMC2 [13], a modern open-architecture control system for machine tools and robots relies on OpenGL-based 3D simulation environment.

Developed system consists of online and offline module. Online module is integral part of robot control system and works in real-time, while the robot is active. Offline module is used for simulation and

verification of robot programs and is independent from the robot. Both modules utilize virtual graphical environment for visualisation of robot models and their surroundings.

2. VIRTUAL MODEL

It wasn't possible to use some commercially available 3D CAD/CAM software (Dassault Catia, SolidWorks) for development of desired models since graphical models needed to be application independent and highly customizable. Therefore, implemented 3D robot and environment models were all made using OpenGL.

2.1 OpenGL

OpenGL stands for “Open Graphics Library” and represents a set of software tools that enable the user to interact with computer's graphics hardware. Virtual scene and virtual camera are the basic concepts that are integrated into OpenGL. Available graphical primitives (points, lines and triangles) are defined and placed on the scene by using adequate mathematical operations. The virtual camera is positioned and oriented towards the objects on the scene. After rendering through OpenGL pipeline, the final result is displayed on the computer screen, as an image of a virtual scene that is generated through the virtual camera.

2.2 Robot model

Using only OpenGL points, lines and triangles for modelling of an object as complex as an industrial robot showed to be unwieldy. Special primitive objects (sphere, prism, cone, pyramid, cylinder etc.) were constructed and used as building blocks, to avoid unnecessary complexity of the modelling process. Accurate, interactive 3D graphical representation of a real industrial robot was made by combining primitive objects.

Modelling of a virtual robot was done in steps, segment at a time. All segments were dimensioned according to the blueprints (technical drawings) of the robot. Modelling approach is described in Fig. 1.

After the modelling was complete, kinematic relations and constraints were defined for every segment of the virtual robot. C++ was used for this operation. Also, coordinate systems were assigned to segments in correspondence with Denavit-Hartenberg parameters. Virtual and real robot possess identical kinematic structure. Virtual robot is not able to move in a way which is impossible for a real robot.

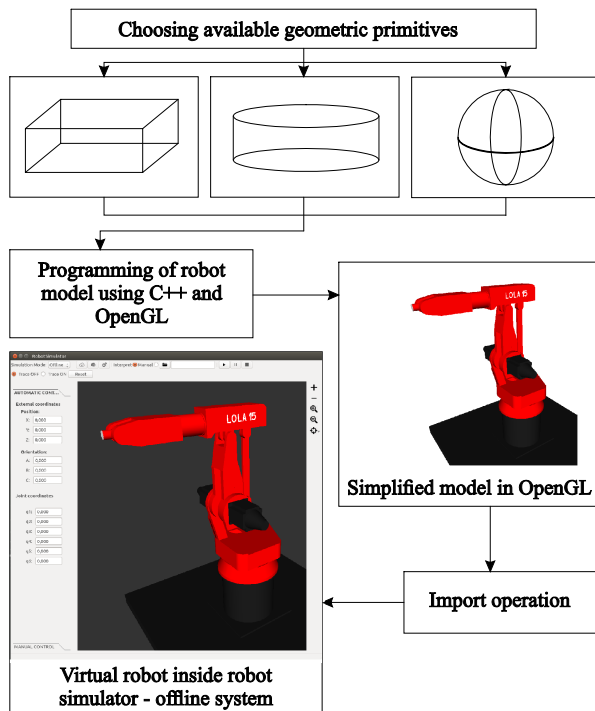


Fig. 1: Algorithm for creation of virtual model.

The core of the simulator is universal, which enables the user to work with different robot models or different machines. Every model must have its own header file with correct kinematics parameters – lengths of segments, ratios for transmissions used in joints and calibration parameters. Once the model and the headers are compiled in C++, simulation can be started by running the application. Developed model of a robot cell is shown in Fig. 2.

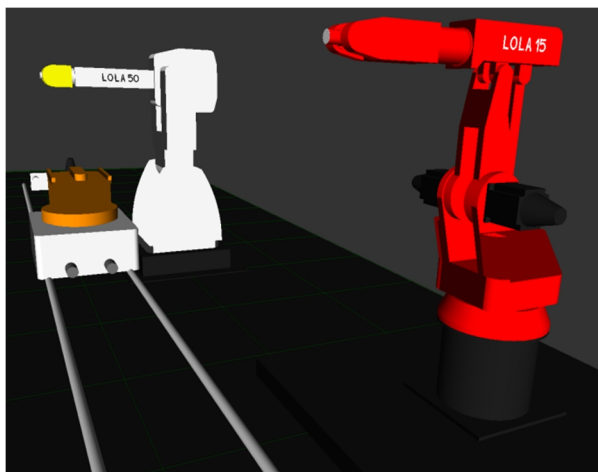


Fig. 2: Supervision module with robots "Lola15", "Lola50" and guided vehicle "Robo1000".

3. SOFTWARE SYSTEM

3.1 Online (supervision) module

Online module acts like an extension of the control system. Online module encompasses 3D graphical environment, which enables visualization of a selected robot or an entire cell. The 3D model of the selected robot moves on the screen in accordance to the feedback received from the motor encoders of the real robot. Therefore, if the real robot moves in a certain pattern, the virtual robot must move in the same way during the execution of the robot program. Described behaviour enables the online module to be used as a tool for remote supervision of a selected robot.

3.2 Offline module

Offline module, or simulation module, is part of the system that is used for testing and verification of robot programs. It doesn't require a link to the robot control system to function properly and it can operate on any PC.

In general, robots are programmed using special robot languages. In this case, LOLA-IRL (Industrial Robot Language) was used. Language compiler generates object code file. Object code file represents input for the simulation system.

To start a simulation, one must first select and import desired robot model onto the scene, shown in Fig. 3.

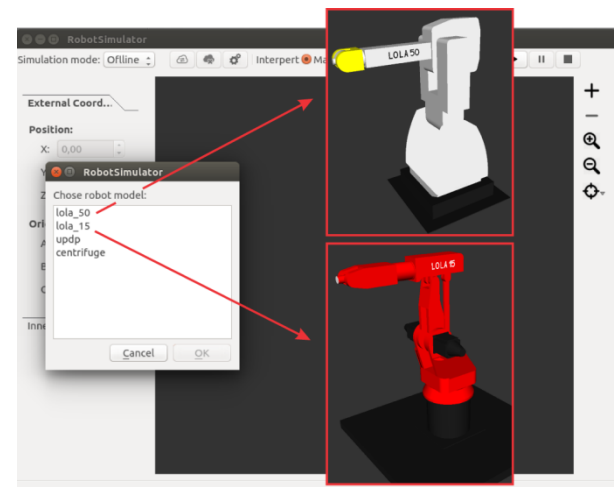


Fig. 3: Selection of available 3D robot models.

Then, object code is loaded for the selected robot. Simulation module moves segments of the virtual robot in accordance to the instructions from the object code (Fig. 4). This manner of operation enables the user to detect possible unwanted events or irregularities in the robot code in virtual environment, without the danger of causing damage or harm. To further simplify the task of program verification, a trace function was added to the simulation module. This function draws trajectory of the robot end-effector during the simulation of the given robot code, which aids detection of programming errors. In case that error was detected, user must correct it in robot source code, recompile and restart the simulation with new object code.

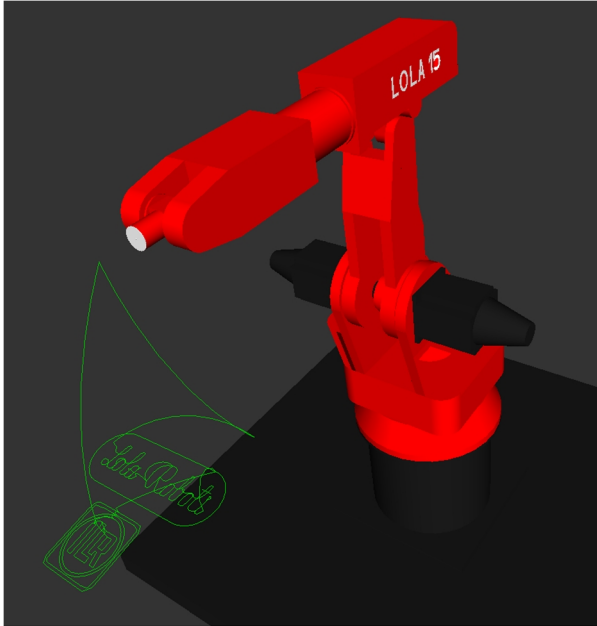


Fig. 4: Lola15 with trace of tip after simulation.

4. SYSTEM VERIFICATION

New system was tested with six axis vertical robots, “Lola15” and “Lola50”, at the Laboratory for machine tools and robotics of Lola Institute from Belgrade.

Real-time Linux Ubuntu is installed on PC robot control units, together with the robot control software and online (supervision) software module. Simulation software is installed on a remote PC, since the connection with the robot is not necessary for simulation of robot programs.

When the compiled object code is supplied to the robot control system, execution of the program can begin. The process may be tracked by looking at the real robot or by looking at the virtual model on the computer screen. The movements are identical.

4.1 Hardware

Hardware base for the developed system is a high performance PC. Necessary addition to a stock PC configuration are “motenc” PCI cards, which control robot’s servo motors. Specially developed, external watchdog timer monitors the communication channel between the control system and motor drivers. Watchdog is set up to momentarily stop the robot if the control system fails.

Software base for the control system is real-time version of Linux Ubuntu OS. Open-source real-time operating system offers high performance, suitable for (robot) control tasks, while it is flexible enough to enable quick and fairly simple means of control software customization. Real-time operating system is configured to prioritize control tasks and to classify user-based interrupts as lower priority. This configuration increases robustness of the control system. The whole control system is enclosed in electrical cabinet of the industrial robot. User interface consists of standard computer monitor, keyboard and a mouse.

4.2 Software

Core of the system is robot control software, based on OROCOS [14] platform. Online module can be installed directly on the PC control unit, besides OROCOS, or it can be installed on remote real-time workstation, where it can be used for supervision. Since this is distributed control system, consisting out of few different segments, implementation of a common object request broker architecture (CORBA) is a must.

OmniORB is an open-source version of the CORBA protocol that was used. CORBA protocol is technology of distributed objects, which enables programming language independence. CORBA represents a concept which enables different parts of the same application to be run on different computers, to be written in different programming languages and still be able to run together as one application or service. ORB (Object Request Broker) is the central part, which handles the communication between the objects (Fig. 5).

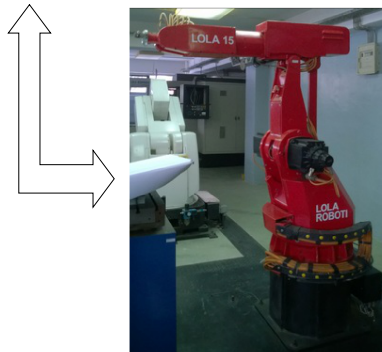
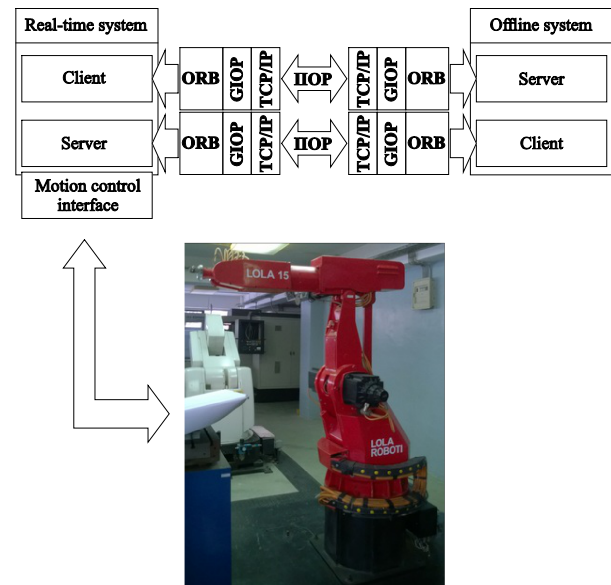


Fig. 5: Description of OmniORB interface.

In this case, CORBA enables the communication between the core of the robot control system and the online supervision software module, since they are not written in the same programming language and are not integrated within one application.

QGLViewer is used for interaction with virtual graphical environment. It enables commands like panning, rotation and zooming of the 3D models. During model development, it simplifies attaching coordinate systems to robotic segments and definition of kinematics parameters.

4.3 Verification

For the sake of simplicity, only experiment conducted on “Lola15” will be described (Fig. 6), since the techniques used are the same for both robots.

Procedure starts with robot source code, written in Lola-IRL. After source code is compiled, resulting object code is input into offline system. Simulation is

run and if no errors are found, the object code is safe for implementation on the real robot.

Verified object code is then loaded into PC robot control system. At the start of the code execution, virtual robot on the screen and real robot simultaneously start performing in a way that was previously seen during simulation. At the end of the program, robot is in standby mode and is awaiting instructions. Online supervision system must be refreshed (in order to delete end-effector traces from the previous run) and it is ready for the next task.



Fig. 6: Vertical six-axis industrial robot "Lola15"

5. CONCLUSION

Main goal of this paper is to present a new approach to modelling, simulation and supervision of robots and robotic cells, by utilizing universal hardware and open-source software. Robot models built using OpenGL were presented. Background (supporting) technologies were discussed – OmniORB and QGLViewer, together with C++ programming language, which was used as an integration method. Developed offline system for robot programs verification and online system for robot supervision were demonstrated. The system as a whole simplifies robot programming process and aids the programmer in generating error-free code, thus reducing the risk of potential damage or harm caused by a flaw in a robot program.

Further research and development of the presented system is geared towards simultaneous supervision of multiple robots, collision detection and cooperation of two robots.

This paper is a part of research that is supported by the Ministry of Science and Technological Development of Serbia, number TR35023.

6. REFERENCES

[1] Neto, P.; Mendes, N.; Araújo, R.; Pires, JN. Moreira AP. *High-level robot programming based on CAD: dealing with unpredictable environments*,

Industrial Robot: An International Journal 39.3 (2012), pages 294-303.

- [2] Milutinovic, D.; Slavkovic, N.; Zivanovic, S.; Glavonjic, M.: *Low-cost control and programming system for five-axis machining by articulated robots with 5 and 6 dof*, Proceedings of 5th International Conference on Manufacturing Engineering ICME, Thessaloniki - Greece, 2014, pages 133-142.
- [3] Živanovi, S.; Dimi, Z.; Slavkovi, N.; Milutinovi, D.; Glavonji, M.: *Configuring of virtual robot for machining and application in off-line programming and education*, Proceedings of 1st International Scientific Conference on Mechanical Engineering Technologies and Applications COMETA, Jahorina, B&H, 2012, pages 125-132.
- [4] Robotmaster. URL: <http://www.robotmaster.com/>
- [5] RobotStudio. URL: <http://new.abb.com/products/robotics/robotstudio>
- [6] VR URL: www.instantreality.org
- [7] Dave Shreiner, Graham Sellers, John Kessenich, Bill Licea-Kane – *OpenGL Programming Guide*, Eighth Edition, ISBN: 978-0-321-77303-6
- [8] Lutovac, M., Dimi, Z., Ferenc, G., Vidakovi, J., Kvrgi, V.: *Distribuirani sistem za kontrolu robota korišćenjem CORBA protokola*, Lola Institut, Beograd.
- [9] Greg Ippolito - CORBA, C++ and Linux, YoLinux.com, <http://www.yolinux.com/TUTORIALS/CORBA.html>
- [10] QGLViewer URL: <http://www.libqglviewer.com>
- [11] Živanovi, S., Glavonji, M., Dimi, Z.: *Konfigurisanje virtuelne mašine troosne glodalice sa paralelnom kinematikom za simulaciju i verifikaciju upravljanja i programiranja*, INFOTEH – Jahorina, Vol. 11, March 2012, pages 464 – 469.
- [12] Rong Shean L., Yan Hong L.: *Development of universal environment for constructing 5-axis virtual machine tool based on modified D-H notation and OpenGL*, *Robotics and Computer, Integrated Manufacturing*, issue 26, 2010, pages 253 – 262.
- [13] EMC2 URL: <http://www.linuxcnc.org/index.php/english/about/>
- [14] OROCOS URL: <http://www.orocos.org/>

All URLs functionality checked on 16.7.2015.

Authors: Mitrovi Stefan, research trainee, Dimi Zoran, research assistant, Vidakovi Jelena, research assistant, Lutovac Maja, research assistant, Kvrgi Vladimir, senior research fellow, Lola Institute Ltd, Kneza Višeslava 70a, 11030, Belgrade, Serbia.

Phone: +381 11 254 64 23

Fax: +381 11 254 40 96.

E-mail: stefan.mitrovic@li.rs; zoran.dimic@li.rs; jelena.vidakovic@li.rs; maja.lutovac@li.rs; vladimir.kvrgic@li.rs

AN IMPROVED MODEL FOR DETERMINING THE THERMAL PRELOAD OF BALL BEARINGS WITH ANGULAR CONTACT

Abstract: Development high speed spindle is conditionally development high speed bearings. New bearings with ceramic balls (hybrids bearings) for support main spindle have minimal increasing temperature up ensuring sufficient main spindle stiffness. Although high bearing temperatures are one of the main factors in bearing failure, the increase of heat in the spindle affects machine errors. This paper presents an improved approach for determining thermal preload of the ball bearings with angular contact. Unlike previous research mathematical model presented in this paper is taken into account the contact angle changes under the influence of thermal deformations, preload and inertial force (centrifugal force and gyroscopic moment). Based on results presented in this paper can be concluded that thermal expansion element bearings is significantly affected by the increase in preload, on the one hand. On the other hand it can be concluded that the increase in the preload and radial stiffness compensates by the influence of inertial forces.

Key words: Ball bearing, Bearing stiffness, Thermal preload

1. INTRODUCTION

Mechanical and thermal processes within the bearing are mutually dependent. This connection is manifested through thermal expansion of the components and the change of mechanical characteristics due to heat flow through the bearing. While the bearings are working, a change in temperature occurs, due to the friction between the ball and the raceway. The heat generated changes in time, which causes thermal expansions on balls and the rings [5]. Thermal expansion causes the change of the contact load in the bearing, which changes and affects the boundary conditions such as heat developed, the thermal contact conductivity, dynamic stiffness, damping properties and etc. The initial negative clearance creates initial contact loads on the raceway of the bearing. As the thermal gradient changes along the radial direction with time and working conditions, leads to increase contact loads, which influence on the increase in preload.

The contact forces within the bearing consist of four interconnected components: initial axial preload, thermal preload, external load and the inertial force (e.g. centrifugal force). Thermal growth on the spindle shaft, housing and bearings causes a change in preload, which is related to friction, static and dynamic stiffness of the bearing. The increase of heat on these elements creates additional thermal load of the bearing, also known as thermal preload [5].

This paper presents the mathematical model (thermal expansion model) for determining the thermal preloading of ball bearings with angular contact bearings for support of the spindles for machine tools. This mathematical model has been based on the work of Lin et al. [5], while the model in this paper has been expanded in order to account for the contact angle changes under the influence of thermal deformations,

preload and inertial force (centrifugal force and gyroscopic moment).

2. THERMAL EXPANSION MODEL-THERMAL PRELOAD

Typically, bearing preload can be established as the sum of initial preload and thermally-induced preload. The initial preload in these cases consists of the internal contact forces which occur during the installation of the bearing on the shaft and housing, including lock nut loads. The thermal preload generally depends on uneven expansion of the bearing components, because the heat generation inside the bearing causes different operating temperatures. The increase of temperatures of the outer ring/the housing/distance ring, inner ring/spindle shaft, and balls due to heat generated in the bearings, causes the expansion of distance rings, balls and spindle shaft in axial and radial direction, resulting in thermal preload.

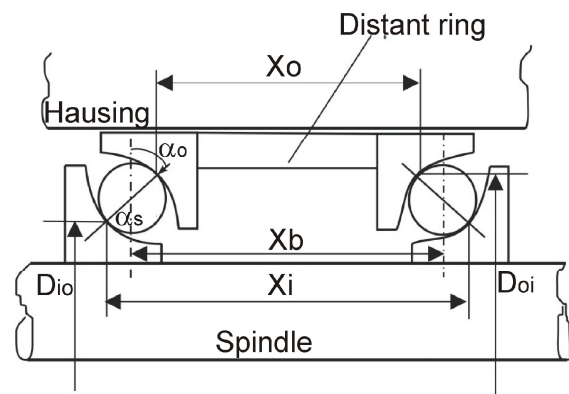


Fig. 1. Components of thermal preload of the bearing

Based on the temperature field obtained by computer analysis or experimental tests it is possible to

define a mathematical model to determine the increase of the preload due to thermal expansion of the bearing elements. In Figure 1 shows the size required for the determination of the thermal preload of the bearings with angular contact.

Thermal expansion of the inner and outer ring in radial and axial directions, as well as the thermal expansion of the ball can be presented as:

$$\delta_{\varepsilon R} = \frac{1}{2} \alpha_s [D_{io}(\Delta T_{ir}) - D_{oi}(\Delta T_{or})] \quad (1)$$

$$\delta_{\varepsilon A} = \alpha_s [x_i(\Delta T_i) - x_o(\Delta T_o)]$$

$$\varepsilon_b = \frac{1}{2} \alpha_b d_b \Delta T_b$$

where α_s is the coefficient of linear expansion of the spindle shaft and rings, α_b is the coefficient of the linear expansion of the ball, T_{ir} and T_{or} are the temperature difference of the inner ring and outer ring, respectively, T_i and T_o are the temperature difference of the shaft and housing/distant ring respectively, while D_{io} and D_{oi} are the inner diameters of the outer ring and outer diameter of inner ring, respectively.

The distance of the contact point between the paired bearings of inner and outer rings x_i and x_o would be [5]

$$x_i = x_b + \frac{1}{2} d_b \sin \alpha_i \quad (2)$$

$$x_o = x_b - \frac{1}{2} d_b \sin \alpha_o$$

The contact angles with the outer (α_o) and inner raceway (α_i) can be determined from [5] as:

$$\tan \alpha_{oj} = X_{1j} / X_{2j} \quad (3)$$

$$\tan \alpha_{ij} = (A_{1j} - X_{1j}) / (A_{2j} - X_{2j})$$

In accordance with Figure 2, while taking into account the contact angle after applying the initial preload the radial (A_{2j}) and axial distance (A_{1j}) between the position of raceway curvature centers is:

$$A_{1j} = A_N \sin \alpha_p + u_x + \theta_y R_i \sin(\psi_j) \quad (4)$$

$$A_{2j} = A_N \cos \alpha_p + u_y \cos(\psi_j)$$

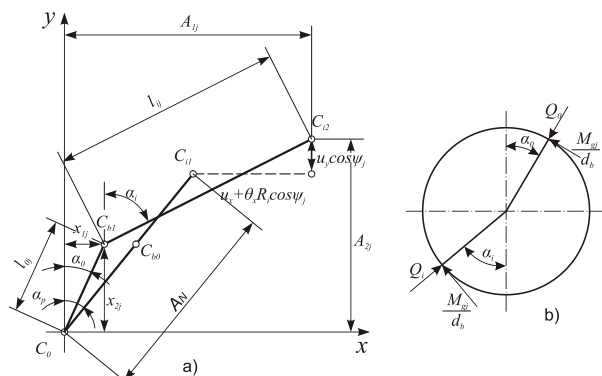


Fig. 2. (a) Position of raceway curvature centers, (b) Ball loading at angular position ψ_j

While under effect of inertial forces on the ball, and due to difference in contact angles between the ball and the raceway, the line of action between the raceway

groove curvature centers will not be collinear, as can be seen on Figure 2a. On Figure 2a, it is assumed that the outer raceway groove curvature center (C_o) is fixed in space, and that the center of inner raceway groove curvature (C_i) is relatively moved when compared to the fixed center. From Figure 2a, the equation of kinematic constraints between the ball and the raceway can be established:

$$[A_{1j} - X_{1j}]^2 + [A_{2j} - X_{2j}]^2 + l_{ij}^2 = 0 \quad (5)$$

$$X_{1j}^2 + X_{2j}^2 + l_{oj}^2 = 0$$

Ball equilibrium equation from Figure 2b is:

$$Q_{oj} \cos \alpha_{oj} - Q_{ij} \cos \alpha_{ij} - \frac{M_{gj}}{d_b} (\sin \alpha_o - \sin \alpha_i) - F_{cj} = 0 \quad (6)$$

$$Q_{oj} \sin \alpha_{oj} - Q_{ij} \sin \alpha_{ij} + \frac{M_{gj}}{d_b} (\sin \alpha_o - \sin \alpha_i) = 0$$

The method of determining the centrifugal force and gyroscopic moment is shown in papers [3], [4] in greater detail.

The relation between Hertz's contact forces and contact deformation for each point of contact with the inner/outer raceways can be written as [1]:

$$Q_{i,o(j)} = K_{i,o} (\delta_{i,o}^{3/2})_j \quad (7)$$

The formulation of Hertz's contact stiffness ($K_{i,o}$) is available in [2].

Four parameters X_{1j} , X_{2j} , $\delta_{i(j)}$, $\delta_{o(j)}$ were obtained by solving the relations (5), (6) through the use of Newton-Raphson's method for every position of the ball, with the assumed values of relative ring displacement (u_x , u_y , u_z). Permissible error with Newton-Raphson's iterations is 10^{-12} . Then, from the equation (3) can be determined by new the contacts angle with the outer and inner raceway.

Total thermal deformation of the bearing in the direction of the line of contact can be determined as the following, with the condition that the contact angles with the inner and outer raceway change because of thermal expansion of the rings and balls, and that $2 \alpha_p = \alpha_o + \alpha_i$ [9]:

$$\Delta_T = \varepsilon_b + \delta_{\varepsilon R} \cos\left(\frac{\alpha_o + \alpha_i}{2}\right) - \delta_{\varepsilon A} \sin\left(\frac{\alpha_o + \alpha_i}{2}\right) \quad (8)$$

Based on the aforementioned, thermal preload can be calculated as:

$$F_{p,T} = \left(\left(\frac{1}{K_i} \right)^{2/3} + \left(\frac{1}{K_o} \right)^{2/3} \right)^{-3/2} \cdot \Delta_T^{1.5} \quad (9)$$

3. RESULTS

Analysis of the thermal preload is done for hybrid angular contact ball bearing SKF 7011 CDGA/HC P4. in a "0" arrangement The bearings are with lock-ring preload. The initial preload is 194 N. Characteristics analyzed bearings are given in Table 1. The analysis was performed in the range of 0 to 6000 rpm.

The heat source assumption is used from Ref. [9]. The temperature information needed for Eqs. (1) are obtained from a thermal model by Zivkovic et al. [9,10].

Outer ring [mm]	90
Inner ring [mm]	55
Ugao dodira [°]	15
Initial preload [N]	194
Axial stiffness [N/μm]	61.9
Radial stiffness [N/μm]	386
No. of balls	18
Diametar of the ball [mm]	11.11

Table 1. Characteristics bearings SKF 7011 CDGA/HC P4

The predicted change of thermal preload for different rotation speeds and 3000 N in radial load has been shown in Figure 3. Thermal preload abruptly increases for the first 20 min. of operation, only to later incrementally decrease until it reaches stationary state. In stationary thermal state for 6000 rpm the increase in preload is 22 %, while for 2000 rpm there is practically no change in preload compared to the initial value.

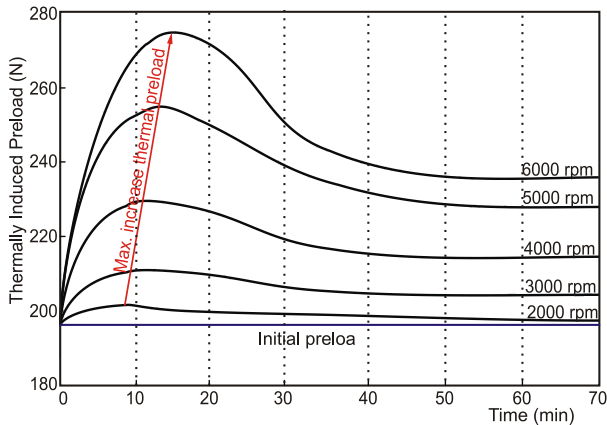


Fig. 3. Prediction of thermal preload of the bearing

Based on thermal analysis, it can be concluded that in initial conditions a large part of generated heat transfers between the balls due to the small mass of balls compared to the other elements.

Thus, the temperatures of the balls are larger than the temperatures of the raceways. As time passes, the larger amount of generated heat goes through the housing and the spindle, and the temperature between the balls and the raceways decreases. All of this causes larger or smaller changes of the bearing elements.

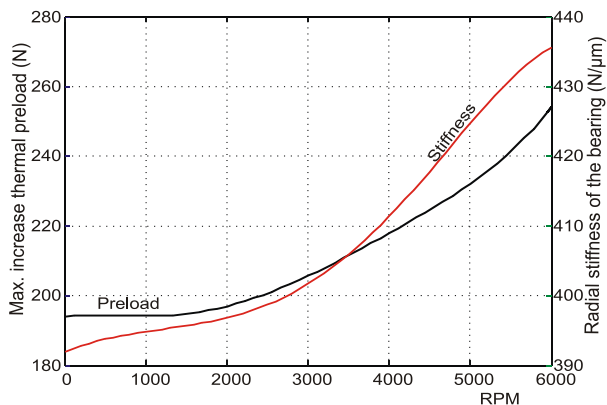


Fig. 4. Maximum thermal preload and radial stiffness of the bearing

By taking the maximal increase in preload from Figure 3, the change in radial bearing stiffness has been determined for different rotation speeds. From Figure 4, it can be seen that the initial preload of the bearing is 194 N when the spindle does not rotate with the corresponding stiffness of 392 N/μm.

Preload then increases to 274 N, as shown in Figure 4, for 6000 rpm with the stiffness of 435.6 N/μm. As the result of increase in maximal thermal preload by 41.23 % for 6000 rpm, the bearing stiffness increases by 11 %.

Finally, after reaching the stationary thermal state, the bearing elements' expansion is nearly constant, therefore it can be said that the change in preload for stationary thermal state is negligibly small. Similar non-stationary change in preload and stiffness has been established in papers [5, 6, 7], as well.

On the other hand from the Figure 5, it can be concluded that increasing the number of revolutions causes a significant decrease in of radial stiffness of the bearing due to inertial force.

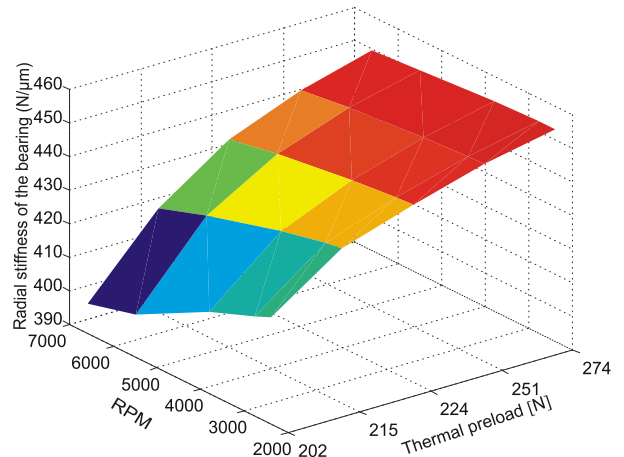


Fig. 5. Change of radial stiffness depending on the number of revolutions and thermal preload

There are two main reasons for the reduction in bearing stiffness due to the inertial forces. The first reason is because the centrifugal forces reduce the contact load between rolling elements and the inner and outer ring. Since the Hertz's contact stiffness is proportionally to contact load, stiffness of outer raceway will be declining while the stiffness of the inner raceway will grow with an increase of the number of revolutions. Another reason for the decrease of stiffness lies in the fact that due to the inertia force there is a difference in contact angle between rolling elements and outside and inside ring.

4. CONCLUSIONS

This paper presents a new approach for determining the thermal preload of ball bearings with angular contact. The thermal expansion of bearing elements causes changes of contact forces and deformations, which directly affects of the contact angle change and increasing preload of the bearings, also known in literature as thermal preload. On the other hand, the increase in preload and stiffness caused by thermal

expansion are compensated due to the effect of inertial forces.

Based on the analysis in this paper, can be concluded that, the rotational speed, boundary conditions and inner construction of the bearing have a significant influence of the thermal preload behavior.

It must be noted here, that the described behavior depends on the arrangement of the bearings and on the operational conditions, as well as on the configuration of the spindle. The previous analysis is applicable exclusively for lock-ring preload bearings.

Acknowledgments: In this paper some results of the project: *Contemporary approaches to the development of special solutions related to bearing supports in mechanical engineering and medical prosthetics* – TR 35025, carried out by the Faculty of Technical Sciences, University of Novi Sad, Serbia, are presented. The project is supported by the Ministry of Science and Technological Development of the Republic of Serbia.

5. REFERENCES

- [1] Harris T. A, Michael, N. K.: *Rolling bearing analysis: Advanced Concepts of Bearing Technology*, Taylor & Francis Group, 2007.
- [2] Harris T. A, Michael, N. K.: *Rolling bearing analysis: Essential Concepts of Bearing Technology*. Taylor & Francis Group, 2007.
- [3] Jang G, Jeong S-W: *Vibration analysis of a rotating system due to the effect of ball bearing waviness*. Journal of Sound and Vibration 269 (3–5):709-726, 2004.
- [4] Li H, Shin Y. C: *Integrated dynamic thermo-mechanical modeling of high-speed spindles, part 1: Model development*, Journal of Manufacturing Science and Engineering, Transactions of the ASME 126 (1):148-158, 2004
- [5] Lin C.W, Tu J.F, Kamman J.: *An integrated thermo-mechanical-dynamic model to characterize motorized machine tool spindles during very high-speed rotation*. International Journal of Machine Tools and Manufacture 43 (10):1035-1050, 2003
- [6] Stein J. L, Tu J. F.: *State-space model for monitoring thermally induced preload in anti-friction spindle bearings of high-speed machine tools*. Journal of Dynamic Systems, Measurement and Control, Transactions of the ASME 116 (3):372-386, 1994.
- [7] Takabi J, Khonsari M. M.: *Experimental testing and thermal analysis of ball bearings*. Tribology International 60 (0):93-103, 2013
- [8] Zivkovic, A.: *Computer and experimental analysis of behaviour ball bearings for special applications*, Doctoral dissertation, Faculty of technical sciences, Univesrity of Novi Sad, Novi Sad, 2013.
- [9] Zivkovic, A., Zeljkovic, M. Tabakovic, S., Milojevic, Z.: *Mathematical modeling and experimental testing of high-speed spindle behavior*, Int J Adv Manuf Technol 77: 1071-1086, 2015.

Authors: Doc. dr Aleksandar Živkovi Prof. dr Milan Zeljkovi , Prof. dr Slobodan Tabakovi , M.Sc. Cvijetin Mla enovi , University of Novi Sad, Faculty of Technical Sciences, Department for Production Engineering, Trg Dositeja Obradovica 6, 21000 Novi Sad, Serbia, Phone.: +381 21 485-23-30, Fax: +381 21 454-495.

E-mail: acoz@uns.ac.rs, milanz@uns.ac.rs; tabak@uns.ac.rs; mladja@uns.ac.rs

Tabakovi , S., Živanovi , S., Zeljkovi , M.

THE APPLICATION OF VIRTUAL PROTOTYPE IN DESIGN OF A HYBRID MECHANISM BASED MACHINE TOOLS

Abstract: Designing of products by using of virtual prototypes in modern conditions allows much faster and cheaper selection of elements and optimisation of construction.

The paper presents the application of virtual prototype of manufacturing capabilities verification process in case of machine tools with kinematic structure which is based on O-X hybrid mechanism.

Key words: Virtual prototype, hybrid mechanism, CNC

1. INTRODUCTION

Development of a product with a large number of moving elements, before building of physical prototype, involves various types of analysis of exploitation conditions in the goal of verification and optimisation of conceptual design.

Machine tools with a large number moving components and exploitation in different conditions is a typical representative of this group of products. A key role in the choice of components, in process of its development, has an analysis of the working of machine tools in the operating conditions.

Developing of a virtual prototype using DMU (Digital Mock Up) concept is more often replacing physical prototype and allows the combination of CAD and CAE technology to optimize product [1]. Usage of DMU technology in optimization allows analysis of kinematic parameters through collision detection and singularities in mechanism work and analysis of the workpiece machining borders before making a physical prototype.

This paper describes a part of the research of patented O-X mechanism usage possibilities [2], [3] as a base for machine tools through the analysis of machining characteristic capabilities forms on the workpiece by using DMU technology.

2. CHARACTERISTICS OF THE O-X MECHANISM

The base of virtual prototype is hybrid O-X glide mechanism composed of planar parallel kinematic mechanism and support structure that enables translational movement (Fig. 1). [3]

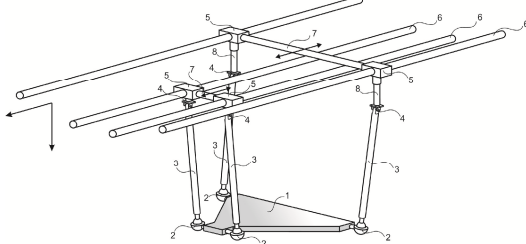


Fig. 1. Planar parallel mechanism

Figure presents planar parallel mechanism whose base is movable platform (1), connected with four struts (3) using spherical joints. Struts are at the other end attached to the sliders (5) over the joints with one rotary degree of freedom (4). Each of sliders can move at own guide (6). Sliders are grouped into pairs that are connected with rigid connection (7) thus providing their same speed and acceleration. In order to increase the autonomy movement of the slider, they are positioned at different distances in the direction of the vertical axis, which allows their passing in the plane, and the duality of movement of the mechanism. That are the movement in the extended (O) and the crossed (X) position. Compensation of differences in the distances between the slider and moving platforms is performed by introducing vertical compensating elements (8), at higher sliders.

Primary specificity of O-X glide mechanism makes the duality of its structure in a plane element. This enables it to work in extended and crossed form. Except this, dimensions of the workspace are larger than similar mechanisms, because of hybrid structure.

The geometric model of parallel mechanism (Fig. 2), which is base of a hybrid O-X glide mechanism, can be presented in a simpler form using of a parallelogram $A'B'C'D'$, which is connected with constant length struts. At the other end the struts are connected with sliders AB and CD, moving on horizontal guides ($D''D, A''A, B''B, C''C$).

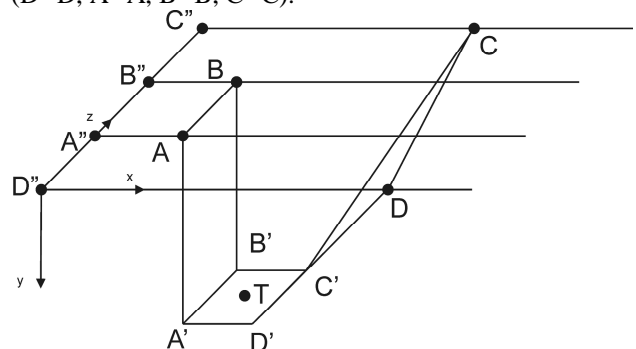


Fig. 2. Simplified geometrical model of a parallel mechanism

Based on the this, we can write vector equations of parallel mechanism

$$\begin{aligned}\overline{OD} + \overline{DD'} &= \overline{TD'} + \overline{OT'} \\ \overline{OA'} + \overline{A''A} + \overline{AA'} &= \overline{OT'} + \overline{TA'} \\ \overline{OB''} + \overline{B''B} + \overline{BB'} &= \overline{OT'} + \overline{TB'} \\ \overline{OC''} + \overline{C''C} + \overline{CC'} &= \overline{OT'} + \overline{TC'}\end{aligned}$$

Assuming that:

$$\begin{aligned}\overline{OD''} &= \vec{0}; & \overline{OA''} &= \begin{pmatrix} 0 \\ 0 \\ a \end{pmatrix}; & \overline{OB''} &= \begin{pmatrix} 0 \\ 0 \\ 2a \end{pmatrix}; \\ \overline{OC''} &= \begin{pmatrix} 0 \\ 0 \\ 3a \end{pmatrix}.\end{aligned}$$

Where is

a – distance between horizontal sliders

In addition, the structure of the planar mechanism imposes certain restrictions:

$$\begin{aligned}\overline{A''A} &= \overline{B''B} \\ \overline{C''C} &= \overline{D''D}\end{aligned}$$

3. KINEMATIC ANALYSIS OF THE O-X GLIDE MECHANISM

3.1 Inverse kinematics

The general expression for inverse kinematic chain is:

$$P_{A,B,C,D} = f(x_T, y_T, z_T)$$

Because of the O-X glide mechanism kinematic analysis is carried out in two configurations.

3.1.1 Extended form

Fig. 3 presents planar projection of extended form of the O-X glide mechanism for which is carried out the inverse kinematic analysis

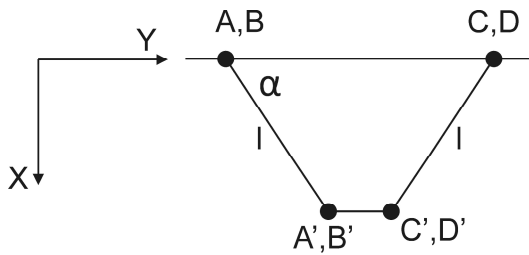


Fig. 3. Planar projection of extended form of O - X glide mechanism

The position of points A and B, can be expressed as follows:

$$\begin{aligned}x_{A,B} &= x_T - \frac{s}{2} - l \cos \alpha = x_T - \frac{s}{2} - l \sqrt{1 - \left(\frac{y_T}{l}\right)^2}, \\ x_{A,B} &= x_T - \frac{s}{2} - \sqrt{l^2 - y_T^2}.\end{aligned}$$

The position of the points C and D in the same manner can be expressed as:

$$\begin{aligned}x_{C,D} &= l \cos \alpha + \frac{s}{2} + x_T = l \sqrt{1 - \left(\frac{y_T}{l}\right)^2} + \frac{s}{2} + x_T, \\ x_{C,D} &= \sqrt{l^2 - y_T^2} + \frac{s}{2} + x_T.\end{aligned}$$

Where are:

- l – length of struts
- s – width of mobile platform
- a – distance between horizontal guides
- α – angle between the struts and horizontal guides

3.1.2 Crossed form

Fig. 4 presents planar projection of crossed form of the O-X mechanism and his inverse kinematic analysis.

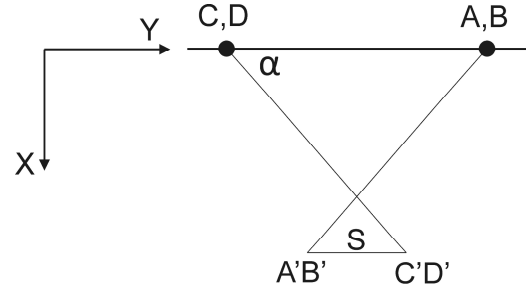


Fig. 4. Planar projection of crossed form of the O-X mechanism

Position of the points A, B, C and D can be expressed as follows:

$$\begin{aligned}x_{A,B} &= x_T - \frac{s}{2} + l \cos \alpha = x_T - \frac{s}{2} + l \sqrt{1 - \left(\frac{y_T}{l}\right)^2}, \\ x_{A,B} &= x_T - \frac{s}{2} + \sqrt{l^2 - y_T^2};\end{aligned}$$

$$\begin{aligned}x_{C,D} &= \frac{s}{2} + x_T - l \cos \alpha = \frac{s}{2} + x_T - l \sqrt{1 - \left(\frac{y_T}{l}\right)^2}, \\ x_{C,D} &= \frac{s}{2} + x_T - \sqrt{l^2 - y_T^2}.\end{aligned}$$

3.2 Direct kinematic

Direct kinematic chain can be expressed as follows:

$$P_T = f(x_A, x_B, x_C, x_D)$$

Generally, the inverse kinematics of parallel mechanisms is quite simple, while direct kinematics often very complex. However, because of simple construction in the case of the O-X glide mechanism direct and inverse kinematics are very simple.

3.2.1 Extended form

Direct kinematics analysis of extended form of the O-X mechanism (Figure 3), explains position of the point T depending on the position of points A, B, C and D can be represented as follows:

$$\begin{pmatrix} 0 \\ 0 \\ a \end{pmatrix} + \begin{pmatrix} x_A \\ 0 \\ 0 \end{pmatrix} + \begin{pmatrix} l \cos \alpha \\ l \sin \alpha \\ 0 \end{pmatrix} = \begin{pmatrix} TA'_x \\ TA'_y \\ TA'_z \end{pmatrix} + \begin{pmatrix} x_T \\ y_T \\ z_T \end{pmatrix}.$$

3.2.2 Crossed form

Similarly as in the previous case, the position of the point T on the movable platform for crossed form of the O-X glide mechanism (Figure 5) can be represented as follows:

$$\begin{pmatrix} 0 \\ 0 \\ a \end{pmatrix} + \begin{pmatrix} x_A \\ 0 \\ 0 \end{pmatrix} + \begin{pmatrix} -l \cos \alpha \\ l \sin \alpha \\ 0 \end{pmatrix} = \begin{pmatrix} TA'_x \\ TA'_y \\ TA'_z \end{pmatrix} + \begin{pmatrix} x_T \\ y_T \\ z_T \end{pmatrix}.$$

4. STRUCTURE OF THE VIRTUAL PROTOTYPE

The final version of the virtual prototype differs from the concept caused by the physical dimensions of the elements of the prototype. In the final version changes in elements such as the position of the slider, length of the struts and the like are introduced. Figure 5 presents adopted solution of the virtual prototype of the hybrid mechanism.

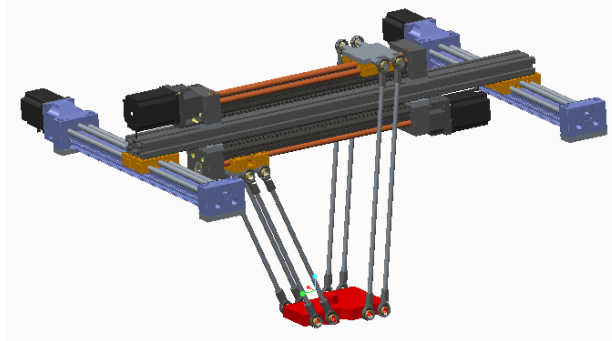


Fig. 5. Virtual prototype of the hybrid mechanism

The virtual prototype which is defined in this way has been subjected to tests that include analysis of capabilities of machining geometric shapes characteristic for the milling. For simulations workpiece with shape based on the NCG recommendations is used.

5. SIMULATION OF MACHINING

Machine simulation by running the program is possible due to the applied modelling of the O-X glide parallel mechanism with all kinematic connections between the components, which allows the motion of a virtual model as a system of rigid bodies.

Fig. 6 shows a detailed virtual prototype of O-X glide parallel mechanism with all kinematic relationships.

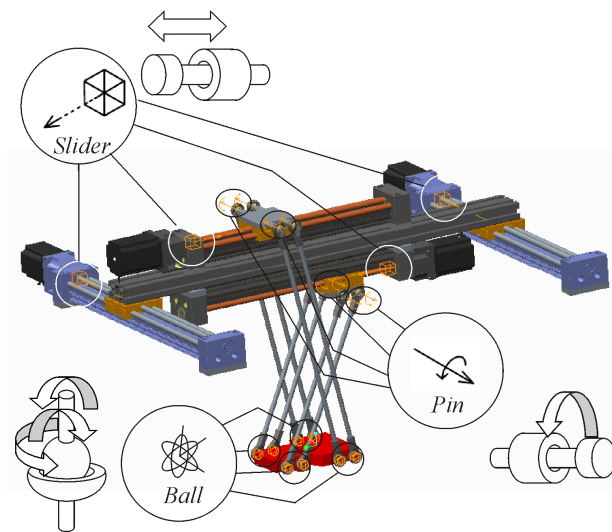


Fig. 6. CAD model for the simulation of parallel mechanism kinematics

This assembly enables the motion of models in the range defined for each connection, which is of particular importance for the identification of possible collisions during the work of the parallel mechanism.

Machining simulation of the virtual prototype allows the motion of movable segments with a tool at the end. The tool path is a result of the execution program obtained by programming using the CAD/CAM system PTC Creo 2.

For the test, a scaled ISO test workpiece whose dimensions are 150×150×40mm is used. Because of the particular shape and size of the workspace of parallel kinematics machines, attention should be paid when setting up a workpiece, which must be within the limits of the workspace of the machine. For the test workpiece shown in Fig. 7, the zero point in the middle of the underside of the workpiece has been adopted, with the coordinate axes x , y , z as has been used in the vertical 3-axis milling machine, marked as MACH_ZERO. The identical zero point exists on the machine (on the working table) on which the workpiece is placed, Fig. 7. Matching these two coordinate systems is accomplished by setting the workpiece on the machine during the machining simulation. Fig. 7 also presents the simulated tool path on the scaled ISO test workpiece, based on the generated CL file. The tool coordinate system is defined in the same way as the workpiece coordinate system and marked as a TOOL_POINT.

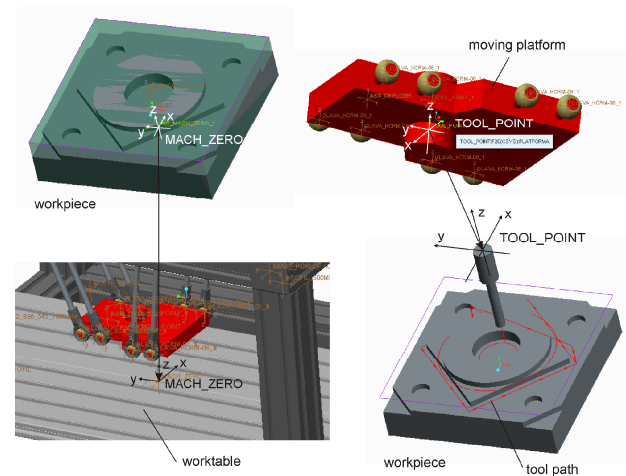


Fig. 7. Coordinate system of the workpiece and tool with tool path simulation

During the simulation of tool paths, a complete prototype of the virtual machine can be included into the simulation, with a machine play option. An example of machine simulation for O-X glide virtual prototype is shown in Fig. 8 for an ISO test workpiece.

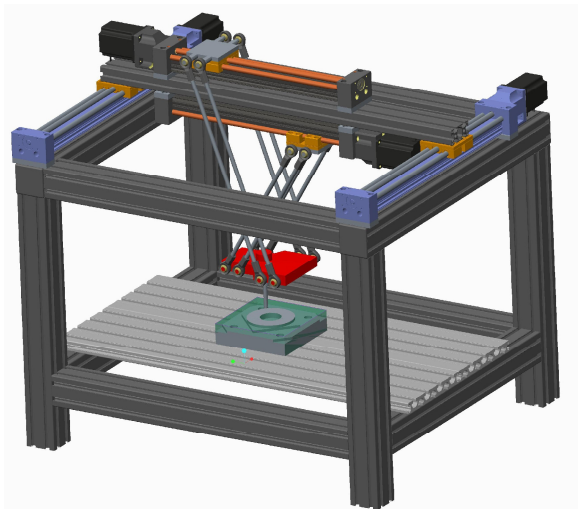


Fig. 8. Machining simulation in the CAD/CAM system

6. RESULTS

Tested workpiece is based on the test workpieces for analyzing of the accuracy of machine tools with numerical control with a three-axis. They could be produced by four characteristic sequence of machining in which had been combined all movements which are expected in the structure of modern machine tools (linear and circular). The dimensions of the workpiece are selected based on the maximum dimensions of the workspace of a parallel mechanism. Results are presented in table 1.

No	Type of moving of the tools/ platform	Successfully completed
1	Face milling, linear movement	
2	Profile milling, linear movement	
3	Profile milling, circular movement 50	
	Profile milling, circular movement 250	
4	Combined milling, linear movement	
5	Combined milling, circular movement 50	
6	Combined milling, circular movement 250	
7	Hole machining	

Tab. 1 Successfulness of machining on virtual machine tool

7. DISCUSSION AND CONCLUSIONS

Conducted research indicates that the virtual prototypes methods application might decrease machine tools development time especially the time needed for the selection of machine components. In addition, analysis of kinematic and dynamic motion parameters and machining capabilities indicate problems that may occur during the machining of pre-defined shapes. This provides a wide range of

possibilities during the design of special type of machines [4] [5].

Present stage of the research identified a number of disadvantages of the initial configuration of machines such as the length and position of the slider struts. All of them were corrected and formed functional virtual prototype. Currently the project is in final stages of building of the physical prototype.

Acknowledgements: In this paper are presented some results of the project: Contemporary approaches to the development of special solutions related to bearing supports in mechanical engineering and medical prosthetics – TR 35025. The project is supported by the Ministry of Science and Technological Development of the Republic of Serbia.

5. REFERENCES

- [1] Altintas, Y., Brecher, C., Week, M., Witt, S.: *Virtual Machine Tool*, CIRP Annals - Manufacturing Technology Volume 54, Issue 2, 2005, Pages 651-674
- [2] Mla enovi C., Tabakovi S., Zeljkovi M.: *Kinematic analysis of machine tool based on O-X glide hybrid mechanism using a symbolic virtual model*, Journal of Production Engineering, Vol. 15, No. 1, Str. 37-40, ISSN: 1821-4932 Faculty of technical sciences;
- [3] Tabakovi, S., Zeljkovi, M., Gatalo, R., Mla enovi, C.: *Ure aj za manipulaciju radnim predmetima ili alatima kod mašina alatki i industrijskih manipulatora*, Glasnik intelektualne svojine, Br. 2/2012, Zavod za intelektualnu svojinu Republike Srbije, Beograd, Broj: 20111243
- [4] Fortunato, A., Ascari, A.: *The virtual design of machining centers for HSM*, Towards new integrated tools, Mechatronics, Volume 23, Issue 3, April 2013, Pages 264-278
- [5] Zivanovic, S., Glavonjic, M., Milutinovic, D.: *Configuring A Mini-Laboratory and Desktop 3-Axis Parallel Kinematic Milling Machine*, Strojniški vestnik - Journal of Mechanical Engineering, Vol.61, No1, pp. 33-42 (2015), DOI:10.5545/sv-jme.2013.1619, 2015.

Authors: Prof. dr Slobodan Tabakovi, Prof. dr Milan Zeljkovi, University of Novi Sad, Faculty of Technical Sciences, Department for Production Engineering, Trg Dositeja Obradovi a 6, 21000 Novi Sad, Serbia, Phone.: +381 21 485-23-30, Fax: +381 21 454-495. E-mail: tabak@uns.ac.rs; milanz@uns.ac.rs;

Doc. dr Saša Zivanovi, University of Belgrade, Faculty of Mechanical Engineering, Production Engineering Department, Kraljice Marije 16, 11120 Belgrade, Serbia, Phone.: +381 11 3302-423, Fax: +381 11 3370-364. E-mail: szivanovic@mas.bg.ac.rs



Anti , A., Šari , T., Miloševi , M.

A MODULE FOR FEATURE EXTRACTION WITHIN THE NEURO-FUZZY SYSTEM FOR TOOL WEAR RECOGNITION

Abstract: The paper presents a model of the developed fuzzy system for tool wear classification. The system comprises of three modules: module for data acquisition and processing, module for tool wear classification, and module for decision-making. The selected method for feature extraction is presented within the module for data classification and processing. The selected model for the fuzzy classifier and classification in experimental laboratory conditions is shown within the data classification and clustering. The proposed model has been tested in longitudinal and transversal machining operations.

Key words: tool wear, feature extraction, signal processing

1. INTRODUCTION

With the development in information technologies and signal processing technologies, a wide specter of on-line sensors has been incorporated in order to receive information relevant for tool condition. Likewise, the obtained information is more and more significant for process control. The signals obtained from diverse sensors have to be transformed into data containing relevant information on the fundamental processes. A large amount of data acquired from multi-sensor systems enables the extraction of diverse features, creating in that manner enough diverse features that are to be used with the purpose of tool condition classification in tool monitoring systems. The development of the monitoring systems that operate in a real time provides the basis for tool condition monitoring in the contemporary automated manufacturing. Qualitative information on the degree of tool wear in the real time presents a necessary requirement for tool durability identification. The acquisition and selection of significant information from a process, by applying the adequate sensors, significantly increases the quality and productivity of the machining process. Apart from a positive influence on the stability of the machining process and the quality of the processed workpiece, this method of processing provides a higher degree of productivity and the maximal tool usability in the sense of a working cycle.

The conventional methods in cutting tool wear monitoring are based on well-known physical principles, as well as the visual, auditory and intellectual abilities of the operator, which are utilized in order to recognize tool wearing. Contemporary intelligent systems for cutting tool wear monitoring are supposed to employ their characteristics to replace and upgrade human drawbacks and provide possibilities in the sense of a continual, fast and precise determination of tool wear condition, leading to the following:

- Increasing the degree of the process system stability, which is especially evident in the

situations of the high degree of wearing and tool breakage;

- Optimization of the processing parameters related to the demanded tool durability, with the considerations of technological process limitations;
- Quality control of the processed surface and demanded dimensional accuracy of the workpiece; and
- Additional rationalization of the production costs.

More intensive research related to the development of “intelligent” systems for cutting tool monitoring began in the 1990s by applying the multi-sensor approach, i.e. wearing classifiers based on the artificial intelligence algorithms. The beginning of the research in the area assumed that the application of these methods should result in the industrially applicable solutions for cutting tool wear monitoring.

2. APPLICATION OF FUZZY SYSTEMS IN TOOL WEAR MONITORING

The combination of diverse signal analyses, several sensor technologies, and artificial intelligence algorithms, based on the fuzzy logic, leads towards the solution that will be able to answer the demands of high performances and provide an adequate solution for tool wear monitoring [1,2]. Fuzzy decision-making is a process of making decisions from a set of insufficiently precise premises. In the last years, most researchers have used fuzzy decision-making systems for tool wear classifications. One of the attempts is presented by Sharma et al. [3] by applying the fuzzy system for tool wear estimation. The defined decision-making rules form a base used for making decisions. The process of fuzzy decision-making includes the membership functions, fuzzy logic operators and if-then rules. The membership function is a curve defining the manner each point in the input information field is positioned in relation to the membership value (or membership degree) between 0 and 1. If the given variable is more susceptible to noise, then its observation field is larger, as well as the membership function width.

3. PROGRAM SOLUTION FOR FEATURE EXTRACTION

On analyzing the diverse presented models, advantages and drawbacks of individual models have been observed, and therefore considered in developing a new model. Having in mind the observed models, the following demands have been set for the development of a new laboratory system:

- Application of the sensor for vibration acceleration measurement in order to detect the dynamic properties of the cutting process better, as well as their implementation into the monitoring system.
- Usage of new artificial intelligence algorithms in the field of tool wear monitoring based on the application of the a priori knowledge on the tool wear condition.
- Finding the adequate methods for input characteristic vector extraction by applying transformations in the time-frequency domain.

Feature extraction is based, according to the authors' knowledge, on a completely new approach comprising the application of the short-time discrete Fourier transform (STFT) over the specter of a determined vibration signal, which is observed as a 2D "image" texture. Time scale is identified as the first dimension, while the frequency scale is the second dimension. The intention is to utilize the influence of differences in the structure of the set segment textures onto the class discrimination of tool wear conditions. Possible changes can occur in the texture shape and properties on certain image segments, yet at the same time with a significantly small number of parameters, in order to obtain the description robustness of the observed processes. The hypothesis, which is experimentally confirmed, is that the dominant physical process of the tool wear condition change is closely related to the structure of the obtained 2D texture after the signal processing by applying the developed method. Based on the above, the application of certain filter banks is proposed, which is widely used in texture recognition problems in order to efficiently extract information in the form of robust features.

The proposed feature selection is based on using the Least Absolute Shrinkage and Selection Operator (LASSO) regression method, proposed by Tibshirani [4], which is widely used in the feature selection tasks [5]. This method finds the optimal features related to the observed data set in order to obtain compromises between the representation error (e.g. square error) and the numbers that are not zero coefficients yet match the most significant functions, which in our case are mostly discriminative. Feature set becomes more robust, even in the case of a limited training data set, based on the conducted experiments.

A majority of features obtained using the 2D method, out of the total number of features selected by the Lasso regression, prove the significance and the robustness of the extracted 2D features in the developed tool wear monitoring systems.

Let $F(x, y)$ be the image texture matching the identified spectrogram STDFT of the observed sensor signal s , where the STDFT is the spectrogram

$|S(k, \omega)|^2$ defined as:

$$S(k, \omega) = \sum_{n=-K/2}^{K/2} s(n)w(k-n)e^{-ikn} \quad (1)$$

where k is a discrete time frame, ω is a discrete time frequency, i.e., discrete frequency of the covered zones, while w is a window sequence used (Hamming function is utilized), with the length K . The discrete time window k , for $k = 0, \dots, k_{\max}$, is identified as the x axis of the image texture, so that $x_{\max} = k_{\max}$. Likewise, ω , for $\omega = 0, \dots, \omega_{\max}$ is identified as the y axis, hence $y_{\max} = \omega_{\max}$. Now, the following stands:

$$F(x, y) = |S(k, \omega)|^2 \quad (2)$$

$$x = 0, \dots, x_{\max}, \quad y = 0, \dots, y_{\max}$$

$$k = 0, \dots, k_{\max}, \quad \omega = 0, \dots, \omega_{\max}$$

All further analyses are conducted over the image texture $F(x, y)$, and are obtained from the above stated procedure; for the reason of simplicity, without the loss of generalization, the continual variables $x \in [0, x_{\max}]$ and $y \in [0, y_{\max}]$ are observed. Then,

$$G(\sigma_1, \sigma_2, \theta, x, y) = \frac{1}{2\pi\sigma_1\sigma_2} e^{(A(\theta)^T [x \ y]) \begin{bmatrix} \sigma_1 & 0 \\ 0 & \sigma_2 \end{bmatrix} (A(\theta) \begin{bmatrix} x \\ y \end{bmatrix})} \quad (3)$$

is directed towards the anisotropic Gauss core. The fixed values $\sigma_1 > 0$ and $\sigma_2 > 0$ determine the scale $x \in [0, x_{\max}]$, $y \in [0, y_{\max}]$ and the direction respectively, while θ and $A(\theta) = \begin{bmatrix} \cos\theta & -\sin\theta \\ \sin\theta & \cos\theta \end{bmatrix}$ for $\theta \in [0, 2\pi]$ determine the kernel orientation (3) and its 2D rotational matrix, respectively. A filter bank is obtained and applied over the certain image textures with the signal $F(x, y)$ defined in (2), using the Laplacian kernel (3), i.e., bar detector, in several diverse scales $S_k = \{(\sigma_1^{(i)}, \sigma_2^{(i)})\}_{i=1, \dots, R}$. Only the changes of the vertical orientation of image texture are being considered, since those alterations bear the information content related to the discrimination in the classification task of interest. Namely, only $\theta = \pi/2$ is used, thus considering only the vertically oriented anisotropic core components (3). $[0, y_{\max}]$ is divided into M subintervals $\{[y_{i-1}, y_i] \mid i = 1, \dots, M\}$ in the fixed time frame k , and $[y_{i-1}, y_i]$, which correspond at appropriate frequencies $|S(k, \omega)|^2$. i -th band of the filter bank is equivalent to the interval $[y_{i-1}, y_i]$ and comprises R vertical components and LM MR8 filter banks [LM], applied to three priori defined scales. An individual vector for a fixed time frame k is obtained by applying the proposed filter banks on the k -th texton $F_k(x, y)$, $x \in [k, k+1]$ acquired from the image texture $F(x, y)$, $x \in [0, x_{\max}]$, over the time frame k . Actually, for every k , new R components are added, each for a different scale, onto the previously processed vector. The components are calculated as follows:

$$v_{k,i} = G(\sigma_1^{(i)}, \sigma_2^{(i)}, \pi/2, x, y) * F_k(x, y) \Big|_{x=k, y=y_{i-1}} \quad (4)$$

for $i = 1, \dots, R$

Based on the above, a set of pre-processed features of the sub-vector $V_k = [v_{k,1} \dots v_{k,R}]$ is obtained. From every extracted feature u , q_u is selected, and the pre-processed vector V_k^u , $k = 1, \dots, q_u$ is formed. Vector V is in this case a random variable, hence V_k^u are its realizations for every time frame k . Further on, the

compactification and robustification of features is conducted, by utilizing the representation via statistic moments, which presents a method to simultaneously conduct the reduction of the model dimensionality. A motive is a fact that a satisfactory number of moments (averaging per time) can be used to present the distribution V . Actually, it can be observed (considering the continual time t instead of the discrete time frame k), that there is a unique correspondence between the distributions of probabilities p_{V^u} and k_{V^u} , with the characteristic function being as follows:

$$k_{V^u}(t) = E e^{iV^u t} = \sum_{j=0}^{\infty} \frac{(it)^j}{j!} E((V^u)^j) \quad (5)$$

4. VERIFICATION OF THE DEVELOPED MODEL

The verification of the proposed model was performed on experimental data divided into two groups – a training set containing approximately three quarters of experimental data, and a test set containing the remaining one quarter of data. All data were gathered during a series of experimental research. Data sets were carefully organized so that each contains data from all combinations of processing parameters and tool wear degrees.

The presented classification method utilized for the classification of the extracted features forms clusters on the basis of the classification matrix. After the feature extraction is performed using the presented method, the next step is to cluster the input data into apriori clusters. The classification, i.e. feature gathering, is performed simultaneously in three dimensions defined via three vectors, i.e. three central moments: variance, skewness and Kurtosis. The analyses have shown that, for the selected feature extraction method, the combinations of their correlations provide the best results. The classification model is evaluated using the training function which is set by defining six cluster centers, one cluster centre for every wearing group in three diverse scales shown of figures 1, 2 and 3.

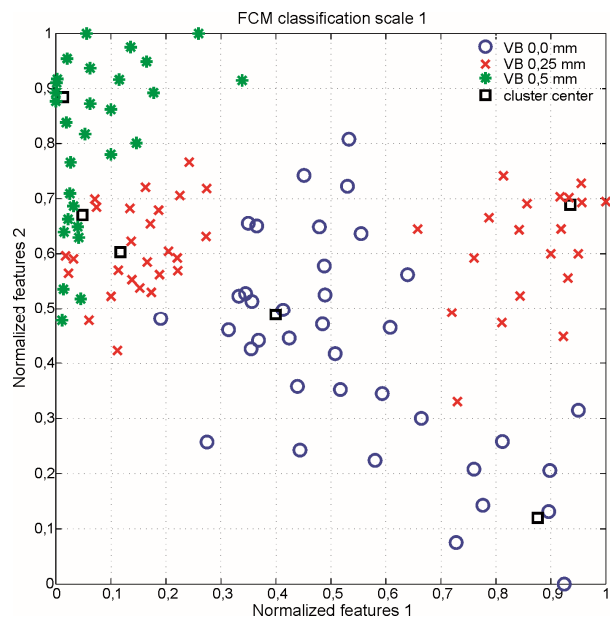


Fig. 1. Distribution of normalized feature vectors in the

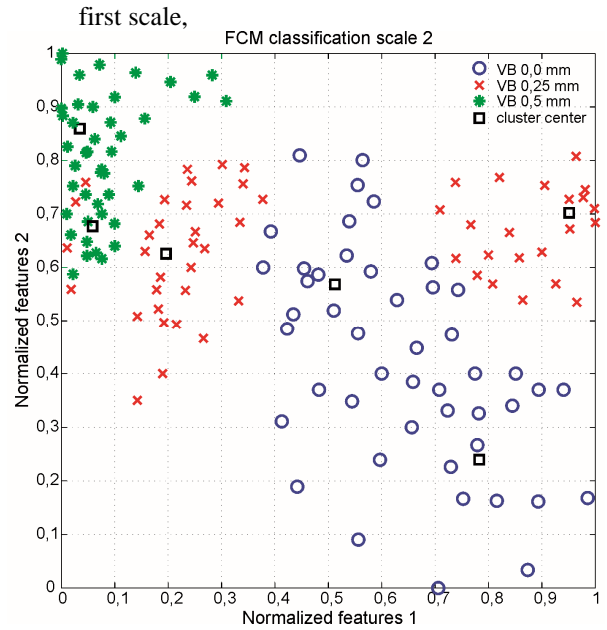


Fig. 2. Distribution of normalized feature vectors in the second scale

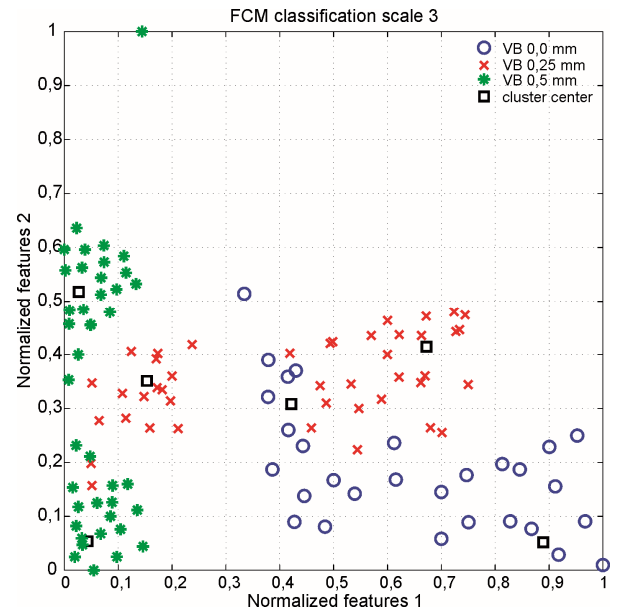


Fig. 3. Distribution of normalized feature vectors in the third scale

In order to estimate the successfulness of the classification, i.e. the number of successfully classified features in individual scales, a statistic validation of the representation of well classified features per scale has been conducted. Figure 4, 5 and 6 presents the percentage of the representation of successfully classified features per individual scales by applying the algorithm, in relation to the apriori classification for individual cutting tool wearing conditions. From the Figures, it can be observed a somewhat lower percentage of the accurately classified features for the tool from the second group in the first scale. On Figures is shows, spindle speed, feed rate and cutting depth combination. However, for other scales, it can be noted that the percentage of the representations of successfully classified features is significantly increased; hence the average percentage value can be

considered to be satisfactory.

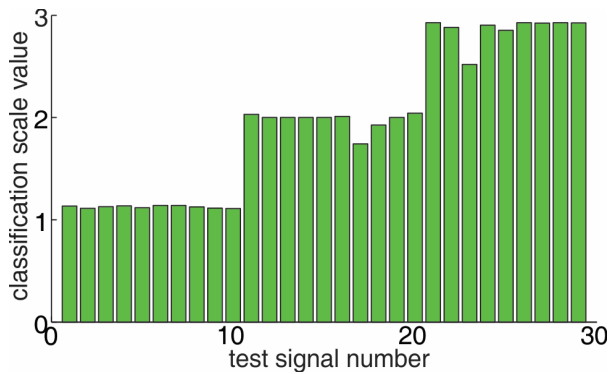


Fig.4. Presents the percentage of the representation of successfully classified features, $v=180\text{m/min}$, $f=0.2\text{mm/rev}$, $a=1.5\text{mm}$

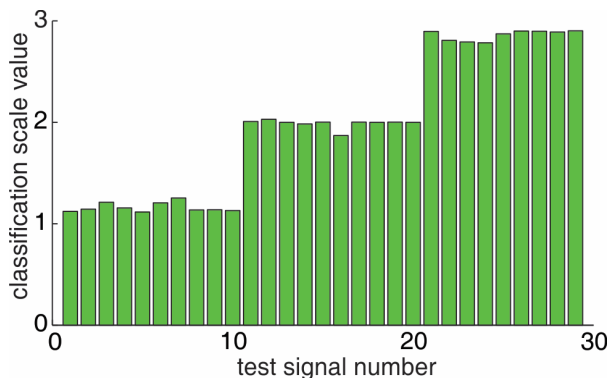


Fig.5. Presents the percentage of the representation of successfully classified features, $v=200\text{m/min}$, $f=0.25\text{mm/rev}$, $a=1.5\text{mm}$

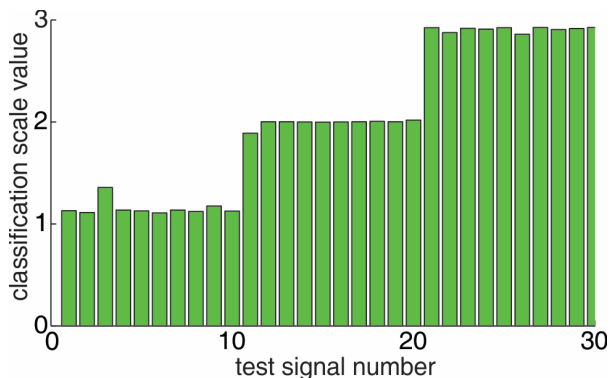


Fig.6. Presents the percentage of the representation of successfully classified features, $v=220\text{m/min}$, $f=0.2\text{mm/rev}$, $a=2\text{mm}$

5. CONCLUSION

This approach uses the robust method to classify the tool wear condition. The experiment results demonstrate that this approach surpasses the standard methods in tool condition monitoring. Furthermore, the proposed procedure can also be utilized in condition estimation of other machining processes, such as drilling and milling. As a drawback in using the method, one could state a demand for high performances of a computer system in the training

stage. In the future, certain improvements are to be conducted in increasing the feature extraction performances and model flexibility. Likewise, the procedure of feature extraction from wavelet and time domains can contribute to a better overview of the dynamics of the tool cutting geometry degradation, i.e. the tool wear process and the increase in resolutions.

11. REFERENCES

- [1] Kunpeng, Z., Yoke San, W., Geok Soon, H.: *Wavelet analysis of sensor signals for tool condition monitoring: A review and some new results*, International Journal of Machine Tools & Manufacture 49, pp 537–553, 2009.
- [2] Rehorn, A.G., Jiang, J., Orban, P.E., *State of the art methods and results in tool condition monitoring: a review*, International Journal of Advance Manufacturing Technology 26, pp 693–710, 2005.
- [3] Sharma, V.S., Sharma, S. K., Sharma, A.K.: *Cutting tool wear estimation for turning*, Journal of Intelligent Manufacturing 19, pp 99–108, 2008.
- [4] Tibshirany, R.: *Regression Shrinkage and Selection with LASSO*, J. R. Statics. Soc. B, 58, 1, pp 267-288, 1996.
- [5] Meinshausen, N., Yu, B.: *Lasso-Type Recovery of Sparse Representations for High-Dimensional Data*, The Annals of Statistics, 37, 1, pp 246–270, 2009.

Acknowledgments

This paper presents a segment of the research on the project "Contemporary approaches in the development of special solutions bearing in mechanical engineering and medical prosthetics", project number TR 35025, financed by the Ministry of Education and Science of the Republic of Serbia, and research over mobility and scholarships in the scope of the network CEEPUS III RO- 0202.

Authors: Assistant Professor DrSc Aco Anti , Assistant DrSc Professor Mijodrag Milošević , University of Novi Sad, Faculty of Technical Sciences, Department for Production Engineering, Trg Dositeja Obradovica 6, 21000 Novi Sad, Serbia, Phone.: +381 21 485 2312, +381 21 485 2346, Fax: +381 21 454-495.

Professor DrSc Tomislav Šari , University J.J. Strossmayer in Osijek, Mechanical Engineering Faculty, Trg Ivane Brli Mažurani 2 35000 Slavonski Brod, Phone.: +385 35 448 264, Fax: +385 35 446 446

E-mail: antica@uns.ac.rs; mido@uns.ac.rs; tsaric@sfsb.hr

IDENTIFICATION OF DYNAMICAL CONTACT PARAMETERS FOR SPINDLE-HOLDER-TOOL ASSEMBLY

Abstract: With the fast advances in computing technology accurate identification of contact dynamics in spindle-holder-tool assemblies is of great importance for predicting tool point frequency response function and evaluating the cutting process stability. This paper describes the mathematical formulation of the Levenberg-Marquardt method which was applied to identify the unknown parameters at spindle-holder and holder-tool interfaces. In order to verify the proposed mathematical model numerical and experimental analysis of the spindle-holder-tool assembly was carried out.

Key words: Parameter identification, contact dynamics

1. INTRODUCTION

Spindle-holder-tool assembly is one of the most important machine tool components because its static and dynamic behavior, strength, speed, among many others, have a significant impact on machine tools overall performance. Regenerative chatter is a well-known machining problem caused by cutting tool-workpiece dynamic interaction that could result in process instability, reduced material removal rate and poor surface quality. In order to identify the stable and unstable cutting zone in the machining process stability lobe diagrams of spindle-holder-tool assemblies have been used for decades. For generation of these diagrams frequency response function (FRF) of the assembly should be achieved firstly. The tool point FRF is typically obtained by experimental modal analysis. However, due to the large number of holder and tool combinations, in order to minimize time-consuming modal testing many researchers have developed semi-analytically approaches for obtain tool point FRF. The accuracy of these models strongly depends on the accurate identification of dynamical contact parameters at the spindle-holder and holder-tool interfaces. Therefore, the identification dynamical contact parameters of spindle assemblies is of great importance for obtaining the accurate tool point FRF. Erturk et al. [1] proposed and experimentally verified analytical model for predicting tool point FRF by combining the receptance coupling and structural modification techniques where all components of the spindle-holder-tool assembly were modeled analytically with Timoshenko beam theory. Schmitz et al. [2] introduced off-diagonal elements to the diagonal joint stiffness matrix to account for the translations imposed by moments and rotations caused by forces.

In this paper Levenberg-Marquardt method was applied to identify the unknown parameters of a spindle-holder-tool assembly. Proposed mathematical model is first used in a case study for analytical demonstration. Then, it is verified experimentally for a spindle-holder-tool assembly.

2. MATHEMATICAL MODEL

Analysis of complex dynamical systems such as spindle assemblies can be simplified by breaking a global system down to a set of interconnected subsystems. Therefore, in this paper the problem referring to dynamic properties of the spindle-holder-tool assembly can be simplified so that instead of viewing it as single, the specified system is regarded as the one composed of three separate subsystems, namely: a spindle, holder and tool. Components of these assembly should be coupled elastically due to flexibility and damping introduced by contact parameters at spindle-holder and holder-tool interfaces. In this paper, we applied the approach [1], where part of the holder inside the spindle is considered rigidly joined to the spindle (Fig. 1a) and the part of the tool inside the holder is considered rigidly joined to the holder (Fig. 1b).

Complex stiffness matrix, representing the spindle-holder interface dynamics, has the following form:

$${}_{SH}\mathbf{K} = \begin{bmatrix} {}_{SH}k_t + i \cdot \omega \cdot {}_{SH}c_t & 0 \\ 0 & {}_{SH}k_r + i \cdot \omega \cdot {}_{SH}c_r \end{bmatrix} \quad (1)$$

Here, ${}_{SH}k_t$ is the translational stiffness, ${}_{SH}c_t$ is the translational damping, ${}_{SH}k_r$ is the rotational stiffness and ${}_{SH}c_r$ is the rotational damping at the spindle-holder interface.

Assuming that response matrices of the subsystem S (spindle with bearings) and subsystem H (holder) are known, then it is possible by using a method of receptance coupling, to obtain the global system response matrix SH (spindle-holder) at the holder tip:

$$\mathbf{SH}_{ii} = \mathbf{H}_{ii} - \mathbf{H}_{ic} \cdot (\mathbf{H}_{cc} + \mathbf{S}_{cc} + {}_{SH}\mathbf{K}^{-1})^{-1} \cdot \mathbf{H}_{ci} \quad (2)$$

The interface dynamics between the holder and the tool can be expressed in Eq. (3):

$${}_{HT}\mathbf{K} = \begin{bmatrix} {}_{HT}k_t + i \cdot \omega \cdot {}_{HT}c_t & 0 \\ 0 & {}_{HT}k_r + i \cdot \omega \cdot {}_{HT}c_r \end{bmatrix} \quad (3)$$

Here, ${}_{HT}k_t$ and ${}_{HT}c_t$ are the translational stiffness and damping at the holder-tool interface, respectively. And ${}_{HT}k_r$ and ${}_{HT}c_r$ are the rotational stiffness and damping at

the holder-tool interface, respectively.

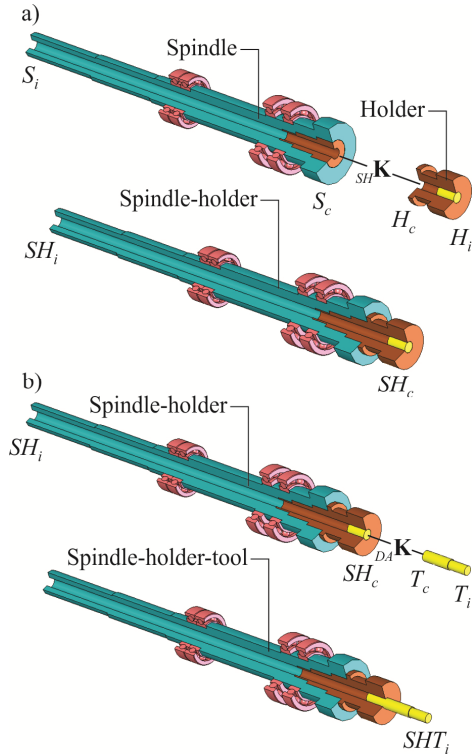


Fig. 1. Elastic coupling of spindle, holder and tool

Receptance matrix of the global system SHT (spindle-holder-tool) at the tool tip is obtained by Eq. (4):

$$\mathbf{SHT}_{ii} = \mathbf{T}_{ii} - \mathbf{T}_{ic} \cdot (\mathbf{T}_{cc} + \mathbf{SH}_{cc} + {}_{HT}\mathbf{K}^{-1})^{-1} \cdot \mathbf{T}_{ci} \quad (4)$$

In order to be able to use equations (2) and (4) to predict the frequency response function at the holder and at the tool tip, respectively, it is necessary to recognize all unknowns, namely, the translational stiffness, the translational damping, the rotational stiffness and the rotational damping at the spindle-holder and holder-tool interface. The following section presents methodology for identification these parameters.

3. PARAMETER IDENTIFICATION OF THE SPINDLE-HOLDER-TOOL ASSEMBLY

3.1 Mathematical background

Fig. 2 shows the general approach to the problem of parameters identification, from problem definition to achieving optimal solutions. A system that is optimized should be presented by appropriate mathematical model (e.g. a system of differential equations), after which should be defined analysis objectives. In order to optimize the system, it is necessary to enable the changes of its form and structure.

The assumption is that the mathematical model can be described by a system of differential equations:

$$\mathbf{D}\dot{\mathbf{y}} = \mathbf{f}(t, \mathbf{y}, \boldsymbol{\theta}), \quad \mathbf{y}(t_0, \boldsymbol{\theta}) = \mathbf{y}_0(\boldsymbol{\theta}) \quad (5)$$

Here, $\boldsymbol{\theta}$ is vector of unknown parameters, \mathbf{y} is dependent state vector of t and \mathbf{f} is generally, nonlinear function, \mathbf{D} is $n \times n$ constant diagonal matrix.

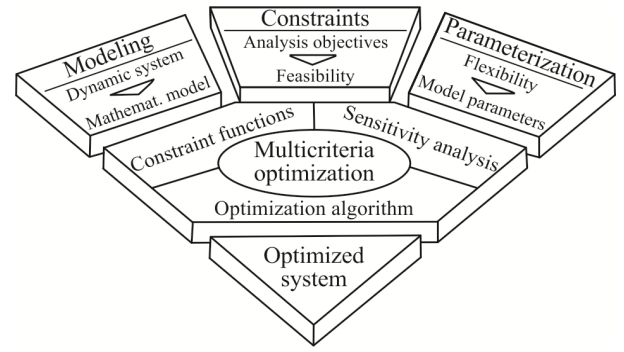


Fig. 2. Process of parameter identification

Each measurement can be defined by following parameters:

$$(c_i, t_i, \tilde{y}_i), \quad i = 1, 2, \dots, m \quad (6)$$

Here, c_i is component vector \mathbf{y} which is measured, t_i is time of measurement, \tilde{y}_i is measured value and m is total number of measurements. The solution of Eq. (5) for c_i component at a time t_i , which corresponds to the i -th measurement, is marked with $y_{c_i}(t_i, \boldsymbol{\theta})$. The general approach to the problem of parameter identification is to minimize the differences between the results obtained by measuring and by the mathematical model, i.e.:

$$r_i(\boldsymbol{\theta}) = y_{c_i}(t_i, \boldsymbol{\theta}) - \tilde{y}_i \quad (7)$$

One of the most widely used method of parameter identification is the least squares method, where the estimates of the constants of the models are chosen such that the sum of the squared residuals is minimized. Differences between the results experimentally obtained and using the mathematical model can be represented as a vector \mathbf{r} :

$$\mathbf{r}(\boldsymbol{\theta}) = [r_1(\boldsymbol{\theta}) \quad r_2(\boldsymbol{\theta}) \quad \dots \quad r_m(\boldsymbol{\theta})]^T \quad (8)$$

which is a basis to obtain an expression for the objective function:

$$f(\boldsymbol{\theta}) = \frac{1}{2} \|\mathbf{r}(\boldsymbol{\theta})\|^2 = \frac{1}{2} \mathbf{r}(\boldsymbol{\theta})^T \mathbf{r}(\boldsymbol{\theta}) \quad (9)$$

Identification of the parameters can be formulated as follows:

$$\boldsymbol{\theta}^* = \arg \min_{\boldsymbol{\theta}} f(\boldsymbol{\theta}) \quad (10)$$

Here, $\boldsymbol{\theta}$ is vector of parameters and $\boldsymbol{\theta}^*$ is vector that minimizes the objective function. If objective function is twice continuously differentiable, then the following Taylor expansion for f applies:

$$f(\boldsymbol{\theta} + \mathbf{h}) = f(\boldsymbol{\theta}) + \nabla f^T(\boldsymbol{\theta}) \mathbf{h} + \frac{1}{2} \mathbf{h}^T \nabla^2 f(\boldsymbol{\theta}) \mathbf{h} + o\|\mathbf{h}^3\| \quad (11)$$

Gradient \mathbf{g} and Hessian matrix \mathbf{H} are defined as follows:

$$\mathbf{g} = \nabla f(\boldsymbol{\theta}) = \left[\frac{\partial f}{\partial \theta_1} \quad \frac{\partial f}{\partial \theta_2} \quad \dots \quad \frac{\partial f}{\partial \theta_{n_p}} \right]^T \quad (12)$$

$$\mathbf{H} = \nabla^2 f(\cdot) = \begin{bmatrix} \frac{\partial^2 f(\cdot)}{\partial \theta_1^2} & \frac{\partial^2 f(\cdot)}{\partial \theta_1 \partial \theta_2} & \dots & \frac{\partial^2 f(\cdot)}{\partial \theta_1 \partial \theta_{n_p}} \\ \frac{\partial^2 f(\cdot)}{\partial \theta_2 \partial \theta_1} & \frac{\partial^2 f(\cdot)}{\partial \theta_2^2} & \dots & \frac{\partial^2 f(\cdot)}{\partial \theta_2 \partial \theta_{n_p}} \\ \vdots & \vdots & \ddots & \vdots \\ \frac{\partial^2 f(\cdot)}{\partial \theta_{n_p} \partial \theta_1} & \frac{\partial^2 f(\cdot)}{\partial \theta_{n_p} \partial \theta_2} & \dots & \frac{\partial^2 f(\cdot)}{\partial \theta_{n_p}^2} \end{bmatrix} \quad (13)$$

For the objective function the gradient and Hessian matrix are:

$$\mathbf{g} = \nabla f(\cdot) = \sum_{i=1}^m r_i(\cdot) \nabla r_i(\cdot) = \mathbf{J}(\cdot)^T \mathbf{r}(\cdot) \quad (14)$$

$$\mathbf{H} = \mathbf{J}(\cdot)^T \mathbf{J}(\cdot) + \sum_{i=1}^m r_i(\cdot) \nabla^2 r_i(\cdot) \quad (15)$$

Here, $\mathbf{J}(\cdot)$ denotes the Jacobian matrix.

Levenberg-Marquardt algorithm is based on the assumption that the error $\mathbf{r}(\cdot)$ around the point (k) may approximate by the first two members of Taylor's series:

$$\mathbf{r}^*(\cdot) \cong \tilde{\mathbf{r}}^*(\cdot) = \mathbf{r}^*(\cdot)^{(k)} + \nabla \mathbf{r}^*(\cdot)^{(k)} \cdot (\cdot - \cdot)^{(k)} \quad (16)$$

Then, instead of minimizing the objective function, its approximation is minimized:

$$\tilde{f}(\cdot) = \frac{1}{2} \tilde{\mathbf{r}}^{*T}(\cdot) \cdot \tilde{\mathbf{r}}^*(\cdot) \quad (17)$$

Equating the previous equation to zero, the following expression which minimizes the function (17) is obtained:

$$\mathbf{J}^T(\cdot)^{(k)} \cdot \mathbf{J}(\cdot)^{(k)} \cdot (\cdot - \cdot)^{(k)} + \mathbf{J}^T(\cdot)^{(k)} \cdot \mathbf{r}^*(\cdot)^{(k)} = \mathbf{0} \quad (18)$$

Adding the learning coefficient $\alpha^{(k)}$, with $\alpha^{(k)} = \alpha^{(k+1)}$, it is possible to obtain the following equation:

$$\alpha^{(k+1)} = \alpha^{(k)} - \alpha^{(k)} \left[\mathbf{J}^T(\cdot)^{(k)} \cdot \mathbf{J}(\cdot)^{(k)} \right]^{-1} \mathbf{J}^T(\cdot)^{(k)} \cdot \mathbf{r}^*(\cdot)^{(k)} \quad (19)$$

In literature these equation represent Gauss-Newton algorithm for $\alpha^{(k)} = 1$, that is, Gauss-Newton damped algorithm for variable $\alpha^{(k)} < 1$, where the Hessian matrix is replaced by a matrix:

$$\tilde{\mathbf{H}}(\cdot)^{(k)} = \mathbf{J}^T(\cdot)^{(k)} \cdot \mathbf{J}(\cdot)^{(k)} \quad (20)$$

Levenberg introduced the approximate matrix of the Hessian matrix:

$$\tilde{\mathbf{H}}(\cdot)^{(k)} = \mathbf{J}^T(\cdot)^{(k)} \cdot \mathbf{J}(\cdot)^{(k)} + \mu \mathbf{I} \quad (21)$$

By replacing the Hessian matrix with Levenberg matrix, the final expression for calculation of the parameters is obtained:

$$\alpha^{(k+1)} = \alpha^{(k)} - \tilde{\mathbf{H}}^{-1}(\cdot)^{(k)} \cdot \mathbf{J}^T(\cdot)^{(k)} \cdot \mathbf{r}^*(\cdot)^{(k)} \quad (22)$$

Based on the presented mathematical model, a program for identification of unknown parameters was written in the MATLAB software package.

3.2 Numerical case study

In this section, an numerical case study for the identification approach described is provided. Geometry of the spindle-holder-tool assembly used for numerical simulation, bearings and interface dynamics properties and all other information related to FEM model are given in [3]. Values of identified parameters

are shown in Table 1, together with errors of identification. Fig. 3a and 3b shows the comparison of FRF at the tip of the tool holder and at the tip of the tool with the identified and real values, respectively. As shown in Fig. 3, the accuracy of the identified parameters is more than satisfactory. Somewhat larger errors are encountered in the identification of the rotational stiffness, because this parameter has no significant impact in the synthesis of dynamic subsystems. The most dominant factor in the synthesis of dynamic subsystems is translational stiffness, and this values are most accurately identified.

	Exact value	Identified value	Relative error [%]
shk_t [N/m]	$6.5 \cdot 10^7$	$6.47984 \cdot 10^7$	0.31
shk_r [Nm/rad]	$3.5 \cdot 10^6$	$3.7393 \cdot 10^6$	6.84
shc_t [Ns/m]	50	44.8	10.24
shc_r [Nms/rad]	7	3.8	45.71
htk_t [N/m]	$2.1 \cdot 10^7$	$2.10254 \cdot 10^7$	0.12
htk_r [Nm/rad]	$1.4 \cdot 10^6$	$1.26983 \cdot 10^6$	9.3
htc_t [Ns/m]	15	12.24	18.4
htc_r [Nms/rad]	3	2.11	29.67

Table 1. Identified contact parameters of the spindle-holder-tool system

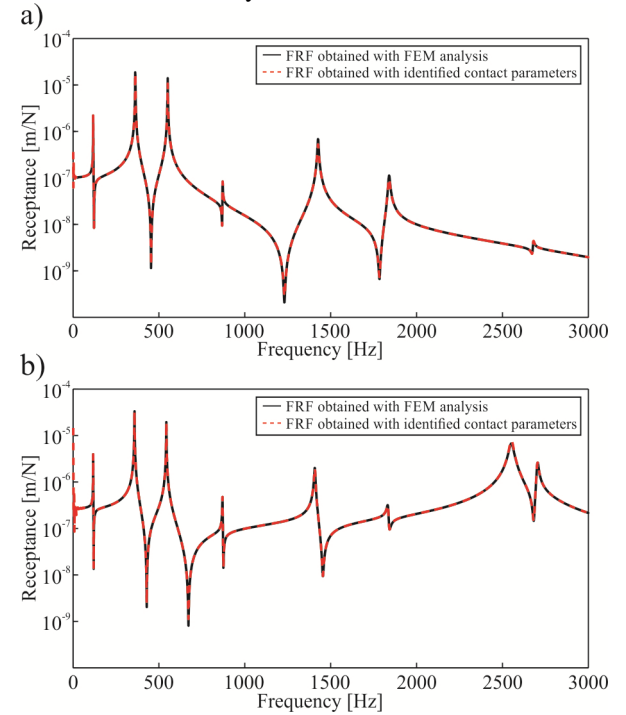


Fig. 3. FRF of the spindle-holder (a) and spindle-holder-tool (b) system with identified contact parameters

3.3 Experimental case study

In this section in addition to the analytical case study, an experimental case study for the parameter identification approach is described, combining experimental and FEM data. The spindle-holder-tool assembly shown in Fig. 4 is suspended to obtain free-free end conditions for performing an impact tests. Experiments were performed with ISO 30 type holder, in which carbide tools with different combination of tool diameters ($D = 9-30$ mm) and different tool overhang lengths ($L = 16-83$ mm). These two

parameters have the strongest influence on their values.

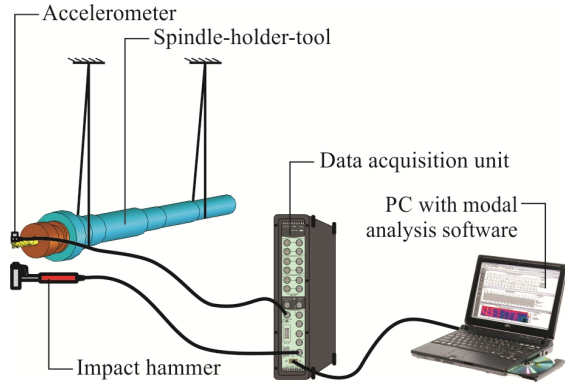


Fig. 4. Schematic layout of experimental setup

In order to provide sufficient data for analysis of the connection parameters at the holder-tool interface 178 measurements was made with different combinations of spindle-holder-tool assembly. Fig. 5 and Fig. 6 shows the result identified translational stiffness and damping at the holder-tool interface, respectively. From these figures it can be concluded that with increasing diameter and tool overhang length occur increase size of translational stiffness at holder-tool interface. On the other hand, it is not possible to derive general conclusions on the impact of these parameters on translational damping.

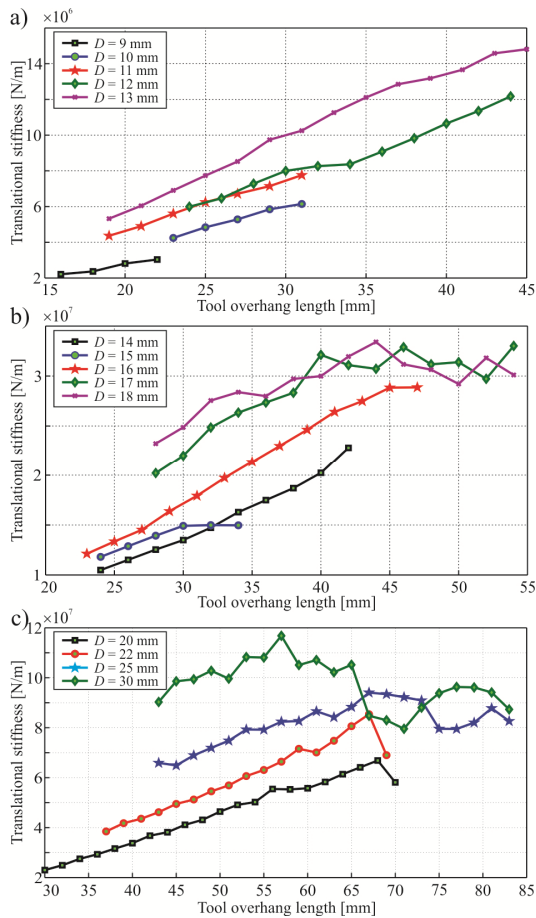


Fig. 5. Identified translational stiffness

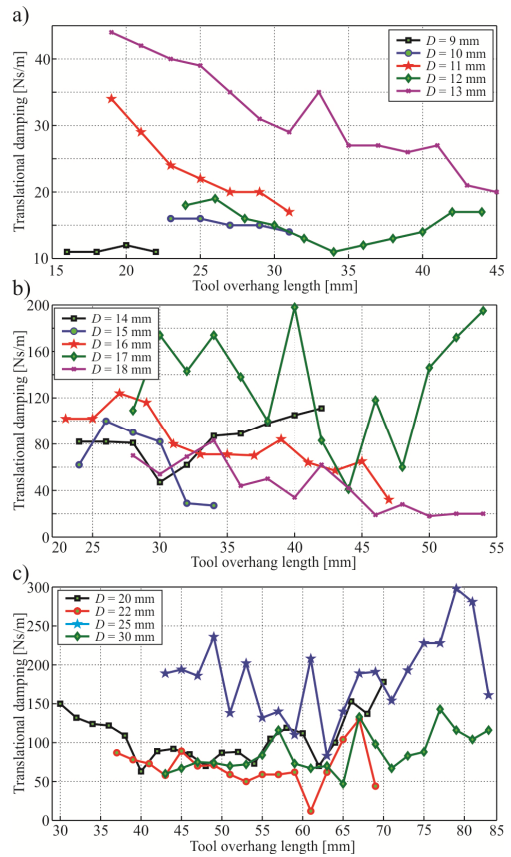


Fig. 6. Identified translational damping

4. CONCLUSIONS

One of the most important requirements in exploitation of the spindle assembly is its dynamic behavior, so the main aim of this study was to develop a mathematical model for identification of the contact parameters at spindle-holder and holder-tool interfaces. The proposed model was analytically and experimentally verified and satisfactory accuracy of the identified parameters was concluded.

5. REFERENCES

- [1] Erturk, A, Ozguven, H., Budak, E.: *Analytical modeling of spindle-tool dynamics on machine tools using Timoshenko beam model and receptance coupling for the prediction of tool point FRF*, International Journal of Machine Tools & Manufacture, 46(15), p.p. 1901-1912, 2006.
- [2] Schmitz, T.; Donaldson, R.: *Predicting high-speed machining dynamics by substructure analysis*, Annals of the CIRP, 49(1), p.p. 303-308, 2000.
- [3] i a, .: *Modeling dynamic behavior spindle - tool holder - tool assembly*, PhD thesis, Faculty of Mechanical Engineering, Banja Luka, 2010, (in Serbian).

Authors: or e i a, Assistant Professor, Prof. dr Milan Zeljkovi, M.Sc. Branislav Sredanovi, Dr. Sc. Stevo Borojevi, University of Banja Luka, Faculty of Mechanical Engineering, Stepe Stepanovica 75, 78000 Banja Luka, BiH, Phone.: +381 21 450-366, E-mail: djordjecica@gmail.com; milanz@uns.ac.rs;

Prodanovi , S., Nedi , N., Luki , Lj.

POSSIBILITIES FOR DISTURBANCE REJECTION IN THE DECOUPLED TITO PROCESS

Abstract: Proper behavior of multivariable process isn't guaranteed only through the disabling influence of its mutual coupling (interaction), but also compensation of disturbance has very important role. Investigation of disturbance that can be rejected by previously decoupled 2x2 process has been presented in this paper. Considered flow tank, as a multivariable process, was controlled using PI controllers. The aim was to determine limit of disturbance intensity under whose influence system can operate correctly, and in that way additionally check validity of designed decoupler, i.e. chosen control strategy. General expression for periodic rising signal that can be introduced into process in order to present array of disturbances has been derived, too. Investigation is very useful and applicable in electrical discharge machining and it was supported by simulations.

Key words: disturbance, decoupling control, PI controller, flow tank

1. INTRODUCTION

Numerous researches have been presented the advantages of the control systems containing decoupler in its controller over approach where mutual coupling wasn't taken into consideration. In one of them [1], control system of level and temperature in 2x2 flow tank has been investigated due to its similarity with many devices in industry, for example, EDM (electrical discharge machining) machines with electrode where state of electrolyte is monitored. Analysis of interaction among its inputs and outputs was carried out using theory given in [2] and decoupler has been designed like in [3]. Previously, process was modeled in [4] using physical laws and experiential data. Parameters of PI controller were determined based on principles given in [5] without need for repeating relay feedback test like in [6]. Besides reference tracking, researched and confirmed in [1], another very significant indicator of control quality is process ability to reject disturbances that occur during its operating. That is the main subject of this research. Here will be considered four cases of disturbance that should serve to determine limits of its intensity which system can compensate.

2. PROCESS AND ITS MODEL

Various types of plants in the chemical, pharmaceutical, food and other industries contain some kind of flow tanks where two fluids are mixed in order to obtain their blend. Flow tank with water as a fluid

that come through the two valves, 1 and 2, whose temperatures are $t_1=15$ °C and $t_2=70$ °C, respectively, was researched. Water is mixed on the constant number of revolutions. One or more properties of final fluid through the outlet valve 3 (on/off type, flow rate Q_3) can be controlled. Therefore, in present 2x2 process, inputs are flow rates (Q_1 or Q_2) through the valves 1 and 2. Outputs are level h and temperature t . Reference values are taken to be 1 m for level, and 30 °C for temperature. Mathematical model for this type of flow tank, derived in [4], is expressed with following transfer function matrix:

$$G(s) = \begin{bmatrix} g_{11}(s) & g_{12}(s) \\ g_{21}(s) & g_{22}(s) \end{bmatrix} = \begin{bmatrix} \frac{K}{Ts+1} & \frac{K}{Ts+1} \\ \frac{K_1}{T_1s+1} e^{-L_1s} & \frac{K_2}{T_2s+1} e^{-L_2s} \end{bmatrix} \quad (1)$$

where: $g_{ij}(s)$ – elements of transfer function matrix, K , K_1 and K_2 – gains, T , T_1 and T_2 – time constants, L_1 and L_2 – delay times.

3. ANALYSIS OF DISTURBANCE

Analysis of process behaviour in the presence of disturbance is extension in checking of control strategy for considered flow tank. General form of used disturbance is expressed by equation (2).

$$d = \begin{cases} 0, & t \in (0, t_0) \\ \sum_{j=1}^n U(t_0 + t_p(j-1) + t, t_0 + t_p j) U(t_0 + t_p n, +\infty) \\ [0, i], & t = t_0 + t_p(i-1) \\ i, & t \in (t_0 + t_p(i-1), t_0 + t_p(i-1) + t) \\ [i, 0], & t = t_0 + t_p(i-1) + t \end{cases}, \quad i = 1, 2, \dots, n \quad (2)$$

where are: t_0 – time of introducing of the first disturbance, t_p – period between starts of the adjacent disturbances, t – disturbance duration, i – disturbance intensity, d_i – ordinal number of disturbance, n – number of iterations. Square shape of disturbance was taken and it is assumed that they appear in the steady state. To enhance efficiency of test, the disturbances were introduced sequentially with defined period and in rising order of their intensity (more precisely, its absolute value). Whereas disturbances aren't measured, the feedback control is necessary here. The meanings of values in equation (2) are shown in Fig. 1.a). The part b) of this figure shows opposite direction of disturbance influence. Hence, this form can be used to determine limits of disturbance intensity.

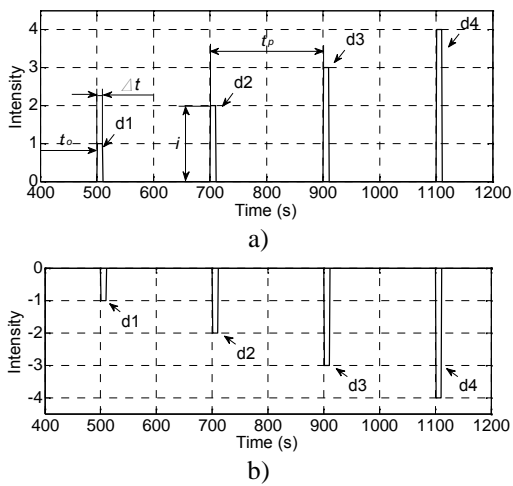


Fig. 1. Array of square disturbances: a) positive direction, b) negative direction

It offers opportunities for researching wide range of their intensity, but then they have to be scaled. In this survey following values have been chosen: $t_0=500$ s, $t_p=200$ s, $t=10$ s, $n=4$. Boundary for

acceptable intensity are 10 % of overshoot and undershoot. Analysis was performed through the considering process responses in presence of disturbance. That was realised using simulations, which need configuration in Fig. 2. and block diagram of entire control system shown in Fig. 3. This block diagram, except disturbance, was formed in [1,4], where I/P transducer is current-pneumatic transducer and U and X_i are manipulated and controlled variable, respectively.

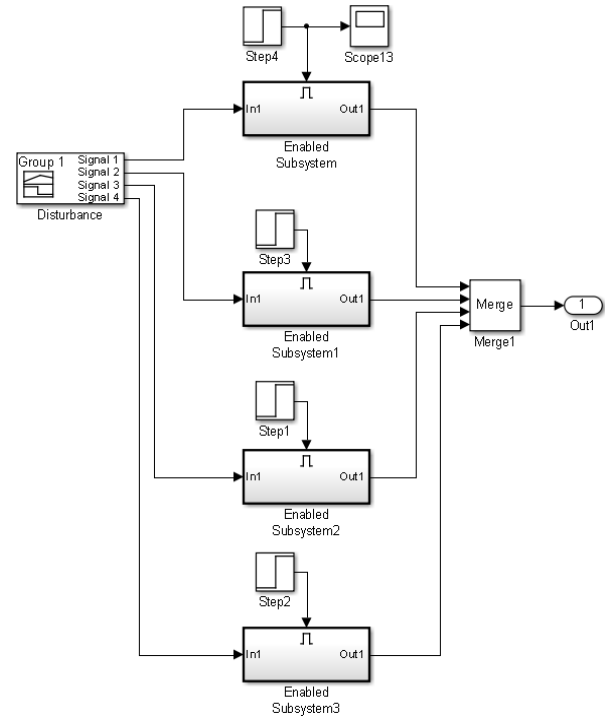


Fig. 2. Configuration for introduction of disturbance

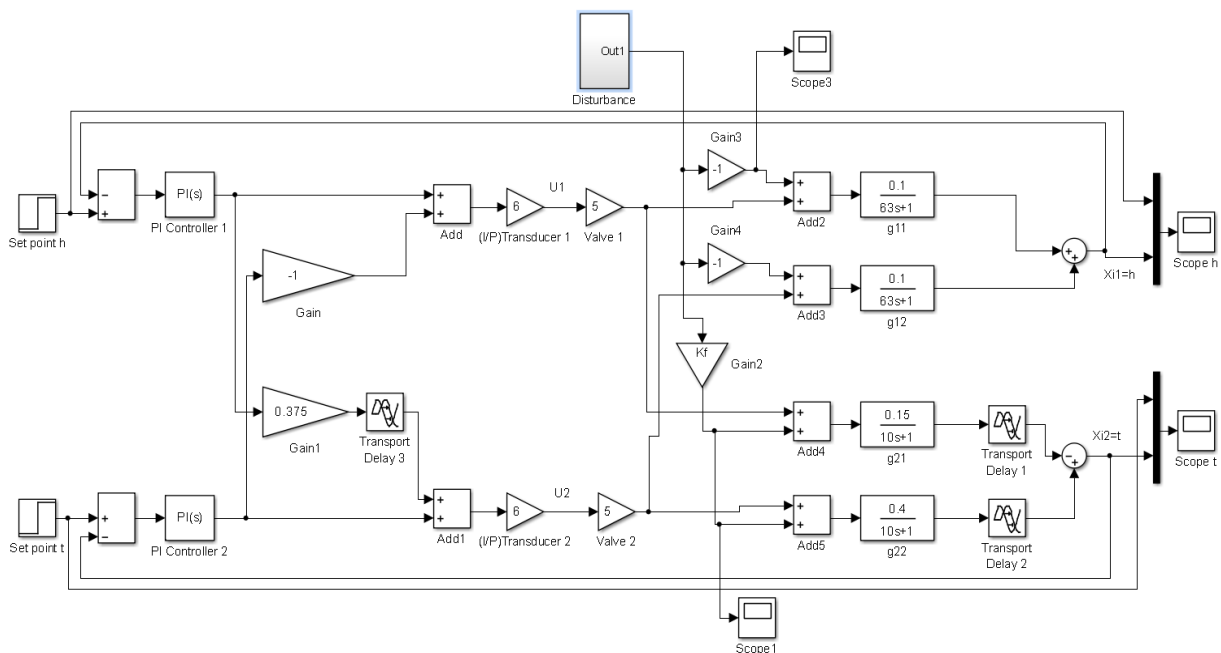


Fig. 3. Block diagram of the control system of level and temperature in decoupled flow tank under disturbance

For increasing of clearness, here should be emphasized, that this approach can be used regardless of type of fluid, whether it is being mixed or not (one or two fluids) and whether disturbance is introduced by adding or removing of fluid.

3.1 First case – increasing of level and temperature ($h+$, $t+$)

Hot water on temperature of 100 °C is adding into tank with flow rate which scaled values are between (1–4). Exact ratio between disturbance and its scaled value can be determined experimentally. That implies its scheduling till equalization of process responses obtained from simulations with its real equivalent, whereupon it can be related with certain value i in equation (2). Effects of disturbance on the process outputs depend on terms in transfer function matrix, too. But for completing definition of disturbance effect, relation between fluid volume and temperature should be calculated and it is presented through the correction factor K_f . This is carried out using law of conservation of energy, which for this flow tank is expressed by equation $t_{r+1}=(V_r t_r+V_d t_d)/(V_r+V_d)$, where: t_{r+1} – temperature of blend after influence of disturbance, t_r – temperature of blend before influence of disturbance, t_d – temperature of added water, V_r – volume in flow tank, V_d – volume of added water. Now correction factor is $K_f=[(t_{r+1} - t_r)/ t_r] 100$.

This way can also be utilized for determining (scaling) of disturbance impact on similar processes. Such approach gives more possibilities for disturbance investigation, because it enables work using simulations when experimentally scaling was previously carried out.

In this first case $K_f=2,3$. Simulations of four values of disturbance intensity, without gains 3 and 4 in Fig. 3, give level in flow tank in Fig. 4, while Fig. 5. and 6. contain temperature and its enlarged view, respectively.

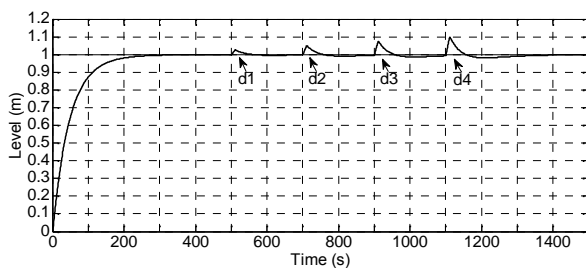


Fig. 4. Level in flow tank under influence of disturbance ($h+$, $t+$)

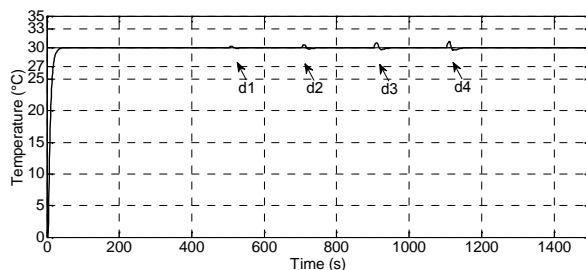


Fig. 5. Temperature in flow tank under influence of disturbance ($h+$, $t+$)

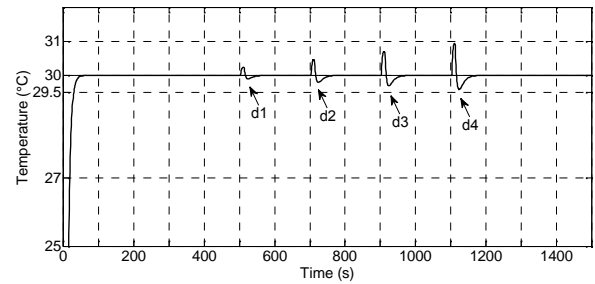


Fig. 6. Enlarged view of temperature in flow tank under influence of disturbance ($h+$, $t+$)

Therefore, to avoid repetition of similar figure (here Fig. 3.), their diversities within these four cases are particularly emphasized in belonging subchapters.

3.2 Second case - increasing of level and decreasing of temperature ($h+$, $t-$)

Equal volumes of mixed water and ice as in first case, but here on temperature of 0°C are adding into tank. Therefore, level is the same like in first case (Fig. 4) and temperature, obtained after simulations of four values of disturbance intensity, without gains 3 and 4 in Fig. 3, is shown in Fig. 7. In this case correction factor is $K_f=-1$. It is important to say that different, but also too small impact of water temperature (100 °C and 0 °C) on its volume in tank is neglected in this research.

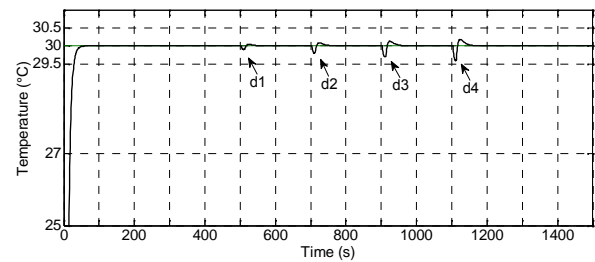


Fig. 7. Enlarged view of temperature in flow tank under influence of disturbance ($h+$, $t-$)

3.3 Third case - decreasing of level and increasing of temperature ($h-$, $t+$)

This case describes drop flow through the valve 1, and because of that, at the initial moment, more water come from valve 2. Temperature of that water is 70 °C and it increases temperature of blend t_r . In this case correction factor is $K_f=1,3$. Simulations carried out according block diagram in Fig. 3. give level and temperature in flow tank shown in Fig. 8. and 9, respectively.

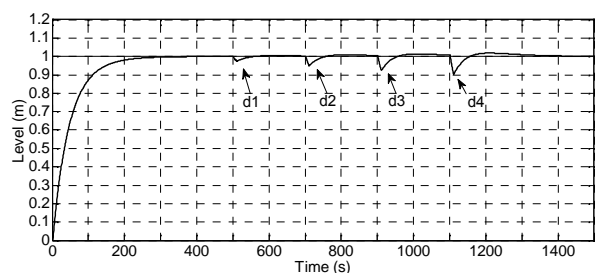


Fig. 8. Level in flow tank under influence of disturbance ($h-$, $t+$)

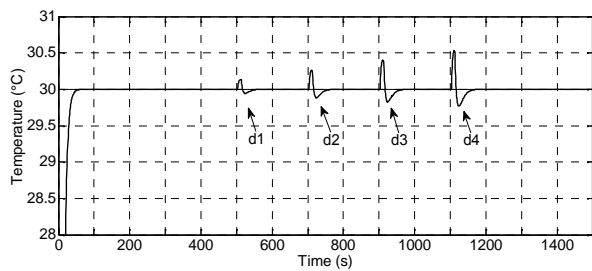


Fig. 9. Enlarged view of temperature in flow tank under influence of disturbance (h -, t +))

3.4 Fourth case – decreasing of level and temperature (h -, t -)

Drop flow (equal as in third case) but through the valve 2 was simulated here according Fig. 3, and because of that, at the initial moment, more water come from valve 1. Temperature of that water is 15 °C and it decreases temperature of blend t_r . In this case correction factor is $K_f = -0,5$. Level is the same like in third case (Fig. 8) and temperature is shown in Fig. 10.

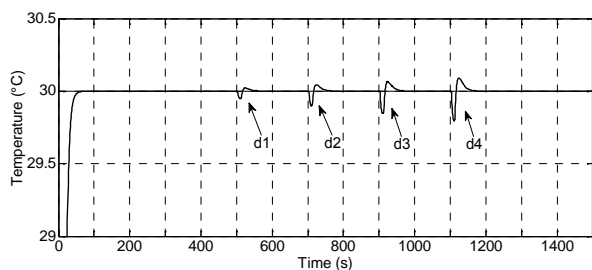


Fig. 10. Enlarged view of temperature in flow tank under influence of disturbance (h -, t -)

3.5 Discussion of results

As stated, limits within which response can be taken as good are $\pm 10\%$. Thus, for level limits are $(0,9 \div 1,1)\text{m}$ and for temperature $(27 \div 33)^\circ\text{C}$. To determine settling time after influence of disturbance T_s , steady state error was defined $s = \pm 2\%$. It is: for level $s = (0,98 \div 1,02)\text{m}$ and for temperature $s = (29,4 \div 30,6)^\circ\text{C}$. Taking into account these limits and simulated responses, it is noticeable that disturbance has larger influence to the level. Due to that, and taking into account simultaneity of disturbance effects on both outputs, the first limitation is in level. Numerous values of disturbance intensity were varied and it was found that responses (better to say level) weren't overcome overshoot limits up to forth level of intensity, as it shown in Fig. 4-10. Another favorable result is that responses, which overcome steady state error, have very short settling time measured from the moment of disturbance occurrence (highest in the level in first case $T_s = 39,5\text{ s}$). Based on this, after mentioned scaling, the real values of water volume and its temperature, which can be added into flow tank as disturbance without undermining the good work of process, can be determined.

4. CONCLUSION

This research supports efforts in forming general model for determining range for certain kind of disturbance that can be compensated by the feedback decoupling control system. In this regard, general model of rising disturbance in square form occurring in equal intervals has been derived, because it well enough represents the nature of disturbance, that have been considered in listed four cases. Considering flow tank, rejection will be better with larger $Q_{3\text{max}}$, because for higher disturbance intensities drainage flow rate should be higher, too. Regarding temperature, larger flexibility of control system can be enabled with valves which satisfy ratio $Q_{3\text{max}} = 2 \cdot Q_{1\text{max}} = 2 \cdot Q_{2\text{max}}$. This flow tank can serve as some kind of universal example, where various machines and processes with similar components in production industry can be investigated. So, in this way, time separated disturbances in level and temperature in a concrete types of devices, can also be researched in future.

5. REFERENCES

- [1] Prodanovi, S., Nedi, N.: *Non-conventional control of level and temperature in the flow tank*, COMETA2014 Conference Proceedings, B&H, p.p. 421-428, Jahorina, 2014. (in Serbian)
- [2] Skogestad, S. and Postlethwaite, I.: *Multivariable Feedback Control: Analysis and Design*, 2nd ed. John Wiley & Sons, Chichester, 2005.
- [3] Morilla, F., Garrido, J., Vázquez, F.: *Multivariable decoupling control*, Revista Iberoamericana de Automática e Informática Industrial, vol. 10, p.p. 3-17, 2013. (In Spanish)
- [4] Prodanovi, S. Lj., Nedi, N. N. and Braši, V. S.: *Some Considerations of Mutual Coupling in Multivariable Processes*, SAUM 2014 Conference Proceedings, p.p. 257-260, Niš, Serbia, 2014.
- [5] Filipovi, V. Ž., Nedi, N. N.: *PID Controllers*, University of Kragujevac, Faculty of Mechanical Engineering, Kraljevo, 2008. (in Serbian).
- [6] Menani, S. and Koivo, H.: *New approach on the automatic tuning of multivariable PI controllers using relay feedback*. International Journal of Systems Science, vol. 34, no. 2, p.p. 93-110, 2003.

Authors:

Mr Saša Prodanovi, University of East Sarajevo, Faculty of Mechanical Engineering, Vuka Karadžića 30, 71123 East Sarajevo, Bosnia and Herzegovina
Phone.: +387 57 340-847, Fax: +387 57 340-847.

Prof. dr Novak Nedi, **Prof. dr Ljubomir Luki**, Faculty of Mechanical and Civil Engineering in Kraljevo, Dositejeva 19, 36000 Kraljevo, Serbia,
Phone.: +381 36 383-377, Fax: +381 36 383-378.

E-mail: sasa.prodanovic77@gmail.com;

nedic.n@mfkv.kg.ac.rs; ljubomir.s.lukic@gmail.com

12th INTERNATIONAL SCIENTIFIC CONFERENCE MMA 2015 -
FLEXIBLE TECHNOLOGIES

PROCEEDINGS



Section C:

**METROLOGY, QUALITY, FIXTURES, METAL
CUTTING TOOLS AND TRIBOLOGY**

Novi Sad, 25-26 September 2015

Luji , R., Nikoli I., Juki , J., Sari , T., Simunovi , G., Simunovi , K., Galzina, V., Svalina I.

APPLICATION OF KAIZEN METHOD THROUGH IMPLEMENTATION OF VISUAL SYSTEM FOR PRODUCTION CONTROL

Abstract: The article describes the process of improving the production process through the implementation of visual control system for the production (control of adhesive application on pneumatic stop switch) based on Kaizen philosophy. The visual control system consists of high-resolution camera, light source, hardware and software for "a visual builder for automated control".

Made visual system in practice has proven to be a good solution that could significantly improve production. Created system is very flexible and with a small modification can be used for other product controls (check mark on the goods, controlling of measures and deviations, etc.).

Key words: Kaizen, visual system, Petri nets

1. INTRODUCTION

Improvement of the production process with accepting investments today could contribute with faster and better production and become the aim of slow growing economies. The answer on such a kind of question is Kaizen approach.

Kaizen is basis of the Japanese production, the most important business philosophy that makes business fundamentals solid and more competitive. The word Kaizen can be translated as a continuous improvement, in which the continuous involvement of all company employees. Kaizen company activities have to be well-designed cycle of activities.

Kaizen philosophy is advisedly implementation of the visual control system for quality control without large investments, extra costs for education of workers or major changes in the existing production process.

An important feature of the visual control system is its flexibility and applicability to different models of control. In the production with more types of products is possible to use visual control systems for a variety of models, which also has a positive impact on the economic feasibility of the implementation of the visual control system.

2. KAIZEN PHILOSOPHY

Lots of article cover Kaizen philosophy in different production areas [1, 2, 3, 4, 5].

Circle of Kaizen activities involves standardization of operation, measurement of the operation, customization, innovation, raising of productivity and standardization of new improved operations. Planning of large scale and extensive projects with high risk and uncertainty through Kaizen approach will be replaced with a number of smaller projects with very large amount of small improvements [6].

Kaizen can be displayed like an umbrella that covers various continuous improvement inside of any organization (figure 1. [7]). Kaizen is not only the type of access to more competitive production but also

"everybody's business", because its strategy is based on the assumption that each person has an interest in improving.

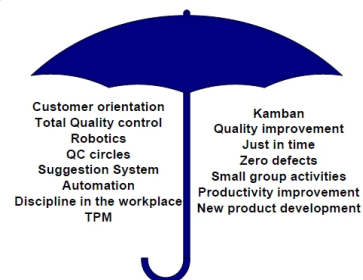


Fig. 1. Umbrella concept [7]

3. QUALITY CONTROL BY USING COMPUTER VISUAL CONTROL SYSTEM

Today's industrial automation systems are almost unthinkable without visual control in the process. The overall visual control process from the supply of images, processing, analysis and measurements can be seen as an integrated process. Systems for computer vision can be divided into several segments: light sources, cameras, software, computers, I/O (input - output) units, sensors and observers (figure 2.).

Depending on the purpose of the visual system, the main goal is to receive a signal from the object to be tested, so that can be determined the geometry and properties, and based on the obtained and processed data to program an action. [8]

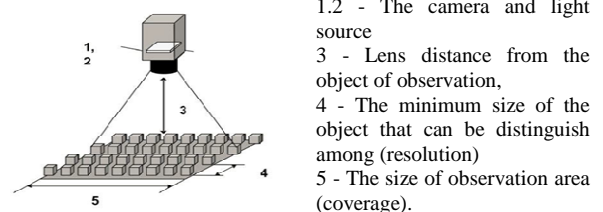


Fig. 2. The basic parameters of the visual control system,

In visual control system, the object that has to be checked is necessary to be lead in control area and associated with program for image processing (figure 3.). As a unit for the fetching of images is recommended to use the digital industrial cameras with high resolution. Depending on the type of measurement and control, the camera has to be calibrated for prescribed conditions (distance the lens from the surface of observation, color recognition and segments of the observed object). It is very important a constant and uninterrupted source of light (intention not to change the conditions in image processing during the process). After computer image processing control, one of the programmed action followed depending on the results of a visual control that the computer sends to the terminal, LAN, PLC, printer and so on.

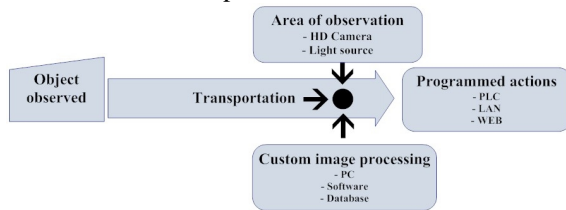


Fig. 3. The principle of verification of the product by using the visual system

“A visual builder for automated control” (Vision Builder AI - VBAI) from National Instruments has in features which allows that system can be quickly installed and implemented as standalone visual control system.

For controls that require conditional decisions or repetitive actions, VBAI works through model and processes diagrams. Through model can be configured that each state performs a specific action: from fetching of images, over text reading till the communication with external devices. The results of these steps are determined which transition that will be used for the next state. Using diagrams it can be can created very complex computer applications for visual control, where the flexibility of programming is better with using ready-made objects (graphical programming) [9]. State and process diagrams work on Petri nets (PN) principle.

Universality is one of PN advantage. The principles are the same, only the necessary knowledge of the rules of each element (subsystem) within the system to assign a specific meaning. In this way, the connections and the characteristic behavior of asynchronous, concurrent, discrete systems have become very transparent.

For the modeling of events-discrete-dynamic system should be taken into consideration conditions and the events that can lead to the change of state. Net status is described through set of variables that represent local conditions. Furthermore, the net points out clearly the existence of the transition and the network structure is based on two sets of objects: positions and transitions.

Positions and transitions are linked through weight relations. Structure of Petrie net is defined by the weight, bi-parity and graph that consists of the positions, transitions and arcs. Petri nets are graphical

method that used the circle to display the position and lines to show the transitions. Input-output connections are shown by arrows between positions and transitions, Figure 4. shows a simple PN model [10].

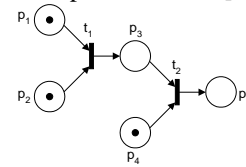


Fig. 4. Simple PN-model [10]

Weights, positions and transitions got a specific meaning with the goal of correct interpretation of the model. For example: In the production system positions typically represent resources (machines, work pieces, information...); weight in a position means that the resource is available, and the lack of weight means it is not available; and position can be used to set the conditions. If such a position has a weight, a condition is true; otherwise it is false (logic 1 or 0).

The transition is usually used to represent the beginning or end of the event (e.g. the machine is repaired...).

Today exists different variants of PN basic structure mainly with simple upgrades. The aim of the upgrades is to improve its functions. Such variants of PN are AMI, Aadli, Artifex, Algebraic etc. [10, 11, 12]

4. VBAI PROGRAMMING INTERFACE AND FEATURES

VBAI interface is composed of the main window that shows the current picture or diagram; the auxiliary window; the window for defining individual states from the diagram; the menu bar; testing and inspection program bar; bar in which can be defined the steps for each part of the program (installation, diagram, cleaning of variables, selection of control) (figure 5.).

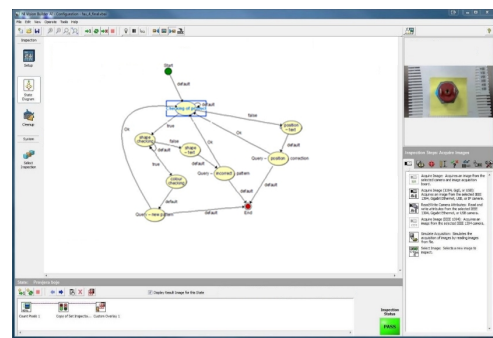


Fig. 5. Development program interface VBAI

After the application is started the program firstly looks for camera signal, then check the object of observation (existence and position). After that program checks the shape of the object (proper form). If everything is OK than program check the color (checks if the observed subject target surface covered with glue or not).

In case of any negative status the program on the screen-prints an error message (no object, incorrectly position of the object, wrong shape of the object, no glue or control is not passed).

Figure 6. shows state diagram for control of glue on pneumatic stop switch, while figure 7. presents necessary control steps for the checking of observed object. The steps are: Simulate Acquisition (figure 8.), Create Region of Interest (figure 9.), Find Edges (figure 10.) and Logic Calculator (figure 11.).

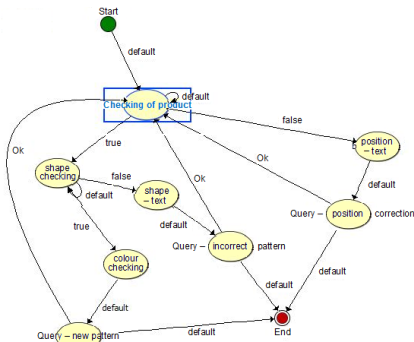


Fig. 6. State diagram for control of glue

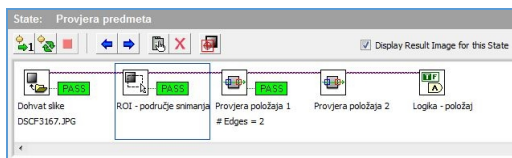


Fig. 7. Steps for control of observed object

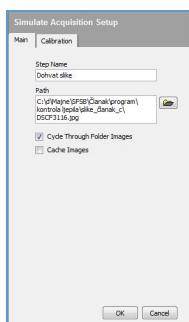


Fig. 8. Simulate Acquisition

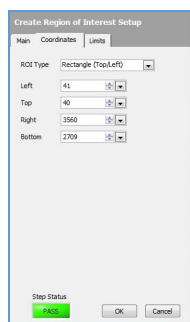


Fig. 9. ROI

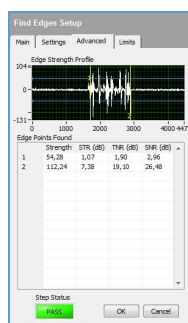
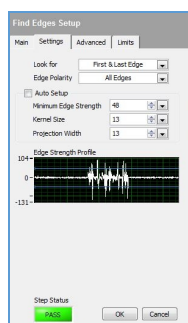
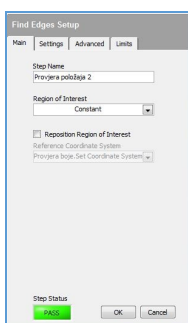


Fig. 10. Find Edges

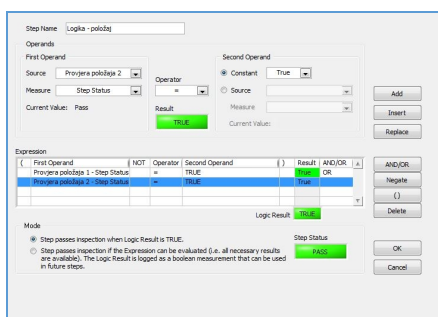


Fig. 11. Logic Calculator

After previous step, the following step is checking the colour (figure 12.). The steps are following: Match Colour Pattern (figure 13.), Coordinate System Setup (figure 14.), Count Pixels (figure 15.), Set Inspection Status (figure 16.) and Custom Overlay (figure 17.).

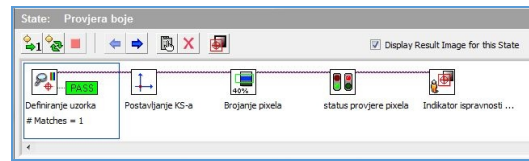


Fig. 12. Checking the colour

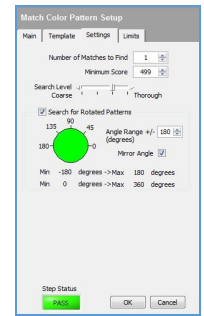
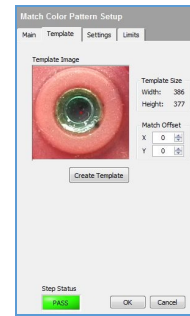
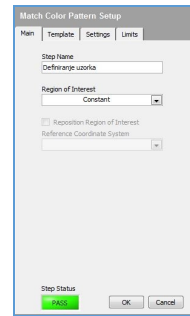


Fig. 13. Match Colour Pattern

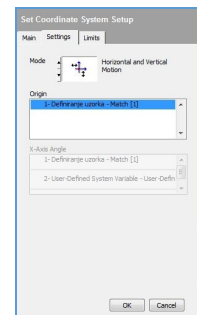
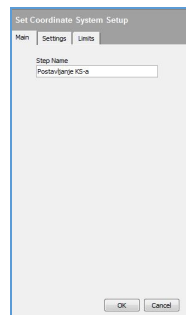


Fig. 14. Coordinate System Setup

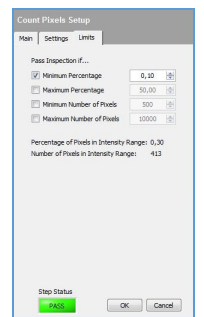
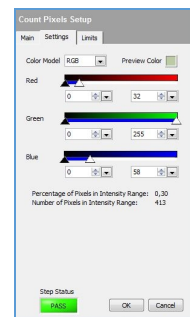
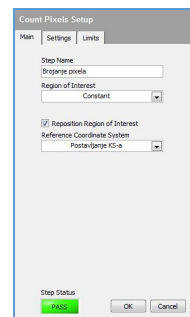


Fig. 15. Count Pixels

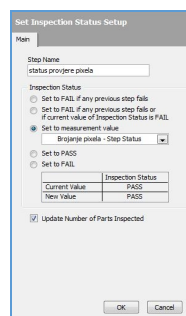


Fig. 16. Set Inspection Status

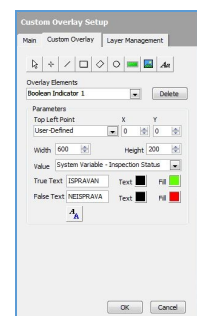


Fig. 17. Custom Overlay

When the subject meets all state controls and program steps, the program will show the text in the green field "TRUE". The subject is identified as correct pattern. Figure 18. shows the user interface in the case of correct pattern identification.

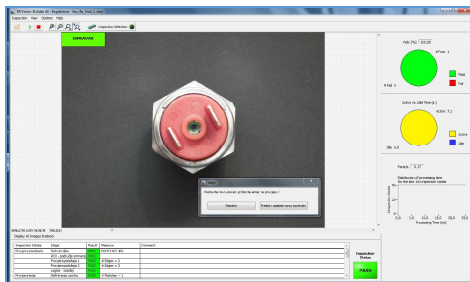


Fig. 18. The appearance of the control interface in the correct pattern

5. CONCLUSION

The purpose of the mission was to improve a particular segment of the manufacturing process with reasonable investment, which will contribute to faster and better manufacturing (Kaizen approach). Visual quality control system is the optimal solution that does not require large investments, additional training of workers or major changes in the existing production process.

The data are taken from Croatian company ELODA. Data are from 2012. when company produced 102.600 pieces of pneumatic switches – 1.246 pieces of waste.

Total installation and control time for 1,000 items is 17.6 hours. Testing and emulating the work of the visual system have been done in 1000 passage of the observed object. Total savings on 102,600 pieces was 3.16 hours, which is not a drastic savings in time, but reduction of discards items was 0.3362%. Current number of product wastes is around 1%, (10.000 ppm) and the goal is less than 1,000 ppm. Every step in reduction of rejects items is step forward.

The advantage of the introduction of the visual system is to improve quality control (high repeatability, reduction of waste etc.) and to improve informatisation and automation of the plant, which is very important for maintaining and getting new certification.

The system is very accurate and possible errors are the factors in the environment, such as changes in lighting, dust and moisture on the lens of camera etc.

Visual system showed that in terms of production need industrial high-resolution camera with advanced features. Another important factor is the light source that must be unobstructed and well-focused on the control field because any major changes in lighting can significantly affect on the results.

6. REFERENCES

[1] Mano, Y., Akoten, J., Yoshino, Y., Sonobe, T.: *Teaching KAIZEN to small business owners: An experiment in a metalworking cluster in Nairobi*, Journal of the Japanese and International Economies, Volume 33, pp 25-42, September

2014.

- [2] Cemrenur, T., Zeynep, A.: *Kaizen-educational: An Awareness-raising and Motivational-enhancement Group Counseling Model*, Procedia - Social and Behavioral Sciences, Volume 84, pp 1356-1360, 9 July.
- [3] Dotoli, M., Epicoco, N., Falagario M., Costantino, N., Turchiano, B.: *An integrated approach for warehouse analysis and optimization: A case study*, Computers in Industry, Volume 70, pp 56-69, June 2015.
- [4] Chan, F.T.S., Lau, H.C.W.; Ip, R.W.L.; Chan, H.K., Kong, S.: *Implementation of total productive maintenance: A case study*, Int. J. Production Economics 95, pp. 71–94, 2005.
- [5] Venkataraman, K., Vijaya Ramnath, B., Muthu Kumar, V., Elanchezhian, C.: *Application of Value Stream Mapping for Reduction of Cycle Time in a Machining Process*. Procedia Materials Science 6, pp 1187 – 1196, 2014.
- [6] Liker, J.K., Meier, D.: *The Toyota Way Fieldbook*, McGraw-Hill, 2005.
- [7] *Kaizen definition & principles in brief*, http://www.michailolidis.gr/index_en.html, Michail Lolidis, 42 pages, (03.07.2015.).
- [8] Jahne, B., Haubecker, H.: *Computer Vision and applications*, Academic Press, 2000.
- [9] National Instruments: *Configurable Machine Vision Software*, http://www.ni.com/pdf/products/us/vbai_datasheet.pdf, (03.07.2015).
- [10] Petri, C.A.: *Kommunikation mit Automaten*, PhD thesis, Institut für instrumentelle Mathematik, Bonn, 1962., 123 pages.
- [11] Valette, R.: *Analysis of Petri Nets by Stepwise Refinement*, Journal of Computer and System Sciences, 18, pp. 35-46, 1979.
- [12] Faculty of Mathematics, Informatics und Natural Sciences, University of Hamburg: www.informatik.uni-hamburg.de/TGI/PetriNets, (10.08.2014.).

Authors: Prof. dr Roberto Lujic, Tomislav Saric, Goran Simunovic, Katica Simunovic, Assistant Ilija Svalina, Student Ivan Nikolic, Josip Juraj Strossmayer University of Osijek, the Mechanical Engineering Faculty in Slavonski Brod, Trg I.B. Mazuranic 2, 35000 Slavonski Brod, Croatia, Phone.: +385 35 446-188, Fax: +385 35 446-443.
E-mail: roberto.lujic@sfsb.hr; tomislav.saric@sfsb.hr; goran.simunovic@sfsb.hr; katica.simunovic@sfsb.hr; ilija.svalina@sfsb.hr; ivan.nikolic@sfsb.hr

Assistant Professor Vjekoslav Galzina, Josip Juraj Strossmayer University of Osijek, Faculty of Education, Cara Hadrijana 10, 31000 Osijek, Phone.: +385 31 321-700, Fax: +385 3 31 321-899
E-mail: vjekoslav.galzina@foozos.hr

MSc. Josip Jukic, College of Slavonski Brod, Dr. Mile Budaka 1, 35000 Slavonski Brod, Croatia, Phone.: +385 35 492-801.

E-mail: josip.jukic@vusb.hr

OPTIMISATION OF THE INSERT TOP CLAMPING SYSTEM USED AT TURNING TOOLS

Abstract: Modern tools used on the machining centres have indexable hardmetal inserts fixed with mechanical systems. The intensive cutting parameters determines stresses that can decrease the stability and the reability of the inserts. The paper analyses the optimal clamping point of the inserts top clamping system used at turning tools. Both square and triangle inserts are studied. The finite element method allows the internal insert stresses analysing. The study is useful for the design improvement of the inserts top clamping systems.

Key words: turning tool, insert, clamping, lever clamping, stresses, design.

1. INTRODUCTION

Current machining systems are faced with increasing requirements for machinability, quality and tool life. The machining systems consist of a machine tool, a work piece clamping device, a work piece, a tool and a tool clamping device. The tools are all made entirely of cemented carbides (hard metal), or have changeable inserts by cemented carbide.

A number of authors have sought to analyse clamping devices of blanks and to optimize them. Leminen [3] analyses requirements and criteria of modularization and standardization of the work piece clamping devices. Mara eková [4] focused on deviations generated during the turning process due to blank clamping pressure. Todorovic [5] analyses a fixture-work piece system with different types of clamping elements.

Technical literature analyses little of inserts clamping on cutting tools. Brindasu [1] analyse a wide range of problems which appear at cutting tools and try to give solution using creativity and finite element method analyses.

The insert clamping system on the tool body must meet a number of needs:

- Small costs per volume unit of machined material;
- High durability of the inserts and their clamping elements;
- Maintaining the positioning dimension of the cutting edge after reconditioning;
- Easy and quick changing of the insert;
- The stability of the insert position on the tool body. The direction and magnitude of the cutting force can vary and dislodge the insert. In this situation its processing precision and tool life decreases.

To meet these needs, the insert clamping system on the tool body must satisfy a number of functional requirements:

- Shapes of the insert, insert seat and clamping elements must ensure the stability of the insert position on the tool body.
- The application position of the clamping force must be well-established to provide insert stability and not to introduce unfavourable tensions in the insert.

- The value of the clamping force must be large enough to provide a rigid grip but small enough not to destroy the clamping screw thread and to produce deformation of the clamping elements or unfavourable tensions in the insert.
- Favourable stresses in the insert in order to obtain better durability.

Until now, cutting tools firms produced some clamping system for the carbide inserts, without fixing hole used for turning. The most usual are presented in figure 1.

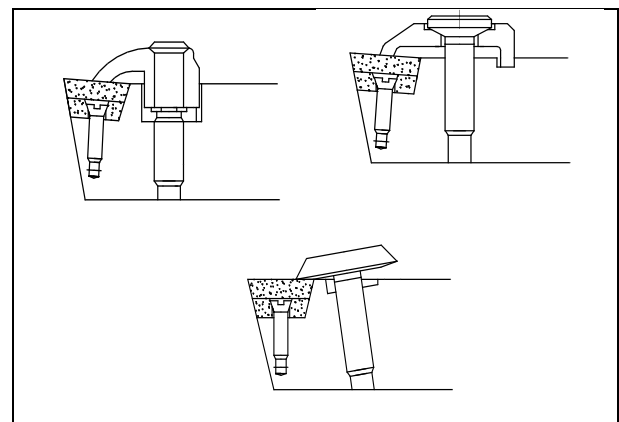


Fig. 1. Top clamping systems

Technical literature doesn't analyse details related with these systems. For a correct design some information are necessary to be known. The following problems will be analysed:

- clamping force value;
- clamping force point of application and direction;
- insert stresses.

2. CLAMPING FORCE ESTIMATION

To estimate the clamping force, a model presented in figure 2 was used. The clamping element is fixed by a screw. The worker applies a torque moment in order to fasten the screw. The clamping element presses the insert with a P force. The value of the torque moment is

indicated in the technical literature [6] (table 1).

Screw	The length of the screw [mm]	Torque [Nm]
M3	7...8.5	1.2
M3.5	12	3
	9.4	2
	5.2	1.2
M4	8.5...13	3
M5	10...17	5
M6	20	7.5

Table 1 Torque moment for a range of clamping screws

The parameters are:

- M_t - torque moment;
- P - clamping force;
- l_p - clamping system parameter (5...10 mm);
- σ_{ac} - compression strength for cemented carbide (2500-5000 MPa);
- A_c - contact area between the insert and the clamping element.

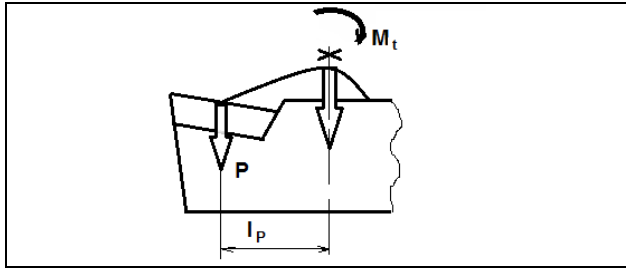


Fig. 2. Clamping force estimation

The following equations can be written [2]:

$$M_t = 0.2 * P * l_p \quad (1)$$

For a M4 screw, the torque is 3Nm. Considering $l_p=7\text{mm}$, the clamping force is:

$$P = \frac{M_t}{0.2 \cdot l_p} \approx 2100\text{N} \quad (2)$$

For a M5 screw (torque is 5Nm), the clamping force is 2500 N.

Contact area between the insert and the clamping system depends on the shape of the clamping element. It is generally greater than 1mm^2 :

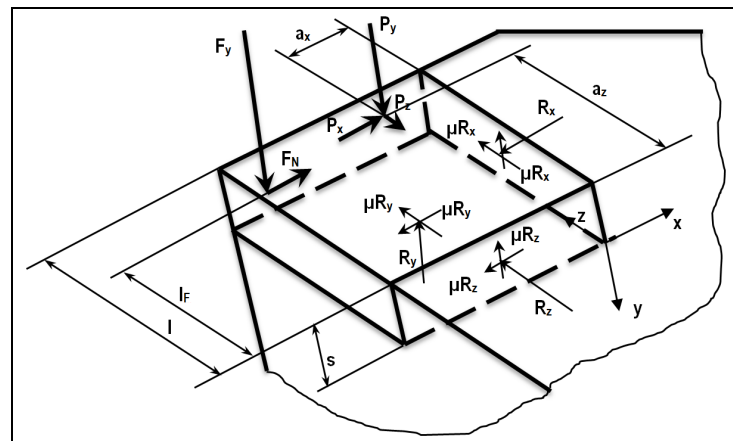


Fig.3 Force equilibrium model of a square insert at turning

In the following study clamping force was considered to be $P=2000\text{ N}$ for finishing and $P=2500\text{ N}$ for roughing.

3. CLAMPING POINT POSITION FOR SQUARE INSERTS

In order to compute the best point position for insert clamping the figure 3 is used. The insert is described in the Oxyz orthogonal system. It has supports on the bottom surface and on two lateral surface opposites to the cutting edge. The cutting force point application is considered to be at the middle of the chip width. We want to establish the best position of the clamping point for different cutting parameter.

The defined parameters are:

- l is insert length;
- s - insert thickness;
- $P(P_x, P_y, P_z)$ clamping force;
- $A(-a_x, -s, a_z)$ insert clamping force position;
- $F(F_N, F_y, 0)$ - cutting force;
- $B(-l, -s, l_p)$ -cutting force position;
- R_x, R_y, R_z - reaction forces in supports.

The force and momentum of equilibrium equations are:

$$F_N + P_x - R_x - \mu R_y - \mu R_z = 0 \quad (3)$$

$$F_y + P_y - \mu R_x - R_y - \mu R_z = 0 \quad (4)$$

$$P_z - \mu R_x - \mu R_y - R_z = 0 \quad (5)$$

$$F_y \cdot l + P_y \cdot a_z - P_z \cdot s + 0.5 \cdot \mu \cdot R_x \cdot s - 0.5 \cdot \mu \cdot R_x \cdot l - 0.5 \cdot R_y \cdot l + 0.5 \cdot R_z \cdot s = 0 \quad (6)$$

$$F_N \cdot l + P_x \cdot a_z - P_z \cdot a_x - 0.5 \cdot R_x \cdot l - 0.5 \cdot \mu \cdot R_y \cdot l + 0.5 \cdot \mu \cdot R_z \cdot l + 0.5 \cdot R_z \cdot l = 0 \quad (7)$$

$$F_y \cdot l - F_N \cdot s + P_y \cdot a_x - P_x \cdot s + 0.5 \cdot R_x \cdot s - 0.5 \cdot R_y \cdot l + 0.5 \cdot \mu \cdot R_z \cdot s - 0.5 \cdot R_z \cdot l = 0 \quad (8)$$

From the equations 3 to 5, the values of reaction forces in supports were computed. With these values, from equations 6 and 8 was possible to establish the expression for a_x and a_z coordinates (clamping force point of application).

In order to improve the equation shape we consider:

$$m = 0.5 \cdot (1 + \mu) / (1 - \mu) / (1 + 2\mu)$$

$$n = 0.5 \cdot \mu / (1 - \mu) / (1 + 2\mu)$$

Clamping force point of application coordinates are:

$$ax = m \cdot l + n \cdot s + Fy/Py [l(m-1) + n \cdot s] + FN/Py [s(1-m) - n \cdot l] + Px/Py [s(1-m) - n \cdot l] \quad (9)$$

$$az = m \cdot l + n \cdot s + Fy/Py (m \cdot l + n \cdot s - lF) + Pz/Py [s(1-m) - n \cdot l] \quad (10)$$

For a friction coefficient $\mu = 0.25$ and a normal cutting $F_N = 0.2 Fy$, clamping force point of application coordinates are:

$$ax = 0.55 \cdot l + 0.11 \cdot s + Fy/Py (0.2 \cdot s - 0.47 \cdot l) + Px/Py (0.45 \cdot s - 0.11 \cdot l) \quad (11)$$

$$az = 0.55 \cdot l + 0.11 \cdot s + Fy/Py (0.55 \cdot l + 0.11 \cdot s - lF) + Pz/Py (0.45 \cdot s - 0.11 \cdot l) \quad (12)$$

For an insert with $l=12.7\text{mm}$ and $s=4.76\text{mm}$, $\mu = 0.25$ and a normal cutting $F_N = 0.2 Fy$ at finishing for $Fy = 500\text{N}$, $l_F = 0.91$ and $Py=2000\text{N}$, the best point position for the clamping force is $ax = 6.25\text{mm}$, $az = 6.6\text{mm}$.

At roughing for $Fy = 1000\text{N}$, $l_F = 0.61$ and $Py=2500\text{N}$, the best point position for the clamping force is $ax = 5.5\text{mm}$, $az = 7.2\text{mm}$.

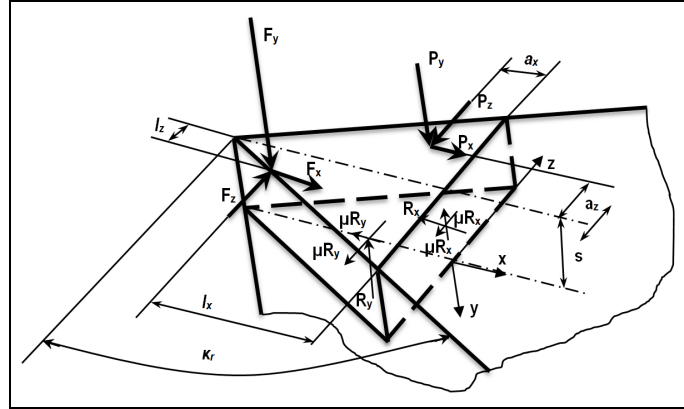


Fig.4 Force equilibrium model of a triangle insert at turning

4. CLAMPING POINT POSITION FOR TRIANGLE INSERTS

The triangle insert is described in the Oxyz orthogonal system (fig.4). It has supports on the bottom surface and on one lateral surface opposite to the cutting edge. The cutting force point application is considered to be at the middle of the chip width. We want to establish the best clamping position for different cutting parameters.

The defined parameters are:

- l is insert length;
- s - insert thickness;
- P(Px, Py, Pz) clamping force;
- A(-ax, -s, az) insert clamping force position;
- F(Fx, Fy, Fz) - cutting force;
- B(-lx, -s, lz) -cutting force position;
- Rx, Ry, - reaction forces in supports.

The force and momentum of equilibrium equations are:

$$Fx + Px - Rx - \mu \cdot Ry = 0 \quad (13)$$

$$Fy + Py - \mu \cdot Rx - Ry = 0 \quad (14)$$

$$Fz - Pz - \mu \cdot Rx - \mu \cdot Ry = 0 \quad (15)$$

$$Fz \cdot s - Fy \cdot lz + Py \cdot az - Pz \cdot s = 0 \quad (16)$$

$$Fx \cdot lz - Fz \cdot lx - Pz \cdot ax - \mu \cdot \sqrt{3}/6 \cdot Ry \cdot l - Px \cdot az = 0 \quad (17)$$

$$Fy \cdot lx - Fx \cdot s + Py \cdot ax - Px \cdot s - \sqrt{3}/6 \cdot Ry \cdot l + 0.5 \cdot \mu \cdot Rx \cdot s = 0 \quad (18)$$

From the equations 13 and 15, the values of

reaction forces in supports (Rx, Ry) were computed. Their values are:

$$Rx = \frac{Fx - \mu \cdot Fy + Px - \mu Py}{1 - \mu^2} \quad (19)$$

$$Ry = \frac{Fy - \mu \cdot Fx + Py - \mu Px}{1 - \mu^2} \quad (20)$$

With these values, from equations 16 and 18 was possible to establish the expression for ax and az coordinates (clamping force point of application).

Clamping force point of application coordinates is:

$$ax = \frac{s \cdot Fx - lx \cdot Fy + s \cdot Px + \sqrt{3}/6 \cdot l \cdot Ry - 0.5 \cdot \mu \cdot s \cdot Rx}{Py} \quad (21)$$

$$az = \frac{s \cdot Pz + lz \cdot Fy - s \cdot Fz}{Py} \quad (22)$$

The forces Fx and Fy are: $Fx = F_N \cdot \cos \kappa_r$ and $Fz = F_N \cdot \sin \kappa_r$, where κ_r is the approach angle of the cutting edge.

For a friction coefficient $\mu = 0.25$ and a normal cutting $F_N = 0.2 Fy$, $\kappa_r = 60^\circ$ an insert with $l=16.5\text{mm}$ and $s=4.76\text{mm}$, at finishing for $Fy = 500\text{N}$ and $Py = 2000\text{N}$, the best point position for the clamping force is given by $ax = 4.3\text{mm}$, $az = 0.9\text{mm}$.

At roughing for $Fy = 600\text{N}$ and $Py = 2500\text{N}$, the best point position for the clamping force is $ax = 5.1\text{mm}$, $az = 1.2\text{mm}$.

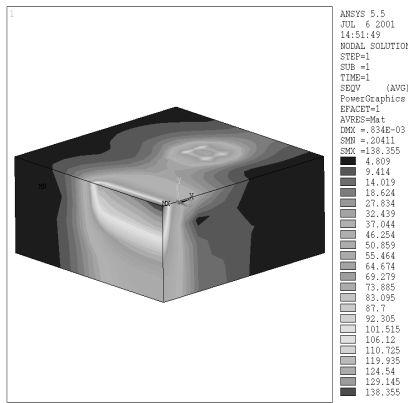
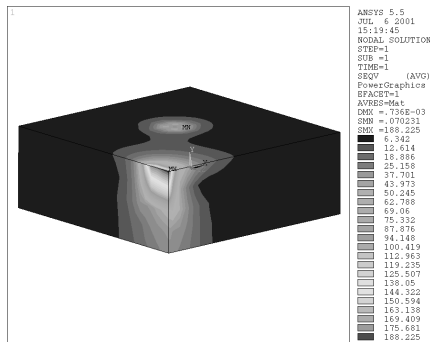


Fig.6 Von Mises stresses for roughing manufacturing insert

5. INSERTS INTERNAL STRESSES

In order to analyse the internal stresses of the inserts in the cutting process, the finite element method was



Bojani , M., Hadžistevi , M., Mladenovi , C.

STRAIGHTNESS EXAMINATION OF CMM AXES

Abstract: It is generally known that the parts with tight tolerances can only be measured on precise, or accurate measuring machines. Accuracy is one of the indicators of quality of measuring equipment. By controlling the parameters of accuracy from the very beginning of machine life cycle, it is possible to maintain the permissible limits of its quality characteristics. The straightness deviation represents line flow in two perpendicular planes. The straightness is one of the essential characteristics of exploitation that must be strictly controlled. Measurement of straightness is applied in many areas such as manufacturing and testing of precision instruments, measuring dimensions of large objects, assembly and adjustment of large equipment.

In this paper, the emphasis is placed on the straightness of the numerically controlled measuring machines (CMM) elements movement along the X and Y axes. The measurement is carried out by laser measuring system (LMS).

Key words: CMM, Straightness, Laser measuring system

1. INTRODUCTION

The paper describes numerically controlled measuring machines, and presents some of experimental results obtained during the straightness examination of coordinate measuring machine elements along the X and Y axes, on the example of Carl Zeiss Contura G2. All results are presented graphically.

Methods for determining the work table moving straightness can be realized by measuring the angle deviation or lateral displacement of the table during the movement. An auto-collimator, precision level, or laser interferometer can be adopted to determine the angle deviations, whereas a straightedge, taut-wire and microscope, alignment telescope, four-quadrant photo-detector, or laser interferometer can be used to determine the lateral displacements.

Although some other methods have been proposed, the laser interferometer for lateral displacement measurements is widely used due to the advantages of high signal to noise ratio, high linearity, high resolution, non-contact, and direct measurement. Laser interferometer was used in the experiment, which was carried out in this paper.

Numerically controlled measuring machines are complex metrology systems. Key elements for the development of CMM are computers, sensors and micro electrical engineering. Numerically controlled measuring machines have two primary applications. The first application of CMM is for measuring and control of all types of tolerance, and second is for adaptive conformity quality management.

The basic characteristics of CMM are [1]:

- Metrological universality
- High resolution, accuracy and reliability compared to conventional measurement technique
- High productivity
- Complete automation of almost all the work cycles
- High flexibility
- Low total cost of metrology process

- Relatively simple and quick preparation process, calibration, adjustable measuring objects, programming and handling CMM system

The parameters that determine the quality of a CMM are shown in Figure 1 [1].

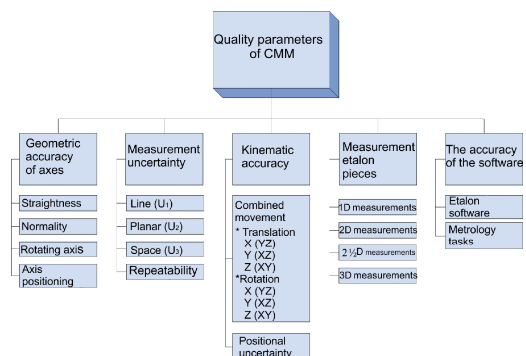


Fig. 1. Elements of CMM quality parameters [1]

2. AXES STRAIGHTNESS

The straightness represents deviation of line flow in the two perpendicular planes (Figure 2). Figure 2a) and 2b) shows parameters of deviation from straightness and Figure 2c) shows the straightness measurement results.

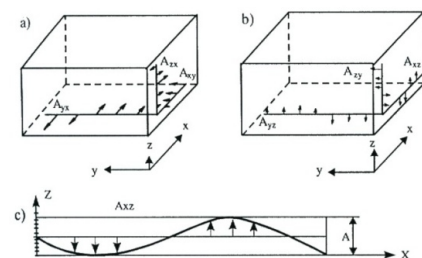


Fig. 2. The parameters and the presentation of axes straightness measurement results [2]

In this way is obtained 6 straightness parameters:

- A_{xy} - straightness of X axis measured in the Y direction
- A_{zx} - straightness of Z axis measured in the X direction
- A_{yx} - straightness of Y axis measured in the X direction
- A_{xz} - straightness of X axis measured in the Z direction
- A_{zy} - straightness of Z axis measured in the Y direction
- A_{yz} - straightness of Y axis measured in the Z direction

By SRPS standard straightness testing includes:

- The line straightness in two planes
- The straightness of the machine parts (components)
- The straightness of movement (movement paths of machine elements)

Path straightness testing is crucial for examination the straightness of machines slide and base. The path straightness of the machine can be defined as parallelism of machine element movement trajectory and the reference line, which is parallel to a measured axis.

Testing can be done in several ways, such as trial by using a measuring ruler and measuring comparator, using stretched wire and a microscope, and using a laser alignment, or a laser interferometer.

As already mentioned, in this paper straightness is measured by the LMS. During the measurement the laser beam passes through the interferometer (Wollaston prism) and being separates in two beams at an angle . These beams are normally deduced from the reflector and return to the laser head, passing through the interferometer, where they are again combined into a single beam. It should be noted that the reflector consists of two rigidly connected mirrors under precise angle. The lateral movement of the interferometer relative to the axis of the reflector is detected inside laser head, and sent to data recording device (Figure 3).

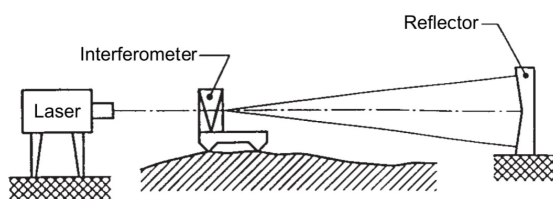


Fig. 3. Testing straightness by using laser interferometer [3]

3. MEASURING INSTRUMENTS

Testing the straightness of above mentioned CMM (Carl Zeiss Contura G2) elements along the X and Y axes was carried out using a laser measuring system (LMS) 5526 A, produced by "Hewlett-Packard", with the accuracy of $0.5 \mu\text{m/m} \pm 0.2 \mu\text{m/m}$ (Figure 4). This system consists of:

- Laser head (He- Ne gas laser)- 5500 C
- Automatic compensator- 5510A
- Laser display HP- 5505A
- Straightness adapter

- Optical components

Laser head 5500C is one of the first HP laser for metrology which has an integrated optical receiver for the return laser beam [4].

Automatic compensator 5510 A is used to correct the influence of environmental factors such as temperature, humidity and air pressure. These factors are measured by using the appropriate sensors connected to the compensator.

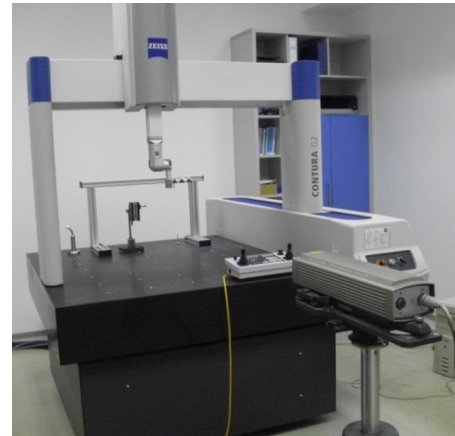


Fig. 4. Numerically controlled measuring machine with mounted LMS

Straightness adapter (Figure 5) consists of partially transmissive mirror that turns the reflected laser beam to the lower opening on the laser head. The laser beam passes through the de-modular polarizer to photo decoder where further signal processing is performed in the usual way.



Fig. 5. Straightness adapter [4]

Optical components for measuring straightness are used:

- *Straightness interferometer* (Figure 6), depending on the length of the measuring way can be used short range and long range interferometer. In this case is used short range interferometer that allows examination of straightness from 100 mm up to 30 m.
- *Straightness reflector* (Figure 6), as well as an interferometer, can be for a short and for a long range examination. It consists of a pair of flat mirrors rigidly connected under the precise angle. The difference between the short and long range straightness reflector is in the angle between mirrors. In this case, is used short range reflector.



Fig. 6. Straightness interferometer and straightness reflector [4]

4. STRAIGHTNESS TEST RESULTS OF THE MEASUREMENT SENSOR CARRIER MOVEMENT

To test the straightness of above mentioned CMM elements along the X and Y axes is used already described laser measuring system, while collecting and processing data are carried out with computer system.

Measuring the straightness of CMM elements moving along X direction is done in relation to the two planes XY and XZ plane. The only difference in these two measurements is in adjustment of the LMS, i.e. straightness reflector.

Total measuring way in the X direction is 700 mm, and the distance between the measuring position is $L_i = 70$ mm. The movement of the measuring sensor carrier was performed in linear cycle (Figure 8), and the first passage is used to test the program. After this passage, measurements were carried out five times in both horizontal and vertical planes. Measured straightness values for measuring sensor movement along the X axis, measured relative to the Z axis, are shown in Table 1. The calculated values of deviations from straightness are shown in Table 2 and graphically in Figure 9.

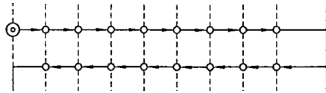


Fig. 8. Segment of linear measuring cycle [7]

Redni broj	I merenje	II merenje	III merenje	IV merenje	V merenje
0	0	-0,0108	-0,0144	-0,018	-0,018
1	-0,036	-0,0432	-0,0432	-0,0468	-0,0468
2	-0,0648	-0,072	-0,0756	-0,0756	-0,0756
3	-0,0972	-0,1008	-0,1044	-0,1044	-0,1044
4	-0,1296	-0,1332	-0,1368	-0,1332	-0,1332
5	-0,1584	-0,162	-0,1656	-0,162	-0,162
6	-0,1908	-0,1908	-0,1944	-0,1908	-0,1908
7	-0,2232	-0,2232	-0,2232	-0,2232	-0,2196
8	-0,252	-0,252	-0,2556	-0,252	-0,252
9	-0,2808	-0,2844	-0,2808	-0,2844	-0,2808
10	-0,3132	-0,3132	-0,3132	-0,3096	-0,3132

Table 1. The measured straightness for movement along the X axis

Redni broj i_i	Položaj x_i	Odstupanje od pravosti	
		Srednje izmerene vrednosti [mm]	ΔP_{X_i} [μm]
0	100	-0,01476	0
1	170	-0,04428	-0,144
2	240	-0,07308	-1,008
3	310	-0,1026	-1,152
4	380	-0,13248	-0,936
5	450	-0,16164	-1,44
6	520	-0,19116	-1,584
7	590	-0,22176	-0,648
8	660	-0,25128	-0,792
9	730	-0,28152	-0,216
10	800	-0,3114	0

Table 2. Calculated values of deviations from straightness

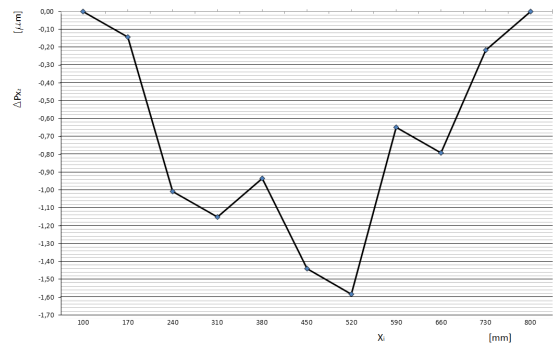


Fig. 7. Graphical representation of deviation from straightness of the X axis in relation to the Z axis

Due to lack of space below will not be displayed measurement results and calculated values of deviations from straightness, but only graphical presentation. Figure 9 shows the deviation from straightness of the X axis in relation to Y.

Measuring the motion straightness of CMM elements in the Y direction is also carried out in relation to the two planes. Total measurement length is 800 mm, and the distance between the measuring positions are $L_i = 80$ mm. The movement of the portal was performed using a PC, the measurement was also performed by linear cycles and the first pass is used to test the program. After this passage, measurements were carried out five times in the YX and YZ planes.

In Figures 10 and 11, are graphs showing deviation of the Y axis in relation to the X and Z axes.

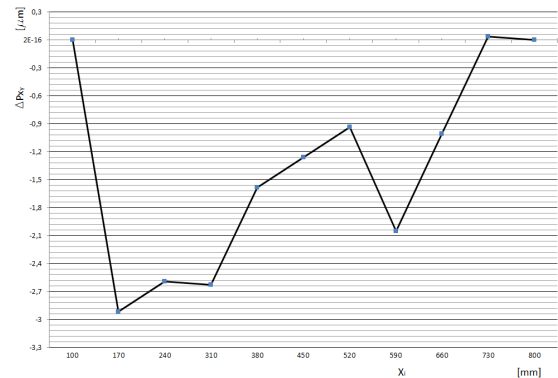


Fig. 9. Graphical representation of deviation from straightness of the X axis in relation to the Y axis

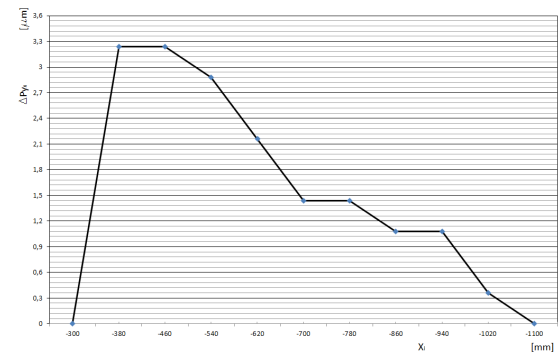


Fig. 10. Graphical representation of deviation from straightness of the Y axis in relation to the X axis

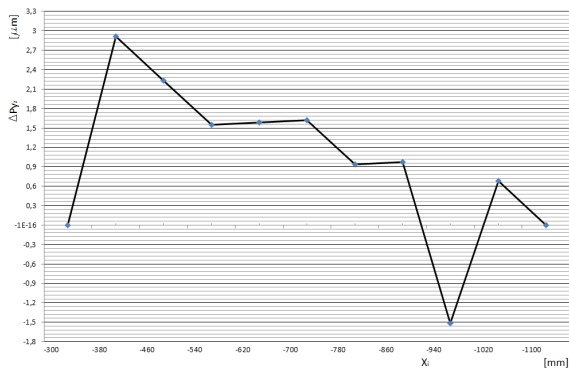


Fig. 11. Graphical representation of deviation from straightness of the Y axis in relation to the Z axis

Data on deviation from straightness by individual axes are obtained based on the movement of coordinate measuring machine movable elements along the X and Y axes. Total deviation from straightness measured for the X axis is displayed spatially, and on the same chart are showed value variation in the two axes, Y and Z (Figure 12). Deviation from straightness along Y axis, relative to the axes X and Z, is displayed in the same way (Figure 13).

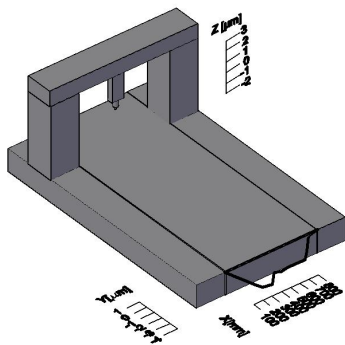


Fig. 12. Spatial graphical representation of the total deviation from straightness of the X axis

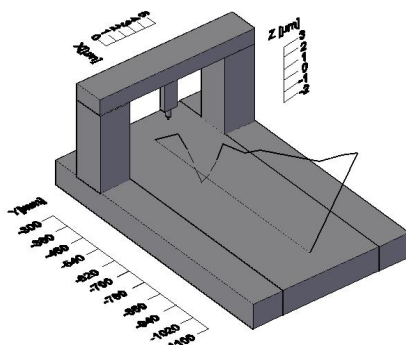


Fig.13. Spatial graphical representation of the total deviation from straightness of the Y axis

5. CONCLUSION

The application of numerically controlled measuring machines is becoming more common in modern industrial systems. To ensure the implementation of various CMM metrology tasks and

high accuracy, the machine itself must possess a high level of quality.

The issues presented in this paper deals with examination of straightness of CMM elements motion. Since the value of the deviations from straightness on numerically controlled machines are very small, they can be carried out only by a laser measurement system.

Testing was performed by moving the measurement sensor along the X and Y axes, and the deviation from straightness is measured in the direction of Y, and Z axes, i.e. in the direction of X and Z axes.

Along the X axis with respect to the Y axis is obtained maximum deviation of $-2.916 \mu\text{m}$, and with respect to the Z axis is obtained deviation $-1.584 \mu\text{m}$.

The maximum values of deviations from straightness for movement along the Y axis, with respect to the X axis are $3.24 \mu\text{m}$, and with respect to the Z axis $2.916 \mu\text{m}$.

The obtained results show that the straightness of the machine is at a satisfactory level.

6. REFERENCES

- [1] Majstorovi , V., Hodoli , J.: *Numeri ki upravljane merne mašine*, Fakultet tehni kih nauka, Institut za proizvodno mašinstvo, Novi Sad, 1998.
- [2] CMMA, *Accuracy Specification for Coordinate Measuring machines*, Entwurf, 1989.
- [3] ISO 230-1: *Prüfregeln für Werkzeugmaschinen, Teil 1: Geometrische Genauigkeit von Maschinen, die ohne Last oder unter Schlichtbedingungen arbeiten*, 1996
- [4] Laser Measurement System 5526A, *Operator's handbook supplement for straightness interferometers*, Hewllet Packard, Santa Clara, 1982.
- [5] Bojani , M.: *Ispitivanje pravosti pomeranja elemenata numeri ki upravljanih mernih mašina*, Ispitni rad, Fakultet tehni kih nauka, Novi Sad, 2012.
- [6] Chen, Q., Lin, D., Wu, J., Yan, J., Yin, C.: *Straightness/coaxiality measurement system with transverse Zeman dual-frequency laser*, Measurement Science and Technology, Volume 16, p.p. 2030-2037, 2005.
- [7] You, F., Zhang,B., Feng Q.: *A novel laser straightness measurement method with beam bend compensation*, Optik, Volume 122, Issue 17, p.p. 1530– 1534, 2011.

ACKNOWLEDGEMENTS

The work is part of research project on "Modern approaches in the development of special bearings in mechanical engineering and medical prosthetics," TR 35025, supported by the Ministry of Education, Science and Technological Development, Republic of Serbia.

Authors: M.Sc. Mirjana Bojani , Prof. dr Miodrag Hadžistevi , M.Sc. Cvijetin Mla enovic, University of Novi Sad, Faculty of Technical Sciences, Trg Dositeja Obradovica 6, 21000 Novi Sad, Serbia, Phone.: +381 21 450-366, Fax: +381 21 454-495.
E-mail: bojanicm@uns.ac.rs; miodrags@uns.ac.rs; mladja@uns.ac.rs

Joti G., Hadžistevi M., Pejašinovi Ž., Štrbac B.

DETERMINATION OF CMM UNCERTAINTY USING CALIBRATED WORKPIECES

Abstract: Coordinate measuring machines (CMMs) are widely used to check geometry of mechanical objects. While applying a coordinate measuring machine to measure a mechanical element, many factors affect the measurement uncertainty. There are a few techniques for assessing uncertainty of measurement, as defined in the ISO Guide to the Expression of Uncertainty in Measurement (GUM). This paper presents a technique for the assessment of measurement uncertainty for measurement results obtained by a CMM and by using calibrated workpieces. The appropriate conclusions will be made based on the analysis of the measurement results.

Key words: CMM, uncertainty of measurement, calibrated workpieces

1. INTRODUCTION

Coordinate measuring machines (CMMs) are one of the best dimensional and geometrical measurement instruments. They are widely used to measure the product's dimensions in industry. Using an instrument with good performance does not imply good measurement results will be obtained. This is due to the fact that the reliability of measurement results is not only attributed to the instrument, but also the operator, method and environment are involved. A better way for characterization reliability of measurement results is to use the concept of uncertainty of measurement. A complete measurement result should consist of the measured value and its uncertainty. Knowledge about the uncertainty of measurement is of fundamental importance to users of these results, because it provides quality assessment and confidence in the results and to their mutual comparison. There are two standardizing documents that consider the uncertainty of coordinate measurements [1,2]. The most significant difference between the documents is that in the first case it is necessary to have a calibrated workpiece and for the second case – a simulation software.

While applying a coordinate measuring machine to measure a mechanical element, many factors affect the measurement uncertainty. This paper presents a technique for the assessment of measurement uncertainty for measurement results obtained by a CMM and by using calibrated workpieces. Uncertainty budget was developed in accordance with ISO GUM and ISO 15530-3. Error sources were found to estimate their standard uncertainties separately. The combined standard uncertainty was then calculated.

2. UNCERTAINTY OF MEASUREMENT

Measurement uncertainty is a parameter that joins the measurement result and which is characterized by dispersion of the values that can reasonably be attributed to the measured value. The parameter could be, for example, a standard deviation or a given multiple of half-width of the interval with the indicated confidence level. This means that the measurement

result is not merely one measurand, but instead measurement uncertainty defines an interval that includes a large number of values, which can claim to represent the measurand with some probability (Fig. 1).

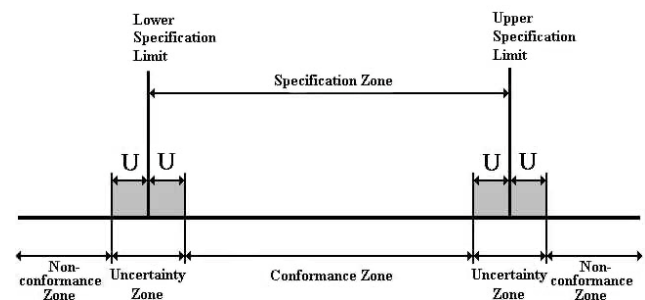


Fig. 1. Interval of acceptable values

Measurement uncertainty is a quantitative indicator of the quality of measurement results, which allows the comparison of measurement results obtained from different sources, different methods in different laboratories. The official definition of measurement uncertainty is [2]: “measurement uncertainty is parameter, which is not negative, is characterized by dispersion of the values attributed to the measurand, which is based on useful information.”

Estimation of measurement uncertainty is significant, it is commonly used in:

- quality control;
- alignment with the regulations;
- assessment of compliance with the requirements;
- research in science and engineering;
- calibration within the national metrology system;
- development, maintenance and comparison of national referent standards;
- laboratory accreditation, etc.

2.1. Uncertainty classification

Standard uncertainty u

Measurement uncertainty is a combination of several components (sources) that contribute to its overall value. Some of these components can be determined based on the statistical distribution of results of a series of repeated measurements and show

by experimental standard deviations – type A evaluation of standard uncertainty [3]:

$$u_A(y) = \frac{s(y)}{\sqrt{n}} = \sqrt{\frac{1}{n(n-1)} \sum_{i=1}^n (y_i - \bar{y})^2} \quad (1)$$

\bar{x} - mean

n - number of repeated measurements

Other components can be determined based on experience or other information – type B evaluation of standard uncertainty. Mentioned information can include [3]:

- previous measurement data;
- experience with or general knowledge of the behaviour and properties of relevant materials and instruments;
- manufacturer's specifications;
- data provided in calibration and other certificates;
- uncertainties assigned to reference data taken from handbooks, etc.

Combined standard uncertainty u_c

The combined measurement uncertainty u_c is applied to estimate the uncertainties indirect measurands.

$$\text{combined uncertainty} = \sqrt{a^2 + b^2 + c^2 + \dots} \quad (2)$$

a, b, c - indirect measurands

Expanded uncertainty U

The expanded uncertainty U is obtained by multiplying the combined standard uncertainty u_c by a coverage factor k :

$$U = k \cdot u_c \quad (3)$$

The result of a measurement is then conveniently expressed as $Y = \bar{y} \pm U$, which is interpreted to mean that the best estimate of the value attributable to the measurand Y is y , and that $\bar{y} - U$ to $\bar{y} + U$ is an interval that may be expected to encompass a large fraction of the distribution of values that could reasonably be attributed to Y [3].

2.2. Techniques for determining CMM measurement uncertainty

When the measurement result Y can be written as an analytic function $Y = f(X_1, X_2, \dots, X_N)$ of its inputs X_i , the measurement uncertainty can be evaluated according to ISO GUM [1]. In case of CMMs, it is not possible to obtain an analytical model of the measurement process. Other methods can be used to determine CMM measurement uncertainties, some of them are also described in ISO/TS 15530-0. Methods regularly used are [4]:

- use of multiple measurements strategies;
- use of calibrated workpieces or standards ISO/TS 15530-3;
- use of computer simulation ISO/TS 15530-4;
- use of expert judgment.

The first two methods allow for very reliable uncertainty evaluations because of their experimental approach. They are easy to perform but very time consuming. The use of computer simulation asks for a

considerable implementation effort, but can be very useful. Regarding the complexity of CMM measurements, expert judgment will not always be reliable, but is recommended when no other methods are available.

3. EVALUATION OF MEASUREMENT UNCERTAINTY USING CALIBRATED WORKPIECES

3.1. Principle and procedure

Before starting the measurements, initialize the CMM and perform procedures such as probe configuration and probe qualification according to the conditions specified in the manufacturer's operating manual. Method requires similarity conditions of the following [1]:

- the dimension and geometry of the workpiece or measurement standard used in the actual measurements and the calibrated workpiece or measurement standard used in the evaluation of measurement uncertainty;
- the measurement procedure of the evaluation of measurement uncertainty and the actual measurement;
- the environmental conditions (including all variations) during evaluation of measurement uncertainty and actual measurement.

The evaluation of measurement uncertainty is a sequence of measurements, performed in the same way and under the same conditions as the actual measurements. The differences between the results obtained by the measurement and the known calibration values of these calibrated workpieces are used to estimate the uncertainty of the measurements.

The uncertainty of the measurement consists of uncertainty contributions [1]:

- due to the measurement procedure;
- from the calibration of the calibrated workpiece;
- due to the variations of the measured workpieces (changing form deviations, expansion coefficient and surface texture).

When performing the measurements, three uncertainty contributions shall basically be taken into account, described by the following standard uncertainties (table 1) [1]:

- u_{cal} standard uncertainty associated with the uncertainty of the calibration of the calibrated workpiece stated in the calibration certificate;
- u_p standard uncertainty associated with the measurement procedure;
- u_w standard uncertainty associated with material and manufacturing variations.

The expanded measuring uncertainty, U , of any measured parameter is calculated from these standard uncertainties as [1]:

$$U = k \sqrt{u_{cal}^2 + u_p^2 + u_w^2} + |b| \quad (4)$$

b - systematic error

Uncertainty component	Method of evaluation	Designation
Geometrical errors of CMM	A	u_p
Temperature of CMM		
Drift of CMM		
Temperature of workpiece		
Systematic errors of probing system		
Repeatability of the CMM		
Scale resolution of the CMM		
Temperature gradients of the CMM		
Random errors of the probing system		
Probe changing uncertainty		
Errors induced by the procedure (clamping, handling, etc.)		
Errors induced by dirt		
Calibration uncertainty of the calibrated workpiece	B	u_{cal}
Differences among workpieces and the calibrated workpiece in - roughness; - form: - elasticity.	A ili B	u_w

Table 1. Uncertainty components and their consideration in the uncertainty assessment

3.2. Experimental work

Experimental measurements were performed with three CMMs, type Carl Zeiss CONTURA G2, at three different locations NS, K and Z. The CONTURA G2 is a mid-range bridge type CMM with advanced features and design strengths (Fig. 2). All axes have 4-sided Carl Zeiss air bearings providing maximum stability and a very precise measurement. Ceramic guideways are thermally stable, minimizing the effect of temperature variation. This experiment utilizes the RDS turning measuring head with the combination of a VAST XXT scanning head with the combination of a VAST XXT scanning measuring sensor. As a replacement for trigger sensors, the VAST XXT offers the unmatched measurement capability, reliability, and accuracy.

	Measurement points							
	1	2	3	4	5	6	7	8
C1	0.0	0.0	0.0	0.0	0.0	0.1	0.1	0.2
	0.1	0.1	0.1	0.1	0.0	0.1	0.1	0.3
	0.1	0.0	0.0	0.1	0.0	0.1	0.1	0.2

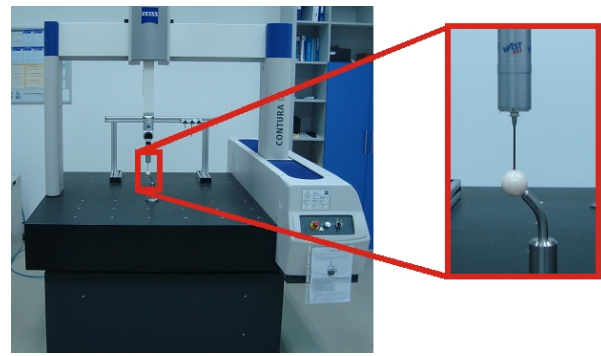


Fig. 2. CMM Carl Zeiss CONTURA G2 RDS, reference sphere and probe

It is important to note that in all three locations the same probe (diameter 3mm), scanning measuring sensor VAST XXT and calibrated workpiece were used. A ceramic calibration sphere with 25 mm diameter (Fig. 2) was used as a calibrated workpiece. The user of a CMM has a high degree of freedom to design the measurement strategy according to the technical requirements (Fig. 3).

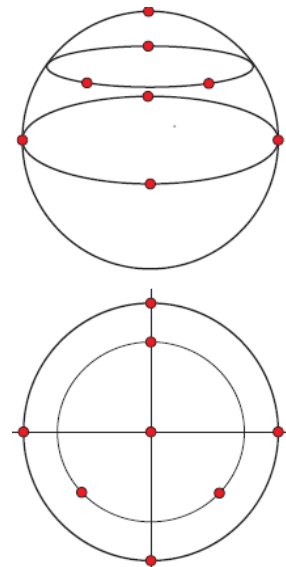


Fig. 3. Measurement strategy

One cycle of an actual measurement consists of the handling of workpieces and one or more measurements of workpieces. Calibration was performed through four cycles of measurements (C1, C2, C3, C4), i.e. four different orientations of the calibrated workpiece. Eight measurements per cycle were performed, the calibration of each point was repeated six times, a total of 192 measurements (Table 3, 4 and 5).

	0.0	0.0	0.1	0.0	0.1	0.1	0.1	0.3
	0.0	0.1	0.0	0.1	0.0	0.1	0.0	0.5
	0.1	0.1	0.1	0.1	0.1	0.1	0.1	0.1
C2	0.1	0.1	0.1	0.1	0.2	0.2	0.1	0.3
	0.0	0.1	0.5	0.1	0.2	0.1	0.4	0.2
	0.0	0.1	0.2	0.3	0.1	0.1	0.2	0.1
	0.0	0.1	0.1	0.2	0.4	0.2	0.1	0.1

	0.1	0.1	0.1	0.1	0.3	0.2	0.1	0.2
	0.1	0.1	0.1	0.1	0.1	0.3	0.1	0.2
C3	0.0	0.2	0.2	0.2	0.2	0.2	0.2	0.3
	0.2	0.2	0.2	0.2	0.2	0.1	0.2	0.2
	0.2	0.2	0.1	0.2	0.2	0.1	0.2	0.2
	0.2	0.1	0.2	0.1	0.1	0.2	0.1	0.1
	0.1	0.1	0.1	0.2	0.2	0.1	0.1	0.1
	0.2	0.1	0.1	0.1	0.1	0.1	0.1	0.1
C4	0.2	0.4	0.3	0.4	0.3	0.3	0.4	0.4
	0.4	0.4	0.4	0.3	0.4	0.4	0.4	0.3
	0.4	0.3	0.3	0.3	0.3	0.3	0.3	0.3
	0.4	0.3	0.4	0.3	0.3	0.3	0.4	0.4
	0.4	0.3	0.3	0.3	0.3	0.3	0.4	0.3
	0.4	0.4	0.4	0.3	0.4	0.4	0.3	0.3

Table 2. Standard deviation, location NS

1.13	1.13	1.1	1.07	1.12	1.11	1.05	1.24
1.11	1.11	1.05	1.08	1.08	1.11	1.06	1.27
1.21	1.14	1.1	1.15	0.98	1.02	1.08	1.1
1.05	1.05	1.09	1.05	1.07	1.06	1.12	1.05
1.07	1.16	1.06	1.09	1.1	1.11	1.07	1.09
1.12	1.12	1.08	1.06	1.17	1.06	1.08	1.12
1.06	1.11	0.94	1.05	1.05	1.1	1.09	1.17
1.1	1.05	1.02	1.17	1.15	1.03	1.16	1.12
1.29	1.2	1.16	1.1	1.23	1.15	1.15	1.23
1.12	1.15	1.19	1.16	1.12	1.21	1.14	1.28
1.04	1.08	1.16	1.1	1.24	1.18	1.1	1.19
1.12	1.14	1.2	1.24	1.12	1.12	1.16	1.24
1.09	1.18	1.12	1.18	1.28	1.1	1.22	1.24
1.1	1.22	1.09	1.11	0.98	1.14	1.28	1.29

Table 4. Standard deviation, location Z

	Measurement points							
	1	2	3	4	5	6	7	8
C1	0.2	0.2	0.2	0.1	0.1	0.1	0.1	0.1
	0.1	0.1	0.1	0.1	0.1	0.1	0.1	0.1
	0.1	0.1	0.1	0.1	0.1	0.1	0.1	0.1
	0.1	0.1	0.1	0.1	0.1	0.1	0.1	0.1
	0.1	0.1	0.1	0.1	0.1	0.1	0.1	0.1
	0.1	0.1	0.1	0.1	0.1	0.0	0.1	0.0
C2	0.0	0.0	0.0	0.0	0.0	0.0	0.0	0.1
	0.0	0.0	0.1	0.0	0.0	0.1	0.1	0.1
	0.0	0.0	0.0	0.0	0.0	0.0	0.0	0.0
	0.0	0.0	0.0	0.1	0.0	0.0	0.0	0.0
	0.0	0.0	0.1	0.0	0.0	0.0	0.0	0.0
	0.0	0.0	0.0	0.0	0.0	0.0	0.0	0.0
C3	0.1	0.0	0.0	0.1	0.1	0.0	0.0	0.0
	0.0	0.0	0.0	0.0	0.0	0.0	0.0	0.0
	0.1	0.1	0.0	0.0	0.0	0.1	0.1	0.0
	0.0	0.0	0.0	0.0	0.0	0.0	0.0	0.0
	0.0	0.0	0.0	0.0	0.0	0.0	0.0	0.0
	0.0	0.0	0.0	0.0	0.0	0.0	0.0	0.0
C4	0.1	0.1	0.0	0.1	0.1	0.0	0.1	0.1
	0.0	0.0	0.1	0.1	0.1	0.1	0.1	0.1
	0.0	0.1	0.1	0.0	0.1	0.1	0.1	0.1
	0.0	0.0	0.0	0.1	0.1	0.1	0.1	0.1
	0.0	0.0	0.1	0.1	0.1	0.1	0.1	0.1
	0.0	0.1	0.0	0.0	0.0	0.1	0.0	0.0

Table 3. Standard deviation, location K

Measurement points							
1	2	3	4	5	6	7	8
0.83	0.85	0.82	0.9	0.83	0.82	0.84	0.81
0.69	0.66	0.65	0.67	0.67	0.74	0.69	0.66
0.64	0.45	0.94	1.01	1	1.08	0.99	1.01
1.01	1.01	1	1.03	0.98	1.05	1.09	0.97
0.99	1.07	1.04	0.99	1.01	0.97	1	1.02
1.02	1.02	1.04	1.01	1.02	1	1.01	1.04
1.25	1.23	1.24	1.26	1.2	1.18	1.22	1.26
1.26	1.25	1.16	1.23	1.19	1.18	1.17	1.29
1.18	1.2	1.14	1.17	1.15	1.11	1.16	1.31
1.07	1.09	1.09	1.15	1.14	1.14	1.13	1.3

3.3. Calculation of the uncertainty

Standard uncertainty of calibrated workpiece u_{cal} , sphere $R = 12.4813$ mm is determined on the basis of an extended measurement uncertainty given in the certificate of calibration sphere [1, 5]:

$$u_{cal} = \frac{U_{cal}}{k} = \frac{0,096}{2} = 0,048 \mu m \quad (5)$$

Standard uncertainty associated with the measurement procedure u_p is determined by expression (1) and shown in table 5. Standard uncertainty associated with material and manufacturing variations u_w is determined by expression (6) and shown in table 5 :

$$u_w = (T - 20^\circ C) \cdot u_\alpha \cdot d \quad (6)$$

T - average temperature of the measurement standard
 $u_\alpha = 0,035 \cdot 10^{-6} 1^\circ C$ - uncertainty of the thermal expansion coefficient

d - diameter of the measurement standard
 In most cases, a systematic deviation b between the indicated value of the CMM and the calibrated value of calibrated workpieces may be observed:

$$b = u_p - u_{cal} \quad (7)$$

Contributors	Locations		
	NS	K	Z
u_{cal}	0,048	0,048	0,048
u_p	0,124	0,053	0,141
u_w	0,000873	0,000873	0,000873
$ b $	0,076	0,005	0,093
$U(k=2)$	0,343	0,148	0,391

Table 5. Results of evaluation of measurement uncertainty

Results of evaluation of expanded standard measurement uncertainty are presented in Fig. 4, for all three locations. The result of a measurement is then conveniently expressed as $Y = \bar{y} \pm U$.

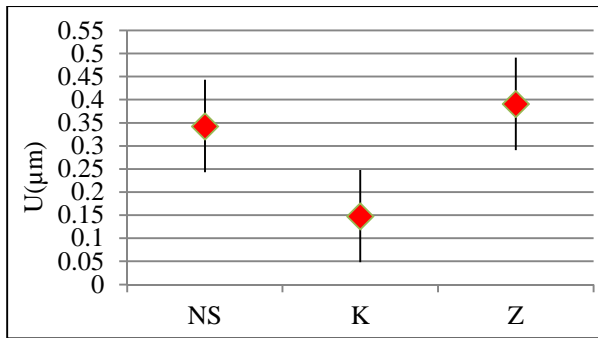


Fig. 4. Results of expanded measurement uncertainty

Fig. 5 gives the results of systematic errors. If these systematic errors are not corrected due to economical or practical reasons, they have to be added to the expanded uncertainty as shown in expression (4).

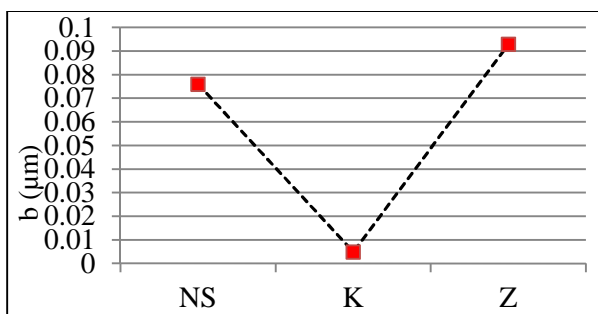


Fig. 5. Systematic errors

4. CONCLUSION

This paper presented a method of determining measurement uncertainty on CMMs. The method is based on the method of using calibrated workpieces or standards. Expanded standard measurement uncertainty was determined for all three CMMs, locations NS, K and Z respectively. Results are reported in Table 5 and presented in Fig. 4. On location K, the CMM has the smallest uncertainty, followed by the CMM on location NS and the CMM on location Z. The same conclusion can be reached by observing the values of systematic errors (Fig. 5).

The method has been completely implemented for measurement of lengths. This allows for unambiguous checking of tolerances. Uncertainty of other geometric tolerances (angle, tolerance features) could be the subject of future research.

5. REFERENCES

- [1] ISO/TS 15530-3:2004 Geometrical Product Specifications (GPS). Coordinate Measuring Machines (CMM): *Technique for Determining the Uncertainty of Measurement*. Part 3: Use of Calibrated Workpieces or Standards.
- [2] *Guide to the Expression of Uncertainty in Measurement (GUM)*. International Organisation for Standardization (ISO), Geneva, 1995.
- [3] Evaluation of measurement data — Guide to the expression of uncertainty in measurement JCGM 100:2008 GUM 1995 with minor corrections.

- [4] Kan-Pierre, K., Van Gestel, N., Bleys, P., Welkenhuyzen, F., (2009). *Uncertainty determination for CMMs by Monte Carlo simulation integrating feature form deviations*, CIRP Annals-Manufacturing Technology, 58, 463-466.
- [5] Certificate of kalibration, issued by spheric-trafalgar limited date of issue 10 March, 2013, certificate number 85566.



Majstorovi , D.V., Stojadinovi , M.S.

CYBER-PHYSIAL MANUFACTURING – INTELLIGENT MODEL FOR INSPECTION PLANNING ON CMM

Abstract: *Cyber-Physical System (CPS) are systems of collaborating computational entities which are in intensive connection with the surrounding physical world and its on-going processes, providing and using, at the same time, data-accessing and data-processing services available on the internet. Cyber-Physical Manufacturing System (CPMS), relying on the newest and foreseeable further developments of computer science, information and communication technologies, on the one hand, and of manufacturing science and technology, on the other hand, may lead to the 4th Industrial Revolution. In order for that to happen we must face the challenges of operating sensor networks, handling big bulks of data, as well as the questions of information retrieval, representation, and interpretation, with special emphasis on security aspects. Novel modes of man-machine communication are to be realized in the course of establishing CPMS.*

In our Laboratory , now we have following researches areas: (i) Digital Manufacturing – Towards Cloud Manufacturing (base for CPMS), (ii) CPMS – Cyber-Physical Quality Model (CPQM) our approach and (iii) Intelligent model for Inspection Planning on CMM as part of Cyber-Physical Manufacturing Metrology Model (CPM³) concept. In this paper we shall show some research results for third direction.

Digital quality, as a key technology for CPMs represents virtual simulation of digital inspection in digital company, based on a global model of interoperable products (GMIP). GMIP represents the integration CAD-CAM-CAI models in the digital environment. The essence of this research is solved the concept of metrology integration into GIMP for the coordinate measuring machine (CMM) inspection planning, based on CPM³.

Key words: *Cyber-Physical Manufacturing, Digital Quality, CMM*

1. INTRODUCTION REMARKS

Today's business structure is much more complex and dynamic than ever before, because market demands of the industry's rapid changes in new products, which is directly reflected in the factory. On the other hand, digitalization and information technology (IT) provide new, unimagined possibilities, engineers in the field of design and planning. The two approaches have led to two concepts that have since emerged: digital factory and digital manufacturing [1,2,13-17].

Developed and implement "advanced manufacturing concept" as a base for Cyber - Physical Manufacturing Systems (CPMSs), will be to evolve along five directions [1,3,26]: (i) on – demand manufacturing: Fast change demand from internet based customers requires mass-customized products. The increasing trend to last-minute purchases and online deals requires from manufactures to be able to deliver products rapidly and on-demand to customers; (ii) optimal and sustainable manufacturing: Producing products with superior quality, environmental consciousness, high security and durability, competitively priced. Envisaging product lifecycle management for optimal and interoperable product design, including value added after-sales services; (iii) human - centric manufacturing: Moving away from a production-centric towards a human-centric activity with great emphasis on generating core value for humans and better integration with life, e.g. production and cites; (iv) innovative products: From laboratory prototype to full scale production – thereby giving

competitors a chance to overtake enterprises through speed, and (v) green products: for example Manufacturing Strategy 2020/30 needs focused initiatives to reduce energy footprints on shop floors and increase awareness of end-of-life (EoL) product use. There are framework for CPMSs.

For a manufacturing system with typical machining operations, factory-wide engineering knowledge integration requires an connection CAD-CAPP-CAM-CNC-CAI and integration with other production-related information systems such as enterprise resource planning (ERP), manufacturing execution system (MES), advanced planning and scheduling (APS), etc [3,4]. A standard for the exchange of product data model (STEP), along with a STEP compliant numerical control (STEP-NC), has been developed to enable integration and exchange of design and manufacturing numerical data. STEP is based on feature technology, and it provides a neutral and interoperable format of product data, independent of any system and suitable for transfer, processing and communication among different systems. Feature technology provides us to associate not only geometric and topological information, but also form features and tolerances that could be used in CAD-CAPP-CAM-CNC-CAI chain [5, 6,14-21].

2. CYBER PHYSICAL MANUFACTURING SYSTEMS (CPMSs) - BASIC FACTS

Cyber-physical systems (CPSs) are enabling technologies which bring the virtual and physical

worlds together to create a truly networked world in which intelligent objects communicate and interact with each other [7]. Together with the internet and the data and services available online, embedded systems join to form cyber-physical systems. CPSs also are a paradigm from existing business and market models, as revolutionary new applications, service providers and value chains become possible [5–7,17-21,26].

The merging of the virtual and the physical worlds through CPSs and the resulting fusion of manufacturing processes and business processes are leading the way to a new industrial age best defined by the INDUSTRIE 4.0 project’s “smart factory” concept [6,7,22].

Smart factory manufacture brings with it numerous advantages over conventional manufacture, as example [5–7,23-26]: (i) CPS - optimized manufacturing processes: smart factory “units” are able to determine and identify their field(s) of activity, configuration options and manufacture conditions as well as communicate independently and wirelessly with other units; (ii) Optimized individual customer product manufacturing via intelligent compilation of ideal production system which factors account product properties, costs, logistics, security, reliability, time, and sustainability considerations; (iii) Resource efficient production; and (iv) Tailored adjustments to the human workforce so that the machine adapts to the human work cycle.

This approach as a manufacturing revolution in terms of both innovation and cost and time savings and the creation of a “bottom-up” manufacturing value creation model whose networking capacity creates new and more market opportunities.

3. RESEARCH IN THE FIELD OF CYBER-PHYSICAL MANUFACTURING METROLOGY MODEL (CPM³) IN OUR LAB

In MEF, Belgrade on Lab for Production Metrology

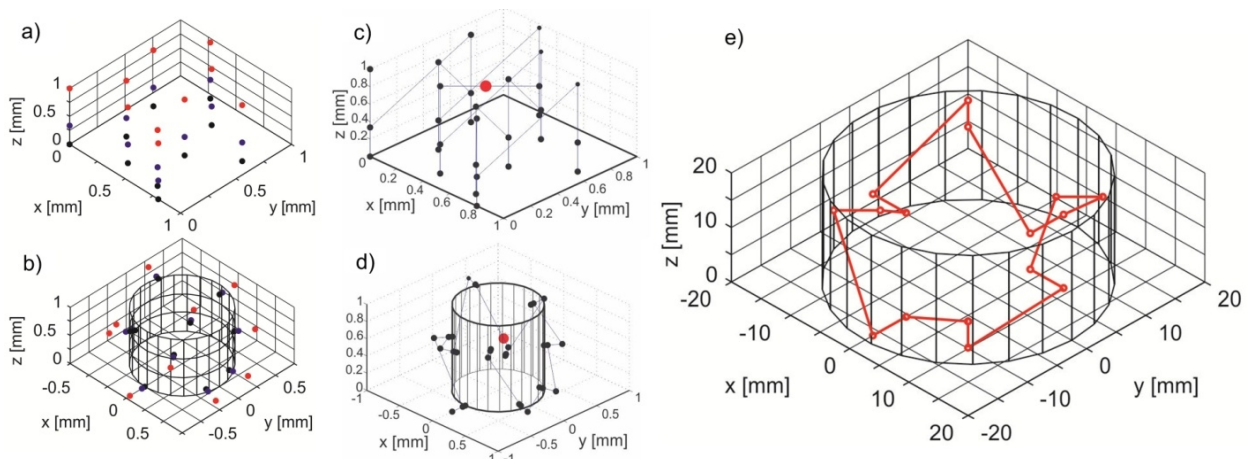


Fig. 1. Principle distribution measuring points (a) plane and b) cylinder), simulation (d) plane and e) cylinder) and optimized measuring path (e))

Based on STL model for the presentation of PP geometry, the tolerances of PP, the coordinates of the last point $P_{(N_{F1})}$ of a feature F1 and the coordinates of the first point $P_{(N_{F2})}$ of a feature F2, the simplified

and TQM, we doing following researches areas: (i) Digital Manufacturing – Towards Cloud Manufacturing (base for CPMs), (ii) Intelligent model for Inspection Planning (IMIP) on CMM as part of CPM concept, and (iii) CPMS – CPQM our approach. In this paper we shall show some research results for second direction [8–12].

The development IMIP for prismatic parts involve following activities: (i) development ontological knowledge base presented in [7,8]; (ii) local and global inspection plan, and (iii) optimize path of measuring sensor. Output from the local and global inspection plan (LGIP) is initial measuring path. The first element LGIP’s is sampling strategy or model for the distribution of measuring points for features presented in [3,4], and second element define the principle for collision avoidance between workpiece and measured probe. By modifying the Hemmersly sequences [12], we define the distribution of measuring points for basic geometric features such as plane, circle, cylinder, cone, hemisphere, truncated hemisphere and truncated cone.

For example the equations for calculation of measuring point coordinates for cylinder are:

$$s_i = R \cos\left(-\frac{\pi}{2} - \frac{2\pi}{N} \cdot i\right) \quad (1)$$

$$t_i = R \sin\left(-\frac{\pi}{2} - \frac{2\pi}{N} \cdot i\right) \quad (2)$$

$$w_i = \left(\sum_{j=0}^{k-1} \left[\left[\frac{i}{2^j}\right] \text{Mod} 2\right] \cdot 2^{-(j+1)}\right) \cdot h \quad (3)$$

where, s_i , t_i , w_i correspond x_i , y_i , z_i respectively and h [mm] is the height of a cylinder.

In Figure 1 are presented distribution points, windows of simulation for plane and cylinder and optimizing path by solving TSP using ants colony.

principle of collision avoidance between work piece and probe at parallelism tolerance inspection is presented in Figure 2.

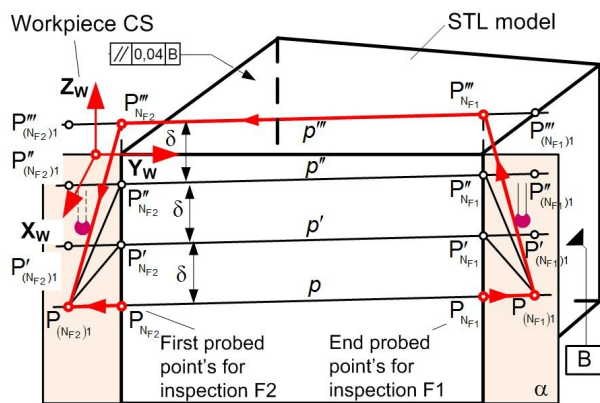
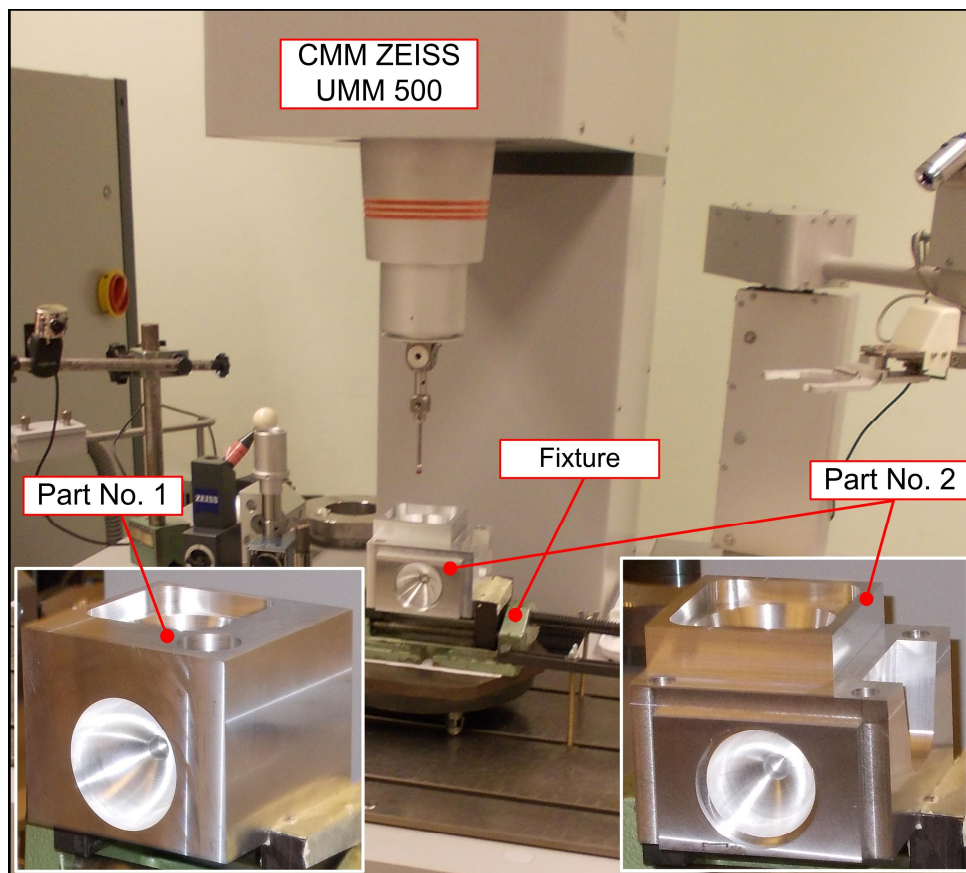


Fig. 2. Principe collision avoidance

The principle is iterative and consists from moving line p for distance δ until line became collision free (line segment p'').

Experiment involves measurement of two PPs that are produced for this research. In comparison to the simpler workpiece PP1 and more complex workpiece PP2 contains new types of tolerances that should be tested. Experimental setups for the measurement of PP1 and PP2 are shown in Figure 3. The measurement of both parts is performed in a single clamp, and the measuring probe configurations are shown at the figures. Experiment is performed on the coordinated measuring machine ZEISS UMM 500.



Technical characteristics of CMM “ZEISS UMM500”

- Number of axis: 3 (X,Y,Z)
- Measuring range in [mm]: 500x200x300
- Automatic change of measurement sensor: yes
- Maximum weight of workpiece in [kg]: 150
- Resolution in [μ m]: 0.1
- Software: ZEISS UMESS
- MPE in [μ m]: $0.4+L/600$
- Assurance in [μ m]: 0,2

Fig. 3. Experimental setup for the measurement of prismatic part no. 1 and no. 2

4. CONCLUSIONS

In the above presented of SPMSs for quality as a CAI model, it is important to consider the newly developed AP242 that is designed to improve the interoperability in STEP, support model-based GD&T and allows for CMM programming based on the inspection features. AP242 enables 3D product manufacturing information (PMI) with semantic representation and 3D model-based design and data sharing on service-oriented architecture (SOA).

The complex geometry of the PP by IMIP changes to the set of points whose sequence defines the measuring path of sensors without collision with workpiece. Presenting measuring path by set of points with a defined order is optimizing by solving TSP with ants colony. Finding the shortest measuring path, the main criteria for optimization, influence to the reduction of the total measurement time, which is one of the goals of this research. The ISIP is especially suitable for use in case of measuring path planning for geometrically complex PPs with large numbers of

tolerances. The simulation provides a visual check of the measuring path.

5. ACKNOWLEDGEMENT

Some of the presented experimental researches was supported by the Ministry of Education, Science and Technological Development of the Republic of Serbia, by Project TR 35022.

6. REFERENCES

- [1] Westkämper, E.: *Manufuture and Sustainable Manufacturing*, Proceedings of CIRP Conference on Manufacturing Systems, pp. 20-28, Paris, 2012, Paris.
- [2] Mattucci, M.: *Factories of the Future*, COMAU, EFFRA, Milano, 2012.
- [3] www.efra.eu (accessed June 2015).
- [4] *HORIZON 2020 - The New EU Framework Programme for Research and Innovation 2014 - 2020*, Brussels, 2014.
- [5] <http://www.bmbf.de/en/19955.php> (accessed June 2015).
- [6] <http://www.plattform-i40.de/> (accessed June 2015).
- [7] *Industrie 4.0, Smart Manufacturing for the Future*, Berlin, 2014.
- [8] Majstorovic, D. V., Stojadinovic, M. S.: *Research and Development of Knowledge Base for Inspection Planning Prismatic Parts on CMM*, 11th International Symposium on Measurement and Quality Control, p.p. 46-52, Cracow-Kielce, Poland, September 11-13, 2013.
- [9] Stojadinovic, M. S., Majstorovic, D. V., *Developing engineering ontology for domain coordinate metrology*, FME Transactions, Faculty of Mechanical Engineering, Vol.42, No.3, pp.249-255, 2014.
- [10] Stojadinovic, S., Majstorovic, V.: *Towards the Development of Feature – Based Ontology for Inspection Planning System on CMM*, Journal of Machine Engineering, Editorial Institution of the Wroclaw Board of Scientific Technical Societies Federation NOT, Wroclaw, Poland, Vol.12, No.1, pp.89-98, 2012.
- [11] Stojadinovic, S., Majstorovic, V.: *Metrological primitives in production metrology–ontological approach*, Proceedings of the 34th International Conference on Production Engineering, pp. 29-30, Nis, Serbia, 28– 30th September, 2011.
- [12] Lee G., Mou J., Shen Y.: *Sampling strategy design for dimensional measurement of geometric features using coordinate measuring machine*, Int. J. Mach. Tools Manufact., Great Britain, Vol.37, No.7, pp.917-934, 1997.
- [13] Wang, L., et al, *Current status and advancement of cyber-physical systems in manufacturing*, Journal of Manufacturing Systems, Article in Press, 2015.
- [14] Wu, D., et al, *Cloud manufacturing: Strategic vision and state-of-the-art*, Journal of Manufacturing Systems, 32 (2013), 564-579.
- [15] Wu, D., et al, *Cloud-based design and manufacturing: A new paradigm in digital manufacturing and design innovation*, Computer-Aided Design 50 (2015), 1-14.
- [16] Lu, Y., *Development of a Hybrid Manufacturing Cloud*, Journal of Manufacturing Systems 33 (2014) 551–566.
- [17] Dworschak, B., Zaiser, H., *Competences for cyber-physical systems in manufacturing – first findings and scenarios*, Procedia CIRP 25 (2014) 345 – 350.
- [18] Herterich, M., *The Impact of Cyber-Physical Systems on Industrial Services in Manufacturing*, Procedia CIRP 30 (2015) 323 – 328.
- [19] Wu, Z., et al, *Tolerance Design and Adjustment of Complex Customized Product Based on Cloud Manufacturing*, Procedia CIRP 27 (2015) 169 – 175.
- [20] Mourtzis D., et al, *Cloud-based integrated shop-floor planning and control of manufacturing operations for mass customisation*, Procedia CIRP 33 (2015) 9 – 16.
- [21] Thramboulidis, K., *A cyber–physical system-based approach for industrial automation systems*, Computers in Industry 72 (2015) 92–102.
- [22] Lee, J., et al, *A Cyber-Physical Systems architecture for Industry 4.0-based manufacturing systems*, Manufacturing Letters 3 (2015) 18–23.
- [23] Wang, L., *Machine availability monitoring and machining process planning towards Cloud manufacturing*, CIRP Journal of Manufacturing Science and Technology 6 (2013) 263–273.
- [24] Wright, P., *Cyber-physical product manufacturing*, Manufacturing Letters 2 (2014) 49–53.
- [25] Xu, X., *From cloud computing to cloud manufacturing*, Robotics and Computer-Integrated Manufacturing 28(2012)75–86.
- [26] Monostori, L., *Cyber-physical production systems: Roots, expectations and R&D challenges*, Procedia CIRP 17 (2014) 9 – 13.

Authors: Prof. dr Vidosav D. Majstorovic, Slavenko M. Stojadinovic, Assistant, University of Belgrade, Faculty of Mechanical Engineering, Department for Production Engineering, Kraljice Marije 16, 11120 Beograd 35, Serbia, Phone.: +381 11 33 02 407, Fax: +381 11 33 70 364.
E-mail: vidosav.majstorovic@sbb.rs;
stojadinovic@mas.bg.ac.rs



Štrbac, B., Radlova ki, V., Spasi – Joki , V., Matin, I, Hadžistevi , M.

ESTIMATING TOTAL UNCERTAINTY OF MEASURING FLATNESS IN ACCORDANCE WITH GPS STANDARDS USING CMM

Abstract: *The measurement result if expressed without confidence interval estimate it is not complete. Confidence Interval is characterized as uncertainty and is a quantitative indicator of the measurement result quality. Measurement uncertainty is mainly caused by factors such as measuring instrument, operator, workpiece, applied strategy and/or measurement conditions. GPS, a standard defining geometrical specification and product verification, integrates the entire product geometry description and defines uncertainty at each stage. The result is a total uncertainty which is usually significantly greater than measurement uncertainty (sometimes twice greater). This study provides a method for estimating total measurement uncertainty of determining flatness error using coordinate measuring machines (CMM).*

Key words: *geometrical product specification (GPS), uncertainty, flatness, coordinate measurement machine (CMM)*

1. INTRODUCTION

The modern industrial world sometimes imposes very narrow tolerances at assemblies and sub - assemblies in order to enable application of functional requirements. Workpieces paired for the purpose of sealing or sliding or those that have to be appropriately oriented, often have to be subjected to estimating flatness errors. Flatness error verified by a measuring equipment with estimated measuring uncertainty, has to be within a field of specification if a compliance with ISO 14253-1 [1] is required. Lately, coordinate measuring machines are the most commonly used measuring instrument for assessing flatness errors because of their flexibility. However, due to many factors and their interactions, evaluation of uncertainty of CMM measurement is a complex task. This is one of the trendiest research topics in the field of production metrology in the last two decades. Research efforts of leading metrology institutes and a number of EU projects resulted in creating and implementation of standardized methods for estimating measuring uncertainty for CMM with the support of ISO [2, 3]. The new generation of geometrical product specifications went a step further in relation to the term "uncertainty". The GPS concept connects the entire course of the geometry of the product, from functionality, specification, production, to verification and represents the workpiece in three different "worlds" - operators [4]. The *first* operator is nominal - ideal model. The *second* specification operator or "Skin" model is the nominal model in combination with the allowed tolerances, while the *third* operator is represented by verification procedures on real workpiece. Presentation of the geometry of the workpiece in this way corresponds to the steps of the CAD / CAM / CAQ systems. Checking the workpiece quality conformity is performed by comparing the specification and verification operators. An approach based on operators and operations significantly

improves the management of data related to the workpiece, so that the minimization of uncertainty is in relation to probable interpretations of geometric specifications. As a guarantee of the best description of the workpiece and estimate of its correspondence with the functional requirements, GPS language introduces defining new factors of uncertainty that are able to characterize products in various stages of its life cycle. In the improved GPS system, besides the measurement uncertainty, the uncertainty of correlation, uncertainty of specification, uncertainty of conformity and total uncertainty are defined.

Therefore, the decision of conformity / nonconformity of a product should be based on the total uncertainty and not, as it has usually been the practice, on the measurement uncertainty. This issue certainly did not attract sufficient attention and research efforts. Wen et al. carried out the estimation of uncertainty for measuring flatness on CMM in accordance with GPS, but they did not define uncertainty of specifications and conformity [5]. Ruffa et al. estimated the total uncertainty [6] for estimating roundness error. This research describes how to minimize the uncertainty of specifications, correlation and conformity. For the evaluation of uncertainty, analytical GUM method and computer bootstrap were used. Ricci et al. have made the most comprehensive approach on estimating the total uncertainty for measuring flatness error using CMM [7].

The research aims are to present a methodology for the estimating the total uncertainty in accordance with the standard instruction for estimating total uncertainty (GUM) [8] on a concrete example of measuring flatness error using CMM.

2. SPECIFICATION AND VERIFICATION OF FLATNESS

According to ISO 12781-1, flatness error is defined as the area between the two parallel planes All points

sampled from the measured surface must be placed within the space limited by two planes, i.e. tolerance space [9].

According to GPS, a complete specification operator for flatness executes all operations necessary for testing the conformity of an actual plane as imagined by the designer. A specification operator consists of the following operations: partition, extraction, filtration, association and evaluation. Partition is used in order to identify the boundaries of geometric primitives (point, line, circle, plane, cylinder) obtained from actual surfaces. The operation of extraction includes describing realistic geometry via the position of sampling points obtained by a measuring instrument. The operation of extraction is performed according to a previously determined measuring strategy. Filtration of the measured values includes separating deviations of various origin (shape deviation, waviness, roughness). It is also used for the elimination of accidental measurement deviations. The operation of association uses fit algorithms for mathematical representation of a surface based on sampling points. Evaluation is used for determining errors, in this case flatness error.

A complete specification operator implies the existence of a tolerance frame in technical documentation, as shown in Fig.1.

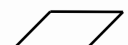
	0.0004	$\lambda_c=2.5$	LS
------------------------------------------------------------------------------------	--------	-----------------	----

Fig.1. A completely defined specification operator for flatness tolerance

A metrologist needs to, unambiguously and in accordance with the principle of duality, apply the operations from the specification operator in the verification operator. In the picture, the parameter „ $c=2.5$ “ defines the operations of extraction and filtration. According to ISO 12781-2 [10], an appropriate filter with cut-off wavelength c has to be chosen with the aim of extraction of the component error of a form required by the geometric specification. Likewise, the accepted filter value defines, for the chosen diameter of the top of the measuring probe, the minimum number of points that needs to be sampled in the “grid” measuring strategy. It is worth mentioning that in the cases when sampling is performed in the discrete mode, the operation of filtration will only be efficient in the ideal verification operator. However, in most case, this can hardly be applied in practice due to the problems of time and price. Therefore, simplified verification operators with a reduced number of measuring points are introduced. In such operators, filtration will not affect measurement results and it will cause uncertainty. The parameter designated as LS (least square) in the picture denotes the fit method or the algorithm used for obtaining, in this case, the plane of reference. Besides the LS method, the minimum zone (MZ) method can also be used. There is no unanimous opinion among scientists and professionals on the choice of the associative criterion. LS has been used more frequently, whereas in MZ the flatness error is usually smaller and the method has been

recommended by ISO 1101 [11].

Finally, form deviation can be explained as the difference between the maximum and minimum local flatness deviation..

Flatness error is defined as [12]:

$$= \max_{i \ i \ n} \{d_i\} - \min_{i \ i \ n} \{d_i\} \quad (1)$$

where d_i represents the maximum and minimum distance of extreme points in relation to the plane of reference and is presented as an equation:

$$d_i = \frac{z_i - ax_i - by_i - c}{\sqrt{1 + a^2 + b^2}} \quad (2)$$

with flatness error:

$$= \frac{(z_{max} - z_{min}) - a(x_{max} - x_{min}) - b(y_{max} - y_{min})}{\sqrt{1 + a^2 + b^2}} \quad (3).$$

The two points that are farthest apart in relation to the plane of reference are presented in coordinates $(x_{max}, y_{max}, z_{max})$ and $(x_{min}, y_{min}, z_{min})$.

This way, an ideal specification operator is defined, and according to the principle of duality, an ideal verification operator can be derived from it. Only in such a scenario can the total uncertainty be equated to measurement uncertainty. In all other cases, other factors of total uncertainty should be considered.

3. TOTAL UNCERTAINTY AND METHODOLOGY OF ITS ESTIMATION

The factors of total uncertainty are presented in ISO 17450-2 as shown in Fig.2[13,14]. Correlation uncertainty is a measure of the ability of geometric specifications to guarantee the functional requirements of what it is intended for. The role of specification uncertainty is to quantify ambiguity in specification operators and this is the case when the specification operator is not complete or when a metrologist introduces a simplified verification operator. Measurement uncertainty gathers all uncertainties generated in the use of a real verification operator. This corresponds to the classic concept of measurement uncertainty and consists of the sum (according to GUM) of the uncertainty of the applied method and implementation uncertainty. Measurement uncertainty takes into account the imperfections of measuring instruments and deliberate deviations from the ideal verification operator.

In our example, there is full compliance with the ideal verification operator and total uncertainty can only be ascribed to implementation uncertainty. Uncertainties generated as a result of temperature or temperature gradient have been neglected because the experiment is carried out in an air-conditioned laboratory. In that case, uncertainty will be affected by CMM point sampling by means of hardware and probe system, and uncertainty in the operation of association when the referential plane is being determined. Uncertainty can be calculated in the following equation:

$$u^2 = \frac{u_{x_1}^2}{x_1^2} + \frac{u_{x_2}^2}{x_2^2} + \frac{u_{y_1}^2}{y_1^2} + \frac{u_{y_2}^2}{y_2^2} + 2 \frac{u_a u_b}{a b} + \frac{u_{z_1}^2}{z_1^2} + \frac{u_{z_2}^2}{z_2^2} + \frac{u_a^2}{a^2} + \frac{u_b^2}{b^2} + \dots \quad (4)$$

The first two rows in formula (4) refer to uncertainty in extreme points of sampling generated by hardware components of a CMM and probe system, whereas the third row refers to the uncertainty of the applied associative method.

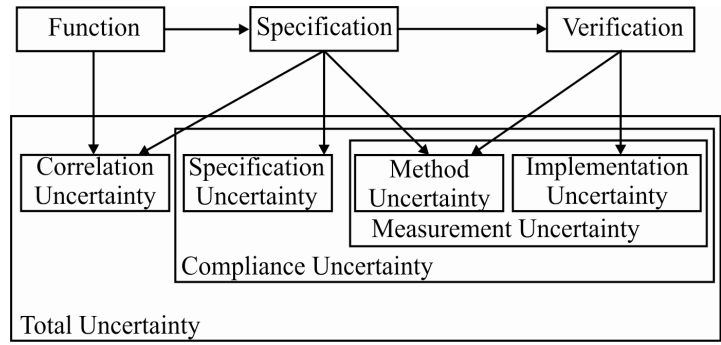


Fig. 2. Factors of total uncertainty [14]

4. CASE STUDY

The verification of the proposed method has been performed on a CMM Carl Zeiss CONTURA g2 RDS (MPE_E= 1.9+L/330) while measuring the flatness of a optical flat d=60mm (Fig.3). This workpiece can be said to represent the artifact of flatness. Is the specified flatness error is = 0.0004 mm. This error is under the domain of accuracy CMM and in this way was eliminated contribution uncertainty - form error. This is important because some studies have shown that this factor in the interactions to the uncertainty of sample points can be one of the most influential on measurement uncertainty [15]. According to the specification operator, for the defined value c, the measured object needs to be measured in 21876 points at the distance of d=0.357mm, with a probe tip r=0.55mm. For the filtration of points, i.e. for

eliminating the frequencies of shorter wavelengths such as roughness and waviness, a Gaussian filter is used according to ISO 16610-21/28[16]. The transfer at limit wavelength is 50%. After sampling, the parameters of the referential plane were obtained and the flatness error was determined. The error was much greater than the measure on the optical flat (Fig.4). The expanded uncertainty, which in this case refers only to implementation uncertainty, using formula (4) and coverage factor k=2, amounts to U=0.6µm. It needs to be mentioned that simplification was introduced here and that the uncertainty of the extreme sampled points was taken as MPE_E/6. The obtained result of uncertainty should be verified in a more precise calibration procedure such as interferometry. Also, more effort is required for the investigation of hardware errors, which is probably different from the applied simplification.



Fig. 3. Experimental setup

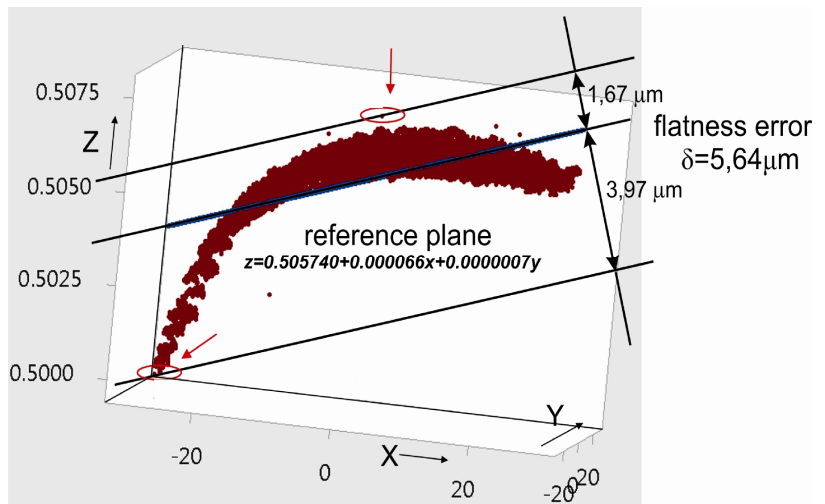


Fig. 4. Sampling points, reference plane (LS) and flatness error

5. CONCLUSION

Being acquainted with the value of total uncertainty is the most important concept according to a new generation of geometrical product specifications and is the basis for making decisions about accepting or rejecting workpieces. Total uncertainty is not very common in industry so it should be promoted as much as possible.

5. REFERENCES

- [1] ISO 14253-1:1998. *Geometrical Product Specifications (GPS) – Inspection by measurement of workpieces and measuring equipment – Part 1: Decision rules for proving conformance or non – conformance with specifications*, ISO, 1998.
- [2] ISO/TS 15530-3:2004. *Geometrical Product Specifications (GPS) – Coordinate measuring machines (CMM): Technique for determining the uncertainty of measurement – Part 3: Use of calibrated workpieces or standards*, 2004.
- [3] ISO, 2004. ISO/TS 15530-4:2008. *Geometrical Product Specifications (GPS) – Coordinate measuring machines (CMM): Technique for determining the uncertainty of measurement – Part 4: Evaluating task-specific measurement uncertainty using simulation*. ISO, 2008.
- [4] Humienny, Z., „State of art in standardization in GPS area“ CIRP Journal of Manufacturing Science and Technology, Vol 2, No 1, p.p. 1-7, 2009.
- [5] Wen, X-L., Zhu, X-C., Zhao, B-Y., Wang, D-X, Wang, F-L.: *Flatness error evaluation and verification based on new generation geometrical product specification (GPS)*, Precision Engineering, Vol. 36, pp. 70-76, 2012.
- [6] Ruffa, S., Panciani, G.D., Ricci, F., Vicario, G.: *Assessing Measurement Uncertainty in CMM measurements: Comparison of Different Approaches*, International Journal of Metrology and Quality Engineering, Vol. 4, pp. 163-168, 2013.
- [7] Ricci, F., Scott, J.P., Jiang, X.: *A categorical model for uncertainty and cost management within the Geometrical Product Specification (GPS) Framework*, Precision Engineering, Vol. 37, pp. 265-274, 2013.
- [8] ISO/IEC Guide 98-3:2008. *Uncertainty of measurement – Part 3: Guide to the expression of uncertainty in measurement (GUM:1995)*. ISO/IEC, 2008.
- [9] ISO 12781-1, *Geometrical product specifications (GPS) — Flatness — Part 1: Vocabulary and parameters of flatness*, 2011.
- [10] ISO 12781-2: *Geometrical product specifications (GPS) — Flatness — Part 2: Specification operators*, 2011.
- [11] ISO 1101: *Geometrical product specifications (GPS) - Geometrical tolerancing - Tolerances of form, orientation, location and run-out*, 2012.
- [12] Cui, C., Fu, S., Huang, F.: *Research on the uncertainties from different form error evaluation methods by CMM sampling*, International Journal of Advanced Manufacturing Technology, Vol. 43, pp. 136-145, 2009.
- [13] ISO/TS 17450-2, *Geometrical product specification (GPS) – General concept – Part 2: Basic tenets, specifications, operators and uncertainties*. 2002.
- [14] Wang, J.X., Jiang, X., Ma, L.M., Xu, Z.G., Li, Z.: *Decision rules for workpieces based on total uncertainty*, International Journal of Advanced Manufacturing Technology, Vol. 28, pp. 1169-1174, 2006.
- [15] Kruth, J.P., Van Gestel, N., Bleys, P., Welkenhuyzen, F.: „Uncertainty determination for CMMs by Monte Carlo simulation integrating feature form deviations“, CIRP – Manufacturing Technology, Vol. 58, pp. 463-466, 2009.
- [16] ISO 16610-21, *Geometrical product specifications (GPS) - Filtration - Part 21: Linear profile filters: Gaussian filters*, 2011.

Authors: M.Sc. Branko Štrbac, Vladan Radlova ki, Associate Professor, Prof. dr Vesna Spasi – Joki , dr Ivan Matin, Prof. dr Miodrag Hadžistevi , University of Novi Sad, Faculty of Technical Sciences, Trg Dositeja Obradovica 6, 21000 Novi Sad, Serbia, Phone.: +381 21 450-366, Fax: +381 21 454-495.
E-mail: strbacb@uns.ac.rs; rule@uns.ac.rs; svesna@uns.ac.rs; matini@uns.ac.rs; miodrags@uns.ac.rs

12th INTERNATIONAL SCIENTIFIC CONFERENCE MMA 2015 -
FLEXIBLE TECHNOLOGIES

PROCEEDINGS



Section D:

**AUTOMATIC FLEXIBLE TECHNOLOGICAL
SYSTEMS, CA_x AND
CIM PROCEDURES AND SYSTEMS**

Novi Sad, 25-26 September 2015

osi , I., Katalini , B., Teki , Ž., Lali , B.

RESHAPING THE FUTURE OF MANUFACTURING - FIVE TRENDS FOR THE NEXT TEN YEARS

Abstract: This paper describes trends and challenges, which will shape the future of manufacturing in the next ten years: development of new technologies and convergence of ICT and manufacturing, customization, open innovation, emergence of new competition and growing impact of intellectual property.

1. INTRODUCTION

Technology is a driving force of our civilisation. Trying to get maximal benefits from existing technology our society has been continuously changing and adapting its organisational form. It started as agricultural society with technology based on raw materials and agricultural products; continued as industrial society with technology based on industrial production; and advanced to information society with technology based on information products. Now we live in the knowledge based society and compete in knowledge economy.

Knowledge economy is one in which commercial and non-commercial organisations (including regions and countries) rely dominantly on the generation and exploitation of knowledge and knowledge assets (compared to using natural resources, physical capital and low skill labour) in the creation of wealth [1]. However, it is not simply about pushing back the frontiers of knowledge. In knowledge economy the success of companies depends more on how effectively they use and explore what they

“know”, than on what they “know” [2], [3].

In this paper, we are interested in describing trends and challenges, which will shape the future of manufacturing in the next ten years in order to open up **discussion at the meeting.**

2. NOT A NEW WAVE, TECHNOLOGY TSUNAMI IS COMING

Continued advances in and convergence of technologies coming from outside manufacturing, like big data, cloud computing, the industrial internet (or Industry 4.0), robotics and additive manufacturing will change production and manufacturing in the same way as steam machine or Ford’s conveyor-belt assembly lines changed it years ago. These technologies are game changers with a dramatic ripple effect as they change the nature of jobs, eliminate labor, save energy, and enable high level of customization. Manufacturers will increasingly rely on them to improve agility, responsiveness and reliability of their operations as well as customer services and production efficiency at every level.

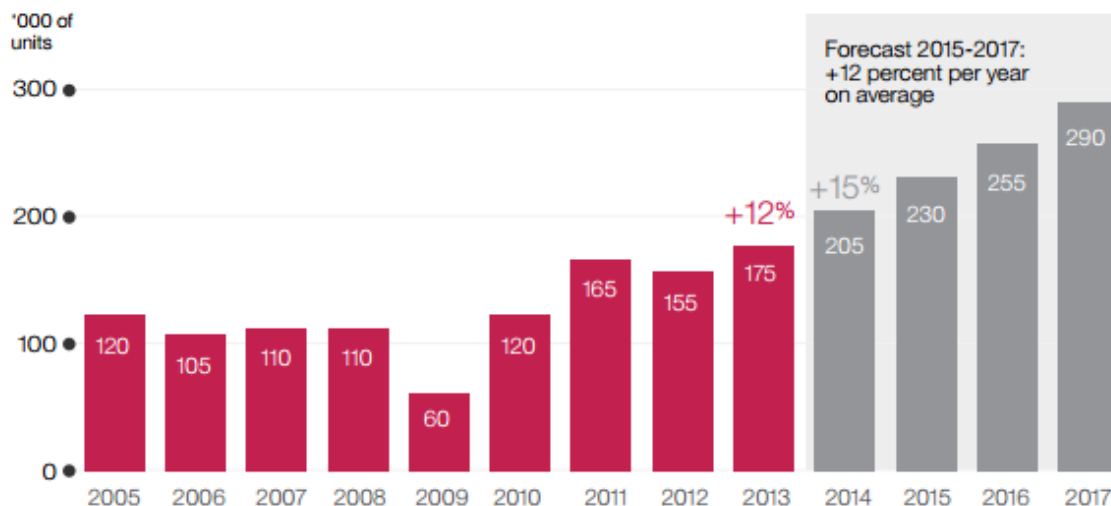


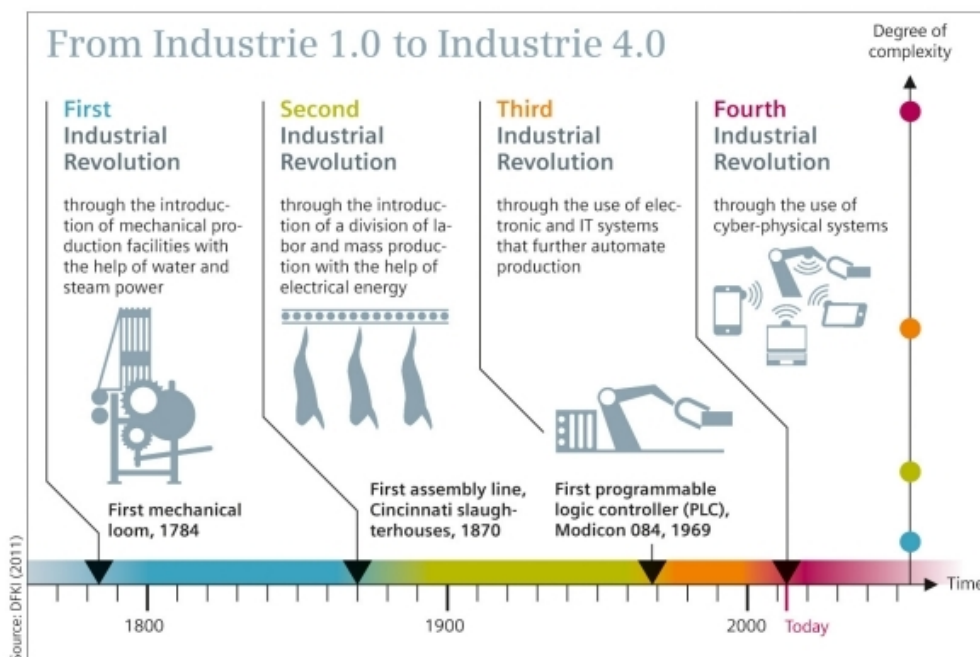
Figure 1. Worldwide annual supply of industrial robots [5]

Although companies have been using computer integration from seventies and applying Internet-based technologies to industrial applications as they have become available over the last decade, the full potential of Internet-based digital technology has yet to be fully realized. In practice, that means: machines/devices

which have the possibility to connect and exchange information with other machines/devices and integrate in larger networks; inventory, which counts itself; containers that detect their contents; self-organized manufacturing assembly; integrated product and production lifecycle processes...

To understand the full potential and impact of new technologies, here are a few findings from recent industry reports:

- Only 4% of manufacturers see no use case for big data analytics in the future. The most likely use cases for big data analytics in the digital factory of the future are related to real-time control and analyses of factory performance, planning and supply chain performance[4].
- In 2012, Intel saved \$3M in manufacturing costs by implementing big data analytics on just a single line. The plan is to extend the process to more chip lines and save an additional \$30M in the next few years[4].
- Boeing is making more than 20,000 3D
- commercial planes. The 787 Dreamliner has 30 3D printed parts, including air ducts and hinges, which is a record for the industry[4].
- The total worldwide stock of operational industrial robots at the end of 2013 was in the range of 1,332,000 and 1,600,000 units. From 2015 to 2017, robot installations are estimated to increase by 12% on average per year[5].
- According to General Electric estimates, full implementation of industrial internet could increase global GDP from \$10 to \$15 trillion by 2030[6].
- Germany's National Academy of Science and Engineering believes that new manufacturing processes will lead to a 30 percent increase in industrial productivity[7].



printed parts for 10 different military and Figure 2: Industry 4.0 [7]

Although the result is not easy to predict, most probably, the majority of machines in the smart factories of the future will be self-organizing, developed in line with the concept of “plug & produce”, with automatically linking supply chains, and directly converting orders into manufacturing information and production action plan.

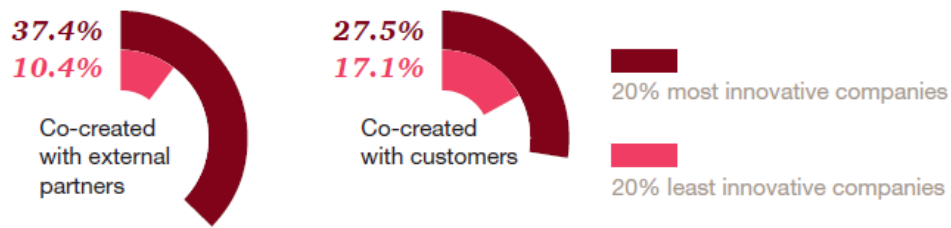
“WORLD N=1”

Individual customer experiences (N=1) becomes the most important focus point for many companies. Thus, they more and more make specific products, in line with the customer's individual wishes. This requires that companies have resilient, dynamic and flexible business processes and ability to customize for and co-create products with users and customers[8]. Big data and strong analytics on one side and ability to build communities and engage users will allow discovery of

trends and unique opportunities and enable the company to engage in product co-creation with their consumer base.

There are numerous examples of customization in car and textile industries. However, in last few years even very complex systems such as the Mars rover Curiosity and the Red Bull's Formula 1 racing car were manufactured in a batch size of one[7].

Flexibility and high responsiveness to customer requests and focus on manufacturing small batches of products will result in factories and machines, which will have to be very differently organized and interconnected. The concept of “plug & produce” will dominate. It will influence high-level compatibility between machines from different manufacturers in order to enable effective and efficient manufacturing of customized products. At the same time, a need for quick and flexible machinery retooling will emerge.



Base: 20% most innovative IM respondents, 46; 20% least innovative IM manufacturing, 57

Figure 3. What percentage of innovative products and services are co-created with customers [12]

3. OPEN INNOVATION APPROACH

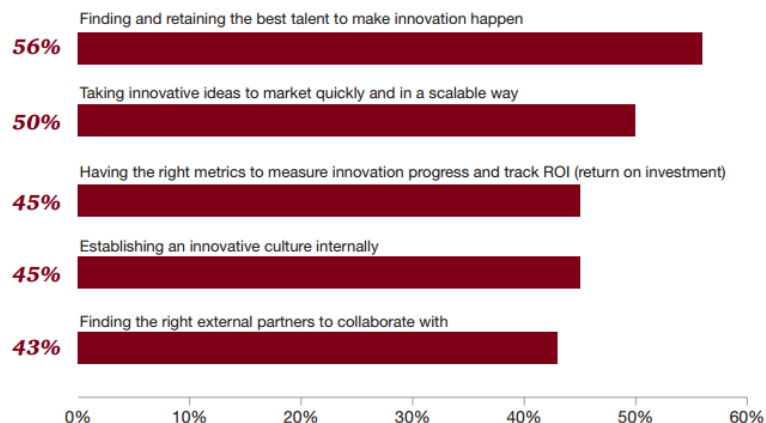
Leading manufacturing companies are increasingly aware that they need to explore and exploit both internal and external knowledge sources to accelerate innovation, since majority of them struggle with a lack of resources and know-how necessary to professionally realize innovation projects. They need to turn to co-creation across innovation processes and allow the flow of knowledge over organizational boundaries, exploiting internal knowledge in more diversified markets, as well as identifying and absorbing external knowledge to support the internal innovation process. Co-creative manufacturing companies are not limiting their innovation potential to what they can devise within their own borders, but open their processes to many diverse participants, whose input can take product and service offerings in unexpected directions that serve a much broader range of needs [9].

Adoption of open innovation principles is a recognition that product development performance can no longer be solely determined by internal R&D functions, but also depends on the contributions of a broad range of external players, from individual customers to large research institutes [10]. Chesbrough argued that different businesses could be located on a continuum, from essentially closed to completely open, and that not all industries were migrating towards open innovation

[11]. However, the results of PwC’s Global Innovation Survey 2013 offered another view on this open innovation trend: 95% of industrial manufacturing executives said their companies had plans to work together with their customers, suppliers, academics, even with the competition— to spur innovation [12]. And open innovation pays off – industrial manufacturing’s most innovative companies are co-creating far more of their products and services.

4. NEW COMPETITORS AND BATTLE FOR TALENT

Who are the main competitors in implementing the manufacturing systems of the future? Big IT companies or traditional manufacturers? Big IT companies, which are to network production processes more strongly, lead the race in countries that outsourced and reduced their production capacities in recent decades. US is the excellent example for this trend. On the other hand, in Germany large and medium-sized manufacturing companies use new automation solutions in order to boost their productivity and remain internationally competitive. The level of industrialization of individual companies in Western economies affects the way they are implementing the manufacturing systems of the future[7]. Should we expect from big IT companies in Serbia and the region to take lead on this?



Source: PwC, *Breakthrough Innovation and Growth*
Base: Industrial manufacturing, 249

Figure 4. Talent – the biggest innovation challenge for industrial manufacturing executives [12]

Finding the right talent can be a big challenge task. Especially, for industrial manufacturing companies. Talent leads the list of innovation challenges for

industrial manufacturing executives – they said finding and retaining the best talent to make innovation happen is the most challenging task. In this context, Uber’s

approach in staffing recently opened the Advanced Technologies Center in Pittsburgh, is not surprising. At the beginning of 2015, Uber, famous for its popular taxi-like services, simply hired a group of some 40 employees from the National Robotics Engineering Center at Carnegie Mellon University[13]. Among these 40 people several were longtime senior lab members. Manufacturing companies will need to make sure they are well-positioned to compete when it comes to attracting and retaining workers with the right skills.

5. INTELLECTUAL PROPERTY

With the emergence of a knowledge economy, importance of knowledge as a driving force of innovation and economic growth worldwide has increased significantly. In the dynamic arena where creativity, knowledge and the production of novel ideas have a central place, traditional manufacturing moves to lower cost economies and new technologies become the most important wheel in global economic trade. In such an economy, intellectual property rights (IPRs) are becoming one of the most important businesses mechanisms in extracting economic value from creativity and encouraging greater investment in innovation[14]. IPRs include patents, trademarks, copyrights, trade secrets, and a number of more specialized instruments.

Where is the problem? Knowledge and knowledge assets are intangible and different from tangible assets that were the critical input in production and primary source of value in the past[2]. This makes companies inexperienced in managing and protecting knowledge. Therefore, in a world dominated by globalisation, deregulation and rapid technological change firms find themselves in the position where their most critical resource (knowledge) is, at the same time, most difficult one to protect[3].

6. CONCLUSION

In this paper, we described five trends and challenges, which will, in our view, shape the future of manufacturing in the next ten years. This list does of trends does not pretend to be final, but to describe a playing field and open discussion.

7. REFERENCES

- [1]I. Brinkley, "Defining the knowledge economy - Knowledge economy programme report," 2006.
- [2]Z. Tekic, B. Katalinic, and I. Cosic, "Key Characteristics of Knowledge," in Annals of DAAAM for 2009 & Proceedings of the 20th International DAAAM Symposium, 2009, pp. 1747–1749.
- [3] Z. Tekic, I. Cosic, and B. Katalinic, "Framing Knowledge in Business Context," in Annals of DAAAM for 2010 & Proceedings of the 21th International DAAAM Symposium, 2010, pp. 555–557.
- [4]P. Manenti, "The Digital Factory: Game-Changing Technologies That Will Transform Manufacturing Industry," 2014.
- [5]IFR, "Industrial Robots," World Robotics 2014, 2014. [Online]. Available: <http://www.ifr.org/industrial-robots/statistics/>.
- [6]P. Evans and M. Annunziata, "Industrial Internet: Pushing the Boundaries of Minds and Machines," General Electric, 2012. [Online]. Available: <http://files.gereports.com/wp-content/uploads/2012/11/ge-industrial-internet-vision-paper.pdf>.
- [7]K. Nikolaus, "Manufacturing: Self-Organizing Factories," Siemens - Digital Factories, 2014. [Online]. Available: <http://www.siemens.com/innovation/en/home/pictures-of-the-future/industry-and-automation/digital-factory-trends-industry-4-0.html>.
- [8]C. K. Prahalad and M. S. Krishnan, The New Age of Innovation. 2008.
- [9] J. S. Brown and J. Hagel, "From push to pull: The next frontier of innovation," 2005. [Online]. Available: http://www.mckinseyquarterly.com/Strategy/Strategic_Thinking/From_push_to_pull_The_next_frontier_of_innovation_1642?gp=1.
- [10]H. Bahemia and B. Squire, "A contingent perspective of open innovation in new product development projects," Int. J. Innov. Manag., vol. 14, no. 4, pp. 603–627, Aug. 2010.
- [11]H. W. Chesbrough, "The Era of Open Innovation," MIT Sloan Management Review, 2003. [Online].
- [12]PWC, "Rethinking innovation in industrial manufacturing," 2013.
- [13]C. Thompson, "Uber Would Like to Buy Your Robotics Department," The New York Times Magazine, 2015. [Online]. Available: http://www.nytimes.com/2015/09/13/magazine/uber-would-like-to-buy-your-robotics-department.html?smid=nytcore-ipad-share&smprod=nytcore-ipad&_r=1.
- [14]Z. Tekic, D. Kukolj, M. Drazic, and M. Vitas, "Towards understanding the role and value of patents in a knowledge-based economy," in DAAAM International Scientific Book 2013, B. Katalinic and Z. Tekic, Eds. Vienna, Austria: DAAAM International, 2013, pp. 389–416.

Authors: Professor Ilija osi , University of Novi Sad, Faculty of Technical Sciences, Department of Industrial Engineering and Engineering Management, Trg Dositeja Obradovica 6, 21000 Novi Sad, Serbia

Professor Branko Katalini , Vienna University of Technology, Institute for Production Engineering and LaserTechnology / Intelligent Manufacturing Systems, Karlsplatz 13/311, A-1040 Vienna, Austria, EU +43-1-58801-31121, branko.katalinic@tuwien.ac.at

Assistant Professor, Zeljko Teki , Skolkovo Institute of Science and Technology, Center for Entrepreneurship and Innovation, Skolkovo Innovation Centre,3 Nobel str., Moscow,143026, RussiaTel. +7 (495) 280 14 81 ext. 3331, z.tekic@skoltech.ru

Assistant Professor Bojan Lali , University of Novi Sad, Faculty of Technical Sciences, Department of Industrial Engineering and Engineering Management, Trg Dositeja Obradovica 6, 21000 Novi Sad, Serbia



Wakhare, M., Šormaz, D.

RULE BASED AUTOMATED SETUP PLANNING WITH TOLERANCE CONSIDERATION

Abstract: Process planning is an important part in design and manufacturing. Setup and fixture planning both are the key functions in process planning. This paper is focused on computer aided setup and fixture planning for prismatic parts using rule based system. Setup planning is the determination of the sequences of the setups of the prismatic part on the machine tools that includes clustering and sequencing of the features in setups. Tool approach directions of the machining features plays an important role in the setup planning, they are generated automatically in this paper. They are considered as vectors in 3D space. Datum precedence relation is proposed in the paper and shown as a graph. Tolerance relationship between features is considered as a main constraint to cluster the features in setups respecting tool approach directions and feature precedence relation. Sequencing of the features within setups and sequencing of setups will be performed to have minimum tool changes. After sequencing of setup optimal setup plan will be generated for 4-axis milling machine. Setup planning for prismatic part is followed by fixture planning and will be considered in this paper. Fixture planning is necessary in manufacturing activities because it ensures the correct positioning and immobility of workpiece related to cutting tools for the complete machining processes. In fixture planning, on the fixturing surfaces of a part locating, clamping and supporting points. will be determined automatically based on workpiece geometry to have good stability of the workpiece on the machine tools while machining. Case study shows the satisfactory results of setup plans.

Key words: Tool approach direction, Geometric and dimensional tolerance analysis, datum precedence, CAPP

1. INTRODUCTION

Currently, in the competitive market companies strive to meet the customer's demand as soon as possible with the better quality of the product and lower cost. Here the need for computer aided process planning arises. The process planning with the aid of computer can save lot of time and money in order to meet the customer's demand. Setup planning is an important task in computer aided process planning. Setup planning task includes identification of total number of setups, feature grouping where tool approach direction is an important criteria, operation sequencing within the setup and setup sequencing. While making setups, tolerance relation between features are mainly taken into consideration to meet the design criteria, however feature precedence also plays an important role while making setups. This paper describes the work done on setup planning and proposes future work. Section 2) describes the work done in the past on setup planning. Section 3) describes the methodology - automated identification of tool approach directions for each features present in the part, datum precedence graph which shows the order of machining the datum, grouping of the features and forming the setups considering tolerance as one of the important constraints. Section 4) shows the case study and its results. Section 5) concludes the paper.

2. LITERATURE REVIEW

In the last three decades, many approaches have been proposed for setup planning such as knowledge based, genetic algorithm, ant colony optimization,

graph-theoretic, group technology etc.

Hazarika and Dixit[1] used expert system and fuzzy set theory to solve setup planning problems. They choose rule based approach which is an expert system to understand and implement easily.

To consider uncertainties such as feature precedence relation, datum selection during setup planning, fuzzy set theory has been used by them. Neerukonda[2] developed a framework for setup planning and used object oriented approach to minimize the number of setups. He considers only geometry data of the part and tool orientation for clustering operations in single setup followed by sequence the operations within the setup. His thesis research doesn't consider tolerance analysis for setup planning.

Sun et al.[3] proposed new directed graph approach for setup planning. The paper focuses to avoid the critical problem which is precedence cycle between setups in setup planning. To overcome this problem the paper shows the generation of the SPG (setup precedence graph) to describe precedence constraint between setups. The paper uses vertex cluster algorithm and checks whether two serial vertex clusters can generate a cycle followed by operation sequencing in setup for minimum tool changes and then setup sequencing for optimal setup plans.

Kumar et al.[4] aims to get optimal setup plan using genetic algorithm approach. The paper reconstructs the GA as the method of representing an operation to be a distinct real number. Chromosomes which are the operation sequences have tendency to loose due to randomness of GA. Therefore to minimize losses, paper uses elitist model for selection of chromosomes. The methodology proposed in the paper doesn't consider

the objective functions of setup planning such as machining time and cost.

Sormaz and Khoshenevis[5] consider process sequencing instead of feature sequencing since there are constraints such as geometrical, technical and economical imposed by design and manufacturing practice. Process sequencing is done in two stages. In first stage process clustering is done based on tool orientation for each processes associated with the features. Features who have same tool orientations are clustered together in same setup. In second stage, process sequencing is done by the best-first search method is implemented to get optimal process sequence.

3. METHODOLOGY

This section describes the methodology used for the setup planning. The approach adopted in this research is to develop the setup planning module that will create an optimal setup plan after performing some crucial tasks such as grouping features to form setups, operations sequencing within the setup and finally sequencing of setups. Tools used in this research are IMPlanner system and Siemens NX.

3.1 IMPlanner System

IMPlanner system[6] is CAPP system which is under development in the Industrial and Systems Engineering department of Ohio University. IMPlanner system provides a test bed for the researchers for research purpose. IMPlanner has some important modules, process plan module, rule based process selection module, feature mapping module, process network module, process visualization module and computer interfaces. All modules in the IMPlanner system are developed using object-oriented modeling. An architecture of an IMPlanner system is shown in figure 1:

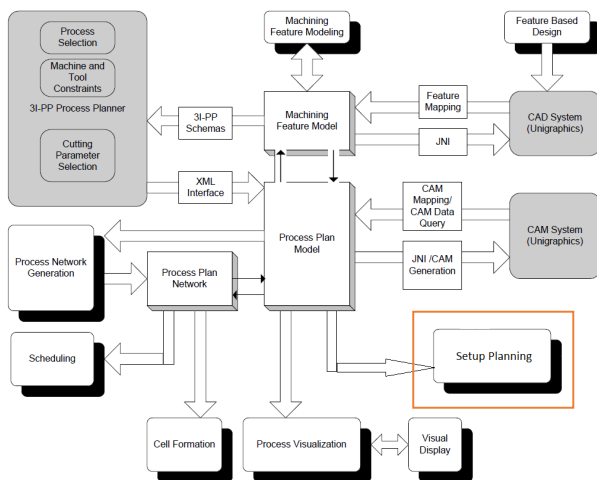


Fig. 1. An Architecture of an IMPlanner System

3.2 Setup Planning Module

The orange square box in fig.1 shows the current area of research. The input of this setup planning

system is feature based part which is actually a Siemens NX part file. The input is processed to map manufacturing features in the IMPlanner system. IMPlanner system converts manufacturing features details into the Jess facts and transfer it to rule based process selection module. These facts are run onto setup planning rules in Jess and finally optimal setup plan is generated for that particular part.

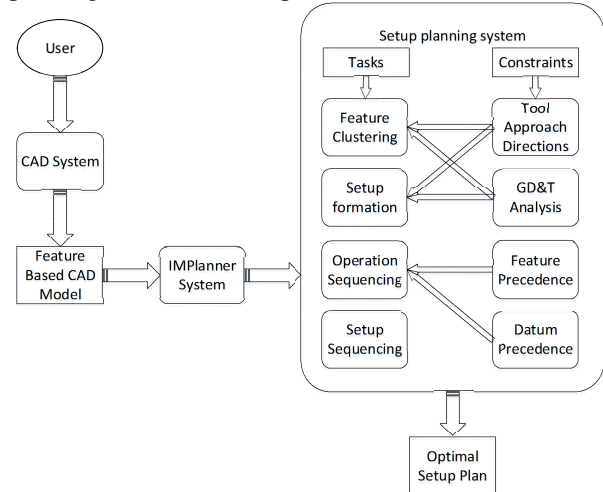


Fig. 2. An Architecture of Setup Planning Module

An architecture of setup planning is shown in fig.2. The setup planning system is developed using rule based system in Jess (Java Expert System Shell). As already discussed, setup planning has sub-tasks such as process clustering, setup formation, operation/process sequencing and setup sequencing. These sub-tasks are influenced by some constraints. These constraints are tool approach directions, GD&T analysis, features precedence and datum precedence. These constraints are explained below:

3.2.1. Tool Approach Direction

Tool approach direction (TAD) of the feature is defined as the free path of the tool over the part to machine the feature without any obstacle. TAD is a primary criteria for grouping the features in setups. For the prismatic parts there are total six tool approach directions. +X, -X, +Y, -Y, +Z and -Z on 3D mill. In this paper we have considered these tool approach directions as vectors in 3D space. Setup planning has an ultimate goal to form minimum setups in such a way that tolerance relation and feature precedence are not violated. Features are represented geometrically with their orientation vectors, and the first step is to active those vectors as TAD objects for all alternate processes selected for each feature. A setup is just a group of features with multiple processes having a common TAD. For a good manufacturing practice group of features with processes having same TAD should be machined in a single setup. If the feature has multiple TADs, it is assigned to single TAD depending upon its tolerance relation with other features. If the feature has multiple TADs and doesn't have tolerance relation with any other feature, then it is assigned to a TAD of a setup where there are maximum number of features.

Figure 3 shows the tool approach directions for different features.

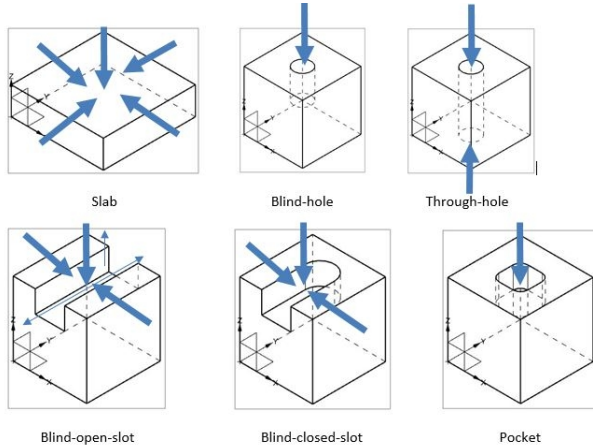


Fig. 3. TADs of different features

For every feature there is one or multiple processes and for every process there is one or multiple TADs. In fig.3 TAD's are shown in thick blue arrows. TAD is not only dependent on the feature but it also depends on the process that we select for the machining the feature. For the slab feature if end-milling process is selected to machine the face, then its TAD is in normal direction (0, 0, 1) vector. However, if the side-milling process is selected then machining of slab can be performed in any direction along X-Y plane. For the blind-hole feature, if drilling process is selected then its TAD will be along hole-axis i.e., (0, 0, 1) vector and blind-hole has only one TAD. Similarly, through hole can be accessible from both directions (0, 0, 1) and (0, 0, -1) vectors. Through hole has two TADs. Slot feature has a normal and sweep, sweep is orthogonal to the normal. Fig.3 shows the normal and sweep for blind-open-slot in thin blue lines. If the end-milling-slotting process is selected to machine the slot then its TAD will be (0, 0, 1) vector (normal direction) while if the side-milling process is selected then its TAD will be along the vectors which are the cross-product of normal and sweep vectors. Blind-open-slot has total three TAD's (one in normal direction and two in directions of cross-product of normal and sweep vectors). Some researchers have considered TAD for a blind-open-slot through sweep directions (0, 1, 0) and (0, -1, 0) but it is not possible unless slot has corner-radius at the bottom.

```
(defrule HoleTAD.Blind.Doesnt.Exist
  (feature (name ?f1) (type HOLE) (bottom YES)
  (holeAxis ?x ?y ?z))
  ?p <- (process (name ?pro) (type drilling) (feature ?f1)
  (TAD $?tadp))
  (not (TAD (vector ?l&: (numberEpsilonEquals ?l ?x)
  ?m&: (numberEpsilonEquals ?m ?y) ?n&:
  (numberEpsilonEquals ?n ?z))))
  =>
  (bind ?l ?x) (bind ?m ?y) (bind ?n ?z)
  (bind ?tad (concatenate ?l ?m ?n))
  (modify ?p (TAD (create$ $?tadp ?tad)))
  (assert (TAD (name ?tad) (features ?f1) (vector ?l ?m
  ?n) (processes ?pro)))
  )
)
```

Figure 4. TAD rule for blind-hole-feature

To identify the TADs for the given features automatically, we have used JESS as a tool in JAVA. JESS is rule based system and has capacity of reasoning for the knowledge we supply in the form of rules[7]. Figure 4 shows the sample rule to identify the TADs of blind-hole feature.

Rule in the figure 4 defines that, when TAD for a feature ?f1 doesn't exist and the feature ?f1 is a type of hole who has a bottom with hole axis of a vector (?x, ?y, ?z), it also has process ?pro which is of drilling type and that process had one or more TADs then assign a new TAD ?tad for the feature ?f1 of vector (?x, ?y ?z) because drilling has to be done along hole-axis.

```
(assert (feature ;Blind Hole
  (name HOLE1)
  (type HOLE)
  (bottom YES)
  (holeAxis 0 0 1)
  ))

(assert (process
  (name drilling1)
  (type drilling)
  (feature HOLE1)
  ))

(assert (feature ;Blind Hole
  (name HOLE2)
  (type HOLE)
  (bottom YES)
  (holeAxis 0 1 0)
  ))

(assert (process
  (name drilling2)
  (type drilling)
  (feature HOLE2)
  ))
```

Figure. 5. Facts for TAD rule of blind-hole feature

Figure 5 shows the facts that run on the TAD rule of blind-hole feature. There are two holes Hole1 and Hole2 and both of them has bottom. Hole1 has drilling1 process and (0, 0, 1) hole axis vector while Hole2 has drilling2 process and (0, 1, 0) hole axis vector.

Result:

```
Jess> (facts)
f-0 (MAIN::feature (name HOLE1) (type HOLE) (TAD
) (bottom YES) (holeAxis 0 0 1))
f-1 (MAIN::process (name drilling1) (type drilling)
(feature HOLE1) (TAD "TAD:0:0:1"))
f-2 (MAIN::feature (name HOLE2) (type HOLE) (TAD
) (bottom YES) (holeAxis 0 1 0))
f-3 (MAIN::process (name drilling2) (type drilling)
(feature HOLE2) (TAD "TAD:0:1:0"))
f-4 (MAIN::TAD (name "TAD:0:1:0") (features
HOLE2) (vector 0 1 0) (processes drilling2))
f-5 (MAIN::TAD (name "TAD:0:0:1") (features
HOLE1) (vector 0 0 1) (processes drilling1))
```

Figure 6. TADs for blind-hole-feature

Figure 6 shows the result that for feature HOLE1 with a process drilling1 and for the HOLE2 with the process drilling2, “TAD:0:0:1” and “TAD:0:1:0” have been created respectively.

Inversely, there is another rule we have written when the same TAD already exists then in that case other feature ?f2 has process ?pro2 who has same TAD then assign feature ?f1 to the that TAD but we also check for the process ?pro if it is the member of the same TAD, if no then add the process ?pro to the same TAD. In the same way TADs would be identified for other type of features and the associated processes for these features would be remembered in their respected TADs

Once all the TADs are identified for all the features of the part, next task of the setup planning is of grouping features based on tolerance relation to make setups.

3.2.2. Geometric and Dimensional tolerance analysis

Consideration of GD&T is a crucial in setup planning. To meet the design specification or for the better quality of the product GD&T plays an important role in setup planning. For grouping of the features in setups one of the three criteria is considered to get critical tolerance relationship between features[3].

Criteria 1: Group two features who have tightest tolerance relationship between each other. This criteria is always preferred since there is no stack-up errors.

Criteria 2: Consider a feature as a datum and machine other. This criteria is less accurate and considered only when it is not possible to machine two features in same setup.

Criteria 3: In this criteria, an intermediate datum is chosen and to machine two features in different setups. This method involves more stack-up errors.

We have considered a datum as a feature since the tolerance relationship is always specified between two features or between datum and a feature.

In this paper criteria 1 has been used to cluster features into setups. Consider an example shown in figure 7 and table 1, which show the tolerance relationship between the features.

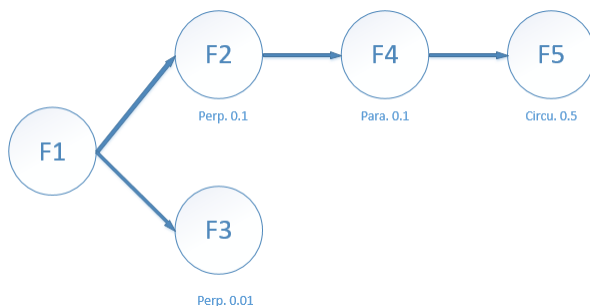


Figure 7. Tolerance relationship between features

Feature F1 has no tolerance. F1 feature is a primary datum for F2 feature and F3 feature. F2 and F3 have a tolerance type perpendicularity and have tolerance value 0.1 and 0.01 respectively with respect to feature F1. F4 has a tolerance type parallelism and has

tolerance value 0.1 with respect to feature F2 since F2 feature is a datum for the feature F4. F5 has tolerance type circularity and has tolerance value 0.5 with respect to feature F4 since F4 feature is a datum for the feature F5.

According to criteria 1, F1 and F3 should be grouped together into the same setup because they have the tightest tolerance relationship. In order to do that there is a need to check if both of them have a common TAD, if yes they can be grouped together in same setup. Conversely, if they don't have common TAD they can't be grouped together and in this case F1 and F3 features will be assigned to different setups. When F1 and F3 are assigned, remaining features are F2, F4 and F5. Among remaining features, F4 has the tightest tolerance relation with feature F2, that's why they should be grouped together if they have a common TAD between them. If they do not have common TAD, F2 and F4 features would be assigned in same fashion as that of F1 and F3 have assigned to different setups. Once F1, F2, F3 and F4 are assigned remaining feature is F5. F4 is a datum for the feature F5. Since the F5 has only tolerance relation with F4, F4 and F5 should be clustered together in same setup if they have a common TAD. If F4 and F5 don't have common TAD then F5 will be assigned to a different setup where there are maximum features of same TAD as that of F5.

We have assumed some processes, TADs for above features to test our feature clustering rules based on tolerance relation:

Features	Tolerance	Processes	TADs
F1		P1	TAD1
			TAD2
		P2	TAD1
			TAD2
P3	TAD1		
	TAD3		
P4	TAD4		
F2	Perp. 0.1	P5	TAD2
			TAD3
F3	Perp. 0.01	P6	TAD3
		P7	TAD4
F4	Para. 0.1	P8	TAD2
F5	Circu. 0.5	P9	TAD5
			TAD2
			TAD4

Table 1. Facts for rule of feature clustering based on tolerance relationship.

In table 1, each feature has one or more processes and each process has one of more TADs. Tolerances specified to some features are also shown in table 1. To cluster the features in same setup having tightest tolerance relationship we have written a rule shown in figure 8:

The rule in figure 8 states that, if a feature ?f1 has

tolerance relation with primary datum ?pd. Feature ?f1 has multiple tolerances and one of them is ?tol of tolerance value ?tv, process ?pro and that process ?pro has multiple TADs and one of TADs is ?tad. Primary.

```
(defrule feature-has-tightest-tolerance-relationship-with-
other-features
  (declare (salience ?*Tolerance-relation_prio*))
  ?f <- (featuresDone (feature $?features)) ;
  (feature (name ?f1&: (not (member$ ?f1 $?features)))
(tolerance $? ?tol $?))
  ?p <- (process (name ?pro) (feature ?f1) (TAD $? ?tad
$?))
  ?t <- (TAD (name ?tad) (features $?feat) (processes
$?prot) (decideFeatures $?decideFea)
(decideProcesses $?decidePro))
  ?to <- (tolerance (name ?tol) (toleranceValue ?tv)
(primaryDatum ?pd)) ;tolerance
  ?d <- (feature (name ?pd&: (not (member$ ?pd
$?features)))) ;datum feature
  ?dp <- (process (name ?pdpro) (feature ?pd) (TAD $?
?tad $?)) ;datum process
  (not (tolerance (name ~?tol) (toleranceValue ?tolval&:
(< ?tolval ?tv))))
  =>
  (modify ?f (feature (create$ $?features ?pd ?f1)))
  (modify ?t (decideProcesses (create$ $decidePro
?pdpro ?pro)))
  (modify ?t (decideFeatures (create$ $decideFea ?pd
?f1))))
```

Figure 8. Rule to cluster features who have tightest tolerance between them

datum ?pd which is also a another feature having the process ?pdpro and ?pdpro has multiple TADs and one of them is same as that of feature ?f1 that is ?tad. We have inserted a condition such that if none of the other feature whose tolerance value is less than ?tv then feature ?f1 and ?pd should be grouped together in a setup of TAD ?tad. On the RHS side of the rule shows that ?pd and ?f1 features are grouped together in 'decideFeatures' slot of TAD template. Moreover, respective processes of both features should also be grouped together and it has been done in 'decideProcesses' slot of TAD template.

```
f-16 (MAIN::TAD (name TAD1) (features F1) (vector )
(processes P1 P2 P3) (decideProcesses ) (decideFeatures
))
f-17 (MAIN::TAD (name TAD2) (features F1 F2 F4
F5) (vector ) (processes P1 P2 P5 P8 P9)
(decideProcesses P8 P9) (decideFeatures F4 F5))
f-18 (MAIN::TAD (name TAD3) (features F1 F2 F3)
(vector ) (processes P3 P5 P6) (decideProcesses P5 P3
P6) (decideFeatures F2 F1 F3))
f-19 (MAIN::TAD (name TAD4) (features F1 F3)
(vector ) (processes P4 P7) (decideProcesses )
(decideFeatures ))
f-20 (MAIN::TAD (name TAD5) (features F4) (vector )
(processes P8) (decideProcesses ) (decideFeatures ))
f-21 (MAIN::TAD (name TAD6) (features F5) (vector )
(processes P9) (decideProcesses ) (decideFeatures ))
```

Figure 9. Setup formation based on tolerance relation

Once both the features are grouped in a setup these

features are remembers in 'featuresDone' template.

The result in figure 9 shows the clustering of above features based on tolerance relationship:

F1 and F3 has the tightest tolerance relation (tolerance value 0.01) and share same TAD 4, hence they both form a setup of TAD 4. Once the F1 and F3 are assigned, among F2, F4 and F5 F2 and F4 has next tightest tolerance relation (tolerance value 0.1) and share same TAD 2, hence both of them form another setup of TAD 2. Now F1, F2, F3 and F4 are assigned. Remaining feature F5 has next tolerance relation with feature F4 (tolerance value 0.5) and F4 and F5 share a same TAD 2, hence F5 is assigned to a setup where F4 is present. Thus total 2 setups TAD4 and TAD2 are formed to machine all these features.

3.2.3. Datum precedence

Datum is a reference for the part to be machined and they are imaginary planes[1]. Datum precedence is another constraint in the setup planning. Tolerance relationship is always represented between a feature and a datum. In this case, datum should be machined before machining the other feature who has a tolerance relation with the datum. Machining all the datum first is a good manufacturing practice and doesn't cause stack up error. In this paper we have shown datum precedence in the form of graph which is generated automatically using Jess and Java tool. Consider the same example mentioned in figure 7. The rule which generates a graph is shown in figure 10:

```
(defrule make-primaryDatum-precedence
  ?f <- (feature (name ?f1) (tolerance ?t) (previous $?ld))
  (tolerance (name ?t) (type ?type) (primaryDatum ?d))
  ?df <- (feature (name ?d&: (not (member$ ?d $?ld)))
(next $?lf))
  (test (not (member$ ?f1 $?lf)))
  =>
  (modify ?df (next (create$ $?lf ?f1)))
  (modify ?f (previous (create$ $?ld ?d)))
  )
```

Figure 10. Rule for datum precedence

When feature ?f1 has tolerance ?t and primary datum ?d then add datum ?d in the 'previous' slot of template feature whose name is ?f1. This indicates, machine the datum ?d first and then feature ?f1.

F1 is a datum for feature F2 and F3. F2 is a datum for feature F4 and F4 is a datum for feature F5. To avoid the stack-up error during changing the setup of the part on machine. F1 should be machined first followed by feature F2 and F3. When F1, F2 and F3 are machined, feature F4 is machined and later feature F5. The sequence of the machining these features depends on feature precedence that has been discussed in the future work section. The generated graph is shown below:

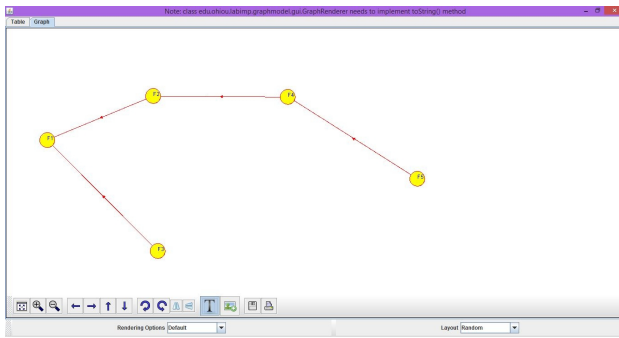


Figure 11. Datum precedence graph

4. CASE STUDY

Currently, our setup planning module is capable to generate Tool approach directions for features extracted from CAD software. It is also capable to produce a datum precedence graph which shows the sequence of the datum to be machined and finally it is capable to cluster features in setups based on the tolerance relationship between the features. We have tested our module on the facts of the ‘Slider’ part shown in figure 12 and result is shown in figure 13 and figure 14.

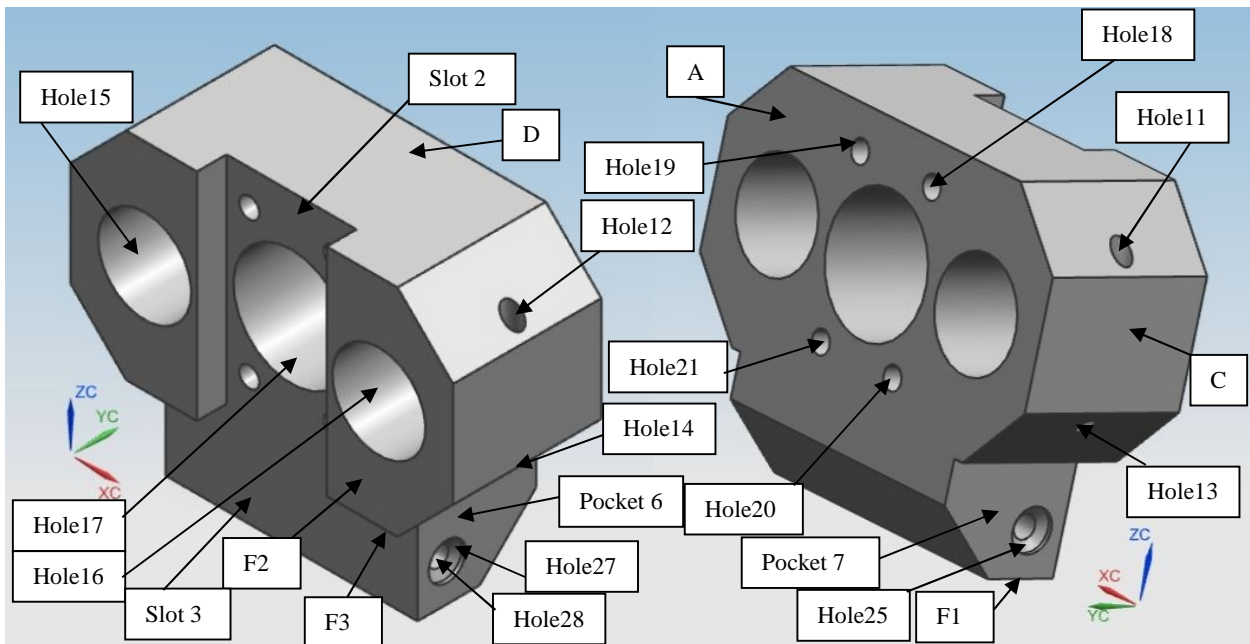


Figure 12. Slider

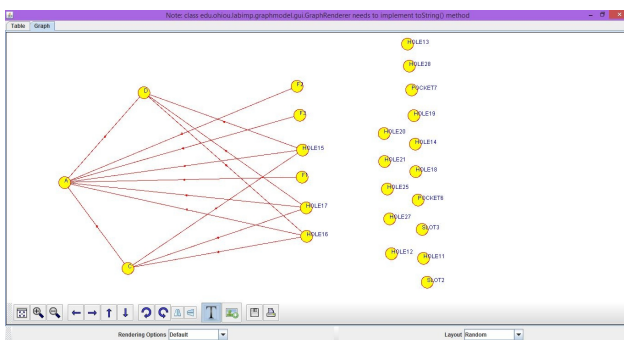


Figure 13. Datum Precedence

Figure 13 shows the datum precedence graph. Feature C is a datum of three features Hole15, Hole16 and Hole17 and these features are in the ‘next’ slot that means feature C has to be machined before these three features, therefore feature C is connected to Hole 15, 16 and 17 by unidirectional line.

Portion of the result of Slider part is shown below:

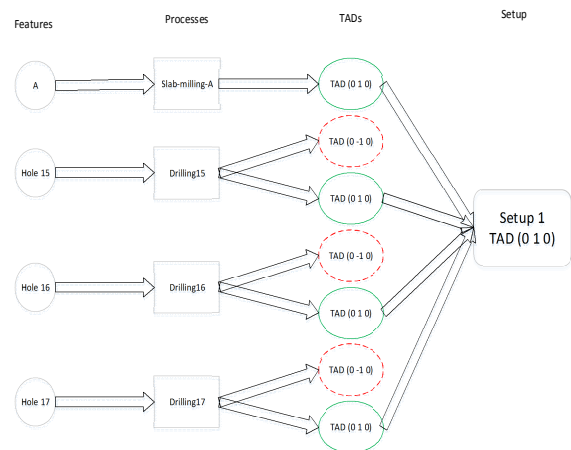


Figure 14. Portion of setup formation of Slider part

Features Hole 15, Hole 16 and Hole 17 have tolerance relationship with feature A. All of them have single process and each process has one or more TADs as shown in figure 14. Since all Hole features have tolerance relationship with feature A, all of them should be clustered together to form one setup if they share common TAD. All Hole features share common TAD (0 -1 0) shown in broken red elliptical shape but feature A doesn't have TAD (0 -1 0). However, TAD (0 1 0) in green elliptical shape is a common TAD for all of them. Hence single setup ‘setup 1’ is formed for

all four features of TAD (0 1 0). Similarly other features form setups accordingly.

f-60	(MAIN::TAD (name "TAD:-1:0:0") (features POCKET8 SLOT2 HOLE28 C HOLE25) (vector -1 0 0))
f-61	(MAIN::TAD (name "TAD:1:0:0") (features HOLE28 SLOT2 POCKET7 HOLE27) (vector 1 0 0))
f-62	(MAIN::TAD (name "TAD:0:-1:0") (features SLOT3 SLOT2 HOLE21 HOLE20 HOLE19 HOLE18 F2 HOLE17 HOLE16 HOLE15))
f-63	(MAIN::TAD (name "TAD:0:1:0") (features HOLE15 HOLE18 HOLE16 HOLE19 HOLE17 HOLE20 HOLE21 A) (vector 0 1 0))
f-64	(MAIN::TAD (name "TAD:0.0:0.0:-1.0") (features SLOT3 HOLE14 HOLE13 F3 F1) (vector 0.0 0.0 -1.0))
f-65	(MAIN::TAD (name "TAD:0:0:1") (features HOLE13 SLOT3 HOLE14 D HOLE12 HOLE11) (vector 0 0 1))

Figure 15. Setup formation of Slider part

Figure 15 shows the final result of feature clustering of Slider part. Fact-60 to fact-65 are the generated setups of their respective TADs. Features, vectors and processes are also shown associated with these TADs.

5. CONCLUSION

Setup planning is an important part of computer aided process planning. In this paper, a knowledge based approach is introduced for setup planning. Tool approach direction is a prime factor for grouping feature is discussed and the method to generate TAD for the features is shown. GD&T is also introduced for setup planning since the quality of the finished product is always important. Datum precedence is introduced in the form of automated generated graph. Datum precedence is important in the setup planning for good manufacturing practice since datum are always machined prior to other features.

Further work will consider FPN (feature precedence network), setup sequencing for 4-axis milling machine and fixture planning. FPN is an important constraint for sequencing operations within the setup. The final task of setup planning is setup sequencing for optimal setup plan.

6. REFERENCES

- [1] M. Hazarika and U. S. Dixit, *Setup Planning for Machining*. Cham: Springer International Publishing, 2015.
- [2] N. Neerukonda, "Automatic Setup Selection and Operation Sequencing for Computer-aided Manufacturing Software," Ohio University, 2005.
- [3] X. Sun, X. Chu, Y. Su, and C. Tang, "A new directed graph approach for automated setup planning in CAPP," *Int. J. Prod. Res.*, vol. 48, no. 22, pp. 6583–6612, Jan. 2010.
- [4] C. Kumar and S. Deb, "Generation of optimal sequence of machining operations in setup planning by genetic algorithms," *J. Adv. Manuf. Syst.*, vol. 11, no. 01, pp. 67–80, Jun. 2012.
- [5] D. N. Šormaz and B. Khoshnevis, "Process

sequencing and process clustering in process planning using state space search," *J. Intell. Manuf.*, vol. 7, no. 3, pp. 189–200, 1996.

[6] D. N. Sormaz, J. Arumugam, and C. Ganduri, "Integration of rule-based process selection with virtual machining for distributed manufacturing planning," in *Process Planning and Scheduling for Distributed Manufacturing*, Springer, 2007, pp. 61–90.

[7] E. Friedman-Hill, *Jess in action: rule-based systems in Java*. Greenwich, CT: Manning, 2003.

Authors: Mayur Wakhare, Dusan Sormaz Ohio University, Industrial and Systems Engineering, Russ college of engineering and technology, Stocker center, Athens, OH, United States – 45701. Phone.: +1-740-593-1545, Fax: 740-593-0778

E-mail: mw594113@ohio.edu;
sormaz@ohio.edu



Cerjakovi , E., Top i , A., Lovri , S., Heri , M.

IMPACT OF PRODUCTION EQUIPMENT SELECTION ON PRODUCTION COSTS

Abstract: *Development and business of manufacturing systems permanently become more complex due to everyday changes that are dictated from the global market. As a results of that fact, there is an everyday need for the adjustment of structure and parameters of manufacturing systems so it could be operated in the most favourable technological and economic conditions. Within this paper, are presents the results of the research that are directed towards the analysis of the impact of the selection of the various production equipment on the production costs for an identical manufacturing process.*

Key words: *production equipment, production costs, simulation studies, flow of material*

1. INTRODUCTION

Development and business of companies, as well as manufacturing systems, permanently become more complex due to everyday changes which are dictated from the global market, production in accordance with the requirements of the customer, increase of volume, quality and complexity of the production, request for the increase of production flexibility, varieties of products, shortened period of development and market lasting of the product, decrease of the production costs etc. All these factors as a consequence have considerable increase of the dynamics of the market where products are required to be of high quality and that they must be delivered at the exact time with the lowest possible production costs. In order to fulfill all these requests, it is necessary that manufacturing systems have a quick response to market requests, which means that they develop every day, with the increase of flexibility and adaption of its structure and performances. Based on above mentioned market conditions companies sometimes lost some of potential business arrangements because of inadequate responses on the market requests. One of possible causes for this is absence of investments into the improvement of production characteristics of the manufacturing systems, as well as into the increase of production capacities in order to fulfill increased market demands and reducing the prices compared to competitive products. On the other side, freezing of its own funds through investment programs during the company's moments of crisis leads to the problems of insolvent that can be deleterious for the existence of the company [1]. So, there is a constant question which structure and equipment, when and in which extent reasonable to invest with the aim of improvement of producing capacities and performances of the manufacturing system, so to reach optimal parameters based on the given criteria.

2. PROBLEM DESCRIPTION

The main issue when it comes to a reconstruction of

manufacturing system through implementation of new production equipment is appearance of various obstacles that can results in inability to consider all the consequences at the end of the reconstruction activities, and that is actually the real problem and the risk. In this paper, it is presented the problem of insufficiently researched area of mutual interaction of technological and economic impacts according to the estimation of potential investment programs for the enlargement of the capacities, as well as projecting new or accomplishment of reengineering working characteristics of manufacturing system, in the serial production, with the aim of improvement of the production characteristics. Koren, Hu, and Weber [2] have demonstrated that the system configuration (the arrangement of the machines and the interconnection among them) has a significant impact on six key performance criteria: 1) investment cost of machines and tools, 2) quality, 3) throughput, 4) capacity scalability, 5) number of product types, and 6) system conversion time. However, if we direct the consideration towards valuing the most favorable equipment for the realization of the specific technological operation in practice, the current approach to this issue is the choice based on partial analysis that does not consider all the possibilities and malfunctions, where consciously suboptimal investment programs are chosen. Cerjakovi et al [3] suggest that relevant investment analysis which will be applied for determination of required structure of manufacturing systems need to include all relevant parameters of direct costs (costs of labor, machinery, tools, emulsions, energy, transportation, quality control, storage, maintenance, montage, etc.) and costs of unused resources i.e. technical indirect production costs of unused resources i.e. technical indirect production costs (appearance of bottlenecks and malfunctions, lack of energy, work resources, production materials, etc.) projected on time of investment repayment. So, it is necessary to apply the methodologies that will as much as possible value the process of investment repayment. Additional issues in the realization of valuing the investment represents stochastic character of

changeable parameters of the manufacturing system, [4].

3. CHARACTERISTICS OF THE OBJECT OF RESEARCH

The polygon of research is manufacturing line which suffered many technological and organization changes during last 12 years. During that time, despite to the changes, manufacturing line kept the manufacturing of an identical products. In fact, during that period are used new technology (tools, manufacturing equipment ...) with the aim to rationalization of the manufacturing process, and it resulted in variation of the structure of technological system and/or the flow of material within observed manufacturing line.

With the aim of showing possible variations of different manufacturing equipment, the operation of drilling on the manufacturing line PLGT2 will be observed, with all its specifications, [1]. It will be presumed that it is necessary to change the equipment on IV technological operation, drilling of the holes on work pieces, (hereinafter TOIV), because it has the biggest impact on forming the total production costs and it has the largest number of applied types of production equipment. In table 1. there are basic characteristics of possible equipment which can be applied for the realization of TOIV which is implemented before. Considering the fact that it is necessary to protect reliable economic indicators of the object of research and to provide authenticity of economic data all economical parameters will be multiplied by x factor.

Production equipment	Shares of certain states in total work time of production equipment (%)			
	Price (x·€)	Power (kW)	Capacity (pcs/shift)	Space (m ²)
M	140.000	40,25	155	14
I	124.000	31	135	22
L	1.000.000	170	520	54
K	1.000.000	60	750	41,75

Table 1. Characteristics of the observed production equipment

For this operation four different types of production equipment during the time were used:

- Production equipment M – CNC single spindle drilling machine (machined 3 workpieces at a time);
- Production equipment I – CNC single spindle drilling machine (machined 3 workpieces at a time) or one workpiece and possesses integrated storage with capacity of 60 workpieces (this solution is used for deburring of holes after treatment on production equipment K);
- Production equipment L – CNC multy spindle drilling machine (machined 8 workpieces at a time);
- Production equipment K – CNC multy spindle drilling machine (machined 6 workpieces at a time) and possesses integrated rotary storage with capacity of 60 workpieces.

For transport of work pieces, kanban pallets with capacity of 60 pieces per unit are used. Working time is in three shifts, 365 days a year with 45 minutes of break (breakfast and cleaning the equipment).

2.1 Preparing for experimental research

In order to provide a needed capacity of observed manufacturing line ($Q=950, \dots, 1200$ pcs/shift), it is necessary to form a complex structure by combining of available production equipment for the realization of the observed technological operation. According to above mentioned criteria, for research are selected following combinations of production equipment for research are selected: K+I+2·M, 8·I, 2·L, K+I+2·I, L+3·M, L+4·I, 7·M, L+2·I+2·M.

Technical parameters (MTTR - Mean Time To Repair, MTBF - Mean Time Between Failures, working availability of production equipment, time of the manufacturing cycle, period and time of changing of tools, period and time of changing semiproducts period and time of quality control) are used for a preparation of the analysis of the observed structure, so they are collected in-site and taken from the data base since 2006. Basic economical parameters that were used within generating the costs are given in the table 2, while others are taken in accordance with the real state (costs of tools, adhere of emulsion...).

Parameter	Value	Unit
Interest rate, inflation, calculated profit of investor (annual level)	17	%
Maintenance (average size)	23	€/h
Amortization (annual level)	20	%
Facility (rent and maintenance on monthly level)	76,7	€/m ²
Workplace (4 shifts)	1915	€
Energy	0,072	€/kWh

Table 2. Basic economical parameters

In order to analyze the operation of the observed facility, it has been done its modelling with the simulation tool Technomatix Plant Simulation. Validation and verification of developed simulation models of the observed manufacturing line was performed by using of method of animation, Desk Checking, partial models tests and the method of comparing with the recorded data, [5]. Obtained data show the authenticity of the created simulation model, with the relative accuracy of the model above 92% compared to the real state, [1]. Working period of observed manufacturing system that was simulated is one year. For evaluation of investment programs is used coefficient of indirect costs K_{ind-tr} , form (1) and coefficient differences of indirect costs in percentage $_{ind-tr}$, forms (2), [3], [1].

$$K_{ind-tr} = \frac{(P_{trj} - \min(P_{tr})) \cdot Q_{pro}}{\min(P_{tr}) \cdot Q_{prj}} + 1 \quad (1)$$

Where are:

K_{ind-tr} – coefficient of indirect costs,

j – number of observed structures ($j=1 \dots m$),
 $\min(P_{tr})$ – minimal recorded value of production costs (€pcs),
 P_{trj} – production costs of the observed structure j (€pcs),
 Q_{prj} – achieved annual production capacity of the observed structure j (pcs./year),
 Q_{pro} – planned annual production, (pcs/year).

$$\Delta_{ind-tr} = \left[K_{ind-tr_j} - \min(K_{ind-tr}) \right] \cdot 100 \quad (2)$$

3. EXPERIMENTAL RESULTS

After processing the results obtained by simulation experiments, relevant data about technological and economic characteristics of previously defined structures of TOIV are presented in table 3. At this point it is important to clarify answer on reasonable question: "Are the technological and economic characteristics of other technological operations have effect on obtained results?". In the order to give the right answer to this question, determination of the size of dispersion of production costs in percentages on other technological operations compared to the average value of these costs for all observed experiments was done. Determined dispersion is with in a diapason from 0,753% to -1,660%, so it can be concluded that there are impacts of production costs of other technological operations on the TOIV production costs, but if we take in to account relations between production costs presented on table 3, these impacts can be disregarded and they can be applied for some further analysis.

TOIV structure	Necessary investment for TOIV (€x)	Production costs for TOIV (€pcs·x)	Accomplished production (pallets/year)
K+I+2·M	1.404.000	1.071	16.825
8·I	992.000	1.009	16.830
2·L	2.000.000	1.439	16.976
K+I+2·I	1.372.000	1.066	16.839
L+3·M	1.420.000	1.157	16.775
L+4·I	1.496.000	1.243	16.828
7·M	980.000	0.966	17.180
L+2·I+2·M	1.528.000	1.249	16.930

Table 3. Techno-economical characteristics of observed structures

Data in Table 3 show that accomplished annual production capacity for some structures is greatly lower when compared to the projected capacity (17.378 ... 21.900 pallets/year) what is directly affected by the level of balancing the whole line and availability of production equipment. If production equipment does not work which is conditioned by waiting for jobs and malfunctions, it results in decrease of planned realization of production volume. This especially has impact on production equipment in starting operations because it can reduce the level of utilization of the equipment in the further technological operations. Furthermore, if table 3 is analyzed, it can be seen that

there is no direct connection between the value of necessary investment and production costs. Previous data show that when the new equipment is purchased, all relevant parameters must be taken to value the investment procedure.

Figure 1 and table 4 presents values of coefficients of indirect costs per observed structures, and the best structure is 7·M, while other structures have a significant increase of the coefficient of indirect costs. The reason for this result can be justified with low purchasing price of the equipment, however, it should be considered that this structure is less sensitive to malfunctions as well as it is needed less time for servicing. In the order of realistic comparison of influences of each type of production equipment in forming of production costs, because of its variety of production equipment and insight in forming manufacturing costs, the following structure L+2·I+2·M is observed.

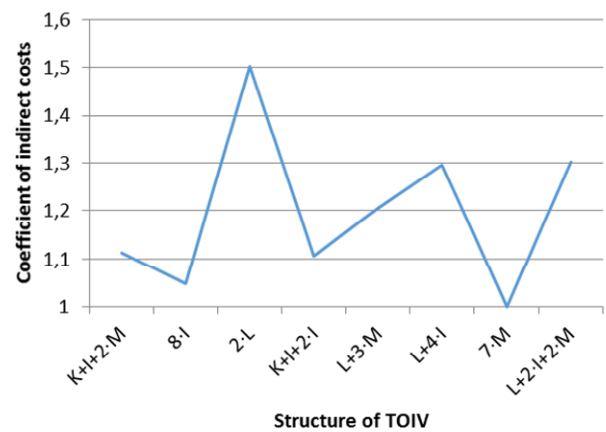


Fig. 1. Coefficient of indirect costs K_{ind-tr}

Structure TOIV	K_{ind-tr}	$ind-tr$ (%)
K+I+2·M	1,113	11,29
8·I	1,047	4,70
2·L	1,503	50,29
K+I+2·I	1,107	10,69
L+3·M	1,206	20,63
L+4·I	1,297	29,66
7·M	1,000	0
L+2·I+2·M	1,303	30,26

Table 4. Value of investment programs

When we compare the distribution of the certain states in the total working time of production equipment in structure L+2·I+2·M, table 5, it can be seen that production equipment type L has significantly higher share in waiting, dismissal state and servicing the equipment when compared with other types of production equipment. This state is described with constructive characteristics of production equipment such as rigidity of a machine, the way of changing tools, maintenance advantages, the way of servicing... With the aim of further analysis, average values of costs and accomplished production will be observed, as well as the relations of each production equipment for structure L+2·I+2·M which is given in table 6.

Production equipment	Shares of specific states in total working period of production equipment (%)				
	Direct work	waiting	States for dismissals	break	service
L	60,53	1,13	8,71	18,74	10,89
I-1	76,49	0,24	0,71	18,74	3,82
I-2	74,43	0,24	2,85	18,74	3,74
M-1	73,04	0,33	3,39	18,74	4,51
M-2	73,76	0,33	2,65	18,74	4,53

Table 5. Shares of certain states in total working period in structure L+2·I+2·M

Differences in average values of costs, given in table 6, for the same type of equipment are conditioned by random events like dismissals states, processing period, period of changing tools, Beside these values, the impact on creating total costs of production has purchase price of the equipment, so if it comes to a completely new investment, ca. 33,17% of total costs goes to investment repayment (principal + interest rate), while, if it comes to the investment of changing the existing manufacturing funds that will be financed from the gathered amortized value during the previous period of production equipment working time, ca. 22,83% of production costs go to the servicing of amortization. So, in this case, ca. 44,00% of total production costs go to direct manufacturing process.

State	Average values of costs (%)				
	L	I-1	I-2	M-1	M-2
TR-1	30,85	6,14	6,30	6,69	6,67
TR-2	18,37	4,45	4,62	4,79	4,77
TR-3	9,77	3,29	3,46	3,48	3,46
GP	39,77	13,55	13,19	14,91	15,05
TR-3/GP	0,246	0,243	0,262	0,233	0,230
TR-3/TR-1	31,69	53,62	54,84	51,98	51,84

Legend.
TR-1 – Total production costs (%)
TR-2 – Production costs without repayment investment costs (%)
TR-3 – Production costs without repayment investment costs and amortization (%)
GP – annual amount of production (%)

Table 6. Techno-economical characteristics of structure L+2·I+2·M

Furthermore, data TR-2 and TR-3 show average values of production costs, if we expect the costs of investment repayment that is the costs of investment repayment and maintenance. These values are presented because of the analysis of the investment amount impact when forming the production costs for different types of production equipment on one side, and the amount of production equipment after the amortization period ends. If we analyze data of total production costs (TR-1) in table 6, it can be easily concluded that percentage ratio is very bad for productive production equipment L, due to the expensive purchase price, however with the analysis of TR-3 it can be seen that the high purchase price is not

the only reason, but also direct production costs and ratio between TR-3/TR-1 (production costs without the costs of investment repayment and amortization with annual amount of production) is adverse when compared to the production equipment of type M for 6,5% where the ratio of purchased price of the observed equipment is K:M=7,14:1.

4. CONCLUSION

The process of choosing production equipment and determining the real value of investment repayment is a complex task which cannot be reduced to the analysis of partial parameters because it requests a complex techno-economical analysis.

The relation of invested-obtained with the purchase of specific production equipment is not a proportional value, so the research points to the sufficient potential for improving characteristics of production, as well as the production costs and enlarging the spectrum of production, changing and optimizing the manufacturing organization without additional investments.

Based on previous conclusions there is the need that in future production equipment should be adjusted to the consumers' requests and not a consumer to the characteristics of production equipment.

5. REFERENCES

- [1] Cerjakovi, E.: *Utjecaj strukture proizvodno-tehnološkog sistema i obima investicije na troškove proizvodnje*, PhD thesis, University of Tuzla, Tuzla, 2012.
- [2] Koren, Y., Hu, J., Weber, T.: *Impact of Manufacturing System Configuration on Performance*, Annals of the CIRP, 47, 1, p.p. 369-378, 1998.
- [3] Cerjakovi, E., Topić, A., Tufekić, Dž., Veža, I.: *Influence of Structure of Manufacturing System and amount of Investment on production cost*, Journal Technical Gazette, 22, 3, p.p. 771-780, 2015.
- [4] Cerjakovi, E., Tufekić, Dž., Topić, A., Šelo, R., elović, Š.: *Stabilisation of production lines by using of simulation study methodology*, International Virtual Journal – MTM, 4, 1-2, p.p. 24-27, 2010.
- [5] Rabe, M., Spieckermann, S., Wenzel, S.: *Verifikation und Validierung für die Simulation in Produktion und Logistik - Vorgehensmodelle und Techniken*, Springer-Verlag, Berlin, 2008.

Authors: Edin Cerjakovi, Assistant Professor, Prof. dr. Alan Topić, M.Sc. Slađan Lovrić, Muhamed Herić, University of Tuzla, Faculty of Mechanical Engineering Tuzla, Univerzitetska 4, 75000 Tuzla, Bosnia and Herzegovina, Phone.: +387 35 320-920, Fax: +387 35 320-921.

E-mail: edin.cerjakovic@untz.ba;
alan.topcic@untz.ba;
sladjan.lovric@untz.ba;
muhamed.heric@untz.ba



A REVIEW ON INTEGRATED PROCESS PLANNING AND PRODUCTION SCHEDULING APPROACH

Abstract: *By tradition, process planning and production scheduling, as two of the most important functions in manufacturing systems, are carried out in sequential way, where scheduling plans are generated after the process plans. However, traditional approach became an obstacle in achieving higher productivity and greater performance of modern manufacturing systems. As result, a tight integration of process planning and scheduling is needed. In this paper, a review of procees planning, scheduling and their integration is given, including advantages and disadvantages of this approach, as well as optimization algorithms used for solving this type of hard combinatorial problems.*

Key words: *integration, process planning, scheduling, optimization algorithms*

1. INTRODUCTION

Process planning and scheduling are two most important functions within modern manufacturing system and represent a key link between Computer aided Design (CAD) and Computer aided Manufacturing (CAM). These functions have a strong influence on profitability of product manufacturing, resource utilization and product delivery time.

Process plans, on one hand, are generated within CAPP (Computer aided Process Planning) system and they specify manufacturing resources and operations used to transform raw material into final shape or final product [1]. The outcome of process planning is the information required for manufacturing processes and identification of tools, machines and fixtures required. Based on complexity of process and number of resources and operations, a part or component may have more than one alternative process plans.

Production scheduling, as other main function, represents the allocation of manufacturing operations to the corresponding resources with indication of start and end times. Scheduling uses process plans as input data and, based on relationships and constraints in process plans, its main task is to generate a scheduling plan (or schedule) that will satisfy given constraints and defined criteria. Process planning and scheduling are strongly interrelated, assuming that both of them are focused on assignment of resources, but regardless of that, many authors claim that the integration of these two functions is still a challenge for both researchers and practitioners [2,3].

By tradition, process planning and scheduling are performed in separate and sequential way, where scheduling plans are generated after the process plans. This approach has several disadvantages that influence the productivity and responsiveness of modern manufacturing systems [4]:

- Process planners usually assume unlimited capacity of resources on the shop floor. They have a tendency to favour some desirable machines and based on that, to

generate most recommended manufacturing processes which can appear to be unrealistic and unfeasible in practice in later stages.

- Fixed process plans generated does not consider alternative machines which can restrict the schedule to only one machine per operation. This can lead to poor resource utilization and create superfluous bottlenecks on shop floor.

- Time delay between planning and execution phase may lead to great changes in constraints that can affect the feasibility of optimized process plans. They may become less optimal or totally invalid. It is assumed that 20-30% of total production plans in this period require modifications to be adapted to the dynamic changes in production environment.

- Usually, both process planning and scheduling consider only one optimization criterion. In real production environment more than one criterion need to be considered simultaneously and their importance may change due to dynamic shop floor conditions.

- Without proper coordinaton process planning and scheduling objectives may create conflicting problems. This is often due to reason process planning is focused on technological requirements of a task, while scheduling emphasizes timing aspects of it.

Mentioned shortcomings of traditional approach can be overcome by consideration of integrated approach to process planning and scheduling, known as IPPS (Integrated Process Planning and Scheduling). The IPPS introduces significant improvements to efficiency and productivity of manufacturing systems through increase of profitability of products, improvement of resource utilization, reduction of scheduling conflicts, reduction of flow time and work in process and adaptation to dynamic shop floor situations. Apart from that, IPPS has a crucial impact on effective realization of computer integrated manufacturing system (CIMS) which tends to integrate various manufacturing functions in a single comprehensive system[2,5].

This purpose of this paper is to give a brief review of integrated approach to process planning and scheduling. Chapter 2 discusses three basic approaches of IPPS with advantages and disadvantages of each. IPPS problem formulation and process plan and scheduling plan representation is represented in Chapter 3. Literature survey of some algorithm-based optimization methods for solving IPPS problems is given in Chapter 4. Chapter 5 is the conclusion of this paper.

2. INTEGRATION APPROACHES OF IPPS

This section introduces three types of general integration approaches based on several models reported in the area of IPPS. These approaches are: Nonlinear process planning and scheduling approach, closed loop process planning and scheduling approach and distributed process planning and scheduling approach.

2.1 Nonlinear approach

Nonlinear approach (NLA) or nonlinear process planning (NLPP) is most basic approach of IPPS. Its methodology is based on generating all possible process plans for each part/job and their ranking according to appropriate process planning optimization criterion/a. Then, when job is required for manufacturing, plan with highest rank is submitted. If that particular plan does not fit well for current shop floor status, plan with second priority rank is provided to the scheduling system. This procedure is repeated until suitable plan is determined from already generated process plans [3,4]. NLA approach methodology is very simple, it has one-way information flow, from process planning (CAPP system) to production scheduling system which are performed in separate ways. This may prevent achieving full optimal results concerning integration of these two functions. Although multiple process plan consideration increases flexibility of this approach and gives more alternatives to process planners, this can also lead to infeasibility of some plans and cause storage problems due to exponential increase in their number. Flow chart of NLA approach is shown in Figure 1.

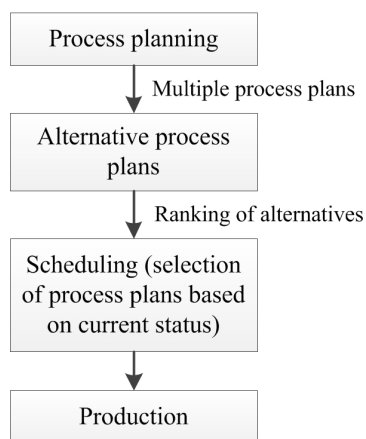


Fig. 1. Nonlinear process planning and scheduling approach [2]

2.2 Closed loop approach

Closed loop approach (CLA) or closed loop process planning (CLPP) generates process plans by using a dynamic feedback from production scheduling and available resources. Production scheduling has a task to tell process planning system about availability of different resources (machines) on the shop floor for current job, so feasibility of all generated process plans is ensured. The real time status of shop floor is crucial element of CLA, so it is sometimes referred to as dynamic process planning or real time process planning approach. Although it possesses significant benefits like real time status consideration, better utilization of alternative process plans and enhanced manipulability of CAPP system, CLA approach also has some drawbacks. Taking into account closer connection between process planning and scheduling departments, their reorganization and reconstruction is inevitable for taking full advantage of CLA. Also, it requires high capacity hardware and software equipment, and some authors claim that approach is very complex and unrealistic in terms of generating real time process plans [3,4]. The basic flow chart of CLA approach is given in Figure 2.

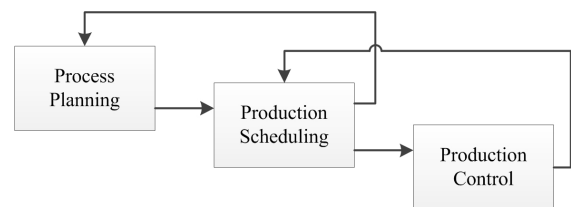


Fig. 2. Closed loop process planning and scheduling approach [3]

2.3 Distributed approach

Distributed approach (DA) or distributed process planning (DPP) works on concurrent engineering principle where process planning and scheduling are performed simultaneously. This model completely integrates these two functions and provides reasonable scheduling plans without generating superfluous process plans. DA approach is divided into two phases. First phase of DA is called initial planning or preplanning phase which is focused on analysis of part/job that need to be manufactured. Simultaneously, machine capabilities are estimated and result of this phase are primary process plans and scheduling plan based on current shop floor status. The second phase is the detailed planning phase which is divided into two subphases. In matching subphase operations are matched with operation capabilities of production resource. After matching is done, the resulting detailed process and scheduling plans are generated [2]. DA approach, like previous two, also has several noteworthy drawbacks. Like CLA, DA requires reorganization and reconstruction of process planning and scheduling departments for successful cooperation. It also requires high capacity and capability from both hardware and software and may cause difficulties in finding feasible plans in reasonable time period for large-sized problems that have vast solution space [3]. In [5] the IPPS model that utilizes advantages of NLA and DA approaches is introduced.

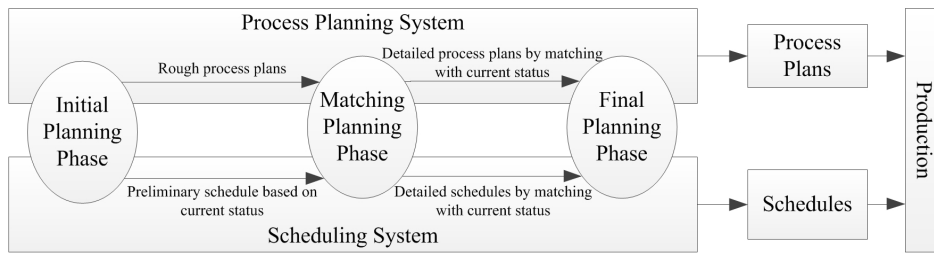


Fig. 3. Distributed process planning and scheduling approach [2]

2.4 Brief comparison of given approaches

All represented approaches have their advantages and disadvantages. In this section they are summarized in Table 1 [2,5].

	Advantages	Disadvantages
NLA	Provides all the alternative process plans and increase flexibility and availability of process plans	Increased flexibility casuses problem to be combinatorial-explosive
CLA	Follows current shop floor status, generate more realistic and useful process plans	Requires real-time data of current status which can cause difficulties if update is needed in every scheduling phase
DA	Interactive, collaborative and cooperative approach	It cannot optimize process plans and scheduling plans as whole

Table 1. Comparison of IPPS approaches

3. FORMULATION AND REPRESENTATION OF IPPS PROBLEM

3.1 Problem formulation

According to the authors [7,8], IPPS problem can be defined in the following way: „Given a set of N parts which are to be processed on machines with operations including alternative manufacturing resources, select suitable manufacturing resources and sequence the operations so as to determine a schedule in which the precedence constraints among operations can be satisfied and the corresponding objectives can be achieved.“

Mathematical modeling of IPPS problem is generally based on the model of job shop scheduling problem which represents one of the classical problems in operations research area. The most often used criteria for scheduling are makespan, job tardiness, job lateness and balanced level of machine utilization. With respect to process planning, manufacturing cost is major used criterion. To avoid conflicting criteria, authors are focused on common criteria in IPPS (i.e. makespan). While solving IPPS problem based on job shop model, some assumptions are usually considered [7]:

- Job preemptions are not allowed and each machine can handle only one job at a time.
- The different operations of one job cannot be processed simultaneously.

- All jobs and machines are available at zero time simultaneously.
- Transportation time is constant; After a job is done on one machine, it is immediately transported to the next machine.
- Setup times are independent of the operation sequence and are included in the processing times.

Complete mathematical model of IPPS based on above assumptions can be found in [7].

3.2 Representation of IPPS problem

Considering process planning covers large number of alternatives, there are three types of flexibilities that need to be taken into account in IPPS [5,6]: operation flexibility, sequencing flexibility and processing flexibility. Process planning optimization include two more types of flexibilities, tool flexibility and TAD (tool approach direction) flexibility which are not covered in this paper. Giving importance to these flexibilities better performance in meeting criteria can be obtained

For describing types of flexilites there are many methods used, such as Petri net, AND/OR graphs and network representations. Figure 4 shows process plan network for one job. There are three nodes in network representation, starting node, ending node, and intermediate node that indicates operation with alternative machines and processing times.

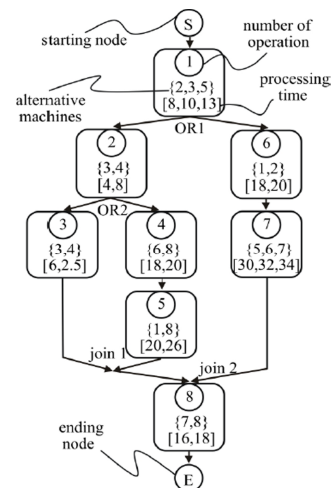


Fig. 4. Process plan network example

Scheduling plans are represented on Gantt charts which shows the order in which the jobs and operations are carried out. X-axis represents time, and Y-axis represents machines and specific arrangement of operations on each machine. Example of Gantt chart for IPPS problem is shown in Fig. 5[5].

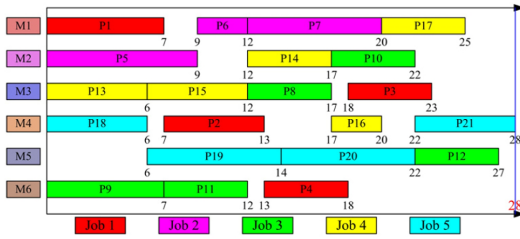


Fig. 5. Gantt chart example

4. OPTIMIZATION ALGORITHMS IN IPPS

Although IPPS approach is more effective and efficient than considered separately, it is more complex. IPPS is NP hard (non-deterministic polynomial) combinatorial optimization problem because number of possible solutions increases exponentially and requires efficient method for finding optimal solution in large search space. There are also many constraints in sequencing operations and manufacturing resource utilization due to manufacturing practice and rules, which additionally increases the difficulty of this problem.

Most popular implementation approaches for solving IPPS combinatorial problems are intelligent algorithm based approaches, usually known as meta-heuristic algorithms like genetic algorithm, simulated annealing, tabu search, particle swarm optimization or ant colony optimization algorithm. Traditional intelligent algorithms have to be modified and improved to be able to solve IPPS problem effectively.

In [5] modified genetic algorithm is introduced for solving IPPS problem. Modifications of simple GA included efficient genetic representations and operator schemes developed for implementation. Experimental results have been used to test the method which gave promising results. Example of hybrid algorithm is proposed in [9] where genetic algorithm and tabu search algorithm are used together and results shown better performance of this HA approach comparing to other methods. Authors [8] developed particle swarm optimization algorithm and implemented for solving operation sequencing and IPPS problem. Achieved results are compared to SA and GA methods where PSO outperformed both GA and SA in the majority of applications. All introduced examples in this chapter are coded in Visual C++ on computers with various configurations.

5. CONCLUSION

The proposed IPPS approach that integrates process planning and scheduling plays a crucial role for performance and efficiency improvements in a manufacturing system. The research presented in this paper provided a brief review of IPPS. Various approaches along with their advantages and disadvantages are introduced. Problem formulation with graph representation of process plans and scheduling plans is shown. Last chapter is focused on reference review of some efficient and robust meta-heuristic methods used for solving IPPS optimization problems. However, many authors claim the integration of these two functions within manufacturing system is still a big challenge for both science and industry.

6. REFERENCES

- [1] Milošević, M., Anti, A., Luki, D., Jović, G., Vukman, J.: *Distributed process planning through web-based collaboration*, The International conference of the Carpathian Euro-region's specialists in industrial systems-CEurSIS, p.p. 147-150, Baia Mare, Romania, 2014.
- [2] Li, X., Gao, L., Zhang, C., Shao, X.: *A review on Integrated Process Planning and Scheduling*, International Journal of Manufacturing Research, Vol. 5, p.p. 161-180, 2010.
- [3] Phanden, K., Jain, A., Verma, R.: *Integration of process planning and scheduling: a state-of-the-art review*, International Journal of Computer Integrated Manufacturing, Vol. 24, p.p. 517-534, May 2011.
- [4] Zhang, H.C., Merchant, M.E.: *IPPM – A Prototype to Integrate Process Planning and Job Shop Scheduling Functions*, CIRP Annals – Manufacturing Technology, Vol. 42, p.p. 513-518, 1993.
- [5] Shao, X., Li, X., Gao, L., Zhang, C.: *Integration of process planning and scheduling – A modified genetic algorithm-based approach*, Computers & Operations Research, Vol. 36, p.p. 2082–2096, 2009.
- [6] Saygin, C., Kilic, S.E.: *Integrating Flexible Process Plans with Scheduling in Flexible Manufacturing Systems*, International Journal of Advanced Manufacturing Technology, Vol. 15, p.p. 268-280, April 1999.
- [7] Li, X., Gao, L., Shao, X., Zhang, C., Wang, C.: *Mathematical modeling and evolutionary algorithm-based approach for integrated process planning and scheduling*, Computers & Operations Research, Vol. 37, p.p. 656-667, 2010.
- [8] Guo, Y.W., Li, W.D., Mileham, A.R., Owen, G.W.: *Applications of particle swarm optimisation in integrated process planning and scheduling*, Robotics and Computer-Integrated Manufacturing, Vol. 25, p.p. 280-288, April 2009.
- [9] Li, X., Shao, X., Gao, L., Qian, W.: *An effective hybrid algorithm for integrated process planning and scheduling*, International Journal of Production Economics, Vol. 126, p.p. 289-298, August 2010.

Authors: MSc Mi a ur ev, Doc. dr Mijodrag Milošević, Doc. dr Dejan Luki, MSc Goran Jović, MSc Jovan Vukman, University of Novi Sad, Faculty of Technical Sciences, Department of Production Engineering, Trg Dositeja Obradovica 6, 21000 Novi Sad, Serbia, Phone.: +381 21 485-2346, Fax: +381 21 454-495.

E-mail: mdjurdjev@live.com; mido@uns.ac.rs;
lukicd@uns.ac.rs; goran.jovicic@uns.ac.rs;
vukman@uns.ac.rs;

Note: This paper is part of a research on project "Modern approaches to the development of special bearings in mechanical engineering and medical prosthetics", TR 35025, supported by the Ministry of Education, Science and Technological Development, Republic of Serbia.



MULTI-AGENT MODELING FOR INTEGRATED PROCESS PLANNING AND SCHEDULING

Abstract: *Multi-agent systems have been used for modelling various problems in the social, biological and technical domain. When comes to technical systems, especially manufacturing systems, agents are most often applied in optimization and scheduling problems. Traditionally, scheduling is done after creation of process plans. In this paper, agent methodology is used for integration of these two functions. The proposed multi-agent architecture provides simultaneous performance of process planning and scheduling and it consists of four intelligent agents: part and job agents, machine agent, and optimization agent. Verification and feasibility of a proposed approach is conducted using agent based simulation in AnyLogic software.*

Key words: *multi-agent systems, process planning, scheduling, integrated process planning and scheduling, simulation*

1. INTRODUCTION

Process planning and scheduling represent two of the most crucial and complex problems in modern manufacturing. Since the introduction of Just-In-Time concept and mass customization, requirements that these activities need to set become more demanding. Deadlines are shorter, variations of products are bigger and batches are smaller. Li et al. [1] outline that traditional process planning and scheduling, which are conducted sequentially, cause several problems. (a) During the process planning resources are assigned on a job without considering the competition for the resources from other jobs. These may lead to unrealistic and infeasible process plans; (b) Fixed process plans may drive scheduling plans to end up with severely unbalance resource load and create superfluous bottlenecks; (c) Process planning emphasizes the technological requirements of a job, while scheduling involves the timing aspects and resource sharing of all jobs. If there is no appropriate coordination, conflicting problems may be created. In order to solve these problems, integration of process planning and scheduling processes have been introduced.

Various technologies that address solutions for integrated process planning and scheduling problems can be found in the literature. Over the years new methods have been added to the traditional technologies, and one of them is agent-based methodology together with the multi-agent systems (MAS). Karageorgos et al. [2] used agent-based approach for supporting logistics and production planning. They developed extended contracting protocol which took into consideration availability and cost of logistic service. Integration of agent-based modeling and particle swarm algorithm in flexible process planning was presented in [3]. Wong et al. [4] developed and compared hybrid-based multi-agent system with the evolutionary algorithms in order to obtain better performance. In the last couple of years

more and more authors are focused on the integrated process planning and scheduling in the dynamic environment. The previous group of authors [5] published their research in which a hybrid-based multi-agent system and Online Hybrid Agent-based Negotiation was used in the dynamic environment under influence of two types of disturbances: part arrival and machine breakdown. He et al. [6] presented a hierarchical agent bidding mechanism that is particularly designed for Make-to-Order manufacturing system. Their goal was to enhance the operational flexibility of manufacturing system in the dynamic business environment.

The aim of this paper is to create multi-agent model that will be capable for performing process planning, scheduling and manufacturing of parts in real time. The remainder of the paper is organized as follows. Section 2 provides problem formulation. In Section 3 definitions and basic characteristics of multi-agent systems are denoted together with the description of the proposed multi-agent architecture. In Section 4 experimental results are presented, while conclusion is shown in Section 5. Section 6 addresses acknowledgements. Section 7 covers references of the paper.

2. PROBLEM FORMULATION

Integration of process planning and job shop scheduling represents a non-polynomial (NP) problem. Guo et al. [7] defined the problem as: "Given a set of n parts which are to be processed on machines with operations including alternative manufacturing resources, select suitable manufacturing resources and sequence the operations so as to determine a schedule in which the precedence constraints among operations can be satisfied and the corresponding objectives can be achieved". In other words, a goal is to process certain number of parts on a predefined number of machines and other resources. Inputs of the system are alternative process plans for each part. These

alternative plans import flexibility into the problem. There are three different types of flexibility connected with the alternative process plans: operation or routing flexibility, sequencing and processing flexibility. The first one defines the possibility of performing one operation on alternative machines with different processing time. Interchanging the sequence of the required operations is defined by the sequencing flexibility. Processing flexibility provides alternative operations or sequences of operations for the same manufacturing feature. Various representation methods are used for describing these flexibilities, but in this paper the AND/OR network is used [8]. Example of an alternative process plans presentation is shown in the Fig. 1.

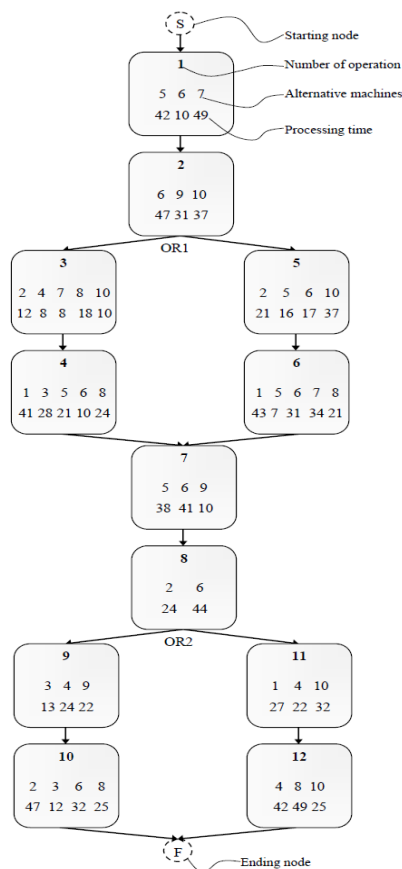


Fig. 1. Alternative process plans for a part [9]

Process planning and scheduling can be conducted in a static and dynamic environment. Static process planning and scheduling problem assumes that all the parameters are known before the start of the process, i.e. number of parts that need to be processed is known at the starting point. In this paper, the dynamic problem is discussed. The stochastic new part arrival is introduced as a dynamic event. Since the decision making is decentralized, the main objective is to find minimum operational time for each operation and for every part. In order to fulfill this objective and meet previously defined constraints in process planning and scheduling, several assumptions must be made. The assumptions are as follows:

- Setup time is included in the processing time;
- Only one operation of one part can be processed

at the time;

- Each machine can only handle one job at the time;
- Every job is independent and each time the job order is launched the auction process for the best processing time must be conducted;
- All machines are available at the start of the simulation;
- Transportation logistics and transportation times are not considered;

3. PROPOSED MAS ARCHITECTURE

Multi-agent systems are formed by a network of computational agents that interact and typically communicate with each other [10]. Proposed MAS architecture consists of four agents: part and job agents, machine agent, and optimization agent. Model is created and implemented in the AnyLogic software.

3.1 Part and job agents

Part and job agents are physically modeled as a two separate agents, but logically can be observed as one. Part agent is used to represent parts that need to be manufactured in the shop floor. Job represents an operation that needs to be processed. Part agent contains information about part number, part ID, current status, current processing time and machine ID that is performing the operation. All agents, and therefore the part agent too, are modeled using state chart diagrams.

Part agent has one entry state, one final state and several intermediate states. Upon arrival, part agent is based in the entry state which is the state of a demand for processing. In that state part agent generate a job agent which represents an order for an execution of an operation. Job agent contains information about part ID and operation that needs to be processed. After the order sending, a part agent stays in the initial state waiting for the results of a bidding process.

Intermediate states are used to represent alternative process plans. Each state represents an operation. Transitions are used to model the precedence between operations. Conditions are used to denote alternative process routes. Part agent goes from initial to one of the intermediate states based on status and machine that performs operation. Machine is assigned to an agent after the successful finish of auction process. Assignment is a trigger for a movement from initial state to one of the intermediate states. When operation is in progress, part agent has an information about machine ID and corresponding processing time obtained through the bidding process. After the operation, agent update its status and goes back to initial state while information about machine ID and processing time is turned to null.

Final state represents finished part. Part is in final state when one of the process plans is applied in full. Tracking changes on the part is conducted using status indicator.

3.2 Machine agent

Machine agent is used for modeling machines. Characteristics of each machine are presented through

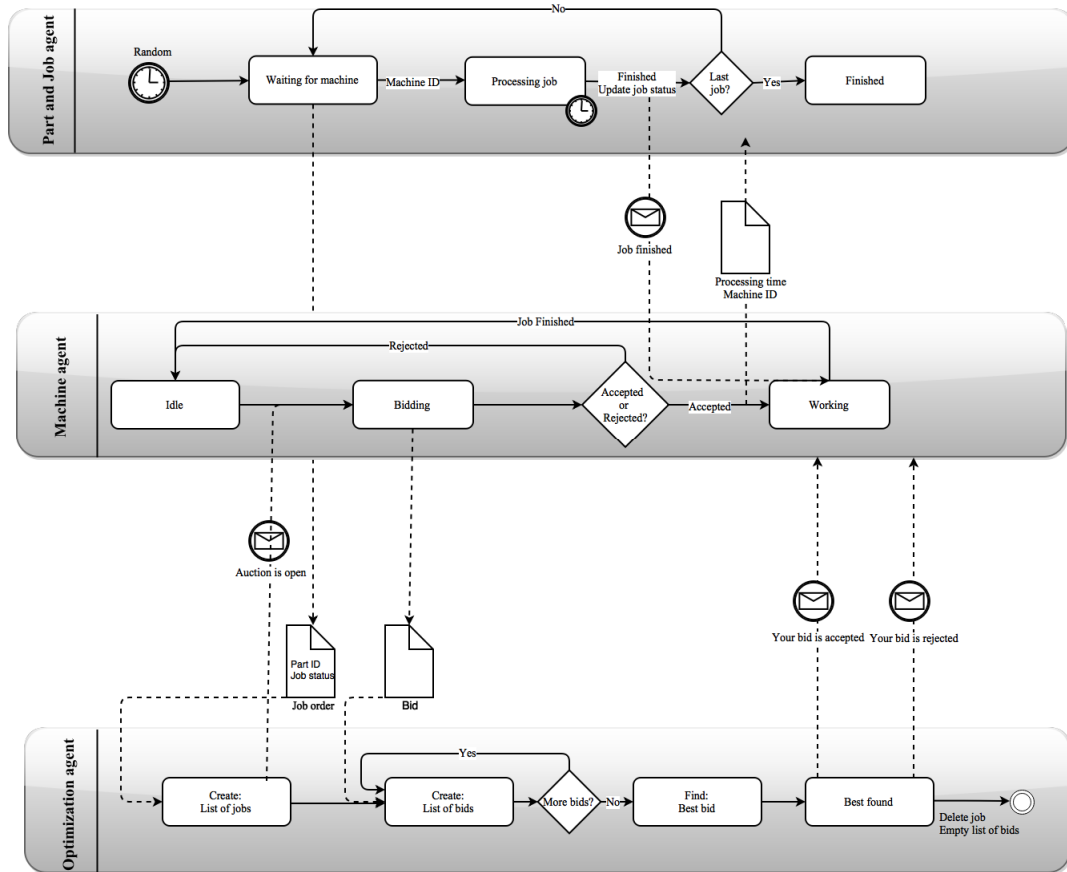


Fig. 2. Communication among agents in the proposed MAS architecture

several parameters: machine ID, processing times for every operation that can be performed on that machine, current processing time, part ID and part status. Machine agent has circular state chart diagram. The diagram contains three different states connected with the transitions.

Entry state of a machine agent is idle state. In that state machine is not active. Idle machines wait for the auction call.

State that follows the auction call is bidding state. Only eligible machines can take part of the auction. Obtaining the call, machines start with the bidding procedure. Machine bids with the corresponding processing time based on the job that needs to be performed. Agent stays in the bidding state as long as auction is open. If machine's bid is the best bid, machine will get the acceptance note. If not, machine will be rejected. Rejected machines go back to initial state. Accepted machine receives the part ID and leaves the bidding state.

Working state is the next state in the state chart diagram. Accepted machine goes from bidding to working state and during this transition sends a message with its ID and processing time to the part agent whose operation will be performed on the machine. When operation is finished the machine receives information from the part agent and goes back to idle state.

3.3 Optimization agent

Optimization agent uses process centric methodology to: (a) enable proper communication

between agents, (b) coordinate auction process, and (c) find the best offer in the bidding process.

Receiving a job order, optimization agent sends auction calls to all machines that are eligible for the job. Only idle, eligible, machines can answer the call. Optimization agent collects all bids into a list of bids and, after the auction is closed, starts with the evaluation. The main evaluation criterion is the minimum processing time for the job. When the minimum is reached, the agent sends acceptance note to the corresponding machine agent and rejects all other machines. If there are no bids for the job, the optimization agent informs the part agent about the case. Part agent launches the order again. This communication among agents, together with the optimization process is graphically interpreted in the Fig. 2.

4. EXPERIMENTAL RESULTS

Feasibility and usability check of the proposed model is conducted in the AnyLogic simulation software. Part with the alternative process plans presented in the Figure 1 is introduced in the shop floor in a stochastic manner in order to simulate dynamic environment. Agents had no prior information about arrival of parts. Several experiments were conducted. In the first one only one part arrived at the 3rd unit of time. In the second one, parts arrived at the 3rd, 13th, 30th, 49th, and 60th unit of time. In the last experiment 10 parts arrived in the following order at: 3rd, 5th, 13th, 22nd, 30th, 36th, 49th, 53rd, 60th, and 75th unit of time.

Obtained makespans are presented in the Table 1. Routings for the first experiment, and Gantt charts for the second and the third experiment are presented in the Fig. 3, respectively.

	Timeline of arrivals	Makespan
Experiment 1	3	119.2
Experiment 2	3 13 30 49 60	254.2
Experiment 3	3 5 13 22 30 36 49 53 60 75	366.7

Table 1. Experimental results

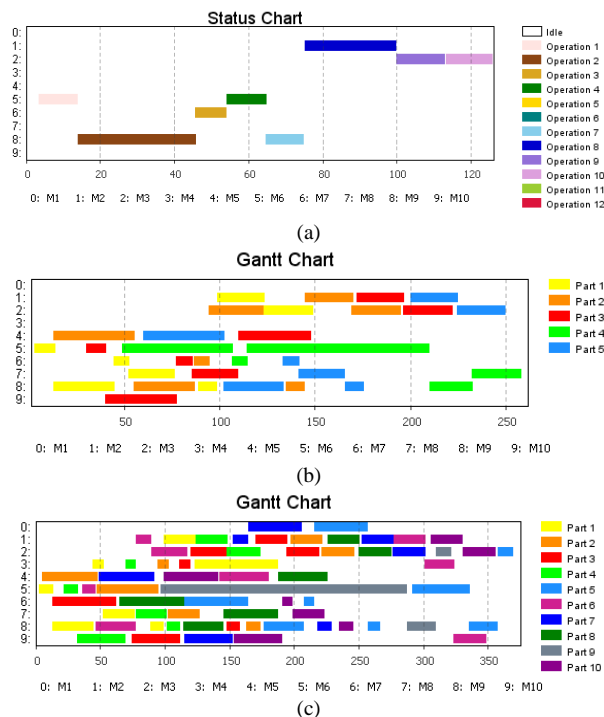


Fig. 3. (a) Part routing; (b) Gantt chart for Experiment 2; (c) Gantt chart for Experiment 3.

5. CONCLUSION

The paper presents multi-agent model for the dynamic integration of process planning and job shop scheduling. The model consists of four agents: part and job agent, machine agent and optimization agent. Process centric negotiation protocol included in the optimization agent is used to gain objectives of the problem and coordination of a decentralized decision making. Proposed model was implemented and verified in the simulation environment using AnyLogic software. Experiments were conducted and the results show that the proposed model is usable in the dynamic environment for integrated process planning and scheduling. Future work will include rescheduling methods upon disturbance caused by a machine failure.

6. ACKNOWLEDGEMENT

This paper is part of the project: *An innovative, ecologically based approach to the implementation of intelligent manufacturing systems for the production of sheet metal parts*, financed by the Ministry of Education, Science and Technological Development of the Serbian Government, Grant TR-35004 (2011-2015).

7. REFERENCES

- [1] Li, X., Zhang, C., Gao, L., Li, W., Shao, X.: *An agent-based approach for integrated process planning and scheduling*, Expert Systems with Applications, 37(2), 1256-1264, 2010.
- [2] Karageorgos, A., Mehandjiev, N., Weichhart, G., Hämmerle, A.: *Agent-based optimisation of logistics and production planning*, Engineering Applications of Artificial Intelligence, 16(4), 335-348, 2003.
- [3] Petronijevi, J., Petrovi, M., Babi, B., Miljkovi, Z.: *Application of multi-agent systems and particle swarm optimization algorithm for flexible process planning*, In: Proceedings of the 39th JUPITER Conference, p.p. 3.114-3.121, 2014.
- [4] Wong, T. N., Leung, C. W., Mak, K. L., Fung, R. Y.: *Dynamic shopfloor scheduling in multi-agent manufacturing systems*, Expert Systems with Applications, 31(3), 486-494, 2006.
- [5] Wong, T. N., Leung, C. W., Mak, K. L., Fung, R. Y. K.: *Integrated process planning and scheduling/rescheduling — an agent-based approach*, International Journal of Production Research, 44(18-19), 3627-3655, 2006.
- [6] He, N., Zhang, D. Z., Li, Q.: *Agent-based hierarchical production planning and scheduling in make-to-order manufacturing system*, International Journal of Production Economics, 149, 117-130, 2014.
- [7] Guo, Y. W., Li, W. D., Mileham, A. R., Owen, G. W.: *Applications of particle swarm and optimization in integrated process planning and scheduling*, Robotics and Computer-Integrated Manufacturing, 25, p.p. 280-288, 2009.
- [8] Kim, Y. K., Park, K., Ko, J.: *A symbiotic evolutionary algorithm for the integration of process planning and job shop scheduling*, Computers & Operations Research, 30 (8), 1151-1171, 2003.
- [9] Kim, Y. K.: *A set of data for FMS production planning and/or scheduling*, <http://syllab.chonnam.ac.kr/links/fmsdata-pp&s.doc>, 2003.
- [10] Monostori, L., Váncza, J., Kumara, S. R.: *Agent-based systems for manufacturing*, CIRP Annals-Manufacturing Technology, 55(2), 697-720, 2006.

Authors: M.Sc. Jelena Petronijevi, M.Sc. Milica Petrovi, Dr. Najdan Vukovi, Dr. Marko Miti, prof. dr. Bojan Babi, prof. dr. Zoran Miljkovi, University of Belgrade, Faculty of Mechanical Engineering, Production Engineering Department, Kraljice Marije 16, 11120 Belgrade 35, Serbia, Phone: +381 11 3302-264, Fax: +381 11 3302-274.

E-mail: jpetronijevic@mas.bg.ac.rs;
mmpetrovic@mas.bg.ac.rs;
nvukovic@mas.bg.ac.rs;
mmitic@mas.bg.ac.rs;
bbabic@mas.bg.ac.rs;
zmiljkovic@mas.bg.ac.rs



Petrovi , M., Petronijevi , J., Miti , M., Vukovi , N., Plemi , A., Miljkovi , Z., Babi , B.

THE ANT LION OPTIMIZATION ALGORITHM FOR FLEXIBLE PROCESS PLANNING

Abstract: *Obtaining an optimal process plan according to all alternative manufacturing resources has become very important task in flexible process planning problem research. In this paper, we use a novel nature-inspired algorithm called Ant Lion Optimizer (ALO) to solve this NP-hard combinatorial optimization problem. The network representation is adopted to describe flexibilities in process planning and mathematical model for the minimization of the total production time and cost is presented. The algorithm is implemented in Matlab environment and run on the 3.10 GHz processor with 2 GBs of RAM memory. The presented experimental results show that the proposed algorithm performs better in comparison with other bio-inspired optimization algorithms.*

Key words: *flexible process planning, ant lion optimizer, particle swarm optimization, genetic algorithms, simulated annealing*

1. INTRODUCTION

Computer Aided Process Planning (CAPP) represents one of the most important research directions in Computer Integrated Manufacturing (CIM). It was developed at the end of the 20th century for the purpose of integrating computer aided design (CAD) and computer aided manufacturing (CAM). Its aim consists of determining detailed methods for manufacturing a part economically and concurrently starting from the initial phase (drawing of the finished part) up to the final phase (the desired shape of the finished part).

As opposed to traditional manufacturing systems, most jobs produced in today's manufacturing systems may have a large number of alternative process plans due to the variety of alternative manufacturing resources. This problem is NP hard (*non deterministic polynomial optimization problems*) which means that time exponentially increases with increase of alternatives. Conventional nonheuristic methods are not able to find optimal solution for this combinatorial problem. In recent years metaheuristic algorithms have been used as primary techniques for obtaining the optimal solutions of process planning problem. Some of the most popular algorithms in this field are: genetic algorithms (GA), genetic programming (GP), simulated annealing (SA), tabu search (TS), swarm intelligence (ant colony optimization (ACO), particle swarm optimization (PSO)) or hybrid algorithms.

Li et al. [1] proposed GP-based approach to optimize flexible process planning with minimum total processing time as criteria. Network representation was adopted to describe flexibility of process plans and efficient genetic representations and operator schemes were also considered. Using the same optimization objective and representation, Shao et al. [2] presented a modified GA-based approach for generating optimal and near optimal process plans. Lv and Qiao [3] proposed new approach called cross-entropy (CE) to optimize flexible process planning. They used

AND/OR network to represented flexibility of process planning and established mathematical model for minimization of total processing time and total cost. Hybrid GA-SA algorithm used to solve flexible process planning problem with the objective of minimizing the production time was presented in [4].

Although these algorithms are able to solve optimization problems, the so-called No Free Lunch theorem [5] allows researchers to propose new algorithms. This paper proposes a new algorithm called Ant Lion Optimizer (ALO) as an alternative approach for solving flexible process planning problem.

The structure of this paper consists of the following sections. In the Section 2 we briefly introduce a flexible process planning problem and describe its representation. Mathematical model of the problem with two objective functions is formulated in Section 3. Section 4 outlines ant lion optimization concept. Section 5 shows comparative results and Section 6 gives concluding remarks. Finally, acknowledgements and references are stated in Section 7 and Section 8, respectively.

2. FLEXIBILITY AND REPRESENTATION

2.1 The flexible process planning problem

In this paper, we consider the following types of flexibility for process planning optimization: machine flexibility, process flexibility, and sequencing flexibility. Machine flexibility relates to the possibility of performing one operation on different alternative machines, with various processing times and costs. Process flexibility refers to the possibility of producing the same part in different ways with alternative operations or sequences of operations. Sequencing flexibility implies the possibility to interchange the ordering of required manufacturing operations.

2.2 Representation of flexible process plans

The flexible process plans representation consists of the information about alternative machines, processing

times, operation sequences, and all the operations needed to manufacture the part. Networks, Petri nets, OR network [1, 2], AND/OR network graphs [3] are some of numerous representation methods used to describe aforementioned types of flexibilities. AND/OR network methodology, described in details in literature [1, 2, 4], is employed to represent flexible process plans.

3. MATHEMATICAL MODELING OF OPTIMIZATION PROBLEM

In this paper, minimization of the total production time and total production cost are two objectives of the optimization problem to be considered. Production time is the one of commonly used minimization criterion in process planning optimization (see e.g. [1, 2]). In this research production time comprises processing time and transportation time.

Processing time (TW) is the time needed to machine a material under some operation(s) and can be computed as:

$$TW = \sum_{i=1}^n TWI(i, j) \quad (1)$$

where n is the (total) number of operations in process plan, $TWI(i, j)$ the processing time of operation i on the alternative machine j .

Transportation time (TT) is the time spent for transport of raw materials, goods, or parts between machines and can be computed as:

$$TT = \sum_{i=1}^{n-1} TTI((i, j_1), (i+1, j_2)) \quad (2)$$

where $TTI(i, j_1), (i+1, j_2)$ is the transportation time between the alternative machine j_1 and j_2 for two consecutive operations.

The total production time (TPT) is defined as:

$$TPT = TW + TT \quad (3)$$

The production cost is another criterion commonly used to select flexible process plans and to quantitatively measure its quality. The total production cost contains the machine cost and the machine change cost, where each cost factor can be described and computed as follows.

Machine cost (MC) is the total cost of the machines selected in flexible process plan and it is computed as:

$$MC = \sum_{i=1}^n MCI_i \quad (4)$$

where n is the total number of operations and MCI_i is the predetermined machine cost index for using machine i , which is a constant for a particular machine.

Machine change cost (MCC) is required to be considered when two consecutive operations are performed on different machines, and it can be computed as:

$$MCC = MCCI \times \sum_{i=1}^n \Omega(M_{i+1} - M_i) \quad (5)$$

where $MCCI$ is the machine change cost index and M_i is the identity of the machine used for operation i .

All this costs are included in the total cost (PC) according to the following equation:

$$PC = MC + MCC \quad (6)$$

4. THE ANT LION OPTIMIZER

Antlions belong to group of insects in the family Myrmeleontidae. The two main phases of the antlions lifecycle are larval stage and adult stage. The antlion larva is often called "doodlebug" because of the trails it leaves in the sand while looking for a good location to build its trap, see Fig. 1. During the process of hunting, antlion makes funnel pits in soft sand and then waits patiently at the bottom of the pit, Fig. 2. Slipping to the bottom, the prey is immediately seized by the antlion. Or, if prey attempts to escape from the trap, antlion throw sands towards the edge of the pit to slide the pray into the bottom of the pit. By throwing up loose sand from the bottom of the pit, the larva also undermines the sides of the pit, causing them to collapse and bring the prey with them. Mathematical modeling of the behavior of antlions and ants is given in the following section [6].



Fig. 1. Pits made by the antlion in soft sand [7]

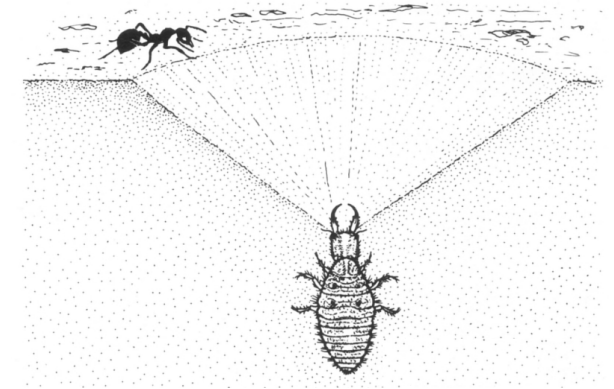


Fig. 2. Hunting behaviour of antlions [8]

4.1 Operators of the ALO algorithm

Random walks of ants when searching food in nature can be described as follows:

$$X(t) = [0, \text{cumsum}(2r(t_1) - 1), \text{cumsum}(2r(t_2) - 1), \dots, \text{cumsum}(2r(t_n) - 1)] \quad (7)$$

where cumsum calculates the cumulative sum, n is the maximum number of iterations, t shows the step of random walk, and $r(t)$ is stochastic function defined

according to the following equation:

$$r(t) = \begin{cases} 1 & \text{if } rand > 0.5 \\ 0 & \text{if } rand \leq 0.5 \end{cases} \quad (8)$$

where t shows the step of random walk and $rand$ is a random number generated according to uniform distribution in the range $[0,1]$.

The position of ants is presented with the matrix:

$$M_{Ant} = \begin{bmatrix} A_{1,1} & A_{1,2} & \dots & A_{1,n} \\ A_{2,1} & A_{2,2} & \dots & A_{2,d} \\ \vdots & \vdots & \ddots & \vdots \\ A_{n,1} & A_{n,2} & \dots & A_{n,d} \end{bmatrix} \quad (9)$$

where M_{Ant} is the matrix for each ant position, $A_{i,j}$ present the value of j -th variable of i -th ant, n is the number of ants, and d is the number of variables.

Fitness function of each ant is saved in the following matrix M_{OA} :

$$M_{OA} = \begin{bmatrix} f([A_{1,1}, A_{1,2}, \dots, A_{1,d}]) \\ f([A_{2,1}, A_{2,2}, \dots, A_{2,d}]) \\ \vdots \\ f([A_{n,1}, A_{n,2}, \dots, A_{n,d}]) \end{bmatrix} \quad (10)$$

where f is objective function (see eq. (3) and (6)).

$$M_{Antlion} = \begin{bmatrix} AL_{1,1} & AL_{1,2} & \dots & AL_{1,n} \\ AL_{2,1} & AL_{2,2} & \dots & AL_{2,d} \\ \vdots & \vdots & \ddots & \vdots \\ AL_{n,1} & AL_{n,2} & \dots & AL_{n,d} \end{bmatrix} \quad (11)$$

where $M_{Antlion}$ is the matrix for each antlion position, $AL_{i,j}$ present the value of j -th variable of i -th antlion, n is the number of antlions, and d is the number of variables.

Analogously, fitness function of each antlion is saved in the following matrix M_{OAL} :

$$M_{OAL} = \begin{bmatrix} f([AL_{1,1}, AL_{1,2}, \dots, AL_{1,d}]) \\ f([AL_{2,1}, AL_{2,2}, \dots, AL_{2,d}]) \\ \vdots \\ f([AL_{n,1}, AL_{n,2}, \dots, AL_{n,d}]) \end{bmatrix} \quad (12)$$

In order to keep random walks of ants inside the search space, they are normalized using the following equation:

$$X_i^t = \frac{(X_i^t - a_i) \times (d_i - c_i^t)}{(d_i^t - a_i)} + c_i \quad (13)$$

where a_i is the minimum of random walk of i -th variable, b_i is the maximum of random walk in i -th variable, c_i^t is the minimum of i -th variable at t -th iteration, and d_i^t is the maximum of i -th variable at t -th iteration.

Mathematical modelling of ants trapping in antlion's pits is given by the following equations:

$$c_i^t = Antlion_j^t + c^t \quad (14)$$

$$d_i^t = Antlion_j^t + d^t \quad (15)$$

where c^t is the minimum of all variables at t -th iteration, d^t is the maximum of all variables at t -th iteration, and $Antlion_j^t$ is the position of the selected j -th antlion at t -th iteration.

Antlion's hunting capability is modelled by fitness proportional roulette wheel selection. The mathematical model that describes the way how the trapped ant slides down towards antlion is given as follows:

$$c^t = \frac{c^t}{I} \quad (16)$$

$$d^t = \frac{d^t}{I} \quad (17)$$

where I is a ratio calculated as:

$$I = 10^w \cdot \frac{t}{T} \quad (18)$$

where t is the current iteration, T is the maximum number of iterations, w is the constant that depends on current iteration as follows:

$$w = \begin{cases} 2 & \text{if } t > 0.1T \\ 3 & \text{if } t > 0.5T \\ 4 & \text{if } t > 0.75T \\ 5 & \text{if } t > 0.9T \\ 6 & \text{if } t > 0.95T \end{cases} \quad (19)$$

Finally, elitism is applied in the following way: the best antlion in each iteration is considered to be elite. It means that every ant randomly walks around selected antlion and has position according to:

$$Ant_i^t = \frac{R_A^t + R_E^t}{2} \quad (20)$$

where R_A^t is the random walk around the antlion selected by the roulette wheel at t -th iteration, and R_E^t is the random walk around the elite antlion at t -th iteration.

5. EXPERIMENTAL RESULTS

In order to evaluate the performance and illustrate the effectiveness of the ALO approach, the algorithm procedure is coded in Matlab software and implemented on a personal computer with a 3.10 GHz processor. In this experiment, job 1 (see Fig. 3) is considered and the transportation time between the machines is given in Table 1. The parameters of algorithm are set as follows: the size of the population is 40 and the number of iterations is 30. The optimization objective is to get an optimal operation sequence that results in minimum production time (eq. (3)) and cost (eq. (6)). Fig. 4a illustrates the convergence curves for the GA, hybrid GA-SA, PSO, and ALO algorithm and Fig. 4b shows error bar plot of production time after 10 runs. The obtained optimal sequence according to minimal production time is (1,2)-(5,3)-(8,7)-(9,8), $TPT=117$, and according to minimal production cost is (1,2)-(5,3)-(8,7)-(9,8), $TPC = 545$.

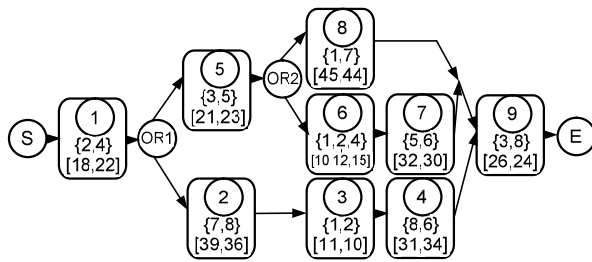


Fig. 3. Alternative process plans network [3]

machine	1	2	3	4	5	6	7	8
1	0	3	7	10	3	5	8	12
2	3	0	4	7	5	3	5	8
3	7	4	0	3	8	5	3	5
4	10	7	3	0	10	8	5	3
5	3	5	8	10	0	3	7	10
6	5	3	5	8	3	0	4	7
7	8	5	3	5	7	4	0	3
8	12	8	5	3	10	7	3	0

Table 1. Transportation time between machines [3]

machine	M ₁	M ₂	M ₃	M ₄	M ₅	M ₆	M ₇	M ₈
cost	30	10	30	40	100	60	10	15
MCCI	160							

Table 2. Machine cost and machine change cost

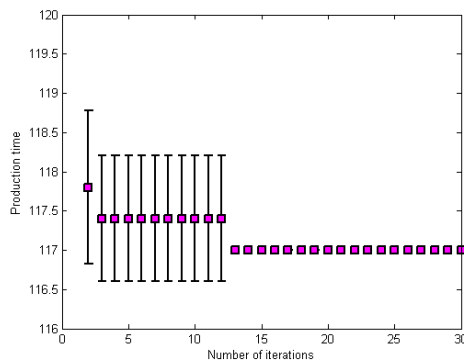
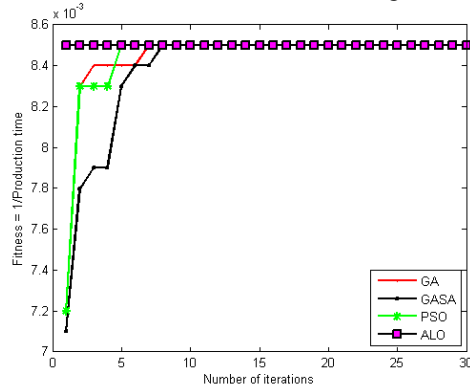


Fig. 4. (a) Comparison of the GA, hybrid GA-SA, PSO and ALO algorithm; (b) Error bar plot of production time

6. CONCLUSION

In this paper, new approach based on Ant Lion Optimization (ALO) algorithm is proposed to optimize combinatorial NP-hard flexible process planning problem. The network representation method is adopted to describe process flexibility, sequencing flexibility, and machine flexibility. The main steps of ALO algorithms are implemented on process planning

problem. The performance of the presented ALO algorithm are verified and evaluated in comparison with the results obtained with GA, SA, and PSO standalone algorithms as well as hybrid GA-SA algorithm. Experimental results indicate that the proposed algorithm performs better in comparison with other bio-inspired optimization algorithms.

7. ACKNOWLEDGMENT

This paper is part of the project: *An innovative, ecologically based approach to the implementation of intelligent manufacturing systems for the production of sheet metal parts*, financed by the Ministry of Education, Science and Technological Development of the Serbian Government, Grant TR-35004 (2011-2015).

8. REFERENCES

- [1] Li, X.Y., Shao, X.Y., Gao, L.: *Optimization of flexible process planning by genetic programming*, International Journal of Advanced Manufacturing Technology 38(1-2), pp. 143–153, 2008.
- [2] Shao, X., Li, X., Gao, L., Zhang, C.: *Integration of process planning and scheduling—a modified genetic algorithm-based approach*, Computers and Operations Research 36(6), pp. 2082–2096, 2009.
- [3] Lv, S., Qiao, L.: *A cross-entropy-based approach for the optimization of flexible process planning*, International Journal of Advanced Manufacturing Technology 68(9-12), pp. 2099–2110, 2013.
- [4] Petrovi, M., Miljkovi, Z., Babi, B.: *Optimization of Operation Sequencing in CAPP Using Hybrid Genetic Algorithm and Simulated Annealing Approach*, In: Proceedings of the 11th International Scientific Conference MMA 2012 – Advanced Production Technologies, Novi Sad, Serbia, pp. 285–288, 2012.
- [5] Wolpert, D.H., Macready, W.G.: *No free lunch theorems for optimization*, Evolutionary Computation, IEEE Transactions, 1(1), pp. 67-82, 1997.
- [6] Mirjalili, S.: *The ant lion optimizer*, Advances in Engineering Software, 83, pp. 80-98, 2015.
- [7] <http://www.asknature.org/media/image/3305>
- [8] <http://oldblockwriter.blogspot.com/2012/02/ant-lions-and-angle-of-rest.html>

Authors: M.Sc. Milica Petrovi, M.Sc. Jelena Petronijevic, Dr. Marko Miti, Dr. Najdan Vukovi, Aleksandar Plemi, prof. dr. Zoran Miljkovi, prof. dr. Bojan Babi, University of Belgrade, Faculty of Mechanical Engineering, Production Engineering Department, Kraljice Marije 16, 11120 Belgrade 35, Serbia, Phone: +381 11 3302-264, Fax: +381 11 3302-274.

E-mail: mmpetrovic@mas.bg.ac.rs;
jpetronijevic@mas.bg.ac.rs;
mmitic@mas.bg.ac.rs;
nvukovic@mas.bg.ac.rs;
aleksandarplemic@gmail.com;
zmiljkovic@mas.bg.ac.rs;
bbabic@mas.bg.ac.rs;



Šormaz, D., Wakhare, M.

AN EXTENDABLE CAPP KNOWLEDGE MODEL AND RULE-BASED METHOD OF PROCESS SELECTION FOR DIFFERENT MANUFACTURING FEATURES

Abstract: *In this paper we demonstrate methodology to extend the manufacturing knowledge by introducing new features into a CAPP model known as IMPlanner. An IMPlanner model was initially capable to map Hole, Pockets, Rectangular Slot and Feature sets/Feature instances from feature based design (CAD) model and used rule based reasoning in Jess to generate manufacturing operations for those feature types. Two kinds of rules are used for process selection: specific rules, where knowledge is coded into rules and facts, and general rules in which knowledge is imported from external files, and rules govern only reasoning procedure in flexible way. Both kinds of rules are explained and illustrated on examples. This paper then applies the same methodology but for extended types of features: Ball End Slot, Bull End Slot, and Chamfer. The methodology includes mapping of these design features into manufacturing features, developments of feature processing rules in Jess and finally generation of manufacturing processes for different dimensions of slots features along with respective machines and tools. The current methodology has been integrated with the Siemens NX CAD system and it has been developed into IMPlanner. The manufacturing parts having these new features have been verified in the IMPlanner prototype and satisfactory results have been achieved.*

Key words: *CAPP, process planning, manufacturing features, process selection, rule based systems.*

1. INTRODUCTION

Computer Aided Process Planning (CAPP) is critical gap between Computer Aided Design (CAD) and Computer Aided Manufacturing (CAM). From CAD model CAPP basically extracts the necessary information such as geometry of the workpiece, manufacturing features in the part, geometrical and dimensional tolerances in order to find appropriate processes, machines and tools required to manufacture the given part. Thus CAPP is the tool which generates the set of sequence of the manufacturing instructions needed to manufacture the part with a good quality. This paper describes the work done on automated process selection for different manufacturing features in an existing CAPP prototype known as IMPlanner (Intelligent Manufacturing Planner). Section 2 describes the previous work done on process planning with focus on process selection research. Section 3 describes the methodology which includes IMPlanner framework, knowledge model, and both specific and general rules Section 4 explains procedure for extending reasoning for new features and section 5 describes a case study results. Section 6 concludes the paper.

2. PREVIOUS WORK

Research in Computer aided process planning (CAPP) has been reported in numerous papers in last decades. The review of knowledge-based systems that includes more than 50 prototypes is given in [1] while more recent reports present new approaches like distributed process planning [2], CAPP as integration tool [3], or CAPP in the context of virtual

manufacturing [4].

Process selection is that part of the process-planning task in which a set of alternative processes is selected for a given feature [1]. The process selection module of a CAPP system verifies the process if it can satisfy tolerance, dimensional and surface requirements for considered feature either completely or partially. This module should select multiple processes for generating a feature when no one process can completely manufacture the required feature. It usually estimates the time and machining cost involved for the selected process.

There are three levels of process knowledge: universal level, a shop level and a machine level [6]. The universal level disregards the knowledge specific to a process or machine shop. This kind of information is available in handbooks and is used when specific details of a process are not available. In the shop level the specific machine or cutters are considered to predict the required accuracy. The machine level takes into consideration only capability applicable to a certain machine. This knowledge is important for selecting the specific machine to perform a specific process. This paper takes into consideration only the universal level for the system, however, the approach is flexible enough to take any detailed information in a specific format.

Process selection has been part of many research efforts as a required component for any CAPP system. Specific research results that address process selection are described below. Paper [7] presents the selection of hole making operations using hierarchical abstraction and backward reasoning. While the paper described an iterative algorithm for selection of multiple processes for holes it did not address the position of the algorithm within integrated CAPP system. The paper describes

automated process planning system that focuses mainly and only on hole manufacturing. Process selection for hole making and milling and building of appropriate knowledge bases are topic of the papers [8] [9] [10]. Authors implemented isolated rule based system to verify and test knowledge base for both hole making and milling. Knowledge base from [9] is so far most comprehensive collection of process capabilities of hole making operations and it has served as primary knowledge source in our work. Work described in [5] presents an integrated approach for inclusion of process selection into overall process planning and optimization system.

Most of reported research papers encode process knowledge into implementation language, making knowledge base extensions and/or modification of reasoning rules in such systems very difficult if not impossible

3. METHODOLOGY

This section describes development of a rule based the methodology in process selection for the manufacturing of part features. The section starts with an explanation of the IMPlanner [13], a CAPP system which is a platform for research in manufacturing planning, intelligent manufacturing integration, and knowledge management in process planning. Then we explain CAPP Knowledge model and two modes of rule based process selection: specific rules, and general rules

3.1 IMPlanner System

IMPlanner system [13] is a CAPP knowledge-based framework built for the purpose of providing distributed and alternate process plans to process manufacturing engineers to make their tasks more flexible and efficient. The generated process plans consists of alternate processes, machines and tools needed to manufacture the specific part. IMPlanner framework consists of manufacturing planning data model, planning modules, and interfaces to external applications. Data model consists of object oriented representation of features, process and related entities [14]. Important planning modules are feature mapping module, process selection module, process network module, setup planning module, simulation module, and process visualization module. All modules in the IMPlanner system are developed using object-oriented modeling. Interfaces to external applications include JNI and Java based interface to CAD and CAM applications; interface to Jess, a rule based engine; and XML interface for saving and retrieving process plans in XML format. The architecture of an IMPlanner system is shown in figure 1.

Processing of a part with IMPlanner starts with importing a CAD model and mapping its design features into manufacturing features. After that, rule based process selection module runs in Jess to perform selection of alternate processes for all features. In the next stage, process plan network (PPN) generation, alternate process candidates for features are clustered

for tools and machines into the PPN, which is optimized in order to select the best process plan, which completes the core IMPlanner functionality. IMPlanner supports several modules aimed in integration of process plans into other manufacturing planning functions, such as cell formation, scheduling, FMS simulation, and process visualization. It has been currently extended to include the module for setup planning. IMPlanner currently interfaces with Siemens NX for both geometry and operation interfaces using both JNI and NX's Java interface.

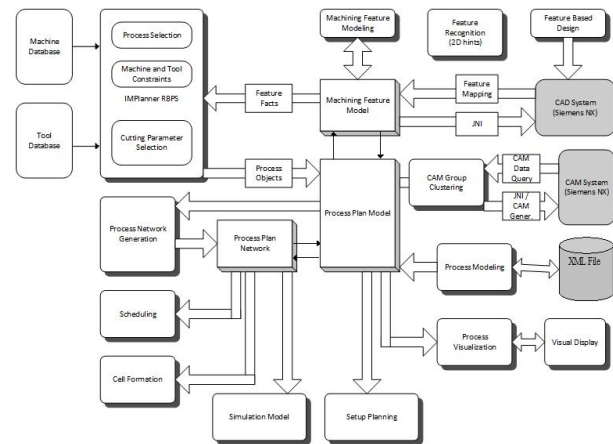


Fig. 1. An Architecture of IMPlanner v2.0

Initially, IMPlanner system was capable to map prismatic features (hole, slots, and pockets). This papers shows the extension of CAPP knowledge model and rule based process selection by adding more different features as it will explained in section 4.

3.2 CAPP Knowledge Model

CAPP knowledge model is basically a representation of process planning data needed during manufacturing activities such as sequencing, scheduling etc. The benefit of the CAPP knowledge model is such that it helps reduce the manufacturing algorithm development time. The model can store necessary data that will be required in manufacturing planning functions. The components of the CAPP knowledge model are manufacturing process model, manufacturing planning object model, feature object model, and process object model. In this section only feature object model and process object models are explained in details since the focus of the paper are different features and the selection processes to manufacture them.

3.2.1 Machining Feature Object Model

Feature object model represents the hierarchy of the machining features and relations between them (see Figure 2). The main class of the hierarchy here is *MfgFeature*. The class *MfgFeature* represents all the common properties associated with all the features. Common properties of all the features include feature name, tolerance relations between them, alternative processes, and feature precedence relations.

The major class *MfgFeature* is further extended to different subtypes (machining features) such as *Hole*, *Slot* and *Pocket* for prismatic parts that are considered. At this level different data properties are associated with each feature such as feature type, dimensions, and tolerances. The feature object model also supports feature sets as common design tool in CAD systems. Figure 2 represents the extended feature model that includes chamfer and several subtypes of slots and their inclusion will be explained in Section 4.

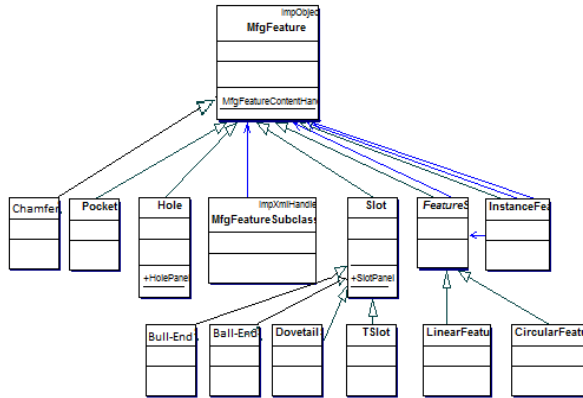


Fig. 2. Machining feature object model

3.2.2 Machining Process Object Model

Machining process object model is implemented in object-oriented environment (Figure 3). In order to map the knowledge representation about machining processes, they are categorized based on their properties. In Figure 3 *MfgProcess* is a major class which carries all the common properties associated with individual processes such as stock, workpiece, and feature references, cutting parameters, tool type and tool approach directions, and tool and machine references.

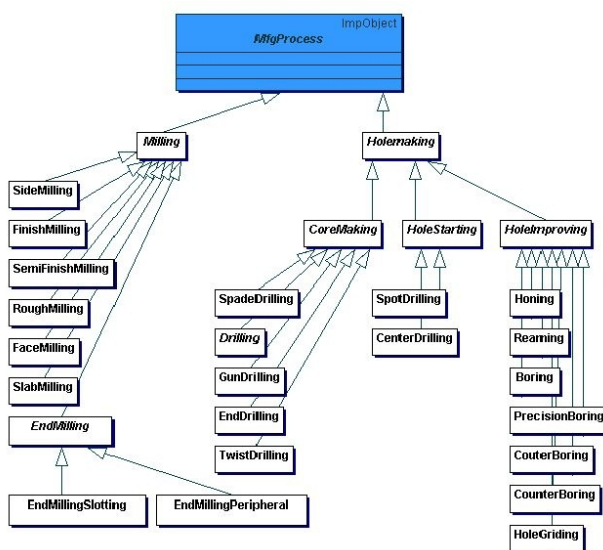


Fig. 3. Machining process object model

The class *MfgProcess* is extended into two classes: *HoleMaking* which represents all hole making processes and *Milling* as a superclass of all specific

milling processes. *HoleMaking* class is further divided into *CoreMaking*, *HoleStarting* and *HoleImproving* classes. The classes under *Milling*, *CoreMaking*, *HoleStarting* and *HoleImproving* are the actual machining processes (for example, *Boring* under the class *HoleImproving* and *SideMilling* under the *Milling* class). Therefore, *SideMilling* process represents the specific process information for side milling process and also inherits all properties of *MfgProcess* and *Milling*.

MfgProcess class has GUI (Graphical User Interface) components to show information about machining processes as well as graphical interface to display a process.

3.3 Rule Based Process Selection

Process selection is an integral part of the process planning function where set of alternate process plans are generated to manufacture the given feature. To generate feasible alternate process plans for the given feature, process selection module verifies process capabilities with the satisfaction of GD&T requirements as well as other parameters such as tool and machine availability.

The IMPlanner system uses Jess rule engine [11] for process selection. Jess is developed in Java and it is a good tool for adding rules. Rules are basically IF-THEN statements. IF part is the left side of the rule known as antecedent and THEN part is the right side of the rule and represent the action to be taken based on the antecedent.

There are several reasoning areas for which rules are developed in the IMPlanner system in different phases of process planning. These areas are given below [16]:

- 1) Rules for feature precedence relation between them based on spatial, quality and tolerance relation between them. Feature precedence relation represents the machining order of features.
- 2) Rules to decide the machining the processes to manufacture the feature and create related operations.
- 3) Rules for selection machines and tools from the database for selected processes.
- 4) Rules for selection of resting face of workpiece considering the fixturing and tool approach directions constraints.
- 5) Rules for sequencing the processes based on the feature precedence relations.

The rules in areas 2 and 3 belong to process selection module. Rules in area 1 are related to feature recognition and modeling while rules in areas 4 and 5 are related to setup planning and sequencing. Rules in areas 1, 4 and 5 are out of scope of this paper.

We have implemented two sets of rules: a) specific rules, in which knowledge is coded into the rules, for example tolerance requirements, b) general rules, in which the knowledge is loaded from external files and rules govern only reasoning in incremental process selection.

3.3.1 Specific Rules

Knowledge required in process selection represents understanding of relations between various manufacturing features, operations, tools and machines. Those relationship may be represented as connections between those points as shown in Figure 4. Feature has two way connection with an operation which corresponds to the knowledge of which operations are capable of making a particular feature shape, for example drilling can make holes.

Operation has a two way connection with machines and tools, which represents facts that the operation needs the tool to make a shape, and it needs a machine to provide kinematics of the process. Finally, tool and machine are also connected, which represents the fact that tool's geometry has to be compatible with machine toolhead.

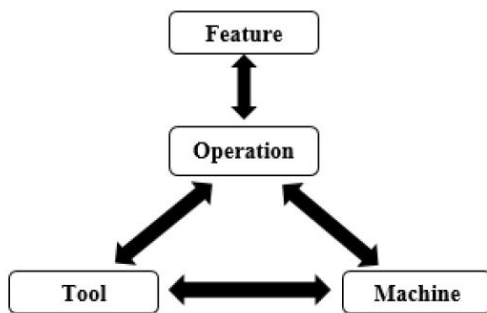


Fig. 4. Representation of relationships in knowledgebase [17]

Relationships from Figure 4 need to be represented in a rule based process selection in some form, either in rules or facts. To illustrate set of specific rule implemented as RBPP module of IMPlanner we represent and explain the rule for selection of machining processes for slots, and the rule for selection of tools for hole improving operations.

The rule in Figure 5 states that if there exists a fact of template feature in a working memory of Jess with name *?f1* which is a type of *slot* having status *input* and the quality less than or equal to *30*, then modify fact identifier *?f* status to *process* and assert new fact of template *operation*. First fact of operation is *end-milling-slotting* and second fact of operation is *side-milling* and both the processes are linked to the feature *?f1*. The feature *?f1* requires another set of processing due to high quality (cut is *double*).

```

(defrule slot2.fine
  ?f <- (feature (name ?f1) (type slot) (status input)
          (quality ?quality& (<= ?quality 30)))
  =>
  (modify ?f (status process) )
  (assert (operation (feature ?f1) (cut double)
                    (process end-milling-slotting)))
  (assert (operation (feature ?f1) (cut double)
                    (process side-milling)))
)
  
```

Fig. 5. Rule for selection of manufacturing processes for slots

Figure 6 shows the rule to select the tool for *boring/drilling/reaming* processes. It states that when a feature *?f1* of dim1 *?d1* has an operation with (type) process *?p1* which is one of *boring/drilling/reaming*, it is performed on machine *?m1* and uses tool *?n2*, when there is a tool whose name *?n1* is different from *?n2*, it is used for the process *?p1* and has diameter *?d2* equals to *?d1*, and the machine *?m1* has the *?n1* tool in the tool list, and the tool *?n1* has not been selected for the feature, then assert another operation on feature *?f1* of process *?p1* on machine *?m1* and assign tool *?n1* to it.

```

(defrule tool-rule-boring/drilling/reaming
  (feature (name ?f1) (dim1 ?d1) )
  (operation (feature ?f1)
    (process ?p1 & boring | drilling | reaming)
    (machine ?m1) (tool ?n2 & ~nil) )
  (tool (name ?n1 & ~?n2) (for-process ?p1)
    (diameter ?d2&(call Gtk epsilonEquals ?d1 ?d2)))
  (machine (name ?m1)
    (tool-list $?tools&(member$ ?n1 $?tools)))
  (not (operation (feature ?f1) (process ?p1)
    (machine ?m1) (tool ?n1) ) )
  =>
  (assert (operation (feature ?f1) (process ?p1)
    (machine ?m1) (tool ?n1) ) )
  )
  
```

Fig. 6. Rule for tool selection for the specific process

We have implemented such rules for feature, process, machine and tool combination for manufacturing of prismatic parts and tested in on collection of complex examples. In case if there are changes in the knowledge for example if the manufacturing a feature requires high quality then the it requires further recoding of the rule. We will explain method for expanding rule base later in section 4.

3.3.2 General Rules

Analysis of the rules shown in section 3.3.1 can easily reveal that the knowledge is coded into the rules, for example, in Fig 5. slot quality should be less than 30 and only two kinds of manufacturing processes are considered. Any modification or extension requires recoding of the rules. For those reasons we have implemented another set of rules, general rules.

General rules address following issues not covered by the specific rules:

- Complete tolerance and process capability consideration, with inclusion of GD&T specifications,
- Process precedence and preference relations,
- Verification of process capabilities and selection of a set of processes for a single feature when required by tolerances.

Complete tolerance consideration is enabled by adding tolerance object model that includes all GD&T specifications and representing some features as tolerance datum. Process capability is include in the form of process capability file (an external XML file which contains details of process capabilities) defined from data reported in [15].

Process precedence and preference are represented as an external XML file which is loaded into rule engine database (facts) before reasoning starts. Illustration of process precedences for hole making operations is shown in Fig 7 (from [15]). Figure 7 shows that there may be up to five hole making operation in order to manufacture a hole of desired quality. Some of those operation may be optional (eg, spot drilling depends on the hole tolerance, while core making depends on the fact that hole is precast or not).

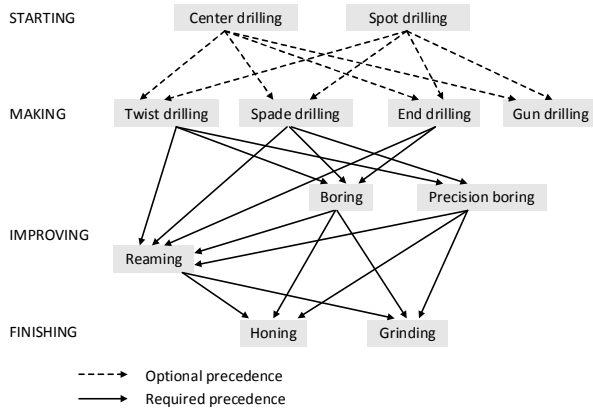


Fig. 7 Hole making precedence

Selection of a set of processes for a single feature is accomplished by implementing rules that consult precedence facts loaded into rule engine from external file. The rules follow incremental process selection which is based on complete or partial satisfaction of required tolerances. The illustration of this approach is shown in Fig 8, which shows a rule for selecting manufacturing process in case that it completely satisfies required tolerances.

```
(defrule SelectHMProcessCompleteMatch
  ?jh <- (Hole (mayBeMachinedBy ?mrbmb)
            processes ?processList) (OBJECT ?o)
            (featureName ?fName) (partModel ?part))
  ?pc <- (ProcessCapability (name ?processName)
            (OBJECT ?pcObj))
  ?nf <- (Hole (OBJECT ?nfObj))
  ?do <- (ProcessFeatureRelation (oldFeature
  ?jh)(newFeature ?nf)(processCap ?pc)(status 1))
=>
  (modify ?do (status 5))
  (bind ?processInstance (createProcessInstance ?jh
  ?processName))
  (addProcessToPart ?part ?processInstance)

  (retract ?nf)
)
```

Fig. 8 Rule for a complete match [16]

The Rule in Figure 8 for process complete match explains that “For hole *?jh*, process capability *?pc* for process *?processName*, and process/feature relation with status of 1 (COMPLETE MATCH), modify the process/feature relation status to 5 (SOLVED), create a new process instance of the *?processName* class on feature *?jh*, add this instance to the part *?part*, and

delete (retract) the in-process feature *?nf*”. It can be observed that all template slot values are represented as variables, which signifies a general rule on facts that are generated from an external file.

4. MODEL EXTENSIONS

IMPlanner and its RBPS (process selection module) have been built to be extendable. The goal was that new research can be applied and new machining features and manufacturing processes can be added within unchanged framework.

In this section we illustrate this concept to extend an existing CAPP model by adding several new features and rules in order to generate alternate processes and related machine and tool data. The steps to include model extension are as follows: CAD feature and manufacturing feature definition, process planning rules extension, and machine and tool database extension.

4.1 Feature Definitions

The design feature package is available in many commercial CAD software such as NX, Solidworks etc. Design feature package includes hole, slot, pocket, chamfer, boss, groove, pad etc. Except boss and pad features other features are manufactured by material removal process while boss and pad add material in design. The feature which are manufactured by material removal process, are called as manufacturing features. The features which add material in the design, are called as design features.

Initial IMPlanner has been extended to include chamfer feature and several subtypes of slots. The chamfer extension is described in [17] and in this section we describe slot extensions.

Ball-end slot and Bull-end slot are the sub-classes of feature slot. Ball-end and Bull-end slots are considered as manufacturing features since they are manufactured by material removal process. Figure 10 shows the gemetric definitions of slot types.

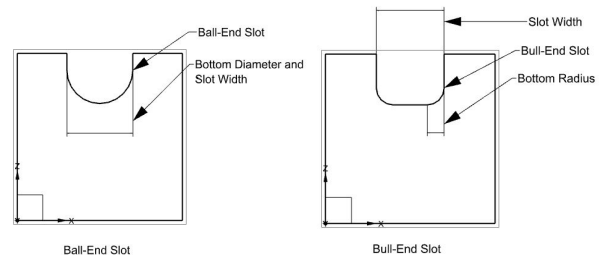


Fig. 10. Ball-End and Bull-End slot features

Ball-end slot has semicircular bottom where the bottom radius is equal to half of the slot width. Bull-end slot has U-shaped bottom where the bottom radius of this slot is less than the half of the slot width.

4.2 Process Planning Rules

When the CAD feature is mapped and the facts are generated then process planning rules run on the facts to find out processes, tools and machines required to manufacture that feature. Different subtypes of slots

have constraints on milling process and corresponding tool in terms of geometry (bottom radius) and milling subclasses are extended by necessary process classes. Rules for new features (slot subtypes) are independent of existing rules, but they operate in the same way. This is illustrated by new rule for ball end slot. The rule (Figure 11) shows that for the fact of template feature with the name *?f1* which has a type of *slot* and sub type value *blind-open ball end slot* with the status *input*, the rule modifies *?f* to status as *process* and asserts two operations with process types *ball-end-slot-end-milling* and *ball-end-slot-side-milling* respectively.

```
(defrule Process-Blind-Open-Ball-End-Slot
  ?f <- (feature (name ?f1) (type slot) (status input))
  (sub-type Blind-Open-Ball-end-Slot)
  =>
  (modify ?f (status process))
  (assert (operation (feature ?f1)
    (process ball-end-slot-end-milling)))
  (assert (operation (feature ?f1)
    (process ball-end-slot-side-milling)))
  )
```

Fig. 11. Rule for selection of Ball-End slot processes

4.3 Machine and Tool Database

Existing CAPP system is extended by adding tools and machine data for the selected processes or operations. For instance, tools are added to the knowledge base with its properties such as name, material, number of teeth, for the process, diameter, width, cost etc. In case of ball-end-slot-end-milling processes the TC501 is selected since its tool diameter (Figure 12) is equal to the slot width and in case of ball-end-slot-side-milling, TC502 (Radius Slotter) is selected since its width (w) (Figure 13) is equal to twice of bottom radius.

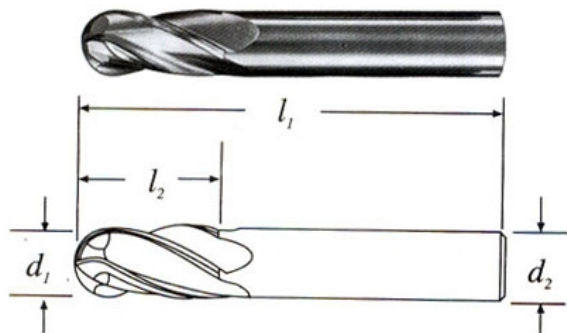


Fig. 12. Ball-End Mill tool for Ball-End-Slot-End-Milling Process (from [18])

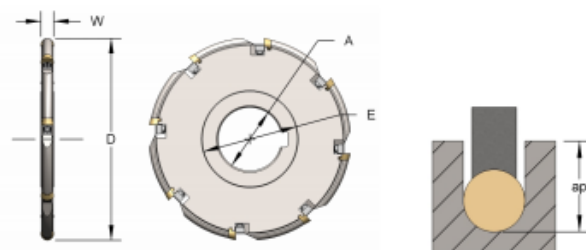


Fig. 13. Radius Slotter for Ball-End-Slot-Side-Milling Process (from [18])

Once the TC501 and TC502 tools are entered into database as facts, CAPP model looks for the machines to be selected to perform the selected processes and where the tools TC501 and TC502 are also members of tool magazine in those machines. For instance, CncVMillFast is in the database for the process ball-end-slot-end-milling-process because it has T501 in its tool magazine. The portion of the fact database that corresponds to relations explained in Figure 4 between tools TC501, TC502 and machine CncVMillFast is shown in figure 14.

We have created similar process selection rules to generate processes for Bull-end slot which is shown in figure 15.

Our CAPP system selects the tools for the selected operations. Tool TC501 is selected for the bull-end-slot-end-milling process where diameter of the tool T1 is equal to the width of the slot. Tool TC502 is selected for the bull-end-slot-side-milling process where width (w) of the tool is equal to the slot width. The next step is to select machines such that they suffice two constraints and those are: compatible to the selected process and have selected tools in tool magazine of the selected machines.

Tool Data
(assert (tool (name T501) (material carbide) (for-process ball-end-slot-end-milling) (diameter 4) (length 5) (life-cycle 200) (cost 15.000)))
Process Data
(assert (process (name ball-end-slot-end-milling) (machine CncVMillFast)))
Machine Data
(assert (machine (name CncVMillFast) (type mill) (toolhead vertical) (bed-size-x 54) (bed-size-y 20) (bed-size-z 10) (setup-time 240) (power 4) (mhandling-time 0.8) (speed-efficiency 1.0) (tool-change-time 40) (unit-cost 1.3) (tool-list T501 T601)))

Fig. 14. Knowledge extension for different slots

```
(defrule Process-Blind-Open-Bull-End-Slot
  ?f <- (feature (name ?f1) (type slot) (status input))
  (sub-type Blind-Open-Bull-end-Slot)
  =>
  (modify ?f (status process))
  (assert (operation (feature ?f1)
    (process bull-end-slot-end-milling)))
  (assert (operation (feature ?f1)
    (process bull-end-slot-side-milling)))
  )
```

Fig. 15. Rule for selection of Bull-End slot processes

5. CASE STUDY

IMPlanner first maps the design features from a CAD model into manufacturing features and then executes the process selection module. Figure 16 and 17 shows the mapped features in an Integration panel, a GUI module of the IMPlanner system.

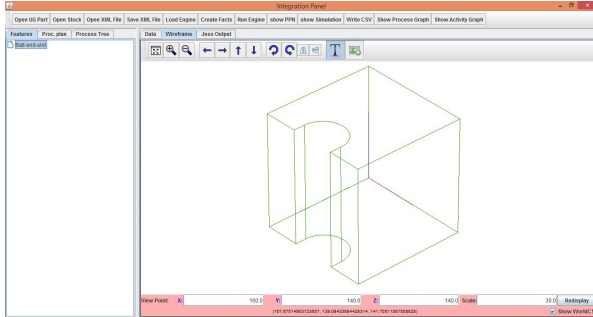


Fig. 16. Mapped Ball-End slot feature from CAD object

Figures 16 and 17 show the graphical user interface (GUI) of an Integration panel with 3D view of the part model. The name of the mapped feature can be seen in left panel while in the right window, wireframe of the CAD model is displayed which has been extracted from the Siemens NX CAD software. Once the features are mapped, process planning rules are activated to select the process plans for the mapped features. Figure 18 shows the fired rules for the mapped features.

Figure 18 shows: Fact f-0 is the information about the stock or raw material such as dimensions, quality, material and batch size. Facts f-1 to f-7 shows the information about the feature, processes required for the specific type of mapped feature, tools required to manufacture the feature and machines which are compatible to the processes and having desired tools. Facts f-8 and f-9 shows the process plan. Fact f-8

shows, to manufacture ball-end-slot 1 feature which is a type of slot feature, use ball-end-slot-milling with the tool T501 on machine CncVMillFast. Fact f9 shows the alternate process plan where it suggests to use ball-end-side-milling process with the tool T502 on machine CncVMillSlow. After the process plan is generated, all the related information is sent back to the IMPlanner system for visual aid.

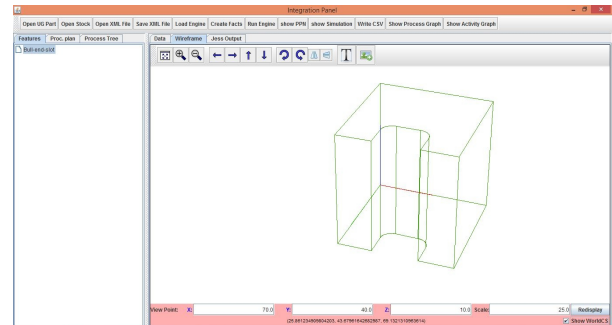


Fig. 17. Mapped Bull-End slot feature from CAD object

6. CONCLUSION

Initially, IMPlanner system was capable to map only Hole, Slot and Pocket features but we have successfully extended our CAPP knowledge model in order to map different manufacturing features and these are chamfer, ball-end and bull end slot from the CAD model designed in Siemens NX. This papers uses same application that is Integration panel to fire the process plans rules over the new mapped features to generate alternate process plans. The existing CAPP model can further be extended by adding other feasible processes to manufacture Chamfer, Ball-end and Bull-end slots features as well as different tools and machines.

```
Jess> (facts)
f-0 (MAIN::part (material CarbonSteel) (x-dim 8.0) (y-dim 8.0) (z-dim 6.0) (quality 20.0) (batch-size 50))
f-1 (MAIN::feature (name ball-end-slot1) (type slot) (sub-type Blind-Open-Ball-end-Slot) (quality 30) (slope 0) (dim1 4) (dim2 4) (dim3 10) (bottomRadius 2) (diam03 0) (status process))
f-2 (MAIN::process (name ball-end-slot-end-milling) (machine CncVMillFast))
f-3 (MAIN::process (name ball-end-slot-side-milling) (machine CncVMillSlow))
f-4 (MAIN::tool (name T501) (material carbide) (for-process ball-end-slot-end-milling) (diameter 4) (width nil) (length 5) (life-cycle 200) (cost 15.0))
f-5 (MAIN::tool (name T502) (material carbide) (for-process ball-end-slot-side-milling) (diameter 10) (width 4) (length 5) (life-cycle 200) (cost 15.0))
f-6 (MAIN::machine (name CncVMillFast) (type mill) (toolhead vertical) (bed-size-x 54) (bed-size-y 20) (bed-size-z 10) (setup-time 240) (power 4) (mhandling-time 0.8) (speed-efficiency 1.0) (tool-change-time 40) (unit-cost 1.3) (tool-list T501 T502))
f-7 (MAIN::machine (name CncVMillSlow) (type mill) (toolhead vertical) (bed-size-x 54) (bed-size-y 20) (bed-size-z 10) (setup-time 240) (power 4) (mhandling-time 0.8) (speed-efficiency 1.0) (tool-change-time 40) (unit-cost 1.3) (tool-list T501 T502))
f-8 (MAIN::operation (feature ball-end-slot1) (process ball-end-slot-end-milling) (machine CncVMillFast) (tool T501))
f-9 (MAIN::operation (feature ball-end-slot1) (process ball-end-slot-side-milling) (machine CncVMillSlow) (tool T502))
```

Fig. 18. Facts of Ball-End slot

7. REFERENCES

- [1] Kiritsis D, A Review Of Knowledge-Based Expert-Systems For Process Planning - Methods And Problems, *International Journal Of Advanced Manufacturing Technology*, 10 (4): 240-262 1995
- [2] Wang, L.H., Shen, W. M., DPP: An agent-based approach for distributed process planning, *J. Intell Manuf* 14 (5): 429-439 Oct 2003
- [3] Xu XW, He Q., Striving for a total integration of CAD, CAPP, CAM and CNC, *Robot Cim-Int Manuf* 20 (2): 101-109 Apr 2004
- [4] Zaeh, M. F., Rudolf, H., Agile process planning considering the continuous reconfiguration of factories *Proceedings of 3rd International Conference of Reconfigurable Manufacturing Systems*, Ann Arbor, MI, May 10-12, 2005
- [5] Khoshnevis B., Sormaz D., and Park J., "An integrated process planning system using feature reasoning and space search-based optimization, *IIE Transactions*, 31(7), 1999, p. 597-616
- [6] Chang T C., *Expert Process Planning for Manufacturing*, Addison-Wesley, Menlo Park, CA, 1991.
- [7] Nau, D.S. Automated process planning using hierarchical abstraction. Texas Instruments call for papers on AI for Industrial Automation, 1987.
- [8] Khoshnevis, B., Tan, W., Rule-based process selection module for milling operations, *Industrial Engineering Research - Conference Proceedings*, 1995
- [9] Khoshnevis, B., Tan, W., Sormaz, D. N., *A process selection rule base for hole-making*, Research Report, Factory Automation Systems Division, National Institute of Standards and Technology, Gaithersburg, MD, 1993.
- [10] Khoshnevis, Behrokh, Tan, Wei Automated process planning for hole-making, *Manufacturing Review*, v 8, n 2, Jun, 1995, p 106-113
- [11] Ernest Friedman-Hill, *Jess In Action*, Manning Publications, 2003.
- [12] Horstman, C.S., Cornell, G., *Core Java*, Volume I, The Sun Microsystems Press, 2000
- [13] D. N. Sormaz, J. Arumugam, and S. Rajaraman, Integrative process plan model and representation for intelligent distributed manufacturing planning, *Int. J. Prod. Res.*, vol. 42, no. 17, pp. 3397-3417, Sep. 2004.
- [14] D. N. Sormaz, B. Khoshnevis, Process Planning Knowledge Representation using an Object-oriented Data Model, *International Journal of Computer Integrated Manufacturing*, Vol. 10, No. 1-4, p. 92-104, 1997
- [15] D. N. Sormaz, P. Khurana, and A. Wadtkar, Rule-Based Process Selection of Hole Making Operations for Integrated Process Planning, *Proceedings of IDETC/CIE 2005 ASME 2005 International Design Engineering Technical Conferences*, September 24-28, 2005, Long Beach, California, USA, vol. 2005, pp. 983-988.
- [16] D. Sormaz, J. Arumugam, C. Ganduri, Integration of Rule-based Process Selection with Virtual Machining in a Distributed Manufacturing Planning System in L. Wang and W. Shen (eds.), *Process Planning and Scheduling for Distributed Manufacturing*, p. 61-90, Springer 2007.
- [17] S. Gamaralalage, Dusan Sormaz, Incremental Expansion of Manufacturing Knowledge Base, *Proceedings of the 2015 ASEE North Central Section Conference*, Cincinnati, April 17-18, 2015.
- [18] http://www.cuttingtooltech.com/catalog/PDF/2009/09_slot.pdf, accessed in August 2015.

Authors: Dušan Šormaz, Mayur Wakhare Ohio University, Industrial and Systems Engineering, Russ College of Engineering and Technology, Stocker center 284, Athens, OH, United States – 45701. Phone.: +1-740-593-1545, Fax: 740-593-0778
E-mail: sormaz@ohio.edu;
mw594113@ohio.edu

Kokotovi , B., Živanovi , S., Jakovljević Ž.

VERIFICATION OF A PROCEDURE FOR FEEDRATE SCHEDULING FOR CONSTANT FORCE IN 2D MILLING OPERATIONS

Abstract: This paper presents a brief overview of the developed procedure for off-line optimization of CNC program. The procedure refers to milling operations in plane $z=const$, using flat end mills. The goal of optimization is to create modified version of part program, using feedrate scheduling, in order to keep desired milling force component on predefined value along tool path. Detailed experimental verification of this procedure is carried out using a representative example and machining test.

Key words: CNC milling, milling forces, optimization, feedrate scheduling

1. INTRODUCTION

Nowadays many research activities in the field of CNC machining are clustered in a concept of Virtual machining (VM) [1]. Besides function of realistic predictions of outputs of machining process through simulation, extremely important function of VM is its ability to perform off-line optimization of designed process. Optimization criteria are different: keeping constant cutting force, maximization of material removal rate, limitation of machining errors, chatter-free machining, etc. The function of CNC program re-planning in order to keep cutting force level constant along tool path is partly implemented in modern CAM software [2,3]. Very impressive results were achieved through re-planning of tool path shape (trochoidal paths and morphing spiral paths in pocket machining) in the software. Such paths assume constant tool/workpiece immersion on the whole path. Another way to keep cutting force constant assumes re-planning of feedrates along programmed path. In CAM systems it is achieved through keeping constant material removal rate. A number of published research results use more precise and more demanding approaches which include milling force prediction based on generated simulation model.

2. PROCEDURE FOR FEEDRATE OPTIMIZATION

Simplified description of the procedure for off-line feedrate optimization is shown in Fig. 1. Such optimization procedure for milling operations in plane ($z=const$), with flat end mills, with helical flutes and arbitrary shape of stock material was developed [4].

Term *adaptation* refers to obtaining the feedrate value which can guarantee keeping the desired level of arbitrary milling force component in specific point of programmed tool path, with predefined workpiece material, cutter geometry, and configuration of tool engagement (engagement map) in the point. Procedure for feedrate adaptation has to be conducted in each point of uniformly discretized tool path. Next step is feedrate *optimization* along tool path. In this step, adapted values are subject to modifications, according to several additional criteria and re-discretization of

tool path with constant feedrate on each path segment described by one block of optimized part program.

For arbitrary set of cutting parameters and engagement map, instant and representative values of milling force components can be identified. Instant values of one force component assume its periodic variation during one spindle revolution. Representative value of this component can be obtained by extraction of min/max/mean values from instant values. Important building block of optimization procedure is a module for reliable milling force prediction, as a part of step K2 (Fig. 1).

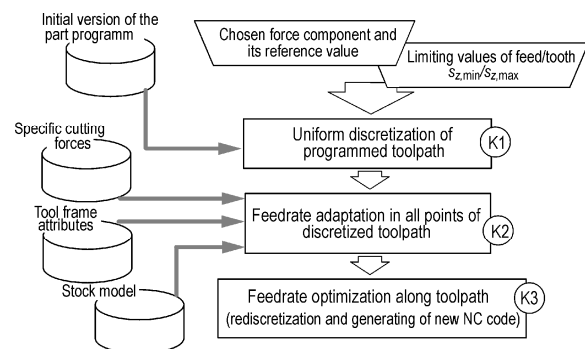


Fig. 1. Basic steps in procedure for feedrate optimization

Many authors [5,6] use procedure for feedrate adaptation which has two steps. In the first step, adaptation process for a given point on the tool path assumes calculation of feedrate based on reference force level F_{ref} , and predicted force value $F_{p(0)}$ for initially programmed feedrate $v_{s,0}$:

$$v_s^{Ad} = v_s^{Ad(1)} = v_{s,0} \frac{F_{ref}}{F_{p(0)}} \quad (1)$$

This feedrate and spindle speed n_{GV} result in a feed/tooth value as input for new simulation of instant force values (1 turn of cutter) for predicting appropriate representative force value $F_{p(1)}$ of a chosen force component. Then, it is possible to obtain adapted value of feedrate in the second step:

$$v_s^{Ad} = v_s^{Ad(2)} = v_s^{Ad(1)} + \frac{(v_s^{Ad(1)} - v_{s,0})(F_{ref} - F_{(0)})}{F_{p(1)} - F_{(0)}} \quad (2)$$

3. AN EXAMPLE OF OFF-LINE FEEDRATE OPTIMIZATION IN END MILLING OF PLANAR CONTOUR

For illustration of functionality of the developed program modules for off-line feedrate optimization, an example of down milling of planar contour is presented in this section. Pre-machined stock and machined part are presented in Fig. 2.

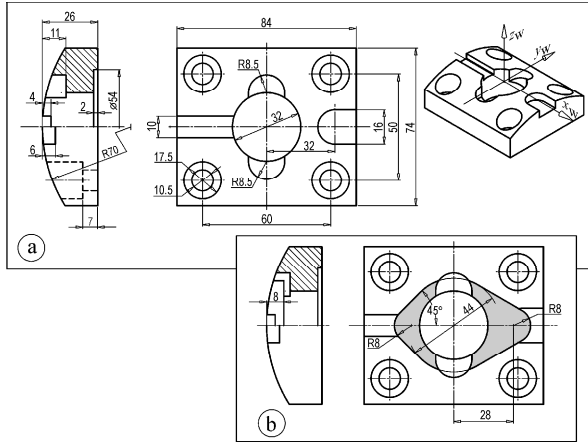


Fig. 2. Dimensions of stock (a) and machined part (b) in representative example

Workpiece coordinate system, contour shape and initial version (with constant feedrate) of the part program are shown in Fig. 3.

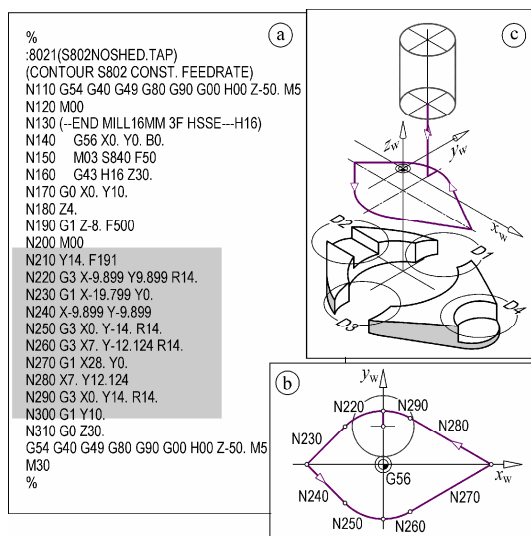


Fig. 3. Example of the feedrate optimization procedure checking: part program (a), tool path (b), and material volume which will be removed (c)

Workpiece material was AlZn4Mg2 (ENAW 7019) with $R_m=390\text{MPa}$ and hardness of 125HB. Tool was DIN327 end mill, HSSE (8%Co) with 3 teeth, $D=16\text{mm}$, helix angle 30° and rake angle 11° . Clamping of tool: ISO40/OZ52 \varnothing 16 collet. Measured runout parameters of the cutter: $\rho_b=0.01\text{mm}$, $\phi_b=81^\circ$. Experimentally identified specific cutting forces [4] for given workpiece material and cutting geometry were:

$$[K_{tc} \ K_{rc}] = [1113.0 \ 384.2] \text{ N/mm}^2,$$

$$[K_{te} \ K_{re}] = [11.1 \ 11.6] \text{ N/mm}.$$

Keeping constant value of the resulting milling force in

xy plane - F_{xy} on the level of 800N, along the tool path, was chosen as optimization criterion.

Form of the stock and shape of the tool path were chosen to ensure rapid changes in cutting depth as well as cutting width along the tool path. Cutting parameters, used in initial version of part program (before feedrate optimization) are shown in Table 1.

[mm]	ns [min^{-1}]	$v_f(0)^{1)}$ [mm/min]	b [mm]	$s_{r,0}^{1)}$ [mm/t]
min. 0 max. 8	796	191	min. 0 max.16	0.08

¹⁾ Programmed in initial version of part programm

Table 1. Parameters of machining test

3.1. Feedrate adaptation

According to flow chart in Fig.1, it was necessary to prepare stock model. This preparation assumes building its Z-map model. Such map, made from STL-file (exported from CAD program) of the stock is shown in Fig.4. Values of other parameters of the procedure for feedrate adaptation are shown in Table 2.

Toolpath discretization increment ΔL_p [mm]	0.5
Increment of the Z-map base Δm [mm]	0.5
Disc thickness of discretized tool h_d [mm]	0.5
Increment for one turn simulation $\Delta \theta$ [$^\circ$]	1.0
Reference force value, F_{ref} [N]	800
Feed limits $s_{z,min}$, $s_{z,max}$ [mm/t]	[0.03, 0.25]

Table 2. Parameters of the procedure for adaptation of the feedrate in points of discretized tool path

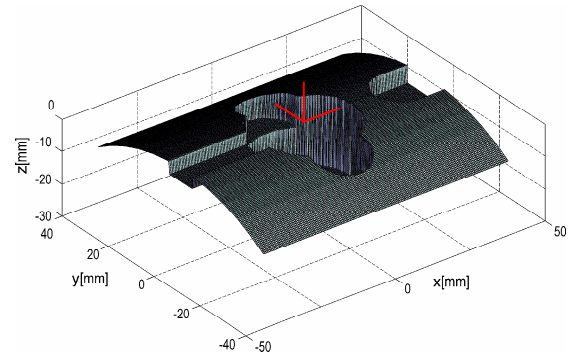


Fig. 4. Z-map of the stock for given example

Totally 250 points were obtained on tool path through its uniform discretization with given increment ΔL_p . Each of these points was a subject of feedrate adaptation (1,2). This procedure assumes calculation of appropriate feedrate which will keep milling force F_{xy} on F_{ref} level, respecting lower $s_{z,min}$ and upper level $s_{z,max}$ of feed per tooth (Tab.2) and specific cutting conditions in this point.

Some details of this procedure for one point are shown in Fig.5: obtaining tool engagement map (using updated workpiece Z-map, tool attributes, instant direction of feedrate vector and position of point), obtaining enter/exit angles for each tool disc in engagement map, and prediction of instant values of milling forces through simulation in single turn of the tool. This simulation has to be carried out two times: for initial feedrate and for feedrate per tooth $s_z^{(Ad1)}$ obtained from (1). It is enough to find required value

for $s_z^{(Ad2)}$ (2). Lower diagram in Fig.5 shows predicted instant values of milling force components for $s_{z,0}$, $s_z^{(Ad1)}$ and finally for $s_z^{(Ad2)}$. Fig 6. shows adapted values of feedrate in all points of discretized tool path, as well as predicted values of representative force, before and after adaptation.

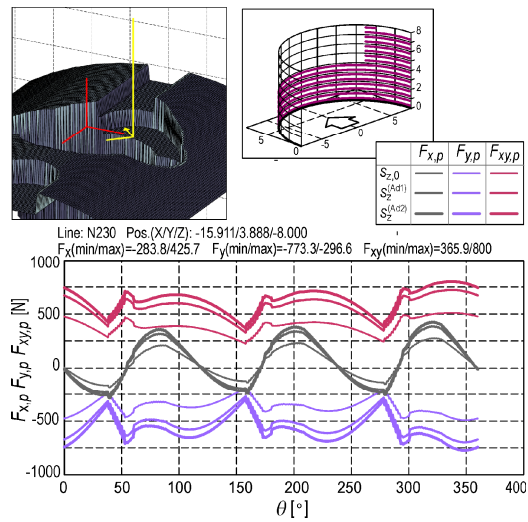


Fig.5. An example of feedrate adaptation in specific point of the tool path

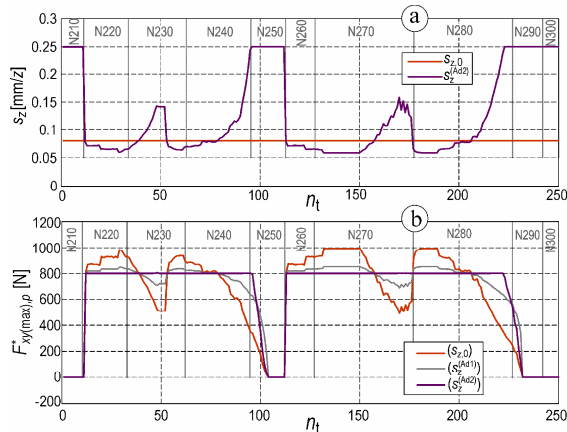


Fig.6. Programmed feedrate and feedrate after adaptation (a) and predicted representative force values (b) for programmed (constant) feedrate and with adapted feedrates

3.2. Feedrate optimization along tool path

Optimization of feedrate along tool path starts from calculated values obtained through adaptation process in points of uniformly discretized path. Keeping such discretization can lead to forming enormously long code of part program and undesirably frequent variation of feedrate on short path segments (high acceleration/deceleration and unstable operation). In this sense, optimization should have the following steps:

- S1. Filtration of feedrate values obtained in process of its adaptation
- S2. Rounding of adapted values of feedrate on discrete values of scale with previously chosen increment and aggregating subsequent path segments (uniform discretization) of the same block of initial program into longer segments with one

value of the feedrate (the first step of re-discretization)

- S3. Second step of re-discretization with modified values obtained in S2 in order to guarantee limited accel/decelerations of machine servo axis.

Through the procedure of feedrate adaptation, regarding initial description of tool path (program of Fig.3a) and according to given parameters (Tab.2) the re-discretization of tool path is carried out. According to steps S1-S3 this re-discretization reduced number of tool path segments from 250 (uniform discretization) to 55. These segments with assigned feedrates are shown in optimized version of the part program (Fig.7) in blocks from N200 to N740.

```

%
:8022(S802RESSHED.TAP)
(SCHEDULING FXY 800N)
(RESHED VSINCR=30MMMIN)
G54 G40 G49 G90 G0 H00 Z0. M5
M00
N130 (- 16MM3F HSSE—H16)
N140 G56 X0. Y0. B0.
N150 M03 S796 F191
N160 G43 H16 Z30.
N170 G0 X0. Y10.
N180 G1 Z-8. F200
N190 M00
N200 G1 X0. Y14.000 F570
N210 G3 X-0.500 Y13.991 R14. F360
N220 G3 X-0.999 Y13.9643 R14. F180
N230 G3 X-7.987 Y11.4979 R14. F150
N240 G3 X-9.543 Y10.2436 R14. F120
N250 G3 X-9.899 Y9.8990 R14. F150
N260 G1 X-11.313 Y8.485 F150
N270 G1 X-12.374 Y7.424 F180
N280 G1 X-13.435 Y6.364 F210
N290 G1 X-13.788 Y6.010 F240
N300 G1 X-14.495 Y5.303 F270
N310 G1 X-15.203 Y4.596 F300
N320 G1 X-16.617 Y3.182 F330
N330 G1 X-16.970 Y2.828 F180
N340 G1 X-19.799 Y0. F150
N350 G1 X-16.970 Y-2.828 F150
N360 G1 X-13.081 Y-6.717 F180
N370 G1 X-12.020 Y-7.778 F210
N380 G1 X-10.960 Y-8.838 F240
N390 G1 X-9.899 Y-9.899 F270
N400 G3 X-9.540 Y-10.247 R14. F330
N410 G3 X-9.168 Y-10.581 R14. F390
N420 G3 X-8.784 Y-10.901 R14. F420
N430 G3 X-8.389 Y-11.208 R14. F480
N440 G3 X0. Y-14.000 R14. F570
N450 G3 X0.500 Y-13.991 R14. F180
N460 G3 X7.000 Y-12.124 R14. F150
N470 G1 X8.7321 Y-11.124 F150
N480 G1 X17.392 Y-6.124 F120
N490 G1 X19.558 Y-4.874 F150
N500 G1 X20.424 Y-4.374 F180
N510 G1 X21.723 Y-3.624 F210
N520 G1 X23.022 Y-2.874 F240
N530 G1 X24.321 Y-2.124 F270
N540 G1 X24.754 Y-1.874 F300
N550 G1 X25.620 Y-1.374 F330
N560 G1 X27.676 Y-0.187 F300
N570 G1 X28.000 Y0. F270
N580 G1 X22.804 Y3.000 F120
N590 G1 X19.340 Y5.000 F150
N600 G1 X14.143 Y8.000 F180
N610 G1 X11.277 Y8.500 F210
N620 G1 X12.844 Y8.750 F240
N630 G1 X11.978 Y9.250 F270
N640 G1 X11.545 Y9.500 F300
N650 G1 X11.112 Y9.750 F330
N660 G1 X10.679 Y10.000 F360
N670 G1 X10.246 Y10.250 F390
N680 G1 X 9.813 Y10.500 F420
N690 G1 X 9.380 Y10.750 F450
N700 G1 X8.947 Y11.000 F510
N710 G1 X8.514 Y11.250 F540
N720 G1 X7.000 Y12.124 F570
N730 G3 X0. Y14.000 R14. F570
N740 G1 X0. Y10.000 F570
N750 G0 Z30.
G54 G40 G49 G90 G0 H00 Z0. M5
M30
%

```

Fig.7. Part program after optimization of feedrates along tool path

4. MACHINING TEST

Quality of the described procedure for off-line feedrate optimization was proven through machining test that was carried on the horizontal machining center (HMC500/40, Lola Corp.). Components of experimental setup were: four component dynamometer with strain gauges (DYN3F1M-M83, KaProM), two displacement sensors (W50, HBM), 4 amplifiers (KWS3082A, HBM), DAQ system (cDAQ9174 + 9215 Voltage module, NI) and computer with software for DAQ (LabView, NI). Workpiece was clamped on the platform of the dynamometer (Fig. 8)

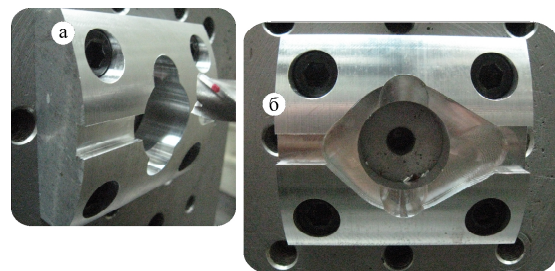


Fig.8. Stock (a), and machined contour (b), in machining test

Experimental setup allows acquisition of two signals from dynamometer (force components along x_w and y_w axes), as well as two signals of actual positions x_w and y_w of machine servo axis. These four signals are enough for reconstruction of changes of resulting milling force F_{xy} , along tool path. Fig.9 shows measured instant values of one force component ($F_{x,w}$) during machining of the contour, according to part program from Fig.7. During experiment a chatter vibrations occurred on some segments of the tool path. It is shown in details (W1 and W2) in Fig.9.

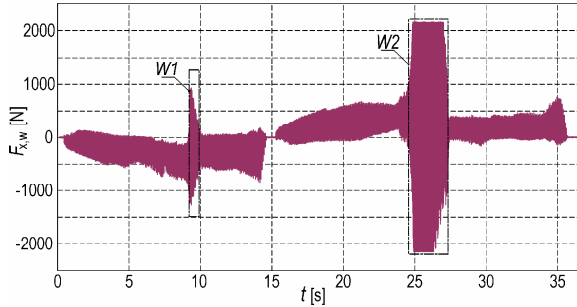


Fig. 9. Instant values of $F_{x,w}$ milling force component (signal from dynamometer) during machining of the contour

Measured positions of machine servo axis (x_w , y_w) during machining test in given example are shown in Fig.10.

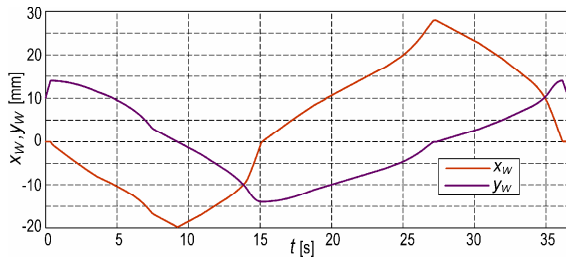


Fig. 10. Measured positions of machine servo axis (x_w , y_w) during machining of the contour

All four signals were collected simultaneously during experiment and allow generation of diagram with distribution of representative cutting force along the tool path. Such diagram is shown in Fig.11. Instant values of milling force, in sample k , were obtained as:

$$F_{xy}(k) = F_{xy,w}(k) = \sqrt{F_{x,w}^2(k) + F_{y,w}^2(k)} \quad (3)$$

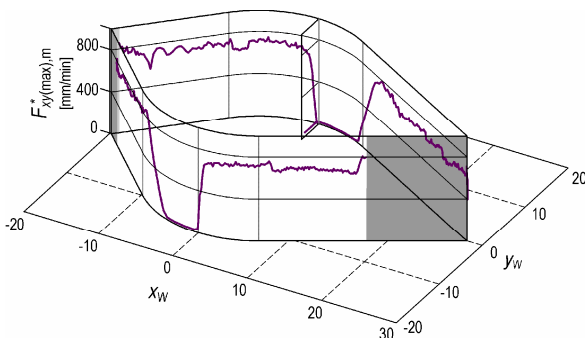


Fig. 11. Distribution of $F_{xy(max),m}$ milling force along tool path, obtained from experiment

Representative values of milling force, extracted for every spindle revolution were obtained as:

$$F_{xy(max),m}^*(q) = \max\{F_{xy,w}(k)\} \quad (4)$$

$$k = (q-1) \cdot n_s + q \cdot n_s, \quad q = 1, 2, \dots$$

Integer n_s denotes the number of samples that refer to one spindle revolution. These values are assigned to points on tool path with coordinates:

$$x_w(q) = x_w(k), \quad y_w(q) = y_w(k), \quad k = q \cdot n_s \quad (5)$$

Diagram in Fig.11 is broken into two tool path segments. These segments are shaded and they refer to chatter which is not included in developed model for milling force prediction.

5. CONCLUSION

This paper presents an example of experimental verification of developed procedure for off line optimization of NC program for a class of milling operations. This optimization is based on feedrate scheduling for keeping the constant milling force level. Good quality of the procedure was shown through machining test. In the trade-off between efficacy and performances of the proposed procedure, arguments are on the latter. Lower efficacy comes from the need of simulation of forces on whole turn of discretized cutter geometry in each point of uniformly discretized tool path. Improvements, in this sense, are the subject of our present research activities.

Acknowledgements. The authors would like to thank the Ministry of Education and Science of the Republic of Serbia for providing financial support that made this work possible.

6. REFERENCES

- [1] Altintas Y., Brecher C., Weck M., Witt S.: *Virtual Machine Tool*, Keynote Paper of STC M, Annals of CIRP, Vol. 54, No2, p.p.651-674, 2005.
- [2] Solid CAM i-machining, from www.solidcam.com, accessed on Sept 2015.
- [3] Open Mind Technologies AG, from www.openmind-tech.com, accessed on Sept 2015.
- [4] Kokotovi B.: *Obrada glodanjem u virtuelnom obradnom sistemu*, doktorska disertacija, Univerzitet u Beogradu, Mašinski fakultet, 2014.
- [5] Boz Y., Demir O., Lazoglu I.: *Model Based Feedrate Scheduling for Free-Form Surface Machining*, Int. J. of Automation Technology, Vol.4, No.3, p.p. 273-283, 2010.
- [6] Kokotovi B., Glavonji M.: *Predicting of milling forces in a virtual manufacturing system*, Tehni ki vjesnik, Vol. 20, No.6, p.p. 1027-1035, 2013.

Authors: Assistant Professor Branko Kokotovi, Assistant Professor Saša Živanovi, Assistant Professor Živana Jakovljevi, University of Belgrade, Faculty of Mechanical Engineering, Production Engineering Department., Kraljice Marije 16, 11120 Belgrade, Serbia, Phone.: +381 11 3302-375, Fax: +381 11 3370-364.

E-mail: bkokotovic@mas.bg.ac.rs
szivanovic@mas.bg.ac.rs
zjakovljevic@mas.bg.ac.rs

Borojevi , S., Joviševi , V., Todi , V., Zeljkovi , M.

PARTS DESIGN BASED ON MANUFACTURING FEATURES

Abstract: This paper presents a methodology of designing the parts based on manufacturing features. The aim of the developed methodology is designing of solid model of part with additional information. Designing of parts is based on developed Elemental Manufacturing Features (EMF). The system parameters which represent holders of geometric, technological and other information are added to attributes of EMF. The developed methodology is implemented as a software application that is integrated into the program system SolidWorks®. Verification of the developed methodology is executed on the example of designing of solid model of the hydraulic cylinder.

Key words: designing of parts, manufacturing features, attributes

1. INTRODUCTION

Computer aided design of product is realizing in the field of application of conventional modeling technology and graphic interpretations of the products, parts or assemblies. The result of conventional modeling technology using a computer is a geometric (solid) model of the product. The geometric model of the product has a number of disadvantages which severely restrict its use in downstream applications. It is used in the process of detailed design of the product and as input to the application for CAE (CAE - eng. Computer Aided Engineering). Information needed in other phases of product development (defining requirements, conceptual design, production scheduling and preparation, realization of production, exploitation, recycling and dismantling) are not contained in the geometric model of the product.

The aforementioned problems of conventional geometric modeling indicate the direction in which the solution is; i.e. some macroscopic entities should be available in explicit form in the model. The macroscopic or high-level modeling entities can provide the hook needed by applications to store and retrieve information. These entities of a higher level are usually identified with entities that are called manufacturing features. These types of features are used in order to provide improvements over the aforementioned disadvantages of the conventional techniques of geometric modeling. Product/part design at a higher semantic level, which uses manufacturing features as entities of macro level, are called a designing based on manufacturing features [1].

2. FEATURES

Most of definitions [2] characterize the features as "entities of a higher semantic level, as opposed to pure geometric elements, which are mainly used in solid modeling."

Approach based on features has a direct relevance and applicability in various production activities that follow the design, such as process planning, programming of computer numerical controlled

machines, product control, etc. [3]. Therefore, it is useful to distinguish between different types of features through their classification. Features, depending on their application, can be roughly divided into: design, structural or shape features, manufacturing features, robotic features, assembly features, production features, quality control features, fixture features and material features [4]. According to Gindy [5], the classification of features was carried out in three basic categories, such as protrusions, depressions and surfaces. On the other hand, Pratt and Wilson [6] proposed a classification of features of explicit and implicit features.

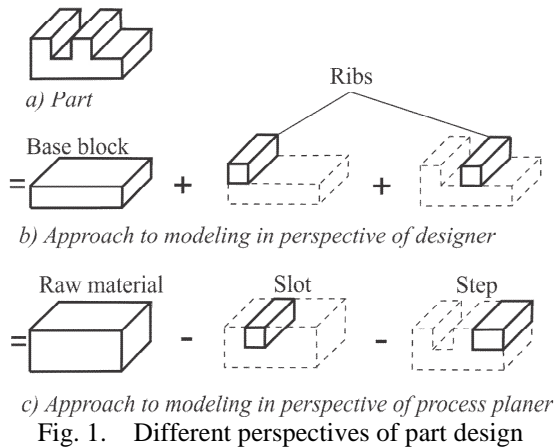
In this work, main attention is focused on the procedure of designing of parts based on manufacturing features.

3. MANUFACTURING FEATURES

Features used for the pure design of parts, often has differ significantly from manufacturing features which has to be used for process planning. The main difference between design and manufacturing features can be most easily seen if we observe the perspective of the design process of the product which is shown in Figure 1 [7]. Approach of part design from the perspective of the designer (Figure 1b) is based on the observation of part from the standpoint of its pure design (modeling), while the approach of part design from the perspective of a process planner (Figure 1c) is based on the observation of part from the standpoint of its manufacturing [7]. Accordingly, the manufacturing features are most frequently associated with the information relating to the volume of material that needs to be removed from the raw material of part using machining processes.

Through a development of information technology it was created the different techniques for procedure of part/product model design based on manufacturing features. These techniques are divided on the basis of whether the manufacturing features was extracted from geometry (FfG - eng. Feature from Geometry), or geometry is created from the manufacturing feature (GfF - eng. Geometry from Features). FfG techniques

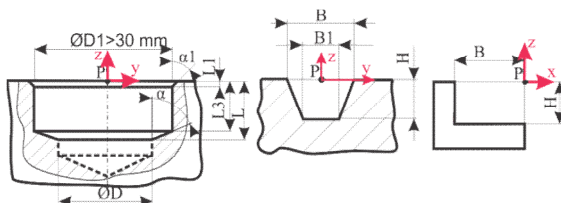
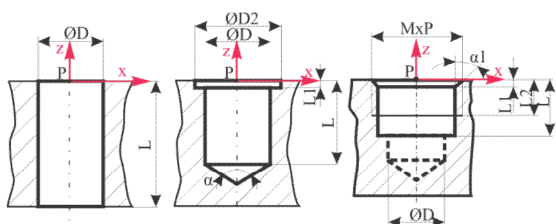
are based on methods for the recognition of the manufacturing features, while the GfF techniques are based on methods for the design of parts based on the manufacturing features [8].



4. DESIGN OF PARTS BASED ON MANUFACTURING FEATURES

Designing of parts with manufacturing features in this paper is based on modeling of parts based on Elementary Manufacturing Features (EMF). Elementary Manufacturing Feature (EMF) is a solid model with unique geometry that makes a functional unit in a manufacturing sense. Elementary Manufacturing Features, in this paper, can be defined as "elementary generic forms with which process planners associate certain attributes, skills and knowledge that apply when designing parts," [9].

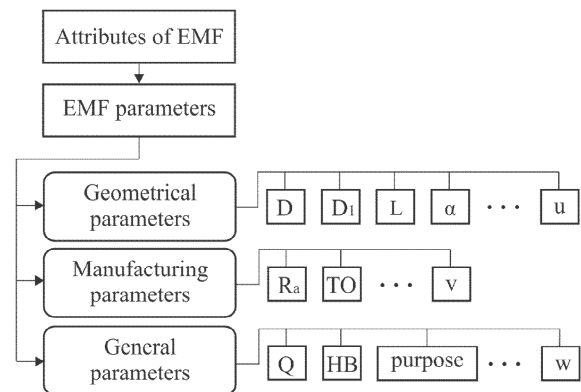
For the operation of milling, the Elementary Manufacturing Features, are shown in Figure 2 and for the drilling operations, EMF are shown in Figure 3. Part modeling with EMF is based on the principle of subtraction of EMF volume from the volume of the raw material part.



Idea concept of design with EMF is based on ability that EMF is "intelligent carrier (source) of information." Implementation of this concept is carried out by introducing and defining the attributes as part of the data structure of the Elementary Manufacturing

Features (Figure 4), in the form of parameters of EMF that are containing:

- geometric,
- manufacturing and
- general parameters.



The structure of the flow chart of the part design based on EMF is shown in Figure 5. The condition for the start of the part design is the previous generated initial solid model of raw material of part with defined overall dimensions and material, as a result of the preliminary part design.

The designer begins the part design with the selection of appropriate Elementary Manufacturing Features from the library of the EMF. After the selection of the EMF, designer adjusts parameters of the EMF. Settings of parameters of the EMF are refers to the setting of: geometric, manufacturing and general parameters.

After setting all parameters of the EMF model, the new solid model of EMF is generated. Generating of new solid model of the EMF (child - model) is done on the basis of generic model (parent - model) which is located in the EMF library. New solid model of the EMF is generated in a solid modeling environment of CAD program system.

A new solid model of the EMF then must be positioned in relation to the solid model of raw material of part. Positioning of EMF solid model is done in an interactive way. After positioning of the EMF solid model, Boolean operation of subtraction was applied. The result of this operation is a model of the raw material of part from whom is subtracted a model of EMF. Information about all parameters from EMF, as well as its position in relation to the origin of the adopted coordinate system of raw material of part, are stored within the developed application for the part design based on the EMF. The result of activities which are related to part design based on the EMF is a detail solid model of part with additional information's.

Designing of parts based on the EMF are closely connected with a library of the Elementary Manufacturing Features. Library of the EMF contains predefined or generic Elementary Manufacturing Features. During the process of part design, Elementary Manufacturing Feature from the library, is possible to use an unlimited number of times with the same or different parameters.

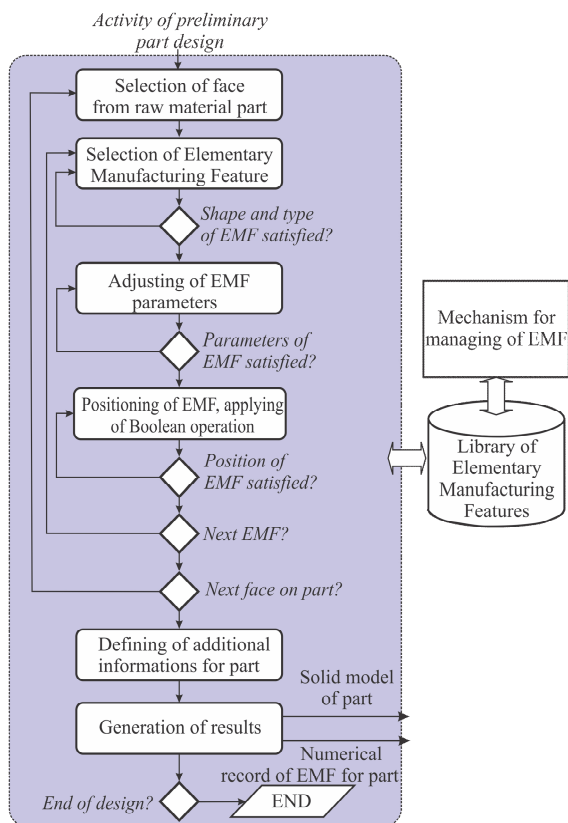


Fig. 5. The basic structure of flow chart for the part design based on the EMF [9]

In order to provide flexibility and scalability of the part design based on the EMF it was developed a mechanism for managing and update of library of the Elementary Manufacturing Features (Figure 6). The mechanism for management of EMF library ensures the input of completely new generic forms or updates the existing Elementary Manufacturing Features.

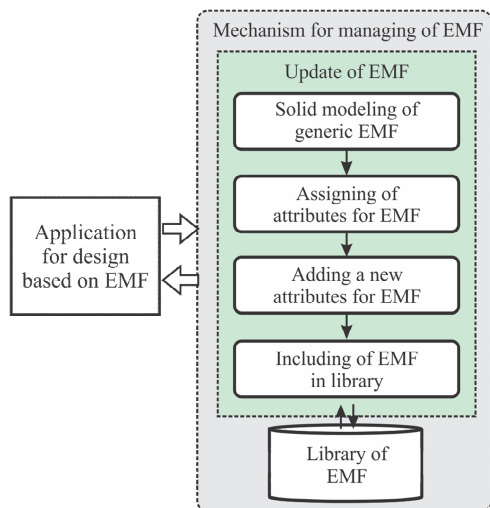


Fig. 6. Basic structure of the mechanism for management of the EMF

The updating process of the EMF library begins with regular solid modeling of new (generic) Elementary Manufacturing Feature within the CAD program system. The solid model of the new EMF then is loaded by a mechanism for managing of the EMF library. The next step is identification and connection

existing geometric attributes with the new (systemic) attributes, as well as the setting of manufacturing and general attributes for a new EMF. Then, the new Elementary Manufacturing Feature, together with the attributes, becomes a part of the EMF library.

5. VERIFICATION OF PARTS DESIGN BASED ON MANUFACTURING FEATURES

Developed application for parts design based on the EMF is integrated into the program system for solid modeling - SolidWorks®. The developed application is an upgrade and provides a functional extension of the program systems SolidWorks®. The basic structure of the application for the part design based on the EMF is shown in Figure 7.

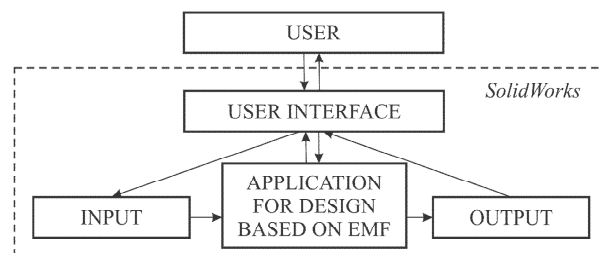


Fig. 7. The basic structure of a developed application for the part design based on the EMF

Verification of the developed applications for the part design based on the EMF is made on the example of designing of a hydraulic cylinder, as realistic industrial part.

The process of designing of the hydraulic cylinder is in accordance with the basic structure of the developed applications which is shown in Figure 5. After generating the initial shape of the raw material of the part in SolidWorks®, starting of the developed application interface for the part design based on the EMF is done at automated manner (Figure 8).

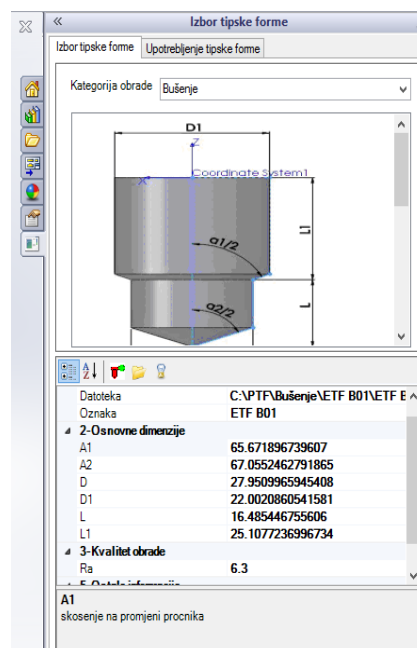


Fig. 8. The developed interface for selection and setup parameters of the EMF [9]

The designer-process planer selects, adjust and generate solid model of the EMF using EMF library. Positioning, with improved program tools based on Boolean operation of subtraction, as well as the inclusion of the EMF in solid model of raw material of the hydraulic cylinder, are next steps in the realization of the detail design of the hydraulic cylinder. After the designer-process planer is placed all solid models of the EMF on the solid model of raw material of the hydraulic cylinder, results from process of design are generated.

Results from design process are generated in the form of solid model and numerical records of the hydraulic cylinder. The solid model of the hydraulic cylinder (Figure 9) consists of 52 Elementary Manufacturing Features (13 Milling EMF and 39 Drilling EMF). From that numbers, it was used a three different types of EMF for drilling and seven different types of EMF for milling.

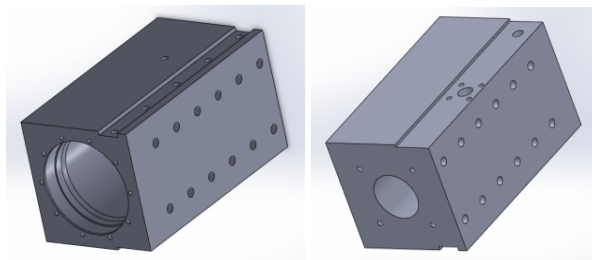


Fig. 9. The solid model of the hydraulic cylinder

Numerical record of the hydraulic cylinder consists of a set of data relating to the information concerning the geometrical and manufacturing parameters of the EMF, volume, positions and normal vector of the EMF in relation to the origin of the coordinate system of the hydraulic cylinder. Segment of the numerical record for hydraulic cylinder is shown in Figure 10.

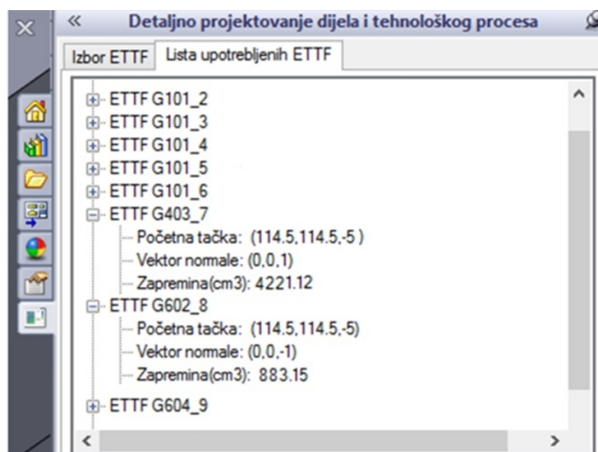


Fig. 10. Segment of output information in a shape of the numerical record for hydraulic cylinder

6. CONCLUSION

In this paper it was presented a methodology for design of parts/products based on manufacturing features, i.e. methodology for parts design from the perspective of the process planer. The result of this methodology for part design allows the inclusion of

additional information to the geometric solid model of parts that are different from the geometric parameters. Additional information is readily available because they have quick and easy access through developed applications. Thus generated additional information can be later used in downstream applications such as process planning, programming of computer numerical controlled machines, quality control, assembly, recycling, etc.

7. REFERENCES

- [1] Todi , V.: *Projektovanje tehnoloških procesa*, Fakultet tehni kih nauka, Novi Sad, 2004.
- [2] Shah, J., Mantyla, M.: *Parametric and Feature based CAD/CAM: Concepts, Techniques and Applications*, New York, 1995.
- [3] Joviševi , V.: *Automatizacija projektovanja tehnoloških procesa*, Mašinski fakultet Banjaluka, 2002.
- [4] Nasr, A.E., Kamrani, A.K.: *Computer-Based Design and Manufacturing: An Information-Based Approach*, Springer Science+Business Media, LLC, New York, 2006.
- [5] Gindy, N. N. Z.: *A hierarchical structure for form features*, Int. J. of Prod. Research. 27(12), 2089-2103. 1989.
- [6] Pratt, M. J., Wilson, P. R.: *Requirements for Support of Form Features in a Solid Modelling System*, CAM-I Inc., Arlington, USA. 1985.
- [7] Luki , D.: *Razvoj opšteg modela tehni ke pripreme proizvodnje*, Doktorska disertacija, Fakultet tehni kih nauka, Novi Sad, 2012.
- [8] Mantyla, M., Nau, D., Shah, J.: *Research challenges in feature based manufacturing*, Communications of ACM, 1996.
- [9] Borojevi , S.: *Razvoj modela za simultano projektovanje proizvoda i tehnoloških procesa*, Doktorska disertacija, Fakultet tehni kih nauka, Novi Sad, 2015.

Authors: Dr Sc. Stevo Borojevi , Prof. dr Vid Joviševi , University of Banjaluka, Faculty of Mechanical Engineering, Stepe Stepanovi a 71, 78000 Banjaluka, RS, B&H, Phone.: +387 51 433-000, Fax: +387 51 465-085.

E-mail: stevoborojevic@hotmail.com;

vid.jovisevic@blic.net

Prof. dr Velimir Todi , Prof. dr Milan Zeljkovi , University of Novi Sad, Faculty of Technical Sciences, Institute for Production Engineering, Trg Dositeja Obradovica 6, 21000 Novi Sad, Serbia, Phone.: +381 21 450-366, Fax: +381 21 454-495.

E-mail: todvel@uns.ac.rs; milanz@uns.ac.rs;

But, A.

VOLUMILL STRATEGY IN GROWING UP THE PRODUCTIVITY ON CNC MANUFACTURING

Abstract: The milling operation is widely used and the results are directly influenced by the milling strategies adopted. The paper presents two processing methods: one classical and one actual, both methods with wide industrial applications. Was made the comparison of these methods in manufacturing, are presented the results that were obtained on a real application. Knowing the milling processes, the new strategies developed by the CAM software, bring more substantial results and efficiency in manufacturing process.

Key words: CNC strategies, volumill, CAM software, milling processes.

1. INTRODUCTION

More milling strategies was develop by the CAM software's with the target to reduce the time of manufacturing and to up grate the surface quality. Some of this news are:

1. Helical Finish:

The Helical Milling strategy is especially useful for milling all around steep cavities or cores, especially in electrodes, (Fig.1).

Benefits:

Higher surface quality
Shorter machining time

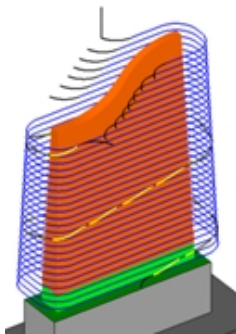


Fig.1 Helical Milling strategy

2. 5X MultiBlade Application

Dedicated application for programming of multi-blade parts. Fig.2

Dedicated 5X-Contiuous Milling Strategies for:

Rough
Finish Floor
Finish Walls.

Benefits

Fast & Simple Programming
Safe, High Quality Toolpath

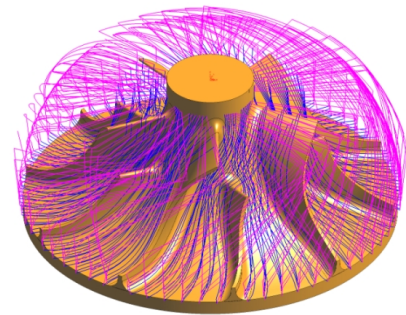


Fig.2 5X MultiBlade Application

3. Finish Surface Quality

New capabilities for better results when machining near a surface's edge:

3.1 Prevent waterfall(Fig.3):

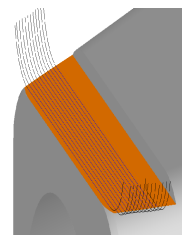


Fig.3 Prevent waterfall

Finish Surface Quality

3.2 Air extension – smooth, natural extension of the toolpath outside the part in all directions (Fig.4)

Extensions Along path + Extra passes

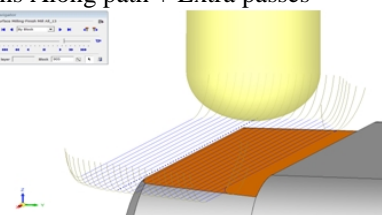


Fig.4 Air extension

Rough VoluMill

New strategy for ultra high volume removal (Fig.5).

Generating an HSM all-rounded toolpath to maintain constant material removal rate

Supports:

Consider updated stock

Consider holder

Execute between layers

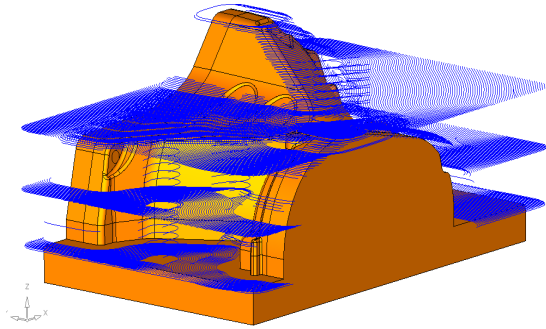


Fig.5 Rough VoluMill

2. BASIC INSTRUCTIONS

Regarding the Volumill strategy in the article was presented the comparison of this with the classical milling method - Z constant.

Was manufacturing one part with one geometry not so complex but with some sharp shapes with narrow channels and with sudden changes of direction. This part is presented in (Fig.6). The target was to confirm with one practical application the manufacturing time and the quality of the surface.

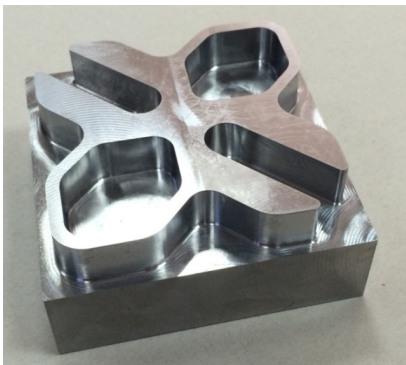


Fig.6 Rough VoluMill The part what was manufacturing for exemplification

The NC programs was made by the CAM software who use the cutting tools parameters was recommended by the cutting tool catalogs for this material.

The raw part is an steel C45 with the dimensions 100 x 100 x 50 mm and the thickness what will be manufacturing by 15mm and was use one end mill cutting tools by 10 mm diameter, with constant Z strategy (Fig. 7).

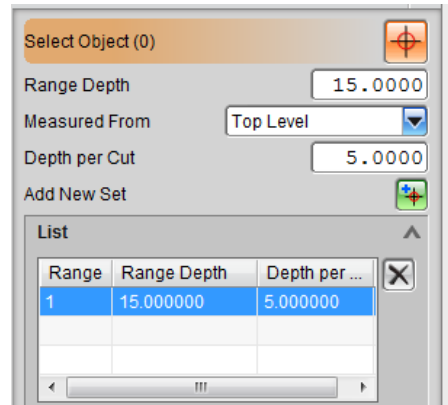
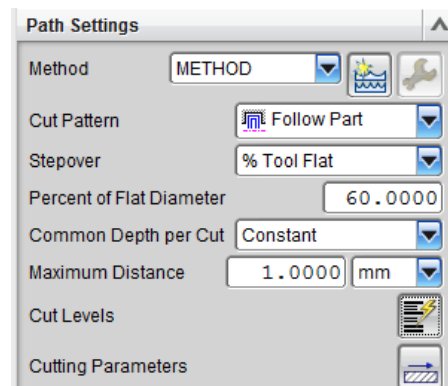


Fig. 7 Constant Z strategy



The thickness (15mm) was divided in 3 constant passes, so the a_p will be 5mm and the radial engagement will be 60% , $a_e=6$ mm. Starting by this informations we will have the cutting tool parameters and the time of manufacturing in (Fig. 8):

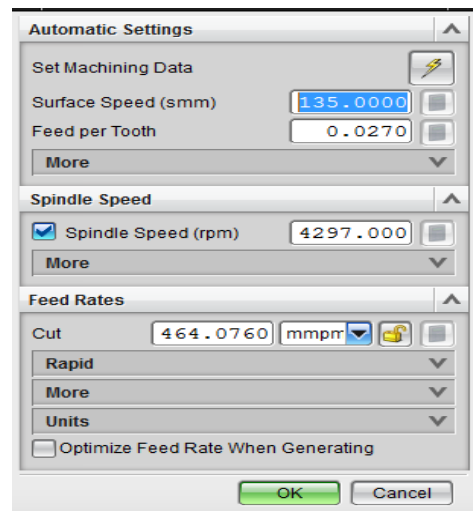


Fig.8. The cutting tool parameters and the time of manufacturing

The cutting speed of the tool will be $V_c=135$ m/min and the feed per tooth is $f_z=0,027$ mm/tooth, and we will use cooling liquid .

The trajectory of the cutting tool is present in (Fig.9)

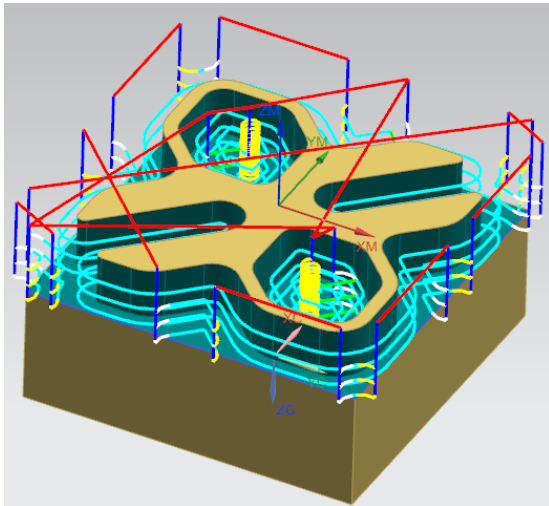


Fig.9 The trajectory of the cutting tool

In (Fig.10) we can see the chip that is around the cutting tool what affect the life of the cutting tool and the surface quality of the part.



Fig.10 The cutting tool and chips

Volumill strategy:

The same raw part was manufacturing with Volumill strategy. Now all the thickness by 15mm will be manufacturing in one single pass: $a_p=15\text{mm}$ and the radial engagement is $10\%/D_c$. The value is $a_e=1\text{mm}$, Fig.11.

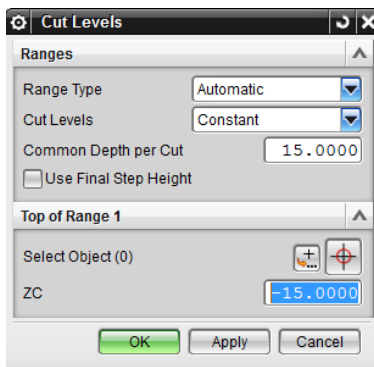
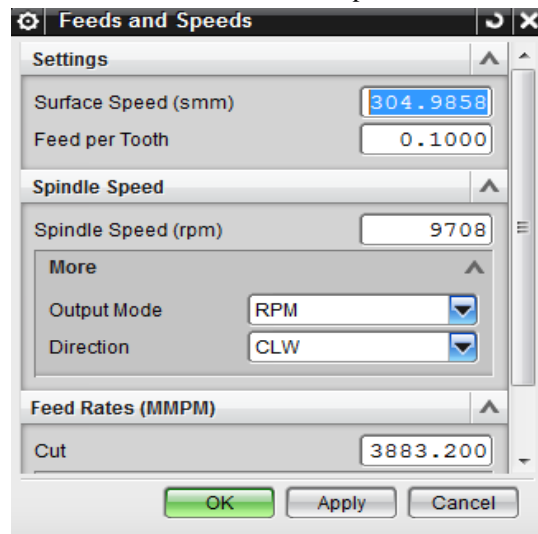


Fig.11 The cutting tools parameters

The radial engagement of the cutting tool is small, the cutting tools trajectory are tangents, the chip volume is minimal so will be possible to use higher



Operation Navigator - Geometry	
Name	Time
GEOMETRY	00:04:31
Unused Items	00:00:00
MCS	00:04:31
WORKPIECE_1	00:04:31
MILL_AREA	00:04:31
VOLUMILL	00:04:31

cutting parameters: spindle speed 9708 rpm., and the spindle speed (Fig. 12).

Fig.12 The cutting tool parameters and the processing time

The cutting tool is very short time in contact with the material- the trajectory is presented in (Fig.13.)

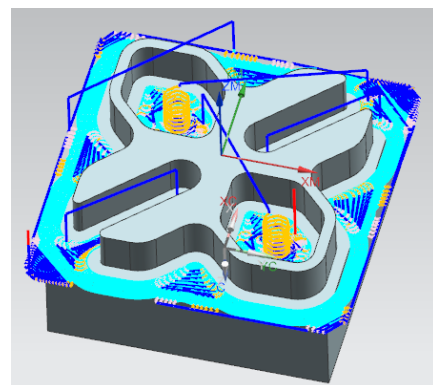


Fig.13 The trajectory of the cutting tool



Fig.14 The cutting tool and chip

3. FINAL REMARKS

After the tests we conclude that Volumill is much more productive, the quality of the surface is much better and the cutting tool life was increase. In Fig. 15 was presented a comparison between the manufacturing time.

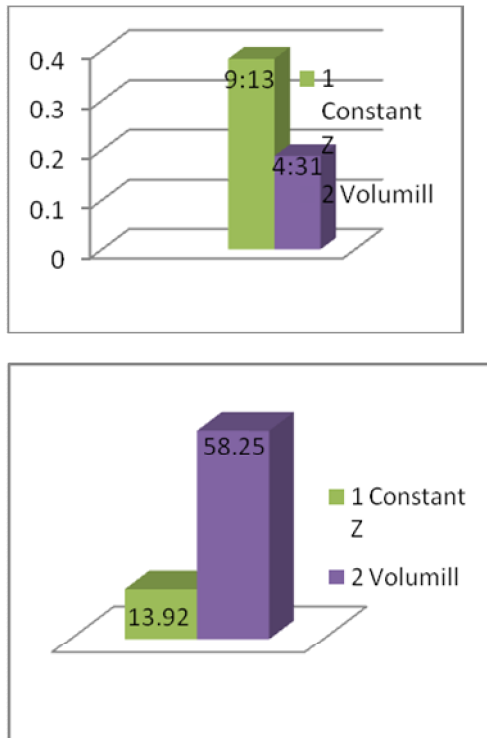


Fig. 15 The manufacturing time and the chip diagram (cm³/min)

All this information's confirm us that the Volumill strategy is much more efficiently who bring more benefits and advantages in comparison with the classical method of manufacturing: cycle time for Z constant is 9 min 13 sec and with Volumill strategy was obtain 4 min and 31 sec. and the accuracy is totally much more better: was obtain in Volumill $R_a = 0.24 \mu\text{m}$ in comparison with Z constant where $R_a = 1,97 \mu\text{m}$.

4. REFERENCES

- [1] But Adrian-(2009) “Advanced machine tools and manufacturing systems.” Editura Politehnica-Timisoara 2009.
- [2] Metal Cutting Technology Training Handbook Sandvik Coromant.
- [3] Metal Cutting Technology Technical guide.

Jakovljevi , Ž., Markovi , V., Živanovi , S.

RECOGNITION OF QUADRICS FROM 3D POINT CLOUDS GENERATED BY SCANNING OF ROTATIONAL PARTS

Abstract: *This paper presents a method for recognition of second order surfaces (quadrics) from point clouds containing information about scanned rotational parts. The method is region growing method that exploits the scatter of data during least squares fitting of quadrics as a region growing criterion. The presented procedure is convenient for segmentation of regions with high (G1 or higher) continuity. Besides, the region seed point is automatically selected which is its comparative advantage to a number of existing methods. The applicability of the proposed method is evaluated using two case studies; the first case study refers to a synthesized signal, and the second presents the applicability of the method on a real world example.*

Key words: *3D point cloud, surface recognition, quadrics segmentation, reverse engineering*

1. INTRODUCTION

Research efforts and practical applications in the field of implementation of 3D scanning devices in on-line manufacturing process control are expanding over the years. Typical examples are assembly automation and robots navigation. The hardware of contemporary 3D scanning devices, and especially optical ones, is characterized by high resolution, speed, and accuracy, and it is suitable for on-line applications. The same holds for algorithms for raw data preprocessing (3D data registration, integration and meshing). However, there is a lack of efficient real-time applicable algorithms for automatic recognition (segmentation and fitting) of geometric primitives from point cloud. During reverse engineering in CAD systems, geometric primitives from point clouds are recognized interactively by user [1], where user recognizes geometric primitives and then annotates a number of points on them. Afterwards, software is capable of fitting the best surfaces through selected points. On the other hand, implementation of 3D scanning devices in control applications requires fully automatic recognition of geometric primitives from point cloud.

Motivated by applications in a number of fields, such as mobile robots navigation [2] and seam pose detection in robotized welding [3], automatic recognition of planes has attracted many research efforts [4, 5]. Besides planar surfaces, in mechanical engineering rotational surfaces are most frequently met. These surfaces usually consist of second order surfaces (quadrics), planes, and general tori. In the focus of this paper is recognition of quadrics from scanned rotational surfaces.

There are a number of algorithms for detection of quadrics from point cloud, and a survey of these methods can be found in [6]. Generally, the methods belong to one of the two classes: 1) edge based, and 2) region based methods. Edge based techniques can be employed for G0 continuous surfaces where there

exists an abrupt change between adjacent regions. Region based methods employ split and/or merge or region growing approach. Region growing approaches start from a seed point and grow region around it using different criteria such as local surface normal [7], average curvature [8], or principle curvature [9].

Recent methods combine edge based approaches for initial segmentation and region based approaches for surface fitting and segmentation of regions with higher continuity. For example, procedure proposed in [10] detects feature edges using dihedral angle; afterwards variational shape approximation is employed for region partition and general shape quadrics are fitted through obtained regions; finally, over-segmented adjacent regions are merged using combination of Euclidean distance and normal deviation as metrics. Another approach from [11] employs tensor voting based method for edges detection and combination of RANSAC, slipping motion analysis, Gauss map and principle curvature for recognition of shapes. An interesting research in the field of recognition of planes, spheres, cones and cylinders from sparse 3D meshes obtained from CAD is presented in [1]. The presented method recognizes feature edges using dihedral angle, and employs region growing based on principal curvature for primitives' extraction.

In this paper we propose a method for automatic recognition of quadrics from point cloud obtained by scanning of rotational parts. The proposed method is in its essence region growing method based on scatter of data during direct least squares fitting of second order surfaces. The presented method is applicable for recognition of G1 (or higher) continuous surfaces.

The remainder of the paper is structured as follows. In Section 2 we provide some theoretical background and present the proposed recognition method and corresponding algorithm. Section 3 presents the implementation of the algorithm on a synthesized point cloud, as well as on a real-world example. Finally, in Section 4 we give some concluding remarks.

2. METHOD FOR RECOGNITION OF QUADRICS FROM SCANNED ROTATIONAL PARTS

The method for recognition of quadrics from scanned rotational parts that is presented in this paper is based on the properties of scatter matrix during least squares fitting of second order surfaces (quadrics). General quadric can be represented by the following equation:

$$a_1x^2 + a_2y^2 + a_3z^2 + a_4xy + a_5yz + a_6xz + a_7x + a_8y + a_9z + a_{10} = 0 \quad (1)$$

where a_i represent surface parameters and $[x y z]$ are the coordinates of a point on quadric. Equation (1) can be represented in matrix form:

$$\mathbf{x} \cdot \mathbf{a} = 0 \quad (2)$$

where $\mathbf{x}=[x^2 y^2 z^2 xy yz xz x y z 1]$, and $\mathbf{a}=[a_1 a_2 \dots a_{10}]^T$ represents the vector of surface parameters.

Coefficients \mathbf{a} can be estimated by solving the following minimization problem [12, 13]:

$$\min \|\mathbf{D}\mathbf{a}\|^2 \quad (3)$$

subject to $\mathbf{a}^T \mathbf{C}\mathbf{a} = 1$

where \mathbf{C} is 10×10 matrix with all elements equal zero except $C(10,10)=1$, and \mathbf{D} is design matrix in the form:

$$\mathbf{D} = \begin{bmatrix} x_1^2 & x_2^2 & x_3^2 & \dots & x_N^2 \\ y_1^2 & y_2^2 & y_3^2 & \dots & y_N^2 \\ z_1^2 & z_2^2 & z_3^2 & \dots & z_N^2 \\ x_1y_1 & x_2y_2 & x_3y_3 & \dots & x_Ny_N \\ y_1z_1 & y_2z_2 & y_3z_3 & \dots & y_Nz_N \\ x_1z_1 & x_2z_2 & x_3z_3 & \dots & x_Nz_N \\ x_1 & x_2 & x_3 & \dots & x_N \\ y_1 & y_2 & y_3 & \dots & y_N \\ z_1 & z_2 & z_3 & \dots & z_N \\ 1 & 1 & 1 & \dots & 1 \end{bmatrix}^T \quad (4)$$

Solution of minimization problem (3) is positive eigen value of

$$\mathbf{S}\mathbf{a} = \lambda \mathbf{C}\mathbf{a} \quad (5)$$

where

$$\mathbf{S} = \mathbf{D}^T \mathbf{D} \quad (6)$$

represents scatter matrix, and λ is Lagrange multiplier.

When all data in design matrix are sampled from one exact quadric, scatter matrix will be singular [12]. On the other hand, when data are sampled from approximate quadric, such as scanned quadric surface, the scatter matrix will be close to singular. As data that do not belong to the particular quadric enter design matrix, matrix \mathbf{S} will be farther from singular matrix. We have exploited this property of scatter matrix to create the method for segmentation of quadrics from considered class of point clouds.

The proposed method is in its essence region growing method. Region growing procedure starts from the first point in the point cloud and adds point by point to the region using reciprocal condition number of

scatter matrix as region growing criterion. When reciprocal condition number of \mathbf{S} passes predefined threshold, a point that does not belong to quadric is detected. In this situation region growing is stopped and the coefficients \mathbf{a} of recognized quadric are estimated. The region is considered a quadric if it contains more than 30 points from the cloud. Otherwise, it is assumed that points do not belong to quadric, but to another type of surface.

When region growing procedure stops, all points that belong to recognized quadric within predefined threshold are excluded from point cloud; for detection of distance between points from the cloud and surface we exploit estimated surface parameters. The parameters estimation and point exclusion procedure is iteratively repeated until no more points are recognized to belong to given quadric. The pseudo-code of the algorithm for implementation of the procedure is presented in Fig. 1.

Since we are dealing with rotational parts, to accelerate and facilitate computational efforts, the algorithm starts with alignment of scanned part's rotation axis with z axis of point cloud, and with sorting of points from point cloud in descending order along z axis. The alignment of rotation axis along z direction is carried out using moments of inertia for all three axes of coordinate system, center of mass, and elementary computer graphics transforms.

```

INPUT:  $\mathbf{x}, \mathbf{y}, \mathbf{z}$  – points from the cloud
         thres1, thres2 – segmentation thresholds


---


put axis of rotation along  $z$  axis
cloud= $[x, y, z]$ ;
sortrows(cloud,-3);
m=0; trials=0;
while trials<30
    m=m+1;
    surfaces(m).surf(1,:)=cloud(1,:);
    for i=1:length(cloud)
        surf_aux= [surfaces(m).surf; cloud(i,:)];
        calculate rcond(S) using surf_aux
        if rcond(S)<thres1
            add cloud(i,:) to surfaces(m).surf; end
    end
    if length(surfaces(m).surf)>30
        l1=0; l2=1000;
        while l1<l2
            l1=length(surfaces(m).surf)
            calculate A
            for i=1:length(cloud)
                if distance<thres2
                    add cloud(i,:) to surfaces(m).surf
                else add cloud(i, :) to new_cloud; end
            end
            l2=length(surfaces(m).surf)
        end
        cloud=new_cloud;
    else trials=trials+1; end
    if length(cloud)<2 trials=31; end
end


---


OUTPUT: surfaces – structure containing segmented quadrics

```

Fig. 1. Pseudo-code of the algorithm for implementation of the method for recognition of quadrics from scanned rotational parts

3. IMPLEMENTATION OF THE PROPOSED METHOD

To illustrate and experimentally verify the proposed procedure, we have implemented it in recognition of second order surfaces in two case studies. The first case study refers to a synthesized point cloud, while the second considers a real world example.

3.1 Case study 1: synthesized point cloud

The point cloud that we use in this case study consists of four second order surfaces, i.e. of one sphere, two ellipsoids (spheroids in particular), and one cylinder. Sphere and cylinder are G0 continuous with adjacent surfaces, while between ellipsoids G1 continuity is achieved. The CAD model of synthesized part is presented in Fig. 2.a, and parameters of synthesized surfaces in Table 1. Synthesized point cloud is noised by white noise with signal to noise ratio of 90dB.

After application of the proposed method, all four surfaces were adequately recognized. Segmentation results are graphically presented in Fig. 2.b, and estimated parameters in Table 1. From Table 1 it can be observed that the algorithm was able to adequately recognize surfaces. The discrepancy between estimated surface parameters and generated surface parameters is less than 0.3%. It should be noted that the parameters of ellipsoids are close and that accurate distinction between these surfaces is a challenging task.

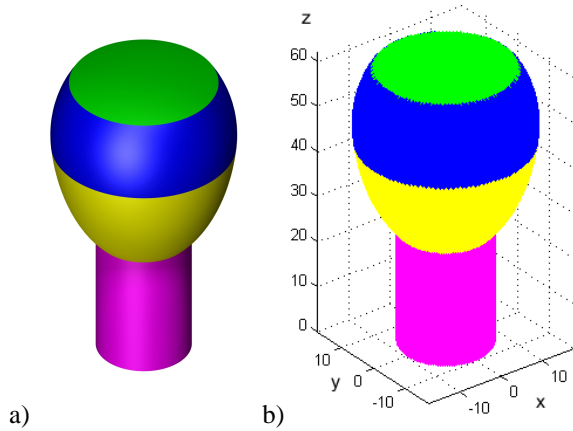


Fig. 2. Case study 1: a) synthesized part; b) segmentation results

	Seg. no	Parameters of quadric $[a_i \times 10^2], i=1, \dots, 10$
generated	1	[0.04 0.04 0.04 0 0 0 0 -0.96 -94.24]
	2	[0.33 0.33 0.25 0 0 0 0 -24 476]
	3	[0.32 0.32 0.11 0 0 0 0 -11.29 186.76]
	4	[1.23 1.23 0 0 0 0 -100]
estimated	1	[0.04 0.04 0.04 0.0 -0.0 -0.0 0.0 -0.96 -94.28]
	2	[0.33 0.33 0.25 -0.0 -0.0 -0.0 0.0 -23.98 474.61]
	3	[0.32 0.32 0.11 -0.0 0.0 -0.0 0.0 -11.29 186.76]
	4	[1.23 1.23 -0.0 0.0 -0.0 -0.0 0.0 0.0 -100.0]

Table 1. Generated and estimated surface parameters in case study 1

3.1 Case study 2: real-world example

In second case study we consider the part presented in Fig. 3. The part consists of ellipsoid, hyperboloid, cone and cylinder.

The parameters of the designed part are presented in Table 2. The part was made on CNC lathe TCN410 – echoENG. The point cloud (Fig. 3.c) is obtained by 3D digitization of the part using ZScanner® 700 [14] handheld laser scanner with resolution of 0.1mm.

As presented in pseudo-code from Fig. 1, the recognition procedure starts by alignment of part's rotation axis with z axis of the coordinate system (Fig. 4). After applying the whole procedure, four quadric surfaces were adequately recognized. Segmentation results are presented in Fig. 5, and estimated parameters in Table 2.

From estimated parameters it can be observed that for all four surfaces adequate surface types (ellipsoid, hyperboloid, cone and cylinder) were recognized. The discrepancy between designed and estimated parameters for all coefficients except for a_3 in cone segment is less than 6%. This discrepancy includes all errors introduced during machining and scanning process, such as interpolation error (ellipse and hyperbola are approximated by circular and linear segments), machining error, scanner accuracy and resolution. It should be noted that the scanner has shown poor performance as presented in Fig. 3c. It has very low accuracy in vicinity of sharp edges and cone segment is located between two sharp edges.

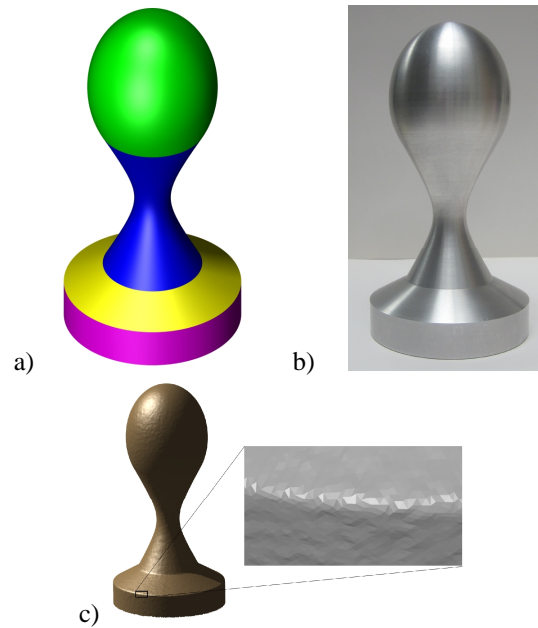


Fig. 3. Part from case study 2: a) designed part; b) photo of real-world part; c) scanned part

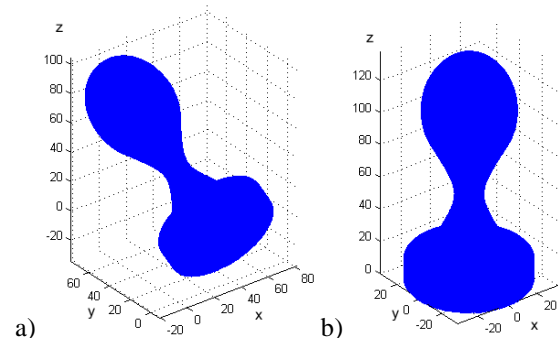


Fig. 4. Point cloud from case study 2: a) before graphic

transforms; b) after alignment

	Seg no	Parameters of quadric [$a_i \times 10^2$], $i=1, \dots, 10$
designed	1	[0.16 0.16 0.09 0 0 0 0 0 -19.78 933.87]
	2	[2.04 2.04 -0.68 0 0 0 0 0 71.46 -1976.42]
	3	[0.33 0.33 1.0 0 0 0 0 0 66.64 1.11e+3]*100
	4	[0.086 0.086 0 0 0 0 0 0 0 -100]
estimated	1	[0.17 0.17 0.09 -0.0 0.0 -0.0 0.04 -0.02 -19.81 930.61]
	2	[2.04 2.04 -0.68 -0.0 0.01 -0.0 0.34 -1.11 72.68 -2033.5]
	3	[0.34 0.34 -0.89 -0.0 0.0 0.0 0.04 -0.29 64.4 -1.13e+3]*100
	4	[0.086 0.086 0.0 0.0 0.0 0.0 0.01 -0.04 0.0 -99.91]

Table 2. Designed and estimated surface parameters in case study 2

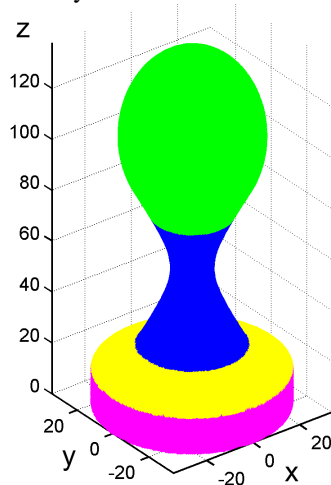


Fig. 5. Segmentation results in case study 2

4. CONCLUSION

In this paper we have presented a method for recognition of quadrics from point clouds generated by scanning of rotational parts. It is a region growing method based on properties of scatter matrix calculated during least squares fitting of second order surfaces. The method is convenient for segmentation of adjacent segments with G1 or higher continuity, and this is its comparative advantage to edge based procedures. Another important property of this method is that seed point is automatically selected as the highest point (point with maximum z coordinate) on the part.

The performances of the method were presented using a synthesized and a real-world point cloud, and the method has shown good recognition results.

To increase the robustness of the method to poor scanner performances, the future work will address the combination of the presented region growing method with edge based segmentation during preprocessing. In addition, recognition of tori, which are also frequently met in rotational parts, will be a part of future research efforts.

4. REFERENCES

[1] Bènière, R., Subsol, G., Gesquière, G., Le Breton, F., Puech, W.: *A comprehensive process of reverse engineering from 3D meshes to CAD models*, Computer-Aided Design, Vol. 45, p.p. 1382–1393, 2013.

[2] Fu, G., Corradi, P., Menciassi, A., Dario, P.: *An*

Integrated Triangulation Laser Scanner for Obstacle Detection of Miniature Mobile Robots in Indoor Environment, IEEE/ASME Transactions on Mechatronics, Vol.16, No.4, p.p.778 – 783, 2011.

[3] Fang, Z., Xu, D., Tan, M.: *A Vision-Based Self-Tuning Fuzzy Controller for Fillet Weld Seam Tracking*, IEEE/ASME Transactions on Mechatronics, Vol.16, No.3, p.p.540 – 550, 2011.

[4] Wang, L., Cao, J, Han, C.: *Multidimensional particle swarm optimization-based unsupervised planar segmentation algorithm of unorganized point clouds*, Pattern Recognition, Vol.45, No.11, p.p. 4034–4043, 2012

[5] Jakovljevic, Z., Puzovic, R., Pajic, M.: *Recognition of Planar Segments in Point Cloud based on Wavelet Transform*, IEEE Trans. on Industrial Informatics, Vol. 11, No. 2 , p.p. 342-352, 2015.

[6] Petitjean, S.: *A Survey of Methods for Recovering Quadrics in Triangle Meshes*, ACM Computing Surveys, Vol.2, No.34, p.p.1-61, 2002.

[7] Rabbani, T., Van den Heuvel, F.A., Vosselman, G.: *Segmentation of point clouds using smoothness constraint*, International Archives of Photogrammetry, Remote Sensing and Spatial Information Sciences, Vol.36, No.5, p.p.248-253, 2006.

[8] Lai, H.C., Chang, Y.H., Lai, J.Y., *Development of feature segmentation algorithms for quadratic surfaces*, Advances in Engineering Software, Vol.40, No.10, p.p.1011–1022, 2009.

[9] Lavoue, G., Dupont F., Baskurt A.: *Curvature Tensor Based Triangle Mesh Segmentation with Boundary Rectification*, Proceedings of the Computer Graphics International, p.p. 10-17, IEEE, 2004.

[10] Yan, D., M., Wang, W., Liu, Y., Yang, Z.: *Variational mesh segmentation via quadric surface fitting*, Computer-Aided Design Vol. 44, pp. 1072–1082, 2012.

[11] Yi, B., Liu, Z., Tan, J., Cheng, F., Duan, G., Liu, L.: *Shape recognition of CAD models via iterative slippage analysis*, Computer-Aided Design Vol. 55, pp. 13–25, 2014.

[12] Fitzgibbon, A., Pilu, M., Fisher R.B.: *Direct Least Square Fitting of Ellipses*, IEEE Transactions on Pattern Analysis, Vol.21, No.5, pp.476-480, 1999.

[13] Rosin, P., L.: *A note on the least squares fitting of ellipses*, Pattern Recognition Letters, Vol. 14, No. 10, p.p. 799–808, 1993.

[14] http://www.zcorp.com/documents/380_ZScanner700_PX_SpecSheet_HiRes.pdf

Authors: Dr. Živana Jakovljević, Assistant Professor, M.Sc. Veljko Marković, Dr. Sasa Zivanović, Assistant Professor, University of Belgrade, Faculty of Mechanical Engineering, Kraljice Marije 16, 11000 Belgrade, Serbia
E-mail: zjakovljevic@mas.bg.ac.rs; vmarkovic@mas.bg.ac.rs; szivanovic@mas.bg.ac.rs;

Acknowledgements. This research was partially supported by Serbian Ministry of Education, Science and Technological Development under research grants TR35007 and TR35020.

MULTI AXIS NC CODE SIMULATION BASED ON THREE-DEXEL MODEL REPRESENTATION AND GPU

Abstract: This paper presents a program system for multi axis NC code simulation based on three-dexel approach. Computing of tool subtraction from a workpiece is done in the GPU (Graphics Processing Unit) as computation power of modern GPU is 10 to 100 times higher than the CPU (Central Processing Unit). Initially, blank workpiece STL model is converted to three-dexel model by depth peeling algorithm. Then, structures for dexels in all three dimensions are transferred into the GPU. Tool movement is approximated by instances between two consecutive positions. For every tool instance, depth and normal textures are generated in all three directions and subtracted from the workpiece model.

Key words: three-dexel model, NC code simulation, GPU computation

1. INTRODUCTION

In the NC (Numerically Controlled) simulation process, workpiece is usually approximated with voxel or dexel elements. The voxel model represents an object with many small cubes, whilst dexel model represents an object with a grid of long columns compacted together. Dexel representation is widely used in NC simulation process, because it is less memory demanding than voxel representation [1].

In Fig. 1a, one circle is represented with dexels in one dexel direction (single dexel representation). The weak point of single dexel representation is that surfaces which are almost parallel with dexel direction can be missed in dexel generation. Much better surface representation for the same number of rays is shown in Fig 1b, where circle is intersected with rays in two orthogonal directions. For three dimensional case presented in Benouamer et al. [1], three dexel model is introduced, where model is approximated with dexels in three orthogonal directions.

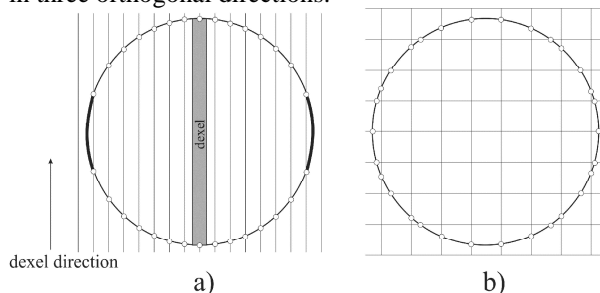


Fig. 1. a) Single dexel representation, b) Dexels generated in two dimensions

Because of simplicity and fast Boolean operations, dexel representation is widely used in program systems where a real-time performance is important, such as, NC machining simulations [2,3,4,5] or virtual sculpting systems [6,7,8,9].

2. MODEL OF THE DEVELOPED PROGRAM SYSTEM

Program system is primarily developed with a goal to simulate free form modelling by hand movement in a virtual environment [9]. User moves tool in space and program system should subtract a tool from workpiece as soon as possible. Also, tool can be of a freeform shape. This program system had two limitations. Model and tool were approximated by a single dexel representation and it was a view dependent. This system is therefore extended with a three-dexel model representation, with subtraction operations now done with the GPU and it is not view dependent. It can also be used in the NC multi axes code simulation, as it is shown in this paper.

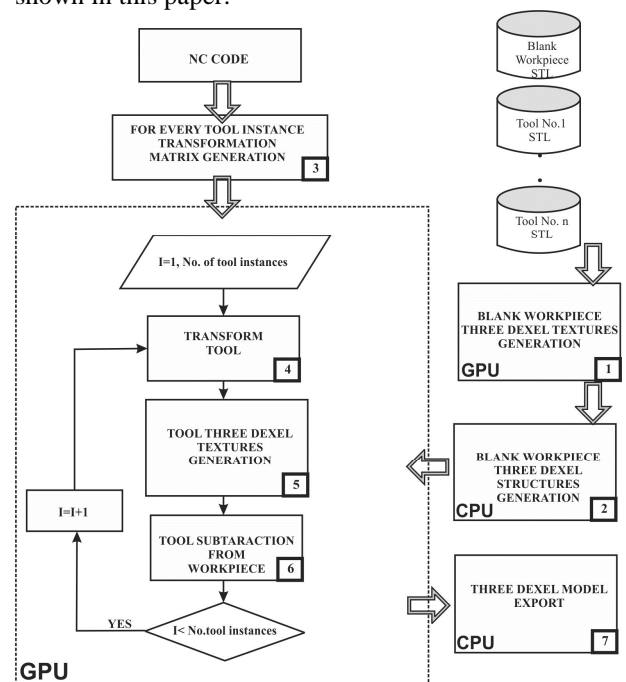


Fig. 2. Model of the developed program system

Model of the developed program system is shown

in Fig. 2. Blank workpiece and tools models are imported in the system as STL files as shown in Fig. 2. Next step presents a generation of three-dexel textures in GPU (Graphics Processing Unit). After that, from generated textures, structures of every dexel are formed by CPU (Central Processing Unit). Matrices of tool instances are generated from the NC code. Then, formed dexel structures are transferred into GPU and complete simulation of tool subtraction from workpiece is performed by the GPU. For every tool instance, model of the tool is transformed by the matrix, and three-dexel textures of the tool are generated. Then, tool instance textures are subtracted from the workpiece and the workpiece is modified. This step is repeated for every tool instance. When computation is done, three-dexel model of machined workpiece can be transferred from the GPU to the main memory, where it can be processed afterwards.

Detailed steps of the procedure explained above are presented in the following sections.

2.1 Blank workpiece STL to three-dexel model conversion

Blank workpiece model is imported in the program system in STL format (as triangle polygon collection where each triangle has a normal). For three-dexel model generation, ray intersection with model in three orthogonal directions should be calculated. This process can be very time consuming (blank workpiece may consist of millions of triangles). To speed up computation, depth peeling algorithm [10] is applied in the program system. Model is rendered in projection as many times as maximal complexity of point in this projection is. In Fig. 3, 2D case is presented.

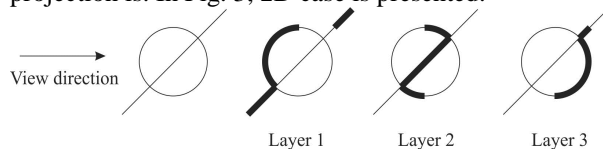


Fig. 3. Depth peeling principle

As shown in Fig. 3, all visible faces are rendered first (Layer 1). After that, these faces are discarded and next visible faces are rendered. Process is finished when there are no faces left to render. Shape shown in Fig. 3 has a complexity of three in the view direction. Surfaces are rendered in images (textures) and every texture pixel has a depth value of surface point in the view direction.

For the model presented in Fig. 4a, rays in x and y direction intersect model in four points (two dexels) when rays in z direction intersect model in two points (one dexel). This means that in depth peeling of the model shown in Fig. 4 number of passes in x and y direction is four, and in z direction is two. Before depth peeling algorithm is applied, bounding view volume should be determined in respect that it covers complete model in all three orthogonal dimensions.

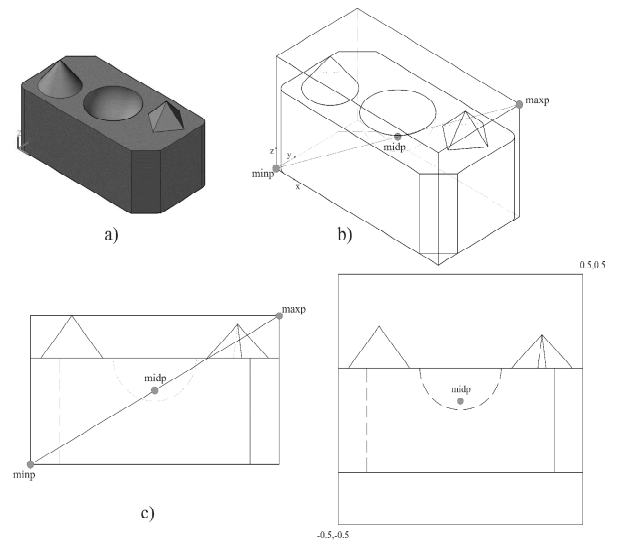


Fig. 4. a) Example model b,c) Bounding box parameters and d) Transformed model prepared for depth peeling

First step presents model bounding box determinations with $minp$, $maxp$ and $midp$ points (Fig. 4b). After that, maximal projection on one of orthogonal axis is determined (Fig. 4c). This projection is an edge of the cube (with center $midp$) from which view bounding box is calculated. Then, model is scaled and transformed in position in such way that $midp$ is transformed in WCS origin and bounding square for texture generation is $(-0.5, -0.5 \div 0.5, 0.5)$. Transformed and scaled model in front view is shown in Fig. 4d. For any depth peel layer model is rendered by the GPU and two images (textures) are generated. In the first texture (depth texture) every pixel contains depth value in the range 0.0-1.0. In the second texture (normal texture) every pixel has a RGB (Red Green Blue) colour, where red, green and blue components contain x, y and z normal information.

Generated depth textures in all three orthogonal directions are shown in Fig. 5. Also, in Fig. 5a, generated normal texture for first layer in z direction is shown.

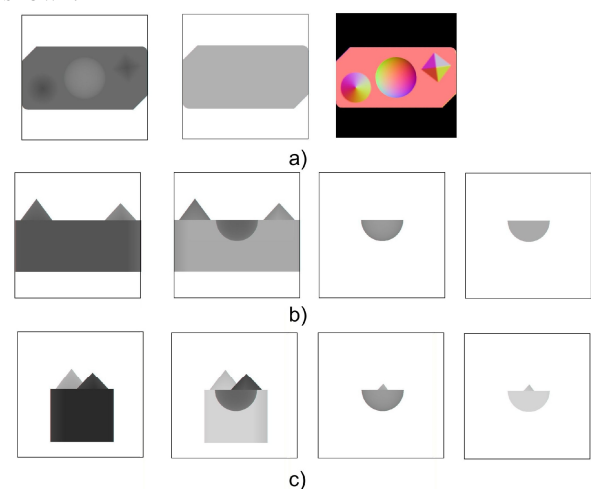


Fig. 5. Generated depth textures a) in z direction with one normal texture, b) in y and c) in x direction

2.2 Three-dexel structure definition

Based on the generated textures in the previous step, structures for dexels in all three dimensions should be generated and transferred into GPU. Parameters for dexel definition are presented in Fig. 6. Every texture has a resolution (*texture resolution*). For dexel presented in Fig. 6a, parameters *depth* and *length* define coordinates of first and last point of dexel in the view direction, when *positionx* and *positiony* define dexel position in a plane. Also, from normal textures every dexel point normals are calculated *normal1* and *normal2*. Two last parameters in dexel structure, *cut1* and *cut2*, give information if blank workpiece dexels are cut in the simulation process.

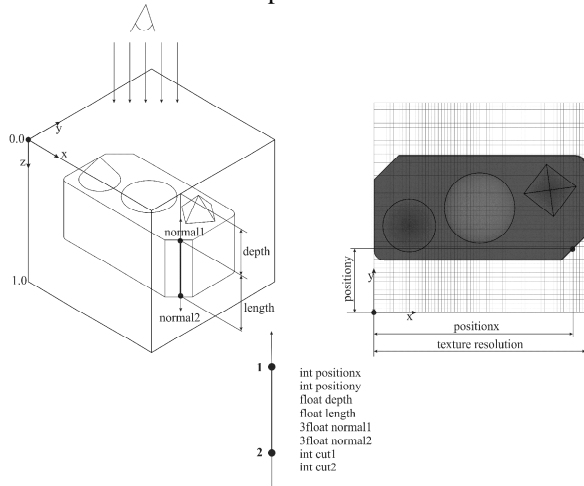


Fig. 6. Dexel structure parameters

When dexel structures for all three directions are generated, they are transferred into GPU as three buffers.

Dexels in all three dimensions generated from textures from Fig. 5 are presented in Fig. 7.

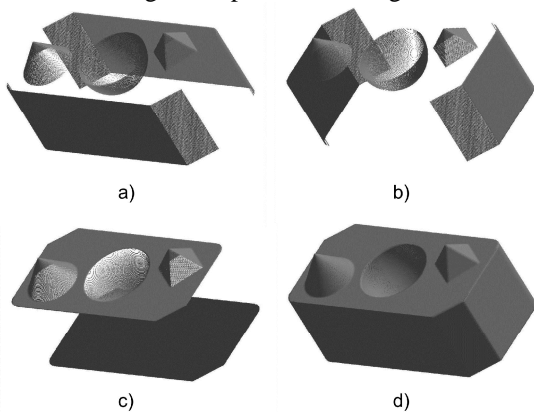


Fig. 7. Generated dexels in y(a), x(b), z(c) directions and a complete three dexel model (d)

2.3 Tool definition in program system

Tool position in the developed program system is presented with instances between two consecutive tool positions. Another approach is to generate tool swept volume and subtract it from a workpiece. Drawback of the second approach is that tool swept volume generation and its subtraction is more time consuming than subtraction of tool instances. Also, for free shape tool, swept volume is very difficult and sometimes

impossible to generate. An example of generated tool instances for different interpolation steps is shown in Fig. 8.

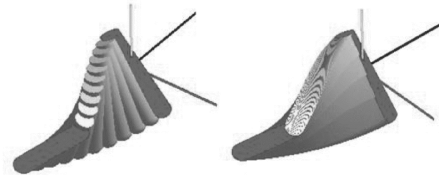


Fig. 8. Tool instances with different interpolation steps

Interpolation of tool positions is done by quaternions and after that position and orientation of every tool instance is presented by 4x4 transformation matrix.

2.4 Subtracting a tool from a workpiece

Tool instance is transformed and rendered in all three directions as a workpiece. As a result, depth and normal textures of tool instance are generated. Subtracting is performed in GPU geometry shader stage and six possible cases are shown in Fig 9.

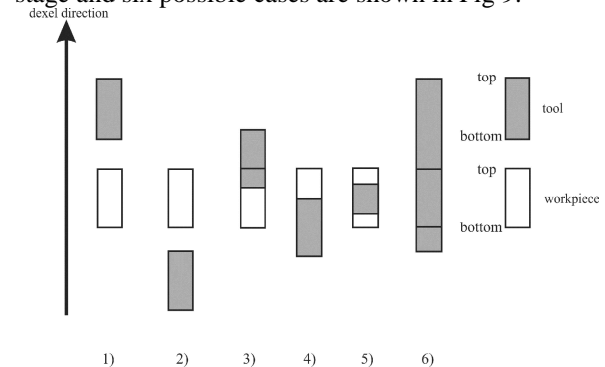


Fig. 9. Possible cases for subtracting tool from workpiece dexels

When tool dexel is above (1) or below (2), intersection does not exist. If tool is cutting workpiece from top (3), top workpiece dexel is set with bottom tool dexel. When tool is cutting workpiece from above (4), bottom workpiece dexel is set with top tool dexel. If a tool dexel divides workpiece (5), then two workpiece dexels are generated. And the last case (6) is when tool dexel completely removes workpiece dexel, then workpiece dexel is deleted from dexel buffer.

3. A SIMULATION EXAMPLE

Simulation example of the developed program system is NC code for five axis milling, which consists of 20976 lines of code. Tools are flat end mill with 10mm diameter and ball end mill with diameter of 5mm. Blank workpiece is box with dimensions 140x80x70mm and it is defined with approximately 7×10^5 dexels.

Simulation is performed on a computer with the following configuration:

- CPU Intel i5 760, 2,8 GHz
- GPU NVidia GTX 660 (960 shader units)
- Memory 4 GB

In Fig. 10 screenshots from this simulation are shown. Simulation is done with 160 fps (frames per

second), which means that operation of tool instance subtraction from workpiece takes 6.25ms.

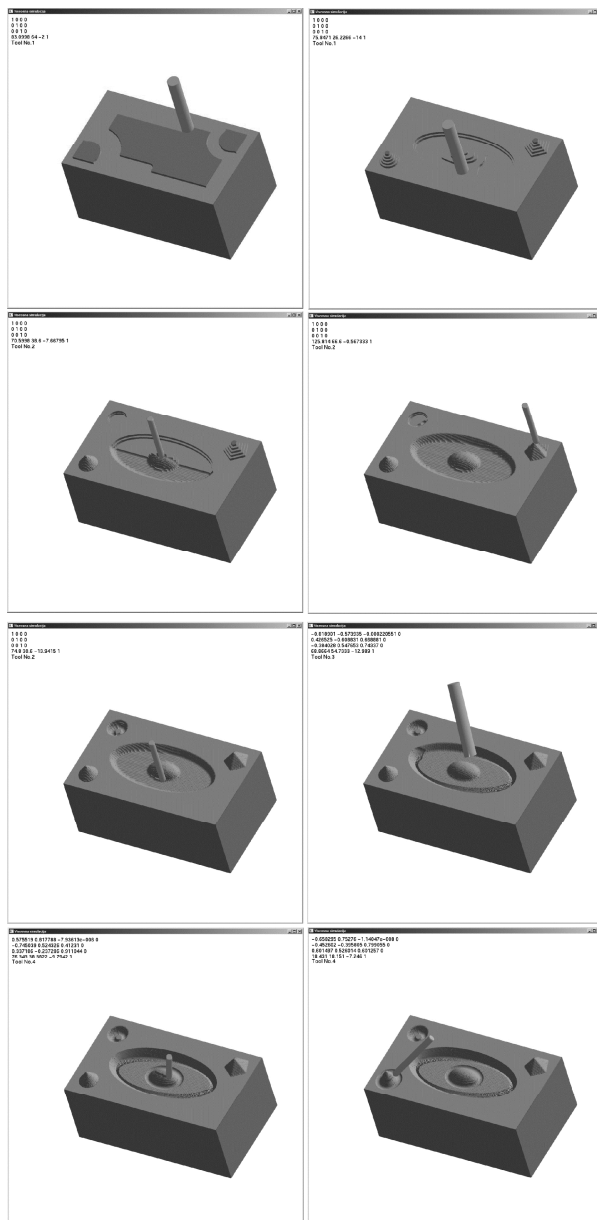


Fig. 10. Program system screenshots of simulated NC code operations

4. CONCLUSION

In this paper, a program system for multi axis NC code simulation based on three-dexel approach is presented. Tool can be a free form shape, which enables program system to be used for free form modelling with very few modifications. Computing of tool subtraction from a workpiece is done by the GPU, which causes very short computation time. Expectation of this system is that with the latest GPU generation subtraction time may be close to 1ms. This will be convenient for free form sculpting and force feedback generation in real time.

5. REFERENCES

[1] Benouamer, M. O., Michelucci, D.: *Bridging the*

Gap between CSG and Brep via a Triple Ray Representation, In Proc. Fourth ACM/Siggraph Symposium on Solid Modeling and Applications, p.p. 68-79, 1997.

- [2] Van Hook, T.: *Real-time shaded NC milling display*, Computer Graphics, SIGGRAPH Proceedings, Vol. 20, No 4, p.p. 15-20, 1986.
- [3] Huang, Y., Oliver, J.H.: *NC milling error assessment and tool path correction*, Computer Graphics Proceedings (SIGGRAPH '94), p.p. 287-294, 1994.
- [4] Muller, H., Surmann, T., Stautner, M., Albersmann, F., Weinert, K.: *Online Sculpting and Visualization of Multi-Dexel Volumes*, Proceedings of the eighth ACM symposium on Solid modeling and applications, p.p. 258-261, 2003.
- [5] Tukora, B., Szalay, T.: *Multi-dexel based material removal simulation and cutting force prediction with the use of general-purpose graphics processing units*, Advances in Engineering Software 43, p.p. 65-70, 2012.
- [6] Zhu, W., Lee, Y.S.: *Dexel-based force-torque rendering and volume updating for 5-DOF haptic product prototyping and virtual sculpting*, Computers in Industry 55, p.p. 125-145, 2004.
- [7] Leu, M. C., Peng, X., Zhang, W.: *Surface Reconstruction for Interactive Modeling of Freeform Solids by Virtual Sculpting*, Annals of CIRP, 54/1, p.p. 131-134, 2005.
- [8] Peng, X., Zhang, W.: *A Virtual Sculpting System Based on Triple Dexel Models with Haptics*, Computer-Aided Design & Applications, 6(5), p.p. 645-659, 2009.
- [9] Milojevic, Z., Navalusic, S., Zeljkovic, M., Tabakovic, S., Vicevic, M., Beju, L.: *Sculpting system based on the dexel approach*, International Conference on Manufacturing Science and Education - MSE2013, p.p. 3-6, Sibiu, Romania, 2013.
- [10] Everitt, C.: *Interactive order-independent transparency*, White paper, nVIDIA 2.6, 2001.

In this paper some results of the project: CONTEMPORARY APPROACHES TO THE DEVELOPMENT OF SPECIAL SOLUTIONS RELATED TO BEARING SUPPORTS IN MECHANICAL ENGINEERING AND MEDICAL PROSTHETICS – R 35025, carried out by the Faculty of Technical Sciences, University of Novi Sad, Serbia, are presented. The project is supported by the Ministry of science and technological development of the Republic of Serbia.

Authors: Assoc. Prof. dr Zoran Milojevi , Assoc. Prof. dr Slobodan Tabakovi , Assist. MSc. Mirjana Bojani , Full Prof. dr Milan Zeljkovi , University of Novi Sad, Faculty of Technical Sciences, Institute for Production Engineering, Trg Dositeja Obradovica 6, 21000 Novi Sad, Serbia, Phone.: +381 21 450-366, Fax: +381 21 454-495.

E-mail: zormil@uns.ac.rs; tabak@uns.ac.rs; bojanicm@uns.ac.rs; milanz@uns.ac.rs

Petrović.A, Ivanović.S, Lukić.Lj

GENERATING PARAMETERS FROM THE NC CODE NEEDED FOR DEFINING THE OPTIMAL TOOL PATH

Abstract: CAM packages are able to generate several different tool paths for multi-axis NC machining of one pocket or contour. Using the optimal toolpath a minimum cutting force, the maximum dynamic stability of the process and minimum tool wear are achieved or some other technological requirements are met. To determine the optimum tool path it is necessary to establish analytical dependence between optimization criteria and machining elements that are determined by specific tool path. In the NC program the basic technological, kinematic and geometric data are contained but not the elements that depend on the tool path, such as cutting depth, width of cut and engagement angle of the cutting tool. This paper presents a NC code transformation methodology and generation of tool path parameters necessary for calculating all elements of contour milling machining process.

Key words: milling, tool path, NC code transformation

1. INTRODUCTION

Most of mechanical parts consist of faces parallel or normal to a single plane and free form objects require a 2.5D rough milling operation of the raw work piece, making 2.5 D pocketing one of the most important milling operations [1]. Using CAM programs for creating tool path for pocket milling, technology designers faces some choices which determine the final shape of tool path. Fig. 1. shows an example of different tool paths generated with the same CAM program for pocket machining.

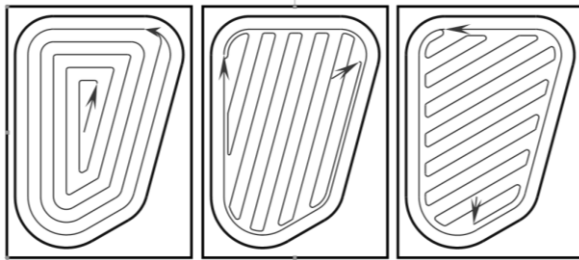


Fig.1. Examples of typical tool paths generated by CAM program

Using the optimal toolpath a minimum cutting force, the maximum dynamic stability of the process and minimum tool wear are achieved or some other technological requirements are met.

The NC program contains basic technological data (specified speed and feed rate), kinematic and geometric data (mode of tool movement and coordinates of points on the tool path). However, cutting process elements, such as engagement angle, depth and width of cut are not contained in the NC programs. Knowledge of these machining elements along the tool path is necessary for checking the adequacy of the generated tool paths from different aspects.

Required elements of the cutting process can be calculated if, in addition to data contained in the generated NC programs, geometric characteristics of blank and geometric and technological characteristics of the tool are defined.

In this paper, NC code transformation methodology and generation of tool path parameters necessary for calculating all elements of contour milling process is presented.

2. NC PROGRAM DATA ANALYSIS

In order to create tool paths database for a given NC programs, transformation of technological, kinematic and geometric tool path data contained in the NC programs into database tables is needed.

3.1 Tehnological data

Used tool data are determined according to NC program blocks which contain program word beginning with T and contain function M06.

$$a_{obr} = f('T'), 'T' \in b_i^{NC}, 'M06' \in b_i^{NC}$$

$$i_1 = i, 'M06' \in b_i^{NC}$$

$$i_0 = i - 1, 'M06' \in b_i^{NC} \quad (1)$$

$$i_0 = i, f(m) \in b_i^{NC}, f(m) = \{M00, M19, M30\}$$

where:

$f('T')$ - is evaluation of tool no.

Value of spindle speed n_{obr} or value of cutting feed s_{obr} is determined according to NC program blocks which contain program word beginning with S or with F [2]:

$$n_{obr} = f('S'), 'S' \in b_i^{NC} \quad (2)$$

$$s_{obr} = f('F'), 'F' \in b_i^{NC} \quad (3)$$

where:

- $f('S')$ is evaluation of spindle speed

- $f('F')$ is evaluation of cutting feed

Spindle speed is changing value in program blocks which contain M-functions:

$$n = \begin{cases} n_{obr}, f(m) \exists b_i^{NC}, i_1 = i, f(m) = \{M03, M04\} \\ 0, f(m) \exists b_i^{NC}, i_0 = i, f(m) = \{M00, M30\} \\ 0, f(m) \exists b_i^{NC}, i_0 = i+1, f(m) = \{M05\} \end{cases} \quad (4)$$

Cutting feed is changing value in program blocks that contain G-functions:

$$s_g = \begin{cases} s_{obr}, f(g) \exists b_i^{NC}, \\ f(g) = \{G01 - G03, G81, G82, \dots\} \\ 0, f(g) \exists b_i^{NC}, f(g) = \{G00, G80\} \end{cases} \quad (5)$$

3.2 Kinematic and geometric data

Kinematic and geometric data, based on coordinates given in current and previous block, are calculated in absolute coordinates for each program block:

x_1, y_1, z_1 - coordinates of start point,

x_2, y_2, z_2 - coordinates of end point,

for functions G00, G01, G02, G03, G81, G82, ..., G89, G98 and G99 (Table 1);

for G90	for G91
$x = \begin{cases} f('X'), 'X' \in b_i^{NC} \\ x_1, 'X' \notin b_i^{NC} \end{cases}$	$x = \begin{cases} f('X'), 'X' \in b_i^{NC} \\ 0, 'X' \notin b_i^{NC} \end{cases}$
$y = \begin{cases} f('Y'), 'Y' \in b_i^{NC} \\ y_1, 'Y' \notin b_i^{NC} \end{cases}$	$y = \begin{cases} f('Y'), 'Y' \in b_i^{NC} \\ 0, 'Y' \notin b_i^{NC} \end{cases}$
$z = \begin{cases} f('Z'), 'Z' \in b_i^{NC} \\ z_1, 'Z' \notin b_i^{NC} \end{cases}$	$z = \begin{cases} f('Z'), 'Z' \in b_i^{NC} \\ 0, 'Z' \notin b_i^{NC} \end{cases}$
$x_2 = x; \quad y_2 = y; \quad z_2 = z$	$x_2 = x_1 + x; \quad y_2 = y_1 + y; \quad z_2 = z_1 - z$
<p>where:</p> <p>x, y, z - are coordinates given in current block;</p> <p>$f('X'), f('Y'), f('Z')$ - is coordinate evaluation according to G20 and G21</p> <p>$f(g) = \{G00, G01\}$</p>	

Table 1 - Coordinates for functions G00 and G01

and:

x_c, y_c, z_c - circular interpolation center coordinates,

r - circular interpolation radius,

α_0 - circular interpolation start angle,

α - circular interpolation angle,

for functions: G02 and G03.

Calculation of circular interpolation parameters for given interpolation center coordinates, for one case is presented in Table 2.

for G02 and G17	for G03 and G17
$i = \begin{cases} f('I'), 'I' \in b_i^{NC} \\ 0, 'I' \notin b_i^{NC} \end{cases}; \quad j = \begin{cases} f('J'), 'J' \in b_i^{NC} \\ 0, 'J' \notin b_i^{NC} \end{cases};$ $r = \sqrt{i^2 + j^2}$	
$x_c = x_1 + i; \quad y_c = y_1 + j; \quad \alpha_0 = \left \arctg \left(\frac{y_1 - y_c}{x_1 - x_c} \right) \right $ $\alpha_0 = \begin{cases} \alpha_0, y_1 - y_c \geq 0 \wedge x_1 - x_c \geq 0 \\ 180 - \alpha_0, y_1 - y_c \geq 0 \wedge x_1 - x_c < 0 \\ 180 + \alpha_0, y_1 - y_c < 0 \wedge x_1 - x_c < 0 \\ 360 - \alpha_0, y_1 - y_c < 0 \wedge x_1 - x_c \geq 0 \end{cases}$ $\alpha_1 = \left \arctg \left(\frac{y_2 - y_c}{x_2 - x_c} \right) \right $ $\alpha_1 = \begin{cases} \alpha_1, y_2 - y_c \geq 0 \wedge x_2 - x_c \geq 0 \\ 180 - \alpha_1, y_2 - y_c \geq 0 \wedge x_2 - x_c < 0 \\ 180 + \alpha_1, y_2 - y_c < 0 \wedge x_2 - x_c < 0 \\ 360 - \alpha_1, y_2 - y_c < 0 \wedge x_2 - x_c \geq 0 \end{cases}$	

Table 2. - Circular interpolation parameters (r, α_0, α) for given interpolation center coordinates x_c, y_c, z_c

If circular interpolation is defined by its radius r , interpolation center coordinates x_c, y_c, z_c , circular interpolation angle α and start angle α_0 have to be calculated. Generally, for given coordinates x_1, y_1, z_1 and x_2, y_2, z_2 and radius r for same type of circular interpolation, there are two possible tool paths (circular arcs corresponding two different center points presented at Fig.2a). For determination of circular interpolation center coordinates x_c, y_c, z_c , rhombus with side r and diagonal corresponding arc chord t is observed (Fig.2b).

For circular interpolations G02 and G03, sign of radius r , and thereby arc center coordinates, is determined by

arc of interpolation (Table 3).

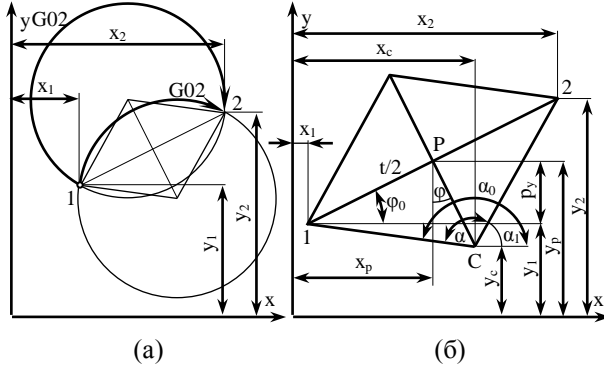


Figure 2. Determination of circular interpolation center coordinates x_c, y_c, z_c ,

Circular interpolation radius r in NC program is positive ($r > 0$) for angle $\alpha \leq 180^\circ$, and negative for angle $180^\circ < \alpha \leq 360^\circ$.

In Table 3, one case of determination of circular interpolation center coordinates is presented.

Case: G17; G02, $r > 0$ and G17; G03, $r < 0$	
$0 \leq \varphi \leq 90^\circ, \varphi = \varphi_0$ $x_c = x_p + p_x; y_c = y_p - p_y$	$90^\circ < \varphi \leq 180^\circ; \varphi = 180 - \varphi_0$ $x_c = x_p + p_x; y_c = y_p + p_y$
$180^\circ < \varphi \leq 270^\circ; \varphi = 180 + \varphi_0$ $x_c = x_p - p_x; y_c = y_p + p_y$	$270^\circ < \varphi < 360^\circ; \varphi = 360 - \varphi_0$ $x_c = x_p - p_x; y_c = y_p - p_y$

Table 3. Circular interpolation center coordinates

By introducing the coefficients:

$$k_g = \begin{cases} 1, & \text{for G02} \\ -1, & \text{for G03} \end{cases} \quad (6)$$

and

$$k_r = \begin{cases} 1, & r > 0 \\ -1, & r < 0 \end{cases} \quad (7)$$

circular interpolation center coordinates x_c, y_c, z_c , are calculated (for G17):

$$\begin{aligned} x_c &= x_p + k_g \cdot k_r \cdot p \cdot \sin \varphi \\ y_c &= y_p - k_g \cdot k_r \cdot p \cdot \cos \varphi \end{aligned} \quad (8)$$

Start angle α_0 is determined as (for G17):

$$\alpha_0 = \left| \arctg \left(\frac{y_1 - y_c}{x_1 - x_c} \right) \right| \quad (9)$$

$$\alpha_0 = \begin{cases} \alpha_0, & y_1 - y_c \geq 0 \wedge x_1 - x_c \geq 0 \\ 180 - \alpha_0, & y_1 - y_c \geq 0 \wedge x_1 - x_c < 0 \\ 180 + \alpha_0, & y_1 - y_c < 0 \wedge x_1 - x_c < 0 \\ 360 - \alpha_0, & y_1 - y_c < 0 \wedge x_1 - x_c \geq 0 \end{cases} \quad (10)$$

Angle α is calculated:

$$\alpha = \begin{cases} 2 \cdot \left| \arccos \frac{p}{r} \right|, & k_r = 1 \\ 360 - 2 \cdot \left| \arccos \frac{p}{r} \right|, & k_r = -1 \end{cases}$$

3. USING OF DATA FROM NC PROGRAMS

Every single NC program block b_i^{NC}

N G X Y Z I J K R F S T M

can be transformed into one record of database table with structure shown as [3]:

NCtabel1(N, G, X, Y, Z, ...)																		
N	G	X	Y	Z	I	J	K	R	F	S	T	M	Tool	interpolation	direction	feed rate f	spindle speed s	...
													mm/	o/min				
...	x_1	y_1	z_1	x_2	y_2	z_2	x_c	y_c	z_c	r	α_0	α						
	mm	mm	mm	mm	mm	mm	mm	mm	mm	mm	°	°						

Table 4. Database table record

In every record (row) of table NCtabel1(N, G, X, Y, Z, ...) according to fields obtained by transformation of data from NC program block (G, X, Y, Z, ...) corresponding fields (feed rate, spindle speed, ...) are calculating. According to this table, records in database tables are created with following structures:

NCprogrami(nazivncprg, ...)				
NC program name	no G01	no G02	no G03	no G8x

Table 4. Structure of database table kinematic records

Alati(nazivncprg, oznalncprg,...)						
NC program name	Tool no	Diametar	Number of flutes	Tool life	Cost index	Shape of tool
		mm		min		

Table 5. Structure of database table technological records

Every record of the table [NCprogrami\(nazivncprg,...\)](#) corresponds to one NC program, with addition of fields related to number of interpolations. One record of the table [Alati\(nazivncprg, oznalncprg, ...\)](#) corresponds to one tool, one cutting feed and one spindle speed in one NC program.

Therefore, NC programs placed in ASCII files are transforming into database tables. First, every NC program block converts into corresponding record of NC table, then in accordance with fields obtained by transformation of data from NC program block (G, X, Y, Z, ...) corresponding fields are calculated (Fig. 3).

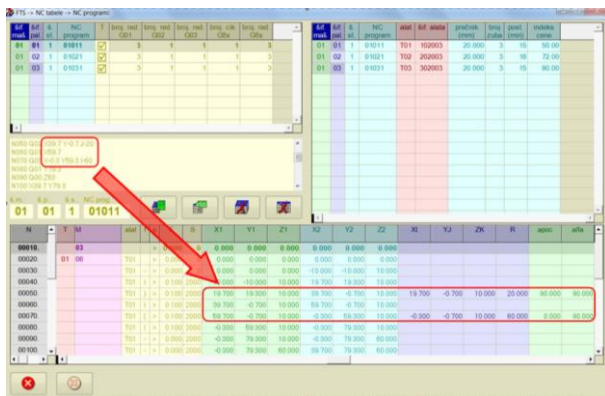


Figure 3. Program blocks transfer and calculation of corresponding fields

For each NC program a single NC database table is created. NC blocks are transferred by decomposition on program words. Firstly, program block no („Nxxxx“) is transferred, and then the block is checked for existence of G function. After G functions, kinematic (X, Y, Z, I, J, K and R) and technological parameters (F and S) are transferred. Then, tool no (T) in tool storage is transferred. Finally, program block is checked for existence of M functions. Based on M functions, tool no (T) is assigned to each record.

4. CONCLUSION

According to the processed data from the NC program and blank geometry, tool path and the cutter location relative to the workpiece can be generated at appropriate spatial intervals along a path, using Matlab program.

The program is developed to track changes in depth and width of the cut and engagement angle along the tool path. On the basis of these variations, cutting force during the milling process can be monitored. Based on the analysis of the cutting force diagram for the different tool paths, a methodology for assessing the tool path and selection of the most appropriate path from the point of minimum cutting force variations can be developed. The analysis can also include other criteria such as tool wear, the total processing time and process stability.

5. REFERENCES

- [1] Dhanik S.: *NC Tool Path Evaluator and Generator for High Speed Milling*, vol. 4533. École Polytechnique Fédérale De Lausanne, Lausanne, Switzerland, p. 201, 2009.
- [2] Ivanović, S. , Lukić Lj.: *Database design from technological and kinematic parameters of NC program for production in flexible manufacturing system*, The Sixth Triennial International Conference Heavy Machinery HM 2008, Mataruška Banja, 26.-29.06.2008.
- [3] Ivanović, S. , Lukić Lj. , Petrović Z.: *Rekonfigurisanje baze podataka fleksibilnog proizvodnog sistema na osnovu parametara iz NC programa*, IMK-14 istraživanje i razvoj- časopis instituta IMK “14. Oktobar “ Kruševac, 28-29, 2008.

Authors: M.Sc. Aleksandra Petrović¹, dr Slobodan Ivanović², Prof. dr Ljubomir Lukić¹

¹Faculty of Mechanical and Civil Engineering in Kraljevo, University of Kragujevac, Dositejeva 19, 36000 Kraljevo, Serbia, Phone: +381 36 383-269

² High technical mechanical school Trstenik, Radoja Krstića 19, 37240 Trstenik, Serbia, Phone:+381 714-121

E-mail: petrovic.a@mfkv.rs;
slobodan.ivanovic@vtmsts.edu.rs;
lukic.lj@mfkv.rs;

Živanovi , S., Kokotovi , B., Jakovljevi , Ž.

TURNING MACHINE SIMULATION FOR PROGRAM VERIFICATION

Abstract: In this paper we discuss the possibilities of application of turning machine simulation and verification of the program before machining. We present the process of new virtual lathes configuring for machine simulation in CAD/CAM environment. Configured virtual lathe is used for the verification of tool path as a part of the off-line programming system, using machine simulation in the CAD/CAM environment. The implementation of developed virtual machine and simulation is presented using a workpiece example. For this test part we have verified machining program using the material removal simulation, and carried out real world machining.

Key words: CAD/CAM, turning machine simulation, program verification

1. INTRODUCTION

Nowadays, machining simulation plays an important role in manufacturing. Machine simulation is the safest and the most cost-effective way to verify tool paths. There are many benefits of machine simulation, and one of the most important is safe and time unlimited testing of machining program. Crashing machine on the computer screen is not a big problem, whereas crashing a real machine is catastrophic [1]. Configuring a virtual machine tool is a complex task which involves the use of huge spectra of methods, models, virtual prototypes, components, and simulations [2].

Machine simulation is an indispensable tool during programming of machines. It gives enormous possibilities in alternatives' testing and enables generation of not only accurate, but also most effective programs. Different cutting strategies, tools and fixtures can be tested in development phase until optimal solution is achieved. All of this is carried out off line on virtual machine, at computer desk, while the current job is in progress on real world machine. Thus, machine simulation is not used only to find errors in the code [1]. It offers many advantages:

- Programming errors are detected immediately.
- During program simulation actual machining time is calculated, and production effort can be estimated more easily.
- Collision checking with actual tools, tool holders and fixtures and machine geometries.
- Workpiece can be programmed and optimized while the current production process on the machine is in progress; developed program can be implemented on the machine immediately.
- Shorter setup times.
- Can be used for training and education.
- New machines can be programmed without any risk.

Program verification process includes the following simulations: toolpath simulation, machine simulation and material removal simulation.

Verification can be carried out based on the CLF (Cutter Location file) or based on the G code.

In this paper we describe the methodology for program verification on lathes. This methodology is implemented on the lathe TCN410-echoENG (Fig.1) for verification of tool path as a part of the off-line programming system, using machine simulation in the CAD/CAM environment.



Fig. 1. TCN410 CNC lathe – (echoENG)

Using basic modules and other components, such as CAD data for the real machine, the machine manufacturer or CAM system manufacturer can create a virtual machine that looks like the real machine as closely as possible [1]. On the other hand, when virtual machine is not provided by manufacturers, the user can develop virtual machine himself, as will be presented in this paper.

The rest of the paper is organized as follows. In Section 2, methodology for program verification on CNC lathes is proposed. Section 3 presents turning machine simulation. In Section 4, one workpiece is machined to experimentally verify the methodology for turning simulation, program verification and configured postprocessor.

2. METHODOLOGY FOR PROGRAM VERIFICATION ON LATHES

Methodology for program verification on lathes will be described using IDEF0 diagrams. IDEF0 is a method designed to model the decisions, actions, and activities of an organization or a system. It is useful in establishing the scope of an analysis, especially for a

functional analysis [3].

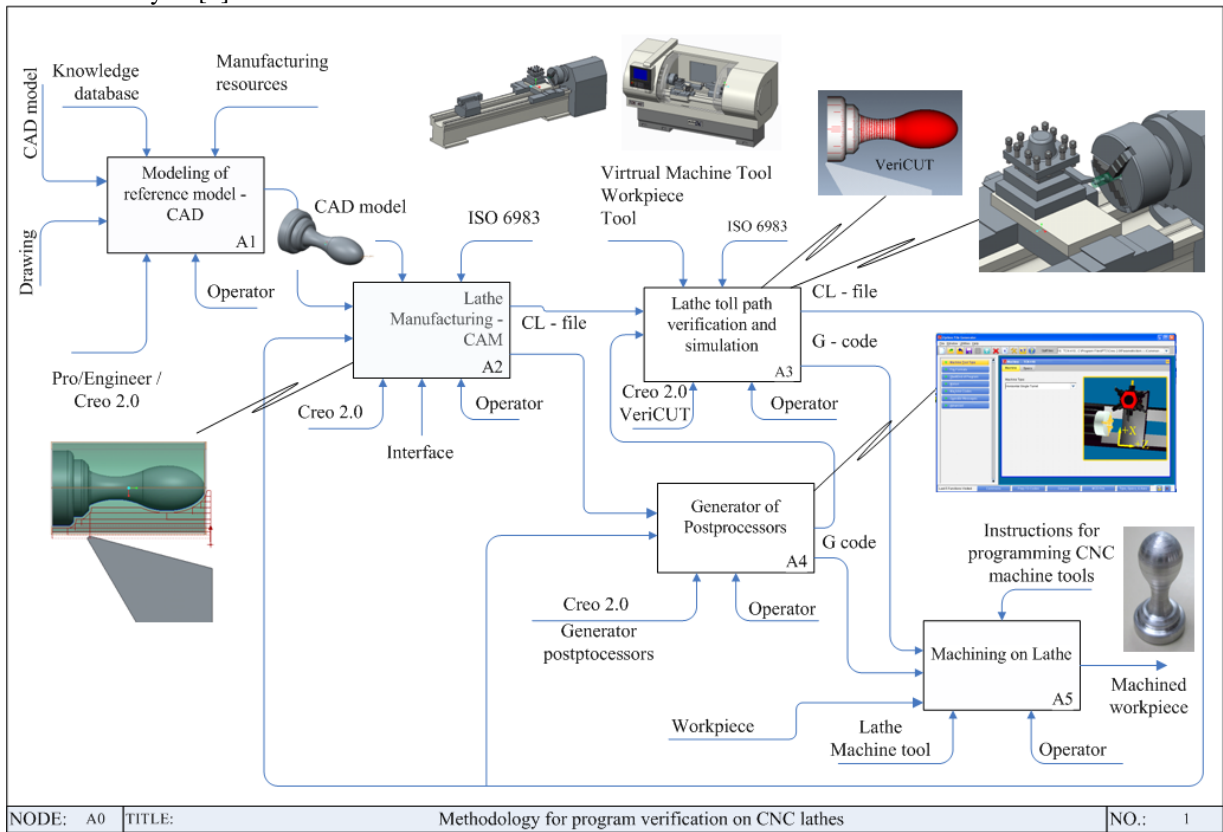


Fig. 2. Basic flow of activities for methodology for program verification on CNC lathes

IDEF0 is used to produce a "function model". The function model is a structured representation of the functions, activities, or processes within the modeled system or subject area. This paper describes the function of turning machine simulation for program verification, using the IDEF0 diagram. Inputs for this methodology can be drawings or CAD model, while the output is machined workpiece. Based on these inputs, preparing reference models for the off-line programming, tool path, and G code are obtained. Verification of G code is carried out by using toolpath simulation, material removal simulation, and machine simulation. Lathe is programmed in G code according to the standard ISO6983.

IDEF0 diagram presented in Figure 2 describes the basic flow of activities (methodology) for program verification on lathes (Fig. 2). The basic activities are: A1 - CAD, A2 - CAM, A3 - Postprocessors, A4 - Tool path verification, and simulation and A5 - Machining. Input for activity A1 is drawing or CAD model that creates reference model for activity A2 (CAM). When the output from activity A2 is obtained (CL-file), it is verified within activity A3 using tool path simulation, material removal simulation and machine simulation. If some errors and collision are identified during the simulation, the activity A2 repeats until CL file is verified. Verified CL-file is an input for the postprocessing activity in the A4. Postprocessor is configured using the postprocessor generator in the CAD/CAM system Creo [4]. In our case study we used 2-Axis Lathe. Obtained G code can be forwarded to the activity A3 to verify the tool path or can be forwarded directly to the machine. After verification of the

program in G code, we can safely pass over to the activity A5, where the machining is achieved on CNC lathe, without additional testing that exists on the machine.

3. TURNING MACHINE SIMULATION

Machine simulation by running the program is possible due to the application of machine mechanism modelling with all kinematic connections between components. That allows the motion of virtual model as a system of rigid bodies. Figure 3 shows a detailed virtual model of lathe mechanism with all kinematic relationships between moving components being defined. Slider connection is used for the movement of two sliders (Apron-Z and cross slide-X).

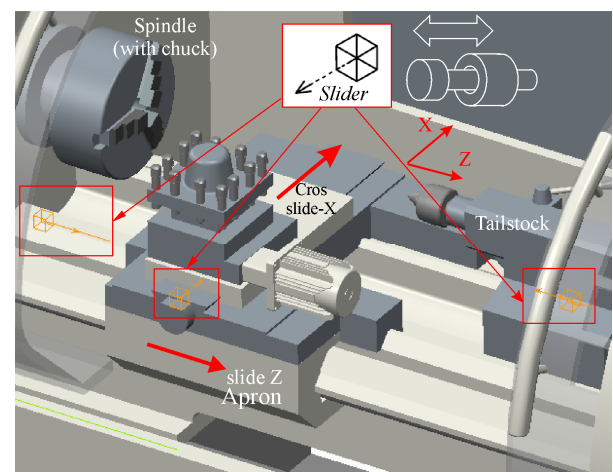


Fig. 3. CNC Lathe machine simulation

Such assembly enables the motion of the model in the range defined for each connection. It has the particular importance for the identification of possible collisions during the operation of the mechanism. Machining simulation of virtual model allows motion of movable segments, with the tool at the tool post.

On the screen, one can see the tool path which is a result of the execution program, created by programming using PTC Creo CAD/CAM system [4]. First of all, it is necessary to prepare a Reference CAD model of the workpiece (Fig. 4), which is used to verify off-line programming system for 2-axis CNC lathe.

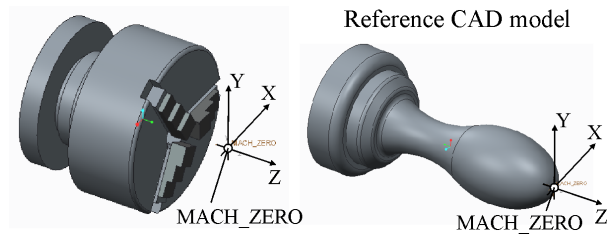


Fig. 4. Coordinate system MACH_ZERO

The identical zero point (MACH_ZERO) exists on the lathe (on spindle with chuck) and on workpiece (Fig.4). Matching of these two coordinate systems is done by setting the workpiece on the machine during the machining simulation.

Tool coordinate systems, on the machine, are marked as a TOOL_POINT. Matching of the tool coordinate system on the tool and on the machine (Tool post), results in setting of the tool into the tool post during the simulation process. Successful simulation is possible if the kinematic connections are correctly defined, as shown in Fig. 3.

After the programming completion, verification of the CL-file is achieved by simulating the tool path, Fig.5.

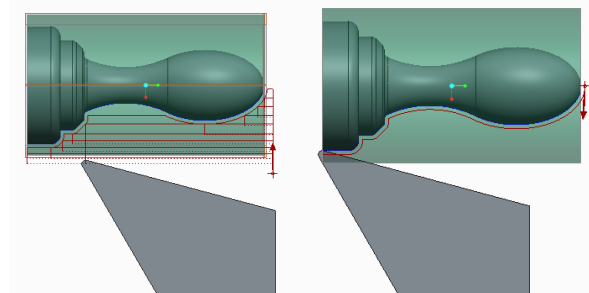


Fig. 5 .Tool path for turning

The TCN410 CNC lathe (echoENG) which is installed at Faculty of Mechanical Engineering in Belgrade, is used for programming and experiment. This lathe is fully modeled in CAD/CAM environment (PTC Creo), with all kinematics joints, in order to be able to include virtual machine model into machining simulation (Fig. 6). During the tool path simulation, complete CAD model of virtual machine can be included into the simulation, with Machine play option, in PTC Creo CAD/CAM system. The completed tool path simulation can be simulated by using rendered solid model of the machine, including fixtures and workpiece. Example of verification by machining

simulation is shown in Fig. 7.

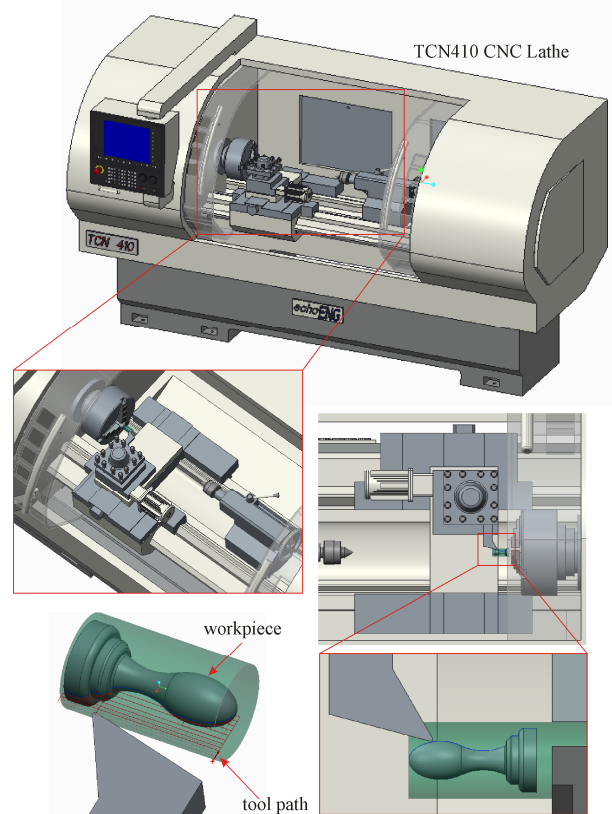


Fig.6. Turning Machine simulation

CAD/CAM system enables: toolpath simulation (Fig.5), machine simulation (Fig.6) and material removal simulation – NC Check [5] (Fig. 7).

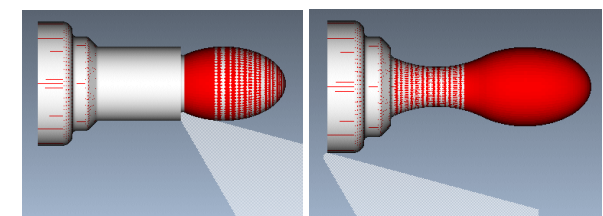


Fig. 7. NC-Check-material removal simulation

After the simulation process is completed, the postprocessing follows. The postprocessor is configured for the TCN410 CNC lathe by using the postprocessor generator from the PTC Creo CAD/CAM system (Fig. 8).

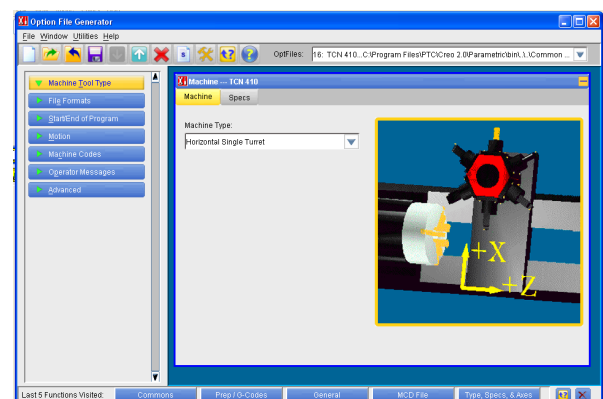


Fig.8. Postprocessor configuring

4. MACHINING TEST

To verify methodology for turning simulation, program verification, and configured postprocessor, we have machined one example of workpiece. Figure 9 presents a screen view of tool path verification on Simens Simumerik 808D control unit. After this final verification we can start safely with program execution on CNC lathe.

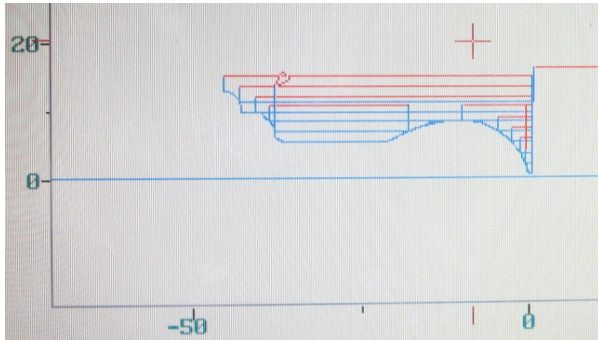


Fig. 9. Program simulation on Simens Sinumerik 808D

The workpiece from Fig. 4, is machined on the TCN410 CNC lathe and it is presented in Fig. 10.

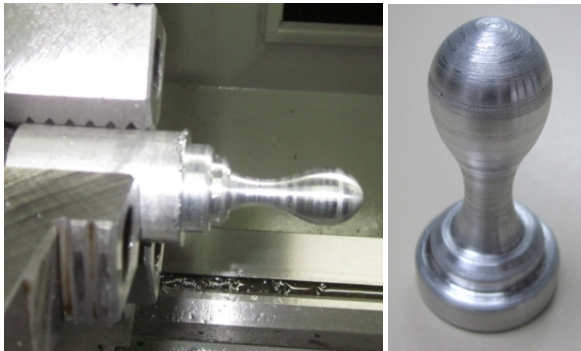


Fig. 10. Machined workpiece

This experiment confirmed that the proposed methodology for program verification which includes all kinds of simulation and configured postprocessor can be directly used by CNC programmers and operators. This is only one of the research challenges in order to realize a fully digitized model of the machine tool.

5. CONCLUSION

This paper presents a methodology for successful establishing of virtual machining environment for off-line programming within a CAD/CAM system that enables tool path simulation, material removal simulation, and machine simulation including the movement of machine parts. Chosen environment that fully meets all requirements is PTC Creo.

At present, machining simulation plays an important role in manufacturing, and this paper presents an integration of the off-line programming and machine simulation in CAD/CAM system Creo. Program verification is established by machining simulation in CAD/CAM system, where the machine

model is working by the running program.

Off-line programming and simulation is very important for increasing the quality level of programming and program verification for CNC lathe.

Off-line programming allows multiple part program verifications, and after such verification part program can be immediately executed on the machine. Further research needs to be related to the applicability of the new method of programming known as STEP-NC [6], for CNC lathes.

Acknowledgements. The authors would like to thank the Ministry of Education and Science of the Republic of Serbia for providing financial support that made this work possible.

6. REFERENCES

- [1] Apro, K.: *Secrets of 5-axis machining*. Industrial Press Inc., New York, Printed by Thomson Press India Limited, 2008.
- [2] Altintas C., Brecher M., Weck M., Witt S.: *Virtual machine tool*, CIRP Annals-Manufacturing Technology, vol. 54, No.2, p.p. 115-138, 2005.
- [3] Kim, S.H., Jang, K.J.: *Designing performance analysis and IDEF0 for enterprise modelling in BPR*, International Journal of Production Economics, vol. 76, No.2, p.p. 121-133, 2002.
- [4] PTC Creo, from, <http://creo.ptc.com>, accessed on April 2013
- [5] VeriCUT, from <http://www.cgtech.com>, accessed on March 2015
- [6] Zhang, X., Liu, R., Nassehi, A., Newman, S.T.: *A STEP-compliant process planning system for CNC turning operations*, Robotics and Computer-Integrated Manufacturing, vol. 27, p.p. 349-356, 2011.

Authors: Assistant Professor Sasa Zivanovic, Assistant Professor Branko Kokotovic, Assistant Professor Zivana Jakovljevic, University of Belgrade, Faculty of Mechanical Engineering, Production Engineering Department,, Kraljice Marije 16, 11120 Belgrade, Serbia, Phone.: +381 11 3302-423, Fax: +381 11 3370-364.

E-mail: szivanovic@mas.bg.ac.rs
bkokotovic@mas.bg.ac.rs
zjakovljevic@mas.bg.ac.rs

12th INTERNATIONAL SCIENTIFIC CONFERENCE MMA 2015 -
FLEXIBLE TECHNOLOGIES

PROCEEDINGS



Section E:

**OTHER PRODUCTION ENGINEERING
TECHNOLOGIES – METAL FORMING
TECHNOLOGIES**

Novi Sad, 25-26 September 2015

Stefanovi , M., Gulišija, Z., Mihailovi , M., Mandi , V., Patari , A.

THE IMPORTANCE OF TRIBO-MODELING IN DEVELOPMENT OF HOT FORGING TECHNOLOGY

Abstract: *The significance of contact friction in hot metal forming processes is very known. The general approach in this area involves the recognition of the influence of the main tribological parameters - pressure, speed and temperature in forming processes. The developed methods are very different for physical modeling of tribological phenomena and influence in a very specific types of metal forming. These methods basically have the appropriate physical model, which imitates local area or a complete work piece in metal forming. The indicators of models can be very different: coefficient of friction, forming limit parameters, temperature distribution, tool wear, etc. This paper gives a review of physical tribo models in hot forging and shows analyzes of models, according to their characteristics and limitations, and describe the high research opportunities of models.*

Keywords: *Metal forming, contact friction, tribo model, hot forging*

1. INTRODUCTION

Modern plastic forming technology is characterized by the production of parts of small mass, high productivity and low cost. Metal forming (MF) process depends on many factors, such as material properties, the structure of the system workpiece / tool, strain rate, the operating pressure and temperature. In addition to these factors, the friction is very important and it affects the forming force, energy consumption and limit deformability, accuracy of design, piece surface quality and tool life.

Tribological system in MF is very complex and it consists of interactive components. The friction between the tool and the piece depends on the various parameters [1,2]:

- Mechanical parameters, such as contact pressure, plastic deformation, strain rate, sliding speed, yield stress of materials,
- Physical parameters such as roughness, temperature, lubricants viscosity, lubricant film thickness,
- Chemical parameters, such as the presence of oxide on contact surfaces, surface energy, types of chemical bonds of lubricants and metal etc.

Friction at MF is highly nonlinear phenomenon that is related to (interacts with) many forming parameters. The following characteristics of friction have a significant and complex influence on the quality of the piece:

- The process of deformation and deformation forces depend on the friction forces and vice versa.
- The friction is generated in the high-pressure conditions, where the pressure is higher than the yield limit in the contact-layer (interface) in many cases.
- Friction is generated at high temperature, where lubricating film has a key role.

- New metal surfaces that appear during forming change with time.

The current development of tribology in MF can be described as progress in:

- Friction tests in MF,
- Characterization of friction,
- Models of friction,
- Controlling and optimization of friction.

Development of suitable friction tests explains the nature of the frictional contact of pieces and tools, optimizes tribological conditions and raises formability.

In general, there are two categories of tribo tests - direct and simulation procedures. All of these methods have their qualities and limitations. In direct tests normal pressure and tangential stress are measured by the sensors which are implanted in the surface of the tool, during real time of processing operations. The method is limited by the sensitivity of the sensor and the selection of measuring points, as well as by the cost of installation.

In the simulation tests in laboratory conditions the loading conditions are different, with mainly the limitations of kinematic conditions. The essential reason for the further development of tribological model is the need for a more complete optimization and controlling of friction in the manufacturing process

Tribometers, as special devices, are used for optimization of technological processes. They are used in the analysis of the phenomenon of friction, wear and lubrication influence in defined tribological conditions. Increase of the efficiency of work processes, achievement of the limit possibilities of process, longer tool life and enhancement of environmental elements are typical goals.

Fig. 1. shows the potential contribution and possibilities of tribo - testing in optimizing the forming process - necessity for tribological tests [3].

Results of tribological investigations are often used for determining the certain parameters in analytical description of the laws of friction and wear. Such data are essential in numerical simulation of the processing.

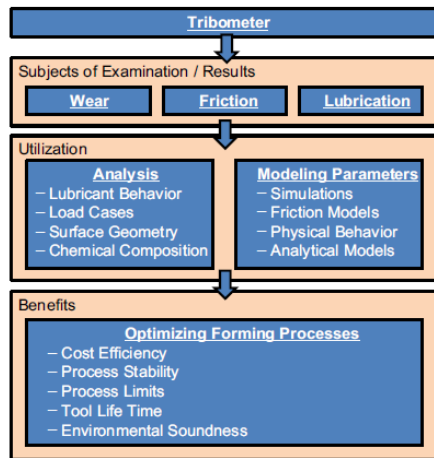


Fig. 1. Necessity for tribological tests [3]

2. TRIBOLOGICAL MODELS IN HOT BULK METAL FORMING

Unlike cold metal forming, tribological modeling in hot operations is complex and more difficult. In this area, friction, heat transfer, lubricants, wear and damage to the tool are of great importance. This is an area of tribology with many opportunities for researchers. In research it is necessary to perform laboratory tests for tribo-simulation, computer modeling and industrial experiments. The interface between tools and materials is crucial for friction and heat transfer. Contact between cold tool and warm piece always leads to complex tribological thermal phenomena. The concluding result must contain a complete description of the interfaces between tools and materials including friction, heat transfer, lubrication and tool damage mechanism.

Final characteristics of the working piece, like dimension, shape, surface quality and structure, depend on system parameters values. Special role in tribological system, in forging, has the lubricant. Fig. 2. show the global approach to hot forging modeling, with specific evaluation on lubricant within the tribological system [4].

During forming the heated material flows over the tool surface, so the tool life is directly dependent on the friction wear intensity in contact. In hot forging, the tool life is limited by the amount of mechanical and thermal strains, where the type of the engraving damage is very different.

Compressing of the ring between flat plates is applied in the area of hot processing. One of the most important tasks in the field of MF tribology in the hot state, as mentioned, is the optimal selection of lubricants.

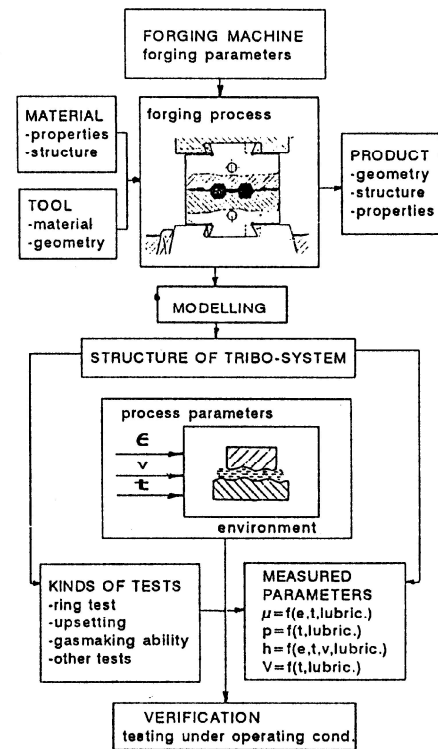


Fig. 2. Hot forging process modeling [4]

The accuracy of the piece, extended tool life and the environment preservation must be provided. Replacement of lubricant based on graphite (code B) with lubricants without graphite (code W) is an old and important task. For this purpose, the most commonly used lubricants are those based on glass, which have a low melting point. Fig. 3. shows the chart of ring compression test at a temperature of forging, with information about the experiment. Fig. 4 and Fig.5. shows the values of the coefficient of friction for different experimental conditions [5].

Ring billet	0.45% carbon steel , 1060°C-1120°C
Original height: inside diameter: out side dia. = 10:15:30	
Dies	SKH51 (Q.T.) , R.T.
Lubricants	Graphite, Non-graphite
Presses	Mechanical press, Hydraulic press
Reduction in height	40% - 49%

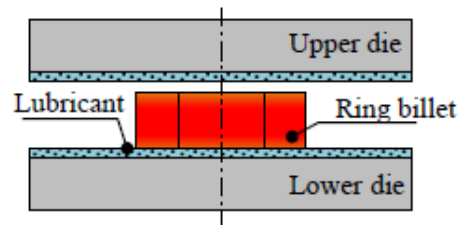


Fig. 3. Setup of ring compression test and testing conditions [5]

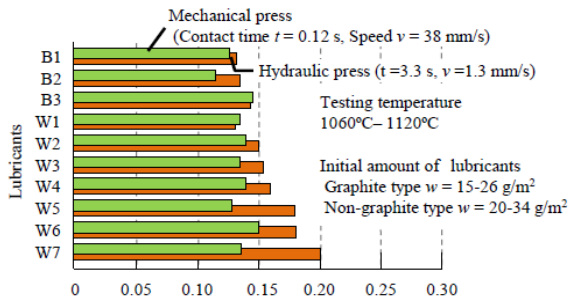


Fig. 4 Coulomb's frictional coefficient by ring compression test [5]

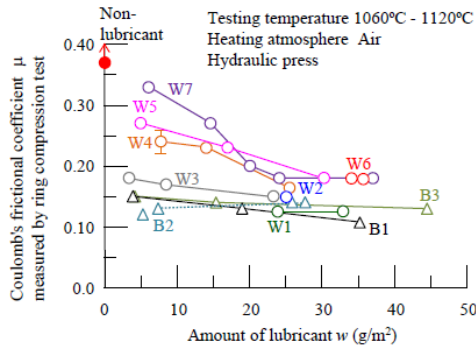


Fig. 5 Influence of amount of lubricants on frictional coefficient [5]

The paper [6] presents a new tribo-test for investigation in the hot state, similar to the test described in the section for the modeling of cold treatment, called Worm and Hot Upsetting Sliding Test (WHUST), Fig. 6. Contactor, which plays the role of tools, can be heated up to 300°C, a specimen can be heated up to 1200°C. The mechanical parameters of the contact at modeling (contact pressure, strain, strain rate, sliding velocity) are adjusted using the test parameters (penetration, geometry of the contactor). Fig.7 shows the change of the coefficient of friction when using different lubricants for hot processing. When using lubricant WL2 on sliding length of 18 mm, the first crack occurs on the surface of the specimens. Limitations of the model, in terms of physical modeling, are related to the small surface area of contact and the nature of sliding in the contact interface.

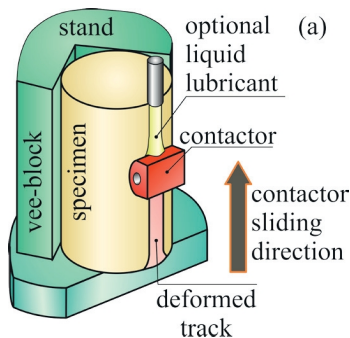


Fig. 6. Schematic view of the WHUST (a), unused contactor (b) and worn contactor (c) [6]

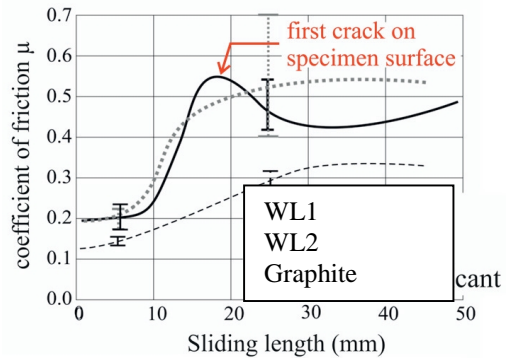


Fig. 7. Coefficient of friction vs sliding length for two white lubricants [6]

The model in Fig. 8 corresponds to conventional tribo-tests, type of block-end disc. According [7], model is used to explore the phenomenon of friction during hot extrusion of aluminum. Heating temperature of the tested material - disk of tribometer is 250-350 °C. The load is 40 N, and sliding speeds of 0.1 m/s. Change of friction coefficient depends significantly from coatings on tool - block tribometer, Fig. 8.b).

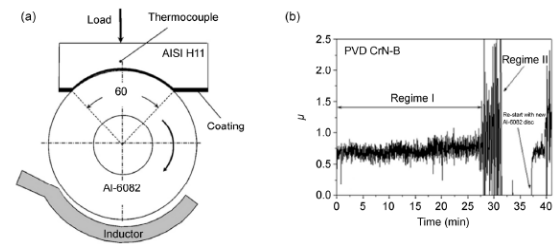


Fig. 8. Block-on-disc test (a); diagram of friction coefficient during the test (b) [7]

Model in Fig. 9 belong to the group of rotational forging tests [7]. Used in tribo - research in the field of hot forging of aluminum at a temperature 250 - 450 °C. In this test specimen is fixed on a rotary disc, compressed by the tool. Friction torque was measured, and calculates the coefficient of friction. The results of lubricants tests for hot forging are shown in Fig.10.c).

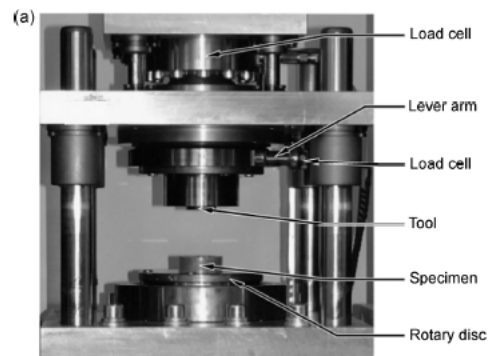


Fig.9. The rotational forging tribometer [7]

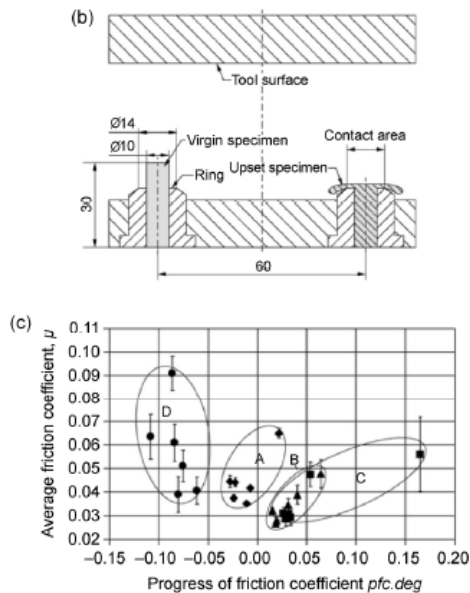


Fig.10. Schematic of the experiment (b), average friction coefficients of lubricants (A, B, C, and D represent different lubricants) (c) [7]

3. CONCLUSION

Tribo system in MF can vary highly from one operation to the other. Chemical, mechanical and micro-structural characteristics of tribo system are very different in hot, warm and cold MF. There are different sliding speeds, contact pressures and temperatures, stress strain states etc. Full modeling of real tribo-conditions in the realization of laboratory tests is usually impossible. The laws of similarity of physical process modeling with recognized limitations and the corresponding results must be complied with.

Unlike the tribology research at cold treatment, for which there are a number of tribometers, hot processing have only a few tribometers. The research of the tribologic influence in metal forming at elevated temperatures is difficult due to the complex nature of thermal and micro structural interaction, and process parameters. Experimental studies are the basic way of study in this area and are a significant part of the development technology of hot forging.

The current development of tribology in MF can be described as progress in the ongoing development of friction tests in the MF, the characterization of friction, friction models, controlling and optimization of friction.

REFERENCES

- [1] Wang D., Yang H., Heng L. *Advance and trend of friction study in plastic forming*, Trans. Nonferrous Met. Soc. China, Vol.24(2014), p.263–1272.
- [2] Stefanovi M., Adamovi D., Gulišija, Z., Aleksandrovi S., Mandi V., Milovanovi M., *Limitations of physical tribo-modeling in metal forming processes*, 12. Intern. Conf. on Accomplishments in Electrical and Mechanical

Eng. and Inf. Technology, DEMI 2015, Banja Luka, Proceed. , pp. 111-118.

- [3] Groche P., Müller C., Stahlmann J., Zan S. *Mechanical conditions in bulk etal forming tribometers—Part one*, Tribology International, Volume 62(2013), p. 223-231.
- [4] Stefanovi M., Stankovi R. *Importance of Tribological Investigations in Hot forging*, YUTRIB 1995, Forth Yugoslav Tribological Conference, Herceg Novi, Proceed., p. 181-182.
- [5] Kazuhito A., Kazuhiko K. *Estimation of frictional property of lubricants for hot forging of steel using low-speed ring compression test*, Procedia Engineering, Vol. 81 (2014), p. 1970 – 1975.
- [6] Dubois A., Dubar M., Dubar L. *Warm and hot upsetting sliding test: tribology of metal processes at high temperature*, Procedia Engineering, Vol. 81(2014), p. 1964 – 1969.
- [7] Dohda K., Boher C., Reyai-Aria F., Mahayotsanun N., *Tribology in metal forming at elevated temperatures.*, Friction 3(1)(2015), 1–27.

Acknowledgement: This paper is a part of the investigation within the project TR 34002 financed by Serbian Ministry of Science and Technological Development.

Authors: Prof. dr Milentije Stefanovi , Faculty of Engineering University of Kragujevac, Serbia, S.Janji 6, 34000 Kragujevac, +381 34 336001, Prof. dr Zvonko Gulišija, ITNMS, Serbia, Franša d Eperea 86, 11000 Beograd, +381 11 3691722, mr Marija Mihailovi , ITNMS, Prof. dr Vesna Mandi , Faculty of Engineering University of Kragujevac, mr Aleksandra Patari , ITNMS.

stefan@kg.ac.rs; zgulisija@itnms.ac.rs;
m.mihailovic@itnms.ac.rs; mandic@kg.ac.rs;
a.pataric@itnms.ac.rs

SOME NEWER ACHIEVEMENTS IN COLD FORGING

Abstract: Cold forging operations are performed below recrystallization temperature of the billet material. This kind of metal forming offers a number of advantages when compared with alternative manufacturing technologies. Main advantages are increased mechanical properties and better surface finish of the workpiece, high production rates, design flexibility, no scrap material (excellent material utility). Limitations are relatively high die loading as well as higher costs of equipment (machine, tooling, dies).

Technologies of cold forging have experienced significant advancement in the development and industrial application in last decades. Current paper gives some view of the newer theoretical and experimental works in the field of this technology. Special attention is placed at the investigations which have been carried out in the Laboratory for Metal Forming at the FTN – University Novi Sad.

Key words: Bulk metal forming, pressure release, bimetallic extrusion, radial extrusion

1. INTRODUCTION

Metal Forming technologies are characterized by high productivity, product quality and, in some cases, by low energy consumption. In many cases products with complex geometries and specific mechanical properties are unobtainable by other processes but metal forming. Bulk metal forming, with many innovations and developments, is establishing itself as a modern tool for production of components of different size and complex shapes in very short time. In this field extensive research and development work is being undertaken with the aim to raise the level of productivity and competitiveness among other production methods. The vital trends in the bulk metal forming sphere are the increased precision and reduced production time. Special attention is paid to ecological issues in connection with metal forming application. Investigations in the theoretical, numerical and experimental fields are being performed in the world metal forming laboratories with the aim to achieve those requirements.

In Metal Forming Laboratory at the FTN – University Novi Sad significant works in bulk metal forming operations have been carried out and completed so far. A number of papers and reports have been published in the reputable journals and at the international conferences.

Current paper outlines some of the newer developments in the bulk metal forming, including theoretical, experimental and numerical methods. Some achievements of the FTN - MF Lab. in this aspect are also presented.

2. LOCAL PRESSURE DETERMINATION BY UBET

UBET stands for Upper Bound Elemental Technique and it is based upon well-known principle of Upper Bound approach [1,2]. But, in the classical

application of this method only total energy and total load, as well as the picture of metal flow could be determined and observed. This fact limited to great extend the application of UBET in many practical and theoretical cases. To overcome this drawback Japanese investigators Kiuchi and Murata in their work [3] proposed one method to obtain local pressure at the contact surface between tool and workpiece using upper bound and introducing velocity change on one imaginary element at the tool/workpiece surface. Further enhancement of this method has been made by Christensen and Bay. They corrected the Kiuchi/Mutara approach by introducing so called “pressure element” which refines the mesh around the points at the contact surface. Authors assumed positive and negative velocity change at the observed point (+ V and - V) and calculated total energy (E_{tot}^+ and E_{tot}^-) using those velocities. After detailed analytical considerations they determined surface pressure as follows:

$$p = \frac{E_{tot}^+ - E_{tot}^-}{S_{i,t} \cdot dV_t} \quad (1)$$

$S_{i,t}$ - Elemental surface

dV_t - Velocity change in time

E_{tot} - Total energy dissipation

Detailed presentation of Christensen and Bay approach can be found elsewhere [4].

Using UBET pressure method contact pressure in backward extrusion between the die wall and workpiece has been determined by the author [5]. In order to verify UBET results, backward extrusion experiment has been performed and contact pressure has been measured Billet material was mild steel ($\sigma_0 = 28 \text{ daN/mm}^2$). In Fig. 1. comparison of results

(UBET – experiment) is shown. As it can be seen fair agreement between those results exists.

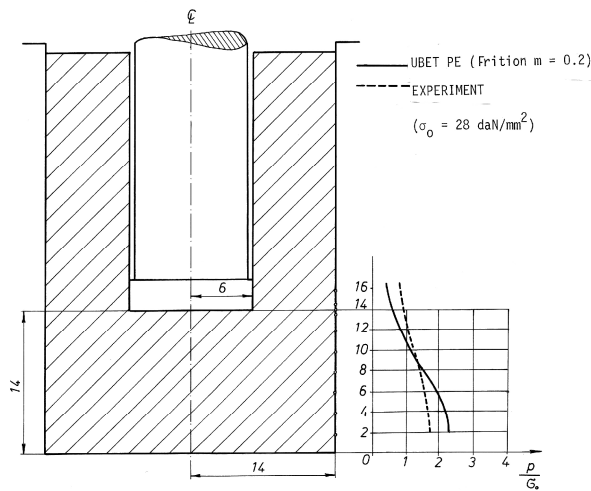


Fig. 1. Contact pressure in backward extrusion: UBET versus experimental results

It should be noticed that the successful practical application of this method is only possible for a relatively simple shapes of workpieces. Further work on this subject should enable usage of UBET pressure program also for more complex component shapes.

3. NEWER WORKS IN COLD EXTRUSION

Cold extrusion is a powerful method to manufacture small and medium size parts, mainly in high batch production. It is applied mostly in automobile industry worldwide. One of the problems which must be solved in practical cold extrusion is high contact pressure between die and workpiece and high working load. This pressure can even limit the usage of cold extrusion in some extreme cases. Also if forming load can be reduced dimensional accuracy of extruded parts can be improved. Therefore, lowering of contact pressure and forming load is one of the big challenges in planning and performing cold extrusion technology.

One solution for this problem is to enable material to flow in such a way that divided flow occurs. Kunogi [6] proposed spread extrusion (Fig. 2.) and Sawabe [7] introduced relief axis method (Fig. 3.), which both provide divided material flow and lowering of forming load and pressure.

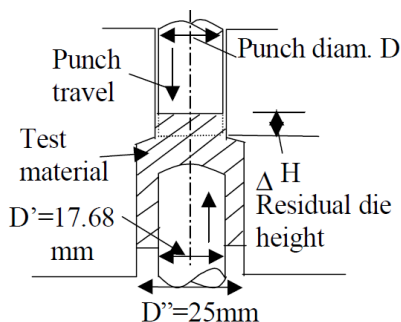


Fig.2. Spread extrusion [7]

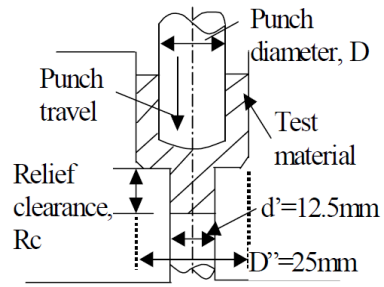


Fig. 3. Relief axis method [7]

Ogha and Kondo further developed this idea [8-10]. Their investigation included theoretical analysis of different extrusion processes and experimental approval of theoretical results including final stage of extrusion process - corner filling. Theoretical solutions based on the Upper Bound Method were applied on two proposed way of obtaining divided material flow - flow relief opening (FRO) and flow relief axis (FRA). Application of FRO and FRA in extrusion of gear are presented in Fig. 4.

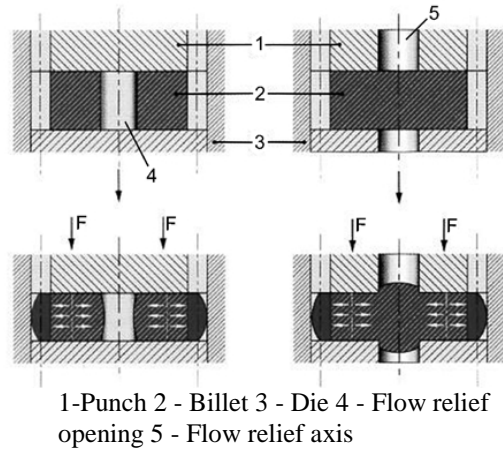


Fig. 4. Application of FRO and FRA in extrusion of gear [5]

Behrens at al. analysed various factors (tool, machine, process parameters) affecting part accuracy in hot forging of gears. They applied principle of flow relief axis where opening was only on the one side of the tool. That opening was also used as a compensating area (Fig. 5).



Fig. 5. Tool sided volume compensation for the gear forging [11]

In the Metal Forming Laboratory at FTN Novi Sad, University of Novi Sad, theoretical and practical work has been performed with the aim to find plausible solution to decrease contact pressure in cold extrusion of gear-like elements [12, 13].

Upper Bound Method was applied for forming load and contact pressure determination for two models of gear-like element extrusion, with relief opening in the center of the billet (Fig. 6) and with the relief opening in the punch (Fig. 7). Both solutions showed that application of relief opening enables decrease of required forming load and punch pressure in extrusion process.

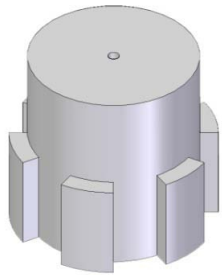


Fig. 6. Gear-like element with flow relief opening in the centre of the billet

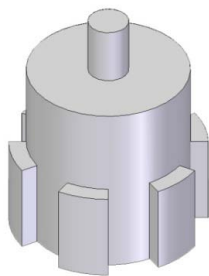


Fig. 7. Gear like element extruded with the relief opening in punch

Results obtained by Upper Bound were verified by numerical analysis and experimental investigation.

Further example which illustrates innovative achievement in the field of cold bulk forming is bi- and multi metallic extrusion. Research has been conducted with the aim to investigate possibilities and limitations of this specific kind of bulk forming as well as to optimize geometrical and technological parameters which influence this process.

One of the most promising types of bimetallic extrusion is manufacturing of shaped components by two different metals (like gears and similar products). Preliminary investigation of gear-like radial bimetallic extrusion was performed at Faculty of technical science.

The billet was composed of outer steel ring and inner aluminium cylinder. The initial idea of this investigation was to obtain an extruded bimetallic part which would have favourable properties compared to aluminium-only and steel-only element. This bimetallic part would have an optimal balance between high strength (contributed by steel segment) and low weight (contributed by aluminium segment).

Numerical simulation of this process was carried out in Simufact Forming 11.0 software. Hydraulic press with 1 mm/s velocity was set as working machine. Both punch and die were set as rigid bodies as deformation of these tools was neglected. Process temperature in simulation was 20° Celsius and standard siMesh Tetra mesher was used for both billets with Tetrahedral elements. During the simulation process remeshing was turned on (at 40° element angle deviation and at 0.4 strain change).

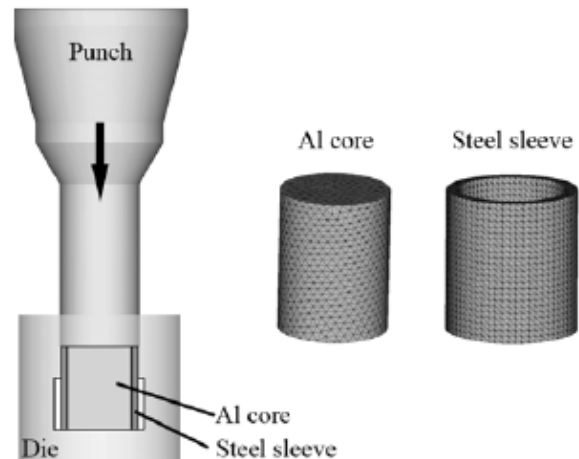


Fig. 8. Modelling of radial bimetallic extrusion in Simufact Forming. left: composition of tools and billets, right: inner and outer billet

Stress – strain curves for both materials were obtained by Rastegajev test:

$$\text{steel} = 1100 \cdot \epsilon^{0,1389}$$

$$\text{al} = 165 \cdot \epsilon^{0,24}$$

Geometry of the die insert used in radial bimetallic extrusion is presented in Fig. 9.

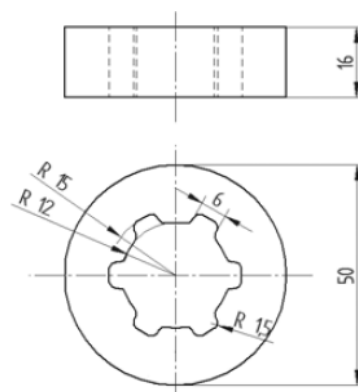


Fig. 9. Geometry of die insert

During this simulation process, three different outer sleeve thicknesses ($s = 1$, $s = 2$ and $s = 3$ mm) were varied and corresponding force – load curves were obtained.

Fig. 10. presents load – stroke diagrams for three different sleeve/core combinations. All diagrams show very similar load growth patterns.

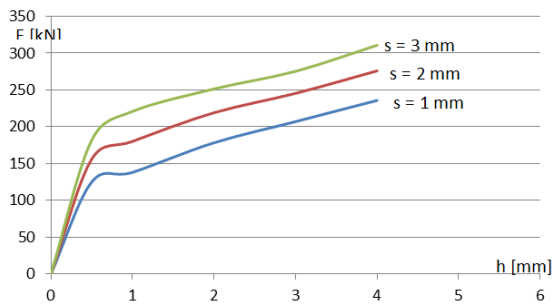


Fig. 10. Load – stroke diagrams for all three outer sleeve thicknesses

Experimental investigation of gear-like bimetallic specimen was performed as well. Initial billet and final shape of the workpiece are presented in Fig. 11.



Fig. 11. Disassembled Al/Steel billet and workpiece after radial extrusion

4. CONCLUSION

Cold bulk metal forming operations represent one of the most important and most widespread groups within metal forming technology. It has wide application in various branches of mechanical and production engineering.

Current paper illustrates some newer trends in this part of metal forming with focus on the operations which were performed at the FTN.

Those are divided flow approach in order to reduce die pressure and bi-metallic extrusion in which product composed of two different materials is produced. Such product has favourable properties compared to one-metal workpiece. Newer theoretical approach to obtain contact pressure as well as verification of this method by experiment is also presented.

Acknowledgments: This paper was created within the Ceepus project CIII-HR-0108 and project TR 035020, financed by the Ministry of Education, Science and Technological Development of the Republic of Serbia.

REFERENCES

- [1] Avitzur, B., *Metal forming: processes and analysis*, McGraw Hill, SAD, 1968.
- [2] Osman, F.H., Bramley A. N., Ghobrial M. I.:

Forging and Preform Design using UBET, Adv. Technology of Plasticity, Vol 1, 1984.

- [3] Kiuchi, Murata: *Simulation of contact pressure on total surface by UBET*, Proceeding 21 International MTDR Conference, pp 13-20, 1980.
- [4] Christiansen, Bay: *Calculation of local surface stresses in drop forging using UBET*, NAMRC Conference, 1986., Birmingham, UK, pp 88-94
- [5] Plancak, M.: *Determination of pressure distribution in forging processes*, Internal Report, University of Bath
- [6] Kunogi, M.: *Spread extrusion method*, Report of science research institute, Vol. 50, 1956., pp 215.
- [7] Sawabe, H., *Relief axis method*, Basic and application on cold forging, Sanpo, 1968.
- [8] Ohga, K., Kondo K.: *Research on precision die forging utilizing divided flow (1st report, theoretical analysis of processes utilizing flow relief-axis and relief-hole)*, Buletin of the JSME, Vol. 25, No. 209, November pp 1828-1835, 1982.
- [9] Ohga, K., Murakoshi, F., Ando, H., Kondo, K., *Precision cold die forging of actual steel gear toothed products utilizing divided flows*, Proceedings of the 5th International Conference on Technology of Plasticity, ICTP, 1996., Ohio, USA, pp 331-336
- [10] Ohga, K., Murakoshi F., Ando H., Miyoshi K., Kondo K.: *Net-shape forging of gear toothed parts utilizing divided flow method*, Proceedings of 6th International conference on technology of plasticity ICTP, Nuremberg, Germany, pp 793-798, 1999.
- [11] Behrens, B. A et al., *Anforderungen an Umformwerkzeuge für das gratlose Präzisionsschmieden*, 2. AutoMetForm/17. Sächische Fachtagung Umformtechnik Tagungsband Freiberg November pp 299-311, 2010.
- [12] Skakun, P., Plan ak M., Ka mar ik I., Ivaniševi a A., Movrin D., Milutinovi M., Viloti D., *One innovative method for load reduction in cold extrusion of gear-like elements*, Journal for Technology of Plasticity, No 1, Vol 40, 2015., pp 57-64
- [13] Skakun, P., *A contribution to the investigation of divided material flow influence to the process parameters of complex shapes cold extrusion*, PhD Thesis, Faculty of technical sciences, Novi Sad, University of Novi Sad, 2015.

Authors: Prof. dr Miroslav Plan ak, Assistant professor dr Plavka Skakun, Igor Ka mar ik, master, Aljoša Ivaniševi , master, Assistant profesor dr Mladimir Milutinovi ., Prof. dr Dragiša Viloti , University of Novi Sad, Faculty of Technical Sciences, Department for Production Engineering, Trg Dositeja Obradovica 6, 21000 Novi Sad, Serbia, Phone.: +381 21 450-366, Fax: +381 21 454-495.

E-mail: plancak@uns.ac.rs
plavkas@uns.ac.rs
ikac@uns.ac.rs
ivanisevic@uns.ac.rs
mladomil@uns.ac.rs
vilotic@uns.ac.rs

Ran elovi , S., Nikoli , S., Milutinovi , M., Taniki , D.

ANALYSIS OF RUNNING SYSTEM AT INJECTION MOLDING TOOL FOR PRODUCTS WITH DIFFERENT GEOMETRY

Abstract: In the industrial processes of injection molding one of the basic requirements is uniformly flow and distribution of thermoplastic to all mold cavity defining a kind of finished product. If it is a simple geometry of the finished work that is not a special request but if one gets a different tool geometries require additional analyzes that offer practical solutions and useful results. Unbalanced schedule unequal molding cavity in space, or in the tool requires FEM process simulation and monitoring parameters in order to achieve the required quality and accuracy of products.

Key words: injection molding, viscosity, tool construction

1. INTRODUCTION

Viscosity is a very important physical feats and parameter of fluid mechanics that are often defined as the resistance to relative motion and flow of the fluid under consideration. In real thermoplastic resin temperature, velocity and shear have a decisive impact on the value of viscosity [1,2]. The viscosity is constant at low values of flow velocity or shear respectively, and decreases with its increase. Also, the viscosity (resistance to flow) decreases when the temperature increases.

2. MATHEMATICAL MODELS OF VISCOSITY THERMOPLASTIC

In the process of injection molding thermoplastic has intensive flow and heat change with tool wall. As plastic flows through the different sections of the machine and the mold, because of drag and frictional effects there is a loss of the applied pressure at the flow front of the thermoplastic. Additionally, as the plastic hits the walls of the mold, it begins to cool increasing the viscosity of the plastic requiring additional pressure to push the plastic. The skin of plastic that is formed at the walls decreases the cross sectional area of the plastic flow that also results in the pressure drop. The molding machine has a limited maximum amount of pressure available to push the screw at the set injection speed. The required pressure to push the screw at the set injection speed should never be more than the maximum available pressure. In this case the process becomes pressure limited [3,4]. During process development, knowing the pressure loss in every section helps in determining the overall pressure loss and the sections where the pressure drops are high. The all mold or running system can then be modified to reduce this pressure drop and achieve a better consistent flow.

Viscosity index is a fluid flow resistance. The viscosity of the most widespread and simplest fluid for analysis, such as water or oil is usually a constant value to the constant temperature. These fluids are generally

behave as Newtonian fluids. Unlike a simple fluid, the viscosity of the thermoplastic in the tool cavity is complex and depends on the chemical structure, composition, and mechanical conditions under which the process takes place alone injection molding. When the basic chemical structure and composition, the viscosity of the thermoplastic depending on the temperature, shear rate, and pressure. To understand the nature of viscosity thermoplastic, you first need to define the shear stress, shear rate and viscosity.

Depending on the chosen material, the major manufacturers of thermoplastic materials provide information of viscosity, and the mathematical model used in FEM analysis. In this study, for the fitting arches Ø75/45 and Ø75/90 chosen material PP Moplen HP548R for which the FEM analysis of viscosity used second Kros mathematical model [5].

The definition of a simple shear fields takes into consideration fluid between stationary and moving parallel plates (fig.1). Near to the movable plate forming a layer of fluid with identical flow rate speed with movable panels [6].

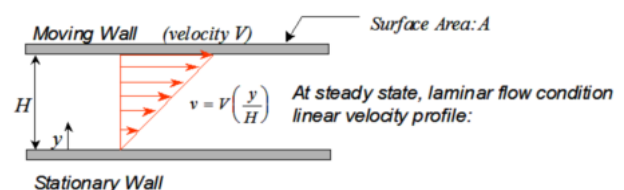


Fig.1. Definition of a simple shear flow field

In steady condition, velocity profile change is a linear function. So, we can define the shear stress τ , and shear rate $\dot{\gamma}$:

$$\tau = \frac{F}{A} \quad (1)$$

$$\dot{\gamma} = \frac{V}{H} \quad (2)$$

From equations (1) and (2) can be defined as the

viscosity η as shear stress τ on shear rate $\dot{\gamma}$. Large shear rate means greater variation of flow velocity in the direction of thickness.

$$\eta = \frac{\tau}{\dot{\gamma}} \quad (3)$$

If the viscosity η higher, will increase the flow resistance and lower shear rate. Otherwise, there will be less resistance to flow. Curve of viscosity of most thermoplastics have the same dependence on shear rate as shown in Fig 2.

Viscosity is approximately constant, at the lower shear rate. It is commonly known as "Upper Newtonian region". The polymer chains are evenly arranged when the shear rate increases, the viscosity decreases. This is called "Shear thinning region". When all the polymer chains completely lined up, then the viscosity becomes insensitive to shear rate. These are the "Lower Newtonian region". The "Upper Newtonian region" and "Shear thinning region" can be observed at the majority of the polymer. "Lower Newtonian region", however, is not as obvious in most thermoplastics, due to molecular degradation due to ultra high-speed shear [7].

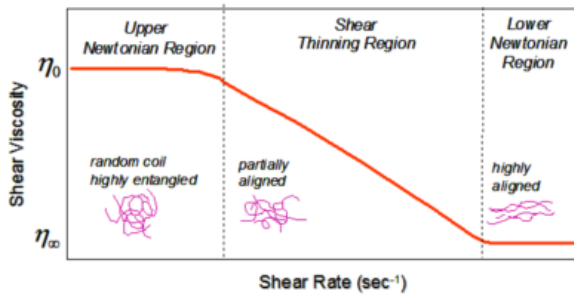


Fig. 2. Characteristics viscosity curve of thermoplastic

Viscosity thermoplastics shows a very large dependence on temperature [8]. Most often, the viscosity rapidly decreases when the temperature rises. Two temperature dependence are commonly used, exponential or "Arheniusov" model and a "William-Landel-Ferry" (WLF) model.

There are various, applicable mathematical models for thermoplastics. Depending on the manufacturer a suitable thermoplastic and data available, applies to some of the mathematical models whose results are available in the software and which represent a good approximation of the real behavior of thermoplastics in the FEM analysis [7,8].

For Newtonian fluid is assumed to be independent of temperature viscosity and shear rate. It has the simplest mathematical formulation and does not take into consideration the non-linear characteristics of thermoplastics. This model is not recommended to simulate the behavior of thermoplastics and is used mainly in order to quickly check network Finite Element appropriate model. In these examples, analysis and mathematical calculation are simplified to the maximum because of the constant viscosity.

$$\eta = \eta_0 \quad (4)$$

where η viscosity and η_0 Newtonian viscosity. Model "power-law" ignores upper Newtonian regions.

The dependence of the viscosity shear rate can be simplified "power-law" equation [8]. When used this model to simulate thermoplastic, results of evaluation of viscosity can be a region of lower rates of shear.

$$\eta = \eta_0 (\dot{\gamma})^{n-1} \quad (5)$$

$$\eta_0 = B \exp\left(\frac{T_b}{T}\right) \quad (6)$$

where n is the "power-law" index with a value between 0 and 1; T_b shows the temperature sensitivity of the material; T melt temperature (K); η_0 is the viscosity at zero shear rate, and B is an index of the consistency.

It is a three - parameter model that reflects the observation that the function of medium - high shear rate almost straight line in log-log coordinate system. Many analytical equations for transformation of the polymer are derived from this model. First Kross mathematical model describing the dependence of the shear rate in the region "upper Newton regions" and "shear thinning region" [7,8].

$$\eta = \frac{\eta_0}{1 + C(\eta_0 \cdot \dot{\gamma})^{1-n}} \quad (7)$$

$$\eta_0 = B \cdot \exp\left(\frac{T_b}{T} + DP\right) \quad (8)$$

where D is a parameter of the pressure corrected for the effect of pressure on viscosity and C is the shear rate parameter.

Second Kross mathematical model is similar to the first Kross model and it also shows the dependence of the shear rate in the "Higher Newtonian region" and "Shear thinning region" It is usually better suited for thermoplastics with a wide distribution of molecular weight (BMWD). On the market are commonly available products with the BMWD data, so that this model is widely present in the standard Moldex3D database. The model has an exponential temperature dependence and is also known as "Kross-Exponential" model [7,8].

$$\eta = \frac{\eta_0}{1 + \left(\frac{\eta_0 \cdot \dot{\gamma}}{\tau^*}\right)^{1-n}} \quad (9)$$

$$\eta_0 = B \cdot \exp\left(\frac{T_b}{T} + DP\right) \quad (10)$$

where is * stress relaxation.

The third Kross mathematical model is a modification of the second. It replaces the temperature dependence of the exponential form to "William-Landel-Ferry" (WLF) form. This model is therefore also known as the "Kross-WLF" model.

$$\eta = \frac{\eta_0}{1 + \left(\frac{\eta_0 \cdot \dot{\gamma}}{\tau^*}\right)^{1-n}} \quad (11)$$

$$\eta_0 = D_1 \cdot \exp\left(\frac{-A_1(T - T_c)}{A_2(T - T_c)}\right) \quad (12)$$

$$T_c = D_2 + D_3P \quad (13)$$

$$A_2 = \tilde{A}_2 + D_3P \quad (14)$$

"Kross-WLF" mathematical model typically has better accuracy is correlated to low temperature and viscosity. If the temperature is below $T_g + 100^\circ \text{C}$, "Kross-WLF" mathematical model is generally better than the "Cross-exponential" model.

"Carreau" model describes the dependence of the shear rate in the "Upper Newtonian regions", and shear in the "Shear thinning region". It is an exponential dependence on temperature, also known as the "Carreau-exponential viscous model."

$$\eta = \frac{\eta_0}{\left(1 + \left(\frac{\eta_0 \cdot \dot{\gamma}}{\tau^*}\right)^2\right)^{\frac{1-n}{2}}} \quad (15)$$

$$\eta_0 = B \cdot \exp\left(\frac{T_b}{T} + DP\right) \quad (16)$$

3. FIELD VISCOSITY ANALYSIS AT INJECTION POLYPROPYLENE

The viscosity index fluid flow resistance and the example of thermoplastic shows a large temperature dependence. The most common viscosity rapidly decreases with increasing temperature. There are various mathematical models to describe the behavior

of the viscosity of the thermoplastic. Most often the chosen material taking physical and chemical characteristics of the manufacture for operating temperature range. For the material of choice in this paper, PP Moplen HP548R, FEM analysis fields viscosity, in the program Moldex3D, was done by the "modified Kross model-2" [9,10].

FEM analysis of the investigated injection molding process was performed using Moldex3D Project module. Mathematical models and assumptions in the field of fluid mechanics and applied in the FEM analysis depend on the type of finite elements mesh. Moldex3D Project module for FEM analysis of injection molding process use three models of finite element mesh for the plastic continuum: solid model, shell model and e-design model.

At the first model of tool, the viscosity of the material at the end of the process of filling both the mold cavity, the logarithmic division, ranges from 1,533 to a maximum of 8,064, with an average value of 4.237. Based on the graphic display is observed quite uneven distribution of viscosity in both the molding chamber. Significantly higher values of viscosity at the end of a filling material in the mold cavity port $\varnothing 75/45^\circ$, which is due to the exponential dependence of viscosity on temperature which, according to the shear material when filled, covered "upper Newtonian region" and "shear thinning region" for this polypropylene. Since viscosity is the resistance of a fluid to flow, it can be concluded that this kind of results, much easier to meet the ongoing process of molding chamber arch $\varnothing 75/90^\circ$ (lower viscosity), as confirmed by the analysis of the pressure distribution in the mold cavity.

Due to the unbalanced running system, first to fill the lower mold cavity, to the end of the expiry time fulfill both the molding chamber, there was a arise pressure in it.

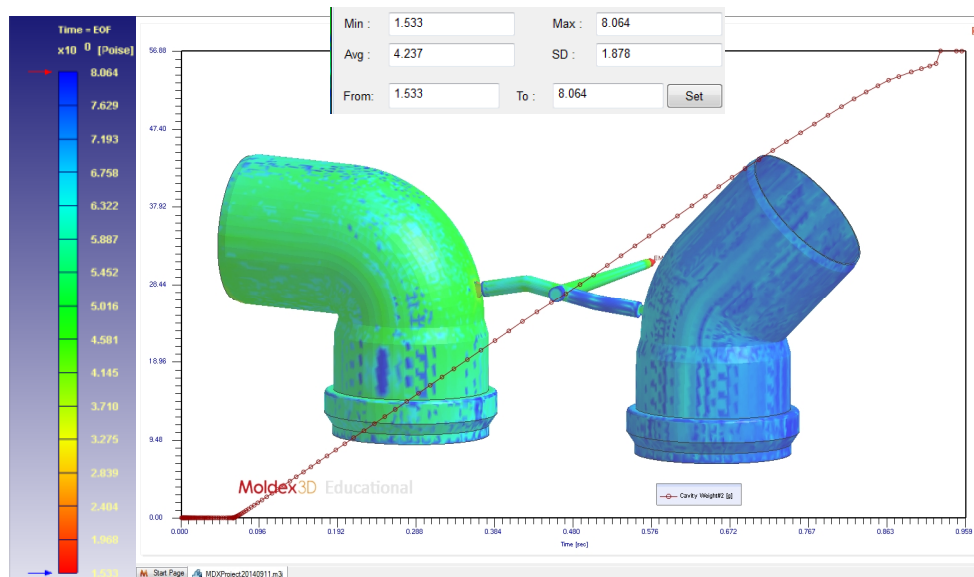


Fig. 3. Field viscosity and chart changes in pressure as a function of time at the first running system

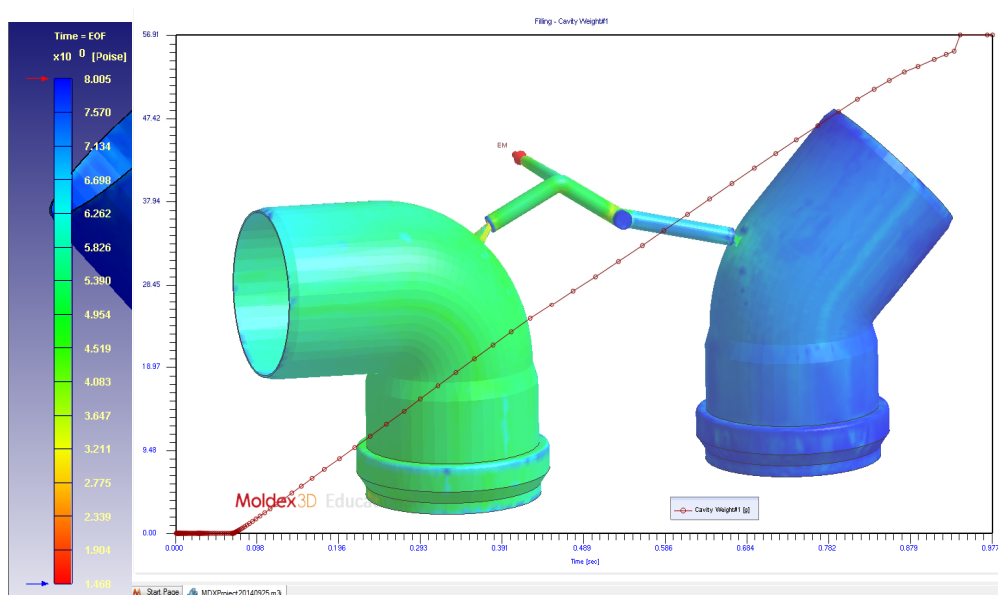


Fig. 4. Field viscosity and chart changes in pressure as a function of time at the second running system

As the greater length of trajectory thermoplastic resin the front against the mold cavity fitting arch $\text{\O}75/90^\circ$ was increased shear rate, which was reflected in a rise in temperature polypropylene in that part of the tool, or a drop in viscosity at the end of time fulfilled.

With constructive change of running system we get a slight increase in the range of viscosities of both the mold cavity, from the minimum value of 1,468 to maximum 8,005. It is observed that higher values of viscosity polypropylene in a small molding cavity, but with a much more even distribution in both the mold cavity (fig.4).

4. CONCLUSION

The results of FEM analysis (MOLDEX3D software) have shown that for initial design of the running system there are significant differences in the field of viscosity for the fittings $\text{\O}75/90^\circ$ and $\text{\O}75/45^\circ$ at first and second tool solutions. Obtained results for accepted running system were balanced and the resin flows under the same conditions (the length of the flow was the same). This finding indicates an increased risk of weld lines occurrence and local weakness of the part strength around the parting line.

With modification in the gate locations of the both tool cavities pressure field becomes more uniform and their maximum values is near equal.

5. REFERENCES

- [1] Shen, Y.K., Yeh, S.L., Chen, S.H.: *Three-dimensional non-Newtonian Computations of Micro-Injection Molding with the Finite Element Method*. Int. Comm. Heat Mass Transfer, 2002, Vol 29, No.5, pp. 643-652, ISSN 0735-1933
- [2] Kemmanno, O, Weber, L, Jeggy, C., Magotte, O.: *Simulation of the Micro Injection Molding Process*. Proceedings of the Annual Technical Conference (ANTEC 2000), Orlando, FL, USA,

pp.576-580, ISBN 1566768551,.

- [3] Lei, X, Longjiang, S., Bingyan, J.: *Modelling and Simulation for Micro Injection Molding Process*, Computational Fluid Dynamics Technologies and Applications, Prof. Igor Minin (Ed.), 2011, pp.317-332
- [4] Liou, A. C., Chen, R. H.: *Injection molding of polymer micro- and sub-micron structures with high aspect ratios*, Int. J. Adv. Manuf. Technol., 2006Vol 28, pp.1097–1103, ISSN 0268- 3768
- [5] Zaikov, G.E., Jimenez, A.: *New Developments in Polymer Analysis, Stabilization and Degradation*. Nova Science Publishers, Inc.,2006.
- [6] <http://help.plastics-u.com/online-help/molding-knowledge/standard-injection-molding>. Accessed on 15.12.2014
- [7] Liang, J.Z., Ness, J.N.: *The calculation of cooling time in injection moulding*, Journal of Materials Processing Technology, Vol. 57, pp. 62-64, 1996.
- [8] Nikoli , S., Ran elovi , S., Milutinovi , M.: *Effect of mold temperature on melt front temperature of thermoplastic resin at injection molding*, Journal for technology of plasticity, vol 39. No.2, ISSN 0354-3870, pp. 55-64, 2014.
- [9] Moldex3D Designer® R12SP2, Core Tech System Co. Ltd. Manuel References
- [10] Moldex3D Project® R12SP2, Core Tech System Co. Ltd. User Manuel

Authors: dr Sasa Randjelovi , Associate Professor, M.Sc. Sasa Nikoli , University of Nis, Faculty of Mechanical Engineering, Aleksandra Medvedeva 14, 18000 Nis, Serbia, Phone +381 18 500629, dr Mladimir Milutinovi , Assistant Professor, University of Novi Sad, Faculty of Technical Sciences, Institute for Production Engineering, Trg Dositeja Obradovica 6, 21000 Novi Sad, Serbia, dr Dejan Taniki , Associate Professor, University of Belgrade, Technical Faculty of Bor, Serbia
E-mail: sassa@masfak.ni.ac.rs

Skakun, P., Planak, M., Kamenik, I., Ivanišević, A., Movrin D., Vilotić, D., Milutinović, M.

FLOW RELIEF OPENINGS IN EXTRUSION OF GEAR-LIKE ELEMENTS - THEORETICAL AND NUMERICAL APPROACH

Abstract: In this paper investigation of cold radial extrusion of gear-like elements with flow relief opening is presented. Flow relief opening is placed in the center of the billet and it helps divided flow to take place during extrusion process. In that way total forming load is lower than in conventional process of extrusion. Geometry of gear like element with straight radial flank profile was considered. Theoretical analysis of process was done by Upper Bound method. Forming load was also determined by numerical simulation. Characteristics of Al 99,5 were used both in the theoretical analysis and numerical simulation.

Key words: cold radial extrusion, flow relief opening

1. INTRODUCTION

Cold extrusion is metal forming process which is applied for production of simple and complex-shaped parts. Application of this method has many advantages such as time, material and energy savings, improved quality of product, etc. Main constraints for implementation of this method are high values of forming load and tool pressure, especially in the process of radial extrusion.

Application of flow relief openings is possible way to reduce this problem. When flow relief opening exists in workpiece, during forming process material simultaneously fills die cavity and relief opening. In that way divided flow occurs. Divided flow means that in the workpiece exists surface where material change direction of flow and it is called neutral surface. When material flows in such a way, deformation load in process is reduced.

Among the first this idea was presented by Kunugi [1] and Sawabe [2], but Ogha and Kondo did overall investigation which include theoretical analysis of different extrusion processes and experimental approval of theoretical results. At the beginning they determined theoretical solution based on Upper bound theorem for final stage of extrusion process - corner filling, for two different position of relief opening, in the billet and in the tool [3]. In [4] they presented extrusion of gear parts with assistance of divided flow.

Zuo et al. [5] and Beherens et al. [6] applied relief openings on the one side of the tool in hot precision forging of the gears.

In Metal forming laboratory at Faculty of technical

sciences, University of Novi Sad, for many years extrusion of gears and gear-like elements are studied [7], [8], [9], [10], [11].

In this paper influence of flow relief opening on the forming load in cold radial extrusion of gear-like element with straight radial flank profile is analysed (Fig 1), Theoretical solution based on Upper Bound method is used for determination of forming load. Theoretical solution is compared with results of numerical simulation of process.

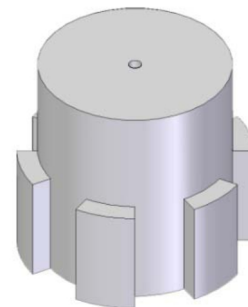


Fig. 1. Gear-like element with straight radial profile and central flow relief opening

2. UPPER BOUND ANALYSIS OF PROCESS

2.1 Upper bound theorem

Based on Upper bound theorem, total power of deformation (\dot{W}_t) can be determined by following expression

$$\dot{W}_t = \dot{W}_d + \dot{W}_s + \dot{W}_f = \frac{2}{\sqrt{3}} \sigma_e \int_V \sqrt{\frac{1}{2} \dot{\epsilon}_{ij} \dot{\epsilon}_{ij}} dV + \int_{A_s} \tau_s |\Delta v| dA_s + \int_{A_f} \tau_f |\Delta v| dA_f \quad (1)$$

First component \dot{W}_d represents internal power of deformation, second component \dot{W}_s is shear loss and third component \dot{W}_f is friction loss.

First step in the Upper bound analysis is to divide forming body into the zones and to predict

kinematically admissible velocity field (velocity components for each zone). Assumed velocity field makes possible to determine total forming load according to Upper Bound theorem [12], [7].

2.2 Theoretical solution

General case of material flow for this shape of workpiece is when neutral surface is between outer cylindrical surface (r_0) and cylindrical surface of the central opening (r_i). In that case of material flow five deformation zones exist (Fig. 2).

Apart from general case of material flow, three more cases of neutral surface position are predicted.

- when neutral surface coincides with inner surface, $r_n = r_i$
- when neutral surface coincides with outer surface or when the teeth are formed before opening is filled with material, $r_n = r_0$ or $r_i = r_{i\max}$ and
- when opening is filled with material before teeth are formed, $r_i = 0$, this is case of conventional radial extrusion.

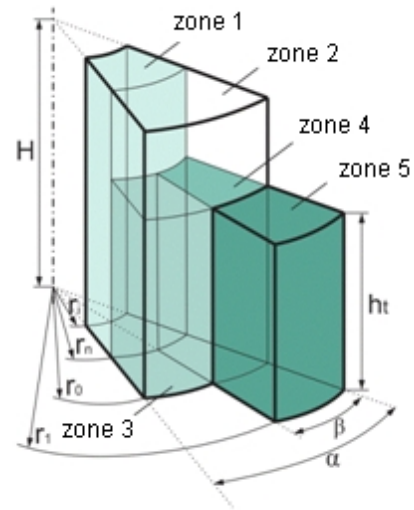


Fig. 2. Deformation zones

In Table 1 predicted components of velocity field for general case of material flow are presented.

Zone 1	$v_z = -\frac{v_0}{H}z$	$v_\theta = 0$	$v_r = -\frac{v_0}{2H} \frac{r^2 - r_n^2}{r}$
Zone 2	$v_z = -v_0$	$v_\theta = 0$	$v_r = 0$
Zone 3	$v_z = -\frac{v_0}{h_t}z$	$v_\theta = -\frac{v_0}{h_t}r(\alpha - \theta)$	$v_r = 0$
Zone 4	$v_z = -\frac{v_0}{h_t}z$	$v_\theta = -\frac{v_0}{h_t} \frac{\alpha - \beta}{\beta} r\theta$	$v_r = \frac{v_0}{h_t} \frac{\alpha}{2\beta} \frac{r^2 - r_n^2}{r}$
Zone 5	$v_z = 0$	$v_\theta = 0$	$v_r = \frac{v_0}{h_t} \frac{\alpha}{2\beta} \frac{r_0^2 - r_n^2}{r}$

Table 1. Components of velocity field

Velocity components from Table 1 are used to determine strain rate components which figure in equation (1).

Neutral radius r_n has the value which minimizes expression (1), which means that neutral surface has position in material which requires minimal forming load. When neutral radius is determined in that way, total power of deformation and forming load can be also determined.

Following parameters were used for determination of forming load: billet diameter $r_0 = 14$ mm, outer radius of gears $r_1 = 17$, angles $\alpha = \pi/6$ and $\beta = \pi/12$ (defined at Fig.2), initial billet height $H_0 = 40$ mm, friction coefficient $\mu = 0,12$. Flow curve was used for Al 99,5 and it has following form:

$$K = 119,39 \cdot \sigma^{0,2048} [\text{MPa}] \quad (2)$$

For stroke increments of 0,5 mm, neutral radius r_n , inner radius r_i , outer radius r_1 and forming load were calculated for two values of initial diameter of billets openings, 5 mm and 8 mm.

Example of calculated values for initial diameter of billet opening of 5mm are presented in Table 2. As it can be seen from the table two cases of theoretical solution appeared for specific material, friction coefficient and geometrical parameters used in calculation.

H [mm]	0	0,5	1	1,5	2	2,5	3	3,5	4	4,46	5,022
r_n [mm]	-	5,376	5,471	5,547	5,604	5,642	5,659	5,655	5,629	5,592	-
r_i [mm]	2,5	2,44	2,38	2,31	2,23	2,15	2,06	1,97	1,87	1,77	0,27
r_1 [mm]	14	14,37	14,73	15,08	15,43	15,76	16,08	16,40	16,72	17	17
F [kN]	0	109,4	119,8	127,5	133,9	139,6	144,8	149,60	154,14	158,15	336,18

Table 2. Forming load for workpiece with initial opening size 5 mm ($r_{i0} = 2,5$ mm)

At the beginning of the process neutral radius had value between r_0 and r_1 , so general case of theoretical solution was used for determination of unknown geometrical variables. This phase ended when outer radius r_1 reached its maximum value which means that teeth were completely formed. From that point material flowed only toward central opening, and mathematical solution for this case of material flow was used.

3. NUMERICAL SIMULATION

Numerical simulation of the radial extrusion process was performed using Simufact Forming 12 software. Geometrical parameters used in theoretical solution were also used to create 3D models of billet and tool in Solid Edge V18 software. Flow curve for Al 99,5 was same as in theoretical solution. Punch and die were modeled as rigid bodies. Between billet material

and die material Coulomb friction with a friction coefficient 0.12 was assumed. Ram stroke of the hydraulic press was 1 mm/s. Element type was hexahedral, size 0,5 mm.

Load-stroke diagrams were obtained by numerical simulation for two different relief openings 5 mm and 8 mm (same as in theoretical solution) and for workpiece without opening (conventional radial extrusion).

4. ANALYSIS OF RESULTS AND DISCUSSION

In Fig. 3 load-stroke diagram obtained by numerical and theoretical solutions for two different relief openings are shown. In order to prove that flow relief opening has influence on load reduction in Fig. 3 load-stroke curve for conventional extrusion process obtained by numerical simulation is also presented.

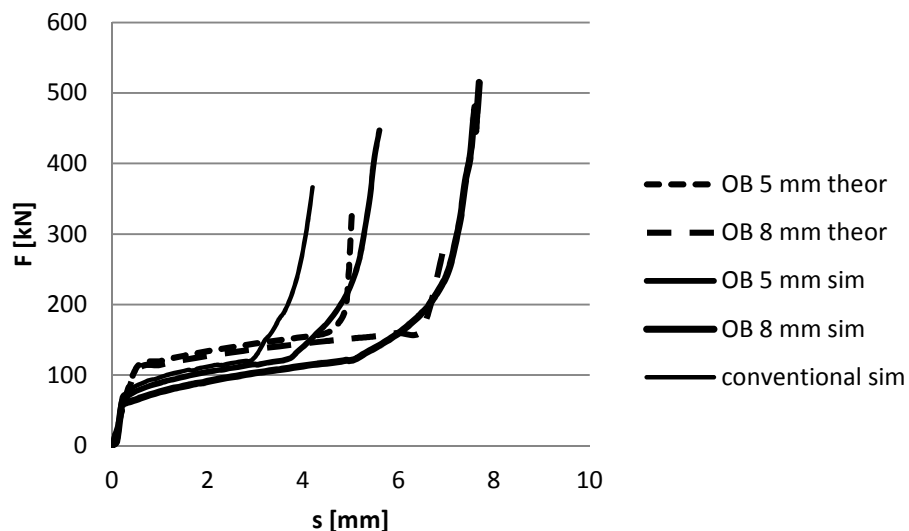


Fig. 3. Load stroke diagram obtained by numerical simulation and theoretical solution

Forming load obtained from theoretical analysis was compared with numerical values. As it can be seen from the diagram on the Fig. 3 process is characterised with three phases. In the first two phases forming load from numerical simulation has lower values, but in the third phase numerical load is higher. Difference in the third phase is consequence of different way of interpretation of the process by theory and by numerical simulation.

Theoretical solution for given conditions predicted general case of material flow (first and second stage of diagram) until teeth were formed. After that material was flowing only towards relief opening (third phase of diagram).

Forming load diagram obtained from numerical simulation has also three stages, but different from theoretical values. Numerical analysis predicted that teeth were formed and flow relief was reduced simultaneously until the very end of the process.

Obtained theoretical and numerical results indicate further directions for investigation of this process. Theoretical solution can be approved by adding new

forming zones, where experimental investigation can help gaining additional information of material flow.

5. REFERENCES

- [1] Kunogi M.: *Spread extrusion method*, Report of science research institute, Vol. 50, pp 215, 1956.
- [2] Sawabe H.: *Relief axis method, Basic and application on cold forging*, Sanpo, 1968.
- [3] Ohga K., Kondo K.: *Research on precision die forging utilizing divided flow (1st report, theoretical analysis of processes utilizing flow relief-axis and relief-hole)*, Buletin of the JSME, Vol. 25, No. 209, November pp 1828-1835, 1982.
- [4] Ohga K., Murakoshi F., Ando H., Miyoshi K., Kondo K.: *Net-shape forging of gear toothed parts utilizing divided flow method*, Proceedings of 6th International conference on technology of plasticity ICTP, Nuremberg, Germany, pp 793-798, 1999.
- [5] Zuo, B., Wang, B., Li, Z., Zheng, M., Zhu, X.: *Design of relief-cavity in closed-precision forging*

- of gears*, Journal of Central South University of Technology, Vol 22, Issue 4, pp 1287-1297, 2015.
- [6] Behrens B. A et al., *Anforderungen an Umformwerkzeuge für das kostenlose Präzisionsschmieden*, 2. AutoMetForm/17. Sächsische Fachtagung Umformtechnik Tagungsband Freiberg November pp 299-311, 2010.
- [7] Plan ak, M., Viloti , D., Skakun, P., *A study of radial gear extrusion*, International journal of forming processes, Vol 6, No 1, pp 71-86, 2003.
- [8] Škunca, M., Skakun, P, Keran, Z., Ši anin, L., Math, M. D., *Relations between numerical simulation and experiment in closed die forging of gear*, Journal of materials processing technology, Vol 177, pp 256-260, 2006.
- [9] Skakun, P., Plan ak, M., Ka mar ik, I., Ivaniševi , A., Movrin , D., Milutinovi , M., Viloti , D.: *One innovative method for load reduction in cold extrusion of gear-like elements*, Journal for Technology of Plasticity, No 1, Vol 40, 2015.
- [10] Plan ak, M., Rosochowska, M., Skakun, P: *Radial extrusion of gear-like components - numerical analysis and experiment*, Technical Gazette, No 5, Vol 20, pp 891-896, 2013.
- [11] Skakun, P.: *A contribution to the investigation of divided material flow influence to the process parameters of complex shapes cold extrusion*, PhD Thesis (in Serbian), Faculty of technical sciences Novi Sad, 2015.
- [12] Avitzur B.: *Metal forming: processes and analysis*, McGraw Hill, SAD, 1968.
- Authors: Asistent dr Plavka Skakun, Prof. dr Miroslav Plan ak, Igor Ka mar ik, master, Aljoša Ivaniševi , master, Asistent mr Dejan Movrin, Assistant profesor dr Mladomir Milutinovi .**, University of Novi Sad, Faculty of Technical Sciences, Department for Production Engineering, Trg Dositeja Obradovica 6, 21000 Novi Sad, Serbia, Phone.: +381 21 450-366, Fax: +381 21 454-495.
E-mail: plavkas@uns.ac.rs
plancak@uns.ac.rs
ikac@uns.ac.rs
ivanisevic@uns.ac.rs
movrin@uns.ac.rs
mladomil@uns.ac.rs

CHARACTERIZATION OF LASER CLEANING OF STEEL SHEETS

Abstract: *The contribution deals with characterization of environmentally friendly laser cleaning of steel sheets. The aim of this contribution is to present the new abilities of cleaning of materials in the future. There are mentioned and compared various material cleaning methods from classic ones to progressive ones and their influence on the environment. Laser cleaning is one of the newest progressive methods of the material cleaning. The results of this technology were recently tested and shown in the Department of Process and Environmental Engineering, Faculty of Mechanical Engineering, Technical University of Kosice together with the firm Trumpf Slovakia, s.r.o.*

The laser cleaning technology can be used in the various fields of industry, in the production sphere, in the renovation of products and materials and also minimised the influence of harmful impact on the environment.

Key words: *laser cleaning, steel sheet, lubrication environment.*

1. INTRODUCTION

In various branches of industries we must lubricate metal materials, their surfaces, components. Equally, the important role as lubrication is also degreasing and scouring of these metal surfaces.

Degreasing of metal materials in the mechanical industry is an important technology for cleaning materials to further processing or as a finishing treatment of surfaces, or is used in the maintenance of machinery parts, tools and the like. By degreasing of metal surfaces not only removes lubricant from surfaces, but also cleans mechanical particles of dust, abrasion and others. With the continuously deteriorating of environment, it is necessary to use such degreasing technologies of materials that have no negative impacts on the environment. Also the environment protection is encompassed by standards and decrees of REACH. [1]

2. CLEANING TECHNOLOGY OF MATERIALS

Cleaning technology of materials should be clear and shortly. We can divide the decreasing of materials according to various methods of degreasing as [3]:

- **Mechanical cleaning technologies** - by WJ technologies, blasting, [2],
- **Chemical cleaning technologies** [4]:
 - degreasing in organic or inorganic solvents,
 - degreasing in alkali solution,
 - degreasing by detergents,
 - emulsion degreasing,
 - degreasing by steam/ vapour,
- **Progressive cleaning technologies:**
 - ultrasonic cleaning technology (with degreasing in solvents or water)
 - dry ice cleaning technology [5], [6], [7],
 - laser cleaning technology.

The degreasing of metal materials by chemical method belongs to the oldest method of the degreasing. This technology requires the using of various degreasers, chemicals, which are very dangerous for the environment both in terms of storage of new and pure chemicals, their utilisation and at the storage of the chemicals [3], [4].

New method as dry ice blast cleaning utilizes a unique combination of forces and ice to powerfully lift surface contaminants without causing of damage or creating harmful secondary waste. similar to sand, bead and soda blasting, dry ice blast cleaning prepares and cleans material surfaces by using a medium accelerated in a pressurized air stream [5], [6].

In the Table 1 is shown the comparison of blasting technologies according to environmental requirements.

CLEANING METHOD	NO SECONDARY	NON-CONDUCTIVE	NON-TOXIC	NON-ABRASIVE
Dry Ice Blasting	•	•	•	•
Sand Blasting*		•	•	
Soda Blasting*		•	•	
Water Blasting*			•	•
Hand Tools	•		•	
Solvents/Chemicals				•

* Upon contact, traditional blasting materials become contaminated when used to clean hazardous substances and objects. These blasting materials are also then classified as toxic waste and require appropriate safe disposal.

Table 1. Blasting technologies according to environmental requirements [7]

3. LASER CLEANING TECHNOLOGY

Laser cleaning safely removes coatings, contaminants, oxides, production residues and more without chemicals, solvents, abrasives, water, or

dust. Cleaning with laser light is highly precise. Treatment can be applied to the exact area required, including 2D shapes and on-the-fly without the need for masking. In contrast to conventional cleaning methods, such as sandblasting or ice pellet blasting, laser cleaning offers the benefit of being very quiet. The technology can easily be integrated on-line into many production processes in a way not possible with other options. Thus time, costs and environmental burdens can be reduced by completing previously outsourced work in-house. Benefits:

- Reduction of solvents (climate protection),
- Reduction of abrasives and chemical cleaners,
- Reduction of nuclear contaminated waste,
- Reduction of process outsourcing burdens,
- Reduction of masking materials, etc.,
- Process can be used safely in the field (e.g. pylons in cropland) and locations when methods such as abrasive blasting are not possible. [8]

Application of laser technique gives possibility of almost full control of the encrustation removal process at the surface of works. Selective and precise interaction of the light beam is a fundamental advantage of non-invasive treatment of more or less tightly connected unwanted surface layers.

Laser cleaning systems are currently in use in the automobile, aerospace, bakery, food, electronics, restoration and other industries. The cleaning surface reflects laser energy and is minimally affected, however, any contaminants on the surface absorb the laser energy and are quickly vaporized, with any fumes or particulates removed by an in-built filter.

When a laser beam irradiates on the material surface, it may be considered that energy flows in only one direction in a semi- infinite body Fig. 5.

The depth the laser energy penetrated into the material surface is constrained by the duration of the laser irradiation. Increasing irradiation time will allow the laser energy to penetrate deeper so as to raise the material substrate temperature.

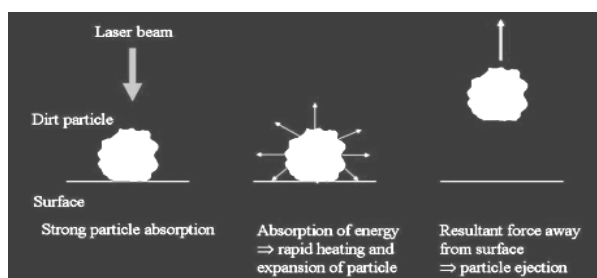


Fig. 5 Working of laser beam [15]

The cleaning of material surface stops when the contaminant is consumed, and consequently there is a minimal heat build-up, avoiding the microscopic roughening and cracking of metal surfaces that can be present when using traditional cleaning methods [9]. The technology steps can be summarized in the following points: [8, 9, 10, 11, 12].

- Powerful, short, rapid, moving laser pulses produce micro-plasma bursts, shockwaves, thermal pressure resulting in sublimation and ejection of the target material.
- A focused laser beam precisely vaporizes the target coating or contaminant.
- Process optimization of the laser beam produces maximum reaction with the target material for speed while, at the same time, does so safely and without harm to the base material.
- Metal surfaces are well-suited for many laser cleaning applications. Metallic and reflective surfaces are ideal although other substrates can be addressed. Optimized beam settings will not metallurgical change or damage the laser treated surface. Laser cleaning systems offer an extremely high level of control and precision.
- Only the coating, residue or oxide targeted for removal is affected as the laser beam is precisely adjusted not to react with the underlying metal surface.
- Laser beam power density is accurately and easily adjusted to achieve cleaning results.

4. EXPERIMENTAL TESTING AND VERIFICATION OF LASER CLEANING TECHNOLOGY

The realization of the first experimental testing was made in the cooperation with Trumpp, Slovakia s.r.o. Materials used for the experiments were:

a) Steel sheet (KOSMALT 190 IF), Table 2, dimension 100 x50 mm, thickness: 2 mm, according to standard STN 038737.

Chemical element	C	Mn	Si _{max.}	P _{max.}	S _{max.}	Al	Cu
Content [%]	max 0,04	max. 0,19	0,01	0,015	0,012	0,02 – 0,06	0,06

Table 2. Chemical composition, KOSMALT 190 IF

b) Synthetic lubrications with various properties (various viscosity):

1. Berutox M21 EPK 420, temperature range: -5 °C to + 200 ~ + 220°C, viscosity of the basic oil: 490 mm².s⁻¹, at the temperature t = 40°C [13]
2. Berutox M 21 KN, temperature range: -5 °C to + 200 ~ + 220 °C, viscosity of the basic oil: 490 mm².s⁻¹, at the temperature 40 °C, [14]
3. Beruplex LI-EP 2, temperature range: -30 °C to + 150 °C [14].

There were used 5 tested pieces for each experiment. In the Fig. 6 are shown dimensions and tested pieces.

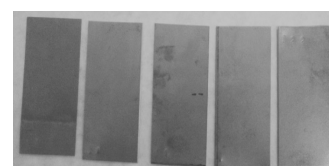


Fig. 6 Rectangular profile of deep-drawn sheet KOSMALT 190

After degreasing with technical white gasoline and US cleaning, the tested samples were weighed on laboratory scales MS, METTLER TOLEDO. The lubricants were applied by a paintbrush and were weighed again. The decreasing of tested samples by laser cleaning were experimentally provided on the laser compact machine TruMarkStation 5000, with the least power, to not do an effect on the surface layer of the metal by hardening. The condition of the laser parameters were: beam source TruMark 6130, optics = F 163, wavelength = 1604 μm , speed of the laser beam $v = 1000 \text{ mm/s}$, frequency = 50 kHz, defocus = 1,5 mm. The example of testing and workplace is shown in the Fig. 7.

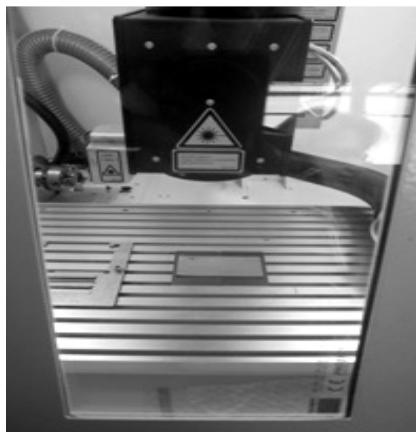


Fig. 7 The example of laser cleaning – position of the sample

After laser cleaning, the tested samples were weighted again and were found the weight loss of tested samples. The weighted values of tested samples are shown in the Table 3.

Sample	weight			
	Degreased sample by white gasoline	Sample + lubrication	Degreased sample by laser	Used lubricant
1	53,189	53,607	53,505	Berutox M 21 EPK 420
2	52,029	53,074	52,77	Berutox M 21 KN
3	53,972	55,518	54,593	Beruplex LI-EP2
4	52,577	53,661	52,598	Berutox M 21 KN

Table 3 Examples of tested samples cleaned by laser beam – sample U1-U5

The results after first planned experiment, where the laser beam passed only once through the surface sample during the laser cleaning, are shown in the Fig. 8 to Fig 13.

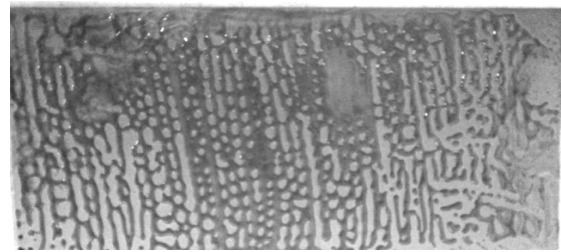


Fig.8 Visual evaluation after laser cleaning (Berutox M 21 EPK 420)

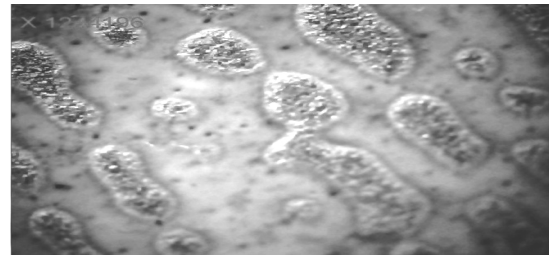


Fig. 9 Detail of degreasing lubricant by lubricant Berutox M 21 EPK 420 by USB microscope

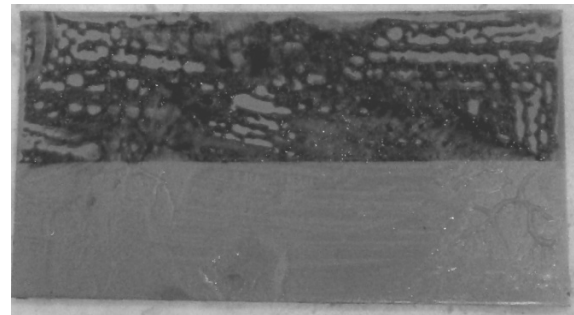


Fig. 10 Tested sample before (light) and after decreasing (dark), Berutox M 21 KN

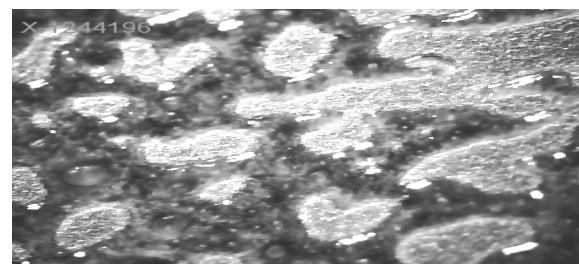


Fig. 11 Detail of degreasing of lubricant Berutox M 21 KN by USB microscope



Fig. 12 The sample after laser cleaning (Beruplex lub.)



Fig.13 Detail of degreasing of lubricant Beruplex LI-EP2 by microscope USB

The results of the comparison of the chosen tested samples weighted on the laboratory scales and cleaned by laser beam are shown in the Fig. 14.

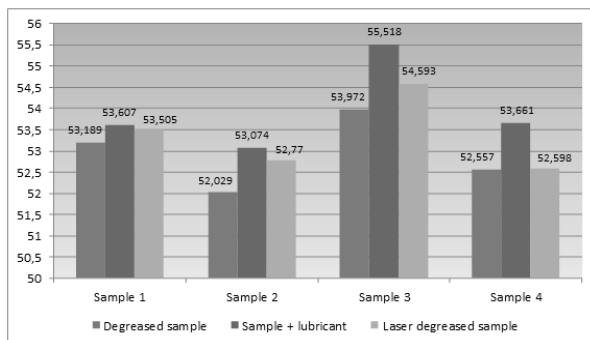


Fig. 14 Degreasing of tested sample by laser beam, sample 1 – Berutox M 21 EPK 420, sample 2 – Berutox M 21 KN, sample 3 – Beruplex LI-EP 2, sample 4 – Berutox M 21 KN

5 CONCLUSION

Due to the ongoing problem of environmental degradation, we try to find ways how to minimize the impact of negative factors on the environment. The engineering industry as a whole is greatly contributes to environmental degradation. One of these ways was to try decrease of the material without the using of chemicals.

In cooperation with TRUMPF Slovakia s.r.o., we tested and verified the possibility of cleaning of the lubricated samples with a laser beam (with the compact machine TruMark 5000) for the first time. The synthetic lubricants were used and laser beam passed only once over the surface of the sample.

From the experiments, we can make a conclusion after visual control that during the laser cleaning tests of the No.4samples reached the best results. The samples were greased by the synthetic lubricant BERUTOX M 21 KN, and on the other hand the worst results were reached with the samples No.1, which were greased by the synthetic lubricant Berutox M 21 EPK 420.

ACKNOWLEDGEMENT

The work was supported by Ministry of Education of Slovak republic KEGA 048TUKE-4/2015.

6 REFERENCES

- [1] BADIDA, M., SOBOTOVÁ, L. et al.. Základy environmentalistiky/ Basic of Enviromentalistics, TU Košice, Slovakia, 2013, pp.301.
- [2] BADIDA, M., SOBOTOVÁ, L. et al. Hydroerosion and Environment, Lüdenscheid: Ram - Verlag, Germany, 2013. pp.131.
- [3] BREZINOVÁ,J et al. Predúpravy povrchov v teórii a praxi. / Surface finishing in theory and practice. TU Košice, Slovakia, 2012, pp.
- [4] Odmas ovacie stroje/ Degreasing machines. STIKA, s.r.o. Slovakia, 2013. http://www.stikasro.sk/sk/odmastovacie_stroje.aspx
- [5] Dry ice cleaning/ Cold Jet catalogue, 2014 www.coldjet.com.
- [6] Dry ice blasting without pellets, Cryo-clean snow. Linde, Slovakia 2014, www.lindeplastics.com
- [7] Dry ice cleaning Applications, Cryonimics, ARTIMPEX N.V., 2014, www.cryonomic.com
- [8] Laser cleaning – Preserve natural resources, 2015, <http://www.cleanlaser.de/wEnglish/funktionsprinzip/umwelt.php>
- [9] JACKSON M.J., ROBINSON G.M., CHEN X. (2006) Laser Surface Preparation of Vitrified Grinding Wheels, In: ASM International, JMEPEG
- [9] Env.Friend. Cleaning with Light Reduces Costs 005 <http://www.prweb.com/releases/2005/06/prweb251764.htm>
- [10]Cleaning with laser light. Clean-Lasersysteme GmbH, Germany, 2014. <http://www.cleanlaser.de>
- [11] Laserové stroje/ Laser machines,2014, TRUMPF Slovakia s.r.o., <http://www.sk.trumpf.com/sk.html>
- [12]Laser cleaning.National Museums Liverpool, 2014. http://www.liverpoolmuseums.org.uk/conservation/departments/sculpture/laser_cleaning.aspx
- [13]Priemyselné mazivá (2014), Lubricant SK s.r.o., <http://www.lubricant.cz/cs/produkty/bechem/prumy slova-maziva/prevodova-maziva/berutox-m-21-epk-420>
- [14]Priemyselné mazivá (2014): Lubricant, <http://www.lubricant.sk/cs/produkty/bechem/prumy slova-maziva/ocelarensky-prumysl/berutox-m-21kn>
- [15] Laser cleaning conservation. <http://www.conservationslasers.com/ourproducts/4533647511>
- [16]Badida,M., Ladomersky, J. Králiková,R., Sobotová,L.,Bartko,L.:Základy environmentalistiky, ELFA,s.r.o., Košice, 2013, p.302, ISBN 978-80- 8086-219-0
- [17] Hodoli ,J., Badida,M., Majernik, M., Šebo,D.: Mašinstvo u inženerstvu zašтите životne sredine, FTH izdavaštvo, Novi Sad, 2003, p.273, ISBN 86-80249-75-0
- [17] Hodoli , J., Badida, M., Majernik, M., Šebo,D.: Mašinstvo u inženerstvu zašтите životne sredine, FTH izdavaštvo, Novi Sad, 2005, p.273, ISBN 86-85211-46-8.

Authors: Sobotova Lydia, Badida Miroslav, Technical university of Kosice, Faculty of Mechanical Engineering, Department og Process and Environmental Engineering, Slovakia.E-mail: lydia.sobotova@tuke.sk
miroslav.badida@tuke.sk

Krašnik M., Viloti , D., Ši anin L., Stefanovi , M.

EXPERIMENTAL AND NUMERIC ANALYSIS OF STEEL C45E FORMABILITY IN THE UPSETTING PROCESSES OF TAPERED SPECIMEN

Abstract: Commercial application of plastic forming technological methods has to be based on the principle of minimal material, time and energy consumption in creation of metal components with high performances. However, design of adequate technological procedure is not simple but, on the contrary, very complex demand to answer and I can not be achieved without prior research focused on the behavior of the material under various forming conditions from the standpoint of achieving maximum strain value. For that reason the forming limit diagram-FLD¹ became the most successful and most widely used tool which enables establishing of optimal and rational production concept.

In this paper is explored the possibility to apply steel C45E tapered specimen upsetting with the aim to more precisely define FLD in the β -factor positive area. Results have shown that there is a need to include tapered specimen upsetting model in the existing methodology of FLD defining.

Key words: Formability, Cold upsetting, Tapered specimen, Stress-strain state, Forming limit diagram

1. INTRODUCTION

Material formability is the ability of permanent change of shape under specific forming conditions without formation of cracks, deformation localization or any other macroscopic contact or free surface damage and internal microstructure damage to the workpiece. Due to the complex impact of various factors which are generally divided into material factors and forming conditions factors, formability function can only be defined in the implicit form:

$$F_M \equiv \varphi_e^l = f \left(H_M, S_M, T_O, \dot{\varphi}, T_\sigma \dots \right) \quad (1)$$

where:

F_M – is formability which is quantitatively expressed with the value of effective strain limit ϵ^l ,

H_M – is chemical composition of the material;

S_M – is microstructure state of the material;

T_O – is forming temperature; $\dot{\varphi}$ – is strain rate;

T_σ – is stress state determined by stress tensor.

If the formability research deals with the material of certain chemical and microstructure state under conditions of cold conventional forming, then equation (1) can be reduced to the expression (2) which points out to the dominant impact of stress state to the size of strain limit:

$$F_M = f(T_\sigma) = f(\beta) \quad (2)$$

where:

β – is indicator of stress state in the critical zone of the specimen.

Graphic interpretation of equation (2) is FLD and there are three basic forming models to define it (uni-axial tension - $\beta=+1$, pure torsion - $\beta=0$ and uni-axial upsetting - $\beta=-1$) [1], Fig. 1. Identical methodology was used in other papers, as in [1-3].

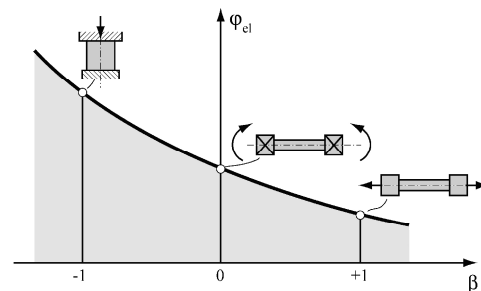


Fig. 1. Forming limit diagram - Basic models [1]

In order to define FLD a different kind of methodology can be used. It is based on establishment of functional dependence between main strains in the moment macroscopic damage to the material occurs [4].

In this paper are presented the results for steel C45E formability in the basic forming models which enabled preliminary definition of FLD. After that, using experimental and numeric approach, the data was obtained and it relates to the process of tapered specimen upsetting with flat plates. Research was realized on specimens in normalized state.

Aim of the research is establishment of possibility to introduce the model of tapered specimen upsetting for the purposes of widening FLD definition in the positive area of stress state indicators. Similar efforts were presented in paper [5], but they are aimed at defining FLD for brass CW603N.

2. THEORETICAL ASPECTS OF DETERMINING STRESS- STRAIN STATE

In order to form functional dependence $\epsilon_e = f(\beta)$ it is necessary to identify changes of stress-strain state in the zone of free surface of the specimen where first

¹ FLD – forming limit diagram

macroscopic damage occurs. In the following lines are presented mathematical formulations based on theoretical and experimental method which aid determination of all the parameters necessary to define FLD. Identical methodology was used in a number of other papers [2-3, 5, 8].

Starting with relation which connects stress-strain components in the area of plastic flow (3), pattern through which hydrostatic stress is defined (4) and using Von Mises yield criterion (5):

$$\frac{d\varphi_\theta}{\sigma_\theta - \sigma_m} = \frac{d\varphi_z}{\sigma_z - \sigma_m} \quad (3)$$

$$\sigma_m = \frac{\sigma_r + \sigma_\theta + \sigma_z}{3} = \frac{\sigma_\theta + \sigma_z}{3} \quad (4)$$

$$\sigma_\theta^2 + \sigma_z^2 - \sigma_\theta \cdot \sigma_z = \sigma_e^2 \quad (5)$$

Vujovi and Shabaik [1] defined equations for defining stress components σ_z and σ_θ in the place where crack occurred:

$$\sigma_z = \pm \sigma_e \cdot \left[1 - \left(\frac{1+2\alpha}{2+\alpha} \right) + \left(\frac{1+2\alpha}{2+\alpha} \right)^2 \right]^{\frac{1}{2}} \quad (6)$$

$$\sigma_\theta = \sigma_z \cdot \left(\frac{1+2\alpha}{2+\alpha} \right) \quad (7)$$

Based on previous equations, indicator of state of stress β can be defined as follows:

$$\beta = \frac{\sigma_r + \sigma_\theta + \sigma_z}{\sigma_e} = - \frac{1 + \frac{1+2\alpha}{2+\alpha}}{\sqrt{1 - \frac{1+2\alpha}{2+\alpha} + \left(\frac{1+2\alpha}{2+\alpha} \right)^2}} \quad (8)$$

Where:

σ_r and σ_z – are components of main stresses in the direction of r , and z axis,

σ_m – is hydrostatic stress,

σ_e – is effective stress.

Coefficient α represents deformation accrual rate and it is defined with the following pattern (9):

$$\alpha = \frac{d\varphi_\theta}{d\varphi_z} \quad (9)$$

In order to apply previous equation it is necessary to determine “strain path” $\varphi_\theta = f(\varphi_z)$. In this paper dependence in question is approximated with second degree polynomial:

$$\varphi_\theta = f(\varphi_z) = A\varphi_z + B\varphi_z^2 \quad (10)$$

Where:

A and B are coefficients of approximated function.

Principal strain components φ_z and φ_r in the critical zone of the specimen are determined according to the height of the marked area Z (Fig. 2) and specimen size in equatorial plane, using incompressibility condition:

$$\varphi_z = \ln \frac{Z_i}{Z_0}, \quad \varphi_\theta = \ln \frac{D_i}{D_0}, \quad \varphi_r = -(\varphi_z + \varphi_\theta) \quad (11)$$

Where:

Z_0 and D_0 – are initial values of marked area height and specimen size,

Z_i and D_i – are values of marked area height and specimen radius after i upsetting phases.

Effective strain at the lace cracks occurred is determined according to the following pattern (12):

$$\varphi_e = \frac{\sqrt{2}}{3} \sqrt{(\varphi_z - \varphi_\theta)^2 + (\varphi_\theta - \varphi_r)^2 + (\varphi_r - \varphi_z)^2} \quad (12)$$

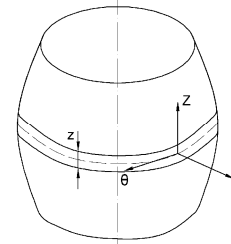


Fig. 2. Cylindrical specimen after deformation [3]

In formability tests which are based on non-monotonous plastic forming processes it is necessary to identify change in state of stress indicators β during forming and during defining FLD it is necessary to use average value β_{av} , which is determined as follows [3, 6]:

$$\beta_{av} = \frac{1}{\varphi_e'} \int_0^{\varphi_e'} \beta(\varphi_e) d\varphi_e \quad (13)$$

Here:

$\beta(\varphi_e)$ – is forming process history which is state of stress indicator of change serving as function of effective strain at the place the crack occurred.

In order to determine average value of state of stress indicator β_{av} we observe that if the critical material damage occurs at the free surface of the specimen, we can also use methodology based on flow theory [6-7].

3. EXPERIMENTAL RESERACH

Normalized steel C45E specimens were used for the research purposes. Microstructure consisted of ferrite grains and lamellar pearlite colonies. Preliminary form of FLD was determined using basic forming models and afterwards the results obtained in the process of tapered specimen upsetting were integrated in the same diagram. In Fig. 3-5 are shown specimens used for defining of FLD.

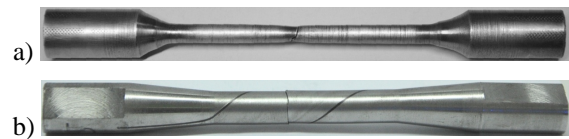


Fig. 3. Specimens after deformation:
a) uni-axial tension, b) torsion

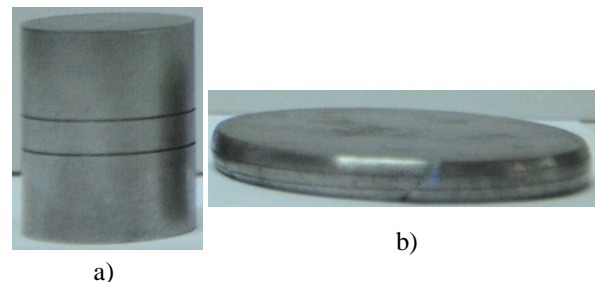


Fig. 4. Upsetting of cylinder by flat plates
a) initial specimen, b) specimen after forming

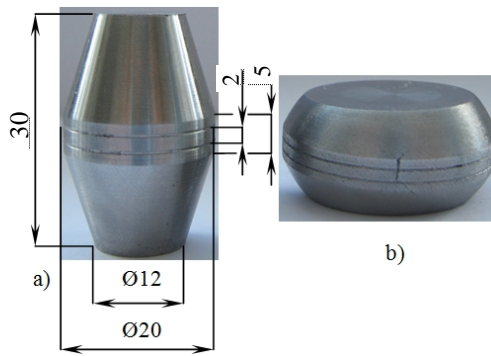


Fig. 5. Upsetting of tapered specimen: a) initial specimen, b) specimen after forming [2, 8]

All experimental research was conducted on Faculty of Technical Sciences in Novi Sad – Department for Production Engineering (Metal Forming Laboratory and Laboratory for Material Testing). Upsetting of the specimens was conducted using hydraulic press with triple action “Sack & Kieselbach“, with nominal force of 6.3 MN.

4. NUMERIC SIMULATIONS

FEM simulations of tapered specimen upsetting with flat plates were conducted using program pack Simufact.Forming 10 in order to make a comprehensive analysis of steel C45E formability. Modeling of the tools' geometry and the workpiece was conducted using software Solid Edge v.18. Tapered workpiece 3D model and upsetting process is shown in Fig. 6.

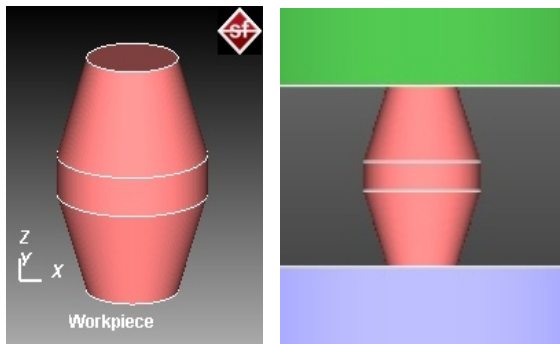


Fig. 6. 3D model – tapered workpiece and upsetting process [2]

Working elements of the tools were modeled as solid bodies and tapered specimens as formable bodies using experimentally determined flow curve in the form of Ludwik relation [2]:

$$K=462.84+451.9177 \cdot 0.3787 \quad (14)$$

Data from the database of Simufact.Forming software database was used in the course of modeling specimen material, and it is as follows: Young's modulus of elasticity $E = 210000$ MPa, material density $= 7800$ kg/m³ and Poisson ratio $\mu = 0.3$. Modeling of contact friction was conducted according to the results from the previous research realized in the Metal Forming Laboratory and Laboratory for Virtual Projecting and Rapid Prototype Production (Department for Production Engineering – Faculty of Technical Sciences Novi Sad). Adopted value of

friction coefficient is $\mu=0.12$.

Choice of machine model (hydraulic press with constant speed of tool movement 0.2 mm/min) was made according to the conditions of experimental research. Numeric simulations were realized in the cold forming conditions with defined temperature of tools and workpiece at 20 °C. Model diskings was conducted using 6351 finite element of Quads type. Mesh was generated automatically using a mesher Advancing Front Quad – Fig. 7.

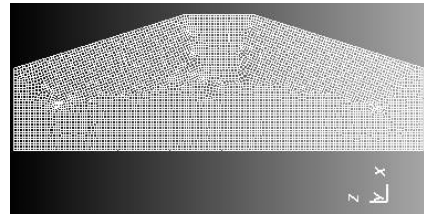


Fig. 7. Appearance of initial mesh of finite elements [2]

The above mentioned type of the finite element and mesher was adopted according to software recommendation but also for simple initial and final workpieces model form.

5. RESULTS

Uni-axial tension and torsion tests were realized in conditions of monotonous forming. After processing experimental data we obtained following information:

- uni-axial tension $\beta=+1$ $\epsilon^1 = 0.0780$
- pure torsion $\beta=0$ $\epsilon^1 = 0.6212$

Due to non-monotonous forming processes, upsetting of tapered and cylindrical specimens was incrementally realized. During the process, in each upsetting phase strain state on outer surface of equatorial area of the specimen was identified. Experimental results made it possible to determine stress state components, forming history, strain limit and β - factor average value according to equations stated in Chapter 2.

Relations of main strains $\varphi = f(\varphi_z)$ at the place the cracks occurred in cylindrical specimens is shown in Fig. 8, and forming history in Fig. 9.

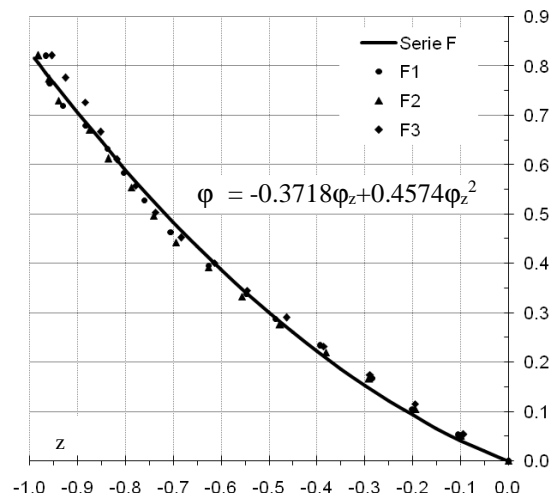


Fig. 8. “Strain path” - upsetting of cylinder by flat plates [2, 8]

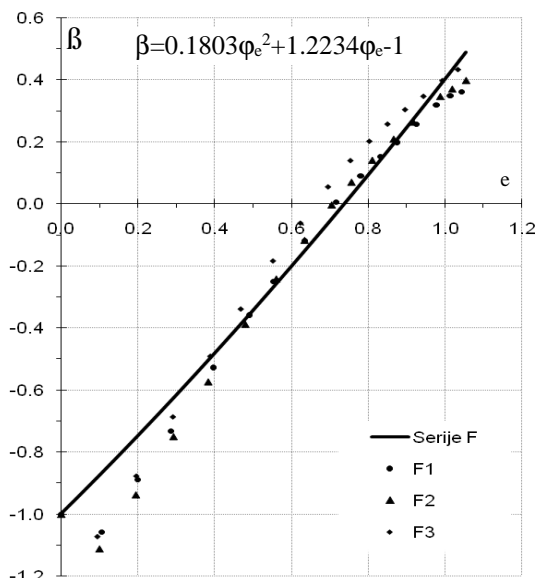


Fig. 9. “Forming history”- upsetting of cylinder by flat plates [2, 8]

Finally, according to equations 12 and 13 and according to test results for three specimens, characteristic values for process of free upsetting of cylinder by flat plates were determined: $\epsilon^l = 1.0434$ and $\beta_{av} = -0.2963$.

Processing of experimental results for the process of upsetting tapered specimens was conducted in the same manner as for the cylindrical specimens. Average values β_{av} and strains limit ϵ^l for individual specimens T₁₋₃ are presented in Table 1. Representative results of experimental research for T series in comparison with FEM analysis results are presented in Table 2.

Specimen mark	β_{av}	ϵ^l
T1	0.2041	0.3565
T2	0.1445	0.3556
T3	0.2073	0.3668

Table 1. β_{av} and ϵ^l – Upsetting of tapered specimens by flat plates [2, 8]

Numeric simulation of upsetting of tapered specimen was realized in order to identify changes in stress-strain state and determination of mutual dependence of strains in the directions of z and θ axis ($\theta = f(z)$) in the critical area of free surface. The third strain component (ϵ_r) was calculated from the law of volume constancy. Criterion of plastic fracture which would enable determination of the exact moment the macroscopic damage on numeric models occurred was not used in simulations. Due to that fact, maximal movement of virtual tools was defined according to data matching strain limits under experimental conditions of the research.

Overall results of FEM analysis of stress-strain state at the place of intersection of equatorial plane and free surface of the model (critical forming zone) were presented in [2]. In Fig. 10 and Fig. 11 is presented a part of results relating to distribution of stress-strain components to limit forming level.

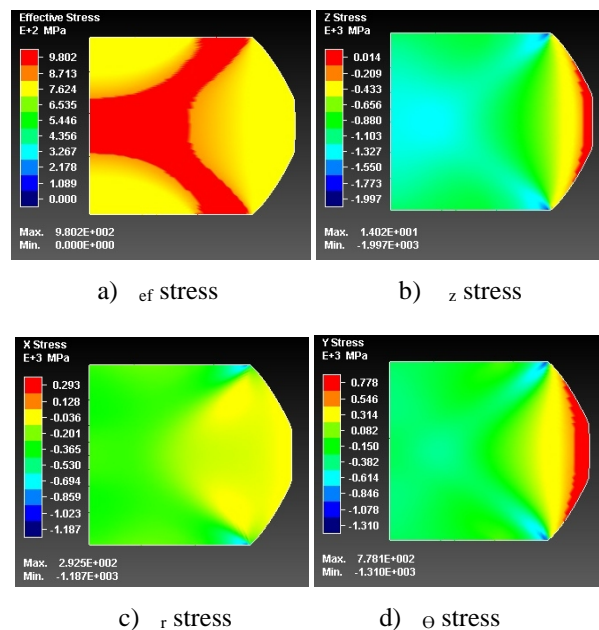


Fig. 10. Distribution of stress components for limit forming level – tapered specimen

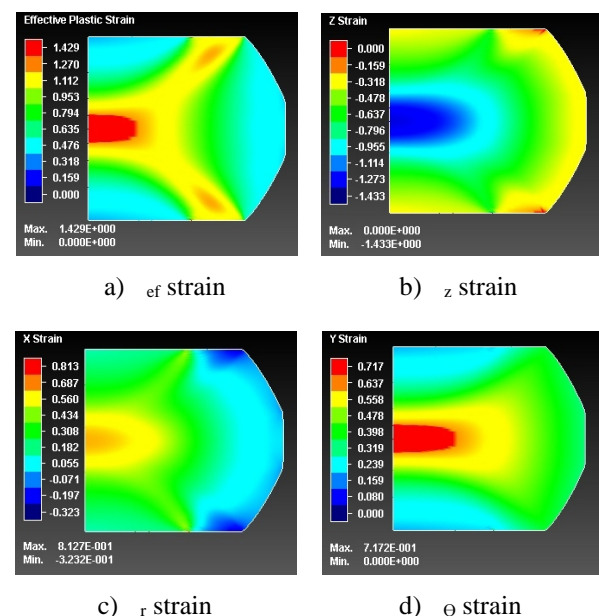


Fig. 11. Distribution of strain components for limit forming level – tapered specimen

Overall research results for the research of process of tapered specimen upsetting by flat plates made it possible to use regressive analysis for the purpose of defining dependence of logarithm strains $\theta = f(z)$, or indicators of stress state of effective strain $\beta = f(\epsilon)$, and then to determine effective strain limits (ϵ^l) and average values of stress state indicators (β_{av}). Theoretical approach based on forming theory was used for the purpose of determining β_{av} .

Sum overview of the results is presented in Table 2. In the following figures is presented graphic comparison of experimental and numeric results: dependence of logarithm strains $\theta = f(z)$ in Fig. 12 and change of stress state indicators depending on effective strain, $\beta = f(\phi_e)$ in Fig. 13.

Series mark	Approximate function $\varphi = f(\varphi_z) = A\varphi_z + B\varphi_z^2$ $\beta = f(\varphi_e) = a\varphi_e^2 + b\varphi_e - 1$	Correlation coefficient - R^2	φ_z^1	φ^1	φ_e^1	β_{av}
Series T _{exp}	$\varphi = -0.3360\varphi_z + 2.5986\varphi_z^2$ $\beta = -9.4133\varphi_e^2 + 8.8553\varphi_e - 1$	0.9799 0.9733	-0.3006	0.3212	0.3595	0.1862
Series T _{sim}	$\varphi = -0.3267\varphi_z + 2.7323\varphi_z^2$ $\beta = -5.5052\varphi_e^2 + 7.7038\varphi_e - 1$	0.9996 0.9757	-0.2945	0.3365	0.3667	0.1658

Table 2 . Analytical forms of functions “strain path” - $\varphi = f(\varphi_z)$, “forming history”- $\beta = f(\varphi_e)$, Strain limit - φ_e^1 and average values of β -factor - β_{av}

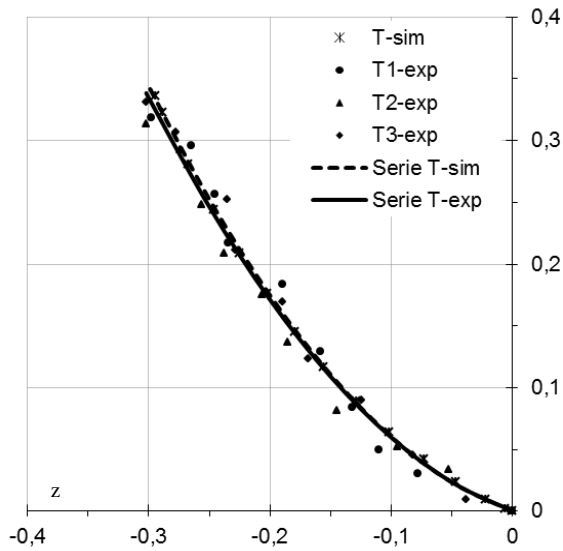


Fig. 12. “Strain path” - upsetting of tapered specimen by flat plates

In Fig. 14 is presented FLD with input of FEM analysis results (β_{av} , e^1). Approximation of forming limit curve was performed according to experimental data and it is aimed to comparison with numeric simulation results.

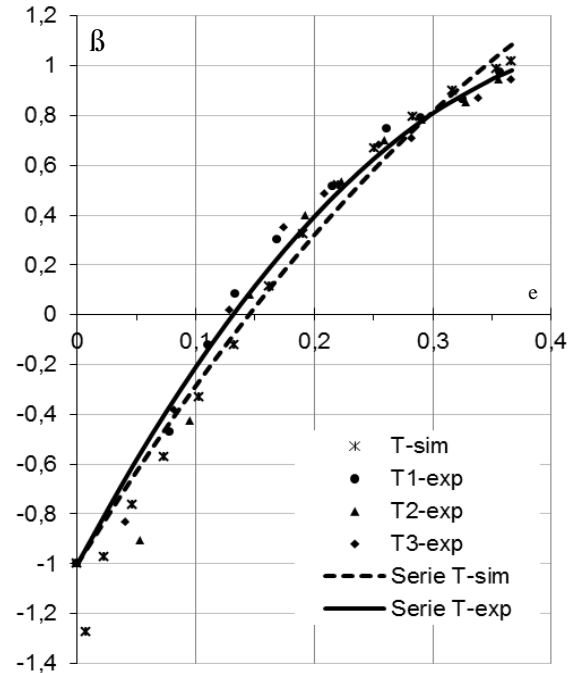


Fig. 13. “Forming history”- upsetting of tapered specimen by flat plates

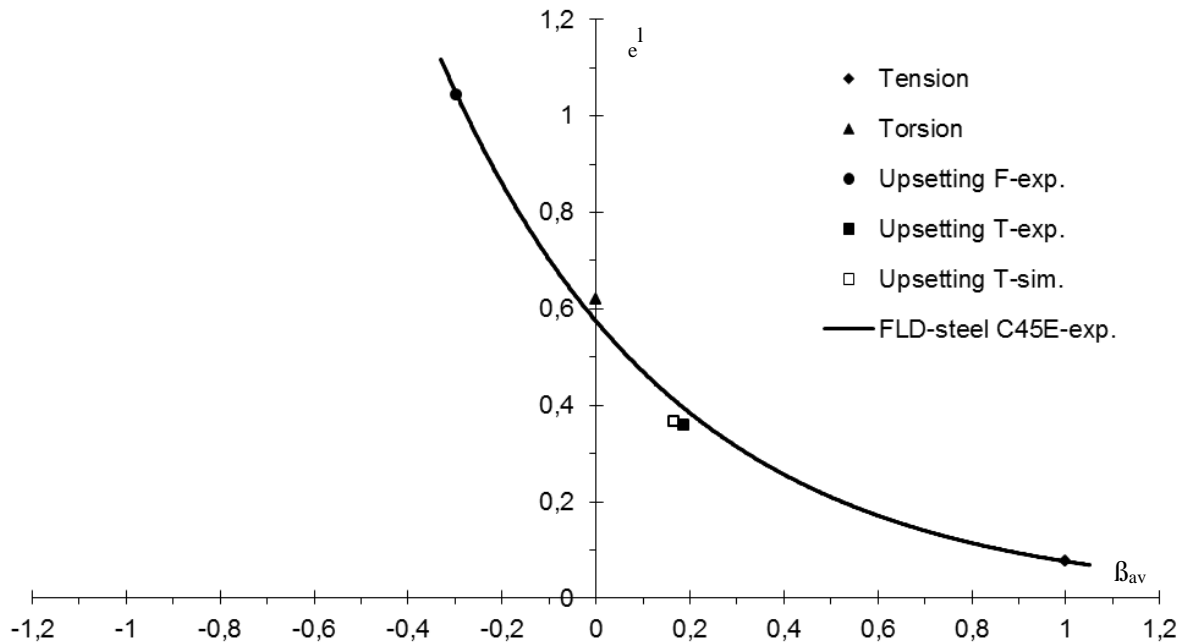


Fig. 14. FLD of steel C45E – comparative overview of experimental and numeric results

Regardless of the approach used, it is evident that the position of tapered specimen upsetting by flat plates in FLD almost identical. Observing it numerically, strain limit obtained through FEM analysis is about 2% larger than experimental value. For that reason we can draw a conclusion that numeric simulation results support general flow of the forming limit curve whose process of defining is based on basic forming models.

6. CONCLUSION

According to experimental research and FEM numeric simulations we can draw following conclusions:

- Stress state identification results on tapered specimen free surface have shown that shape and dimensions of workpieces have strong impact to the changes of stress components.
- Increase of forming limit degree leads to reduction of pressure component of normal stress σ_z , which is more strongly pronounced in the final upsetting phases. On the other hand, value of tangential component of normal stress σ_{θ} is continuously increasing.
- If the trend of changes of stress components on the free surface of the specimen is analyzed in the context of their impact to material formability, it can be noted that in the course of upsetting the tapered specimen a continuous worsening of forming conditions occurs where the dominant impact comes from tangential component of normal stress σ_{θ} whose tension impact accelerates reaching the critical level of accumulated damage to microstructure.
- If we consider the dependence of tangential (tension) stress (σ_{θ}) on intensity of tangential stress on contact surfaces, i.e. friction coefficient, we can hypothetically state that tapered specimens show the same behavior as cylindrical specimens under the condition that the upsetting process of cylindrical specimens by flat plates is realized under the conditions of high coefficients of contact friction. Direct consequence is reduction in steel formability in the processes of tapered specimen upsetting in relation to the process of upsetting the cylinder.
- Average values of stress state indicators ($\sigma_{av}=0,1862$ – exp. and $\sigma_{av}=0,1658$ – FEM) which together with limit values of effective strain ($\epsilon^l=0,3595$ – exp. and $\epsilon^l=0,3667$ – FEM) determine the position of tapered specimen upsetting process in FLD enabled more precise determination of forming limit curve in the positive area of σ_{θ} -factor.
- Finally, model of tapered specimen upsetting by flat plates provides new information of steel C45E formability in relation with basic forming models with justified necessity for its incorporation to the existing FLD defining methodology.

7. REFERENCES

- [1] Vujovi , V., Shabaik A.: *Workability Criteria for Ductile Fracture*. Trans., ASME J. Engng. Mater. Technol., Vol. 108, p.p. 245-249., 1986.
- [2] Kraišnik, M.: *Impact of stress-strain state to development of microstructure damage and material formability in the process of cold bulk forming*, Doctoral dissertation, Faculty of Mechanical Engineering, East Sarajevo, 2014.
- [3] Viloti , D., Alexandrov, S., Plan ak, M., Movrin, D., Ivaniševi A., Viloti , M.: *Material Formability at Upsetting by V-Shape Dies*, Steel research international, p.p. 923-928, Special Edition 10th International Conference on Technology of Plasticity - ICTP, Aachen, Germany, 25th – 30th September 2011.
- [4] Hartley P., Vilotic D., Plancak M.: *Formability maps in cold forging with conical dies*, Proceedings of the 8th ESAFORM Conference on Material Forming, Cluj-Napoca, Romania, pp. 527-530., 2005.
- [5] Ivaniševi A., Viloti D., Ka mar ik I., Milutinovi M.: *Upsetting of brass billets by flat dies*, Journal for Technology of Plasticity, Vol. 38, N_o 2, pp. 191-199., 2013.
- [6] Viloti D., Plan ak M., upkovi ., Alexandrov S., Alexandrova N.: *Free Surface Fracture in Three Upsetting Tests*, Experimental Mechanics Vol.46: p.p. 115–120, 2006.
- [7] Alexandrov, S.: *Fracture prediction in steady ideal plastic flows*, Acta Mechanica Vol.163, p.p. 127–138, 2003.
- [8] Kraišnik M, Viloti D, Ši anin L, Petrovi Ž.: *Initial microstructure state impact to steel C 45E formability*, 11th International Scientific Conference MMA 2012- Advanced Production Technologies, Novi Sad, p.p. 453-458., 2012.

Authors: Assistant Professor, **Milija Kraišnik**, University of East Sarajevo, Faculty of Mechanical Engineering, Vuka Karadžića 30, 71123 East Sarajevo, Phone.:+387 57 340847, **Prof. dr Dragiša Viloti** , **Prof. emeritus dr Leposava Ši anin**, University of Novi Sad, Faculty of Technical Sciences, Department for Production Engineering, Trg Dositeja Obradovića 6, 21000 Novi Sad, Serbia, Phone.: +381 21 4852349, **Prof. dr Milentije Stefanovi** , University of Kragujevac, Faculty of Engineering, Sestre Janjić 6, 34000 Kragujevac, Phone.: +381 34 336001
E-mail: milijakraisnik@yahoo.com
vilotic@uns.ac.rs
lepos@uns.ac.rs
stefan@kg.ac.rs

Kovačević, L., Terek, P., Miletić, A., Kukuruzović, D., Kakaš, D.

APPLICATION OF CASTING SIMULATIONS IN OPTIMIZATION OF GATING SYSTEM WITH VERTICAL RUNNER EXTENSION

Abstract: One of the most influential stages in the production of high quality castings is the mold filling process. During the mold filling, surface turbulence causes entrainment of oxide films into the bulk liquid which have detrimental effect on the integrity of the final product. Avoiding formation of these defects is feasible by applying non-pressurized bottom gating systems. However, for most demanding castings one needs to go a step further and employ a surge control system. The purpose of this research is to investigate benefits of vertical runner extension (VRE) proposed by prof. Campbell. Different variants of gating systems, with and without VRE, are simulated and their effectiveness is analyzed. Based on obtained results, guidelines for implementation of VRE's are given.

Key words: casting simulation, gating system, quality, surge control

1. INTRODUCTION

In recent years there is a considerable and steady increase in non-ferrous castings production. In the period between 2010 and 2013 average annual growth rate of the European non-ferrous industry was 10.5% [1]. More than 50% of this production is related to the automotive industry and its continuous quest to reduce fuel consumption by producing lighter vehicles [2]. Therefore, quality demands on metalcasting facilities are continually increasing and the production of castings almost completely free from defects becomes a necessity.

One of major problems encountered in aluminum alloy castings production is the turbulence during mold filling, which significantly affects the quality and reliability of the final product. Aluminum has extremely high affinity for oxygen. Consequently, aluminum alloys have tendency to form an insoluble oxide films on the molten metal surface. In the case of surface turbulence, when the surface happens to fold, the oxide film becomes entrained in the bulk liquid. Since the oxide film is entrained by a folding action, the resulting defect is a double oxide film called a bifilm. Because the films are necessarily folded dry side to dry side, there is little or no bonding between these dry interfaces, so that the double films act as cracks [3]. As the casting solidifies the bifilm becomes frozen into the casting. Therefore, no matter how clean the metal just prior to pouring, significant damage to the metal can still occur. The presence of bifilms has detrimental effect on the resultant casting's mechanical properties, such as yield strength, tensile strength, elongation and contribution toward a reduction in casting pressure tightness [4].

Green and Campbell [5] found that the tensile strength is controlled by the gating system design. Use of a gating system that promoted surface turbulence and thus formation of large amounts of entrained bifilm defects produced castings with poor reliability with Weibull moduli in the range 11 to 22, which is

approximately the range of engineering ceramic materials. The use of the gating system designed to minimize surface turbulence produced castings with Weibull moduli in the range 38 to 54, which is close to those of aerospace forgings [6]. Similar findings were reported in numerous additional studies [5,7-9].

Therefore, in order to obtain castings that can meet the rigorous quality demands of contemporary automotive industry, one has to design a gating system that is able to maximally suppress the occurrence of surface turbulence. Campbell [3] noted that in order to achieve this task, surface tension of the surface has to be greater than the dynamic pressure within the melt. Therefore, he introduced the concept of critical velocity which is the maximum allowable velocity of the melt that enables obtaining defect free castings. Numerous researches have proven that the value of critical velocity for aluminum alloys is 0.5 m/s [8]. Velocity of 0.5 m/s is achieved by a metal stream falling from a height of approx. 12.5mm. This is extremely small value for all practical purposes, as most of the castings in production have significantly larger dimensions. Consequently, in order to obtain high quality castings, one has to find a way to reduce the velocity of the melt prior to the ingates. This is done by using surge control systems such as: vertical runner extension (VRE), terminal vortex surge riser, vortex sprue, vortex well, vortex runner, diffusing runner and similar systems [3,6,10]. Unfortunately, surge control is relatively novel concept and most of designs are not adequately tested by numerical simulations nor by practical experiments. Therefore, benefits of their use are not completely understood and proven.

The purpose of the presented research is to investigate benefits of the VRE as a surge control system.

2. METHODOLOGY

Geometry selected for this investigation is shown in Fig. 1. It is a medium sized casting and therefore can be selected as a suitable representative to explore

techniques for reducing surface turbulence induced by high speeds encountered in the gate area due to gravitational acceleration. One of the most common aluminum alloys, AlSi7Mg is selected as a casting material for all simulations.

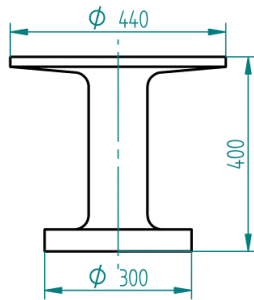


Fig. 1 Drawing of the selected geometry

In order to minimize flow speeds during mold filling stage, the geometry was rotated by 90 degrees. Two different systems were analyzed. First, a naturally pressurized gating system was designed for the selected geometry by following guidelines given by prof. Campbell [3]. It is used as a benchmark in order to adequately assess the benefits of the VRE addition. Second, after the second ingate at the end of the runner, VRE is added in an attempt to slow down the molten metal. Since there are no developed calculations several iterations are used until the optimal size of the VRE was achieved.

A common practice is to make chunky runners in an effort to deliver the metal as quickly as possible, to avoid loss of temperature, cold shuts and misruns [11]. However, recent investigations [3,4] suggest that a thin running system often produces a better quality casting since the surface turbulence is easier to control by surface tension of the molten metal. Therefore, rectangle cross section of the gating system was selected. Whenever possible, aspect ratio of 4:1 was maintained.

The 3D geometries were modeled in Siemens Solid Edge ST8 and then imported into the simulation software. In order to make simulations computationally efficient, models did not include a pouring basin. The simulations were carried out using Magma5 v5.2 from MAGMA Giessereitechnologie GmbH, Germany. In all simulations the pouring temperature was selected to be 700°C and the pouring rate was defined through pressure curve boundary condition. The mold material was green sand and the initial mold temperature was set as 40°C. Values of material properties and heat transfer conditions were selected from internal database of the Magma5.

3. RESULTS AND DISCUSSION

3.1 Naturally pressurized gating system without surge control elements

As expected, classical gating system without surge control was unable to successfully suppress the occurrence of surface turbulence and generation of undesirable bifilm defects. Although, the total area of the ingates was carefully calculated in an effort to limit melt velocity to a value under the critical velocity, this

has not happened. As can be seen in Fig. 2, even with the implementation of tapered runner, momentum of the flowing liquid causes the furthest ingate to be favored. Metal jets into the open mold cavity producing substantial turbulence and leading to irreparable damage to the mechanical properties of the final product.

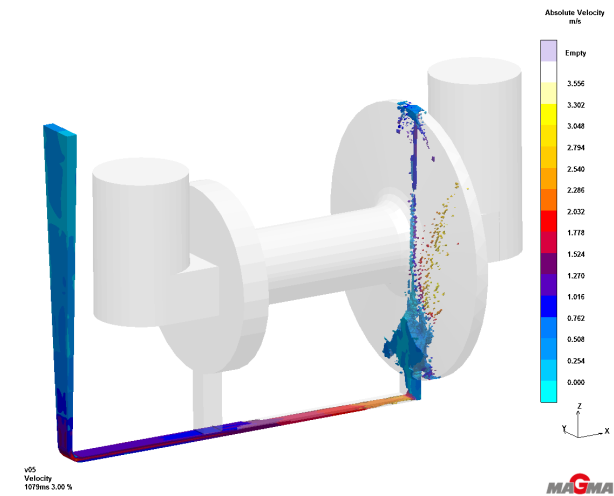


Fig. 2 Calculated absolute velocities at the beginning of the mold filling

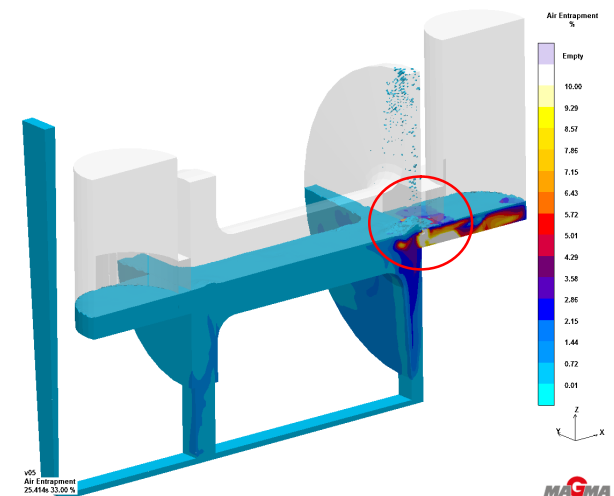


Fig. 3 Calculated air entrapment parameter 25.4 seconds after the start of pouring

Air entrapment parameter field 25.4s after the start of pouring is given in Fig. 3. This time corresponds to 33% filling of mold cavity. Even at this late stage of filling there is evidence of surface turbulence. Small jetting of the incoming melt can be seen protruding from the metal surface. Although, limited in size this jetting is still a potent generator of casting defects, as documented by the value of the air entrapment parameter.

Initial gating system included one more potent source of casting defects, as shown in Fig. 4.

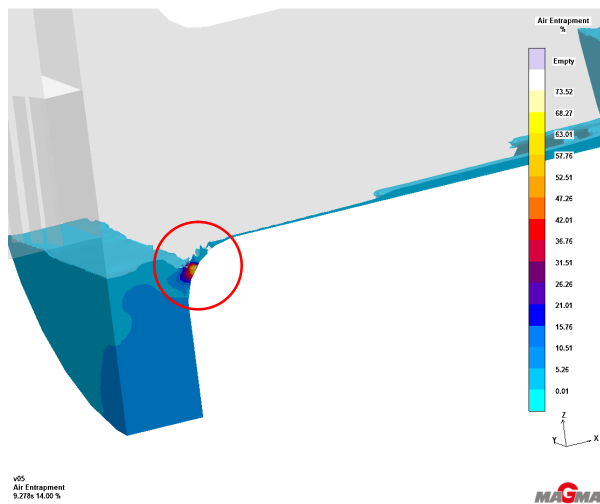


Fig. 4 Air entrapment due to additional fall of molten metal at the moment when the flows from two ingates meet

Usual procedure during design of a filling system with multiple ingates, is to make the ingates approximately equal (as long as geometry allows such connection). This can lead to additional and unnecessary falling of the molten metal inside the mold cavity. In this case, ideal situation would be to make the streams of metal from the two ingates meet at the middle portion of the casting. Unfortunately, since the filling of the left plate through the ingate 1 is somewhat slow, this portion of the casting is starting to be filled by metal from ingate 2. Therefore, there is a need for iterative optimization of the relative size of the two ingates in order to achieve proper filling pattern. This cannot be done through classical calculations and is the perfect illustration for the necessity of using computer simulations in the process of gating system design for high quality castings.

3.1 Gating system with vertical runner extension

Calculated absolute velocities for gating system with VRE, at the moments when the molten metal starts to enter the mold cavity from ingates 1 and 2 are given in Fig. 5 and Fig. 6. Results indicate adequate filling conditions without the air and bifilm entrapments. The only notable surface turbulence is confined to the VRE itself. Flow of metal into the casting is smooth with the surface flow velocities below critical velocity of 0.5m/s. Therefore, results suggest that VRE is not able to completely eliminate generation of casting defects. However, jetting of the molten metal is expelled from the casting and is confined to a gating system, thus resulting in a high quality product.

Presence of the bifilm defects in gating system and in large quantities can provoke quality issues if not properly addressed. In a typical foundry operation, gating system and feeders are remelted after being cut off from the casting. Presence of oxide inclusions in remelted scrap can deteriorate initial melt quality and can cause increased scrap rate if not properly eliminated during melting or consequent molten metal treatment e.g. deoxidation.

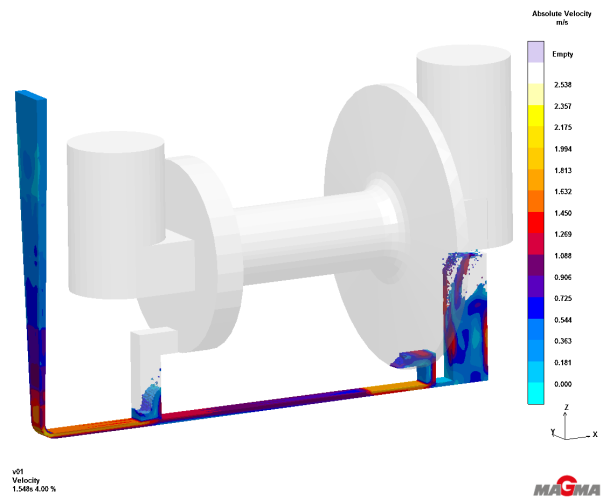


Fig. 5 Calculated absolute velocities at the beginning of the mold filling from the ingate2

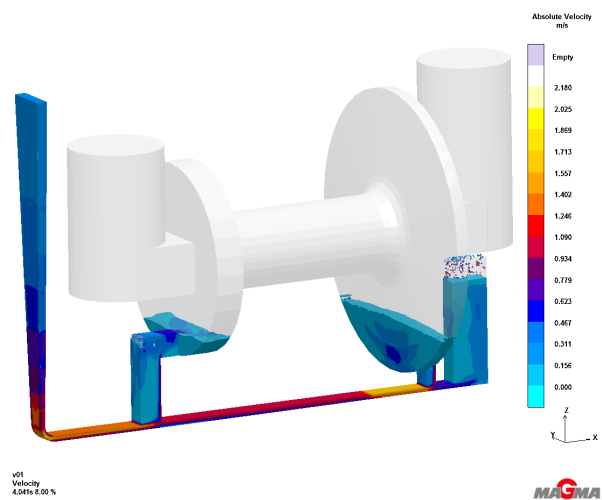


Fig. 6 Calculated absolute velocities at the beginning of the mold filling from the ingate 1

It should be noted that the optimization of VRE was completed through several iterations. First literature assumptions and recommendations for design of the VRE's suggested that there should be minimal size of the reservoir necessary to control the initial surge of molten metal. Further increase in size of the VRE should theoretically only influence the economic aspect of the production (casting yield) without compromising achieved product quality. It was found that this hypothesis was not true in this investigation. When the size of the VRE's was larger than optimal, simulation results registered rise in the ingate velocities. Large size of the reservoir prolonged time until molten metal reached the ingates increasing the total volume of metal located in the VRE at this critical moment. Consequently, height of the metal inside the reservoir also increased, leading to higher pressures and flow velocities inside the ingates.

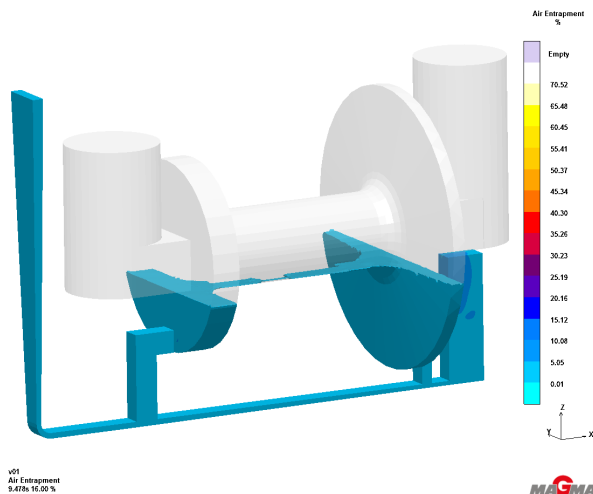


Fig. 7 Calculated air entrapment parameter at the moment when the flows from two ingates meet

By iterative optimization of the area ratio between the two ingates, it was possible to influence filling pattern and completely eliminate the additional falling of the molten metal inside the mold cavity, Fig. 7. Therefore, it can be expected that the resulting casting will have high mechanical properties.

4. ACKNOWLEDGEMENTS

Authors would like to thank MAGMA Giessereitechnologie GmbH, Germany for their generous support through donation of their software Magma5.

5. CONCLUSIONS

Addition of vertical runner extension (VRE) to the naturally pressurized gating system gives a possibility completely eliminates surface turbulence from the casting mold cavity. All turbulence is confined to the VRE.

The optimization of a gating system can be done by different routes. Nevertheless, the numerical simulation offers the possibility of a shorter time and lower investment cost. In the case of VRE, the numerical simulation is the only viable route for optimization of a gating system and production of high quality castings.

6. REFERENCES

- [1] CAEF - The European Foundry Association: *The European Foundry industry 2013*, 2014.
- [2] CAEF - The European Foundry Association: *The European Foundry industry 2011*, 2011.
- [3] Campbell, J.: *Castings Practice: The Ten Rules of Castings*, Elsevier Butterworth-Heinemann, Oxford, 2004.
- [4] Pischel, R.P.: *Calming the Turbulence in Your Runner System*, Modern Casting, 96, p.p. 24–27., 2006.
- [5] Green, N., Campbell, J.: *Influence in oxide film filling defects on the strength of Al-7Si-Mg Alloy Castings*, AFS Transactions, 114, p.p. 341–347, 1994.
- [6] Hsu, F.-Y., Lin, H.-J.: *A Diffusing Runner for Gravity Casting*, Metallurgical and Materials Transactions B, 40, p.p. 833–842, 2009.
- [7] Mi, J., Harding, R.A., Campbell, J.: *Effects of the entrained surface film on the reliability of castings*, Metallurgical and Materials Transactions A, 35, p.p. 2893–2902, 2004.
- [8] Campbell, J., *Complete Casting Handbook: Metal Casting Processes, Techniques and Design*, Elsevier Butterworth-Heinemann, Oxford, 2011.
- [9] Eisaabadi Bozchaloei, G., Varahram, N., Davami, P., Kim, S.K.: *Effect of oxide bifilms on the mechanical properties of cast Al-7Si-0.3Mg alloy and the roll of runner height after filter on their formation*, Materials Science and Engineering: A, 548, p.p. 99–105, 2012.
- [10] Ahmad, R., Talib, N.: *Experimental study of vortex flow induced by a vortex well in sand casting*, Revue de Métallurgie, 108, p.p. 129–139, 2011.
- [11] Gebelin, J.-C., Jolly, M.R., Hsu, F.-Y.: *“Designing-in” controlled filling using numerical simulation for gravity sand casting of aluminium alloys*, International Journal of Cast Metals Research, 19, p.p. 18–25, 2006

Authors: MSc Lazar Kova evi , MSc Pal Terek, MSc Aleksandar Mileti , MSc Dragan Kukuruzovi , Prof. dr Damir Kakaš, University of Novi Sad, Faculty of Technical Sciences, Trg Dositeja Obradovi a 6, 21000 Novi Sad, Serbia, Phone: +381 21 485 2330.

E mail: lazarkov@uns.ac.rs

Relji , V., Milenkovi , I., Šešlija, D., Dudi , S., Šulc, J.

DEVELOPMENT OF REMOTE CONTROLLED PNEUMATIC SPRING

Abstract: Remote controlled pneumatic spring represents a new experimental setup in the field of mechatronics. It is designed to simulate the linear mechanical spring under compression load, under different conditions. The simulation is realized using pneumatic cylinders. The cylinders are remote controlled, via Internet, from any location with Internet access. In addition, presented mechanical structure describes linear spring more realistic than the previous version. This setup will help all users better understanding the basics of spring theory.

Key words: spring, pneumatic, remote control, LabVIEW

1. INTRODUCTION

In order to strengthen cooperation between high schools and faculties, nowadays, researches develop remote labs, which help all students better understanding of theory and introducing in work with elements that are used in industry and manufacturing processes. There are a lot of proofs [1] that remote laboratories for advanced motion control are important tools for teaching students in mechatronics courses of control system engineering and experimentation with a wide range of feedback device. In [2], authors emphasised that online engineering is increasingly important for a growing number of higher education institutions. Also, online experimentation promotes user immersion in virtual environments recreating the real experience [3].

This paper describes newly designed remote experiment called “pneumatic spring” which simulates a mechanical spring under compression load, under different conditions. We have studied spring theory of the basic experiment described in [4]. It will be shown in Section 2.

The work is presented in the following manner. Section 2 gives a detailed description of experimental environment. Section 3 gives report about experimental results. In section 4, we provide concluding remarks and we outline topics for future investigations.

2. EXPERIMENTAL SETUP

Pneumatic spring has previous versions, but some improvements are necessary. In papers [5-7], we have described a way of using a pneumatic spring. In this paper, improved setup of pneumatic spring will be presented in order to help easier and better understanding of spring theory. Remote controlled pneumatic spring is a mechatronic system. It is composed of elements from different engineering fields. The first step was the studying of spring theory. The second step was development of mechanical structure of pneumatic spring. The third step was a realization of new control scheme. Finally, the fourth step encompassed system programming.

2.1 Spring theory

In this paper, we used the basic of linear spring theory. Spring stiffness (k) is calculated from spring's geometry and shear modulus using formula 1 [8]:

$$k = \frac{G \cdot d^4}{8 \cdot D^3 \cdot n_a} \left[\frac{N}{mm} \right] \quad (1)$$

where is:

- G - shear modulus of material $\left[\frac{N}{mm^2} \right]$,
- d - spring wire diameter [mm],
- D - mean diameter of spring [mm], and
- n_a - active coils.

Another formula have to be incorporated in this setup, because of its importance for this system. It is formula for calculating pressure of compressed air. Pressure in our system is calculated using formula 2:

$$p = \frac{F}{d_1^2 \cdot \pi} = \frac{k \cdot x}{d_1^2 \cdot \pi} \quad [bar] \quad (2)$$

where is:

- d_1 – diameter of pneumatic cylinder [mm], and
- x – elongation [mm].

It is necessary to emphasize that the effect of the frictional force in this paper is neglected.

2.2 Mechanical structure of pneumatic spring

Pneumatic spring was realized using two double acting pneumatic cylinders that placed opposite each other. CAD model of the system was developed in software package Solid Works and it is presented in Fig. 1. The first cylinder (Fig. 1, position A) simulates a force which is required to displace the spring from the equilibrium position under compression load. The second cylinder (Fig. 1, position B) simulates the spring behaviour under different conditions.

This improved mechanical structure shows linear spring more realistic then the previous versions. Namely, the previous structure was installed in different way. Pneumatic cylinders were placed one above the other. In that setup it was hard to distinguish

which cylinder simulates the spring and which cylinder simulates force which is required to displace the spring from the equilibrium position.

The installation of newly version of pneumatic spring is quite different. Pneumatic cylinders are connected with the base structure (Fig. 1, position C), made of wood, using a purposeful created couplings (Fig. 1, position D) and connections of screws (Fig. 1, position E). Another important element of the system is an electrical pressure regulator (Fig. 1, position F) which is connected with base structure using connections of screws, too. Cylinders have the mark: Festo DNC-32-100-PPV-A. Electrical pressure regulator has the mark: Festo MS6-LRE-1/4-D7-OP-PI-SK5-VK5-VJBE [9].

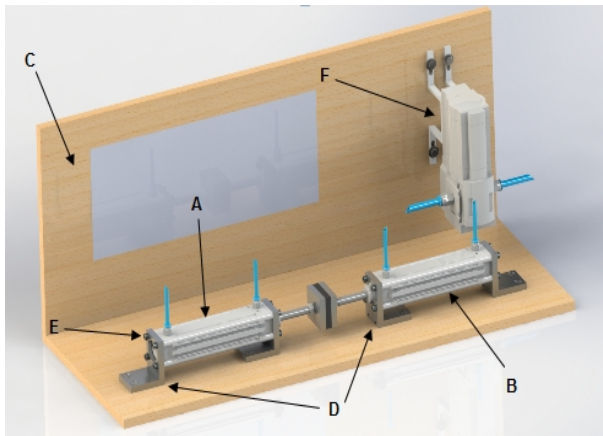


Fig. 1. CAD model of pneumatic spring

2.3 Pneumatic control scheme

A new control scheme is simpler than the previous one which is represented in [5-7]. It is developed in software package Fluid Draw (Fig. 2).

In initial moment, both monostable solenoid 3/2-way valve (Fig. 2, position 1V1 and 1V2) are actuated. On that way, compressed air, with a pressure value of 6 bar, is brought from source (Fig. 2, position P) to piston rod side of cylinder B. On same way, compressed air (a value is equal value of secondary pressure from electrical pressure regulator (Fig. 2, position 1V4), and it lower than 6 bar) is brought to piston side of cylinder A. In initial moment, system is idle.

When programmable logical controller (PLC), as main control device, will deactivate valve 1V2, cylinder B extracts and pushes cylinder A by compressing air in its piston side because there is the non-return valve (Fig. 2, position 1V3) which does not allow air leakage into the atmosphere (simulate of action of force). This process takes a few seconds. After that, PLC will reactive valve 1V2. Cylinder A extracts to the final extended position and pushes cylinder B which retracts in initial position (simulate of action of spring).

At the end of cycle, PLC will deactivate valve 1V1 for three second. It was done in order to drop compressed air from piston rod side of cylinder B into the atmosphere. After that, PLC will reactive valve 1V1 and cylinders will return in initial positions.

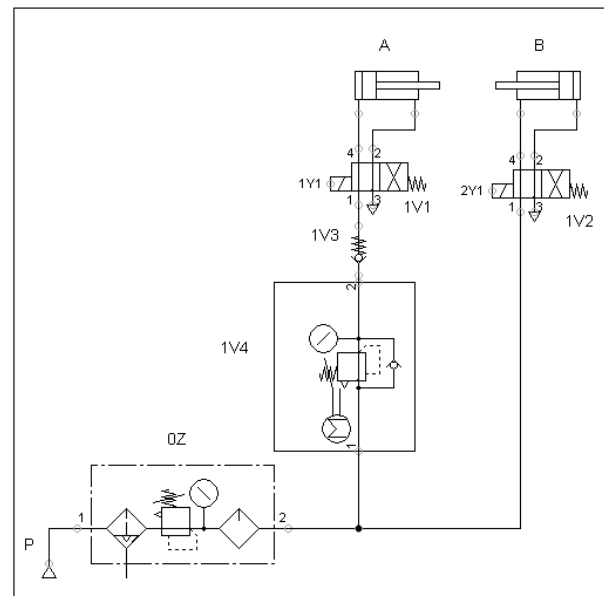


Fig. 2. Pneumatic control scheme

2.4 Remote system control

In version of pneumatic spring described in [6], control was enabled only in local network. In this new version, remote control of pneumatic spring is enabled using object-oriented programmable language called LabVIEW and TCP/IP protocol from any location with Internet access. System is organized in the following manner (Fig. 3). All users (clients) need to install client's application (Fig. 4) on their computers. For running of application, clients must install a LabVIEW Run-Time Engine 2013. It can be downloaded from web page: <http://www.ni.com/download/labview-runtime-engine-2013/4061/en/> [10].



Fig. 3. Organization of system

Before starting application, clients have to sign in to the application with the user name and password. After that, they have to fill in parameters from formula (1) and formula (2). The calculated value of secondary pressure on the electrical pressure regulator will be shown in application. With starting application, clients send the calculated value to the server via Internet,

using TCP/IP protocol. Server sends received data to main control device – PLC using serial communication, RS232. This process is enabled with the the existence of server’s application (Fig. 5) which is also made in LabVIEW. PLC has the mark: Festo FC660 Standard. Code for PLC is written as statement list in software package FST4.10.

When PLC receives data, it adjust them for the secondary pressure on regulator. That is an initial moment. After that, process is carried out according to the procedure described in Section 2.3. Clients can track the system live with the installed web camera that is placed near the system. The camera can be accessed by entering its IP address in any web browser.

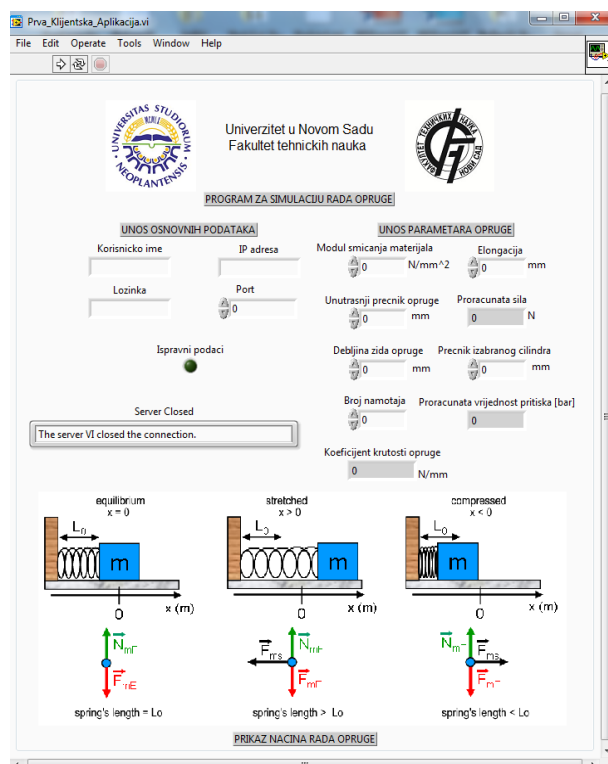


Fig. 4. Client’s application in LabVIEW

Clients can use (not required) recommended values for filling in fields in application. Recommended values are:

- $80000 \left[\frac{N}{mm^2} \right]$ - shear modulus of steel,
- 3-10 [mm] - spring wire diameter,
- 0.5-1.5 [mm] - mean diameter of spring,
- 20-50 - active coils,
- 20-50 [mm] – elongation, and
- 32 [mm] - diameter of pneumatic cylinder.

3. RESULTS AND DISCUSSION

It was found out by testing that the system work exactly as planned. Disadvantages, as control of system only in local network or inability to distinguish “spring” and “force”, which were appeared in previous version, are eliminated with this setup. Now, this setup will enable control from any location with Internet

access. In addition, improved mechanical structure shows linear spring more realistic. Also, the number of elements in pneumatic control scheme was reduced.

4. CONCLUSIONS

In this paper, we designed a new experimental setup called pneumatic spring. It is an example of mechatronic system and it is designed to simulate linear mechanical system under compression load, under different conditions. Remote control of system is enabled via Internet. This setup will help all users (clients) easier understanding basics of spring theory and introduction in elements that used in industry.

Further research would be related to development of similar systems called “circular manipulator”, “biaxial manipulator”, etc. All this system will remote control, via Internet.

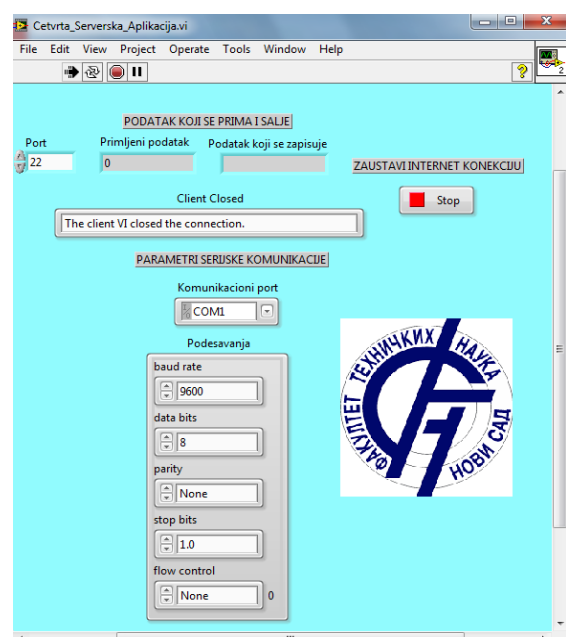


Fig. 5. Server’s application in LabVIEW

5. REFERENCES

- [1] Gadzhanov, S.D., Nafalski, A., Nedic, Z.: *LabVIEW Based Remote Laboratory for Advanced Motion Control*, 11th International Conference on Remote Engineering and Virtual Instrumentation (REV), 130-136, Porto 26.-28.02.2014., Polytechnic of Porto, Porto
- [2] Carpeno, A., Lopez, S., Arriaga, J.: *Using Remote Laboratory eLab3D for a Broader Practical Skills Training in Electronics*, 11th International Conference on Remote Engineering and Virtual Instrumentation (REV), 98-99, Porto 26.-28.02.2014., Polytechnic of Porto, Porto
- [3] Cardoso, A., Restivo, M.T., Quintas, M.R., Chouzal, F., Rasterio, M.G., Marques, J.C., Menzes, P.: *Online experimentation : Experiment@Portugal 2012*, 11th International Conference on Remote Engineering and Virtual Instrumentation (REV), 303-308, Porto 26.-28.02.2014., Polytechnic of Porto, Porto

- [4] Quintas, M.R., Restivo, M.T., Rodrigues, J., Santos, B.: "Feeling force", 11th International Conference on Remote Engineering and Virtual Instrumentation (REV), 326-327, Porto 26.-28.02.2014., Polytechnic of Porto, Porto
- [5] Relji , V., Milenkovi , I., Šešlija, D., Dudi , S., Šulc, J.: *Daljinski upravljana pneumatska opruga*, Tehni ko rešenje, Fakultet tehni kih nauka, Novi Sad, 2015
- [6] Relji , V., Šešlija, D., Šulc, J.: *Razvoj daljinski upravljane pneumatske opruge*, Zbornik radova fakulteta tehni kih nauka, br.8/2014, 1781-1784, Fakultet tehni kih nauka, Novi Sad
- [7] Šulc, J., Šešlija, D., Relji , V., Milenkovi , I., Dudi , S.: *Razvoj i imeplementacija daljinskog upravljanja opruge u kursevima mehatroni kog i industrijskog inženjerstva*, 59. ETRAN, 27-28, Srebrno jezero 08.-11.06.2015., ETRAN, Beograd
- [8] Miltenovi , V.: *Mašinski elementi – oblici, prora un, primena*, Mašinski fakultet, Niš, 2009
- [9] Web page of coroporation of Festo: <http://www.festo.com/net/startpage/>
- [10] Web page of corporation of National Instruments: <http://serbia.ni.com/>
- Authors: Vule Relji , M.Sc., Ivana Milenkovi , Assistant Professor Prof. dr Dragan Šešlija, Slobodan Dudi , Assistant Professor, Jovan Šulc, M.Sc.** University of Novi Sad, Faculty of Technical Sciences, Institute for Mechatronics, Robotics, Automation and Integrated Systems, Trg Dositeja Obradovica 6, 21000 Novi Sad, Serbia, Phone.: +381 21 485-2127
- E-mail: vuketa90@uns.ac.rs; ivanai@uns.ac.rs; seslija@uns.ac.rs; slobodan_dudic@yahoo.com; sulc_jovan@yahoo.com;

Vuki evi , M.

THERMITE WELDING

Abstract. The paper was written with the aim to introduce the professionals, particularly young colleagues – engineers, to one of possible technologies appropriate for welding of rails, no matter whether they are railroad, tram, industrial, forest or any other tracks. It resulted from the ideas that the situation in the national railways should be improved in the coming years and the main task in that process would be to adapt the tracks to high speeds. The interruption in practical and theoretical knowledge occurred due to the so-called transitional processes in which vital industrial national functions were destroyed, and negative consequences were biggest in the railway system.

In the meantime, this technology has grown from a typical casting technology used in the past into an individual, i.e. independent one. Its application is not restricted to open areas any more (a lot of fumes), but it has also expanded to closed areas with electronic and other equipment sensitive to airflow obstruction (computers, telecommunications...).

A network of conductors for protection from natural electrical discharges (lightning rod installations) is welded. The mentioned fields of application are the basis for further presentation.

Key words: thermite process, exothermic process, exothermic reaction, rail welding, welding of electrical conductors, network of conductors for lightning protection system, mould, crucible.

1. INTRODUCTION

The Russian scientist N. N. Beketov was the first who pointed to aluminothermy in 1859^[2]. However, western sources insist on the Hans Goldschmidt process formulated by the German chemist, Prof. Hans Goldschmidt in 1896^[5]. This process was the basis for industrial track welding patented in Germany, in 1901. His corporation named Goldschmidt carried out the first welding of tram tracks in Essen, Germany, in 1899, and in 1904 the same company continued to develop and apply the same technology in the USA^[2]. In Europe, this process boomed especially after the Second World War, in the period of intensive renewal of railway infrastructure in devastated Germany.

Thermite¹⁾ is the general and trade^[1] name for the exothermic reaction²⁾ of mixture of two parts units of aluminum in powder form (name: reducer) and three parts units of iron oxide, also in powder form (name: additional metal, cunder). Burning of thermite releases a large amount of heat and light. As with explosives, it is necessary for thermite to be detonated, i.e. ignited, which implies the use of a mixture of barium peroxide (BaO₂) and aluminium. The initial mixture, or the starting material, is ignited by a flint spark lighter or a flame coming from a magnesium strip, a white-hot steel rod, or an electric spark. Thermite reaction is not explosive and it is homogenized in 15÷30 s (initial delay). Aluminium takes the necessary

amount of oxygen from iron oxide (reduction) for burning and that is why it is not necessary to reduce take it from the air. Therefore, the process can start in any environment (in the presence of air or without it), and when it begins, it cannot be “stifled”, by interrupting the contact with the air, so that, under certain conditions, it can be used for underwater welding. The exothermic chemical process most frequently takes place in a crucible, Figure 1. It has a necessary volume and is made of infusible materials. Its mass is sufficiently small so that it could be easily handled in the field and have a long life (this refers to the crucibles which are repeatedly used). The lining is metallurgically neutral and does not affect the structural compositions in the weld metal.

2. PHASES OF THE PROCESS

Thermite welding is realized, according to Figure 1, through the following phases:

- starting the process, i.e. thermite reaction,
- pouring thermite,
- crystallization of metal,
- weld finishing.

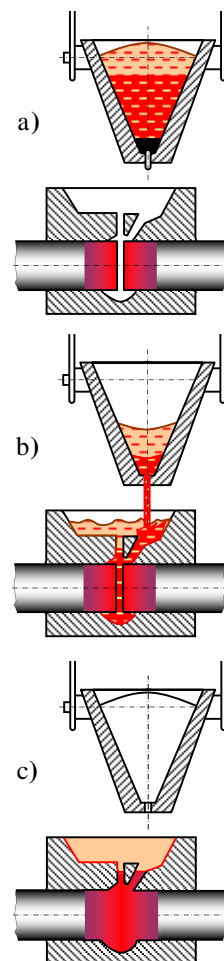


Figure 1. Thermite process phases^[1].

¹⁾ A combustible mixture of aluminium powder and iron oxide powder which, while burning, produces heat of up to 3000°C (welding, combustible aerial bombs, thermite shells...)

²⁾ A chemical reaction in which, while forming a compound, heat is released to the surroundings; its opposite is endothermy.

The welding pieces and the mould are first preheated by using the torch.

After removing the torch, the crucible with the poured thermite mixture and the starting material is placed in the middle of the mould. By using a spark of the starter put in the middle of the powder, or in some other way, the process is initiated. Slag and liquid metal are separated during the reaction. In the meantime, the pin is removed, or the steel plug melts, or the steel plate melts (...), which are placed at the exit of the crucible.

Liquid metal is poured into the mould with the initial laminar flow. At the end, slag flows into the mould and floats on the surface of the liquid metal.

In the next several minutes, the crucible and the mould are not moved from the welding position, which should allow slow crystallization and the use of slag for prolonged protection from the influence of air.

Upon the completion of crystallization of metal and slag, the crucible and the slag tray slag basins (if there are any) are removed. Destruction of the mould is carried out by applying manual tools, but carefully in order not to damage the weld material. As the mould parts are strongly heated, there is a danger of injuring workers or other persons in that area. Therefore, there must be serious precautions.

The weld has larger dimensions than the profiles of the workpieces, so the removal of excess material and shaping of the outer surfaces of the weld are accomplished by applying hydraulic accessories and manual tools for milling and grinding..

3. PROCESS TYPES

Taking into account the method of forming the welding zone, i.e. the way of forming the weld, there are three technological variants of the thermite process:

- a) by pressure,
- b) by casting, and
- c) by brazing.

In the first type, slag, which makes the base metal wet and heated, is first poured into the mould, and a thin film which is kept at the ends of the pieces prevents their immediate contact with the melt additional material. The additional metal represents the source of heat and fills the groove, but does not melt the ends of the base material. After the pieces are heated to the forging temperature, by applying axial pressure, the weld is formed.

In the casting-based variant, molten metal is first poured into the mould. It melts the end zones of the base metal and together with it forms the weld, while slag floats on the surface realizing its protective function and slowing down the cooling.

In the application of the brazing-based process, all additional materials are placed at the joint, and the thermite mixture heats them and the main parts of the joint to the necessary brazing temperature. It is called braze welding because the base metal does not melt, but, as in brazing, fusion is accomplished by solidifying the molten additional material/filler.

4. MAIN CHARACTERISTICS

The main characteristic of thermite welding is the speed of work and simplicity of application. Besides welding steel, it is also used for repair welding of grey cast iron with the addition of ferro-silicon. Thermite mixtures are also made on the basis of Cu, Ni, Cr and Mn, but only copper thermite is used in welding electrical contacts and copper conductors.

Electric current is not used and the application in the field is possible. The welding speed corresponds to the pouring speed. The larger the sections of the pieces to be joined, the more effective the process.

4.1. Advantages of the process

The most important advantage of the process refers to small residual stresses, which is a consequence of natural and slow cooling.

The other advantages are:

- very strong joint,
- the material of the weld is more resistant to corrosion,
- improved electrical properties of the joint; electrical contact resistance is eliminated,
- not so dangerous for operators and other persons,
- allows joining of numerous materials, particularly those with different properties...

4.2. Disadvantages of the process

They are neither numerous, nor primary in determination of its application:

- if compared with other processes, this one is a little more expensive,
- the use of one-off models also adds to the costs of production,
- the process is sensitive to bad weather conditions (increased humidity)...

5. PROCESS PARAMETERS

The main parameter of the process is the composition of thermite mixture on the basis of which typical chemical reactions occur and the other parameters are:

- the groove width, mm,
 - the quantity of additional material, kg/m,
 - the vertical deviation; a ruler which is 1 m long,
 - the lateral deviation; a ruler which is 1 m long,
 - the preheating time, min,
 - the cooling time, min,
 - the thermite reaction time, s,
 - the time of crystallization in the mould, min.
- The secondary auxiliary parameters of the process are:
- the time of manual finishing of the weld, min,
 - the time of machining the weld, min,
 - the tolerance in the vertical direction on the finished weld, mm,
 - the lateral tolerance on the finished weld, mm.

The secondary auxiliary parameters of the process are:

- the time of manual finishing of the weld, min,
- the time of machining the weld, min,
- the tolerance in the vertical direction on the finished weld, mm,
- the lateral tolerance on the finished weld, mm.

6. TRACK WELDING

Thermite casting used in track welding has numerous advantages, among which great comfort and less noise are the most important ones. Certainly, the costs of maintenance of those tracks are reduced.

This type of welding is successfully accomplished at the temperatures over 0°C.

As this type of welding is most frequently done on the already mounted tracks, it is necessary to remove at least two sleepers and elements connecting the rails on the closest sleepers, and to make sure that the length of the rails without those sleepers is greater than the distance between three sleepers, Figure 3.

The position of the rails, in accordance with Figure 4, is adjusted for three directions.

The A-frame, is used for that purpose, Figure 5.

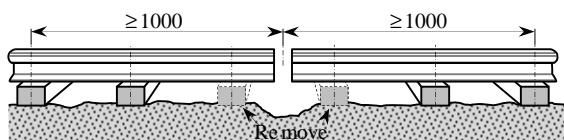


Figure 3. Regulation of the welding zone.

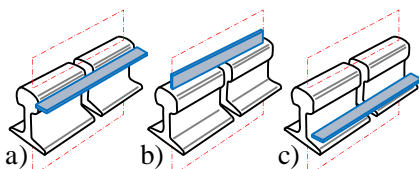


Figure 4. Geometrical parameters of the joint;

- horizontal deviation,
- vertical deviation,
- deviation from straightness (bending, twisting).

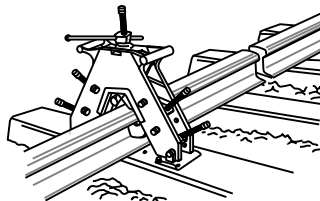


Figure 5. A-frame.

Mounting of the mould starts with the installation of its base, Figure 6a, to which the profiled sides (b) and their steel sheet clamps (c) are mounted. Final activities in the formation of the mould are puttying of the connecting edges, Figure 7a, and its tightening (b).

Preheating of the ends of the rails and the mould is accomplished by a specially designed torch, Figure 8, and after that, Figure 9, the crucible is positioned above the mould and the chemical reaction starts.

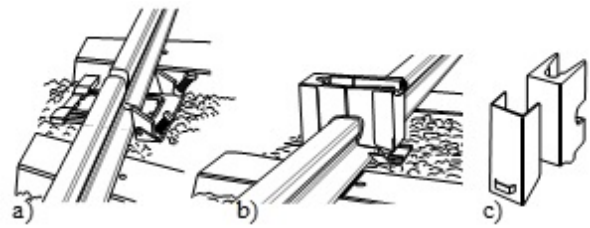


Figure 6. Mould formation:

- instalation of the base
- instalation of the profiled sides
- steel sheet clamps.

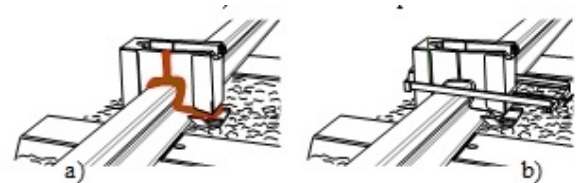


Figure 7. Puttyng of joints (a), and securing of the mould (b)

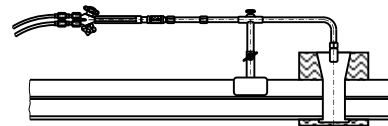


Figure 8. Preheating of the groove and the mould.

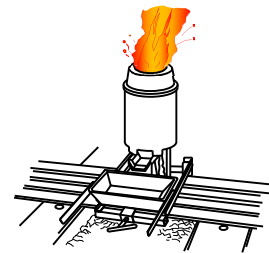


Figure 9. Position of the crucible and the mould.

7. WELDING OF ELECTRICAL CONDUCTORS

It is realized by applying powders of copper-oxide and aluminium. The almost instantaneous result is molten copper and aluminium oxide slag, which, being lighter, floats on the surface of the liquid metal. Temperatures in the welding zones can be even above 2000°C. The weld is formed exclusively on the basis of heat energy of activation. Thermite reaction takes place in a graphite crucible or a crucible with ceramic lining, Figure 10. The mould is designed and made specially for each joint, depending on the shape and dimensions of the pieces to be joined as well as on the weld type, i.e. the type of joint which should be made. The version of mould for repeated application can be used for making 40÷75 welds, and if carefully used - even a larger number of welds can be made, which reduces the costs of the process.

7.1. Preparation of conductors for welding

The conductors should be clean, bright and dry, which creates the preconditions for obtaining a quality weld.

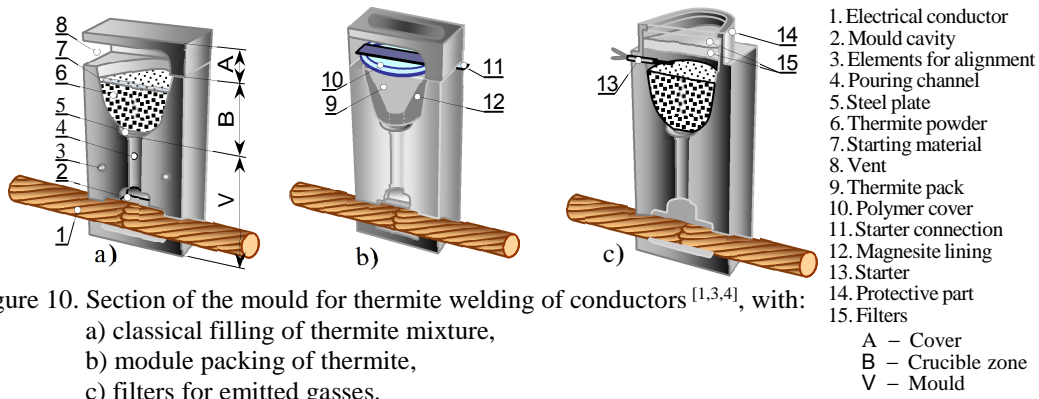


Figure 10. Section of the mould for thermite welding of conductors^[1,3,4], with:
 a) classical filling of thermite mixture,
 b) module packing of thermite,
 c) filters for emitted gasses.

Two or more conductors with equal or different diameters, Figure 11a, are welded to a flat or skewed surface, adhered or at a distance from it (b), pieces of different profiles and mutual positions are joined (c), joints with reinforce rod (d)...

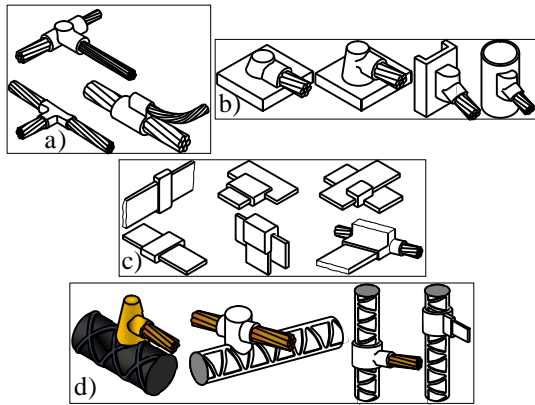


Figure 11. Examples of welded electrical conductors^[1].

Mould positioning is accomplished by applying appropriate ancillary tools, Figure 12, whose construction depends on the shape of the workpiece.

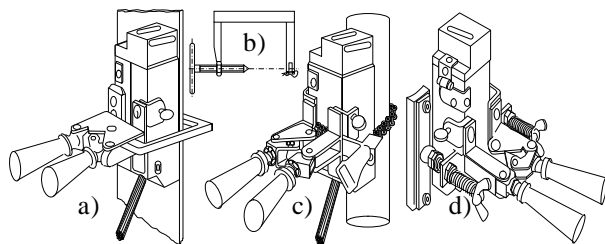


Figure 12. Ancillary tools for positioning the mould for welding of conductors^[1]:

- a) on a flat surface,
- b) a clamp in the form of a stirrup,
- c) on a skewed surface (pipe),
- d) by means of magnets on ferromagnetic materials.

8. CONCLUSIONS

While welding according to the principles of casting and brazing, as well as during crystallization and cooling of the weld metal, there are no removals of pieces, impacts or vibrations. Unlike electric resistance welding by sparking and gas pressure welding, the welding pieces are not shortened (because there is no additional pressure, i.e. welding force), and that is why

this process is used as a final operation in joining pieces.

The structure of equipment is simple and mobile, and its use does not require a high level of training for operators.

9. ACKNOWLEDGEMENT

The paper is realized within the project 37020 funded by the Ministry of Education, Science and Technological Development.

10. REFERENCES

- [1] , , : „ , 2, , , 2015
- [2] Lonsdale, C.: *“Thermite Rail Welding: History, Process Developments, Current Practices and Outlook for the 21st Century”*, Metallurgical Engineer Conrail Technical Services Laboratory, Altoona, 2000
- [3] *“Manual for Fusion Welding of Rails by the Alumino-Thermic Process”*, Government of India, Ministry of Railways, Research Designs&Standards Organisation, Revised-2012
- [4] *“Thermit Welding”*, Process Manuals, section five, GoldShmidt, Thermit Group, Rainham, Essex, 2014
- [5] *“Welding Techniques”*, Indian Railways Institute of Civil Engineering, Pune, India, 2006

Author: prof. dr Miomir Vuki evi , University of Kragujevac, The Faculty of Mechanical and Civil Engineering in Kraljevo, Dositejeva 19, 36000 Kraljevo, Serbia, Phone/Fax.: +381 36 383-337 to 380. E-mail: vukicevic.m@mfkv.rs

12th INTERNATIONAL SCIENTIFIC CONFERENCE MMA 2015 -
FLEXIBLE TECHNOLOGIES

PROCEEDINGS



Section F:
MECHANICAL ENGINEERING AND
ENVIRONMENTAL PROTECTION

Novi Sad, 25-26 September 2015



Vojinovi Miloradov, M., Mihajlovi , I., Miloradov, M., Radoni , J., Turk Sekuli , M., Španik, I.

MASS DISCHARGE OF EMERGING SUBSTANCES BASED ON CONCENTRATION LEVELS IN DANUBE IN THE VICINITY OF NOVI SAD

Abstract: Emerging substances, EmS, have received special attention as pollutants of water bodies due to possible negative effects on humans or on the ecosystem even at very low concentrations. Mass discharge loads/emissions of persistent chemicals from the Danube River to the Black Sea is calculated with the flow rate of 3000 m³/s at the 1255 km of Danube in Novi Sad focused on alkyl phenolic compounds, caffeine and BPA and pharmaceuticals as the typical representatives of EmS. Results indicated mass loads from 0.012 tons/year for nonylphenols to 20.96 tons/year for bisphenol A.

Key words: persistent chemicals, mass discharge, Danube

1. INTRODUCTION

Chemicals are a part of modern life and are present in all compartments of environment and in all spheres of human life. The dominant number of organic chemicals and some of inorganic species belong to the new recognized family of emerging substances of concern. The unique and some specific physico-chemical properties are pseudo persistency, non-monotonic dose response, low and sub-low concentration levels in aquatic media (in the range of ppb to ppt), toxic and hazardous effects as hormone active disruptor chemicals and low removal efficiency by wastewater treatments [1, 2].

EmS are generally polar if their log K_{ow} are < 4.5 and non or semi volatile (Henry coefficient, $K_H < 10^{-3}$ Pa m³mol⁻¹). EmS are also relatively stable towards most chemical reactions in the aqueous environment. Physicochemical properties of EmS (solubility, ad/absorbability, biodegradability, beside others) vary greatly depend on their different molecular structures, number of asymmetric C atoms, stereochemistry, size and shape, hydrophobicity, charge, degree of ionization and others. For the most EmS, there is currently little information about their potential toxicological consequences on ecosystems, particularly from long-term and low-level environmental exposure. The fate and the transport of EmS in natural aquatic media are practically unknown, especially in context of water/soil/sediment distribution and partitioning processes [3-8]. These processes are in the intensive phase of research.

The main generation and input of EmS of concern is by wastewater. They have been detected in influents as well as in effluents. There is no regulation on the concentration levels of EmS in the environment. For this time there is only the NORMAN network list on which the variety types of EmS are divided into 37 classes with subclasses and with each representative of chemical compounds of EmS. More than several hundred and fifty chemicals belong to the NORMAN list of emerging substances [9].

Information and the comprehension of mass discharge load of EmS from the Danube to the Black Sea are very challenging and give useful information about the transport, accumulation and sedimentation to the Black Sea. Knowing the concentrations of persistent emerging chemicals in the river water and the river flow (m³/s) can lead to calculation of the mass load of the EmS emitted to the Black Sea (kg/day or tons/year).

In this paper some results of our research activities within NATO Project are presented focused on the calculations of mass load by Danube to the Black Sea at the 1255 km of Danube in Novi Sad with the river flow of 3000 m³/s and based on the detected concentration levels of presented chemicals.

2. MATERIAL AND METHODS

Within international NATO Project two sampling campaigns of target analyses were conducted after preliminary four screening analyses [6, 8]. Collected samples of surface water at the selected five sampling sites in the river Danube in the vicinity of Novi Sad were analysed in Slovakia.

All samples were collected in plastic and glass bottles and stored at 4°C until analysis. A 800 ml aliquot of water sample were spiked with internal standard (phenanthrene-D10 in case of PAHs and industrial chemicals and propazine or cis-chlordane in case of pesticides and mass labelled PBDE-138 - Wellington laboratories) to achieve final concentration of 1µg/l and extracted with two 50 ml portions of dichloromethane for 20 minutes. After extraction, both extracts were combined and dried with anhydrous sodium sulphate. Small aliquots of copper powder were added into obtained extract to remove elementary sulphur. After filtration, the combined extract was evaporated using Kuderna-Danish apparatus to final volume of 1 ml. A 50 µl of extract was injected into Agilent 6890 gas chromatograph with Agilent 5973 mass spectrometric detector. Helium was used as carrier gas. The MSD was used in SIM mode for all

samples.

The group of pesticides, PAHs, PCBs and some industrial pollutants such as Pentachlorobenzene, DEHP, other phthalates, Nonylphenols (tech. mix.), Octylphenols, Pentachlorophenol, 4-n-Nonylphenol, Bisphenol A, Hexachlorobenzene, 4-tert.- Octylphenol, bensothiazols and methyl jasmonate were analyzed using GC-MS employing large volume injection according to modified ISO 6468 procedure. C10-C13 chloroalkanes, Hexabromocyclododecane and PBDEs were analysed using GC-MS with negative chemical ionization (NCI). ISO/DIS 12010 was used for determination of C10 - C13 chloroalkanes.

A gas chromatographic-mass spectrometric method was used for the quantification of BPA in the Danube surface water samples. A solid-phase extraction procedure with two types of cartridges (C18 and Bond Elut Plexa) was used for preconcentration and removal of interferences. Characteristic chromatogram was obtained in SIM mode (retention time 15.054 min).

Simazine, Atrazine, Isoproturon, Diuron and hormones were analysed using SPE-HPLC-DAD according to modified ISO 11369 procedure.

All standards of individual analytes used to produce the standard calibration curves were of a quality given in 'Reference Materials for Residue Analysis' obtained from Dr. Ehrenstorfer (Seelze, Germany).

For mathematical calculations very simple relation between river flow and known concentration levels of selected EmS of concern has been chosen.

3. RESULTS AND DISCUSSION

Target analysis was defined according to the qualitative screening analyses. Within screening analyses more than 300 different dominant organic compounds were detected. The most frequently occurring compounds in studied water samples were phthalates, phenols, PAHs and other aromatics, esters of fatty acids, alkanes and alkenes.

Phthalates are used as plasticizers, industrial and lubricating oils, defoaming agents, cosmetics and insect repellents. Di-(ethylhexyl)-phthalate belongs to the most common phthalate plasticizers, due to its suitable properties and low cost, it is widely used in manufacturing of articles made of PVC. It is also used as hydraulic fluid and as a dielectric fluid in capacitors, as solvent in glow sticks and as plasticizer in medical devices. Plastics may contain 1 % to 40 % of DEHP. DEHP is highly soluble in oil, but not in water. The possible sources of contamination with DEHP are unsanitary dumpsites, as well as mixture of waste oils as the consequence of their high solubility in oil. DEHP is potential endocrine disruptor, androgen antagonist (not as pseudo-estrogen) and the reason for dramatically lower sperm counts in men. DEHP hydrolyses to MEHP and subsequently to phthalate salts, hence detection of fatty acids could be the result of oxidation of released alcohol in DEHP hydrolysis to aldehyde and carboxylic acid. 1,2-benzthiazole enter the environment from a number of sources such as the leaching of rubber products, fine particles of automobile tires, and antifreeze, and also it is gaining

in popularity in the wood and leather industries. Since benzothiazoles are water soluble, it is unlikely that they will sorb to particles, settle to sediments, or be bioaccumulated. 1,2-benzthiazole is currently entering rivers from urban runoff.

In all samples of Danube River water diethyl phthalate, diisobutylphthalat, dibutyl phthalate and diisooctyl phthalate have been detected and were also subject of target analysis. Some of the detected phthalates are already on the NORMAN list of emerging substances (Diethyl phthalate and Dibutyl phthalate).

Special groups detected in all river water samples were terpenes like nerol, citronellol, menthol, ionone and other compounds like camphor, ethyl citrate or methyl jasmonate that could occur in cosmetics, care products, and home cleaning products. Wide variety of hormones, derivatives of benzene and polycyclic aromatic hydrocarbons (PAHs) were detected in many studied water samples. Presence of hormones in all samples of surface water indicates human or animal faecal pollution and the presence of bacteria in the Danube River could also be expected.

Phenols were identified practically in all studied samples independently of their source. Considering activities performed in vicinity of sampling areas, identified phenols could originate from the biodegradation processes of higher phenols like octylphenols, nonylphenols or alkylphenoxyoxylates, as well as from processing of coal and wood or crude oil.

Bisphenol A (BPA) is identified as the suspected endocrine disrupter (ED) and is on the NORMAN list of emerging substances and is also on the list of substances for further investigation reported by the US EPA and European Union. Although BPA arouses a considerable public health concern, there is a general lack of the information on the levels of EDs in the countries of the Western Balkan region. bisphenol A (BPA) is identified as a suspected endocrine disrupter [10, 11].

BPA is an industrial chemical, mostly used in the production of polycarbonate plastics and epoxy resins, unsaturated polyester-styrene resins and flame retardants. They are used in a wide range of products such as reusable baby bottles and toys, metallic food and drink cans, electronic equipment, sports safety equipment, dental sealants, etc. [12, 13, 14]. BPA releasing into the aquatic environment and food is mostly during manufacturing or by leaching from the final product due to the hydrolysis of the polymers at high temperature or under acidic/basic conditions. The main adverse effects of BPA presence in the environment on human health are fertility problems (decrease in sperm production), obesity, endocrine dysfunction and increasing carcinogenic risk [15-17]. BPA concentration levels ranged from < 6 ng/L to 221.6 ng/L. The study confirmed the presence and the high frequency of detection of BPA, the endocrine disrupter, in the Danube water samples near Novi Sad. Based on the concentration levels within target analyses (Fig 1.) industrial EmS of concern (phtalates, pharmaceuticals, bisfenol A, cofein) were chosen for

calculation of mass discharge loads from Danube to the Black Sea [18].

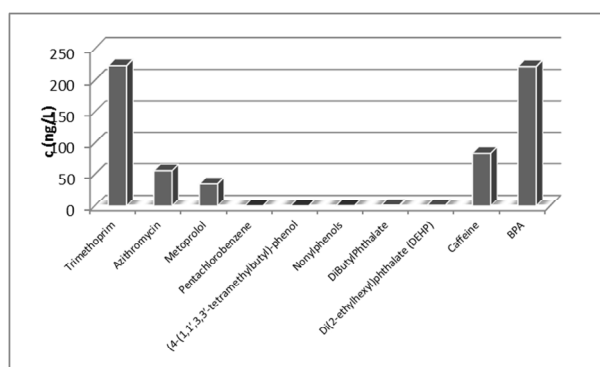


Fig 1. Concentration levels of EmS in Danube at 1255 km

According to the literature data, Loos was the first tried to calculate input in tones per year of emerging substances, showing that the high concentrations in tons could be theoretically deposited to the Black Sea. For our results of target analyses, we have firstly given the calculations of EmS deposition to the Black Sea based on the river flow of 3000 m³/s at the selected location, at 1255km of Danube in the vicinity of Novi Sad (Table 1). Loos et al. [19] calculated mass load for the whole Danube by using the average river flow of 6000 m³/s.

Compound	Concentration [ng/L]	Mass load [t/year]
Trimethoprim	223	21.1
Azithromycin	56	5.3
Metoprolol	35	3.3
Pentachlorobenzene	0.010	0.001
(4-(1,1,3,3-tetramethylbutyl)-phenol	0.02	0.002
Nonylphenols	0.13	0.012
DiButylPhthalate	1.16	0.11
Di(2-ethylhexyl)phthalate (DEHP)	0.77	0.073
Caffeine	84	7.95
BPA	221.6	20.96

Table 1. Mass discharge loads of emerging persistent chemicals from the Danube river to the Black Sea with flow rate of 3000 m³/s at the Novi Sad

The highest concentrations in Danube were detected for trimethoprim and BPA. Hence, the highest mass loads of 21.1 and 20.96 tons/year were calculated for those substances.

This calculation and assessment of mass load of EmS deposited in the Black Sea are with relatively high level of uncertainty due to the limited and short period of monitoring data. Anyway, they pointed out to the high depositions of those toxic chemicals to the Black Sea.

4. CONCLUSIONS

EmS are pollutants with growing concern of their occurrence in environment, toxic effect at very low

concentrations, with possible negative effects on humans and bioindicator aquatic ecosystem. Paper presented general and specific phyco-chemical properties of EmS with focus onto mass load through river basin to the Black Sea. Those calculations has a certain degree of uncertainty, but they point out to the high mass loads of EmS in tons per year to the Black Sea.

The pollution of the Danube could be influenced by wastewater directly discharged in the vicinity of Novi Sad. Pollution of the Danube in the vicinity of Novi Sad could influence on chemical and eco toxicological status in the downstream part of the Danube in Romania and Bulgaria as well as in the Black sea.

The data generated during this research activities, which constitutes one of the first studies in Balkan countries to report mass discharges for a variety of EmS based on concentration levels in surface water, could be used in the future to identify these compounds of potential significance and worthy of further investigation. Research in EmS and priority pollutants needs to continue as it is one of the most needed and challenging aspects of environmental issues.

Acknowledgement: The research is supported by NATO Project DriWaQ-NS (ESP.EAP.SFP 984087) and project of the Ministry of Education, Science and Technological Development (III46009 and Bilateral Project 680-00-140/2012-09/13).

REFERENCES

- [1] Stamm, C., Alder, A.C., Fenner, K., Hollender, J., Krauss, M., McArdell, C.S., Ort, C., Schneider, M.K. *Spatial and Temporal Patterns of Pharmaceuticals in the Aquatic Environment: A Review*. Geography Compass 2/3, pp. 920-955, 2008.
- [2] Verlicchi, P., Al Aukidy, M., Zambello, E. *Occurrence of pharmaceutical compounds in urban wastewater: removal, mass load and environmental risk after a secondary treatment—a review*. Sci Total Environ., Vol. 429, pp. 123–155, 2012.
- [3] Gruji Leti, N., Mili, N., Turk Sekuli, M., Radoni, J., Milanovi, M., Mihajlovi, I., Vojinovi-Miloradov, M. *Quantification of emerging organic contaminants in the Danube River samples by HPLC*. Chemicke Listy, Vol. 106, pp. 264-266, 2012, ISSN 1213-7103.
- [4] Mili, N., Milanovi, M., Gruji Leti, N., Turk Sekuli, M., Radoni, J., Mihajlovi, I., Vojinovi Miloradov, M. *Occurrence of antibiotics as emerging contaminant substances in aquatic environment*. Int J Environ Health Res., 1-15, 2012. DOI:10.1080/09603123.2012.733934.
- [5] Vojinovi Miloradov, M., Turk Sekuli, M., Radoni, J., Mili, N., Gruji Leti, N., Mihajlovi, I., Milanovi, M. *Industrial emerging chemicals in the environment*. 2013. Chem Ind. DOI:10.2298/HEMIND121110028V
- [6] Vojinovi Miloradov, M., Mihajlovi, I.,

- Vyviurska, O., Cacho, F., Radoni, J., Mili, N., Spanik, I. *Impact of wastewater discharges to Danube surface water pollution by emerging and priority pollutants in the vicinity of Novi Sad, Serbia*. Fresenius Environmental Bulletin, Vol 23, No. 9, pp. 2137-2145, 2014.
- [7] Gruji Leti, N., Milanovi, M., Mili, N., Vojinovi Miloradov, M., Radoni, J., Mihajlovi, I., Turk Sekuli, M. *Determination of Emerging Substances in the Danube and Potential Risk Evaluation*. CLEAN – Soil, Air, Water, ISSN: 1863-0669, 2014. DOI: 10.1002/clen.201400402.
- [8] Mili, N., Spanik, I., Radoni, J., Turk Sekuli, M., Gruji, N., Vyviurska, O., Milanovi, M., Srema ki, M., Vojinovi Miloradov, M. *Screening analyses of wastewater and Danube surface water in Novi Sad locality, Serbia*. Fresenius Environmental Bulletin, Vol 23, No. 2: 372-377, 2014.
- [9] Network of Reference Laboratories for Monitoring of Emerging Environmental Pollutants, "The Norman Database on Emerging Substances", <http://www.norman-network.net> (accessed 02/03/2012).
- [10] Groshart, C.H., Okkerman, P.C., European Commission DG ENV, Informe M0355008/1786Q/10/11/00, 2000.
- [11] US Environmental Protection Agency, Office of Research and Development: Multi-Year Plan (FY2000-2012) for Endocrine Disruptor, December 2003, <http://www.epa.gov/osp/myep/edc.pdf>.
- [12] Vandenberg, L.N., Colborn T., Hayes T.B., Heindel, J.J., Jacobs, D.R., Lee, D.H., Shioda, T., Soto, A.M., vom Saal, F.S., Welshons, W.V., Zoeller, R.T., Myers, J.P. *Hormones and Endocrine Disrupting Chemicals: Low-Dose Effects and Nonmonotonic Dose Responses*, Endocr. Rev., Vol. 33, pp. 378-455, 2012.
- [13] Rykowska, I., Wasiak, W. *Properties, threats, and methods of analysis of bisphenol A and its derivative*, Acta Chromatogr., Vol. 16, pp. 7-20, 2006.
- [14] Ballesteros, O., Zafra, A., Navalón, A., Vílchez, J.L., *Sensitive gas chromatographic-mass spectrometric method for the determination of phthalate esters, alkylphenols, bisphenol A and their chlorinated derivatives in wastewater samples*, J. Chromatogr. A, Vol. 1121, pp. 154-162, 2006.
- [15] Huang, Y.Q., Wong, C.K., Zheng, J.S., Bouwman, H., Barra, R., Wahlström, B., Neretin, L., Wong, M.H., *Bisphenol A (BPA) in China: A review of sources, environmental levels, and potential human health impacts*, Environ. Int., Vol. 42. pp. 91-99, 2012.
- [16] Hu, J.Y., Yuan, T., Ong, S.L., Song, L.F., Ng, W.J., *Identification and quantification of bisphenol A by gas chromatography and mass spectrometry in a lab-scale dual membrane system*, J. Environ. Monit., Vol. 5, pp. 141-144, 2003.
- [17] Cunha, S.C., Fernandes, J.O., *Quantification of free and total bisphenol A and bisphenol B in human urine by dispersive liquid-liquid microextraction (DLLME) and heart-cutting multidimensional gas chromatography-mass spectrometry (MD-GC/MS)*, Talanta, Vol. 83, pp. 117-125, 2010.
- [18] Kova evi, S., Dimki, M., Vojinovi -Miloradov, M., Majki, B., ogo, M., Radoni, J., Turk Sekuli, M. *Occurrence and behavior of selected pharmaceuticals during bank filtration in Danube river- a three year survey in Serbia*. Proceedings of the papers, ISBN 978-80-227-3955-9, International Conference Engineering of Environment Protection - TOP2013, Bratislava, The Slovak Republic, June 11-13, 2013, 151-156.
- [19] Loos, R., Locoro, G., Contini, S. *Occurrence of polar organic contaminants in the dissolved water phase of the Danube River and its major tributaries using SPE-LC-MS 2 analysis*. Water res, Vol. 44(7), pp. 2325-2335, 2010.

Authors: Prof. emeritus Mirjana Vojinovi Miloradov¹, Assistant Professor Ivana Mihajlovi¹, dr Milorad Miloradov², Associate Professor Jelena Radoni¹, Associate Professor Maja Turk Sekuli¹, Associate Professor Ivan Španik³

¹University of Novi Sad, Faculty of Technical sciences, Department of Environmental Engineering and Occupational Safety and Health, Trg Dositeja Obradovica 6, 21000 Novi Sad, Serbia, Phone.: +381 21 485-2405, Fax: +381 21 455-672.

²Vojvodina Academy of Sciences and Arts

³Institute of Analytical Chemistry, Slovak University of Technology in Bratislava

E-mail: miloradov@uns.ac.rs;

ivanamihajlovic@uns.ac.rs; milons@eunet.rs;

jelenaradonic@uns.ac.rs; majaturk@uns.ac.rs;

ivan.spanik@stuba.sk



Adamovi , D., Vojinovi Miloradov, M., Dori , J., Miloradov, M., Adamovi S.

OPTIMAL WORKING REGIME OF IC ENGINE FROM THE POINT OF EMISSION CHARACTERISTICS

Abstract: Investigations conducted in this paper are the result of testing of emission characteristics of internal combustion (IC) engine. Emission characteristics of Fiat 1.1 EFI engine were examined at different engine speed, variable load, varying the air-fuel ratio in the supply mixture. During this research the individual and joint effect of operating parameters of the experimental engine to the concentration levels of BTEX compounds was observed. Exhausts were sampled directly at the tail pipe. Analysis of exhaust gas samples was conducted using gas chromatography technique in combination with photoionization detector (GC/PID).

Key words: IC engine, BTEX compounds, exhaust gas, air pollution

1. INTRODUCTION

The fate of chemicals in the environment is controlled by their physico chemical properties, the nature of introduction of the chemical in the environment and also by the environmental conditions. [1]

Volatile organic compounds (VOCs) are omnipresent in lower urban atmosphere. Benzene, toluene, ethyl benzene and xylene (BTEX) in accordance with the physico chemical characteristics, belong to the group of volatile organic compounds. Due to their toxicity and ambient air concentrations, they are regarded as hazardous air pollutants (HAP's) [2]. The monoaromatic volatile compounds like BTEX, emitted to the ambient air, constantly take part in partitioning and distribution between the major environmental compartments like water, soil, vegetation etc. or it may entail partitioning between phases within an environmental compartment [3]. Aside from independent toxicity, BTEX also serve as precursors of secondary ambient air pollutants such as peroxyacetylnitrite, ozone, free radicals and nitrogen oxides [4]. Generally, the origin of BTEX in the environment is through vaporization and incomplete combustion of these compounds in motor vehicles [5].

According to toxicological studies, all BTEX compounds are neurotoxins and irritants. Studies of chronic exposure to BTEX constituents have shown a range of potential health effects. These range from increased risk of myeloid leukemia as a result of exposure to benzene, to a range of central nervous system disorders (headaches, dizziness, loss of balance or muscular control) and possible effects on blood, liver or kidneys associated with chronic exposure to benzene, toluene, ethylbenzene and xylene.

BTEX are some of the most common air toxics found in urban areas [6, 7]. They are emitted from a range of sources and monitoring has shown elevated concentrations in urban air [8]. Sources include combustion products of wood and fuels, industrial paints, adhesives, degreasing agents, and aerosols. Traffic is considered an important source of benzene

for both indoor and outdoor exposure [9,10,11]. Members of the community are therefore exposed to a potentially large number of BTEX sources with varying concentrations.

2. EXHAUST GASES OF MOTOR VEHICLES

Most of the world's vehicles use internal combustion engines, burning petrol or diesel or gas hydrocarbon fuels for their energy supply. Air pollution studies have shown that certain constituents in exhaust gases from automotive vehicles may react in the atmosphere to form smog-type pollutants. The exhaust gases from internal combustion engines are complex mixtures consisting principally of the products of complete and incomplete combustion, small amounts of the oxidation products of sulfur and nitrogen, and compounds derived from the fuel and lubricant [12]. Out of all the available sources, the internal combustion engines are the major consumer of fossil fuel around the globe. Out of the total heat supplied to the engine in the form of fuel, approximately, 30 to 40% is converted into useful mechanical work [13]. The remaining heat is expelled to the environment through exhaust gases and engine cooling systems, resulting in to entropy rise and serious environmental pollution. Undesirable emissions in internal combustion engines are of major concern because of their negative impact on air quality, human health, and global warming. These emissions include unburned hydrocarbons (HC), carbon monoxide (CO), nitrogen oxides (NO_x), and particulate matter (PM).

Gasoline and diesel fuels are mixtures of hydrocarbons, compounds which contain hydrogen and carbon atoms. Hydrocarbon emissions result when fuel molecules in the engine do not burn or burn only partially. Hydrocarbons react in the presence of nitrogen oxides and sunlight to form ground-level ozone, a major component of smog [14].

In a "perfect" engine, oxygen in the air would convert all the hydrogen in the fuel to water and all the carbon in the fuel to carbon dioxide. Nitrogen in the air would remain unaffected. In reality, the combustion process

cannot be perfect and automotive engines emit several types of pollutants.

Additives are added to gasoline to enhance different properties in its storage and use. Tetraethyl lead was a common additive for several decades as an anti-knocking agent. Unfortunately, lead is a toxic heavy metal to which the nervous systems of babies and children are particularly sensitive [15]. Tetraalkyl lead is absorbed through the respiratory tract and through the skin, and then metabolized in the liver to trialkyl lead, the most toxic metabolite. It has effects on neurological development, particularly in children. Due to the extremely high toxicity of lead and harmful effects on the environment alternative solutions for lead as anti-detonator were sought. The presence of large amounts of aromatic hydrocarbons in the exhaust of motor vehicles is the result of substitution of alkyl-lead derivatives with aromatic compounds in order to increase the octane number of fuel or the resistance of fuel to detonate combustion. If detonation is allowed to persist under extreme conditions or over many engine cycles, engine parts can be damaged or destroyed. The high content of aromatic compounds is characteristic of unleaded gasoline. Benzene and alkylated benzenes are found in considerable quantities in gasoline and in the exhaust gas of gasoline engines, whereas the contributions from diesel evaporation and combustion are expected to be less important.

BTEX components are currently the most common additives to gasoline in the United States. They are added as an inexpensive way to increase the octane ratings. The average blend of gasoline contains between 12 and 18% BTEX by volume. This value is higher in the winter time because higher concentrations of volatile components are added to improve engine performance in cold weather. The EPA has set the limit of benzene concentration in gasoline to be $<0.62\%$ (v/v) [16].

2.1 Air-fuel ratio

One of the most important variables in determining IC engine emission is the fuel air equivalence ratio [17]. The IC engine is always operated at stoichiometric or slightly rich mixture. At the starting of the engine, very rich mixture is supplied as vaporization is very slow. Thus, until the engine warms up and this enrichment is stopped, CO and HC emissions are high. At part load conditions, lean mixture can be used which will reduce HC and CO emissions and moderate NO_x emissions.

All the gaseous emissions vary systematically with air-fuel ratio, as shown in Figure 1. This variation is central to understanding recent developments in engine management and emission reduction. The chemically optimal air-fuel ratio, regardless of air pollution production, is called stoichiometric, and is indicated by the vertical dashed line. The stoichiometric ratio corresponds to the mass of air needed to oxidize completely a mass of fuel. This ratio is typically about 14.7 kg air per kg fuel, although it varies with fuel composition. At this ratio, NO production is close to a peak, while CO and HC are both low. With

richer mixtures (lower air-fuel ratio), there is not enough oxygen to fully combust the available fuel, so CO and HC increase [17]. Less energy is released, so less NO is created in the cooler conditions.

When the air-fuel ratio is increased above 1 (leaner combustion), there is excess oxygen so that CO and HC stay low.

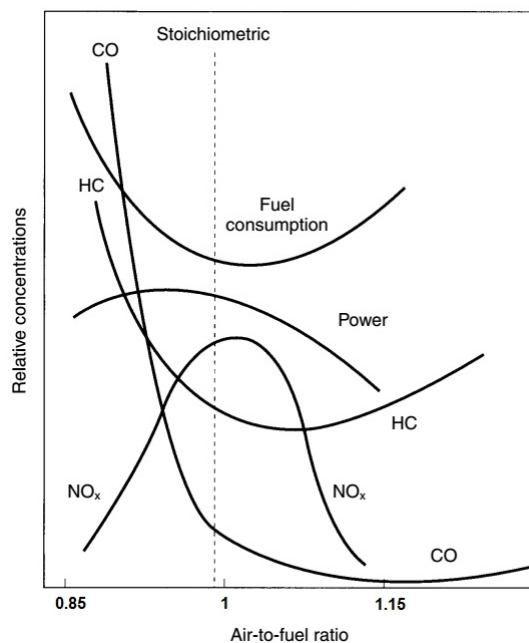


Fig. 1. The variation of NO_x, CO, and HC emissions with air-fuel ratio [17].

However, excess air is also being imported into the combustion chamber, warmed up and exhausted. This reduces the temperature and again lowers NO production. Running the engine at non-stoichiometric conditions also reduces thermal efficiency, so that more fuel is burned to offset any reductions in emission concentration. Hence $\phi=1$ is the label for a stoichiometric mixture of air with any fuel (regardless of composition), less than one for a rich mixture and greater than one for a lean mixture.

2.2 Hydrocarbon emissions

Hydrocarbon emissions (HC) result from incomplete combustion or from fuel evaporation. The incomplete combustion in motor vehicles can be due to several causes. For example, for a lack of O₂, or because fuel can collect in the crevices of the cylinder, or because some fuel species burn at a higher temperature, thus do not completely combust. In stoichiometric and enrichment conditions, HC emissions are usually proportional to fuel rate consumption. HC puffs can be emitted under enleanment conditions, which can occur during long deceleration events [18] and transients [19]. During decelerations, the dramatic drop in fuel results in a cessation of combustion, and hence virtually all of the remaining fuel is emitted unburned. However this fuel excess is typically oxidized in the catalyst. This is an example of a history effect. Evaporative emissions

related to motor vehicles can be: diurnal emissions, caused by the diurnal temperature while the vehicle is not being driven; hot-soak emissions, occurring for about one hour after the end of the trip due to the high temperature of the fuel system; running losses, occurring during the trip due to the higher temperature and pressure of the fuel system; resting losses of gasoline vapor through faulty connections, gas tanks, etc.; refueling emissions.

Hydrocarbons react in the presence of NO and sunlight to form ground-level ozone and contribute to the formation of smog, which has deleterious health and greenhouse effects. A number of aromatic hydrocarbons, such as benzene, are carcinogens [20].

The EPA estimates that on-road mobile sources contribute 29% of the total HC emitted in the US [21].

3. EXPERIMENTAL

The experimental part of this paper was carried out at the Laboratory for Engines and Vehicles, Department of Mechanization and Design Engineering on the Faculty of Technical Sciences in Novi Sad. In order to define the optimal parameters of experimental engine, from the point of emission characteristics, laboratory equipment which owns Department for Environmental Engineering and Occupational Safety and Health was used.

During the experimental measurements concentration levels of BTEX compounds in exhaust gases were monitored at different speeds, variable load of experimental engine, with the varied ratio of air-fuel mixture in the supply.

During experimental studies the emission characteristics of IC engine with electronic fuel injection 1.1 EFI (Electronic Fuel Injection) have been examined. Specifications for the test engine are shown in Table 1.

Engine type	1,1 EFI
Manufacturer	Fiat
Number of cylinders	4
Number of valves (per cylinder)	2
Working volume	1116 cm ³
Maximum engine power	45 kW at 5600 min ⁻¹
Maximum torque	85 Nm at 3800 min ⁻¹
Cooling	by water
The fuel supply	BOSCH M4.6
Compression ratio	9,2
Piston diameter	80 mm

Table 1. Characteristics of the experimental engine

The target compounds have been analyzed in exhaust air samples by the Perkin Elmer Photovac Voyager-mobile GC.

The Voyager uses the principles of gas chromatography (GC) to separate and identify volatile organic compounds. For the separation of sample components the Supelcowax10-Polyethylene glycol (PEG) column has been used. The BTEX compounds have been identified by GC retention time in comparison with the authentic Messer standard.

4. RESULTS AND DISCUSSION

Laboratory tests in this paper were carried out in order to determine the functional dependence of the concentration levels of BTEX compounds emitted during movement of passenger car in urban driving conditions and operating parameters of the experimental engine. The measurements of the concentration levels of BTEX compounds have been conducted on an experimental engine exhaust pipe.

During laboratory tests the three working parameters of the experimental engine were monitored: engine speed (in range from 2000 to 3500 rpm), air-fuel ratio (from 0.85 to 1.15) and engine load (from 10 to 50%). The individual and combined effects of operating parameters on the concentration levels of BTEX compounds in the exhaust gas mixture have been observed.

In order to approach more detailed statistical processing, first of all, descriptive statistical analysis of the dependent variables (concentration of components) for each measured concentration of BTEX components was performed. During the experimental measurements 150 analysis of each parameter were carried out. Descriptive indicators of dependent variables are shown in Table 2.

Compound	N	M	SD	Sk	Ku
Benzene	150	20,15	10,42	0,53	0,14
Toluene	150	39,89	26,12	0,71	-0,28
Ethylbenzene	150	8,35	4,55	0,38	-0,91
m,p-xylene	150	27,04	17,82	0,65	-0,73
o-xylene	150	9,11	5,51	0,57	-0,58

N-number of analysis, M- middle value, SD- standard deviation, Sk- skewness, Ku- kurtosis

Table 2. Descriptive indicators of dependent variables (concentration of components)

During experimental measurements the dominant influence of the coefficient of air excess to lowering of the concentration levels of all compounds from the BTEX group was noticed. Analyzing the differences in the concentration levels of components of exhaust gases, compared to the coefficient of air excess, it is evident that the concentrations differ significantly in the three factor levels for all five components observed in this experiment. Graphic representation of differences in the concentration levels of BTEX compounds for different values of the coefficient of excess air is presented in Figure 2.

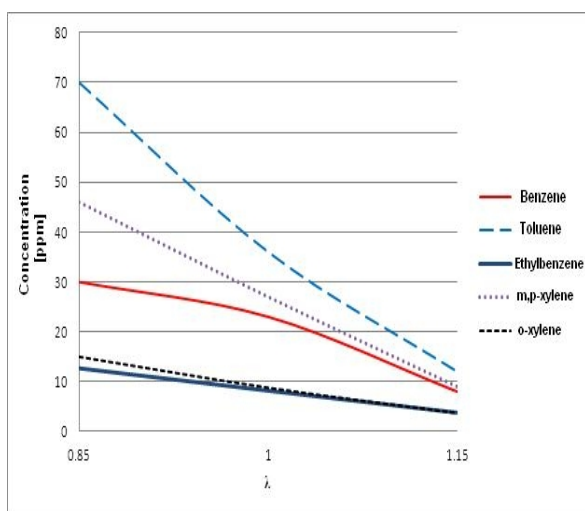


Fig. 1. The concentrations of the compounds of BTEX as a function of λ factor.

Increasing of λ factor generates favorable conditions in the combustion chamber, which results in lowering the concentration levels of all compounds from BTEX group. The most significant effect of increasing the amount of air in the supply mixture was achieved through the reduction of concentration levels of toluene in the mixture of exhaust gases by approximately 85% compared to the initial conditions, which correspond to the rich air-fuel mixture. Significant reduction of the concentration levels also have been achieved in the case of benzene and p-xylene, while the smallest effect of increasing of λ factor was observed in the case of ethylbenzene and o-xylene.

5. CONCLUSION

The presence of high concentration levels of BTEX compounds in the exhaust of motor vehicles occur as a result of substitution of alkyl-lead derivatives, as anti-knock agents, with aromatic compounds in unleaded gasoline.

The presence of high concentration levels of BTEX in the exhaust gas mixtures occurs primarily as a result of incomplete combustion of rich supply mixture.

Increasing the engine speed, engine load and the air content in the supply air-fuel mixture affects the reduction of concentration levels of BTEX in the mixture of exhaust gases, which indicates the ability to control the emission characteristics by varying the appropriate operating parameters of the engine.

Acknowledgement: This research was supported by Ministry of Education, Science and Technological Development, Republic of Serbia (III46009).

6. REFERENCES

[1] Mackay, D., Shin, W. Y., Ma, K. C.: *Illustrated Hand-book of Physical Chemical Properties and Environmental Fate of Organic Chemicals*, CRC Press, Florida, 1997.

[2] Field, R. A., Goldstone, M. E., Lester J. N., Perry R.: *The sources and behaviour of tropospheric anthropogenic volatile hydrocarbons*. Atmospheric Environment, 26A, p.p. 2983-96. 1992.

[3] Manahan, S. E.: *Environmental Chemistry*, CRC Press, Florida. 2004.

[4] Rappengluck, B., Oyola, P., Olaeta, I., Fabian P.: *The Evolution of Photochemical Smog in the Metropolitan Area of Santiago de Chile*, Journal of Applied Meteorology, 39(3), p.p. 275-90, 1998.

[5] Ching-Chang L.: *Exposure assessment on organic volatile compounds (VOCs) for Tollway station workers via direct and indirect approaches*, Journal of Occupational Health, 44, p.p. 294- 300, 2002.

[6] Lee, S.C., Chiu, M.Y., Ho, K.F., Zou, S.C., Wang, X.: *Volatile organic compounds (VOCs) in urban atmosphere of Hong Kong*, Chemosphere 48, p.p. 375-382, 2002.

[7] Bono, R., Scursatone, E., Schiliro, T., Gilli, G.: *Ambient air levels and occupational exposure to benzene, toluene, and xylenes in northwestern Italy*, J. Toxicol. Environ. Health, A 66, p.p. 519-531, 2003.

[8] Environment Australia: *A Status Report to the Community: Living Cities – Air Toxics Program*, Department of the Environment and Heritage, Commonwealth of Australia, Canberra. 2002.

[9] Jo, W.K., Park, K.H.: *Concentrations of volatile organic compounds in the passenger side and the back seat of automobiles*, J.Expo. Anal. Environ. Epidemiol. 9, p.p. 217-227, 1999.

[10] Crebelli, R., Tomei, F., Zijno, A., Ghittori, S., Imbriani, M., Gamberale, D.: *Exposure to benzene in urban workers: environmental and biological monitoring of traffic police in Rome*, Occup. Environ. Med. 58, p.p. 165-171. 2001.

[11] Kim, Y.M., Harrad, S., Harrison, R.M.: *Concentrations and sources of VOCs in urban domestic and public microenvironments*, Environ. Sci. Technol. 35, p.p. 997-1004, 2001.

[12] Elliott, M. A., Nebel, G. J., Rounds F. G.: *The Composition of Exhaust Gases from Diesel, Gasoline and Propane Powered Motor Coaches*, Journal of the Air Pollution Control Association, p.p. 103-108, 2012.

[13] Jadhao, J. S., Thombare D. G.: *Review on Exhaust Gas Heat Recovery for I.C. Engine*, International Journal of Engineering and Innovative Technology (IJEIT) Volume 2, Issue 12, p.p. 93-100, 2013.

[14] Sharaf J.: *Exhaust Emissions and Its Control Technology for an Internal Combustion Engine*, International Journal of Engineering Research and Applications, Vol. 3, Issue 4, p.p. 947-960, 2013.

[15] Robbins, N., Zhang, Z. F., Sun, J. Ketterer, E. M., Lalumandier, A. J., Shulze A. R.: *Childhood lead exposure and uptake in teeth in the Cleveland area during the era of leaded gasoline*, Science of The Total Environment, Volume 408, Issue 19, p.p. 4118-4127, 2010.

[16] Control of Hazardous Air Pollutants From Mobile Sources (final rule).” Federal Register 40:80,US EPA, Washington, DC, 589-668, 2006.

[17] Adamovic, D.: *Model detekcije benzena, toluena, etilbenzena i ksilena u izduvnim gasovima motornih vozila primenom gasne hromatografije u funkciji procene zagadjenja ambijentalnog vazduha*, Doktorska disertacija, FTN Novi Sad, 2015.

[18] An F., Barth, M., Scora, G., Ross M.: *Modeling leanment emissions for light duty vehicles*, Transportation Research Record 1641, 1998.

[19] Nam E. K.: *Understanding and modeling NOx emissions from light driving vehicles during hot operation*. PhD thesis. University of Michigan, Ann Arbor, Michigan, 1999.

[20] Degobert P.: *Automobile and pollution*, Editions Technip. Paris, France, 1995.

[21] EPA: *National air quality and emission trends report, 1999*, United States Environmental Protection Agency, 2001.

Gluvakov, Z., Agarski, B., Košut, Z., Hodoli, J., Kosec, B., Miliji, V.

MULTI-CRITERIA ASSESSMENT OF AGRICULTURAL AND WOOD BIOMASS PELLETS FROM ENVIRONMENTAL AND ENERGY PERSPECTIVE

Abstract: In modern life, where the emphasis is placed on sustainable development and environmental protection, fuels produced from biomass are increasingly gaining importance. Therefore, it is necessary to consider the quality of the final product obtained from biomass, from environmental and energy perspective. In this paper, six types of biomass pellets have been assessed after pressing and cooling with multi-criteria analysis on the basis of present European standards and laboratory methods. Conducted assessment revealed that the biomass pellets made from beech and mixture of beech, pine and soybean were best ranked in multi-criteria analysis from environmental and energetic perspective.

Key words: biomass pellets, multi-criteria analysis, methods of quality, environment, energy

1. INTRODUCTION

Pellets quality parameters can be distinguished as: biological, chemical-thermic, and physical. Biological parameters are defined with biomass type, structure, anatomic structure, and fragmentation (particle size) [1]. Physical-mechanical parameters indicate pellets geometry, density, abrasion, and pressure resistance. Chemical-thermic parameters are defined with pellets content of specific chemical elements, ash, moisture, and pellets calorific value [2]. Producers, suppliers and consumers of solid biofuels, where energy biomass pellets are included also, need quality biofuels in order to obtain safer management.

The aim of this paper is to assess the energy biomass pellets, on the basis of European standards and laboratory methods, with multi-criteria analysis (MCA) from environmental and energy perspective.

2. MATERIALS AND METHODS

Observed pellets were made from agricultural and wood biomass from Vojvodina region in Serbia. Used materials for MCA are biomass pellets from various raw materials [3, 4]. Raw materials in production process for obtaining of final product (pellets) are:

- pine,
- beech,
- wheat straw,
- soybean straw,
- mixture 1 (beech 50%, pine 30%, and soybean straw 20%), and
- mixture 2 (beech 30%, pine 50%, and soybean straw 20%).

The parameters for evaluating the biomass pellets are: moisture content, ash content, thermal power, bulk density, attrition, and small particles (less than 3.15 mm). The parameters values are obtained through the following methods:

- Method for measuring the moisture content

determination in energy pellets - Moisture content in biomass pellets is the "loss" of mass that a chipped pellet mass loses during two hours of the drying process at temperature of 105 °C. Moisture content determination in pellets was carried out according to the standard SRPS E. B8. 012.

- Method for determination of the calorific value of energy pellets - Calorific value of pellets is determined calorimetrically according to the standard CEN/TS 14918.
- Method for determination of ash content in energy pellets - Ash content of the sample is the mass of energy pellets remaining after complete combustion of the sample at a temperature of 575 ± 25 °C, expressed as a percentage, according to SRPS H.N8.136.
- Method for determination of energy pellets attrition - Resistance of energy pellets to attrition (wear) is determined in rotational container according to ASAE standard 269.2.
- Method for determination of fine particles in energy pellets - Fine particles in energy pellets (sample) are particles (impurities) smaller than 3.15 mm, as well as dust in the sample [5].
- Method for bulk mass determination in energy pellets - Bulk mass (bulk density) is a parameter which is easy to determine, and is the mass and total volume of energy pellets ratio, according to [6] and [7].

TOPSIS (Technique for Order Preference by Similarity to an Ideal Solution) method [8] has been used to assess the biomass pellets. The basic principle is that the chosen alternative should have the shortest distance from the ideal solution and the farthest distance from the negative-ideal solution. The TOPSIS procedure consists of six steps:

1. *Normalization of the performance matrix.* The performance matrix $X_{(n,m)}$ has number values that in general have different metrics. Each matrix row corresponds to one alternative, and each column to a

single criterion. Therefore, normalization is performed by relation (1) to obtain normalized matrix $R_{(n,m)}$:

$$r_{ij} = \frac{x_{ij}}{\sqrt{\sum_{i=1}^n x_{ij}^2}} \quad i = 1, \dots, n, \quad j = 1, \dots, m \quad (1)$$

2. *Calculation of weighted normalized performance matrix.* Weighted normalized performance matrix values v_{ij} are calculated (2) as:

$$v_{ij} = w_j r_{ij} \quad (2)$$

where w_j is the criteria weight and $w_j=1$.

3. *Determining the ideal and anti-ideal solution.* The ideal solution A^+ and anti-ideal solution A^- are determined by relations (3) and (4).

$$A^+ = \{(\max v_{ij} | j \in G), (\min v_{ij} | j \in G'), i = 1, \dots, n\} \\ = \{v_1^+, v_2^+, \dots, v_m^+\} \quad (3)$$

$$A^- = \{(\min v_{ij} | j \in G), (\max v_{ij} | j \in G'), i = 1, \dots, n\} \\ = \{v_1^-, v_2^-, \dots, v_m^-\} \quad (4)$$

Where:

$G = \{j = 1, 2, \dots, m \mid j \text{ belongs to criteria that have to be maximized}\}$

$G' = \{j = 1, 2, \dots, m \mid j \text{ belongs to criteria that have to be minimized}\}$

The best alternative is the one that has the largest v_{ij} value for the criteria that has to be maximized and the minimum v_{ij} values for the criteria that has to be minimized. A^+ indicates the best alternative - the ideal solution, while A^- indicates the anti-ideal solution.

4. *Calculation of distance from the ideal and anti-ideal solution.* In this step, using the relation (5) and (6) n -dimensional Euclidean distance for all alternatives from the ideal and anti-ideal solutions is calculated.

$$D_i^+ = \sqrt{\sum_{j=1}^m (v_{ij} - v_j^+)^2}, \quad i = 1, \dots, n \quad (5)$$

$$D_i^- = \sqrt{\sum_{j=1}^m (v_{ij} - v_j^-)^2}, \quad i = 1, \dots, n \quad (6)$$

5. *Calculation of relative closeness to ideal solution.* For each alternative relative closeness is determined by equation (7).

$$RC_i^+ = \frac{D_i^-}{D_i^+ + D_i^-}, \quad i = 1, \dots, n \quad (7)$$

where $0 < RC_i^+ < 1$. Alternative A_i is closer to ideal solution if RC_i^+ is closer to value 1, or at the same time, if D_i^+ is closer to 0.

6. *Ranking alternatives.* Alternatives are ranked by descending values of RC_i^+ .

3. RESULTS

Performance matrix for MCA with parameters values for each biomass pellet is provided in table 1. Observing the values from biomass pellets samples provided in table 1, and comparing them with EN 14961-1 standard, it can be concluded that there are no significant deviations of moisture content (<15% according to standard), ash content (10% according to standard), content of fine particles (3% according to standard), and bulk mass (>550 kg/m³ according to standard). Calorific values in EN 14961-1 standard are not defined, however, they present minimal value that is necessary to quote, as net calorific value according to EN 14918 standard. Attrition is not defined by EN 14961-1 standard.

Comparing the values from table 1 with ENplus standard the following can be concluded:

- According to standard, moisture content should be 10%, less deviations are present in case of pellets made from beech and biomass mixtures 1 and 2 (beech, pine, soybean);
- According to standard, ash content should be 3%, significant deviations are present in agricultural biomass (wheat and soybean straw);
- According to standard calorific value should be 16.0 MJ/kg, small deviations are present in all biomass pellets but pine;
- According to standard, bulk mass should be 600 kg/m³, small deviations are present in biomass mixtures 1 and 2;
- According to standard, fine particles should be 1%, deviations are present in wood biomass;
- Attrition is not defined in ENplus standard.

	Moisture [%]	Ash [%]	Calorific value [MJ/kg]	Bulk mass [kg/dm ³]	Attrition [%]	Fine particles [%]
Pine	9.54	1.17	16.40	0.735	2.03	1.74
Beech	10.63	0.64	15.00	0.655	3.75	3.07
Wheat straw	7.78	8.63	14.70	0.734	0.19	0.05
Soybean straw	7.71	7.43	15.41	0.697	0.25	0.17
Biomass mixture 1	8.85	2.39	15.57	0.554	0.55	0.22
Biomass mixture 2	11.48	1.59	15.64	0.573	1.39	0.45

Table 1. Performance matrix

Two weighting factors perspectives (table 2) have been assigned in order to obtain multi-criteria analysis (MCA) results from environmental and energy point of view. In environmental weighting factors perspective the highest weighting factor value is assigned to ash content (0.25) since ash represents waste. In energy weighting factors perspective the highest weighting factor value is assigned to thermal power (0.25) and moisture content (0.25) since these properties are the most important for the biomass pellets as boiler fuel. Lower weighting factors values have been assigned to

bulk density (0.15), rubbing properties (0.10), and small particles (0.10) in both weighting factors perspectives.

Normalization results are shown in figure 1, while the final MCA results are in figure 2. Figure 1 shows the normalization results from MCA where weighting factors are excluded, and this figure presents the “default” assessment state without the decision maker’s preferences.

	Moisture [%]	Ash [%]	Calorific value [MJ/kg]	Bulk mass [kg/dm ³]	Attrition [%]	Fine particles [%]
Criteria type	Min.	Min.	Max.	Max.	Min.	Min.
Weighting factors – Environmental perspective	0.20	0.25	0.20	0.15	0.10	0.10
Weighting factors – Energy perspective	0.25	0.15	0.25	0.15	0.10	0.10

Table 2. Criteria type and weighting factors perspective

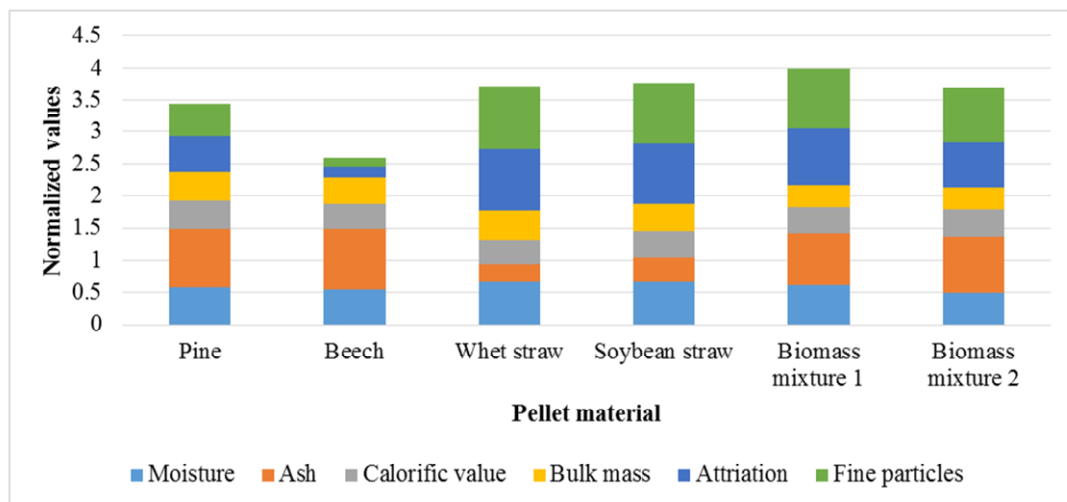


Fig. 1 Normalized values (vector normalization)

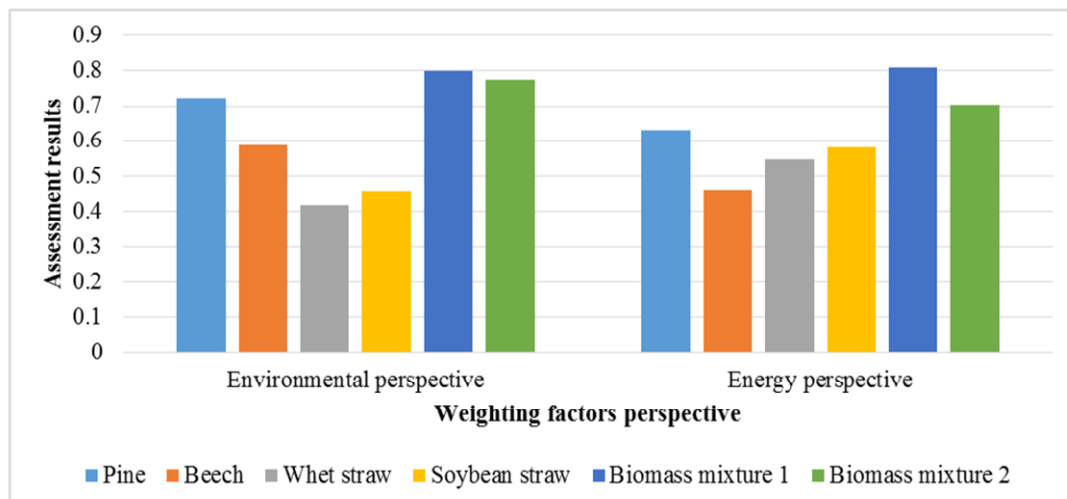


Fig. 2. Biomass pellets assessment results from environmental and energy perspective

4. CONCLUSION

It is necessary to have in mind that European standards are related mostly to energy pellets from wood biomass. Ash content in agricultural pellets depends on factors such as: location, agro-technical methods, material structure and so on. Furthermore, when biomass is collected it is important not to take dirt and other materials, which leads to ash increase in energy pellets.

Normalization results from MCA (figure 1) show the perspective where weighting factors are excluded, and this figure presents the “default” assessment state without the decision maker’s preferences. Comparing the normalization results (figure 1) with MCA results (figure 2), very similar ranking can be seen where the biomass mixture 1 has the highest ranking while other pellets ranks slightly change.

Observing the MCA results provided on figure 2, it can be concluded that in both weighting factors perspectives pine, mixture 1 and 2 pellets have the same, highest rankings. Pine, mixture 1 and 2 pellets are the best alternatives from environmental and energy perspectives. However, rankings of beech, wheat straw, and soybean straw pellets change with different weighting factor perspectives. In the environmental perspective, beech pellets are higher ranked than wheat and soybean straw pellets, while in the energy perspective these rankings are in reverse order. This change of rankings can be explained with the fact that the beech pellets have significantly lower ash content than the wheat and soybean straw pellets, thus effecting the beech pellets rankings since ash content has the highest weighting factor in environmental perspective (0.25) and lower in energy perspective (0.15).

Acknowledgements:

The results presented in this paper are part of the research project "Development and improvement of technologies for energy-efficient use of multiple forms of agricultural and forest biomass in an environmentally acceptable manner, with the possibility of cogeneration" (No. III-42011) funded by the Ministry of Education, Science and Technological Development of the Republic of Serbia.

A part of results presented in this paper is obtained in the framework of project “The platform for building the network of LCA centers and R&D institutes from Central and Southeastern Europe”, TR 114-451-1924/2011-02, supported by Provincial secretariat for science and technological development of Autonomous Province of Vojvodina, Republic of Serbia.

5. REFERENCES

[1] Gluvakov, Z., Brki, M., Jani, T.: *Metode za određivanje kvaliteta energetskih peleta od biomase*, Meunarodna nauka na konferencija, Obnovljivi i raspoloživi izvori energije, Fruška gora, Andrevlje, 2012.

[2] Urbanovića, O.: *Hodnotenie technologických parametrov výroby tuhých biopalív na báze biomasy*, Dizertácia na prácu, Nitra, 2011.

[3] Prvulović, S., Gluvakov, Z., Tolmac, J., Tolmac, D., Matic, M., Brkić, M.: *Methods for Determination of Biomass Energy Pellet Quality*, Energy and Fuels, 28(3), pp. 2013-2018, 2014.

[4] Gluvakov, Z., Agarski, B., Košut, Z., Hodoli, J., Imamović, N., Miljić, V.: *Vrednovanje peleta od poljoprivredne i drvne biomase višekriterijumskom analizom*, ETIKUM 2015 conference, Novi Sad, Serbia, June 19-20, 2015.

[5] Gluvakov, Z.: *Methods of energy pellets from biomass*, Master work, Faculty of Agriculture, Novi Sad, 2012.

[6] Mohesenin, N. N.: *Structure, physical characteristics and mechanical properties plant and animal materials*, Gordon and Breach Press, New York 1980.

[7] Singh, K. K., Goswami, T. K.: *Physical properties of cumin seed*, Journal of Agricultural Engineering Research. 1996.

[8] Hwang, C.L., Yoon, K.: *Multiple Attribute Decision Making*, In: Lecture Notes in Economics and Mathematical Systems 186. Springer-Verlag, Berlin, 1981.

Authors: MSc Zorica Gluvakov¹⁾, Dr Boris Agarski²⁾, MSc Zlatko Košut³⁾, Prof. Dr Janko Hodoli²⁾, Prof. Dr Borut Kosec⁴⁾, Vojislav Miljić, dipl. ing⁴⁾

¹⁾ University of Novi Sad, Faculty of agriculture, Trg Dositeja Obradovića 8, 21000 Novi Sad, Serbia,

²⁾ University of Novi Sad, Faculty of Technical Sciences, Institute for Production Engineering, Trg Dositeja Obradovića 6, 21000 Novi Sad, Serbia, Phone.: +381 21 485 2306, Fax: +381 21 454-495.

³⁾ Victoria Starch, 23000 Zrenjanin, Serbia,

⁴⁾ University of Ljubljana, Faculty of Natural Sciences and Engineering, Aškerova 12, 1000 Ljubljana, Slovenia, Phone.: +386 1 2000410, Fax: +386 1 4704560.

⁵⁾ Foragrobio, 24000 Subotica, Serbia.

E-mail: zorica.gluvakov@live.com
agarski@uns.ac.rs
zlatko.kosut@victoriagroup.rs
hodolic@uns.ac.rs
borut.kosec@omm.ntf.uni-lj.si
vojislav.milijic@foragrobio.rs



Mora a, S., Fajsi, A., Beker, I., Ševi , D.

THE SUSTAINABLE PRODUCT DESIGN AND MANUFACTURING PROCESS

Abstract: Companies are constantly asked to improve performances in order to get the chance to retain or to improve own market position and financial situation. Within the last two decades or so, business processes have had a huge impact on environment and companies have the task to reduce these impacts by using environment-oriented methods and techniques. Eco-design presents one of the most used methods focused on the environmental protection over the entire life-cycle of the product, and the purpose of this article is to analyze its aspects in the term of environment protection.

Key words: Product design, industrial development, sustainability, eco design, product life cycle

1. INTRODUCTION

Competitiveness in today's economy is predetermined by intensifying globalization process, and requires from companies to get closer to customers through the increasing market segmentation. Market requirements in the 21st century are revolved toward big variance of products and services, so the company cannot rely on cost reducing strategy, applying mass production of small number of products. Instead of that, company has to find way to produce as big as possible quantity of products (per customer requirements), with less costs. Another problem is the respect of environmental standards for processes and products. Realization of that requirement means constant changes in technical-technological sense, also in all processes in the company [1].

In modern global economy, companies are facing ever increasing challenges for short time-to-market to enter into the market early, for reduced time-to-volume to occupy the market quickly, and for decreased time-to-profit to get return from market shortly. These business requirements drive technology needs [1] to speed up product development to enhance manufacturing and supply capability and capacity, and to improve revenue from lifecycle efficiency.

Business world of the 21st century witnesses an expanding global competition with increased variety of products and low demand. Old manufacturing technologies fail to meet the increasing demand for customization production and environmental aspects. On the other hand, increased product variety, customized and instable product designs, and international competition lead to the development of new manufacturing technologies. Ecology, productivity, quality, and flexibility are critical measures of manufacturing performance for justifying the investment in manufacturing systems [2]. Flexibility, eco-design and bionics are the key concept used in the design of modern manufacturing systems. Thinking in terms of product life cycles is one of the challenges facing manufacturers today

2. ENVIRONMENT-ORIENTED PRODUCT DEVELOPMENT

The issue of environment protection during product life cycle is becoming one of the main problems for each company. Analysis of the current state in the field of environmental management shows correlation between technological activities and business performances. Reduction of negative impacts of technological activities on environment improves product competitiveness and production efficiency.

Today companies have confronted with typical five critical factors [3]:

1. a rising consumption of natural resources,
2. the dramatic increase of world-population,
3. environmental impacts i.e. limited natural resources (energy, materials),
4. global communication networks based on standards and
5. an unstoppable worldwide globalization.

It can be said with certainty that today environment protection problem has an influence on almost all segments of human life and work. The networking and common cooperation between stakeholders are defined as a key to problem solving.

When we speak about various numbers of ecological aspects, it is not rare for stakeholders to get into a conflict. For that reason, there must be compromise between main stakeholders, especially in the objective process definition.

There are identified five groups of stakeholders:

1. Financiers (owners, shareholders, creditors, investors, etc.). According to their interests each company need to:
 - Increase sales and profitability;
 - Reduce costs and increase productivity
 - Use rational means of production.
2. Customers, they have own expectations what need to be done by company:

- Production of high quality ecological products that are high customized according to the customer requirements;
- Reduction of negative impacts of their own products and processes and raising awareness of environmental issues.

3. Management and employees. Their main interests, in terms of ecology, are focused on:

- Reduction of resources per unit of product;
- Reduction of waste generated in the production and all other units;
- Improving the quality of the work environment;
- Development of eco innovations;
- Integration of organizational, managerial and process structure regarding environment protection;
- Informing the public about results.

4. Society, which act through defining and modifying national policies. According to them, the company need to:

- Define and implement environment protection policy and have open minded attitude towards this issue based on mutual trust and cooperation;
- Be available for dialogue with the public.
- Organize internal audit in order to check level of implementation of ecological principles and standards;
- Provide ecological risk assesments and undertake measures for reduction of identified risks.

5. Environment. This group includes all living creatures and their natural environment. The organization is obligatory to support following principles in order to reduce negative impacts on the biosphere:

- Using rational earth resources;
- Reduction of negative impacts on biodiversity;
- Water quality maintenance (including drinking water);
- Air quality maintenance.

Effective use of ecological measures within the company level can provide only a partial answer for these demands. Based on above definitions and statements, we define ecodesign as a solution which can provide contradictory demands. It should be emphasized that the most important thing is eco-design imlementation during whole product life cycle, even to its disassembling and recycling of component parts.

3. ECO-DESIGN IN INDUSTRY

Industry has a significant impact on the environment, and one way in which it can be reduced is adoption of 'eco-efficiency' approaches. In particular, 'eco-design' is increasingly viewed as being key to sustainable and improved product development. By design, we mean not any "solution" or "design", but, according to the definition, ecology formative project activities to build

a harmonious world of objects with the use of industrial capacity and technology. In this case, a deep internal contradiction arises, so to speak, in the heart of "green" projects - they are created in an industrial environment, but should be useful not only to consumers but also nature, moreover, throughout the life cycle. From the interpretation of the basic concepts of the sequence depends on the implementation of "green" design units, especially the use of materials, style accents. In recent years, more and more talk about sustainable design, which has a clear meaning border, raises the issue of compliance, and so on. In theory it is possible to note the presence of "wandering" definitions when the same characteristics ascribed to the stable, the environmental and green design (not to mention the more specific forms, such as biodesign, green design, and so on).

-design - an integrative and ecologically responsible design discipline. It helps unite disparate efforts in green manufacturing, sustainable production, eco-engineering and other fields. Based on the approach that emerged in the "design with environmental component", the author proves the impossibility of separation sustainable design and typology of traditional engineering criteria forming [4].

Ecodesign - design direction, focus on key environmental protection over the entire life-cycle of the product. Taken into account in the complex, all aspects of the creation, use and disposal of the product. Eco-design, along with the obvious and common requirements of beauty, comfort and price, pays particular attention to:

- Consumption of resources in the design, manufacture, use and disposal.
- Origin materials. It is taken into account many aspects, starting with the protection of the environment by the manufacturer (supplier) to the respect for the rights of workers in enterprises, correct attitude towards farmers, etc. There are different kinds of certification, such as the one which carries the Forest Stewardship Council.
- Security in the use of the product, the absence of injury, to minimize noise emission, radiation, vibration, and so on.
- Simple and safe disposal, reuse of materials with minimal environmental damage [4].
- Developed special methods and standards to conduct a comprehensive analysis of all these aspects.

We can often say that environmental strategies are too expensive for enterprises, but in many cases ecodesign makes easy economizing. For example materials, energy and waste production minimizing give direct advantages for manufacturer. Apart from economizing achievement ecodesign gives the possibility of products obtainment which enlarge the user safety, they are unfailling and better quality. Ecodesign improvement option only stands a chance, if it is supported by stimuli other than the expected environmental benefit alone. Those ecodesign improvement options were most successful that were supported by several strong internal and external stimuli and not blocked by any no-go barriers (Fig. 1) [4].

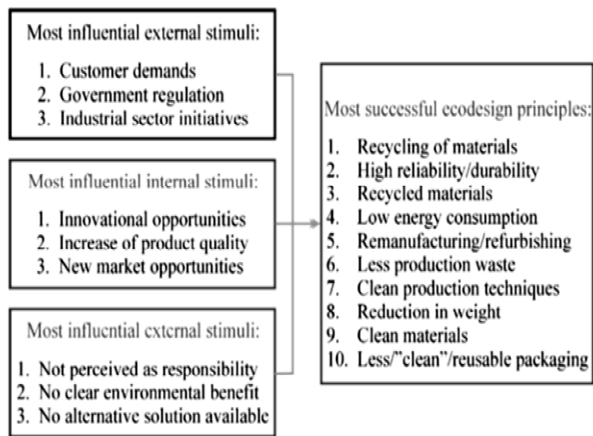


Fig 1. The most influential stimuli and barriers[4]

Product life thinking involves systematic approach to product development that gives the company important charting of every product life stage, together with the various stakeholders and situations that the product is likely to meet during its lifetime. An important step in the process of systematic environmental improvement is to gain insight into the product's life cycle.

By forming a picture of the whole life cycle of the product, we can ensure that each stage in the product's life becomes as environmentally benign as possible. This activity is called product life thinking.

When the product life cycle is revealed to the product developer, it is possible to identify environmental problems and potential solutions for the whole life cycle [4]. But other stakeholders from the company must also join in. This process requires involvement of all interests group.

As the environmental demands on a company's activities and products increase, product life thinking can be used to ensure that the company's environmental responsibility is integrated into the manufacturing processes, logistics and also the actual use of the products which are launched onto the market. It is obvious that by adopting a focus on the whole product life cycle, new competitive dimensions or even whole business models can be formed.

Implementation of eco-design principles consists of eight activities which are presented in the table below (Table 1).

Table 1. Basic algorithm in Eco-design process

Number	Activities	Description of activities
1.	Analysis - search for a problem (ecology, time, quality, costs...)	Finding, taking into account the data from the process or product analyzing, real problems, existing solutions to optimize or emerging needs that can be met with the ecology considerations identified.
2.	Problem identification	Observation of business, technology, economic and ecological aspect and identification of potential solutions, existing product, materials or technology properties with outstanding characteristics, eligible for transfer for application to our problems.
3.	Analysis of the solution	Analysis and layout of a number of factors that allow perceiving the shape, structure, organization and principles of the solution. - Extraction of the fundamental principles that motivate the solution.
4.	Reformulation of the solution	Deduction of general principles, obtained in the previous step, in particular and in greater details and considering possible links between the biological behaviour of the solution and mechanical behaviour.
5.	Design brief and association principles	Identification and outline of the general and specific principles for the operation of the product, the requirements and constraints of the problem and the ecological and environmental aspects to be considered for subsequent association with properties extracted from the analysis of the solution.
6.	Generating concepts	Development of ideas and concepts (in the form of sketches and 3D models) based on conceptual models and following the guidelines and principles obtained in steps of analysis and definition of the ecological solution and the problem.
7.	Validation	Verification of compliance with the requirements of the problem and validating the gains introduced by the ecologic concepts developed through the validation process of the corresponding relationship between the requirements and objectives of the project to achieve the goals established. - Selecting the most appropriate concepts for the next step.
8.	Detail and finish	Making technical drawings for construction, detailed descriptions of components, materials, manufacturing processes and all the considerations necessary for the type and purpose of the project. - Construction of prototype and presentation of results.

When we speak about reducing impact on the environment it is necessary to close the material cycle taking into consideration both primary and secondary resources. Primary resources are required to provide for the input of material needed for the manufacture of technical products. To reduce the impact on the environment, secondary resources including refurbished parts and recycled materials can be used.

Application level of eco-design into product life cycle depends on the level of product development. In the table below there are listed different levels of product deployment and their definition.

Level	Definition
1. Product improvement	Progressive and incremental improvement of the product, e.g. through re-styling using fewer materials
2. Product redesign	A new product, designed on the basis of an existing product
3. New product concept definition	An innovation 'rupture' (as technical functions to fulfill product functionality are different)
4. New production system definition	Occurs when innovation in the production system is necessary

Table 2. Levels of product development [6] [7]

Different levels of product development require different approaches. Product life cycle planning (LCP) aims to set target specifications for the product and its life cycle, and to establish eco-design concepts [8] [9]. Design has a significant role in the field of environmental management. Some scholars state that design is responsible for most of environmental impacts. Although traditionally, the design process itself consumes few resources, about 15% of manufacturing costs, it is responsible for committing the remaining 85% [6].

4. FINAL REMARKS

Environment protection management is selected as a priority issue in contemporary economic and social development. In order to protect environment the society need to change current behavior on the individual and group level. It requires development of methods which will be oriented on ecological aspects for each phase of product life cycle.

The purpose of this article is to analyze the basic concepts that characterize the eco-design solutions at the present stage, and provide the basis of criteria at deducing professional evaluation of products' design with the environmental component.

The importance of this article lies on the necessity of implementation of Eco design concept within product life cycle. Implications for further research might be oriented on application of eco-design tools and methods by small and medium-sized enterprises. Authors Baumann and Schischke indicates that implementation of this approach into SMEs is limited due to resource limitation [10] [11]. How SMEs can implement eco-design due to limited resources and lack of financial and government support represents question for further research.

ACKNOWLEDGMENT

Research presented in this paper was supported by Ministry of Science and Technological Development of Republic of Serbia, Grant TR-35050, Title: "Development of software to manage repair and installation of brake systems for rail vehicles", for the period 2011th-2015th year.

REFERENCES

- [1] Hadžistevi, M., & Mora a, S. (2009). Networks And Quality Improvement. *International Journal for Quality research*, 4(3)
- [2] Engineering design center at Cambridge University. <http://www-edc.eng.cam.ac.uk>
- [3] Westkämper, E., Alting, L., & Arndt, G. (2001). Life cycle management and assessment: approaches and visions towards sustainable manufacturing. *Proceedings of the Institution of Mechanical Engineers, Part B: Journal of Engineering Manufacture*, 215(5), 599-626
- [4] C. van Hemel, J. Cramer, Barriers and stimuli for ecodesign in SMEs, *Journal of Cleaner Production* 10 (2002) 439-453
- [5] McAloone, T. C. & Bey, N. (2009), Environmental improvement through product development — a guide, Danish EPA, Copenhagen Denmark, ISBN 978-87-7052-950-1, ISBE: 978-87-7052-949-5, 46
- [6] Knight, P., & Jenkins, J. O. (2009). Adopting and applying eco-design techniques: a practitioners perspective. *Journal of cleaner production*, 17(5), 549-558
- [7] Parliament UK. Securing the future, delivering UK sustainable development strategy. CM6467. London: HMSO; 2005
- [8] Kobayashi, H. (2005). Strategic evolution of eco-products: a product life cycle planning methodology. *Research in Engineering Design*, 16(1-2), 1-16
- [9] Kobayashi, H. (2000). A method of life cycle planning for product eco-improvement. *International Journal of Environmentally Conscious Design & Manufacturing*, 8(4), 27-37.
- [10] Baumann, H., Boons, F., & Bragd, A. (2002). Mapping the green product development field: engineering, policy and business perspectives. *Journal of Cleaner Production*, 10(5), 409-425.
- [11] Schischke, K., Deubzer, O., Griese, H., & Stobbe, I. (2002, May). LCA for Environmental Management and Eco-Design in the Electronics Industry-State of the Art and Screening Approaches. In internet-based InLCA/LCM conference, May (pp. 20-25).

Authors: Doc. dr Slobodan Moraca, M.Sc. Angela Fajsi, Assoc. Prof. Ivan Beker, doc. dr Dragoljub Ševi

University of Novi Sad, Faculty of Technical Sciences, Department of Industrial Engineering and Management, Trg Dositeja Obradovica 6, 21000 Novi Sad, Serbia

E-mail: moraca@uns.ac.rs;
asladic@uns.ac.rs;

Muránsky, J.

QUALITY OF ENVIRONMENT AND ITS QUANTITATIVE DETERMINATION IN MECHANICAL ENGINEERING

Abstract : A mathematical method is applied to the solution of this problem. The individual factors of environmental and economic character have been expressed before, in the other publications, by means of different equations having universal validity. The progress in this field is the quantitative expression of the quality of environment in the local level. The presented method is applied in the field of mechanical engineering. Each of summarized criterions is represented by its graphical form. The final results can be presented in the percentual and monetary form, too. An application in the automotive industry closes the paper.

Key words: quantitative expression of the quality of environment, mathematical modeling, graphical presentation, automotive industry.

1. INTRODUCTION

Operational Program (OP) – Quality of Environment, [1], [2] is a research program, what has been approved by the European Commission for the Slovak Republic. About 4,3 billion € will be disposable from the European Structural and Capital Funds for this OP, during the years 2014 – 2020, including the slovakian co-financing. The Slovak Ministry of Environment will be co-operate in this research program with lot of institutes as

- Slovak Agency of Environment,
- Department of Home Affairs,
- Slovak Agency for Innovations and Energy, and some others.

This OP has an integral characteristic, because it supports activities concentrated to

- waste management,
- water management,
- preservation of air quality standards and its improvement,
- decontamination of environmental ballasts, and nature preservation.

Mechanical engineering represents in the Slovak economy its significant part. It is a key innovative industry and, as such, any European industrial policy must consider mechanical engineering as a strategic sector [3]. The question is – what an influences has mechanical engineering on the quality of environment ?

There are a lot of methods an approaches, how this problem express, for example exactly, or as a declaration. It would be suitable to find some method for the quantitative expression of the quality of environment, as one of the results of mechanical engineering production processes.

A lot of analytical methods are suitable, how to solve this problem [4]. One of them is described in this paper – [5], [6].

2. THE BASIC ENVIRONMENTAL AND ECONOMIC FACTORS AND THEIR EXPRESSION

According to the formulas presented in [5], the most important ones are the following :

$$K_1(x) = C_1/x \quad (1),$$

where C_1 is a disposable quantity of natural capital during a year, for production of x products in a mechanical engineering works.

The total costs for environment protection, signified as $K_2(x)$, is defined as

$$K_2(x) = C_2 \cdot x + INV + SAN \quad (2),$$

where

$$C_2 = V + ODP + EMO + EMV + IM \quad (3),$$

and V – manufacturing costs per one unit of product,
 ODP – quantity of solid wastes,
 EMO – quantity of emissions,
 EMV – quantity of liquid wastes,
 IM – quantity of imissions inside the factory,
 INV – capital expenditure in connection to the environment protection,
 SAN – costs depending from the environment degradation (fines, fees, etc.)

The total costs for the manufacturing of x products in a factory, can be expressed as

$K(x) = K_1(x) + K_2(x)$, and applying the substitutions – including $C_3 = INV + SAN$ too, the following equation is obtained

$$K(x) = C_1/x + C_2 \cdot x + C_3. \quad (4)$$

After the differentiation of the equation (4), the optimal number of products $x = x_{opt}$, and the corresponding quality of environment, in connection to the factory influences are defined, as

$$x_{opt} = \sqrt{\frac{C_1}{C_2}}. \quad (5)$$

The graphical interpretation of this results are illustrated in Fig. 1.

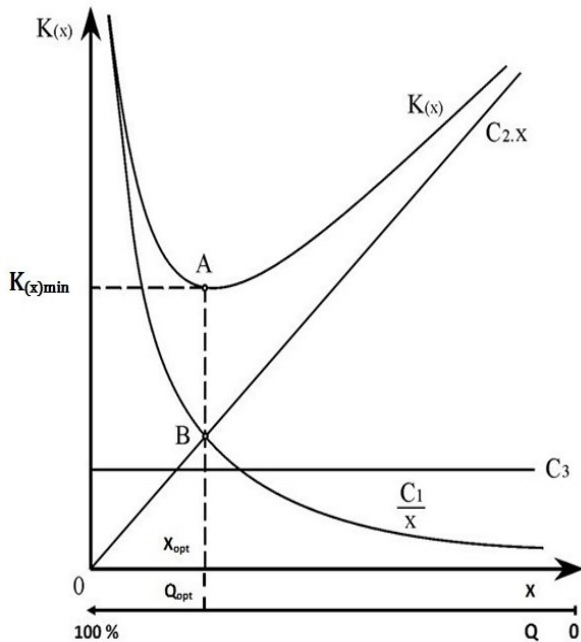


Fig. 1 Graphical interpretation of the compromise solution between the economic and the environmental demands in the mechanical engineering industry.

3. DISCUSSION

- The curve $K(x)$ sometime called as **the curve of the sustainable development** - has its minimum (point A), and represents, according to some approach, the compromise solution between the economic and the environmental demands on the micro-economic level.
- Consumption of the natural capital (habitually per annum) is gradually reduced by growing production, which is compensated with costs - to eliminate this consumption. Point B represents equality of both - costs and thus the **economic optimum of the environment quality - Q_{opt}** .
- The environment quality in this case is in connection to the concrete mechanical engineering factory. If the $x = 0$, $C_2 = 0$ too, the

corresponding $Q = 100\%$, and the natural capital C_1 has not been consumed, too.

- The environment protection costs have their initiation part of the constant value, which consists of the capital expenditure part **INV** and constant payments **SAN**. It is presumed that **SAN = const**, to the $x = x_{opt}$ value. If $x > x_{opt}$, it will be probably depend from the other concrete conditions.
- Perhaps, the presented method and approach, can be applied to some parts in the LCC (Life Cycle Costing) analysis.

4. AN APPLICATION IN THE AUTOMOTIVE INDUSTRY

The basic input data, according to the [7], [8] are the following :

$C_1 = 1,8 \cdot 10^{20}$ €/ year, $C_2 = 1,65 \cdot 10^9$ €/ year, and C_3 has a marginal value. The corresponding graph is illustrated in figure 2.

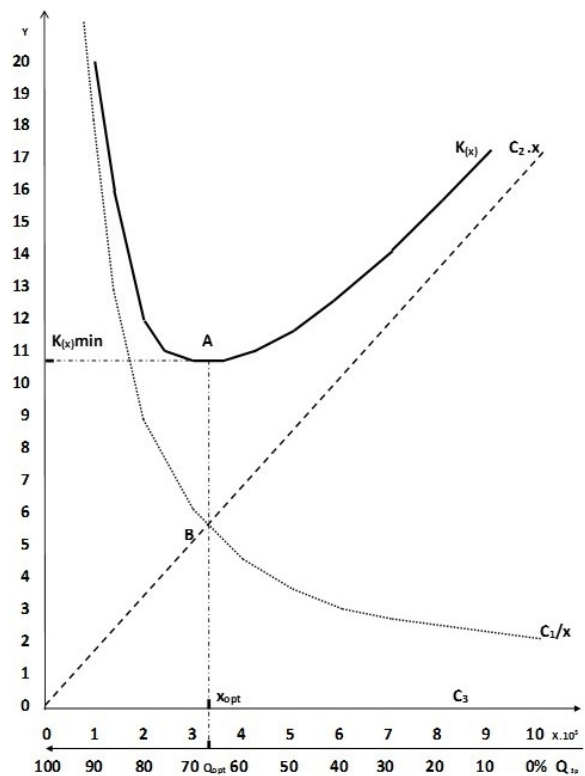


Fig. 2 Results from the personal car production in a ME factory, illustrated in this graph:

$x_{opt} = 330\ 000$ cars/year, quality of environment for the given conditions : $Q_{opt} = 67\%$.

If the theoretical value of the environment quality $Q_t = 100\%$, then it is reduced according to the formula :

$$Q_t - Q_{opt} = 100\% - 67\% = 33\%. \quad (6)$$

Of course, the financial quantification and expression of these data is possible too. It depends from the monetary system.

It is possible to declare according to the applied procedure : **the quality of environment has the quantitative value !**

5. CONCLUSION

There is the need for systematic approach to organize a factory in such a way, that improving the environmental and economic performance of their products across product life cycles becomes an integrated part of operations and strategy [1]. Determination of the optimal quality of environment and the optimal production volume for the given conditions has operational and strategic purpose, too [7]. The described method represents the way , how to determine them. An application, for example, in the automotive industry this approach can bring not only environmental, but also economic benefits [8],[10].

At the present time, the research program in this field is continuing, and is concentrated and applied in some factories in Slovakia for personal cars production.

REFERENCES

- [1] Žiga, P.: Operational Program – Quality of Environment (in Slovak). Enviromagazín, 5/2014, p.7, ISSN 1335-1877
- [2] Húska, M.: Priority is – Better Quality of Environment (in Slovak). Enviromagazín, 5/2014, pp.8-9, ISSN 1335-1877
- [3] Opinion of the European Economic and Social Committee on Industrial Change in Mechanical Engineering Sector (2005/C 267/02)
- [4] Gray, M.: Geodiversity : *Valuing and Conserving Abiotic Nature*. J.Wiley & Sons, Chichester, 2010, 260p.
- [5] Muránsky, J.: *Determination of the Optimal Production Volume Respecting the Environmental and Economic Criteria*. In: **maa 2012**, 11th Int. Scient. Conf., Novi Sad, Serbia, Sept. 20-21,2012, pp.373-376, ISBN 978-86-7892-429-3
- [6] Muránsky, J.: *Environmental Evaluation of Mechanical Engineering Works*. In : **Etikum 2014**, Int. Scient. Conf., Novy Sad, Serbia, June 2014, ISBN 978-86-7892-616-7
- [7] Available from: <http://www.portal.statistic.sk/showdoc.do?docid=37945>
- [8] Available from : http://www.teeb.ecosyst/stud/eu-0810/an_2010^
- [9] Muránsky, J.: *Environmental Compatibility of the Mechanical Engineering Products (in Slovak)*. SD(VLK), 2008, p.300, ISBN 978-80-96988-9-2
- [10] Available from : <http://www.cecs.pdx.edu/~herm/capstone/mee9899/491stuff/mon7/37945>

Author: Prof. Ing. Juraj Muránsky, PhD., External specialist of the Slovak Ministry of Environment, working place : Rož avská 15, 04011 Košice, Slovakia, phone : 0944 160 860, e-mail : jurmur@netkosice.sk

12th INTERNATIONAL SCIENTIFIC CONFERENCE MMA 2015 -
FLEXIBLE TECHNOLOGIES

PROCEEDINGS



Section G:
BIO-MEDICAL ENGINEERING

Novi Sad, 25-26 September 2015

3D MODELING OF SPINAL DEFORMITIES SHAPES USING 5TH DEGREE B-SPLINES

Abstract: In this article, we present a new methodology to model spinal deformities in patients with idiopathic scoliosis. This approach uses a 5th degree B-spline to characterize the deformities by taking central spinal line as a reference for positioning and orienting vertebrae. Generic 3D model of the spine and 3D optical scans of dorsal surfaces were used to generate the control vertices required to generate the central spinal line. B-spline based mathematical representation of central spinal line provides a set of quantitative measures to assess spinal deformities. This methodology was applied on a representative dataset consists 372 adolescent idiopathic scoliosis patients and tested for its effectiveness.

Key words: Scoliosis, B-spline Curves, Adolescents, CAD, 3D Spinal Model

1. INTRODUCTION

Adolescent Idiopathic Scoliosis (AIS) is a spinal deformity that can be characterized by lateral deformities of the dorsal surface and trunk. This deformity causes various health problems for these patients with continuous progression in addition to being unaesthetic, so the secondary lifestyle diseases, like clinical depression and difficulties of doing activities in the workplace also increases. The current clinical standard for diagnosis and monitoring of these patients is based on Cobb's angles, measured using sagittal and frontal radiographic images. Significant technical and procedural advances in non-invasive imaging modalities offer new avenues to diagnose and monitor scoliosis [1]. One of these modalities is 3D optical scan that digitize dorsal surfaces using traditional raster-stereography principle with modern equipment.

In this study, we have used generic 3D model of spine and 3D optical scan to generate central spinal line. To represent an intricate 3D shapes and curves in computer aided design (CAD) environment, we tested various freeform curves including μ -splines, -splines, nonlinear splines, exponential splines, splines in tension, and B-splines. Although B-spline curves are the most widely used, due to easy handling and computational efficiency [2], we have adopted them for modeling spinal deformities.

1.1 Characteristics of B-spline Curves

This section describes the main characteristics of B-spline curves that are needed to model spinal deformities in patients with AIS. If there are positive integer parameters k and n , wherein $k < n + 2$, and known knot vector $(t_0 < t_1 < \dots < t_n < t_{n+1} < \dots < t_{n+k})$, as well as the $n+1$ points of the control polygon: a_0, a_1, \dots, a_n , then the parametric curve c represented by the function $p(t)$ in formula (1) is B-spline curve, defined on the control knot polygon a_0, a_1, \dots, a_n and

by the node vector (t_0, \dots, t_{n+k}) . Points denoted as a_i are control points of the control knot polygon, or de Boor's points, $N_{i,j}(t)$ is basic spline function [3]. If the node interval is $[t_i, t_{i+1}]$ and if lengths between corresponding nodes are equal, the node vector is then uniform. B-spline curve created by this property is called uniform B-spline curve (Figure 1). The node vector with non-uniform distribution of nodes defines the non-uniform B-spline (non-uniform B-spline curve). Parameter n in (1) represents degree of B-spline curve.

$$p(t) = \sum_{i=0}^n N_{i,j}(t) \cdot a_i \text{ for } t \in [t_{k-1}, t_{n+1}], \quad (1)$$

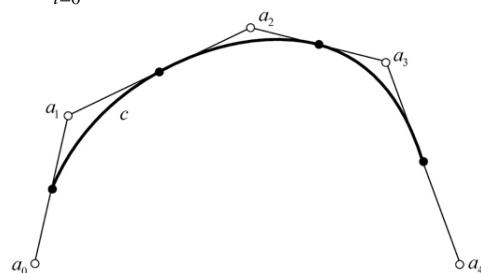


Fig. 1. Uniform B-spline curve for $n = 4$ and $k = 3$

In accordance with mentioned, main characteristics of the B-spline curves are:

- For $t \in [t_l, t_{l+1}]$ applies that segment of B-spline defined on the interval $[t_l, t_{l+1}]$ depends only on the k control points: a_{l-k+1}, \dots, a_l , and then it can be described as follows:

$$p(t) = \sum_{i=0}^n N_{i,j}(t) \cdot a_i = \sum_{i=l-k+1}^l N_{i,k}(t) \cdot a_i \quad (2)$$

- Curve is invariantly associated with the control polygon a_0, \dots, a_n by affine transformations;

- If B-spline curve is smooth at each subinterval of interval $[t_i, t_{i+1}]$, then B-spline curves are C^{k-2} continuous in points $p(t_i)$.

In order to represent and analyze the central spinal line and shape for diagnosis as well as characterization of the spinal deformity in adolescent patients with idiopathic scoliosis, after testing on 372 patients, we propose the use of 5th degree B-splines [4].

2. MATERIALS AND METHODS

2.1 Central Spinal Line Representation

To achieve an optimum smoothness of the central spinal line and symmetry line of the dorsal surface, we have performed interpolation of vertices obtained by scanner using simple spline curves [5]. Then we obtained best-fit curves for the interpolated set of points. This interpolation enables us to have sufficient number of vertices to perform deformity analysis on the spinal line.

A set of focal points on the transverse profiles that was derived from the 3D scans of dorsal surface was used to measure “symmetry” as shown in figure 2. The line connecting these focal points may be single, double or triple curved depending on the angle of deformity and in ideal case it coincides with the line of spinal processus [1].

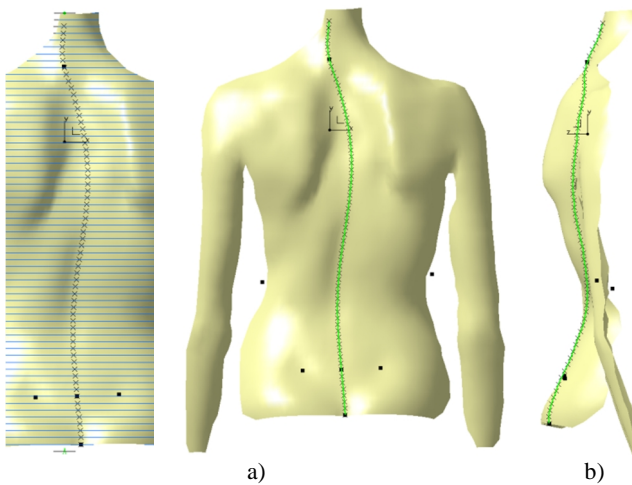


Fig. 2. Interpolation of points of the symmetry line on dorsal surface a) posterior and b) sagittal view

We have defined the “angle of deformity (degrees)” as an angle at an instance (vertices) in the frontal plane, measured similar to Cobb’s angle measurement method [4].

Central spinal line was derived by connecting centroids of all vertebral bodies in both frontal and sagittal plane [6, 7]. Its mathematical representation allows us to localize inflection vertices for downstream curvature analysis of the spine and also to measure Cobb’s angles to characterize idiopathic scoliosis (Figure 3). By projecting the spinal line on two planes (sagittal and frontal) analysis of its projections inflection points can be determined in places where the 2nd derivative is equal to Zero. Then the radius of the osculating circle becomes infinite. Analysis of the

central spinal curve of deformity or its projections enables generation of a set of quantitative measures for physicians to determine positions and orientations of dislocated vertebrae, structure of deformity, and other postural parameters [6]. Having in mind that most of deformities occur between the spinal levels from L5 to C7, obtained 3D curve is segmented from projected fix_C7 to fix_DM points (Figure 3) [8].

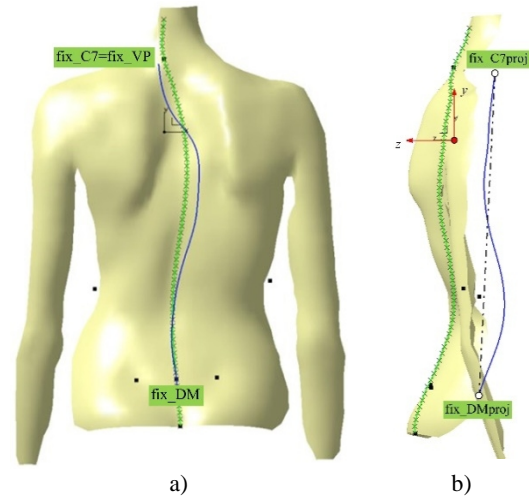


Fig. 3. Segmentation of the spinal curve from fix_C7 to fix_DM a) posterior and b) sagittal view

Interpolation of the large number of near points consequently causes many changes of its curvatures. Approximation of the spinal curve in order to improve its smoothness is performed in PLM system CATIA using 5th degree of B-spline curve (Figure 4).

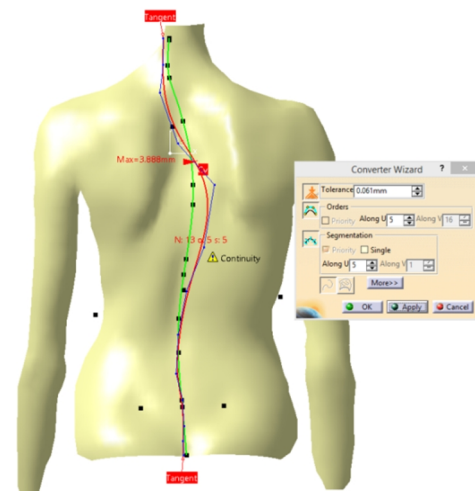


Fig. 4. Approximation of spinal line by B-spline

This step is essential because the parameter of the segmented length determines the parameter of vertebral scaling factor. Unit scaling factor is normalized according to the Panjabi’s anthropometric measures and recommendations [8]. In addition, the resulting curve segment $Split_L$ is base for generating the skeletal CAD model (3D geometrical set) or reference 3D model to regenerate master model of the spine, inflection points, Cobb’s and SOSORT-these angles in the sagittal and frontal plane, and also axial rotation of each vertebrae in the transverse plane.

2.2 Influence of Order of Degrees of B-spline on Spinal Curve Approximation

The process of generating the spinal shape from 2D radiographic (x-rays) images is a complex one. Many authors have used a set of known anatomical landmarks which are easily recognizable in radiographic images to determine the inflection points (I_1, I_2, I_3, I_4 in Figure 5a) and the position of apex vertebrae of each segment (F_{12}, F_{23}, F_{34} in Figure 5d), required to represent the curve, curve's control vertices (lines of control polygon). For a detailed representation of the spinal profile on the frontal plane projection, the central spinal line should pass through the centroids of the vertebral bodies in x-rays, from 6 to 9 (8 to 10) representative points and should have C^2 continuity [9, 10] (Figure 5).

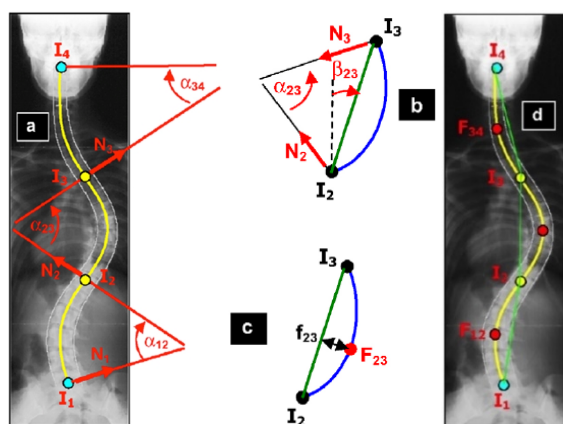


Fig. 5. Segmentation of frontal projection of spinal line by planar B-spline, adopted from [9]

The approximation of central spinal line was realized automatically to eliminate physicians' bias. The control vertices are generated directly from the 3D optical scan data of the dorsal surface. Reference lines, required to quantify Cobb's angle or angle of deformity, were automatically generated. Quality of the central spinal line - depends on the quality of interpolation and approximations of spinal line by B-spline and inflection points. Central spinal line in frontal plane is described by the ($n = 5$) 5th degree of polynomial line and a method of analysis and generation of analytical Cobb's angles, as described in [10]. In this study we have used n^{th} degree spatial curve and quality control was performed with different degrees in approximation phase itself.

3. RESULTS AND DISCUSSION

3.1 Effect of Degrees of Approximation on Cobb's Angle Measurement

Table 1 provides a sensitivity of the central spinal curve of a patient, with different degrees of approximation ($n = 6$ to $n = 4$). A similar sensitivity analysis was performed on sagittal projection of spinal line as well, but not given here. After testing we concluded that for 3D representation of central spinal line in the space, 5th degree B-spline is the most suitable [4]. By decreasing degree of B-spline, the form of the initial interpolation line will be significantly distorted, and by increasing, system will generate

greater number of inflection points and unrepresentative Cobb's angles.

B-spline	Frontal plane	Spinal line
	Maximal Cobb angle: 40.36° , T11-T6 9 referent lines	
Degree 6 $n = 6$		
	Maximal Cobb angle: 53.21° , T11-T4 8 referent lines	
Degree 5 $n = 5$		
	Maximal Cobb angle: 42.42° , T11-T4 6 referent lines	
Degree 4 $n = 4$		

Table 1. The influence of the degree of B-spline approximation on the smoothness and number of Cobb's angles

3.2 Deformity Curve Measures

Segment of the 3D spinal line denoted as a *Split_L* between dorsal anatomical markers *fix_C7* to *fix_DM* allows calculation of *ScalingFactor* parameter.

Those internal parameters of the spinal line are presented for 231 female and 141 male adolescents in table 2.

Descriptive statistics of spinal line lengths and scale factor for female and male adolescents

	N	Range	Min.	Max.	Mean	Std. Dev.
ScalingFactor Female	231	.39	.67	1.07	.89	.06
ScalingFactor Male	141	.44	.66	1.11	.93	.08
Split_L Female	231	197.73	336.73	534.46	442.2	32.17
Split_L Male	141	220.37	331.06	551.44	466.14	44.65

Table 2. Descriptive statistics of spinal curve parameters for 372 adolescents

3.3 Cobb's Angles in Frontal Plane

In table 1 comparative review of frontal spinal line projection for the same patient is presented. Cobb's angles in frontal plane were measured based on the generated segment *Split_L* of the spinal line. In the case of 6th degree of B-spline, software generated 5 different Cobb's angles (max=40.36°, T11-T6). In the case of 5th degree of B-spline, software generated 4 different Cobb's angles (max=53.21°, T11-T4). In the case of 4th degree of B-spline software generated 3 different Cobb's angles (max=42.42°, T11-T4). After testing, we concluded that 5th degree B-spline best fits given points, make smooth curve and doesn't distort projection as in a case of higher and lower degrees. Similar analysis can be performed in sagittal plane in order to quantify kyphosis and lordosis.

4. CONCLUSIONS

The diagnosis and treatment of adolescent idiopathic scoliosis rely on characterization of the spinal deformity. We have proposed a new method to quantitative measure the spinal deformity based on central spinal line that was computed from (i) generic 3D spine model, (ii) radiographic images, and (iii) 3D optical scan of dorsal surface. The central spinal line was generated in both frontal and sagittal planes to measure angular deformity of each segment of spinal curve (Cobb's angle). We have approximated and represented the central spinal line using 5th degree B-splines. Sensitivity analysis of degree and parameters on the deformity line was studied and found to be reproducible and satisfactory. Proposed methodology leads to more precise diagnosis and automated Cobb angles extracting in two planes, based on optical scans, compared to traditional methods where angles are measured manually on dimmed x-rays with low interobserver and intraobserver reliability. The representation needs to be evaluated on a larger data set with additional quantitative measures to be able to translate to clinical settings acceptable in daily praxis.

ACKNOWLEDGMENTS

This research work is supported by the Serbian Ministry of Science and Technology under the grant III-41007: "Application of Biomedical Engineering in Preclinical and Clinical Practice".

5. REFERENCES

- [1] Devedži, G., Lukovi, S., Lukovi, V., Milošević, D., Subburaj, K., Lukovi, T.: *ScolioMedIS: Web-oriented information system for idiopathic scoliosis visualization and monitoring*, Computer Methods and Programs in Biomedicine, vol. 108, no. 2, p.p. 736-749, 2012.
- [2] Piegler, L., Wayne, T.: *The NURBS Book*, 2nd ed., University of South Florida: Springer-Verlag Berlin, Heidelberg, 1997.
- [3] Munira, M., Nur, N., Fazilah, A., Noorazedfiza, Z.: *Review on Non Uniform Rational B-spline (NURBS): Concept and Optimization*, in International Manufacturing Engineering Conference (IMEC 2013), Bukit Gambang Resort City, Kuantan, Pahang, 2013.
- [4] Lukovi, S., "Non-rigid registration of sculptured surfaces in Internet Environment", Doctoral thesis, University of Kragujevac, Faculty of Engineering, 2015.
- [5] Hana, K., Hak, S., Eun, S., Choon-Sik, Y., Tae-Sub, C., Ho-Taek, S., Jin-Suck, S., Young, H., Sungjun, K.: *Scoliosis Imaging: What Radiologists Should Know*, RadioGraphics, vol. 30, p.p. 1823-1842, 2010.
- [6] Berthonnaud, E., Dimnet, J., Hilmia, R.: *Classification of pelvic and spinal postural patterns in upright position. Specific cases of scoliotic patients*, Journal of Computerized Medical Imaging and Graphics, vol. 33, p.p. 634-643, 2009.
- [7] Stokes, I.: *Three-Dimensional Terminology of Spinal Deformity. A Report Presented to the Scoliosis Research Society by The Scoliosis Research Society Working Group on 3D Terminology of Spinal Deformity*, Spine, vol. 19, no. 2, p.p. 236-248, 1994.
- [8] Cukovic, S., Devedzic, G.: *3D Modeling and Simulation of Scoliosis – an Integrated Knowledge Approach*, in 4th IEEE Mediterranean Conference on Embedded Computing - MECO, Budva, Montenegro, 2015.
- [9] Berthonnaud, E., Dimnet, J.: *Analysis of structural features of deformed spines in frontal and sagittal projections*, Computerized Medical Imaging and Graphics, vol. 31, p.p. 9-16, 2007.
- [10] Kanayama, M., Tadano, S., Kaneda, K., Ukai, T., Abumi, K.: *A Mathematical Expression of Three-Dimensional Configuration of the Scoliotic Spine*, Journal of Biomechanical Engineering, vol. 118, p.p. 247-252, 1996.

Authors: Dr Lukovi Saša¹, Prof. dr Devedži Goran¹, Mr Lukovi Vanja², Prof. dr Nabil Anwer³, Doc. dr Lukovi - Zevi Tanja⁴, Dr. Subburaj Karupppasamy⁵,

¹University of Kragujevac, Faculty of Engineering, Sestre Janji 6, 34000 Kragujevac, Serbia; ²University of Kragujevac, Faculty of Technical Sciences, Svetog Save 65, 32000 Kragujevac, Serbia; ³Paris Nord University, IUT Saint Denis, Place du 8 mai 1945, 93206 Saint-Denis Cedex, France; ⁴Faculty of Medical Sciences, S. Markovića 69, 34000 Kragujevac, Serbia; ⁵Singapore University of Technology and Design (SUTD), (EPD) Pillar, 8 Somapah Road, Singapore – 487372, Singapore.

E-mail: cukovic@kg.ac.rs; devedzic@kg.ac.rs; vanja.lukovic@ftn.kg.ac.rs; nabil.anwer@ens-cachan.fr; tanjalukovic_kg@yahoo.com; subburaj@sutd.edu.sg

CONTROL OF PROCESS OF MACHINING OF AN ARTIFICIAL FEMORAL HEAD

Abstract: The hip joint is one of the most important joints of the musculoskeletal system of man, which facilitates the movement of walking upright. The hip joint is a naturally conceived as a spherical joint. At the proximal part of the femur is the head of the femur, balls, placed at right angles to the vertical axis of the body. Acetabular cup placed in the pelvis and is specially oriented to the vertical axis of the body. Femoral head has a spherical form and allows mobility and rotation in all directions, sufficient to perform the functions of the movement of the locomotive system. This document presents a method for determining the machining parameters and the machining allowance for roughing turning and milling, grinding, sanding and super finishing a function of processing time per operation, and satisfactory dimensional control, surface roughness R_a , micro roughness, centricity and the error forms.

Key words: Hip joint, acetabular cup, femoral head, endoprosthesis

1. INTRODUCTION

The hip joint is one of the most important joints of the musculoskeletal system of man, whose operation allows moving and walking upright. The hip joint is a naturally conceived as a spherical hinge consists of a spherical part and the socket. At the proximal part of the femur is the head of the femur, the ball, which is set at the appropriate angle to the vertical axis of the body. Acetabular cup that is placed in the pelvis is specially oriented to the vertical axis of the body. Femoral head has a spherical form and provides mobility and rotation in all directions, sufficient to perform the functions of the movement of the musculoskeletal system, and occasional acrobatics.

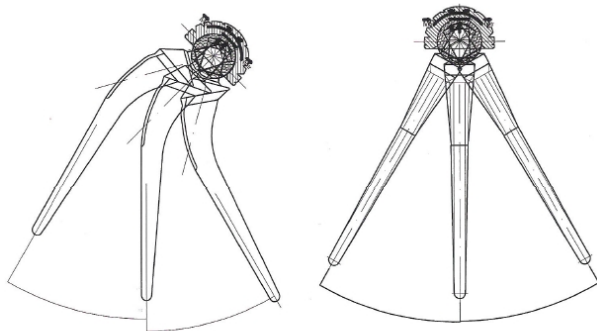


Fig. 1. The possibility of rotation in the hip joint.

Looking kinematic, in the hip joint during movement comes to a mutual sliding between the femoral head and acetabular cups.

The occurrence of degenerative changes in the hip joint, arthritis, necrosis, benign or malignant diseases or mechanical complications, fracture of the proximal part of the femur or pelvis, leading to difficulty or impossibility of displacement in the area of the hip joint, and therefore the displacement of the entire musculoskeletal system is difficult or impossible.



Fig. 2. Degenerative changes and fracture in the hip joint and incorporated endoprosthesis



Fig. 3. Malignant changes in the hip joint and incorporated prosthesis

Restoration of these complications in hip joint is solved successfully by surgical method of removing damaged or diseased parts and installation of endoprosthesis of the hip joint.

Head endoprosthesis and acetabular cup are in constant contact and make tribo-mechanical system in the presence of synovial fluid as lubricants [2].

The main task of acetabular cup and head endoprosthesis is to load, which comes from the mass of the body, upper extremities and additional cargo, transfer with acetabular cup on the head of prosthesis, and then across the body endoprosthesis transfer to the lower extremity and to thereby provide a painless mobility in the hip joint.

Tribological processes in the areas of contact of acetabular cup and head prosthesis are in function of the technological process and the machining parameters used in forming the contact surfaces. Wear between the contact surfaces due to friction depends on the micro roughness, R_a , macro roughness, the error forms, conditions of lubrication, load size due to body weight, BMI and way of sterilization polyethylene acetabular cups.

The main objective of the research described in this document is the determination of cutting data and supplements for roughing scraping and milling, grinding, sanding and super finishing in the function of processing time per operation, and for dimensional control, surface roughness R_a micro roughness, centricity and error forms.

2. MATERIAL AND METHODS

The study observed making head prosthesis $\text{Ø}32\text{k}6$ and

Femoral head	$\text{Ø}32$	$\text{Ø}32$	$\text{Ø}32$	$\text{Ø}32$	$\text{Ø}32$	$\text{Ø}30$	$\text{Ø}30$	$\text{Ø}30$	$\text{Ø}30$	$\text{Ø}30$
Milling	28	26	22	29	28	24	27	28	27	25
Addition material	+0,2	+0,18	+0,2	+0,17	+0,2	+0,17	+0,18	+0,2	+0,19	+0,18
Turning	18	17	20	21	17	17	16	18	17	20
Addition material	+0,17	+0,12	+0,18	+0,17	+0,15	0,18	+0,15	+0,15	0,2	0,17

Table 1. Coarse mashing of the Femoral head

Femoral head	$\text{Ø}32$	$\text{Ø}32$	$\text{Ø}32$	$\text{Ø}32$	$\text{Ø}32$	$\text{Ø}28$	$\text{Ø}28$	$\text{Ø}28$	$\text{Ø}28$	$\text{Ø}28$
Grinding	28	30	29	30	29	30	32	31	30	28
Addition material	+0,08	+0,08	+0,09	+0,07	+0,09	+0,06	+0,09	+0,08	+0,09	+0,09

Table 2. Coarse grinding of the Femoral head

For finishing grinding with rubble 22A320M.

Femoral head	$\text{Ø}32$	$\text{Ø}32$	$\text{Ø}32$	$\text{Ø}32$	$\text{Ø}32$	$\text{Ø}28$	$\text{Ø}28$	$\text{Ø}28$	$\text{Ø}28$	$\text{Ø}28$
Grinding	11	11	12	10	10	12	12	10	18	17
Addition material	+0,05	+0,04	+0,03	+0,05	+0,04	+0,03	+0,03	+0,04	+0,03	+0,03

Table 3. Finishing grinding of the Femoral head

For finishing super finishing with rubble with rubber binder TYROLIT C320-75VB3.

Femoral head	$\text{Ø}32$	$\text{Ø}32$	$\text{Ø}32$	$\text{Ø}32$	$\text{Ø}32$	$\text{Ø}28$	$\text{Ø}28$	$\text{Ø}28$	$\text{Ø}28$	$\text{Ø}28$
Main time	12	15	10	13	15	13	15	12	12	15
Final dimensions	32,00	31,99	32,01	32,00	31,98	28,00	28,00	28,01	27,98	27,98

Table 4. Finishing by super finishing of the femoral head

Figure 3 presents distribution of time in process of mashing of a ariphical femoral head.

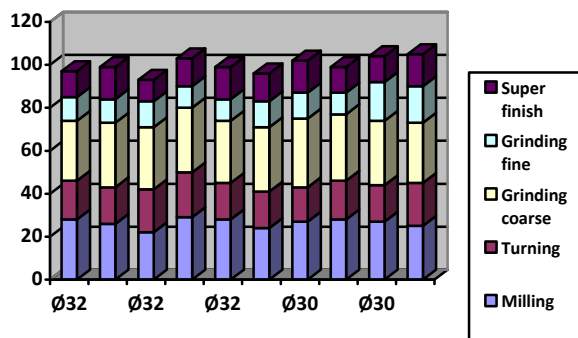


Fig. 3 Distribution of mashing time

$\text{Ø}28\text{k}6$ of materials suitable for making implants, C316 LVM where the raw materials bar $\text{Ø}35$ and $\text{Ø}30$. In doing so, they analyzed all processing operations. The main cut-off time on a lathe is constant. Production of conical holes $\text{Ø}16 / \text{Ø}14$ or $\text{Ø}14 / \text{Ø}12$ is also constant. The main time for this operation cannot be radically shortened regime change processing.

Operation roughing ball turning and milling operations with the presentation of the main time and additional material for the next operation is shown in Table 1.

For the operation of processing coarse grinding with rubble with Bakelite bond 22A46M6JB. The main time and the addition of further operation are shown in Table 2.

Figure 3 shows used grinding wheels.



Fig. 3. The used grinding wheels

Control shape, macro roughness and roughness is made on the device Form Talysuff Taylor Hobson. This device is equipped with a computer system that provides management,

measurement, processing of measured data as well as a visual display on the screen and the ability to print or archiving.



Fig. 4. Machine control macro roughness



Fig. 5. Machine control micro roughness

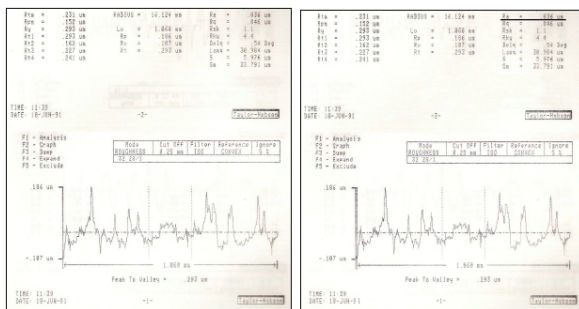


Fig. 6. Numerical and graphical display micro roughness

3. DISCUSSION

By observing the results of the measurements it can be concluded that it is possible to influence the main time of making the choice of equipment, control equipment, treatment regime (for rough scraping or milling). By reducing the addition of a sending is possible to influence the time of rough sending. The main time of the final sanding and super finishing can be considered constant. Appendix for these operations must provide the ability to achieve the required dimensions and surface quality. If the supplement for super finish is bigger, the time of processing is longer. For demanding surface quality, micro roughness ($R_a < 0,05$), the

error forms, macro roughness will be increased. Final control of roundness, macro roughness has established three forms: circle, ellipse, triangular closed fault lines.

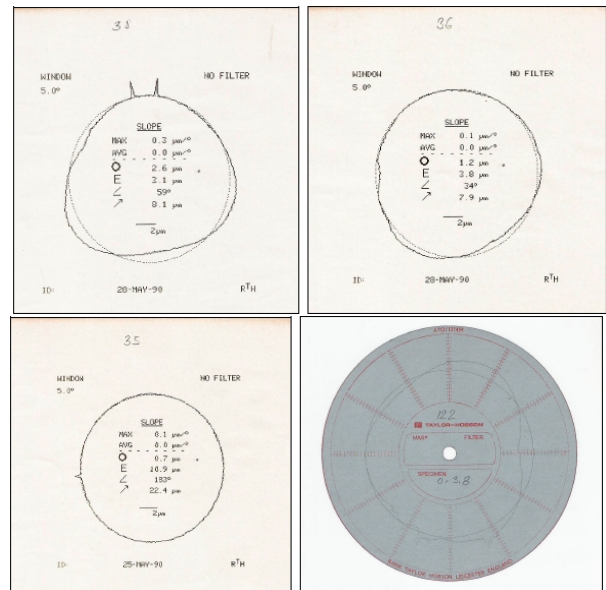


Fig. 7. Graphic errors shape, macro roughness

Spherical head endoprosthesis in the production provides relative rolling between the tool and the work piece. It is necessary to choose the mode of processing, speed tools, shift speed of the work piece, the radius of the blade, grain size and binder binder wheels for milling, turning, grinding or super finishing, so that roughness peaks do not exceed the tolerance zone for the intended operation.

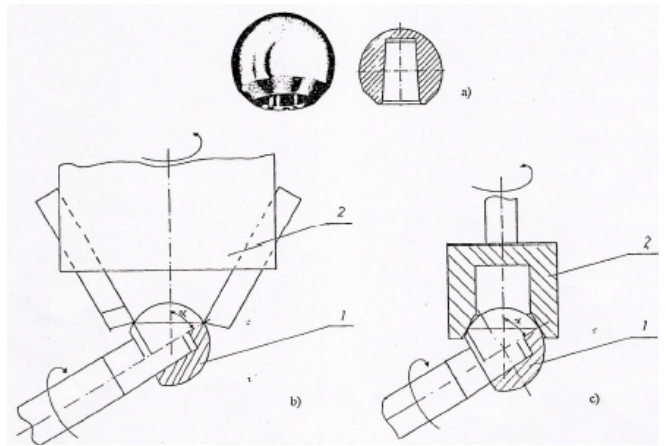


Fig. 8. Scheme of processing sphere (a); milling (b); by grinding (c)

4. CONCLUSION

Looking at the total processing time head prosthesis can decrease the main time for rough machining or milling. The shortening of the running time for fine grinding, especially super finish is insignificant. Supplement for super finish must be sufficient to achieve the required quality processing $R_a < 0,05$. Greater additional material for super finish increases main processing time. The result is greater macro roughness, the error forms.

5. REFERENCES

- [1] Gruji , J.: Ra unarsko modeliranje i eksperimentalno ispitivanje proteze zgloba kuka, *Magistarska teza*, Novi Sad, 2008.
- [2] Gruji , J., Sovilj, B., Krklec, V., Vukeli , B.: Analiza triboloških procesa vešta kog zgloba kuka, Savetovanje tribologije, Kragujevac, 1992.
- [3] Zlati , M., Radojevi , B.: Degenerativna oboljenja kuka i hirurško le enje, Beograd, 1989.

Authors:

Mr Jovan Gruji , Gruji & , Novi Sad, Bul. Vojvode Stepe 6 +381 21 518 381, E-mail: grujicgrujicns@gmail.com

Mr Andrija Rom ek, FKL Temerin, Factory of rolling bearings and cardan shafts, Industrijska zona bb, +381 21 6841 100

Natalija Tabakovic, Technical school Novi Sad, Bulevar kralja Petra I 38, Novi Sad 21000, +381 21 444 606.

E-mail: natalija.tabakovic@gmail.com;

Hotimir Ličen
21131

31

Movrin, D., Spasi, A., Ivanišević, A., Kačmarik, I., Vučajirilović, V., Skakun, P., Milutinović, M.

DETERMINATION OF INFILTRATION DEPTH IN 3D PRINTING TECHNOLOGY BY USING CT TECHNIQUE

Abstract: Nowadays modern additive technology can be used for producing full functional parts. For this reason produced parts have to possess great mechanical properties. In inkjet 3D printing technology depth of infiltration has a direct influence on final characteristic of the produced part. Determination of infiltration depth using standard testing methods is difficult because cutting of tested part is necessary. In this paper determination of the infiltration depth using nondestructive CT method is presented. Medical CT device Siemens Cardiac with three different variation of the image noise were used. Values of CT window level (width and center) in second reconstruction were also tested.

Key words: Additive technology, Inkjet 3D printing, Infiltration, CT

1. INTRODUCTION

Additive technology or additive manufacturing (AM), also referred to as 3D printing, involves manufacturing of a part by depositing material layer-by-layer. This differs from conventional processes such as subtractive processes (i.e., milling or drilling), formative processes (i.e., casting or forging), and joining processes (i.e., welding or fastening). Additive manufacturing has received tremendous attention in recent years. [1]. Large number of systems for AM is developed and they can be divided in four groups according to the material state. Most methods use liquid (photopolymer) as starting material which is subjected to the high power light during processing (laser, UV). This exposure to the high energy light results in solidification of the liquid (through so-called “polymerization”), i.e. building a solid body – model. Powder based systems are very widespread and they use heat (produced by laser or electron beam) or liquid glue for joining particles. Also, sheet form and a gas form of the base materials can be used in AM techniques.

It should be emphasized that RP is used not only in the field of industrial and mechanical engineering, but also in other fields such as medicine [2, 4] architecture, arts etc. Detailed statistics on RP application fields is given in Fig.1.

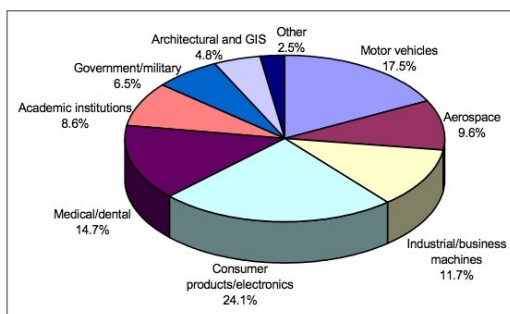


Fig. 1. Application of additive technologies in various fields [5]

In this paper main characteristics of the 3D inkjet printing (3DP) process are described and determination of the infiltration depth using non-conventional and nondestructive technique is presented as well.

3DP technology was invented at MIT and has been licensed to more than five companies for commercialization. 3D printer prints liquid binder at selected regions of the speeded powder, which results in creation of the first solid layer. Hence, in 3DP, only a small portion of the part material is delivered through the print-head; most of the part material is comprised of powder in the powder bed. Typically, binder droplets (80 μm in diameter) form spherical agglomerates of binder liquid and powder particles and they provide bonding to the previously printed layer. Once a layer is printed, the powder bed is lowered and a new layer of powder is spread onto it (typically via counter-rotating rolling mechanism) [3]. This process (printing binder into bed; recoating bed with new layer of powder) is repeated until the part, or array of parts, is completed. A schematic of the 3DP process is shown in Fig. 2

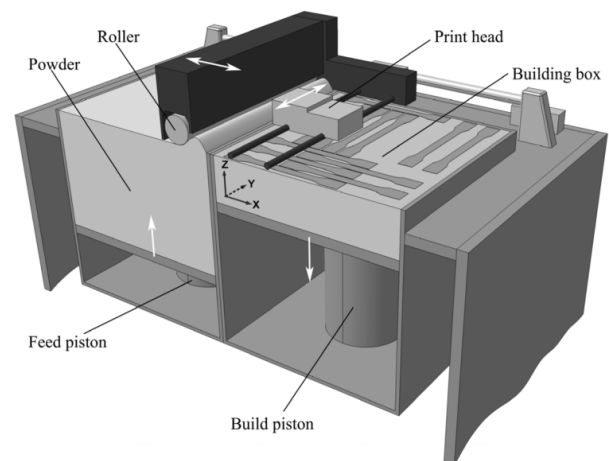


Fig. 2. 3D printing machine [6]

When the printing process is completed infiltration steps are needed to fabricate proper part density or to ensure good mechanical properties. Different types of liquid infiltrants can be used for infiltration; waxes, cyanoacrylates, epoxy resins, etc. For the best mechanical properties epoxy resins should be used. Also, different methods of infiltration are developed for achieving maximal mechanical properties with minimal wasting of the infiltrant and minimal infiltration time. Spraying, submerging and washing are the most commonly used methods of infiltration.

In the literature a large number of researches of the impact of infiltration type and method on the mechanical properties printed parts can be found. In the papers [6-10] impact of the different process parameters and type of infiltrants on mechanical properties of the final part are described. In the case of the thick-wall parts depth of infiltration has a very large influence on final mechanical properties. Determination of the infiltration depth is possible only by destructive (cutting) methods [11]. In this paper nondestructive CT method for infiltration depth determination is presented.

2. EXPERIMENTAL INVESTIGATION

2.1 Equipment

Experiment can be divided in two stages; 3D printing of the specimens and measuring of infiltration depth by CT devices.

For the specimens fabrication, 3D printer Z 310plus (Z corporation - 3D Systems) was used (Fig.3). Powder used in the experiment was ZP 131 with binder zb90 and 0.1 mm layer thickness. Binder/volume ratio in core was 0.0975678 and in the shell and ribs 0.195136. Bleed compensation in all three directions was activated for better accuracy of the specimens.



Fig. 3. 3D printer Z 310plus

SIEMENS Sensation Cardiac 64 medical CT scanner (Fig. 4.) was used for specimens scanning. Following parameters of CT were applied: protocol for head, pixel size 0.385 mm, tube voltage 140kV and three different reconstruction kernels (H30s, H60s and H70h). The reconstruction kernel, also referred to as “filter” or “algorithm” by some CT vendors, is one of the most important parameters that affect the image

quality. Generally, there is a tradeoff between spatial resolution and noise for each kernel. A smooth kernel generates images with lower noise but with reduced spatial resolution. A sharp kernel generates images with higher spatial resolution, but increases the image noise. The selection of reconstruction kernel should be based on specific clinical applications. For example, smooth kernels are usually used in brain exams or liver tumor assessment to reduce image noise and enhance low contrast detectability. On the other hand, sharper kernels are usually used in exams to assess bony structures due to the clinical requirement of better spatial resolution.

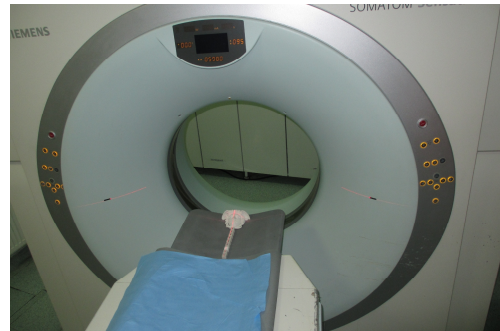


Fig. 4. SIEMENS Sensation Cardiac 64 medical CT scanner with specimens

2.2 Calibration

Specimens which were used for determination of infiltration depth had cubic shape with dimension 15x15x15mm. Infiltration was performed by epoxy resin S5000 (manufacture by Samson-Kamnik, Slovenia) using submerging technique. Because of different density of infiltrated and non-infiltrated volume of specimens, CT technique based on Hounsfield scale has possibilities to detect the size of infiltrated specimen volume. The Hounsfield unit is a way to characterize radiation attenuation in different tissues and thus making it easier to define what a given finding may represent. It measures radio density and is a quantitative scale. Typical values for different elements and tissues range from -1000 for air to more than +1000 for bones.

For second reconstruction and specimens measuring Syngo fastView software was used. Default cross section view with no additional setups is shown in Fig. 5. As can be seen in figure 5, with default values of window width and center, differences between infiltrated and non-infiltrated zone are not clearly visible.

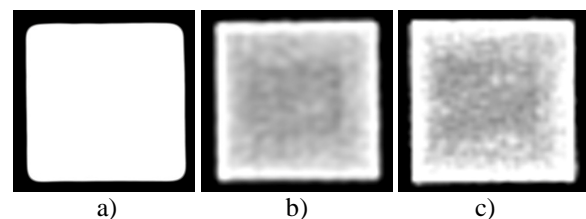


Fig. 5. Default cross section view in different reconstruction kernels: a) H30s, b) H60s, c) H70h

In order to divide two zones of specimens, calibration of values of windows width and center in Syngo fastView software is necessary. Window width is the range of CT numbers displayed with shades of gray, ranging from black to white. Window center is center of the scale. Calibration is performed by using half of cubical specimens from which non-infiltrated volume is removed.

Non-infiltrated volume is removed by clean water, as binder is water-soluble and powder from non-infiltrated zone was easily removed by plastic tools without risk of damage infiltrated zone. After removing powder, specimen is measured by Vernier caliper and obtained dimensions are used for calibration of windows width and center for all three cases of reconstruction kernels (Fig. 6).

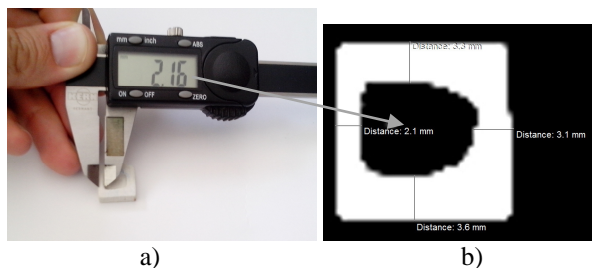


Fig. 6. Measuring of specimen using: a) Vernier caliper, b) Syngo fastView software (H30s)

Best results are obtained by using H30s reconstruction kernel and values for window width 3 and center 880. Kernels H60s and H70h exhibit poor results with lot of noise (artefacts) and very unclear boundary between zones and they are not suitable for measuring (Fig. 7).

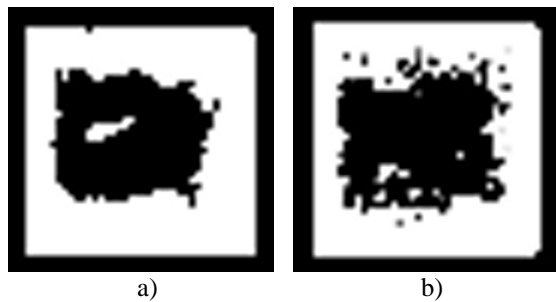


Fig. 7. CT images for reconstruction kernels a) H60s and b) H70h

2.3 Verification

For verification of procedure, the cubic specimen with same dimension as calibration is used. Measured values are given in table 1.

As can be seen in table 1 differences between dimensions measured by software Syngo fastView and Vernier caliper are not significant. According to previous research performed on Faculty of Technical Sciences, average infiltration depth reach by combination epoxy resin and submerging technique is 3-6 mm. According to this and maximal differences between two presented techniques (0.36 mm), nondestructive CT technique has great opportunities for determination of printed parts quality from the standpoint of infiltration depth.

Dimension	Syngo fastView (CT)	Vernier caliper
a	3.5	3.66
b	3.7	3.98
c	3.1	3.46
d	3.7	3.87

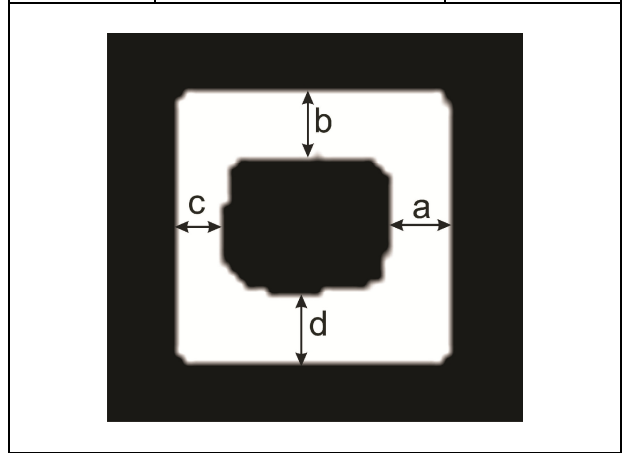


Table 1. Dimensions of infiltrated zone

3. CONCLUSION

Additive manufacturing do not require dies, tools and long preparation time to produce final parts and because of this, it is the most powerful technology in single and small scale production. Also, a wide range of different materials such as polymers, metals, ceramics, wood, composite etc. can be used. In additive manufacturing final parts must have very good mechanical properties.

In 3D ink jet printing, low density, moisture sensitive and very brittle (unusable) so-called green parts are produced in the first stage. Using different post processing technique such as infiltration, parts reach very high mechanical properties. Infiltration by liquid infiltrants which penetrate deep into green parts is necessary in most cases. Mechanical properties of fabricated parts depend on infiltration depth especially in the case of thick-wall components. Controlling of infiltration depth in final parts is possible only by cutting parts and by measuring penetrated zone. This approach has many drawbacks, mainly because it damages the part and in that case part can become useless.

This paper presents non-destructive CT technique for determination of infiltration depth. Because of the difference in density between infiltrated and non-infiltrated volume of the part, CT scanner can detect and divide these two volumes.

In experimental research cubic specimen with 15x15x15 mm dimensions was used. Infiltration was performed by submerging technique and epoxy resin S5000. In CT procedure three different protocols (kernels) are used: H30s, H60s and H70h. During measuring by Syngo fastView software calibration of window width and center was performed and their values were adopted according to dimensions obtain by Vernier caliper. After calibration, verification procedure is performed and results of infiltration depth measured by software and Vernier caliper were

compared. Differences between obtained results are not significant and this technique was proved to be useful for determination of infiltration deep with non-destructive method.

In further investigation industrial CT with higher resolution will be used. Also, for specimens measurement different commercial software package will be used (i.e. 3D Doctor, Mimics, etc).

4. ACKNOWLEDGEMENT

Results of investigation presented in this paper are part of the research realized in the framework of the project "Research and development of modeling methods and approaches in manufacturing of dental recoveries with the application of modern technologies and computer aided systems" – TR 035020, financed by the Ministry of Education, Science and Technological Development of the Republic of Serbia.

5. REFERENCES

- [1] Conner B.P, Manogharan G., Martof A., Rodomsky L.M., Rodomsky C.M., Jordan D.C, Limperos J.W.: *Making sense of 3-D printing: Creating a map of additive manufacturing products and services*, Additive Manufacturing, 1/4, pp. 64-76, 2014.
- [2] Drstvenšek, I.: *Layered technologies*, University of Maribor, Maribor, Slovenia, 2004.
- [3] Gibson, I.; Rosen, D.W.; Stoker, B.: *Additive Manufacturing Technologies, Rapid Prototyping to Direct Digital manufacturing*, Springer, New York, 2010.
- [4] Tabakovi S, Konstantinovi , Radosavljevi R, Movrin D, Hadžistevi M, Hatab N.: *Application of Computer-Aided Designing and Rapid Prototyping Technologies in Reconstruction of Blowout Fractures of the Orbital Floor*, Journal of Craniofacial Surgery, 26/5, pp.1558-1563, 2015.
- [5] Wohlers Report, *Additive Manufacturing and 3D Printing State of Industry, Annual Worldwide Progress Report*, Wohlers Associates, Fort Collins, Colorado, USA, 2014.
- [6] Galeta, T., Kljajin, M., Karakaši , M.: *Geometric accuracy by 2-D printing model*, Strojniski Vestnik, 54, pp. 725–733, 2008.
- [7] Impens, D.: *An Experimental Approach to Assess the Impact of Post Processing Variables on the Mechanical Characteristics of 3D Printed (Powder Binding Process) Parts*, Electronic Theses and Dissertations. Paper 5272, 2015.
- [8] Lužanin, O., Movrin, D., Plan ak M., Tozh-Tascau, M.: *Using factorial design to assess the influence of epoxy brand and preheating on the tensile strength of 3d printed specimens*, The Seventh International Symposium "KOD 2012", pp.431-434, Balatonfüred, Hungary, Faculty of Technical Sciences, Novi Sad, 2012.
- [9] Galeta, T., Kladari , I., Karakaši , M.: *Influence of Processing Factors on Tensile Strength of 3D Printed Models*, Strojarsstvo, 47/6, pp. 149–156, 2011.
- [10] Pilipovic, A., Raos, P., Šercer, M.: *Experimental analysis of properties of materials for rapid prototyping*, The International Journal of Advanced Manufacturing Technology, 40/1, pp.105-115, 2007.
- [11] Faraedon, M. Z., Xiao, K., Noort, R., Yates, J.M.: *Investigation of Elastomer Infiltration into 3D Printed Facial Soft Tissue Prostheses*, Anaplastology, 4/1, pp.1-5, 2015.

Authors: ¹Dejan Movrin, ²Aleksandar Spasi ,
¹Aljoša Ivanišević , ¹Igor Ka mar ik, ²Viktorija
**Vu aj- irilovi Assitent Professor, ¹Plavka Skakun
Assitent Professor, ¹Mladomir Milutinovi Assitent
Professor, ¹University of Novi Sad, Faculty of
Technical Sciences, Institute for Production
Engineering, Trg Dositeja Obradovica 6, 21000 Novi
Sad, Serbia, Phone.: +381 21 450-366, Fax: +381 21
454-495.
²Clinical Center of Vojvodina, Center for Radiology,
Hajduk Veljkova 1, 21000 Novi Sad, Serbia, Phone:
+381 21 484-3484.
E-mail: movrin@uns.ac.rs; a_spasic@yahoo.com;
aljosa@uns.ac.rs; igorkac@uns.ac.rs;
vcirilovic@hotmail.com; plavkas@uns.ac.rs
mladomil@uns.ac.rs**

SOFTWARE SUPPORT FOR FMEA ANALYSIS IN ORTHOPEDIC SURGERY

Abstract: Risk analysis is a systematic tool used for the assessment of the activities within the process of considering the problems that accompany the same. Surgical procedures, in modern orthopedics, involve the use of conventional as well as new solutions, methods, materials and supplies that contribute to efficient operative and postoperative procedures. Each of these interventions entail risks and uncertainties that the patient may have a not-so-small effects in a shorter or longer period.

Key words: orthopedic surgery, software, trochanteric fractures, risk

1. INTRODUCTION

In order to even the most complex development is carried out as soon as possible by applying new methods, materials and supplies surgeon is placed in an unenviable situation. In front of orthopedic surgery in the circumstances today are faced with very complex tasks that carry certain risks. Such surgical procedures requiring teamwork, both during the intervention and in its preparation and in the post operative period. If such risks record, systematize, analyze and continually deduct achieve the real goal of such methods [1]. Developed countries have this method provides also the standards and procedures as an essential part of their health systems (ISO 14971). This raises the level of knowledge and skills of all participants of the health system, which every day becomes more complicated and complex, all with a view to respond to the demands of the high risk [2].

Defining the boundaries of risk is a dynamic process in a time where there is a tendency to increase or decrease this limit with the aim of better quality of the process. One of the most common orthopedic interventions, which are very frequently encountered in orthopedics are surgical treatments trans trochanteric fractures [3]. These are surgical procedure in which a true sense of testing the entire medical system of the orthopedic clinic, both in terms of the health status of the patient, as well as human resources, organizational and technical levels. Each of these factors can not be sorted out separately but in the concrete conditions and environment can perceive certain advantages but also disadvantages which are crucial for the priority value risk.

2. SOFTWARE SUPPORT FOR ORTHOPEDIC FRACTURE ANALYSIS

Bones are rigid, but they do bend or "give" somewhat when an outside force is applied. However, if the force is too great, the bones will break, just as a plastic ruler breaks when it is bent too far.

The severity of a fracture usually depends on the force that caused the break. If the bone's breaking point has been exceeded only slightly, then the bone may crack rather than break all the way through. If the force

is extreme, such as in an automobile crash or a gunshot, the bone may shatter.

If the bone breaks in such a way that bone fragments stick out through the skin, or a wound penetrates down to the broken bone, the fracture is called an "open" fracture. This type of fracture is particularly serious because once the skin is broken, infection in both the wound and the bone can occur.

Common types of fractures include:

- Stable fracture. The broken ends of the bone line up and are barely out of place (Fig. 1).
- Open, compound fracture. The skin may be pierced by the bone or by a blow that breaks the skin at the time of the fracture. The bone may or may not be visible in the wound.
- Transverse fracture. This type of fracture has a horizontal fracture line.
- Oblique fracture. This type of fracture has an angled pattern.
- Comminuted fracture. In this type of fracture, the bone shatters into three or more pieces.



Fig. 1. Input form for software application

The current surgical procedures in orthopedic surgery as well as designing a new medical device or devices inevitably contains a number of questions and problems. They must be solved is usually very fast, and will experience in their later implementation clearly

indicate poor solutions with higher or lower risk. Recommendations for planning quality assurance for manufacturers of medical devices and supplies include two methods for risk analysis:

- FMEA - Failure mode effect analysis
- FMECA - Failure mode critical effect analysis

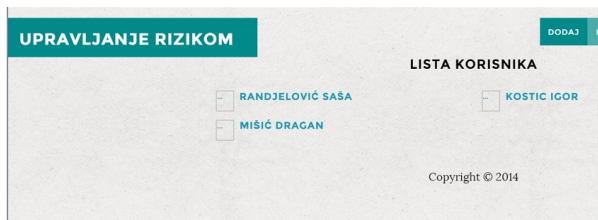


Fig. 2. Risk analysis method and list of user

FMEA is a bottom up approach that assumes the analysis of basic errors at the level of individual components, evaluation of the effect as well as identifying possible solutions. You should be conducted at the beginning of the design process and design solutions to identify potential design weaknesses [4].

FMECA addition adds and probable frequency and severity of errors identified processes. The primary task of FMEA is the early detection of design errors that may have a decisive effect on the safety and characteristics of the bone implantantnog assembly or the patient's condition.

For example trans-trochanteric fractures being illustrated a method of risk assessment that examines the most common group of defects in concrete conditions. On this occasion, the group identified errors that are commonly represented and whose appearance can have significant consequences :

- selection of patients for invasive harvesting intervention
- the choice is not appropriate implant
- the choice is not the appropriate method of fixation.
- usually this fracture
- low level of equipment
- insufficient human potential

These errors represent the complex effects that are not a simple collection activities have the effect of several factors which, in the given circumstances is not easily monitor or resolve [5,6].

The very selection of the patient, his arrival and reporting is not problematic, but when seen in the context of the current health status of the entire patient then it can be a generator of many, very risk, error-free. Most often these are patients with diabetes, chronic renal insufijencijom, high blood pressure, and not rarely there are present malignant tumors, which greatly complicate the process of surgical interventions.

Moguća greška	Uzrok greške	Efekat greške	Ocena greške			Rizik RPN	Aktivnost za smanjenje ili eliminisanje rizika	Napomena	AŽURIRANJE
			O	S	D				
Izbor pacijenta za operaciju sa komorbiditetom	Pacijent boluje od šećerne bolesti	povišen stepen mortaliteta (smrtnosti pacijenta)	5	10	9	450	detaljnija preoperativna priprema pacijenta		AŽURIRANJE
Izbor pacijenta za operaciju sa komorbiditetom	Pacijent ima hroničnu bubrežnu insuficijenciju	povišen stepen mortaliteta (smrtnosti pacijenta)	3	10	8	240	detaljnija preoperativna priprema pacijenta		AŽURIRANJE
		povišen							

Fig. 3. Risk identification and their evaluation

Upravljanje rizikom - Windows Internet Explorer									
http://160.99.21.150:8080/risk/switch.do									
Upravljanje rizikom									
Izbor pacijenta za operaciju sa komorbiditetom	Pacijent boluje od šećerne bolesti	povišen stepen mortaliteta (smrtnosti pacijenta)	5	10	9	450	detaljnija preoperativna priprema pacijenta		AŽURIRANJE
Izbor pacijenta za operaciju sa komorbiditetom	Pacijent ima hroničnu bubrežnu insuficijenciju	povišen stepen mortaliteta (smrtnosti pacijenta)	3	10	8	240	detaljnija preoperativna priprema pacijenta		AŽURIRANJE
Izbor pacijenta za operaciju sa komorbiditetom	Pacijent ima visok krvni pritisak	povišen stepen mortaliteta (smrtnosti pacijenta)	9	10	8	720	detaljnija preoperativna priprema pacijenta		AŽURIRANJE
Izbor pacijenta za operaciju sa komorbiditetom	Pacijent ima prelom nastao kao posledica metastaze tumora	povišen stepen mortaliteta (smrtnosti pacijenta)	3	10	5	150	detaljnija preoperativna priprema pacijenta		AŽURIRANJE
Izbor pacijenta za operaciju sa komorbiditetom	Pacijent u poznim godinama	povišen stepen mortaliteta (smrtnosti pacijenta)	8	9	8	576	detaljnija preoperativna priprema pacijenta		AŽURIRANJE

Fig. 4. Risc identification list and their evaluation

UPRAVLJANJE RIZIKOM
DODAJ LISTA ODJAVA

STAVKA

Moguća greška

Izbor pacijenta za operaciju sa komorbiditetom

Efekat greške

povišen stepen mortaliteta (smrtnosti pacijenta)

Uzrok greške

Pacijent ima hroničnu bubrežnu insuficijenciju

PROCENA GREŠKE I RIZIKA

Učestanost

3

Ozbiljnost

10

Otkrivanje

8

RPN

240

SMANJENJE ILI ELIMINISANJE RIZIKA

Aktivnost za smanjenje ili eliminisanje rizika

detaljnija preoperativna priprema pacijenta

Napomena

OTKAŽI
UPAMTI

Copyright © 2014

Fig. 5. Risc evaluation and corrective action

The choice is not appropriate implant can be very critical and with great risk to the patient. That experience and level of knowledge surgeon and the whole team comes to the fore. For these reasons, in

these circumstances, seeking the best practices and succeeded surgical intervention that would represent a good basis for new interventions. Clinics and surgeons with extensive experience in higher benefits, because a

larger number of interventions and surgical procedures is a good basis for making the right decisions [7,8]. The x-ray shows a healed thighbone fracture treated with intramedullary nailing and the right x-ray, the thighbone fracture has been treated with plates and screws (Fig. 2).

The choice is not the appropriate method of fixation as well as the previous error is closely related to the experience of the individual and the entire orthopedic clinics. External fixation is often used to hold the bones together temporarily when the skin and muscles have been injured (Fig. 3).

For all of these errors and problems to a great extent the solution lies in good organization working clinic for a longer period. Namely, if the experience and knowledge is transferred and processed in a quality manner, over a long period, it can be a good way to achieve a greater number of successful interventions with satisfied patients.

As noted, in addition to the surgical procedure becomes very prominent and postoperative period when a bad decision and recognize that they largely caused by the intervention or medical condition of the system.

One of the most common non or delayed healing of fractures formed. The main cause of the relatively large distance between the fracture surface which is formed by surgery so it is not possible to start his healing and the formation of transient bone tissue. Closely associated with this error is unstable fixation or insufficient stiffness of the entire system that just needs to provide satisfactory postoperative course.

These were errors that occurred as a result of a small lower level of knowledge and experience of the surgical team and its individuals. When we add to these environmental conditions, technical equipment and human potential is obtained by a coherent view of an entire health system.

In the first place is often the case that there are no suitable implant, as a whole or its individual elements. Then he reached for a smaller or larger improvisations whose consequences is difficult or can not be eliminated.

4. CONCLUSION

Identifying errors they may be eliminate or their effects reduced design solutions and corrections before they reach a specific product to the patient, where every mistake can have very serious consequences to the patient and future potential.

Good reasons implementation of such methods of early identification of problems greatly reduces the cost to the design process and later production, where costs can multiply. It offers a measure or level of protection to be reckoned with when it comes to a completely new or improved product.

5. ACKNOWLEDGMENT

This paper is part of project III41017 "Virtual human osteoarticular system and its application in preclinical and clinical practice", funded by the Ministry of Education and Science of Republic of Serbia.

6. REFERENCES

- [1] Morelli, P., Vinci, A., Galetto, L., Magon, G., Maniaci, V., Banfi, G.: *FMECA methodology applied to two pathways in an orthopaedic hospital in Milan*, J Prev Med Hyg, 2007; 48: pp. 54-59
- [2] Henry, O.: *Risk Management in Medical Device Design*. Medical Device & Diagnostic Industry. December, 2009
- [3] *Pharmaceutical cGMPS for the 21st Century—A Risk-Based Approach: Second Progress Report and Implementation Plan*. U.S. Department of Health & Human Services. December, 2009.
- [4] Harvey, R., Sidebottom, C.: *The Role of Risk Management in the New IEC 60601-1*. Medical Device & Diagnostic Industry. 2009.
- [5] Mike, S.: *The Use and Misuse of FMEA in Risk Analysis*, Medical Device & Diagnostic Industry. December, 2009.
- [6] Mitkovi, M., Milenkovi, S., Bumbaširevi, M., Lesi, A., Golubovi, Z., Mladenovi, D., Mici, I., Jovanovi, V.: *Surgical treatment of pertrochanteric fractures using personal external fixation system and technique*, Facta Universitatis, Series: Medicine and Biology Vol.9, No 2, 2002, pp. 188 - 191
- [7] Yoshino, N., Watanabe, Y., Takenaka, N., Watanabe, N., Fukuda, Y., Fujita, N., Maruyama, N., Sumiyoshi, H., Takai, S.: *Implant failure of long Gamma nail in a patient with intertrochanteric-subtrochanteric Fracture*, J Orthop Sci (2006) 11: pp. 638–643
- [8] Milenkovi, S., Mitkovi, M., Radenkovi, M., Mladenovi, D., Golubovi, Z., Stanojlovi, M.: *Surgical treatment of the trochanteric fractures by using the external and internal fixation methods*, Facta Universitatis, Series: Medicine and Biology Vol.10, No 2, 2003, pp. 79 – 83

Authors: dr Saša Randjelovi, Associate Professor, dr Dragan Miši, University of Nis, Faculty of Mechanical Engineering, Aleksandra Medvedeva 14, 18000 Nis, Serbia, Phone +381 18 500629, **Milena Miši**, University of Nis, Faculty of Electronic Engineering, **dr Igor Kostić**, Orthopaedic and Traumatology Clinic, University of Nis, Faculty of Medicine, Nis, Serbia, **dr Dejan Taniki, Associate Professor**, University of Belgrade, Technical Faculty of Bor, Serbia
E-mail: sassa@masfak.ni.ac.rs

Raspuđi , V.

ROTATIONAL KINEMATICS OF LOWER LIMBS DURING STAIR ASCENT USING CAD/CAE

Abstract: *The methodology of combining data captured by optoelectronic systems with the current CAD/CAE computer technologies can be used for biomechanical analysis of different forms of locomotor movements. The goal of this study was to analyze rotational kinematics of human lower limb segments during stair ascent using generated kinematic simulation models and real data of marked points recorded while subjects performed this motion activity. The mobility of the kinematic models is realized through spherical joints between segments, and through cylindrical joints between proximal and distal links in the direction of their longitudinal axis. The general patterns for segment and joint angles, angular velocities and accelerations during stance period have been determined.*

Key words: *biomechanics, computer simulation, kinematic analysis*

1. INTRODUCTION

Current CAD/CAE systems that are widely being used in applications for traditional mechanical design and analysis provide mostly simple simulation and analysis tools for biomechanical motion analysis of human body. Their capabilities are primarily intended for ergonomic or static analysis. The development of methodology for 3D computer simulation that will truly emulate the real human body motion of a recorded magnetic or optical monitoring within the CAD/CAE system can provide a detailed biomechanical analysis of kinematics and dynamics in various aspects of locomotion. This is especially important for the development of products such as prosthetic devices, whose design and motion mechanism are directly dependent on natural locomotion of the human body.

The methodology of combining data captured by the optoelectronic tracking system with the current CAD/CAE computer technologies applied in this study can be used for three-dimensional biomechanical analysis of different forms of locomotor movement, and thus be integrated in the standard computer environment for development and improvement of mechanical design.

Beside the possibility to actively control the amount of damping in artificial joints, modern above-knee prosthesis should be able to generate power. This would enable persons with above-knee amputation to achieve not only biologically realistic kinematics, but also dynamics of locomotion. The problem of natural locomotion for these persons is particularly reflected when climbing stairs, since most available above-knee prosthesis do not give the possibility of obtaining reciprocal way of climbing.

Understanding of normal biological locomotion is a prerequisite for improving design and control concepts of powered prosthetic devices. For this reason, in this study a detailed analysis of rotational kinematics of motion during stair ascent using CAD/CAE has been conducted.

2. METHODS

In biomechanical tests, human body is usually displayed as a mechanism comprised of segments, which are connected in a series of kinematic chains. In this study, a kinematic model of lower extremities consisted of 5 joints and 10 links [Fig. 1]. The mobility of the system is achieved through three rotational degrees of freedom between joints and links (spherical joints), and by one translational and one rotational degree of freedom between all proximal and distal links in the direction of their longitudinal axis (cylindrical joints). These kinematic models have enabled a computer simulation that accurately mimics the captured data with spatial coordinates of markers, and the three-dimensional computer reconstruction of their trajectories and their projections in the sagittal, frontal and transverse plane.

The kinematic analysis has been performed using the automatized method for determination of spatial orientation of lower limb segments. 3D coordinates of the marked points recorded by the optoelectronic measuring system were the input data for the computer simulation, which calculates and reconstructs trajectories of joints and spatial orientation of lower limb segments [1]. The input data were obtained from ten subjects (range 21-39 years), with no apparent abnormalities of the locomotor system. The climbing was performed with the speed that the subjects considered as their normal speed of climbing. Special attention was given to naturalness in walking and a constant walking velocity. Subjects were climbing barefoot on the laboratory staircase (rise height 17 cm, tread length 29 cm). Five markers have been attached to palpable landmarks of lower extremities, and their position is defined according to the procedure described in (Perry, 1992) and (Cappozzo et al., 1995) [2,3]. The markers were placed on the following characteristic landmarks: hip (upper front edge of the great trochanter), knee (top of the fibula), ankle, heel, the root of the little finger (top of the fifth metatarsal).

Orientation of thigh and shank is defined by the angles measured from the vertical to the longitudinal

axis of these segments, with the convention on positive and negative signs of angles as shown in Fig. 1. Orientation of foot segment is defined by the angle between the vertical and the connecting line of the ankle and little foot markers. The angle of knee is defined by the angle between the longitudinal axes of thigh and shank, and the ankle angle as an angle between the longitudinal axis of shank and connecting line of ankle and the root of little finger markers.

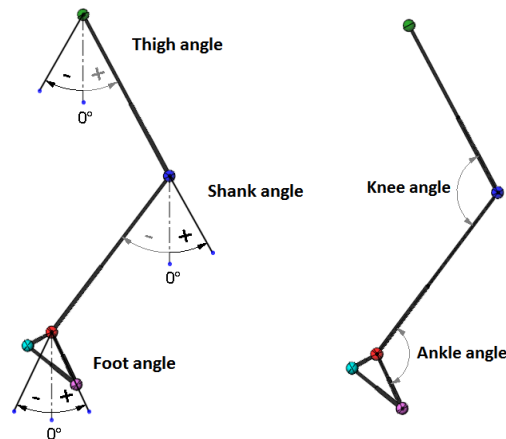


Fig. 1. The angles of lower limb and sign convention

In order to compare the characteristics of climbing, the average values and standard deviations of analysed motion parameters have been determined. For each of the examined subjects and for all measurements conducted, there are three defined patterns: individual, typical and general. An individual pattern represents each functional dependence of the measured parameter on time or on the normalised percentage of stance period (SP) for each of the subjects. From individual patterns of motion characteristics, a typical pattern for every subject has been established. A general pattern for a particular motion has been determined from typical patterns of all subjects.

Determination of the mean value of the curves representing the dependency of selected parameters on the percentage of stance period has been made by the normalization method, dividing one cycle of each curve in equally spaced data points, after which the mean value is determined for all points of the curve. Since the number of data identified by measuring is different depending on the speed of walking, spline interpolation was used to determine 100 equally spaced data points.

Data captured by the optoelectronic measuring system have been transferred to the software package MATLAB using software commands written in Excel Link interface. To prevent the generation of stochastic errors of broad frequency spectrum and to remove "noise" of measurements, the filtering of the measured data is performed in MATLAB by Moving Average filter [4].

Fig. 2 represents the kinematic model in the following characteristic positions during stair ascent:

- The position O1, which marks the beginning of foot contact with the surface;
- The position P1, which marks the maximum inclination of shank, i.e. the rightmost position in the loop of knee trajectory;

- The position P2, which marks the leftmost position in the loop of knee trajectory;
- The position O2, which marks the end of foot contact with the surface.

It has been determined that the characteristic position P1 occurs at 20% SP, and the characteristic position P2 at approximately 60% SP.

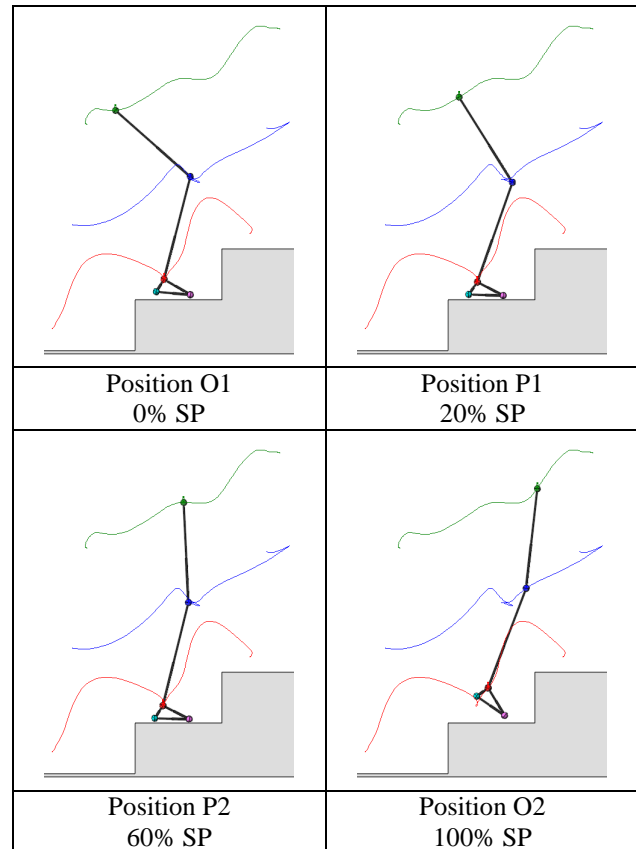


Fig. 2. The characteristic positions during stance period

3. ANALYSIS OF SIMULATION RESULTS

Because the present market solutions of prosthetic knees and feet allow only one rotational degree of freedom around the longitudinal axis of their joints, the rotational kinematics of defined kinematic leg models has been analyzed in the sagittal plane. Fig. 3-8 show general patterns of angles, angular velocity and acceleration of thigh, shank, foot, knee and ankle during the contact of the foot with the ground (stance period).

At the beginning of the stance period (0% SP) the average (general) value of the thigh angle is 47.47° and the average value of the shank angle is -18.12° (Fig. 3). The value of the knee angle is 114.40° and the ankle angle is 100.46° (Fig. 6). From the initial contact of the foot with the step O1 to position P1 (20% SP) the thigh and shank move in negative direction of rotation (Fig. 4). The rotational movement of the thigh accelerates until P1 position, while the shank accelerates during the first 5% SP, after which it begins to decelerate (Fig. 5). The average thigh rotation value is -13.44° , and the shank rotation is -4.00° .

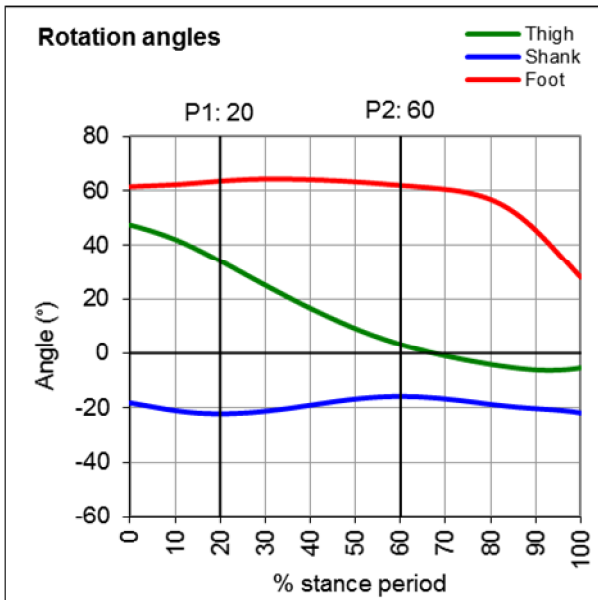


Fig. 3. Rotation angles of thigh, shank and foot

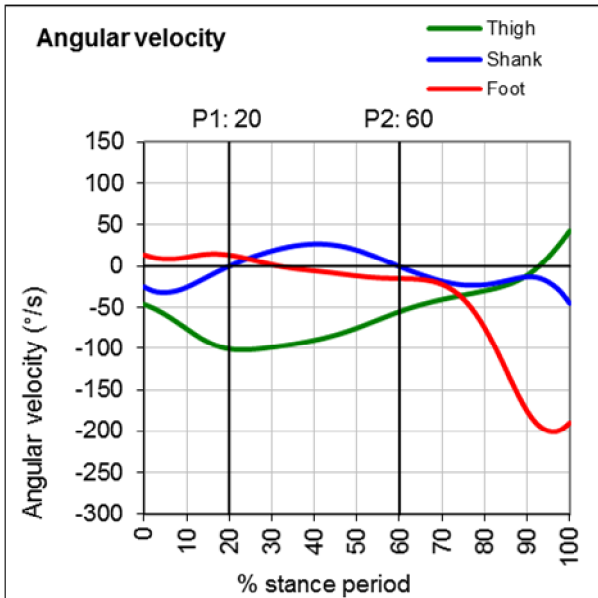


Fig. 4. Angular velocity of thigh, shank and foot

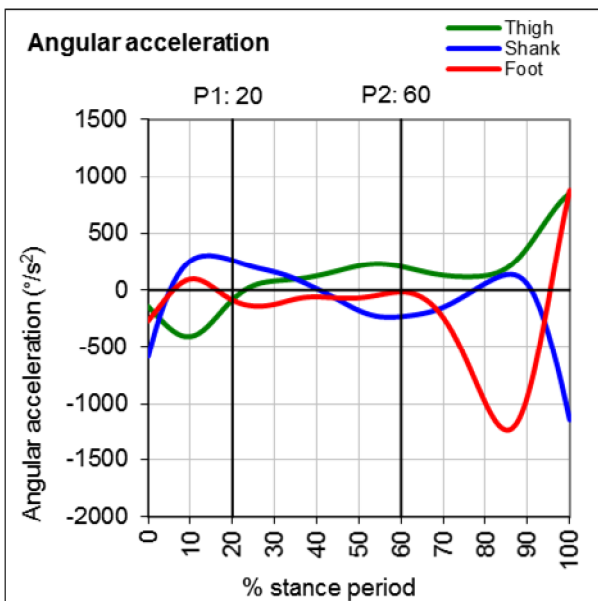


Fig. 5. Angular acceleration of thigh, shank and foot

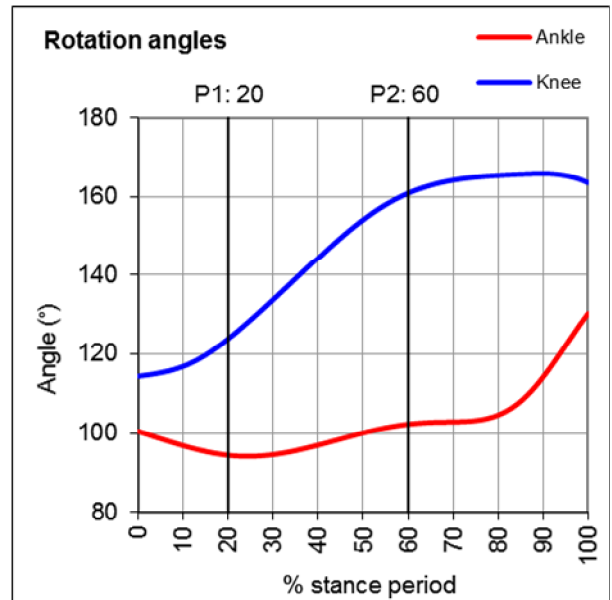


Fig. 6. Rotation angles of ankle and knee joint

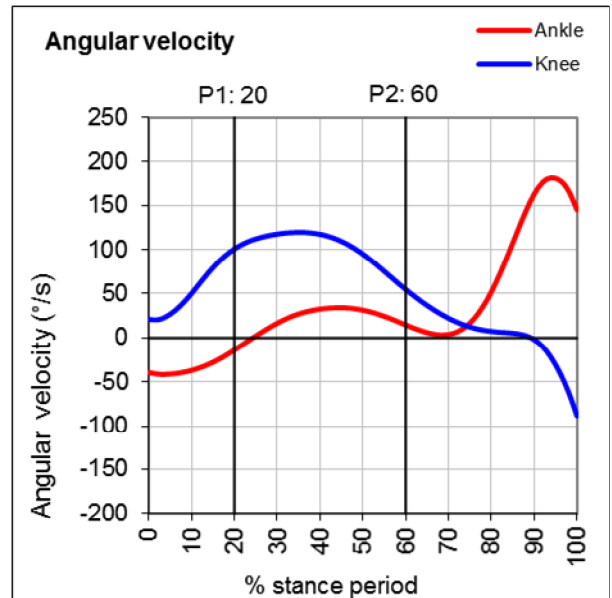


Fig. 7. Angular velocity of ankle and knee joint

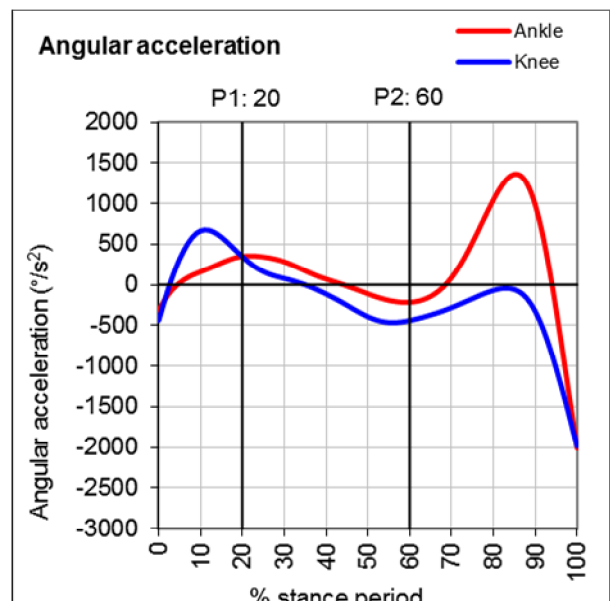


Fig. 8. Angular acceleration of ankle and knee joint

The result of the rapid movement of the thigh and the slower movement of the shank in the negative direction is rapid extension of the knee in an amount of 9.44° , while the ankle joint performs a slow dorsal flexion in the amount of 6.05° .

Positive angular velocity of the thigh, shank and foot segment indicates the counterclockwise rotation, and negative angular velocity indicates rotation in the clockwise direction. Concerning the knee and ankle joints, positive angular velocity indicates the extension of the knee and the plantar flexion of the foot, and a negative angular velocity indicates the knee flexion and the dorsal flexion of the foot.

In the P1 position the shank has taken the maximum angle of inclination from the vertical to the amount of -22.12° , to allow the achievement of the required ground reaction moment arm to generate torques in the knee and ankle joints necessary to raise the weight of the body to a higher level of the following step.

From the P1 to the P2 position it comes to direction change of shank rotation from negative to positive, while the thigh rotation in the negative direction continues. During the first half of this period (20% SP and 40% SP) the shank rotation is accelerated and then slowed down until the P2 position. The rotation of the thigh is made with a slowdown. The average rotation of the thigh is -30.77° and 6.30° of the shank. The average value of the knee extension during this period amounted to 37.05° . Thereby the knee extension takes place rapidly to 35% SP, after which it slows down to move from a knee flexion in extension (90% SP). In the period from the P1 position to approximately 45% SP it occurs rapid plantar flexion in the ankle joint, after which it slows down. The change of the ankle angle in the period P1-P2 was 7.83° .

In the P2 position the thigh has approximately vertical alignment (flexion in the amount of 3.26°). In this position, it comes again to the rotation direction change of the shank from positive to negative. Immediately after the P2 position (67.5% SP) the thigh has a vertical alignment and a hip extension begins. At this point it comes to the change from slow to rapid plantar flexion of the foot and it begins the lifting of the heel from the surface. The maximum value of hip extension (-6.28°) takes in about 90% SP and then the hip flexion re-enters, i.e. there is a change of rotation of the thigh from negative to positive. At this point, rapid knee flexion begins and the foot is preparing to the swing phase.

In the period from the P2 to O2 position, the foot retains its extended position, with a very little value of knee extension in the amount of 2.64° , while there is a maximum of foot plantar flexion, with an increase in the value of the ankle angle in the amount of 28° .

Analysis of rotational kinematics during the stance period has shown that the value of the knee angle is in the range of 114° to 166° , and the value of the ankle angle is in the range of 94° to 130° . Therefore, the biggest change of angle is 52° for the knee and 36° for the ankle joint.

The maximum deviation of individual values compared to the general pattern occurs directly after the capture of the position of maximum inclination of the

shank (P1 position), with a maximum standard deviation of 6° for the knee angle and 4° for the ankle angle.

The greatest angular velocity of the knee joint, amounting to $120^\circ/\text{s}$ (2 rad/s), is achieved in 35% SP, which roughly corresponds to half the interval between typical end positions in the knee loop between which knee moves in the negative longitudinal direction. The maximum angular velocity of the ankle joint, amounting to $180^\circ/\text{s}$ (rad/s), is achieved just before lifting the foot from the ground (95% SP).

4. CONCLUSION

The purpose of this study was to analyze rotational kinematics of lower limb segments during stair ascent. The findings from the current study provide baseline measures for design improvement of powered above-knee prosthesis to allow more natural way of movement. In developing of control concepts for adjustment of prosthesis motion, with information on the values of the joint angles in the characteristic phases of motion, it is important to know the angular velocity of segments and joints. Knowing the angular velocity of segments allows determination of their current rotation direction, while based on knowledge of the angular velocity of the knee and ankle joint it can be concluded whether flexion or extension occurs in these joints.

The motion analysis has been conducted in CAD/CAE environment, in order to provide the possibility of integration of biomechanical kinematic and dynamic data with the standard computer environment for design and motion analysis of prosthesis mechanical components.

5. REFERENCES

- [1] Raspudic V.: *Computer Simulation of Lower Extremities Movement During Stair Climbing*, (407-411), Applied Mechanics and Materials, Vol. 330, 2013.
- [2] Perry J.: *Motion Marker Systems, In: Gait Analysis, Normal and Pathological Function*, (367-370), SLACK Incorporated, ISBN: 1-55642-192-3, USA, 1992.
- [3] Cappozzo A. et al.: *Position and orientation of bones during movement: anatomical frame definition and determination*. Clinical Biomechanics, Vol. 10, No. 4, pp. 171-178, ISSN: 0268-0033, 1995.
- [4] *Documentation for MATLAB*, The Language of Technical Computing, Version 7, 2004.

Author: Doc.dr.sc. Vesna Raspudic, University of Mostar, Faculty of Mechanical Engineering and Computing, Matice hrvatske bb, 88000 Mostar, Bosnia and Herzegovina, Phone.: +387 36 337-028, Fax: +387 36 337-012.

E-mail: vesna.raspudic@sve-mo.ba



Spasi A., Vučajirilovi V., Movrin D., Šokac M., Budak I., Till V.

CT DENSITY OF THE CORTICAL BONE OF ALVEOLAR PROCESS OF MAXILLA

Abstract: Precision of segmentation of CT scans of maxillary alveolar process depends on the sharpness of the outer margin of the bone and its demarcation from surrounding structures. Cortical bone defects and lower densities affect 3D model's similarity to the original. CT scans of the maxilla of twenty five patients were evaluated. ROI was placed on five determined spots of cortical bone on both buccal and palatine side of the alveolar process to obtain CT density (anterior, middle lateral, posterior lateral). Lower densities were measured on: a) edentulous positions compared to positions with preserved teeth; b) lateral buccal positions compared to anterior buccal position; c) buccal side compared to palatine side. Factors influencing cortical bone density are: preservation of the tooth, position on the alveolar process and side of the alveolar process. Segments of lower cortical bone density should be places of increased attention in verification of segmented CT scans. Precision of segmentation of CT scans of maxillary alveolar process depends on the sharpness of the outer margin.

Keywords: CT density, alveolar process, cortical bone.

1. INTRODUCTION

With recent advances in computer – aided technologies (CAx) and their application in different fields, it also allowed vast growth and increasing number of different applications of Computed Tomography (CT) in other industries, beside medicine, such as aviation, railway, military industry and others [1, 2].

The main tool used for extraction of valuable information from the CT images is segmentation process. In a more classical term, segmentation is defined as a process of dividing image on non-overlapping, consistent homogenous regions, in accordance with certain characteristics such as intensity of grayscale or texture. As a result of the segmentation process a binary image is generated where the value 1 represents the region of interest, and 0 represents the background that has been excluded [3].

Rapid prototyping (RP) of maxilla is performed using images of maxilla obtained on computerized tomography (CT) examination. Segmentation of maxilla is process of demarcation of gingival soft tissue from the bone of maxilla on images that are to be used in RP protocol.

With the use of computers, automated and greatly reduced time in segmentation process is achieved due to the use of different computer software.

But, however, automatic segmentation software is prone to an error on regions of maxilla where density of cortical bone is decreased, and demarcation from soft tissues is not perfect. On these positions manual segmentation must be performed. Evaluation of bone density and analysis of places where decrease of density is the greatest should be helpful in process of control of automatic segmentation as a reminder on which places automatic segmentation results should be most meticulously evaluated.

One of many reasons why this is of utmost importance is also the application of segmentation in modeling process of bone grafts of complex shapes [4]. Here the segmentation plays a very important role as the generated 3D model presents a base for bone grafting and later implant planning.

For the purposes of manual segmentation process, the most common type of segmentation algorithm used is the Otsu's thresholding method [5]. Here, the main focus lies in the pixels intensity on the DICOM image which goes from 0 to 4096. By defining the upper and lower threshold value (ie. the pixels intensity values), it is able to differentiate the object of interest from the rest of the image. These values are defined by the user and can successfully extract the predefined object inside a region of interest. The figure 1 below shows interface of the segmentation process used in software called 3D DOCTOR (able software corp.)

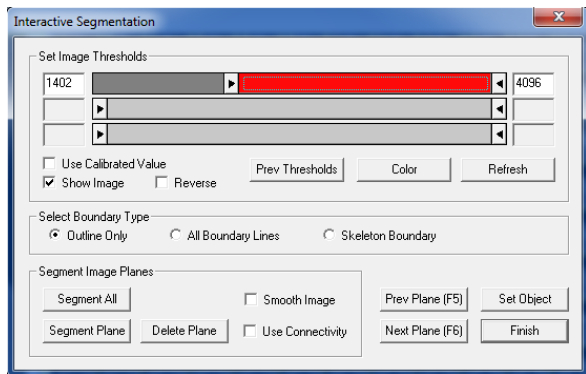


Fig. 1. Segmentation dialog window from 3D DOCTOR software

2. MATERIALS AND METHODES

Twenty five CT examinations of head performed for various neurological reasons were uploaded from picture archiving and communication system. Examinations were performed on CT 64-channel scanner (Definition 64; Siemens, Erlangen, Germany). CT density of alveolar process of maxilla was measured on ten positions, five respectively on buccal and palatine side, placed as follows (tooth position outlined in brackets): right posterior (17), right medial (14), anterior (between 11 and 41), left medial (44), left posterior (47) (Figure 3).

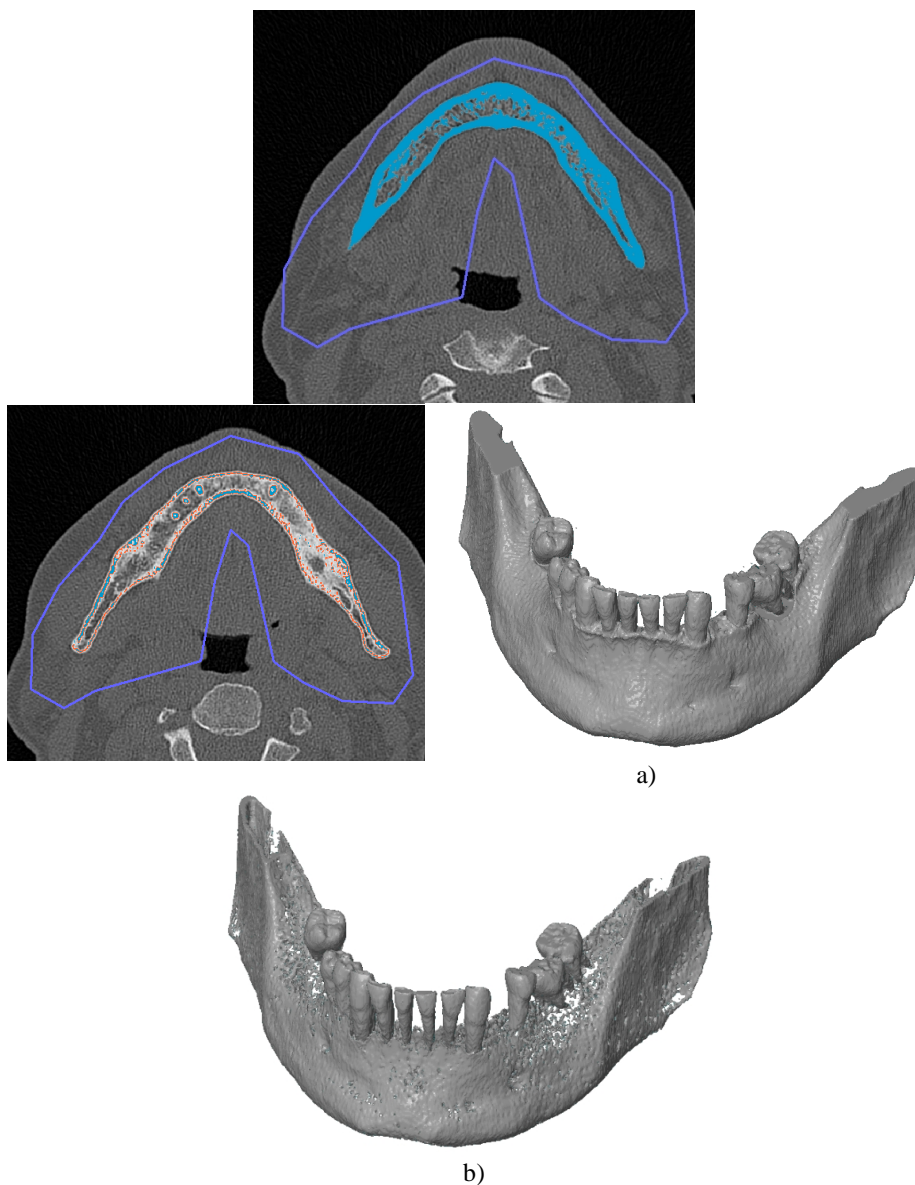


Fig. 2. Results of segmentation a) good and b) not good

But, in order to achieve highly accurate and reliable presentation of segmented 3D model, these parameters must be properly chosen. On the figure 2 below it can be seen how inaccurate results of segmentation can have a negative impact on the end result which is a 3D model of the segmented object.

Circle tool was used to set region of interest (ROI) on cortical bone (Figure 4). CT densities in Hounsfield units (HU) for all ten positions were recorded and average values for each position were calculated.



Fig. 3. Positions on which cortical bone density was measured.

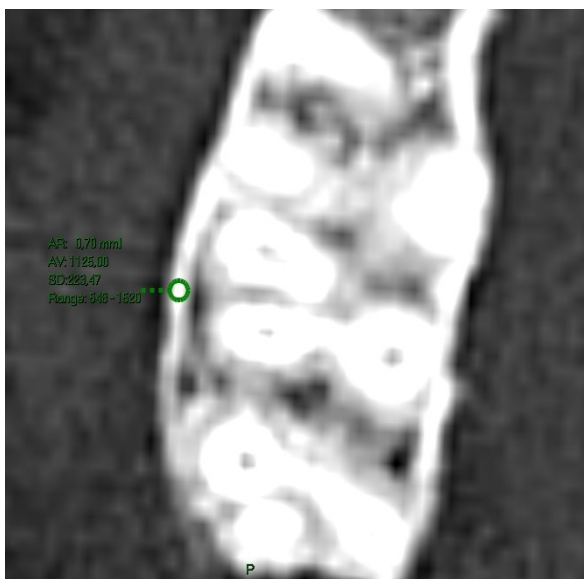


Fig. 4. Circle ROI placement

3. RESULTS

Average densities of cortical bone of alveolar process of maxilla are shown in Table 1.

Significant difference was detected on positions with preserved tooth compared to edentulous positions.

In edentulous positions lower densities were detected on lateral posterior (1, 9) and medial positions (3, 7) compared to other.

In edentulous lateral positions lower densities were detected on positions on buccal (1, 3, 7) compared to positions on palatine side (2, 4, 10).

position	preserved tooth	edentulous
1	983	337
2	1217	658
3	1119	425
4	1365	798
5	1034	898
6	1141	763
7	1161	484
8	1255	792
9	975	625
10	1255	612

Table 1. Cortical bone density in HU

4. DISCUSSION

Bone of alveolar process of maxilla is composed of cortical and cancellous bone. On the surface bone is outlined by cortex. It is heavily calcified tissue and the firmest part of the bone. Due to great amount of calcium its CT density is high. Going towards the depth of the alveolar process cortical bone changes into cancellous bone. Cancellous bone is composed of latticework of branching and connecting strands of osseous tissue called trabeculae [6]. Intertrabecular space of cancellous bone is filled mainly with fat. Hence the density of calcium and consequently CT density in this tissue are much lower than in that of cortical bone.

Two important factors for decrease of density of alveolar process can be highlighted.

Firstly loss of tooth that happens during time of life for various reasons leads to decrease of intensity of jaws chewing function. This is important because loss of teeth produces loss or minimization of various forces and actions such as the chewing forces, the forces of the tongue muscle, and the perioral muscles. This functional reduction may enhance the bone resorption in the maxillary alveolar process and the hard palate. [7]. On the other hand bone function promotes mechanisms for bone creation so when this is not the case resorptive effects will surpass osteogenesive effects.

Secondly loss of tooth in the jaw and atherosclerotic changes leads to decrease of blood volume deployed to the bone. Consequentially lack of blood supply in the absence of the drainage pathway of the crestal mucosa affects periosteal regeneration [8].

In our series edentulous jaws, along with positions on jaws with extracted tooth have shown lower densities of cortex compared to jaws with preserved tooth.

Notable differences in rate and degree of atrophy were observed between anterior and posterior positions, which might be the result of differences in anatomy.

Posterior segments showed a higher frequency and degree of atrophy than anterior segments, which is in concordance with the fact that molars tend to be lost at an earlier age than anterior teeth. Hence, atrophy might develop in the posterior part of the jaw first and progress further [9]. This explains effect that posterior lateral positions mainly had lower CT densities of the cortex compared to anterior positions.

Differentiation of tissues in this kind of CT diagnostic is obtained because of their different CT densities. Tissues that have different density can be readily separated one from another. Main advantage of CT examination of alveolar process for obtaining images to be used for rapid prototyping lies in the fact that there is great difference between densities of soft tissues of gingiva and cortical bone of alveolar process, and in the fact that cortical bone has smooth margin that can be easily segmented from surrounding tissues.

Loss of density of the cortical bone changes the contour of the bone. Ideally it is smooth and covered with dense cortex. In cases of bone density minimization and occurrence of defects of cortical bone contour becomes irregular, and on its surface cancellous bone emerges. Its structure with soft tissues mixed with osseous elements makes it difficult to mark the contour of the bone as its density is not as high as in cortical bone has values closer to the values of CT densities of soft tissues. Additionally contour of the bone becomes irregular with gaps in its structure which makes errors in segmentation more probable.

5. CONCLUSION

Loss of cortex density is observed in all edentulous positions. Edentulous positions compared among themselves have lower densities on buccal medial and posterior compared to anterior positions and on buccal posterior and medial compared to palatine side. Quality of automatic segmentation of CT images should be meticulously analyzed especially on positions with expected lower cortical CT density.

6. ACKNOWLEDGEMENT

Results of investigation presented in this paper are part of the research realized in the framework of the project "Research and development of modeling methods and approaches in manufacturing of dental recoveries with the application of modern technologies and computer aided systems" – TR 035020, financed by the Ministry of Education, Science and Technological Development of the Republic of Serbia.

7. REFERENCES

- [1] Kruth J.P., Bartscher M., Carmignato S., Schmitt R., De Chiffre L., Weckenmann A.: *Computed tomography for dimensional metrology*, CIRP Annals - Manufacturing Technology, 60, p.p. 821–842, 2011.
- [2] Huang R., Ma K., McCormick P., Ward W.: *Visualizing industrial CT volume data for nondestructive testing applications*, Proceedings of the 14th IEEE visualization 2003. IEEE Computer Society; p.p. 547–54, 2003.].
- [3] Cai W., Chen S., Zhang D.: *Fast and Robust Fuzzy C-Means Clustering Algorithms Incorporating Local Information for Image Segmentation*, Pattern Recognition, 40, p.p. 825–838, 2007.
- [4] Mirkovi S., Budak I., Puškar T., Tadi A., Šokac M., Santoši Ž., ur evi -Mirkovi T.: *Application of modern Computer-aided Technologies in the production of individual bone graft*, Vojnosanitetski preglod, (accepted for publishing), 2015.
- [5] Nobuyuki O.: *A threshold selection method from gray-level histograms*. IEEE Trans. Sys., Man., Cyber. 9 (1): 62–66, 1979.
- [6] Gentry S.D., Bramblett C.A.: *The anatomy and biology of human skeleton*, ARR, 1988.
- [7] Suresh S., Sumathy G., Banu M.R., Kamakshi K., Prakash S.: *Morphological analysis of the maxillary arch and hard palate in edentulous maxilla of South Indian dry skulls*, Surg Radiol Anat 34:609–617, 2012.
- [8] S. Ihde.: *Principles of BOI*, Springer Verlag Berlin Heidelberg, 2005.
- [9] Reich K.M., Huber C.D., Lippnig W.R., Ulm C., Watzek G., Tangl S.: *Atrophy of the residual alveolar ridge following tooth loss in an historical population* Oral Diseases 17, 33–44, 2011.

Authors: Aleksandar Spasi¹, Viktorija Vu aj irilovi^{1,2}, Dejan Movrin³, Mario Šokac³, Igor Budak³, Viktor Till^{1,2}. ¹ Center of Radiology, Clinical Center of Vojvodina, Hajduk Veljkova 1, Novi Sad, Serbia, Phone: +381 21 520577,

² University of Novi Sad, Medical Faculty, Hajduk Veljkova 3, Novi Sad, Serbia, Phone: +381 21 3420677,

³ University of Novi Sad, Faculty of Technical Sciences, Institute for Production Engineering, Trg Dositeja Obradovica 6, 21000 Novi Sad, Serbia, Phone: +381 21 450366

E-mail: a_spasic@yahoo.com; veirilovic@hotmail.com
movrin@uns.ac.rs; marios@uns.ac.rs
budaki@uns.ac.rs; vtill@eunet.rs



Vasiljevi , D., Maravi , T., Kantardži , I., Lainovi , T., Blaži , L.

GENERATION OF A CT-SCAN BASED 3D SOLID MODEL OF A SECOND UPPER PREMOLAR TOOTH

Abstract: Finite element analysis (FEA) of three-dimensional (3D) models of biomaterials and human tissues has become increasingly popular in recent decades. The creation of a 3D solid model based on CT scans of a second upper premolar is presented in this paper. All slices obtained from a CT scan of an intact extracted upper second premolar were imported into SolidWorks (SolidWorks Corp., USA) and the realistic 3D model was developed. After a 3D model is completed, it is possible to simulate different dental procedures and calculate values of stress and strain within the tooth and biomaterials using FEA.

Key words: 3D model, finite element analysis, premolar

1. INTRODUCTION (10 PT, CAPITALS)

In recent years there has been an increasing interest in the research of mechanical aspects of biomaterials and human tissues [1–3]. Studies based on laboratory experiments may give some of the answers in this field, but the major problem is that dental and medical research is usually very expensive, ethically questionable and time consuming when conducted on live subjects. Hence, the use of numeric models and in vitro simulations became a valuable means of saving time and resources associated with laboratory and clinical research.

Finite element analysis (FEA) can be applied on a three-dimensional (3D) model of a biological structure and enable calculation of stress and strain within that structure, which is difficult to measure in vivo [4]. For instance, in dental research, FEA can be used in various fields, such as restorative dentistry and endodontics, prosthodontics, implantology, orthodontics and oral surgery [5]. Stress and strain within the tooth structures and biomaterials used for their reconstruction can be calculated. The influence of different restorative materials, different restoration designs and dental procedures on the tooth and the surrounding tissues, the influence of tooth anatomy and morphology of the tooth on the success of certain dental procedures, are just some of the many useful and interesting applications of FEA in dentistry. In order for the FEA to be as precise as possible, a realistic tooth model must be made beforehand.

Previous studies have reported different techniques for generating 3D solid models of teeth [6–8]. Tooth models can be created using data collected from different sources, such as: data from literature, data obtained through direct measurement of an extracted tooth, 3D scans of the outer surface of the tooth, or computed tomography (CT) or nuclear magnetic resonance (NMR). Nowadays, technological development brings us new possibilities for efficient generation of sophisticated 3D models. In recent years these models are designed using different software packages, based on the information gained from CT

scans. [9–12].

The aim of this study was to generate a realistic 3D-FE solid model of a maxillary premolar tooth based on CT data.

2. CONSTRUCTION OF THE HUMAN MAXILLARY PREMOLAR SOLID MODEL

A human upper second premolar was extracted for orthodontic reasons. After the extraction the tooth was scanned using the Sensation 64 Cardiac CT scanner (Siemens, Germany). This is a 64 slice CT scanner and it was possible to obtain 110 slices along the x axis (all slices were positioned in parallel yz planes), 88 slices along y axis and 47 slices along z axis. The resolution of the CT scanner was 0.00976 mm along x and y axis and 0.5 mm along z axis. The contrast recorded by the CT scanner was from -1024 to 3071 which makes total of 4096 levels.

In this paper slices parallel to the xy plane (along the vertical z axis) were used for the creation of the 3D solid model. From the existing 47 slices only 42 slices contained useful information. All the slices obtained from the CT scanner were written in DICOM file format (DICOM – Digital Image and Communications in Medicine). DICOM is a standard file format for distributing and viewing any kind of medical image regardless of the origin. The selected slices were imported to program AMIRA (Visage Imaging Inc. USA). The first step after importing slices in AMIRA was the automatic segmentation using a threshold. In all the slices dentin has lower contrast than enamel, so the threshold is defined in the following way: exterior – dentin threshold 400 and dentin – enamel threshold 2400. The purpose of a threshold is to define a border line between two entities. There were only three thresholds because the pulp is considered as the exterior. Pictures of one of the slices imported and segmented in AMIRA are given on Fig. 1A and 1B. After segmentation and definition of the enamel, the dentin and the pulp, the next step was the alignment of all imported slices. It is very important to align all the slices that are imported to AMIRA in order to properly

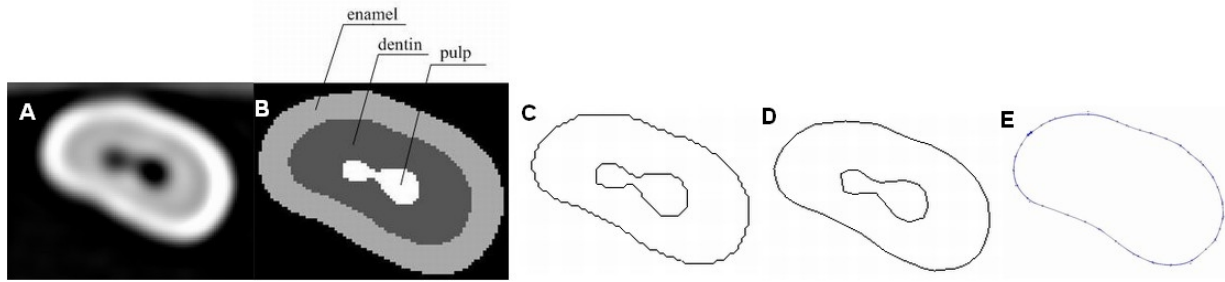


Fig 1. A) Picture of a CT slice imported in AMIRA; B) Picture of the same imported CT slice segmented in AMIRA; C) The contour of dentin computed in the program AMIRA; D) The same contour of dentin after processing in an in-house developed program; E) The spline computed in the program SolidWorks from the outer contour of dentin

form the 3D solid model. The program AMIRA can use several different alignment procedures. For the solid model described in this paper, the alignment of the center of gravity was used. This alignment procedure provides that the centers of gravity of all slices are positioned on the same vertical line. The most important thing in the preparation for the 3D solid model is the computation of contours. In the contour computation procedure, the program AMIRA calculates the sequence of points that make contours (line that divides two entities). It is necessary to compute contours for all entities (enamel, dentin and pulp) and along the selected axis (in this paper – z axis). All these contours were written in series of data files. In order to make it possible to import the contours in program for 3D solid modeling, data files ought to be written in standard file format for CAD exchange. A very popular CAD exchange file formats is DXF (DXF – Drawing eXchange Format) and it is used for transferring data from the program AMIRA to the program SolidWorks (SolidWorks Corp., USA).

The basic idea of the development of a 3D solid model is representing contours with splines and building solid model using “Loft” feature. Example of a dentine contour is shown in Fig. 1C.

From Fig. 1C it can be seen that the dentine contour is not suitable for definition of the spline. On the figure one can see larger and smaller horizontal and vertical lines that splines can’t handle very well. Because of that an in-house developed program was used for preparing dentine contour for splines. Fig. 1(C,D,E) shows picture of the same dentine contour before the use of the program, after the use of the program and finally the spline constructed from the dentine contour, respectively.

The 3D solid model was developed in the program SolidWorks. The program SolidWorks is a very popular program for CAD/CAM (CAD – Computer Aided Design, CAM – Computer Aided Manufacturing). The process of developing a 3D solid model consisted of the following steps:

- definition of required number of horizontal planes (xy planes) positioned at the exact height along the z axis as the contour CT slices,

- importing adequate contours in the defined horizontal plane and definition of spline,
- building a 3D solid body from the splines positioned in horizontal planes by using the “Loft” tool (Fig. 2).

This procedure is repeated for each tooth structure: the enamel, the dentin and the pulp. The 3D solid model of the whole human maxillary premolar with the surrounding tissues is presented in Fig. 3A, 3B, 3C and 3D.

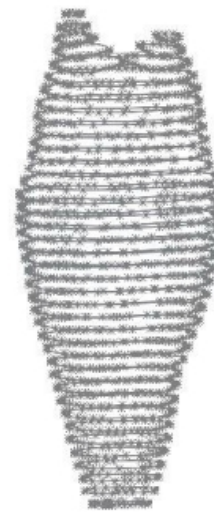


Fig. 2. The 3D solid body of dentin made from the splines positioned in horizontal planes

As in classical mechanical assembly which consists of several parts, the human maxillary premolar was constructed as the assembly from three parts: the enamel, the dentin and the pulp. All parts in the assembly were bonded. The 3D solid model was developed for the research of stress and strain in the human tooth. This can be done using finite element analysis (FEA). Necessary condition for the stress and the strain calculation by the finite element method (FEM) is a definition of boundary conditions. It is not possible to define adequate boundary conditions for the human tooth if the periodontal ligament (PDL) and the

alveolar bone are not added to the 3D solid model of a human tooth. So the complete 3D solid model of the human maxillary premolar consisted of five parts: the enamel, the dentin, the pulp, the periodontal ligament and the alveolar bone. The periodontal ligament was modeled using the “Shell” feature to follow the outer surface of the human maxillary premolar and to have thickness of 0.2 mm. The 3D solid model of the human maxillary premolar with the periodontal ligament and the cortical bone is presented in Fig. 3C and 3D).

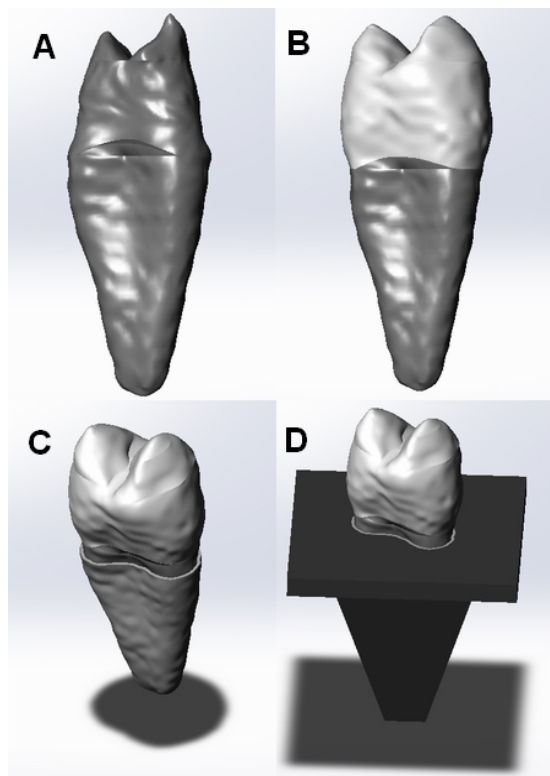


Fig. 3. 3D solid model of the human maxillary premolar. A) Dentin; B) Dentin and enamel; C) Tooth with the PDL; D) Tooth with the surrounding PDL and bone tissue

3. FINITE ELEMENT ANALYSIS OF THE HUMAN MAXILLARY PREMOLAR

After finishing the 3D solid model of the human maxillary premolar, the next step was the definition of parameters for the finite element analysis. The first step was the assignment of material properties. It was assumed that all materials and tooth structures had a linear elastic behavior which can be represented by the Young’s modulus of elasticity and the Poisson’s ratio. The material characteristics are presented in Table 1.

In order to be able to calculate various types of stress and strain in tooth structures, generated by different therapeutic procedures by FEA, one ought to define three necessary things: the fixture, the load and the mesh. In our case, the fixture was standard fixture with fixed geometry. The exterior nodes on all surfaces of the cortical bone were fixed in all directions so they could not move or rotate. The load was applied to the

tooth at three points on the occlusal surface of the premolar (one on the palatal cusp, and the other two on the mesial and distal marginal ridge), mimicking the natural biting position with the resulting force crossing the central position. The intensity of the resulting force was 150 N.

Material	Young’s modulus [Mpa]	Poisson’s ratio [-]
Enamel	84100	0.20
Dentin	18600	0.31
Pulp	2	0.45
Peridontal ligament	70	0.45
Cortical bone	15000	0.30

Table 1. Material characteristics of the tooth tissues [11]

The solid mesh, which was appropriate for complex 3D solid models, was used in this study. The standard mesher which generated parabolic tetrahedral solid elements was used for meshing in the SolidWorks program. The parabolic tetrahedral element is defined by four corner nodes, six mid-side nodes and six edges. In this paper parabolic elements were used because they represent curved boundaries more accurately and they produce better mathematical approximations. After the convergence test the resulting 3D solid model had 116244 nodes and 75231 elements. The meshed 3D solid model is presented in Fig. 4.

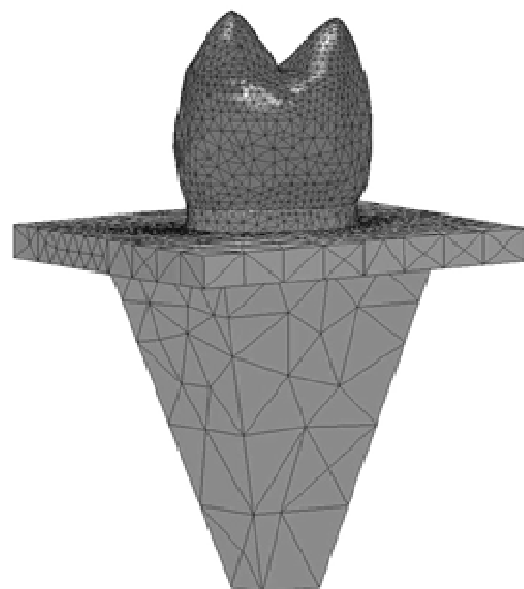


Fig. 4. The 3D solid model of the human maxillary premolar meshed in the program SolidWorks

After the mesh is complete, stress and strain can be

calculated using FEA. As a result, the researchers receive rather precise information about the Von Mises stresses, principal stresses, cuspal deflection, and the distribution of the stresses in tooth structures and biomaterials (Fig. 5).

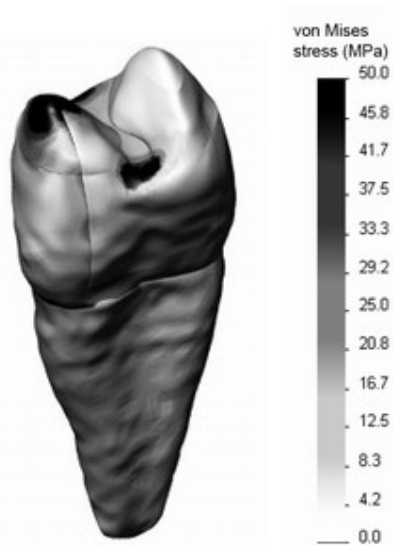


Fig. 5. The example of the calculated Von Mises stresses using FEA on a tooth model restored with mesio-occluso-distal composite filling

4. CONCLUSIONS

A realistic 3D-FE solid model of a maxillary premolar tooth was successfully generated in the Solidworks program using CT data. Overall, the model created in this study presented good results and reproducibility and confirmed FEA to be a valid method for stress and strain calculation in biological structures.

5. REFERENCES

- [1] Bitter, K., Meyer-Lueckel, H., Fotiadis, N., Blunck, U., Neumann, K., Kielbassa, AM., Paris, S.: *Influence of endodontic treatment, post insertion, and ceramic restoration on the fracture resistance of maxillary premolars*, International Endodontic Journal, vol. 43, pp. 469–477, Jun 2010.
- [2] Soares, P.V., Santos-Filho, P.C.F., Queiroz, E.C., Araújo, T.C., Campos, R.E., Araújo, C.A., Soares, C.J.: *Fracture resistance and stress distribution in endodontically treated maxillary premolars restored with composite resin*, Journal of Prosthodontics, vol. 17, pp. 114–9, Feb 2008.
- [3] Jiang, W., Bo, H., YongChun, G., LongXing, N.: *Stress distribution in molars restored with inlays or onlays with or without endodontic treatment: A three-dimensional finite element analysis*, Journal of Prosthetic Dentistry, vol. 103, pp. 6–12, 2010.
- [4] Wakabayashi, N., Ona, M., Suzuki, T., Igarashi, Y.: *Nonlinear finite element analyses: advances and challenges in dental applications*, Journal of Dentistry, vol. 36, pp. 463–71, July 2008.

- [5] Vukadinov, T., Blaži, L., Kantardži, I., Lainovi, T.: *Primena metode kona nih elemenata u stomatološkim istraživanjima*, Medicina danas, vol. 12, pp. 29–33, 2013.
- [6] Lin, C.-L., Chang, Y., Lui, P.: *Multi-factorial analysis of a cusp-replacing adhesive premolar restoration: A finite element study*, Journal of Dentistry, vol. 36, pp. 194–203, 2008.
- [7] Chatvanitkul, C., Lertchirakarn, V.: *Stress distribution with different restorations in teeth with curved roots: a finite element analysis study*, Journal of Endodontics, vol. 36, pp. 115–118, Jan. 2010.
- [8] Dejak, B., Młotkowski, A.: *3D-Finite element analysis of molars restored with endocrowns and posts during masticatory simulation*, Dental Materials, vol. 29, pp. e309–e317, 2013.
- [9] Rodrigues, F., Li, J., Ballester, R., Watts, D.: *Sequential software processing of micro-XCT dental -images for 3D-FE analysis*, Dental Materials, vol. 25, pp. e47–e55, 2009.
- [10] Ausiello, P., Franciosa, P., Martorelli, M., Watts, D.C.: *Numerical fatigue 3D-FE modeling of indirect composite-restored posterior teeth*, Dental Materials, vol. 27, pp. 423–30, May 2011.
- [11] Kantardži, I., Vasiljevi, D., Blaži, L., Puškar, T., Tasi, M.: *Computed-tomography scan-based finite element analysis of stress distribution in premolars restored with composite resin*, Physica Scripta, vol. T149, p. 014075, 2012.
- [12] Kantardži, I., Vasiljevi, D., Blaži, L., Lužanin, O.: *Influence of cavity design preparation on stress values in maxillary premolar: a finite element analysis*, Croatian Medical Journal, vol. 53, pp. 568–576, 2012.

6. ACKNOWLEDGEMENTS

This paper presents part of the research realized in the framework of two research projects financed by the Ministry of Education, Science and Technological Development of the Republic of Serbia (Grant numbers III 45016 and TR 035020)

7. INFORMATION

Authors: Associate Research Professor **Darko Vasiljevi**, MSc, PhD, University of Belgrade, Institute of Physics, 118 Pregrevica, 11000 Belgrade, Serbia, Phone: +381113162067; **Tatjana Maravi**, DMD, Assistant **Ivana Kantardži**, PhD, **Tijana Lainovi**, DMD, University of Novi Sad, Faculty of Medicine, School of Dentistry, 3 Hajduk Veljkova, 21000 Novi Sad, Serbia, Phone: +381216615706; **Full professor Larisa Blaži**, MSc, PhD, University of Novi Sad, Faculty of Medicine, School of Dentistry, Clinic of Dentistry of Vojvodina, 12 Hajduk Veljkova, 21000 Novi Sad, Serbia, Phone: +381216612222; E-mail: darko@ipb.ac.rs; vukadinov.tatjana@gmail.com; ivanakantardzic@gmail.com; tijana.lainovic@gmail.com; larisa.blazic@gmail.com

12th INTERNATIONAL SCIENTIFIC CONFERENCE MMA 2015 -
FLEXIBLE TECHNOLOGIES

PROCEEDINGS



AUTHOR INDEX

Novi Sad, 25-26 September 2015



Author Index

A

Adamovi S.....207
Adamovi , D.207
Agarski, B.211
Anti , A.....63
Anwer, N.....227

B

Babi , B.....121, 125
Badida, M.....181
Barali , J.25
Beju, L.D.....79
Beker, I.....215
Blaži , L.....247
Bojani , M.....83, 153
Borodavko, V.....5
Borojevi , S.....67, 141
Brindasu,P.D.79
Budak, I.....247
But, A.....145

C

Cerjakovi E.....113

Či a,67

Čosi , I.....101
Čukovi , S.....223

D

Devedži , G.....223
Dimi , Z.....51
Dori , J.....207
Dudi , S.195

Đur ev, M.117

F

Fajsi, A.215

G

Gaiko, V.5
Galzina, V.75
Gluvakov, Z.....211
Gostimirovi , M.1, 13, 21, 29
Gruji , J.....227

H

Hadžistevi , M.13, 83, 87, 97
Heri , M.129
Hodoli , J.211

I

Ivaniševi , A.....169, 177, 231
Ivaniševi , S.151

J

Jakovljevi , Ž.137, 149, 161
Ješi , D.21
Joti , G.87
Jovi i , G.....117
Joviševi , V.....141
Juki , J.....75

K

Ka mar ik, I.....169, 177, 231
Kakaš, D.191
Kantardži , I.....247
Katalini , B.101
Kheifetz, M.5, 9

Klimenko, S.	5, 9
Knežev, M.	43
Kokotovi , B.	137, 161
Kopa , J.	1, 29
Košarac, A.	37
Kosec, B.	211
Kosti , I.	247
Košut, Z.	211
Kova , P.	13, 21
Kova evi , L.	191
Kraišnik, M.	185
Kramar, D.	1, 29
Kukuruzovi , D.	191
Kulundži , N.	21
Kvrgi , V.	51

L

Lainovi , T.	247
Lali , B.	101
Lazarevi , D.	47
Li en, H.	227
Lovri , S.	113
Luki , Lj.	71, 157
Luki , D.	117
Lukovi , V.	223
Lutovac, M.	51

M

Majstorovi , D.V.	93
Mandi , V.	165
Maravi , T.	247
Markovi , V.	149
Matin, I.	97
Mihailovi , M.	165
Mihajlovi , I.	203
Milenkovi , I.	195
Mileti , A.	191
Milji , V.	207
Milojevi , Z.	153
Miloradov, M.	203, 207
Miloševi , M.	63, 117
Milutinovi , M.	169, 173, 177, 231
Miljkovi , Z.	121, 125
Miši , D.	247
Miši , M.	247
Miti , M.	121, 125
Mitrovi , S.	51
Mla enovi , C.	37, 43, 55, 83
Mora a, S.	215
Movrin, D.	177, 231, 243
Muránsky, J.	219
Muženi , D.	1

N

Navaluši , S.	79
Nedi , B.	25, 47
Nedi , N.	71

Nikoli , I.	75
Nikolic, S.	173

P

Patari , A.	165
Pejašinovi , Z.	87
Petronijevi , J.	121, 125
Petrovi , A.	157
Petrovi , M.	121, 125
Plan ak, M.	169, 177
Plemi , A.	125
Pozilova, N.	9
Prodanovi , S.	71
Pucovski, V.	13, 29
Pynkin, A.	9

R

Radlova ki, V.	97
Radoni , J.	203
Ran elovi , S.	173, 235
Raspudic, V.	239
Relji , V.	195
Rodi , D.	13, 21
Rom ek, A.	227

S

Sekuli , M.	1, 13, 29
Sekuli , S.	33
Simonovi , S.	17
Skakun, P.	169, 177, 231
Sobotová, L.	181
Spasi – Joki , V.	97
Spasi , A.	231, 243
Sredanovi , B.	67
Stefanovi , M.	165, 185
Stojadinovi , M.S.	93
Subburaj, K.	223
Svalina, I.	75

Š

Šari , T.	63, 75
Šešlja, D.	195
Ševi , D.	215
Ši anin, L.	185
Šimunovi , G.	75
Šimunovi , K.	75
Šokac, M.	243
Šormaz, D.	105, 129
Španik, I.	203
Štrbac, B.	87, 97
Šulc, J.	195

T

Tabakovi , N.....	227
Tabakovi , S.	55, 59, 153
Taniki , D.	173, 235
Tanovi , Lj.....	5, 9
Teki , Ž.....	101
Terek, P.....	191
Till, V.....	247
Todi , V.....	141
Top i , A.....	113
Turk Sekuli , M.	203

V

Vasiljevi , D.	247
Vidakovi , J.	51
Viloti , D.....	169, 177, 185
Vojinovi Miloradov, M.	203, 207
Vu aj irilovi , V.....	231
Vuki evi , M.....	199
Vukman, J.	117
Vukovi , N.....	121, 125

W

Wakhare, M.....	105, 129
-----------------	----------

Z

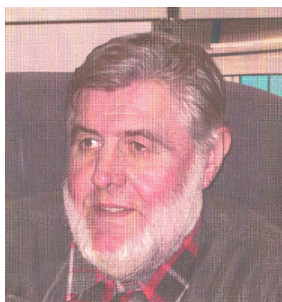
Ze evi -Lukovi , T.....	223
Zeljкови , M.....	37, 55, 59 67, 145, 157

Ž

Živanovi , S.	59, 137, 149, 161
Živkovi , A.	37, 43, 55

IN MEMORIAM

Prof. dr Ratko Gatalo (1941 – 2014)



Tiho, kao što je i živeo, u petak 3. oktobra 2014. godine, nakon kraje i teške bolesti umro je naš uvaženi dr Ratko Gatalo, redovni profesor Fakulteta tehničkih nauka u Novom Sadu.

Ratko Gatalo je rođen je 29.05.1941. godine u Potocima kod Mostara. Osmogodišnju školu završio je 1956. godine u Gajdobri. Industrijsku srednju tehničku školu-mašinski odsek, u Novom Sadu završio je 1960. godine. Diplomirao je na proizvodnom odseku Mašinskog fakulteta u Novom Sadu 1964. godine. Poslediplomske studije za stepen magistra nauka završio je na smeru za proizvodno mašinstvo na Mašinskom fakultetu u Beogradu. Magistarski rad pod nazivom "Primena kompjutera manjeg kapaciteta u tehnologiji izrade delova metalopreraiva u industriji" odbranio je juna 1973. godine. Doktorsku disertaciju pod nazivom "Prilog razvoju integralnog sistema za automatsko projektovanje rotacionih izradaka i njihove tehnologije izrade u metalopreraiva u industriji" odbranio je na Fakultetu tehničkih nauka u Novom Sadu juna 1978. godine.

Radni vek započeo je u preduzeću "Ge-Ge" u Adi 1964. godine, zatim u Birou za projektovanje livnica u preduzeću Centralna remontna radionica DTD u Novom Sadu. Od 01. oktobra 1967. godine radio je kao asistent na Katedri za mašinsku obradu i mašine alatke na Mašinskom fakultetu u Novom Sadu. Godine 1973. izabran je u zvanje docenta, 1980. godine u zvanje vanrednog profesora, a u zvanje redovnog profesora na predmetima Automatsko upravljanje mašinama i Mašine alatke na istom fakultetu izabran je 1986. godine. Pored predavanja na predmetima Mašine alatke, Automatsko upravljanje mašinama i Eksploatacija mašina alatki razvio je i predavao predmete CAD/CAPP/CAM postupci, Automatski fleksibilni tehnološki sistemi i Automatizacija postupaka projektovanja, kao i predmete Automatizacija mašina alatki na VTS u Subotici i Raunarska grafika na Tehničkom fakultetu u Zrenjaninu. Na Mašinskom fakultetu u Istom Sarajevu razvio je i predavao predmet Tehnološki obradni sistemi-CIM, kasnije Fleksibilni tehnološki sistemi, punih deset godina. Na magistarskim studijama razvio je i predavao više kurseva iz područja savremenih mašina alatki, fleksibilnih tehnoloških sistema i automatizacije postupaka projektovanja. Na Fakultetu je poseban doprinos dao razvoju laboratorijske baze. Pod njegovim vodstvom diplomiralo je preko 120 inženjera. Bio je mentor i član komisija za odbranu u preko 50 magistarskih radova i preko 30 doktorskih disertacija. Autor je 6 knjiga, preko 250 naučnih i stručnih radova objavljenih u časopisima i zbornicima radova u zemlji i inostranstvu, preko 50 elaborata naučno-istraživačkih projekata i tema i preko 60 stručnih radova.

U toku rada na Fakultetu bio je prodekan za nastavu, rukovodilac Mašinskog odseka, direktor Instituta za proizvodno mašinstvo, glavni i odgovorni urednik časopisa Proizvodno mašinstvo. Više od petnaest godina bio je šef Katedre za tehnologiju i sisteme obrade skidanjem materijala. Za svoj rad dobio je dve Plakete Fakulteta tehničkih nauka, Plaketu Pokrajinskog komiteta za nauku i informatiku Vojvodine, Oktobarsku nagradu grada Novog Sada i Plaketu i povelju "Prof. dr Pavle Stanković".

Svojim nesebičnim i samopregornim radom doprineo je da današnji laboratorijski kapaciteti Katedre i Instituta za proizvodno mašinstvo ni malo ne zaostaju ni za laboratorijama u najpoznatijim istraživačkim centrima slične namene u svetu.

Odlaskom u penziju krajem 2001. godine Prof. Gatalo ni u jednom trenutku nije prekinuo saradnju sa kolegama, mladim kadrovima u Laboratoriji, na Katedri, Institutu, Fakultetu i šire. Do poslednjih dana je bio aktivan u realizaciji magistarskih i doktorskih studija. Posebnu aktivnost je pokazao u okviru projekata naučno-istraživačkog rada i projekata saradnje sa privredom.

Mi, njegovi saradnici, kolege, nekadašnji studenti, poštovaoci njegovog nesebičnog zalaganja i rada, s poštovanjem omo se sećati profesora Ratka Gatala.

IN MEMORIAM

Prof. dr Ratko Gatalo (1941 - 2014)



Silently, just like he lived his life, on Friday, October the 3rd 2014, our esteemed Dr. Ratko Gatalo, Full Professor at the Faculty of Technical Sciences in Novi Sad had passed after a short illness.

Ratko Gatalo was born on 29.05.1941. in Potoci near Mostar. He finished elementary school in 1956. in Gajdobra. In 1960. he completed Industrial-technical high school - mechanical division in Novi Sad. He graduated at the production department of the Faculty of Mechanical Engineering in Novi Sad in 1964. He finished his postgraduate studies for the degree of Master of Science at the Department of Production Engineering of the Faculty of Mechanical Engineering in Belgrade. In June 1973. he completed his Master's thesis entitled "Application of low capacity computers in the technology of metal-parts industry". In June 1978. he finished his PhD thesis entitled "Contribution to the development of integrated systems for automated design of rotating workpieces and their production technology in the metal industry" at the Faculty of Technical Sciences in Novi Sad.

He started his professional career at the "Ge-Ge" in Ada in 1964, then in the Bureau for the foundry design in the Central repair workshop DTD in Novi Sad. On 1st October 1967 he started his university career as an assistant at the Chair of machining and machine tools at the Faculty of Mechanical Engineering in Novi Sad. In 1973. he was elected assistant professor, in 1980. associate professor, and was elected to a full professorship in 1986. at the same faculty for the subjects of Automatic machines control and Machine tools. In addition to lectures on the subjects of Machine Tools, Automatic machines control and Exploitation of machine tools, he developed and taught following courses: CAD/CAPP/CAM procedures, Automatic flexible manufacturing systems and Automation of design processes, as well as subjects of Automation of machine tools at the Technical College in Subotica and Computer graphics at the Technical Faculty in Zrenjanin. He has developed and taught Technological machining systems-CIM (later known as Flexible manufacturing systems) at the Faculty of Mechanical Engineering in East Sarajevo for ten years. For the Master's degree studies, he had developed and taught several courses in the field of modern machine tools, flexible technological systems and automation of design processes. He was a special contributor to the development of laboratory base at the Faculty. More than 120 engineers have graduated under his leadership. He was a mentor and/or viva committee member for more than 50 master theses and over 30 doctoral dissertations. He was the author of 6 books, over 250 scientific papers published in journals and conference proceedings in the country and abroad, over 50 research projects studies and themes and over 60 professional papers.

During his professional career at the Faculty, he was the Dean for Academic Affairs, Head of the Mechanical Engineering, Director of the Institute for Production Engineering, as well as the editor in chief of the Production Engineering journal. For more than fifteen years he served as the head of Chair of Technology and machining systems. For his work, he received two Awards of the Faculty of Technical Sciences, Award of the Regional Committee of Science and Informatics of Vojvodina, October Award of Novi Sad and the Award plaque "Prof. Dr. Pavle Stankovi".

His selfless and self-sacrificing work has immensely contributed to today's laboratory capacity of the Chair and the Institute for Production Engineering, making it no different than any laboratory in the most prestigious research centers of similar purpose in the world.

Prof. Gatalo's retirement at the end of 2001. has not stopped his cooperation with colleagues, younger personnel in the Laboratory, Department, Institute, Faculty and beyond. Until the last few days of his life he was active in the implementation of master's and doctoral studies. He demonstrated a special activity in the framework of projects of scientific research and cooperation projects with industry.

We, his associates, colleagues, former students and admirers of his selfless commitment and work will respectfully remember Professor Ratko Gatalo.

12th INTERNATIONAL SCIENTIFIC CONFERENCE MMA 2015 -
FLEXIBLE TECHNOLOGIES

PROCEEDINGS



INFORMATION ABOUT DONATORS

Novi Sad, 25-26 September 2015

**MINISTARSTVO PROSVETE,
NAUKE I TEHNOLOŠKOG
RAZVOJA**

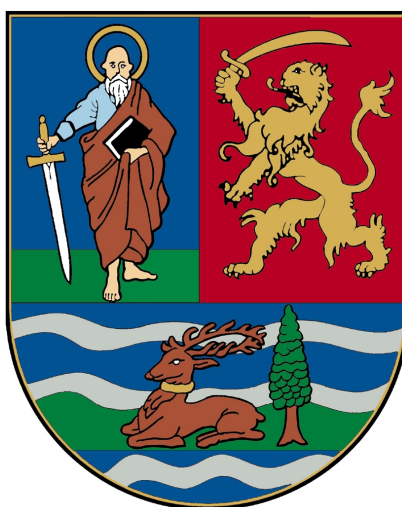


Nemanjina 22-26
11000 Beograd

www.mpn.gov.rs

REPUBLIKA SRBIJA
AP Vojvodine

SEKRETERIJAT ZA NAUKU I TEHNOLOŠKI RAZVOJ AP VOJVODINE



Bulevar Mihajla Pupina 16
21108 Novi Sad

Tel: (021) 487 4641

Fax: (021) 456 044

E-mail: secretary@apv-nauka.ns.ac.rs

<http://apv-nauka.ns.ac.rs/vece/index.jsp>

Univerzitet u Novom Sadu
Fakultet tehni kih nauka
Vladimira Perića-Valtera 2
21000 Novi Sad
Srbija

FAKULTETET TEHNI KIH NAUKA

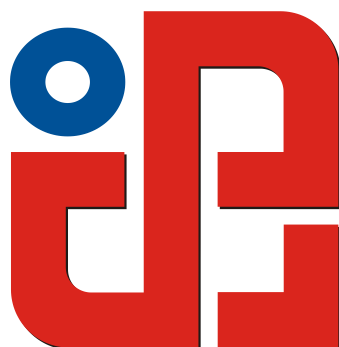


FTN marketing služba:
Tel: (021) 485 20 61
Fax: (021) 458 133
E-mail: agak@uns.ac.rs
www.ftn.uns.ac.rs

POTRAŽITE INFORMATOR!

Univerzitet u Novom Sadu
Fakultet tehničkih nauka
Vladimira Perića-Valtera 2
21000 Novi Sad
Srbija

DEPARTMAN ZA PROIZVODNO MAŠINSTVO

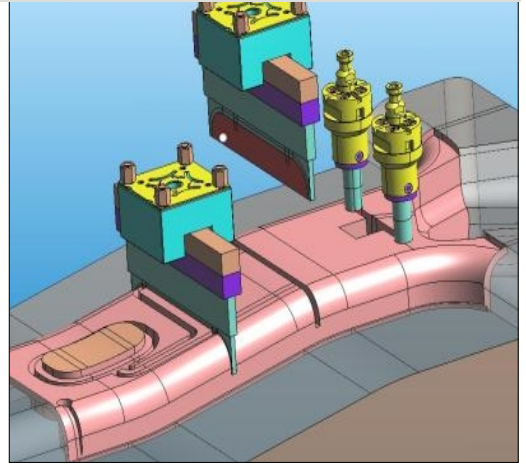
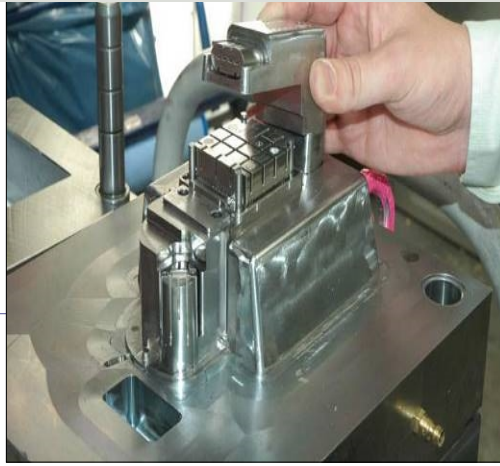
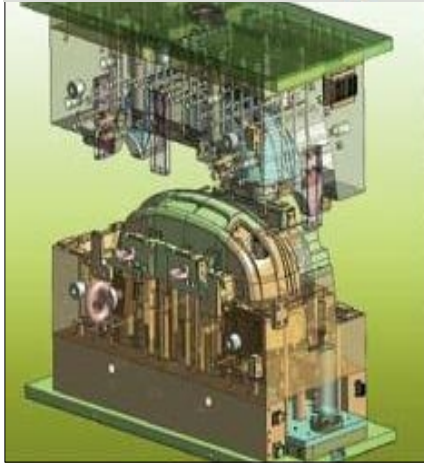


sekreterijat departmana:
Tel: (021) 450-366, 485-23-20
Fax: (021) 454-495
E-mail: ipm@uns.ac.rs
www.ftn.uns.ac.rs
www.dpm.ftn.uns.ac.rs

POTRAŽITE INFORMATOR!

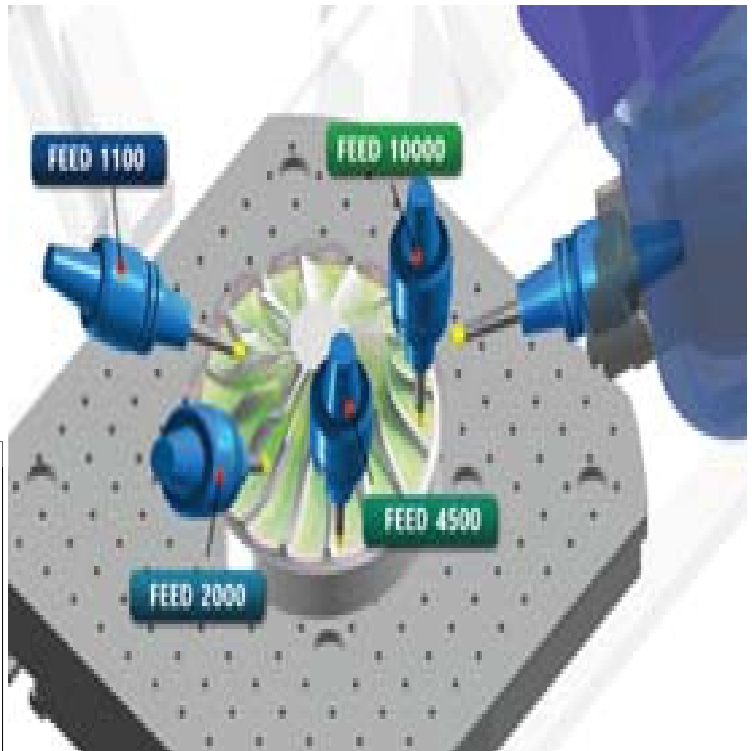
Cimatron^E

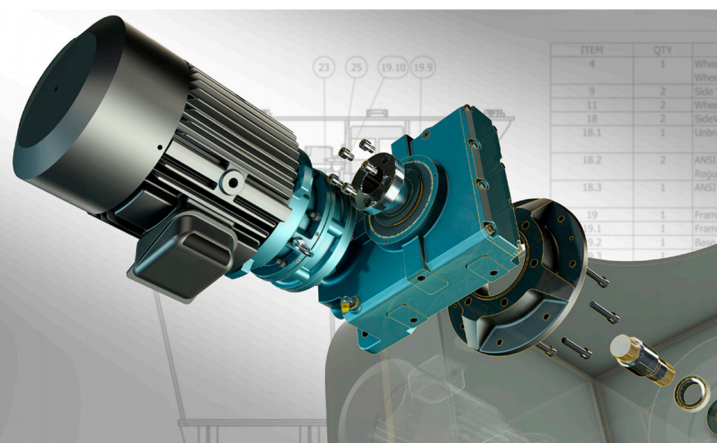
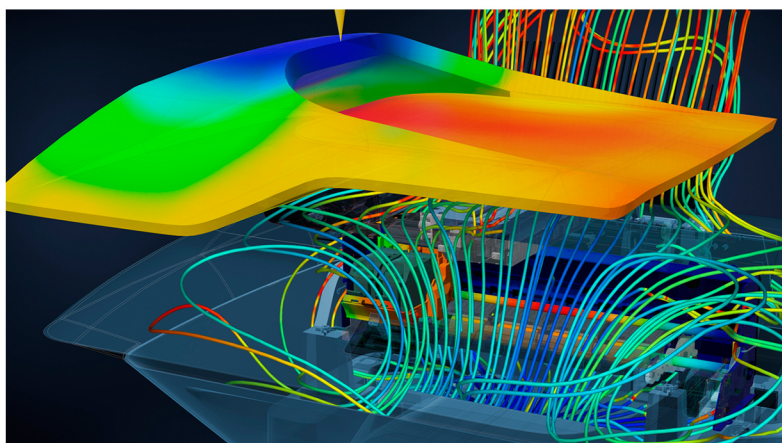
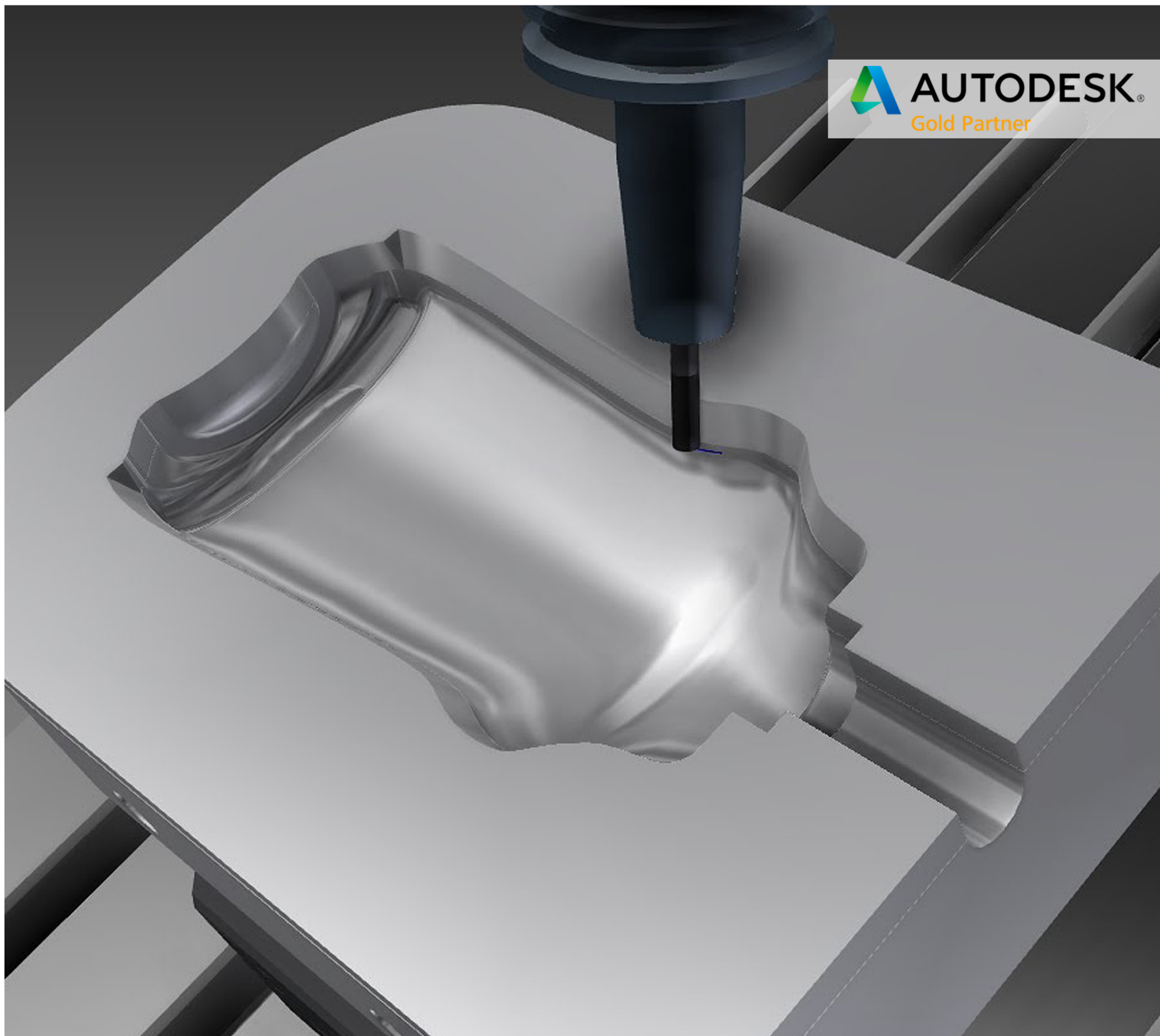
Solution for design and execution of moulds, optimization of CNC programs




NCBRAIN 5X

Software for collision check and optimization of CNC programs





Autodesk nudi zaokruženu paletu programa, koji omogućavaju rešavanje svih problema pri projektovanju u proizvodnom mašinstvu. Paletu čine programi za projektovanje i izradu tehničke dokumentacije, kreiranje digitalnih prototipova, simulacije kretanja i opterećenja, analize i proračune fluida, alate za projektovanje proizvoda od plastike, CAM rešenja, kao i programe za upravljanje **tehničkom dokumentacijom...**



www.teamcad.rs

Bulevar Mihajla Pupina 10g / 254,
11070, Novi Beograd, Srbija

Moldex3D

M O L D I N G I N N O V A T I O N

Moldex3D®

Faster and more reliable plastic injection molding simulation anytime, anywhere

eDesign

Ensure your design

- ▶ Validate and optimize part/mold design with true 3D simulation
- ▶ Minimize cost, design cycle and time to market
- ▶ Maximize productivity and return on investment

Quick & Direct
CAD/CAE
Integration

Robust
Analysis Engine

High-Speed
Computation

Accurate
&
Understandable
Results

CoreTech System Co., Ltd. Headquarters
8F-2, No.32, Taiyuan St., Chupei City,
Hsinchu County 302, Taiwan
Tel: +886-3-560-0199

RESELLER FOR SERBIA, BOSNIA AND HERZEGOVINA, MONTENEGRO

TECHNO MEDICAL SOLUTION CENTER
JOSIFA MARINKOVICA 15
26000 PANCEVO
TEL: +381 64 133 17 44
HTTP://WWW.MOLDEX3D.COM

TMSC

TECHNO-MEDICAL
SOLUTION CENTER

Proizvodni program, proizvodi i usluge su odraz visoke stručnosti i dugogodišnjeg iskustva sopstvenih kadrova u razvoju i proizvodnji opreme i postrojenja za prirodni gas, TNG i naftu.

Stručnost i iskustvo kadra, razvoj i proizvodnja na savremenim mašinama i ispitivanje u sopstvenoj laboratoriji za gasnu tehniku, omogućili su osvajanje široke lepeze proizvoda, koji po svojim performansama zadovoljavaju najoštrije kriterijume domaćih i inostranih standarda.

U cilju kvalitetnog i pouzdanog poslovanja, implementirani su međunarodni standardi ISO 9001:2008, ISO 14001:2005 i OHSAS 18001:2007, izvršena sertifikacija po GOST-u.

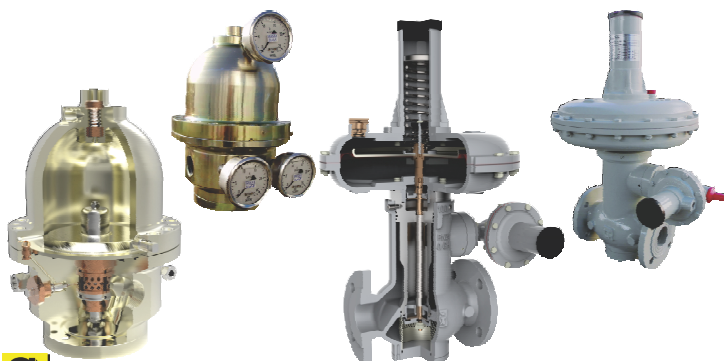


Proizvodnja mašinskih delova za potrebe proizvodnje gasne opreme obavlja se na CNC mašinama visoke tačnosti i performansi, a kapaciteti omogućuju i uslužnu mašinsku obradu na sledećim mašinama:

- sedam strugarskih obradnih centara za struganje, bušenje, glodanje
- četiri horizontalna obradna centra
- jedna koordinatna merna mašina

U „GasTeh“-u se nalazi pogon za procesnu tehniku, gde se vrši zavarivanje i montaža gasno-energetske opreme za potrebe proizvodnje i inženjering poslove.

U pogonu „GasTeh“-a se pored proizvodnje sopstvenih proizvoda, vrši i uslužna mašinska obrada. Isti se obrada pozicija za automobilsku industriju i firme „Audi“ i „BMW“.





DOO "GRUJIĆ I GRUJIĆ"

Bul. Vojvode Stepe 6, NOVI SAD, SRBIJA, Tel/fax: 021/518 381, 021/6403 091
Mob. 063/865 78 79, e-mail:grujicgrujicns@gmail.com

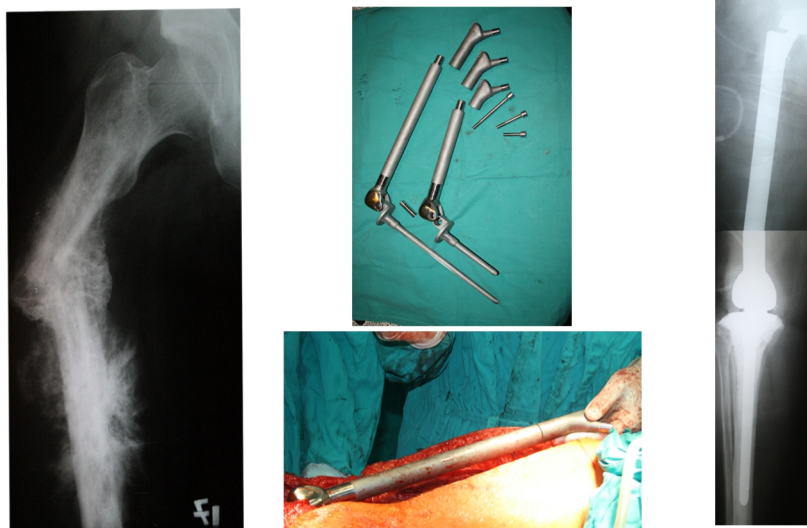
Endoproteza ramena



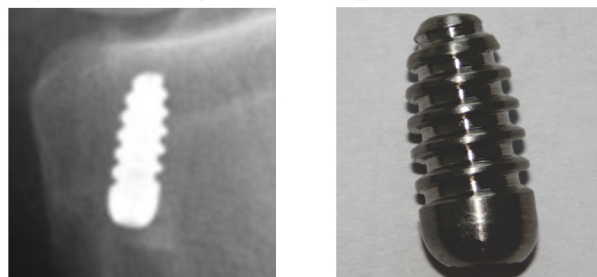
Modularna proteza zgloba kuka



Modularna proteza zgloba kuka i kolena – „total femur”



Vijak za ligamentoplastiku kolena



FKL[®] ∞

FABRIKA KOTRLJAJUĆIH LEŽAJA I KARDANA

Dugogodišnja saradnja sa
Institutom za proizvodno mašinstvo
na primeni CNC mašina i razvoju novih proizvoda

Industrijska zona bb
21235 Temerin

Tel: +381 21 68 41 100

Fax: +381 21 842 650

www.fkl-serbia.com

